Photoinduced Iodoperfluoroalkylation of Unsaturated Hydrocarbons

Inaugural-Dissertation

zur Erlangung des Doktorgrades
der Mathematisch-Naturwissenschaftlichen Fakultät
der Heinrich-Heine-Universität Düsseldorf

vorgelegt von

Lucas Helmecke

aus Solingen

Düsseldorf, Oktober 2020

aus dem Institut für Organische und Makromolekulare Chemie
der Heinrich-Heine-Universität Düsseldorf

Gedruckt mit der Genehmigung der
Mathematisch-Naturwissenschaftlichen Fakultät der
Heinrich-Heine-Universität Düsseldorf

Berichterstatter:

1. Prof. Dr. Constantin Czekelius
2. PD Dr. Klaus Schaper

Tag der mündlichen Prüfung: 14.12.2020

Eidesstattliche Erklärung

Ich versichere an Eides statt, dass die vorliegende Dissertation von mir selbstständig, ohne unzulässige fremde Hilfe unter der Beachtung der "Grundsätze zur Sicherung guter wissenschaftlicher Praxis" an der Heinrich-Heine-Universität Düsseldorf erstellt worden ist. Die aus fremden Quellen direkt oder indirekt übernommenen Gedanken sowie Ergebnisse sind als solche kenntlich gemacht. Die Arbeit wurde bisher weder im Inland noch im Ausland in gleicher oder ähnlicher Form einer anderen Prüfungsbehörde vorgelegt. Es wurden keine früheren erfolglosen Promotionsversuche unternommen.

Düsseldorf, den _____ _____

Lucas Helmecke

Preface

This doctoral thesis is composed of five parts. The first four parts present and summarize four publications, which were published in the context of this doctorate. The fifth part presents unpublished results.

The first part of this thesis presents and summarizes the results of the publication "Mechanistic Insights into FLP-Catalyzed Iodoperfluoroalkylations" and gives insights into a FLP-catalyzed iodoperfluoroalkylation that was published by Czekelius *et al.* in 2016.[1] The publication is attached, reprinted with permission and can be cited as: Spittler, M.; Helmecke, L.; Czekelius, C. *Eur. J. Org. Chem.* **2019**, 458-468; DOI: 10.1002/ejoc.201800866.[2] Copyright (2019) WILEY-VCH.
Further work on this topic was presented in the doctoral thesis of Dr. M. Spittler and can be cited as: Spittler, M. Frustrated Lewis Pair-Catalysed Functionalisation of Alkenes with Iodoperfluoroalkanes and Gold-Catalysed Desymmetrisation of 1,4-Diynes. Heinrich-Heine-Universität Düsseldorf; http://docserv.uni-duesseldorf.de/servlets/DocumentServlet?id=50212, 2018.[3]

The second part of this thesis presents and summarizes the results of the publication "Metal-Free Activation of C–I Bonds and Perfluoroalkylation of Alkenes with Visible Light Using Phosphine Catalysts". It gives insights into photomediated iodoperfluoroalkylation of alkenes and first mechanistic findings. The publication is attached, reprinted with permission and can be cited as: Helmecke, L.; Spittler, M.; Baumgarten, K.; Czekelius, C. *Org. Lett.* **2019**, 21 (19), 7823-7827; DOI: 10.1021/acs.orglett.9b02812.[4] Copyright (2020) American Chemical Society.

The third part of this thesis presents and summarizes the results of the publication "Visible Light-Induced Homolytic Cleavage of Perfluoroalkyl Iodides Mediated by Phosphines" and gives insights through theoretical calculations into the photomediated iodoperfluoroalkylation. The publication is attached and can be cited as: Bracker, M.; Helmecke, L.; Kleinschmidt, M.; Czekelius, C.; Marian, C. M. *Molecules* **2020**, *25* (7), 1606; DOI: 10.3390/molecules25071606.[5]

The fourth part of this thesis presents and summarizes the results of the publication "Metal-free Iodoperfluoroalkylation: Photocatalysis vs. Frustrated Lewis Pair Catalysis" and compares the

FLP-catalyzed with the phosphorus-catalyzed as well as the photomediated iodoperfluoroalkylation. Additionally, the substrate scope was extended to alkynes. Further investigations regarding the photomediated iodoperfluoroalkylation, like the addition of iodide salts, an interval irradiation, a reaction at elevated temperature, a determination of the association constant for $^{t}Bu_3P$, PPh_3, $(MeO)_3P$, were conducted. The manuscript and the Supporting Information are not attached to this doctoral thesis. The publication can be cited as: Helmecke, L.; Spittler, M.; Schmidt, B. M.; Czekelius, C. *Synthesis* **2020**, 6; DOI: 10.1055/s-0040-1707232.[6]

Acknowledgments

This is to acknowledge and thank the people who accompanied and supported me on the way to this dissertation.

First of all, I would like to thank Prof. Constantin Czekelius. After my master thesis in his research group, he not only gave me the opportunity and permission to work in his research group. The whole time he had an "open door" policy and acknowledged my work and fostered it. I was able to learn a lot under his supervision, also beyond my chemical research, which I will take with me on my further scientific path.

Further, I would like to thank PD Dr. Klaus Schaper as second assessor, who has accepted to review this doctoral thesis.

Dr. Michael Spittler already supervised me during my master thesis. During the end of his doctoral studies and the beginning of my doctoral studies, he always challenged and supported me. I would like to thank him for the strenuous but successful initial period of my doctorate and beyond. I was also able to learn a lot apart from laboratory work.

Besides Dr. Michael Spittler, Dr. Kai Baumgarten also supported me since the time of my master thesis. He helped and educated me beyond this time and chemistry.

A heartful thanks to Sabine Houben for lending me a helping hand whenever I was working in the laboratory. I was able to learn new and different working techniques that will help my future work.

I would like to thank Vicky Kemp very much for her support and for staying in touch, even after she finished her studies in germany.

I sincerely thank my parents for their continued and progressive support during my studies and the creation of this dissertation.

Last but not least I would like to thank Genescha Olgar very much for supporting me during the whole time.

Table of Contents

Abbreviations

acac	Acetylacetone
ATR	Atom transfer reaction
ATRA	Atom transfer radical addition
BCF	Tris(pentafluorophenyl)borane
BET	Back electron transfer
BHT	Butylhydroxytoluene
BINAP	2,2′-Bis(diphenylphosphino)-1,1′-binaphthyl
bpy	2,2′-Bipyridine
δ	Chemical shift [ppm]
Cat	Catalyst
CFL	Compact fluorescent lamp
CHD	1,4-Cyclohexadiene
DABCO	1,4-Diazabicyclo[2.2.2]octane
dap	9-Bis(4-anisyl)-1,10-phenanthroline
DBU	1,8-Diazabicyclo[5.4.0]undec-7-ene
DIPEA	Diisopropylamine
DMAc	Dimethylacetamide
DMF	*N,N*-Dimethylformamide
dtbbpy	4,4′-Di-*tert*-butyl-2,2′-dipyridyl
EDA	Electron donor-acceptor
ESI	Electrospray ionization
ee	Enantiomeric excess
ET	Electron transfer
EPR	Electron paramagnetic resonance

equiv	Equivalent(s)
fac	Facial
FLP	Frustrated Lewis pair
GC	Gas chromatography
HAS	Homolytic aromatic substitution
HAT	Hydrogen atom transfer
Hex_F	Tetradecafluorohexane
HOMO	Highest occupied molecular orbital
HRMS	High-resolution mass spectrometry
IR	Infrared spectroscopy
LCD	Liquid-crystal display
LED	Light-emitting diode
LG	Leaving group
LUMO	Lowest unoccupied molecular orbital
m.p.	Melting point
NIS	*N*-Iodosuccinimide
NMM	*N*-Methylmorpholine
NMR	Nuclear magnetic resonance
PC	Photocatalyst
PCET	Proton coupled electron transfer
phen	Phenanthroline
PMP	*p*-Methoxyphenyl
ppm	Parts per million
ppy	2-Phenylpyridine
PTC	Phase-transfer catalyst
RA	Redox auxiliary

R_F	Perfluoroalkyl group/substituent
r.t.	Room temperature
rt	Radical trap
RGB	Red, green, blue
SCE	Saturated calomel electrode
SET	Single-electron transfer
SOMO	Singly occupied molecular orbital
TBAF	Tetrabutylammonium fluoride
TBAI	Tetra-*n*-butylammonium iodide
TBDMSCl	*tert*-Butyldimethylchlorosilane
TBDMS	*tert*-Butyldimethylsilyl
TEA	Triethylamine
TEEDA	*N,N,N′,N′*-Tetraethylethylenediamine
TEMPO	2,2,6,6-Tetramethyl-1-piperidinyloxyl
TFA	Trifluoroacetic acid
TFE	Trifluoroethanol
THF	Tetrahydrofurane
TLC	Thin-layer chromatography
TMEDA	*N,N,N′,N′*-Tetramethylethylendiamine
TMG	1,1,3,3-Tetramethylguanidine
TOF	Time-of-flight
UV-VIS	Ultraviolet-visible

1. Abstract

This doctoral thesis presents results mainly on the topic of photomediated and phosphorus-catalyzed iodoperfluoroalkylations. Previous works to elucidate the reaction mechanism of the FLP-catalyzed iodoperfluoroalkylation, which is described at the beginning of this thesis, led to this efficient photomediated reaction. An investigation and screening of various phosphorus(III) compounds revealed that tri-*tert*-butylphosphine (^{t}Bu$_3$P) was the most effective phosphorus species for this type of reaction. By using catalytic amounts (10 mol%) of ^{t}Bu$_3$P and blue light irradiation (461 nm), various alkenes, as well as alkynes, were transformed into the corresponding addition product. Theoretical calculations supported further understanding of the absorption characteristics, occurring intermediates, as well as the mechanism. Finally, the photomediated reaction was compared to the FLP-catalyzed iodoperfluoroalkylation, which was the starting point for the investigation of this reaction type.

2. Introduction

The introduction of this doctoral dissertation focuses on photochemical fluorinations and perfluoroalkylation. As a start, the advantages of fluorinated products will be illustrated.

2.1. Benefits of fluorine and fluorinated compounds

Fluorinated molecules find significant use in pharmaceutical, agrochemicals, and material science.[7-12] Investigations on organic molecules demonstrated that the replacement of hydrogen or oxygen atoms by fluorine atoms or perfluoroalkyl groups results in advantages regarding reactivity, selectivity, and evidently change the chemical, biological and physical properties of the molecule. This includes the lipophilicity, bioactivity as well as the metabolic stability of the fluorinated compounds in comparison to the non-fluorinated compounds.[12-13] The main reasons for these changes are the high electronegativity of fluorine, a small atomic radius, and the high dipole of a C—F bond.[14-15]

As mentioned previously, the exchange of hydrogen or oxygen atoms by fluorine can be advantageous regarding reactivity and selectivity. In case of changing a CH_3-group (2.0 Å) to a CF_3-group (2.7 Å), the van der Waals radius changes by 0.7 Å.[16] In case of the trifluoromethyl group, the group electronegativity is similar to oxygen.[17-18] Due to the strong negative inductive effect, the expulsion of hydrogen and the introduction of fluorine atoms leads to a substantial increase in the pKs value.[11-12, 15] 50 years ago, there was only about 2% of fluorine-containing drugs on the market.[7] Based on the sales, 30% of the top 30 drugs today contain at least one fluorine atom.[19-20] Additionally, about 20% of the available drugs contain fluorine and 30 - 40% of the agrochemicals (as reported in 2006).[11, 21] In 2012 to 2013, about 40% of the chemical pharmaceutica were fluoroorganic compounds, which were approved in a clinical phase III study.[22-23] Prominent representatives contain a single fluorine molecule, a trifluoro- or perfluoroalkyl group (Scheme 1). Besides, fluorinated and perfluoroalkylated materials are becoming increasingly important in the field of material science.[8, 24-25]

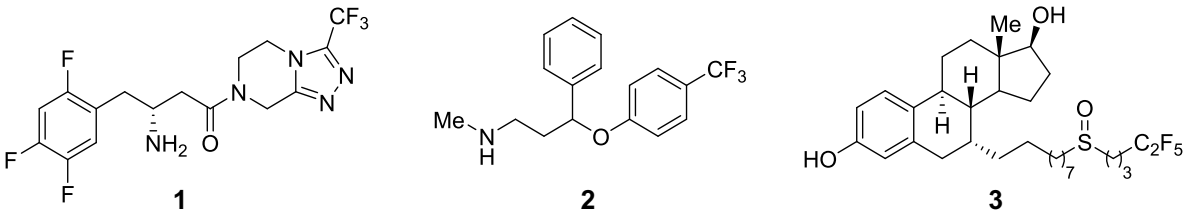

Scheme 1: Prominent representatives which contain fluorine-, trifluoromethyl- or perfluoroalkyl groups.[26-27]

2.2. Photochemistry

When it comes to photochemistry, the first name commonly mentioned is Giacomo Luigi Ciamican (1857 - 1922). Although he was not the first chemist to use sunlight for chemical reactions, he is considered as a pioneer of photochemistry.[28] The image of the photochemical reactions on the rooftop of the University of Bologna, where his reactions were irradiated by sunlight, is still present in many lectures and books. With his quotations at that time, he is now closer than ever to current debates and discussions about the climate crisis and renewable energies.

"Modern civilization is the daughter of coal, for this offers to mankind the solar energy in its most concentrated form [...]. *Modern man uses it with increasing eagerness and thoughtless prodigality for the congest of the world, like the mythical gold of the Rhine* [...]. [...] *But coal is not inexhaustible.* [...] *On the arid lands there will spring up industrial colonies* [...]*; forests of glass tubes will extend over the plains and glass buildings will rise everywhere; inside of these will take place the photochemical processes that hitherto have been the guarded secret of the plant* [...]. *And if in a distant future the supply of coal becomes completely exhausted, civilization will not be cheked by that, for life and civilization will continue as long as the sun shines!"*[28]

Moreover, as described by Ciamican in Science 1912, the industry will continue to move towards photochemical reactions.[28] The continuing popularity in publications and the widespread use of photochemical reactors and photocatalysts is related to the development of different, energy efficient light sources (fluorescent light bulbs, halogen lamps). Pending sufficient sunlight in the past, the development of new irradiation methods aided research investigation of photochemical reactions. The choice of the irradiation source depends on emission of a precisely defined wavelength spectrum which should match the absorption spectrum of the photocatalyst. Since filters in front of the light source had to suffice for a long period, the development of light-emitting diodes (LEDs) with a narrow wavelength and high intensity led to the advancement of photochemistry in the last decades.[29] LED strips and high-power LED lamps made it possible to quickly and easily develop setups for reactions, flow reactors, or photoreactors in the laboratory.[30-31] Since many organic molecules lack an absorption of visible light, the development and improvement of photocatalysts (organic dyes[32] or metal complexes with polyheteroaryl ligands[33-34] and transition metals like Ru, Ir, Cu[34]) contributes to the applicability in organic synthesis. As a result, with new methods at hand, target key steps in organic synthesis were practicable under mild conditions with visible light and photocatalyst.

It is therefore not surprising that the number of publications on photochemistry has been steadily increasing in recent years.[29, 35-36] The separate pioneering works of D. MacMillan, T. Yoon, and C. Stephenson are often referred to as a turning point in literature regarding photochemical reactions. Their publications initiated the interest and renewed the possibilities in photoredox catalysis since about 2008.[34] For example, MacMillan *et al.* presented an asymmetric *α*-alkylation of aldehydes using $Ru(bpy)_3Cl_2$ as photocatalyst.[37] Using the same catalyst, Yoon *et al.* published a [2+2] enone cycloaddition.[38] Stephenson *et al.* published, on the contrary, a photoredox reductive dehalogenation of activated alkyl halides, using $Ru(bpy)_3Cl_2$ as well as Yoon and MacMillan.[39]

2.2.1. Transition Metal Photocatalysis

When it comes to metal-catalyzed and visible-light-induced fluoroalkylation reactions, typically saturated 4d and 5d transition metal complexes are used. The best known ones are the Ru(II) polypyridine complexes and the Ir(III) complexes (Scheme 2).[26]

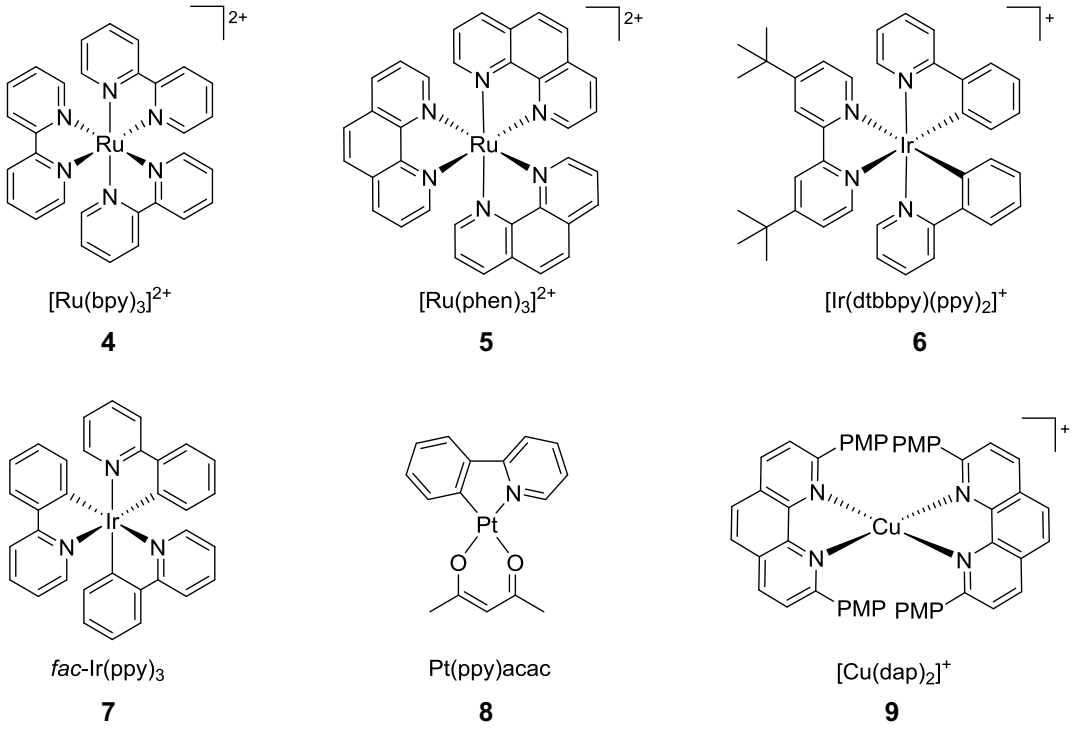

Scheme 2: Metal complexes used in fluoroalkylation reactions and as visible-light photocatalyst.[26]

The generation of radicals with transition metal-based photocatalyst proceeds without highly reactive radical initiators and mostly at room temperature. Reactions can be conducted under extremely mild conditions and very low loadings of the catalyst, mostly 1 mol % or lower. As an irradiation source, often commercially available household light bulbs are used, which is an advantage over high-energy ultraviolet (UV) light sources.[34] The disadvantages of metal catalysts are the high cost and the toxicity of the metal catalyst itself. Many different fluoro-, difluoro-, trifluoro-, arylthiofluoro- and

perfluoroalkyl sources are commercially available and are well tested with different metal catalyst.[26, 40-41] Since photocatalysts (PC) act either as a one-electron-reductant or as a one-electron-oxidant, either an oxidative quenching cycle or a reductive quenching cycle is performed. In advance of this electron transfer, the photocatalysts must enter its excited state (PC*) mediated by visible light (Scheme 3).[42]

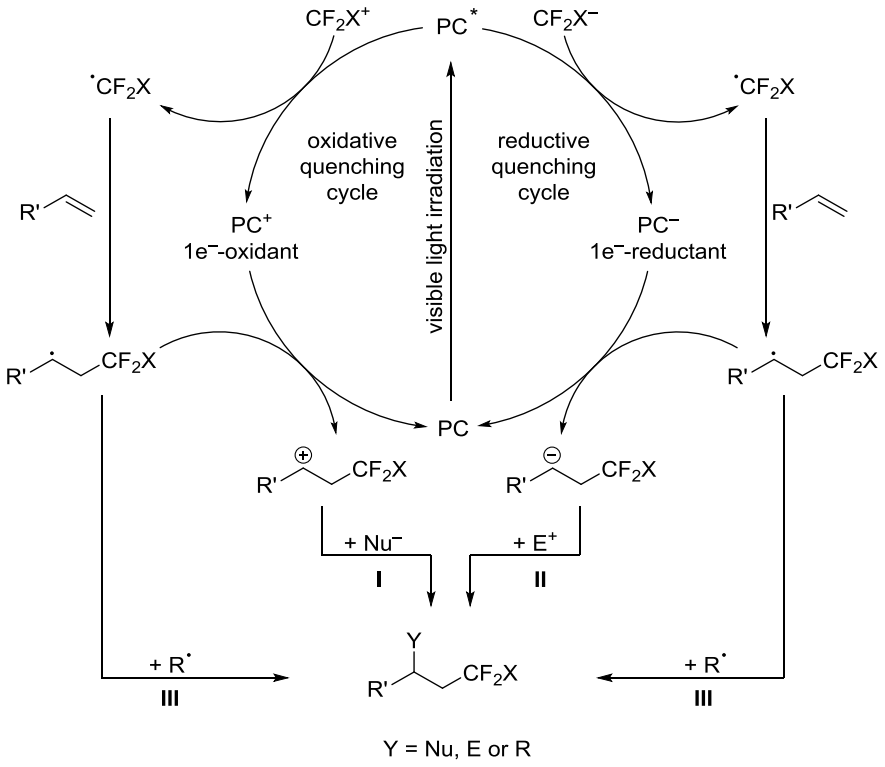

Scheme 3: Oxidative and reductive quenching cycle of an excited photoreactor (PC^*).[42]

Depending on whether an electron-rich (CF_2X^-) or an electron-poor (CF_2X^+) fluoromethylating reagent is used, the photocatalyst passes through one of the two quenching cycles to return to the electronic ground state. The addition of a nucleophile (**I**) or electrophile (**II**) can lead to the desired product. A third radical reactant pathway (**III**) leads either through an atom transfer reaction (ATR), hydrogen atom transfer (HAT), or homolytic aromatic substitution (HAS) to the desired product (Scheme 3).[42] The conception of such a reaction sequence is strongly oriented on the redox potential of the excited photocatalyst. If an electron-deficient CF_2X (X = F, H) species is present in the reaction solution, the oxidation potential of the excited photocatalyst (PC^*) has to be lower than the reduction potential of the CF_2X^+ species. A SET step from the excited photocatalyst (PC^*) to the CF_2X^+ species generates the CF_2X radical ($CF_2X^\bullet$) and the oxidized photocatalyst (PC^+). The formed CF_2X radical ($CF_2X^\bullet$) reacts with the used substrate (i.e., alkene) and undergoes a one-electron-oxidation afterwards with the highly oxidizing catalyst (PC^+), to generate a cationic intermediate and the ground

state photocatalyst (PC). Scavenging of the electrophilic intermediate is achieved by a reaction with a nucleophile (**I**). In the reductive quenching cycle, the photocatalyst (PC) undergoes an one-electron oxidation with the electron-rich CF_2X reagent and the reduced catalyst (PC^-). The reduced photocatalyst (PC^-) then serves as a one-electron reductant to produce a carboanionic intermediate, which can be captured with an electrophile (**II**) (Scheme 3).[42]

MacMillan *et al.* presented an asymmetric *α*-alkylation of aldehydes using $Ru(bpy)_3Cl_2$ **4** as photocatalyst in 2008 and sparked new interest in photochemistry.[37] The group extended this method to an asymmetric *α*-trifluoromethylation and *α*-perfluoroalkylation of aldehydes, changing the catalyst from a ruthenium-catalyst to an iridium-catalyst **6** (Scheme 4).[43]

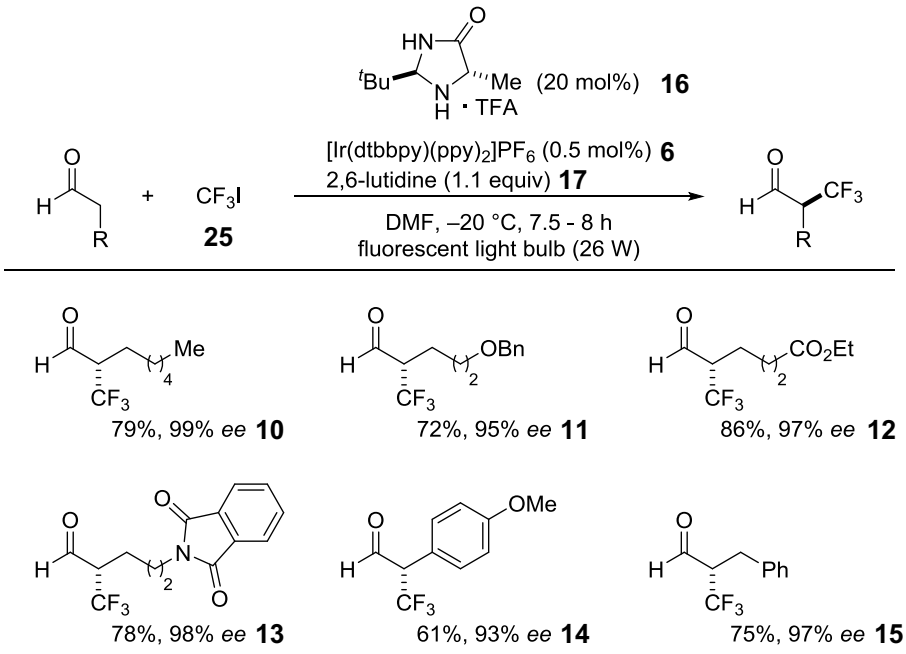

Scheme 4: Asymmetric *α*-alkylation of aldehydes using $[Ir(dtbbpy)(ppy)_2]PF_6$ **6**.[43]

MacMillan *et al.* proposed that the used chiral organocatalyst **16** forms an enamine intermediate with the used aldehyde **18** in the organocatalytic cycle. The resulting enamine **19** reacts with the trifluoromethyl radical **26**, which is formed in the photoredox catalysis cycle, forming the CF_3-coupled radical intermediate **21**. The photoactivated $*[Ir(dtbbpy)(ppy)_2]^+$-catalyst **23**, which was excited by a fluorescent light bulb, undergoes a SET to form the iminium intermediate **22** and iridium reductant **24**. The iridium reductant **24** participates in the mesolysis of CF_3I in a second SET step and provides the mentioned CF_3-radicals **26** and regenerates the photoredox catalyst **6**. Final hydrolysis of the iminium ion **22** releases the final *α*-trifluoromethylated aldehyde **20** and the organocatalyst **16** (Scheme 5).[34, 40, 43]

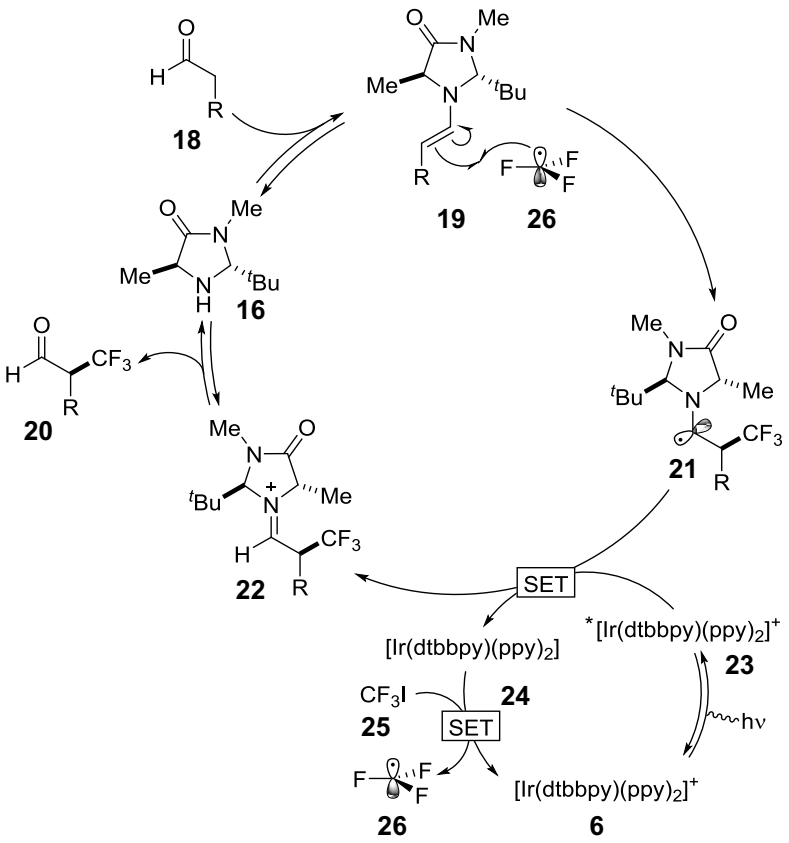

Scheme 5: Proposed mechanism of the asymmetric *α*-alkylation of aldehydes by MacMillan *et al.*[43]

As described above, different trifluoromethyl sources can be used. For example, Gouverneur *et al.* presented the hydrotrifluoromethylation of unactivated alkenes by irradiating $[Ru(bpy)_3Cl_2] \cdot 6\,H_2O$ **4** in methanol and using Umemoto reagent **27** as CF_3-source. Unactivated terminal and monosubstituted alkenes, as well as geminal disubstituted alkenes, were converted effectively (Scheme 6).[44-45]

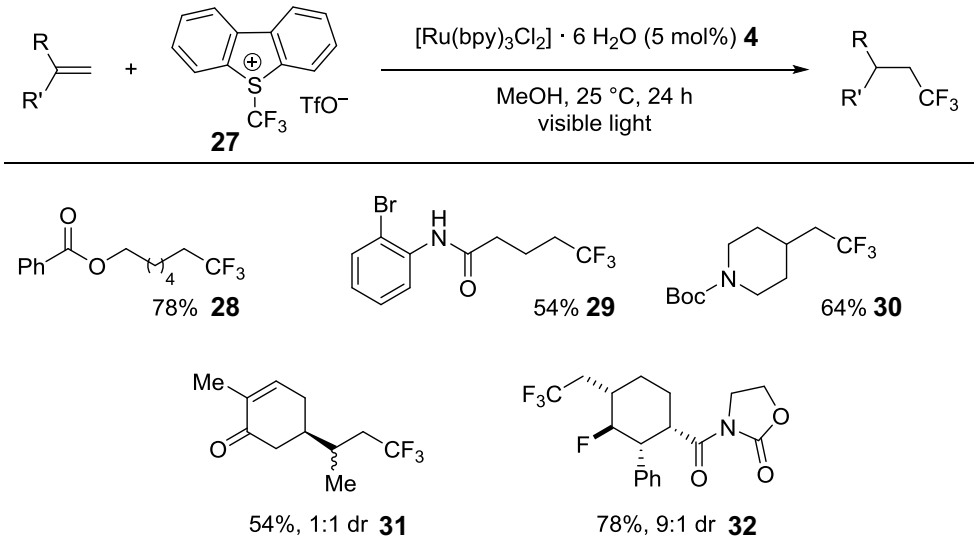

Scheme 6: Hydrotrifluoromethylation of terminal alkenes.[44]

The generation of radicals from the CF_3-source is similar to the presented example of MacMillan *et al.* and the applied iridium catalyst **6** (Scheme 4). Here, the ruthenium catalyst $[Ru(bpy)_3Cl_2]$ **4** is irradiated with visible light, which leads to the excited state of the catalyst **33** followed by the SET reduction of the trifluoromethyl-source **27**. The formed CF_3 radicals **26** add to the double bond of the used substrate. Methanol acts as a hydrogen atom donor and completes the hydrotrifluoromethylation (Scheme 7).[44]

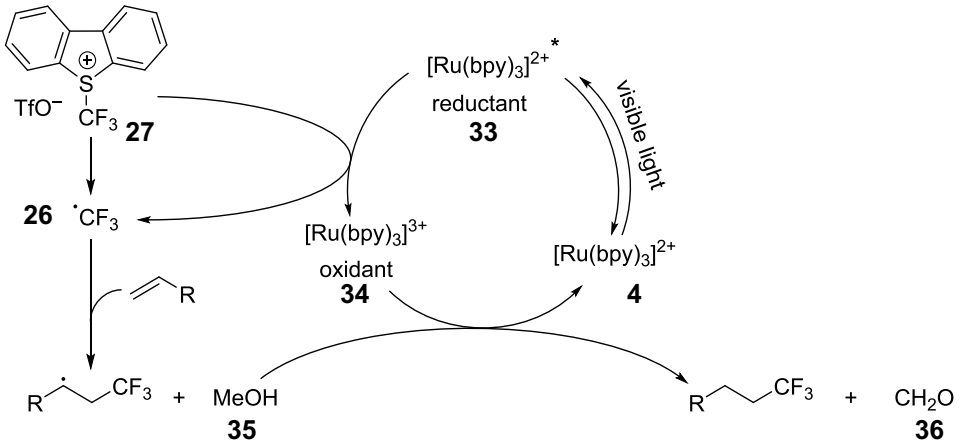

Scheme 7: Reaction mechanism for the hydrotrifluoromethylation of terminal alkenes.[44]

2.2.2. Organic photoredox catalysts

Organic photoredox catalysts provide an alternative to their transition metal counterparts in photoredox catalysis. There are several advantages of organic photoredox catalysis. They are generally inexpensive, nontoxic, easy to remove after the reaction and when it comes to organic dyes, they have a strong chromophoric character.[46] By using organic dyes as catalysts, light sources with specific irradiation wavelengths can be used. Cho *et al.*, for example, published a metal-free visible-light-induced trifluoromethylation of olefins and alkynes. As organic photocatalyst Nile Red (9-diethylamino-5*H*-benzo[α]phenoxazine-5-one) was used, in the presence of different bases and CF_3I **25**. The excitation of Nile Red already occurred at 585 nm (yellow light). As a model substrate, 1-dodecene (**37**) was used. Other organic dyes (Eosin Y, methylene blue, coumarin 6) and the metal complex $[Ru(phen)_3]Cl_2$ **5** were tested (Table 1).[46]

Table 1: Optimization reactions of the trifluoromethylation reaction with different photocatalysts.[46]

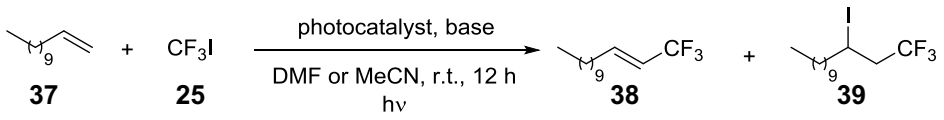

37 **25** **38** **39**

entry	Photocatalyst (1 mol%)	base (2 equiv)	yield [%] 38	39
1[a]	Eosin Y	DBU	90	–
2[a]	Methylene blue	DBU	60	–
3[a]	Coumarin 6	DBU	75	6
4[a]	Nile red	DBU	90	–
5[a]	$[Ru(phen)_3]Cl_2$	DBU	93	–
6[a]	Nile red	K_2CO_3	–	–
7[a]	Nile red	Lutidine	–	–
8[a]	Nile red	TMEDA	15	73
9[a]	Nile red	DIPEA	–	90
10[b]	Nile red	DBU	92	–

a) white fluorescent bulb (23 W); b) yellow LED

Eosin Y, Nile red and literature-known metal complex showed excellent yields (entry 1, 4, 5, Table 1).[46-47] Further studies were conducted with Nile red as a catalyst with light absorbance at higher wavelength compared to Eosin Y. The screening of the different bases showed optimal results when DBU (1,8-diazabicyclo[5.4.0]undec-7-ene) was utilized, yielding product **38** (entry 4, Table 1) in high yield. By changing the base to TMEDA or DIPEA the corresponding trifluoromethylated iodide product **39** was isolated (entry 8, 9, Table 1). As mentioned earlier, the use of Nile red as a photocatalyst made the reaction possible by irradiating the reaction solution with a yellow LED instead of a white fluorescent bulb (23 W) (entry 10, Table 1). Through the excitation of the photocatalyst (Nile red), the CF_3-radical **26** is formed in the first step and adds to the used educt. An atom transfer radical addition (ATRA) with CF_3I **25** forms product **39**. After HI elimination, when DBU is utilized as a base, product **38** is formed. Alternatively, the iodoperfluoroalkylated product **39** is formed by photocatalytic oxidation followed by iodine addition. If a deprotonation step takes place, after the photocatalytic oxidation, the alkenyl trifluoromethylated product **38** is formed (Scheme 8).[46]

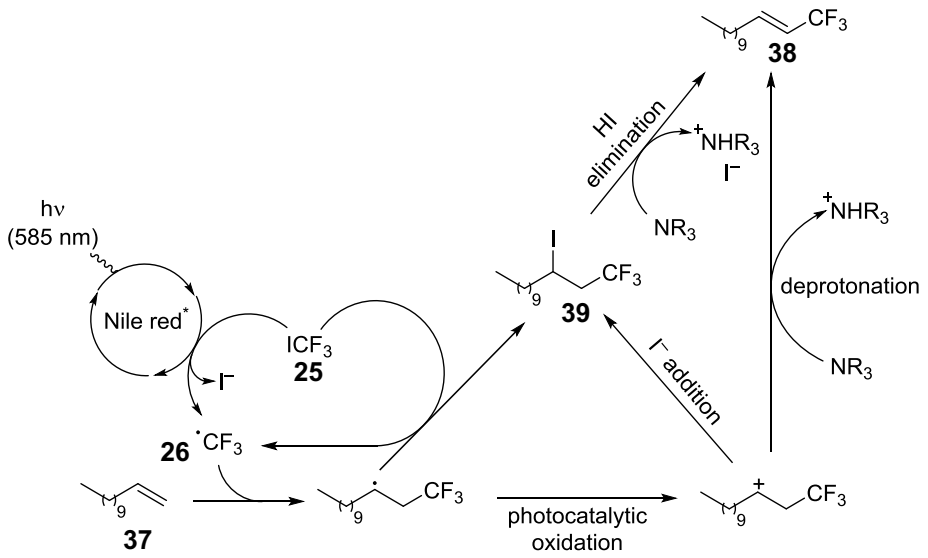

Scheme 8: Proposed reaction mechanism of the Nile red-catalyzed selective trifluoromethylation.[46]

Cho and co-workers also performed the experiment using the tested bases (DBU, DIPEA, TMEDA) solely. For this purpose, they used a white fluorescent bulb. Most likely, this trifluoromethylation reaction was performed by forming an electron donor-acceptor (EDA) complex between the tested base and CF_3I **25**. In this EDA complex, the C—I bond is cleaved homolytically mediated by light irradiation. Instead of using a photocatalyst with a perfluoroalkyl iodide, Scaiano and colleagues used methylene blue **40** as photocatalyst, in combination with the Togni's reagent **41** as CF_3 source. Herein the trifluoro- and hydrotrifluoromethylation of electron-rich heterocycles, as well as terminal alkenes and alkynes, were presented (Scheme 9).[48]

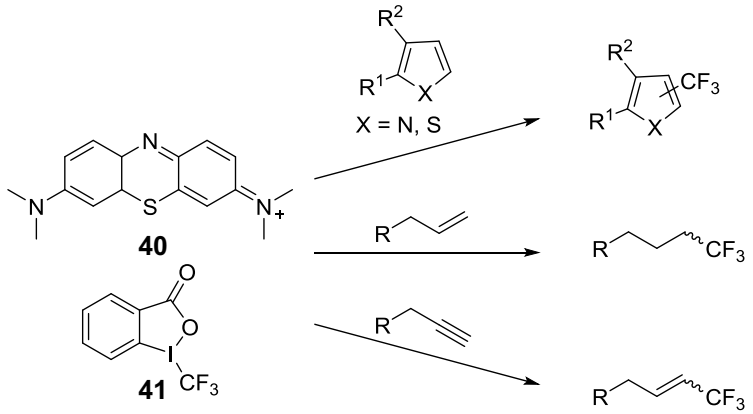

Scheme 9: Methylene blue-catalyzed trifluoromethylation and hydrotrifluoromethylation using the Togni's reagent **41**.[48]

Scaiano and co-workers initially assumed that the Umemoto reagent **27** was the most efficient CF_3 source for the reaction, due to its lower reduction potential in comparison to the Togni reagents **41** and **45**. However, the highest yield was obtained when the Togni (I) reagent **41** was used, instead of the other two CF_3 sources (Table 2).[48]

Table 2: Screening reaction and the reduction potential of the Umemoto and the Togni reagents.[48]

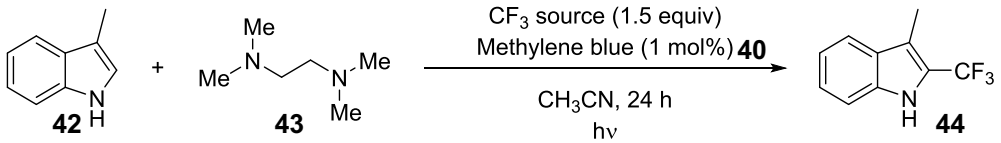

CF_3 source	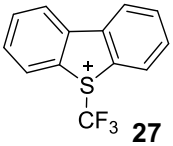 27 Umemoto	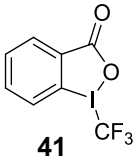 41 Togni I	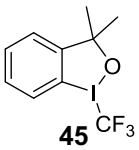 45 Togni II
$E^{red}_{1/2}$ (V vs. SCE)	–0.75	–1.34	–1.49
yield [%]	35	77	47

Noël *et al.* used the aforementioned organic dye Eosin Y to present the perfluoroalkylation of heteroarenes in continuous flow (Scheme 10). In the first step of the proposed mechanism Eosin Y is excited by visible light irradiation. The excited Eosin Y accepts an electron of the used base through a single electron transfer (SET), followed by a second SET, which generates the perfluoroalkyl radical species.[49]

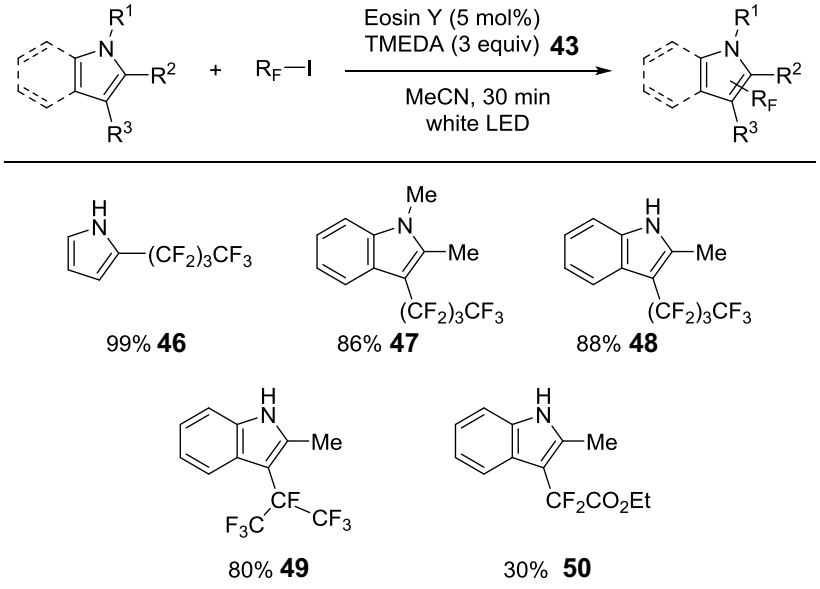

Scheme 10: Perfluoroalkylation of indoles and pyrroles with Eosin Y in continuous flow.[49]

The perfluoroalkyl subsequently adds to the used educt and generates a stabilized carbon radical. The following oxidation step and final deprotonation completed the final perfluoroalkylation of heteroarenes (Scheme 11).[49]

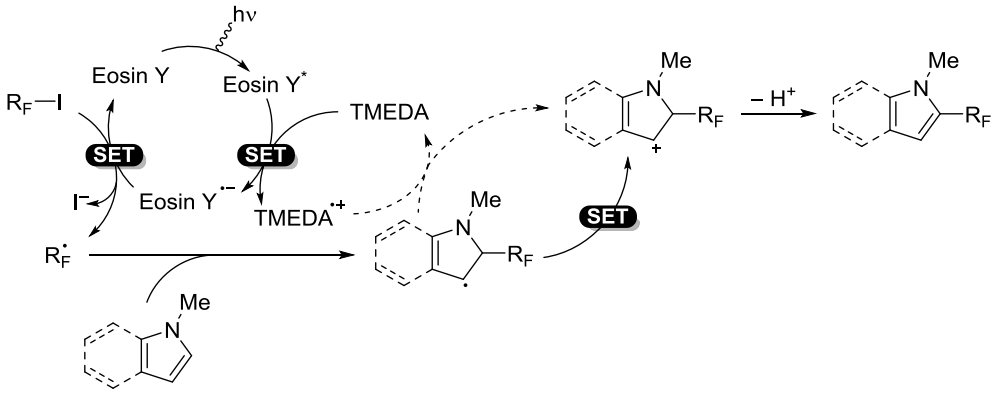

Scheme 11: Proposed reaction mechanism of the Eosin Y-catalyzed perfluoroalkylation of indoles.[49]

2.2.3. Electron Donor-Acceptor complex

In 1950 Mulliken introduced the term electron donor-acceptor complex.[50-51] An electron donor-acceptor complex is the association of an electron-rich donor molecule (D, with a low ionization potential) and an electron-poor molecule acceptor molecule (A, with a high electronic affinity), mostly shortened as EDA complex. The association, through pseudo-electrostatic interactions of the donor and acceptor molecule, is a diffusion-controlled process, wherein both molecules are in their electronic ground state. By irradiation with visible light, the EDA complex gets into an excited state, which allows an electron transfer (ET) without the presence of a photocatalyst.[52-54]

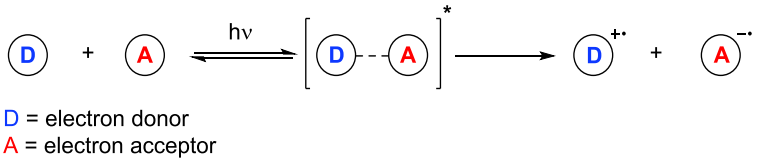

Scheme 12: General concept of an electron donor-acceptor complex.[55]

Compared to colored metal photocatalysts or organic dyes, EDA complexes only show a weak absorption band in the UV-VIS spectrum, associated with an electron transfer transition from the donor to the acceptor.[56] Such absorption can be sufficient enough to show a change in color by mixing two colorless reagents.[53] The photophysical properties of EDA complexes have been studied prior to their use in organic synthesis, as the electron transfer from the donor to the acceptor is fast and reversible.[52, 57] Organic anions or heteroatom electron lone pairs (phosphorus-, nitrogen-, oxygen-, sulfur-centered atoms) can act as an electron donor.[53, 57] In contrast cations, electrophiles and oxidants are able to serve as electron acceptors.[57] Halogens can also function as electron acceptors and interact with the electron donor through a halogen bond.[53] Such a halogen bond bears an analogy to the hydrogen bond. It is described as a non-covalent interaction of a halogen atom (Lewis acid) with a Lewis base.[58-59] The electron transfer occurs from the nonbonding orbital of the Lewis base into the

antibonding orbital of the halogen (n→σ*).[60] The so-called σ-hole,[60-61] a positively charged region or polar flattening of the electron density at a halogen molecule,[62-65] enables the interaction to the nonbonding orbital of the Lewis base.

The halogen bond is stronger for the heavier halogens and consequently weakest for fluorine.[64] However, this type of bond is not limited to halogens, but it is also observable in groups 14 (carbon group), 15 (pnictogen group) and 16 (chalcogen group) of the periodic table.[62] The interaction and formation of an EDA complex can be identified by crystal structure analysis,[66-67] by NMR spectroscopy (*e.g.*, an upfield shift in the ^{19}F-NMR resonance of a CF_2 moiety, when fluorinated electron acceptors are used), UV-VIS and infrared spectroscopy.[68]

Melchiorre *et al.* summarized different synthetic methods in a review on EDA complexes.[54] Two different methods are described. One is the stoichiometric use of donor and acceptor molecules, and the other is the catalytic use of one of the partners to form the EDA complex.

One general concept is the coupling of an electron rich-donor (D) with an electron-poor acceptor (A) in stoichiometric amounts. The donor and electron acceptor used end up in the final product. Critical for this reaction is a suitable leaving group, *e.g.*, halides, attached to one of the substrates, in this case the acceptor (Scheme 13).[54]

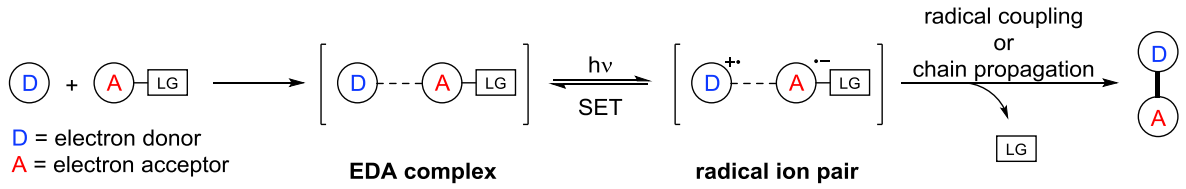

Scheme 13: General concept for the coupling reaction of an electron rich-donor and electron-poor acceptor in stoichiometric amounts *via* EDA complex activation. LG = leaving group.[54]

The reason for the leaving group is, besides the photoinduced SET, an irreversible fragmentation to produce open-shell intermediates leading to the final product. In general, electron-rich aromatic compounds can be used as donors and electron-poor alkyl halides as acceptors. Melchiorre *et al.*, for example, published the reaction of 3-substituted indoles **51** (blue, donor) with electron-accepting benzyl halides **52** (red, acceptor) as C2-alkylation of indoles **53** (Scheme 14).[54, 69]

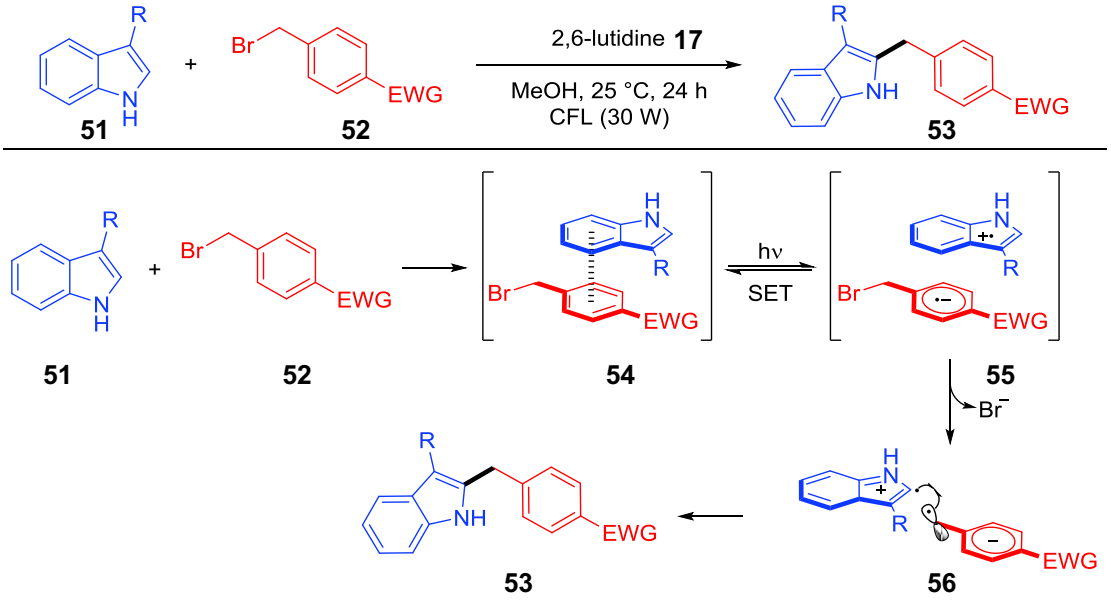

Scheme 14: C2-alkylation of indoles presented by Melchiorre *et al.* as an example for a coupling reaction of an electron-rich donor (blue) and an electron-poor acceptor (red).[54, 69]

Instead of using only a leaving group, the use of a redox auxiliary can decorate the acceptor as an activating group and leaving group. The main core of the substrate does not need to be electronically balanced since the formation of the EDA complex is controlled by the electronic properties of the redox auxiliary.[54]

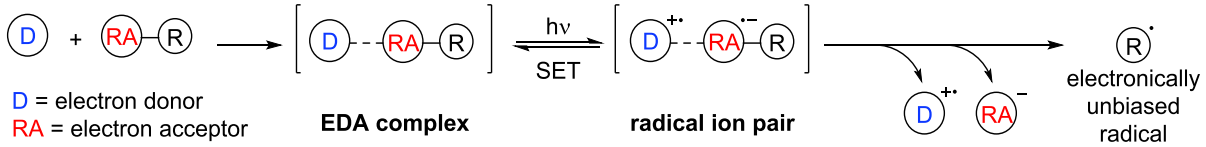

Scheme 15: General concept of the use of redox auxiliary that drives the formation of an EDA complex and the fragmentation to produce radicals. RA = redox auxiliary.[54]

Based on this concept, Leonori *et al.* presented in 2015 a photochemical generation of nitrogen-centered radicals. Functionalized dinitro-substituted *O*-aryl oximes as acceptor **60** were used (Scheme 16).[70] The bench-stable precursor **60** was combined with electron-rich NEt_3 as donor, forming the EDA complex **61**. Through a photoinduced SET, a radical ion pair was formed and the electron auxiliary acts as leaving group. The dinitro-phenoxide **63** is released, and the formed iminyl radical underwent a 5-*exo*-trig cyclization. Either the formed C-centered radical **65** abstracts a hydrogen-atom from added cyclohexadiene (**64**) to form the hydroimination product **58** or it is oxidized by the released dinitro-phenoxide **63** to form the iminohydroxylated cyclization products **59** (Scheme 16).[54, 70]

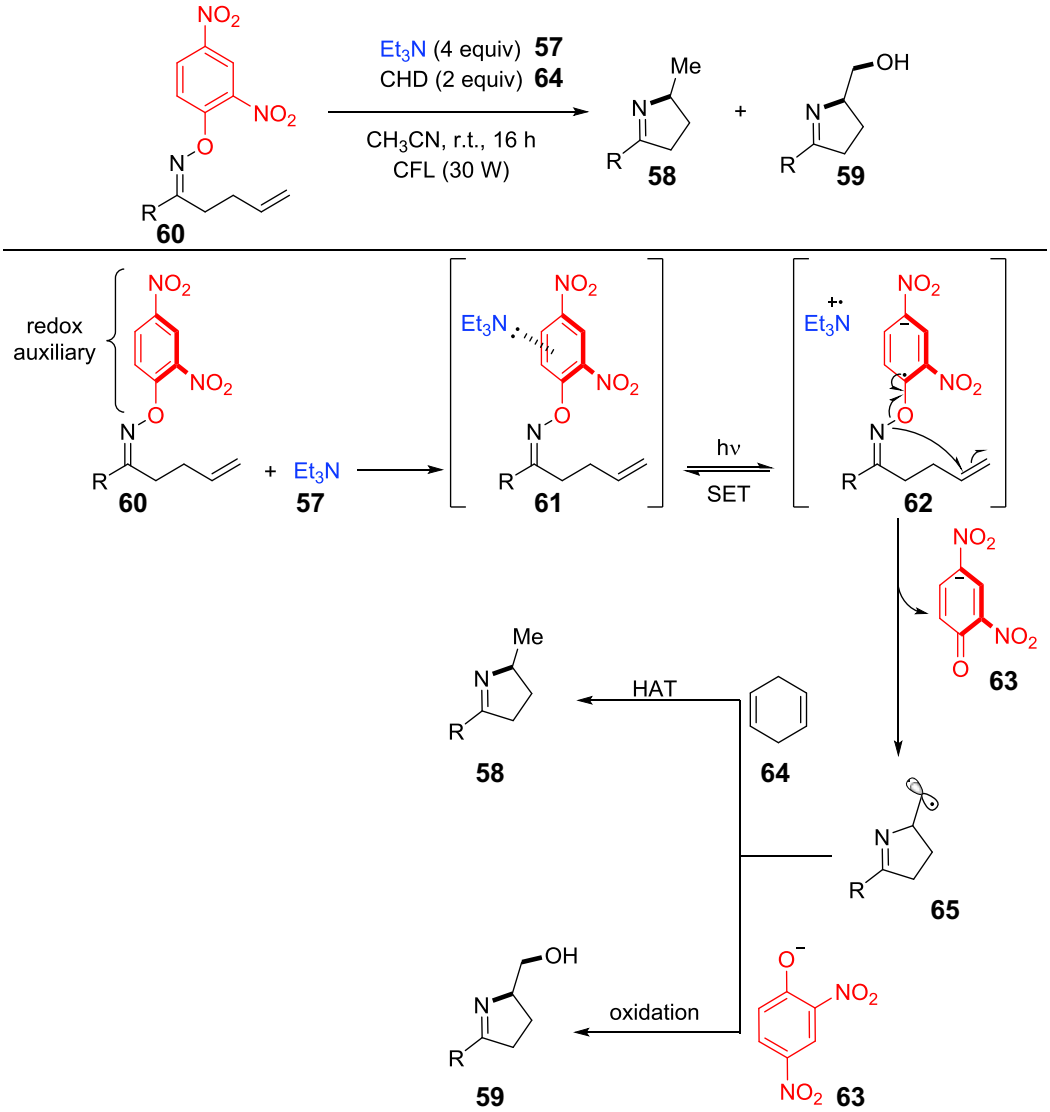

Scheme 16: Proposed mechanism for the visible-light-mediated electron transfer *via* EDA complex for the hydroimination and iminohydroxylation of *O*-aryl oximes. HAT = hydrogen atom transfer, CHD = 1,4-cyclohexadiene.[54, 70]

Another method is the coupling of the donor- or acceptor-moiety with another substrate, a radical trap. The used donor or acceptor is sacrificed and not part of the formed product (Scheme 17).[54] Yu published an example in 2016 regarding to synthesis 2-fluoroalkylated quinoxaline derivatives **67**. Perfluoroalkyl radicals are formed through EDA complex formation of the perfluoroalkyl iodide (acceptor, red) and the sacrificial secondary amine (donor, blue) (Scheme 18).[54, 71]

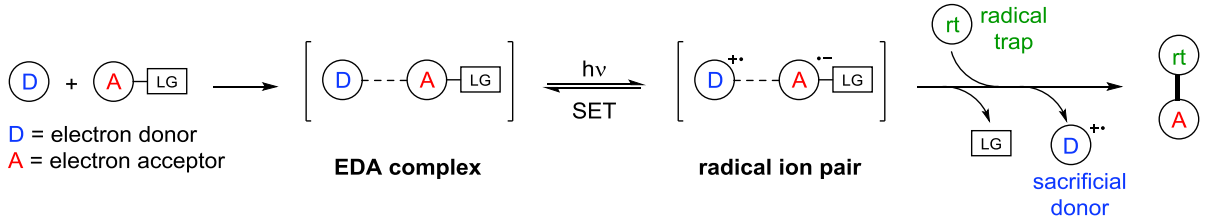

Scheme 17: General scheme for radical formation based on the use of a sacrificial donor or acceptor pair. LG = leaving group.[54]

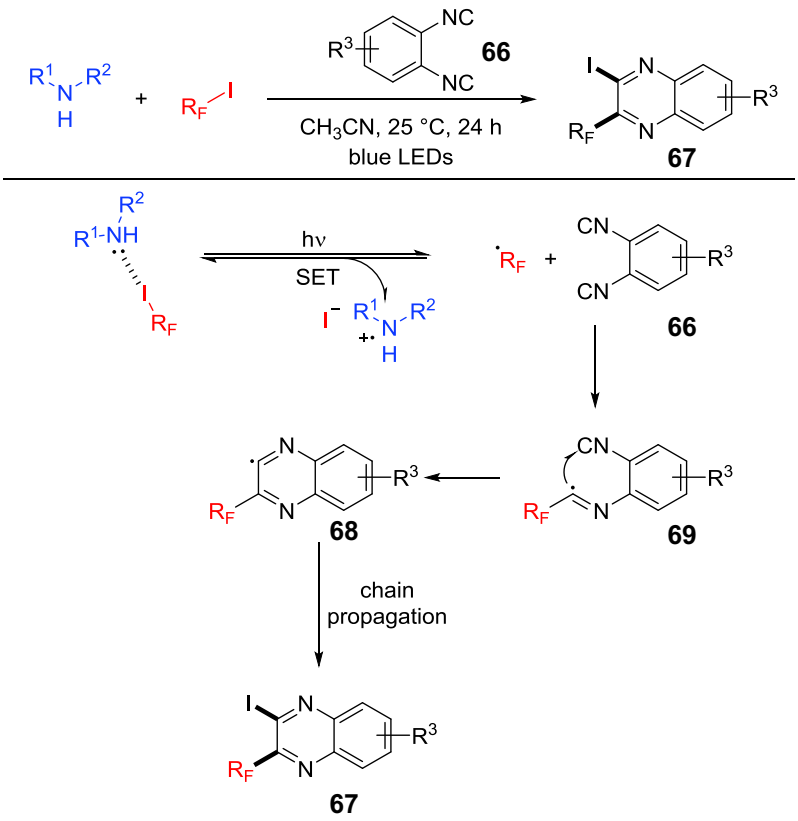

Scheme 18: Photochemical synthesis of 2-fluoroalkylated quinoxalines **67**.[54,71]

Isocyanide **66** acts as a radical trap and triggers a cyclization to intermediate **68**. After iodine abstraction the final quinoxaline product **67** was formed. Later in this introduction, this reaction is described in more detail (see p. 37). Besides a stochiometric use of EDA complexes, an utilization of only catalytic amounts of an EDA complexes is possible as well. Four variations of such a catalytic process are presented. Firstly, an example of an *in situ* generation of a catalytic generated donor intermediate is described (Scheme 19). Secondly, a variant is described, in which the acceptor is formed catalytically as intermediate (Scheme 20). As illustration for this second method, a photocatalytic Stetter reaction is shown (Scheme 21). Thirdly, an intramolecular variation is presented, where previously only intermolecular EDA complexes were present in the reaction solution (Scheme 22). And last but not least, a method in which the donor catalyst generates photochemically radicals and is regenerated afterwards (Scheme 25).

In the first example, a catalyst activates and significantly polarizes one of the used substrates to form an electron donor, and induces the formation of an EDA aggregate with an electron acceptor (Scheme 19).[54]

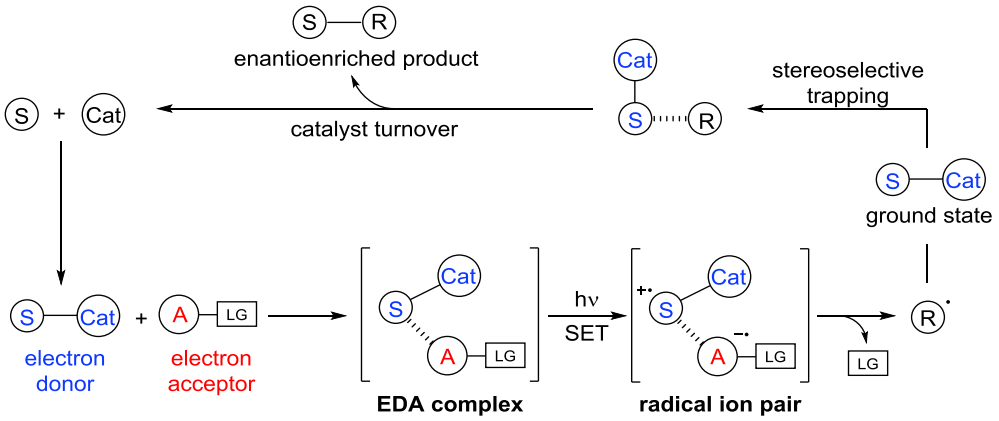

Scheme 19: Example of an *in situ* generation of a catalytic intermediate as donor and forming and EDA complex with an acceptor. R corresponds to the acceptor without the leaving group, whereby the acceptor properties are lost. Cat = catalyst, LG = leaving group, S = substrate.[54]

Even asymmetric radical processes are possible *e.g.* in the presence of a chiral catalyst. The advantage of this method is the activation of only weakly polarized substrates, such as ketones or aldehydes, which can enter into a charge-transfer complex with the used acceptor.[54] The catalyst must not bind to the donor, but can also bind to a substrate and form an acceptor (Scheme 20).

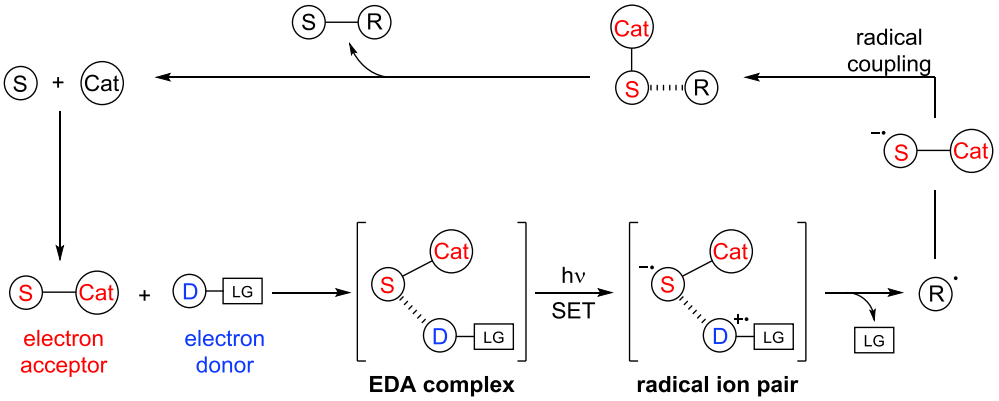

Scheme 20: Catalytic strategy of *in situ* formation of a catalyst and a substrate to form an acceptor. R corresponds to the donor without the leaving group, whereby the acceptor properties are lost. Cat = catalyst, LG = leaving group, S = substrate.[54]

In 2019 Gilmour *et al.* published a photocatalytic radical Stetter reaction. A pyrrolidine-derivative **70** as secondary amine organocatalyst was used to form the EDA complex (Scheme 21). Gilmour *et al.* used an imidazolidinone derivative **70** to form an electron-poor iminium ion **74** in combination with an α,β-unsaturated aldehyde **71**.[54, 72]

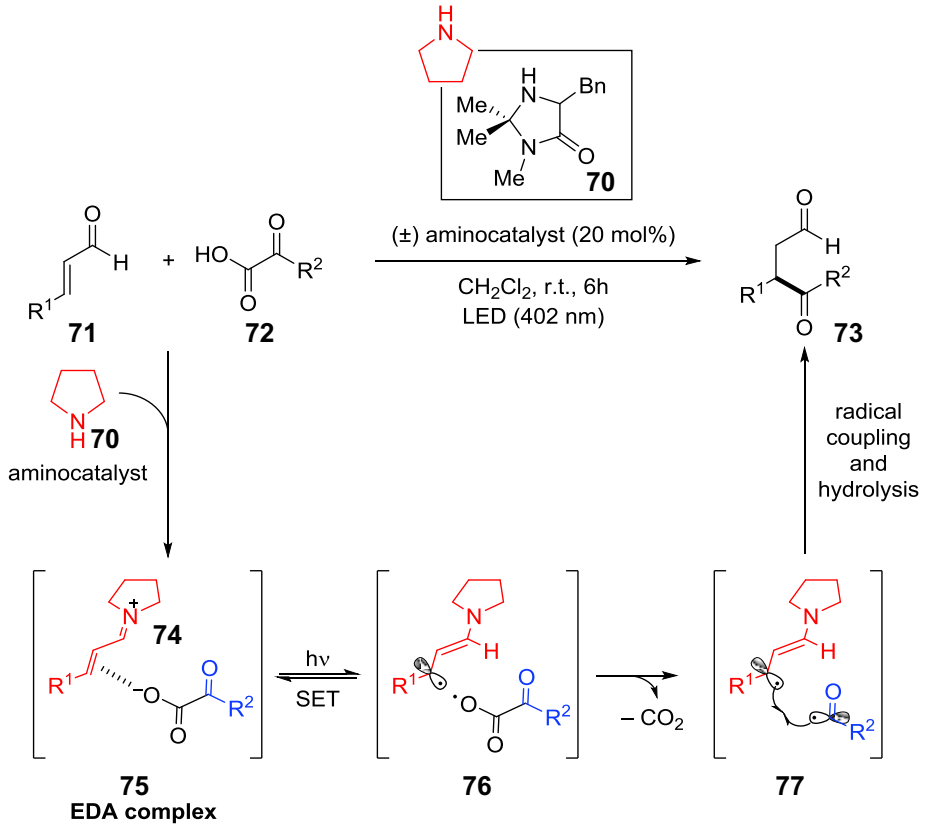

Scheme 21: Photocatalytic Stetter reaction by forming an iminium ion-based EDA complex.[54, 72]

As an electron donor, an α-keto acid **72** was used. However, radicals were only formed in the presence of a suitable light-source (402 nm). By a rapid decarboxylation and generation of an acyl radical, the coupling product **73** was formed.[72] Melchiorre *et al.* presented an intramolecular EDA complex formation, instead of the formation of an intermolecular aggregation of donor and acceptor (Scheme 22).[54]

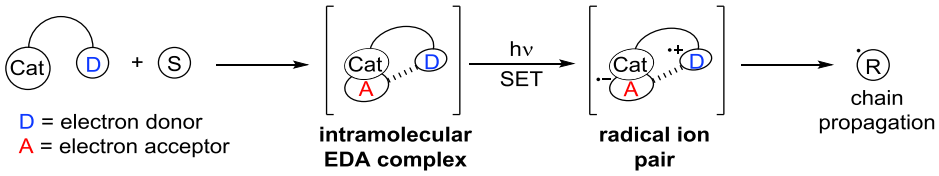

Scheme 22: Connection between catalyst and donor molecule and intramolecular EDA complex formation. Cat = catalyst.[54]

As already shown in another example, an electron-poor iminium ion was generated by condensing a cyclohexanediamine-derivative **78** with a cyclic enone-derivative **80** (Scheme 23). The cyclohexanediamine catalyst **78** had an electron-rich carbazole moiety attached. After formation of the intramolecular EDA complex **83**, confirmed by X-ray crystallographic analysis, the counter-ion pair **84** was formed by a SET through irradiation at 420 nm.[73]

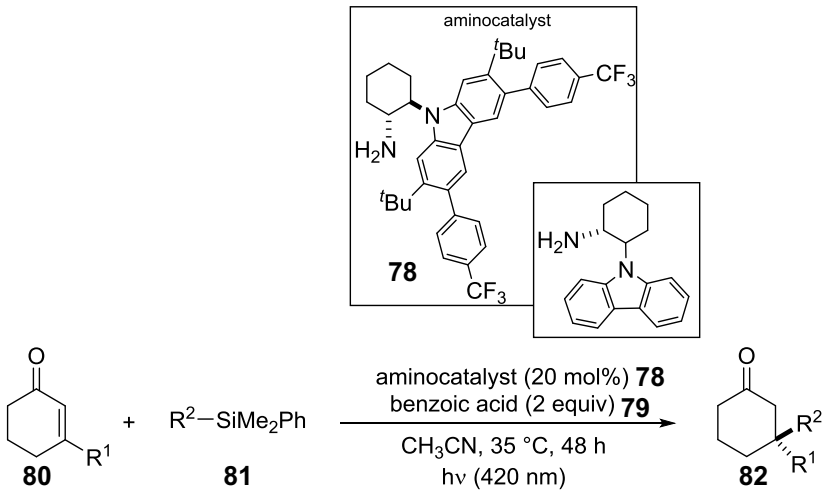

Scheme 23: Enantioselective catalytic radical conjugate addition by formation of an intramolecular EDA complex.[54, 73]

The resulting carbazole radical **84** acted as an effective oxidant to generate a radical through a SET from the electron-rich alkyl silane **81**. The radical was captured by the ground state and electron-poor iminium ion and EDA complex **83**. A following intramolecular SET reduction formed a radical cation **88** at the carbazole moiety and oxidized another alkyl silane **81**. The final hydrolysis generated the neutral imine as catalyst **78** and product **82**.[54, 73]

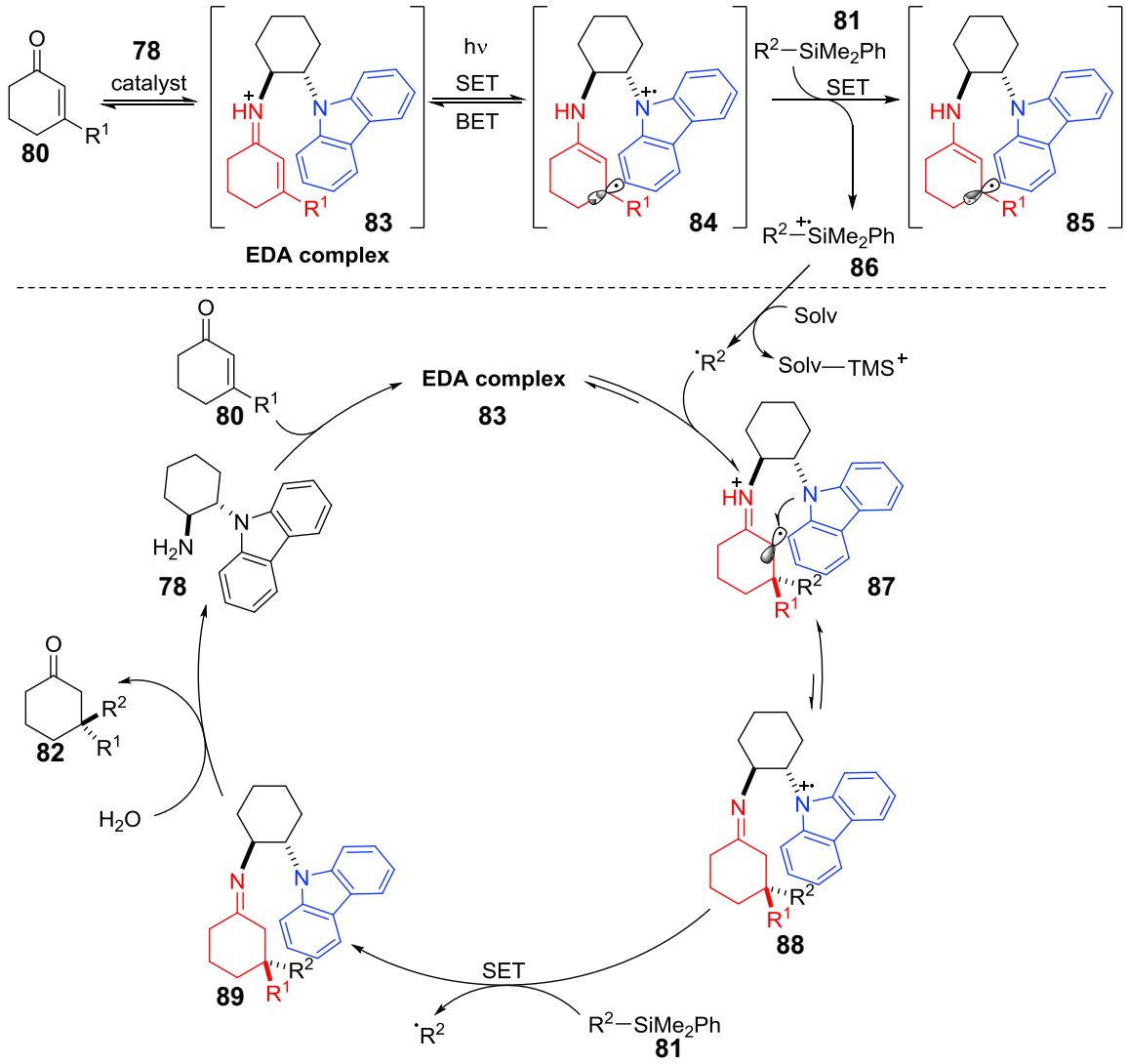

Scheme 24: Proposed reaction mechanism of the radical addition to β-substituted cyclic enones **80** to form quaternary carbon stereocenters *via* intramolecular EDA complex formation.[54, 73]

The demonstrated reactions showed a catalyst that is directly involved in the photochemical radical formation and the trapping of the radical species. A different way is the use of a catalyst that is exclusively involved in the generation of radicals (Scheme 25).[54]

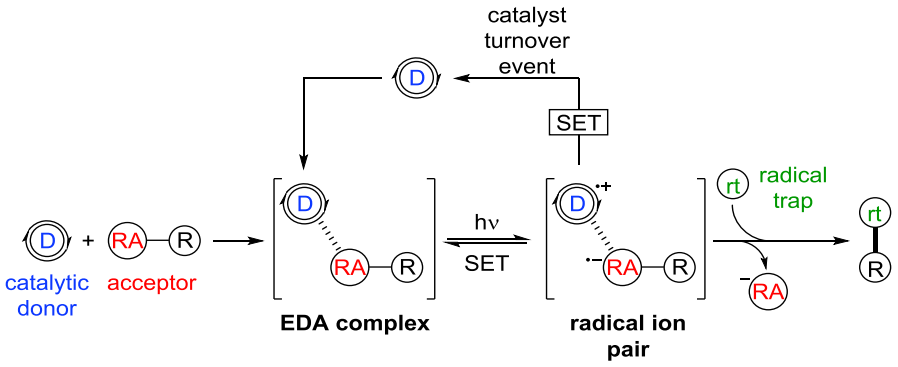

Scheme 25: General strategy for a radical formation and catalyst turnover of the donor molecule. RA = redox auxiliary.[54]

Photocatalytic decarboxylative alkylation with sodium iodide (**90**) as additive and triphenylphosphine (**91**) as catalyst was published by Shang and Fu *et al.*[74] Triphenylphosphine (**91**) and sodium iodide (**90**) triggers the aggregation to a three-component EDA complex **96** with the used phthalimide derivative **93** (Scheme 26).

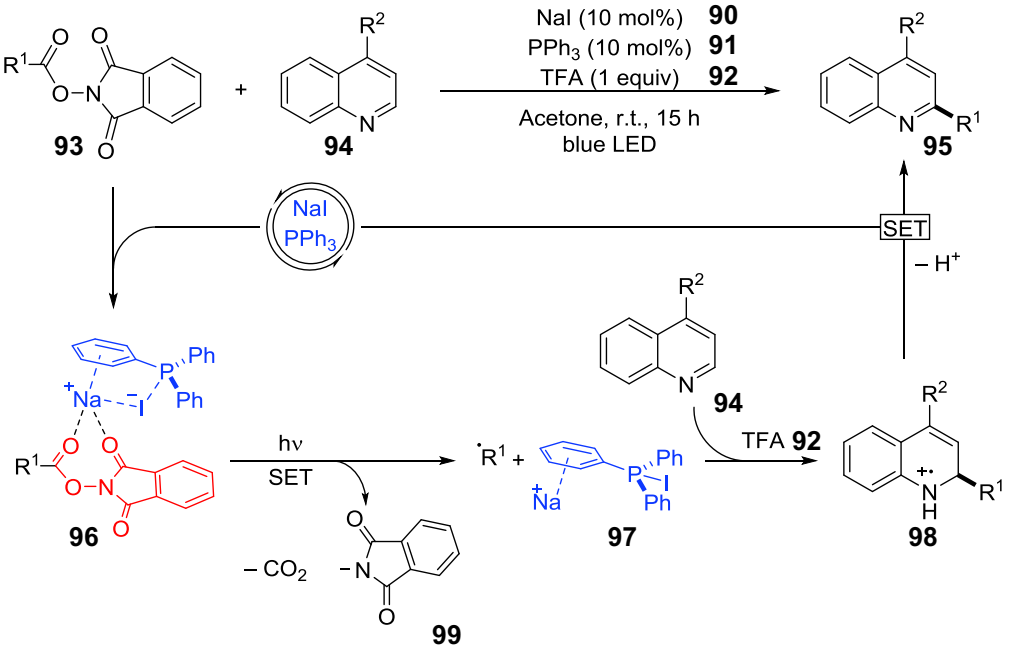

Scheme 26: Photocatalytic decarboxylative alkylation with sodium iodide (**90**) as additive and triphenylphosphine (**91**) as catalyst.[74]

After decarboxylation and cleavage of the phthalimide moiety **99**, the resulting radical reacts with a radical trap, in this case an acid-activated heteroarene **94**. The radical cation **98** is reduced by the PPh_3—I radical intermediate and forms the alkylated heteroaromatic final product **95**. Triphenylphospine (**91**) and sodium iodide (**90**) are used as a catalyst in the next catalytic cycle.[54, 74]

Amine-catalyzed reactions

Chen and co-workers presented a protocol for the perfluoroalkylation of alkenes and alkynes in the presence of a *N,N,N′,N′*-tetraethylethylenediamine (**100**) (TEEDA) (Scheme 27). A comparison of sunlight, UV light (254 nm) and a compact fluorescent lamp (CFL) as an irradiation source was conducted.[75]

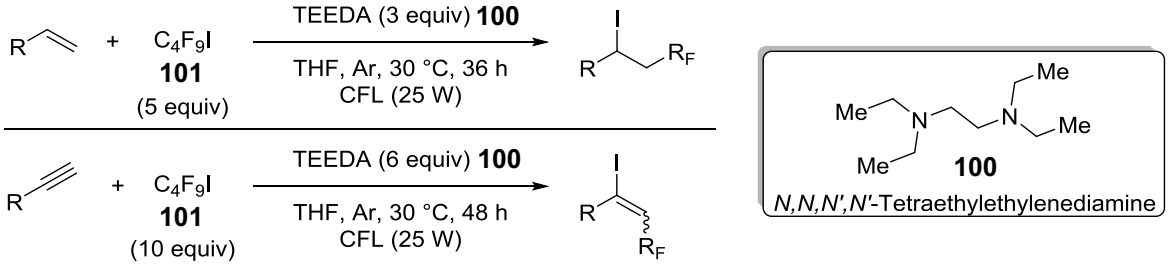

Scheme 27: TEEDA-catalyzed iodoperfluoroalkylation of alkenes and alkynes.[75]

In a phenanthridine **103** synthesis and perfluoroalkylation of alkenes and alkynes, best results were obtained with a CFL lamp. Tests of 28 amines as a promotor for the synthesis of phenanthridine derivatives **103** from 2-isocyanobiphenyl (**102**) and nonafluoro-1-iodobutane (**101**) indicated that tertiary amines are more effective than primary or secondary amines. Electron rich amines promoted the reaction better than electron-poor amines.[75]

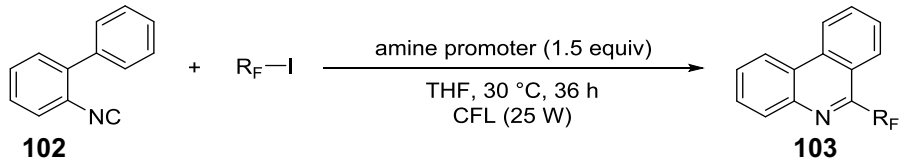

Scheme 28: Phenanthridine synthesis to evaluate the amine promoter.[75]

To investigate the halogen bond, the association constants between Lewis bases and $C_{10}F_{21}I$ were determined. For TEEDA **100** and $C_{10}F_{21}I$ the association constant was determined to be 1.1 M^{-1} and between THF and $C_{10}F_{21}I$ a lower value of 0.28 M^{-1} was observed. Additionally, the tests showed that a 1:1 complex between the solvent THF and $C_{10}F_{21}I$ was present. Thus, the mechanistic investigations demonstrated the promotion of the photochemical perfluoroalkylation by the used amine and the solvent THF.[75]

Lv and Yu *et al.* used TMEDA **43** and a white light bulb to synthesize perfluoroalkyl-substituted benzimidazo[2,1-*a*]isoquinolin-6(5*H*)-ones **108** and indolo[2,1-*a*]isoquinolin-6(5*H*)-ones derivates **110**. The presented synthesis was compared with the known works of Song and co-workers. Song *et al.* presented a Cp*Rh(III)-catalyzed [4+2] annulation reaction and an $AgNO_3$-catalyzed decarboxylative cascade cyclization, that was presented by the authors themselves.[76-77]

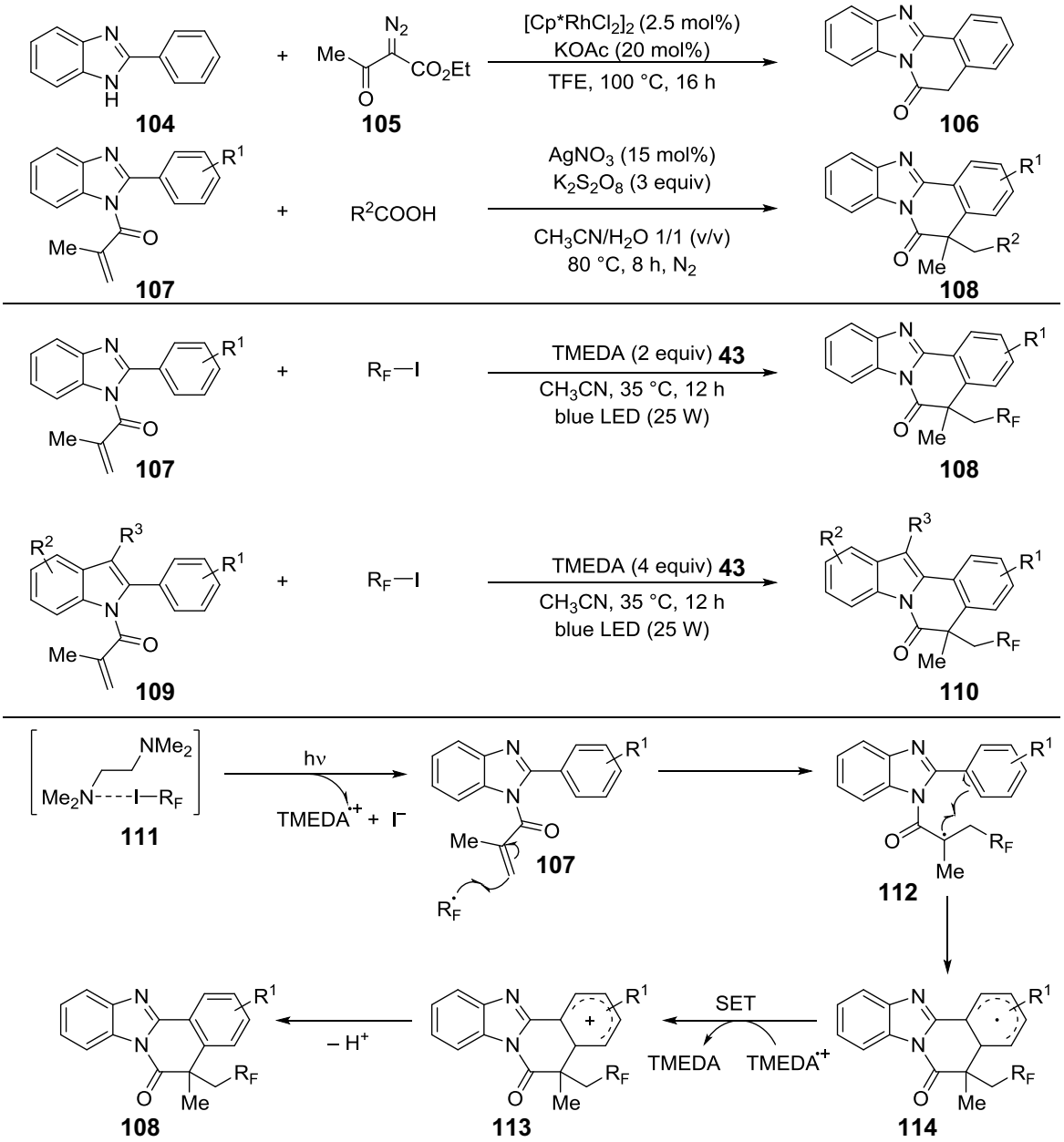

Scheme 29: Synthesis of benzimidazo[2,1-*a*]isoquinoline-6(5*H*)-ones and indolo[2,1-*a*]isoquinolin-6(5*H*)-ones. Metal-catalyzed (top), amine-catalyzed (middle), and the proposed reaction mechanism (bottom).[76]

Compared to the methods already known from literature (Scheme 29, top), the method of Lv and Yu *et al.* requires no expensive metal complexes, stoichiometric oxidant, or high reaction temperatures.[76] As a reaction mechanism, it was suggested that after the addition of the perfluoroalkyl radical to the C=C bond of the educt **107**, the resulting radical undergoes an intramolecular cyclization. After an intermolecular SET, a carbocation is formed, and by final deprotonation, the product **108** can be isolated (Scheme 29, bottom).[76]

As an alternative to the synthesis of 2-perfluoroalkylbenzothiazole **117** and -benzoselenazole **118**, Yu and colleagues presented the reaction using TMEDA **43** (Scheme 30).[78]

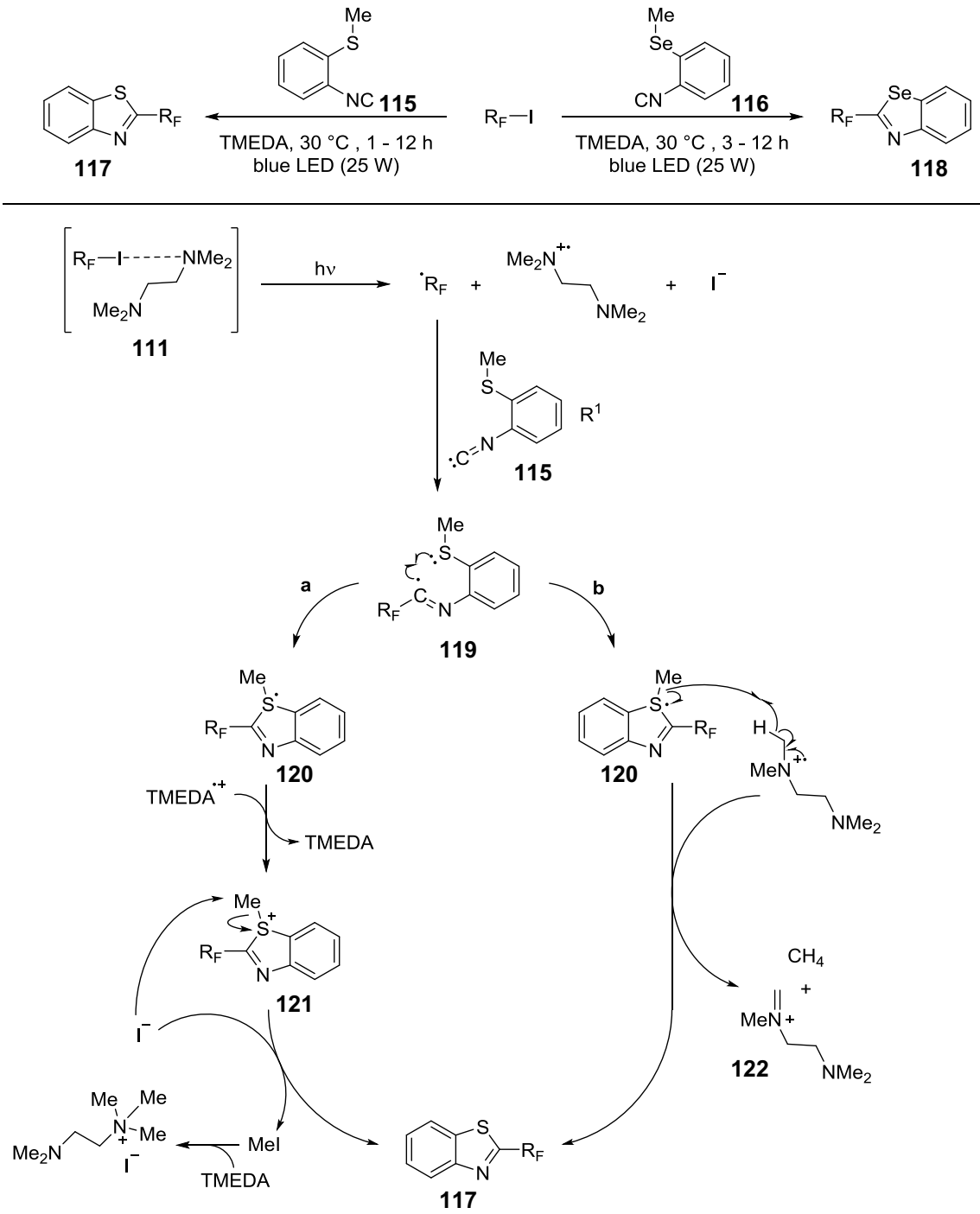

Scheme 30: Synthesis of 2-perfluoroalkylbenzothiazoles **117** and benzoselenazoles **118** by EDA complex using TMEDA (top) and proposed reaction mechanism (bottom).[78]

Benzothiazoles with trifluoromethyl groups in the 2-position are a remarkable compound class and are biologically active (*e.g.* anti-tumor and anti-bacterial agent). Current synthetic methods include traditional condensation reaction, transition metal-catalyzed annulation, intramolecular oxidative cyclization, Sandmeyer trifluoromethylation reaction or photocatalytic CF_3 radical initiated cascade cyclization.[78]

As reaction mechanism, Yu *et al.* proposed that initially, a perfluoroalkyl radical is formed through the formed EDA complex **111**. The formed perfluoroalkyl radical adds to the terminal carbon atom of the isocyano group **115**. After intramolecular cyclization, forming a sulfonium radical **119**, two pathways are possible (**a**, **b**). Following pathway **a**, the formed sulfonium radical is oxidized by the TMEDA radical cation and the sulfonium cation **121** is generated. As a final step, an iodine anion performs a nucleophilic attack at the methyl group of the sulfonium cation **121**, and thereby releases the final perfluoroalkylated product **117** and methyl iodide. Methyl iodide is attacked by TMEDA and forms the quaternary ammonium salt, which was detected by HRMS (ESI-TOF). Following pathway **b**, the formed sulfonium radical **120** reacts with a TMEDA radical cation *via* a concerted proton-coupled electron transfer (PCET), forming the 2-perfluoroalkylbenzothiazole product **117**, methane and a iminium ion **122**, which was detected by HRMS (ESI-TOF).[78]

Yu and co-workers published several contributions on using amine-based EDA complexes. In two publications, they used dibenzylamine (**126**) as catalyst for the synthesis of 2-fluoroalkylated quinoxalines **125**[71] and the halogen-bond-mediated atom transfer radical addition of perfluoroalkyl iodides to alkynes.[79] Furthermore, they presented the hydrotrifluoromethylation of unactivated alkenes and alkynes with the well-known Togni's reagent[80] and the direct aromatic C—H trifluoromethylation with the Umemoto's reagent.[81] *N*-methylmorpholine (NMM) was used in both cases as a tertiary amine, to form the EDA complex with the electron-deficient trifluoromethylating reagents.

When Yu and co-worker investigated the synthesis of 2-fluoroalkylated quinoxalines **125**, they used 1,2-diisocyano-4,5-dimethylbenzene (**123**) as a model substrate and perfluorooctyl iodide (**124**). By the addition of a secondary or tertiary amine, MeCN as the solvent, and irradiation of blue light, the corresponding 2-perfluoroalkylated quinoxaline **125** was isolated. Best results were obtained when dibenzylamine (Bn_2NH, Table 3, entry 2) was used as donor, instead of 1,4-diazabicyclo[2.2.2]octane (DABCO, Table 3, entry 1) or *N*,*N*-diisopropylethylamine (DIPEA, Table 3, entry 3).[71]

Table 3: Examination of the double radical isocyanide insertion reaction.[71]

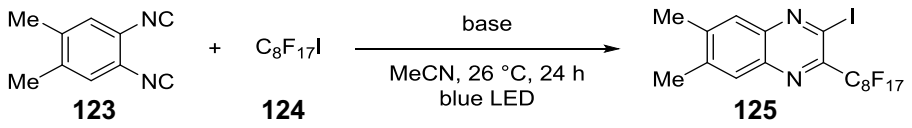

entry	base	yield [%]
1	DABCO	52
2	Bn_2NH	65
3	DIPEA	50
4[a]	Bn_2NH	0
5[b]	Bn_2NH	62
6	none	17

a) no visible-light irradiation; b) The reaction solution was irradiated through a 400 - 650 nm short-pass filter

Without irradiation, no conversion was detected (Table 3, entry 4) and when the reaction solution was irradiated through a short-pass filter (400 - 650 nm) a similar result to the standard reaction setup was obtained (Table 3, entry 5). When no base was added, only a small amount of the desired product was isolated (Table 3, entry 6). Based on this result, a reaction mechanism was proposed by Yu *et al.* (Scheme 31).[71]

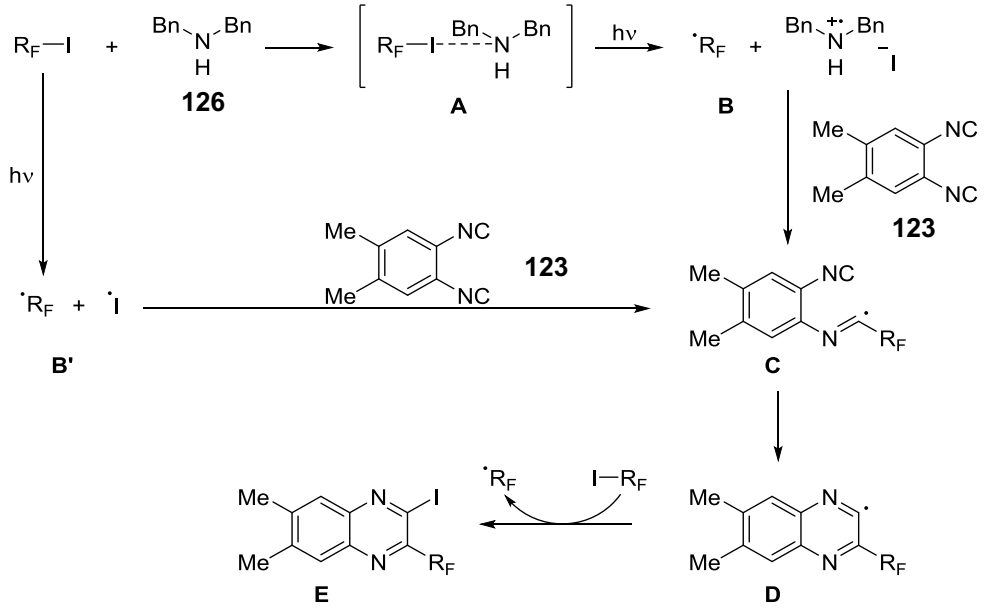

Scheme 31: Proposed mechanism for the double radical isocyanide insertion.[71]

The EDA complex (**A**) is formed between the perfluoroalkyl iodide and the used base. Light irradiation lead to the irreversible fragmentation of the EDA complex and forms the desired perfluoroalkyl radical (**B**). An experiment without the addition of any base (Table 3, entry 6) indicated that the perfluoroalkyl iodide forms radicals just by the irradiation of the used LED (**B'**). After the addition of the perfluoroalkyl radical to the used 1,2-diisocyano-4,5-dimethylbenzene (**123**), the intermediate (**C**) is formed, followed by radical cyclization (**D**). In the final step, an iodine atom is abstracted from

the used perfluoroalkyl iodide to give the final product (**E**).[71] In 2018, Yu and co-worker extended the dibenzylamine-catalyzed iodoperfluoroalkylation to alkynes under blue light irradiation.[79]

Finally, Yu *et al.* demonstrated that these 2-fluoroalkyl-3-iodoquinoxaline (**125**) are suitable substrates for Suzuki, Sonogashira and Buchwald-Hartwig couplings (Scheme 32).[71]

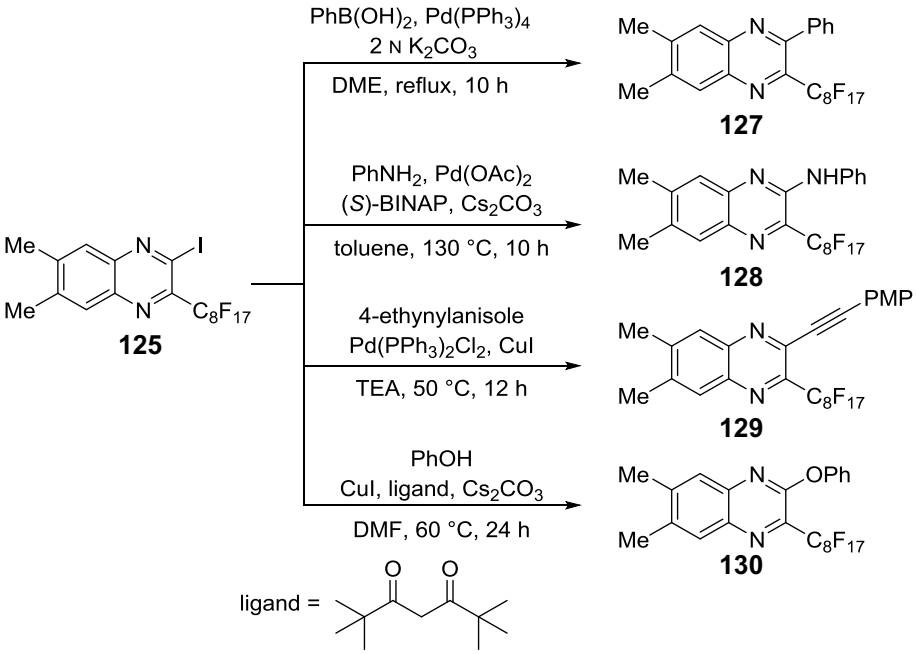

Scheme 32: Synthetic utility of the 2-fluoroalkylated quinoxalines **125**.[71]

Enolate-catalyzed reactions

In 2014, Melchiorre *et al.* presented a direct aromatic perfluoroalkylation and trifluoroalkylation of α-cyano arylacetates by using 1,1,3,3-tetramethylguanidine (**131**) (TMG) as base. As electron acceptor perfluoroalkyl iodides and as electron donor ethyl α-cyano phenylacetate (**132**) were used. Irradiation was conducted by a 23 W CFL bulb (Scheme 33).[82]

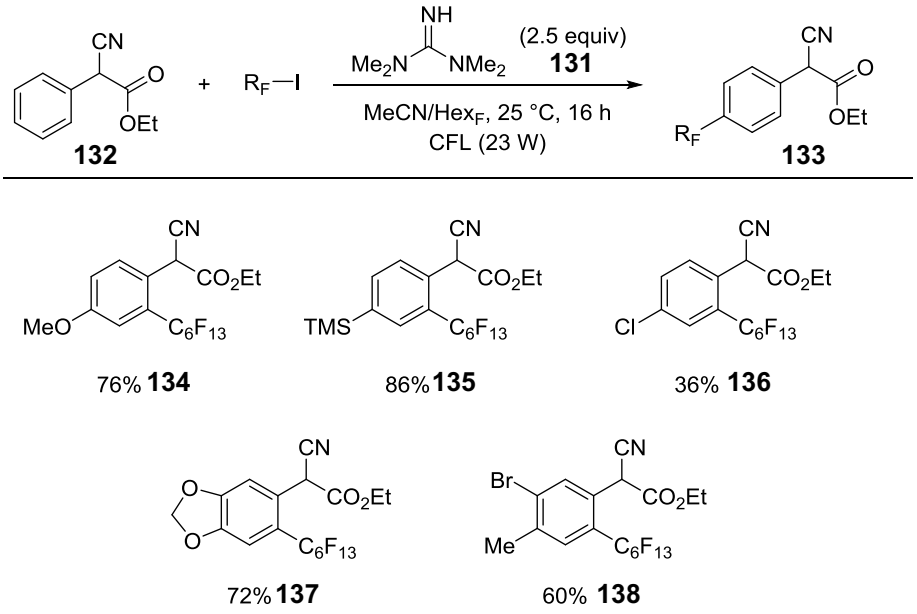

Scheme 33: Metal-free photochemical aromatic perfluoroalkylation of α-cyano arylacetates **132** presendet by Melchiorre *et al.*[82]

Melchiorre *et al.* varied the solvent and base and observed a different product formation (*para/ortho* product). A homolytic aromatic substitution pathway seemed to be a suitable rationale (Table 4). Conducting the reaction in acetonitrile, the *para*- and *ortho*-functionalized products were obtained in a ration of 2:1 (entry 2 - 3, Table 4). Only minor amounts of the bifunctionalized product were formed. Best results were achieved when 1,1,3,3-tetramethylguanidine (**131**) (TMG) was used as base and tetradecafluorohexane (Hex_F) was added to the solvent (entry 7, Table 4). Tetradecafluorohexane was added to collect the generated product in a different phase, since it was observed that the formed enolate has a strong absorption in the visible region and thereby prevented a completion of the reaction. By using the biphasic solvent and TMG **131** as base, not only the yield was increased, the reaction time was shortened from 16 h to 5 h as well.[82]

Table 4: Screening of the perfluoroalkylation reaction.[82]

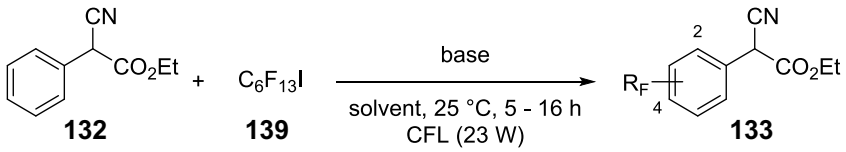

132 **139** **133**

entry	base	solvent	yield [%]	Distribution [%]		
				4	2	2,4
1	none	MeCN	0	–	–	–
2	Cs_2CO_3	MeCN	70	60	33	7
3	TMG	MeCN	62	60	31	9
4	Cs_2CO_3	DMF	45	65	32	3
5	Cs_2CO_3	AcOEt	22	66	31	3
6	Cs_2CO_3	MeCN/Hex_F	73	55	31	14
7	TMG	MeCN/Hex_F	83	58	32	10

Investigation of the substitution pattern of the used substrates demonstrated that electron-donating substituents were tolerated. In contrast, electron-withdrawing groups reduced the electron density on the arene and, as a result the efficiency of the reaction. *para*-Substituted arylacetates were selectively substituted at the *ortho*-position. *ortho*- or *meta*-Substituted arylacetates yielding in moderate regioselectivity and the *para*-isomer was favoured. No *meta*-substituted adduct was detected.[82] Melchiorre *et al.* proposed an enolate formation as the first reaction step and the aggregation to the used perfluoroalkyl iodide forming the EDA complex **141**. An electron transfer leads to the perfluoroalkyl radical (Scheme 34). The addition of the perfluoroalkyl radical to the enolate-type anione **140**, led to the postulation of two final pathways. The formed cyclohexadienyl radical **145** is oxidized by a perfluoroalkyl iodide through a single-electron-transfer (SET). Deprotonation and acidic work-up lead to the final perfluoroalkylated product **133**. A second pathway describes an atom-transfer radical addition (ATRA). After the abstraction of the iodine atom from the perfluoroalkyl iodide, a deiodohydrogenation results in the rearomatisation of the intermediate and acidic workup leads to the final perfluoroalkylated α-cyanoarylacetate **133**.[53, 82]

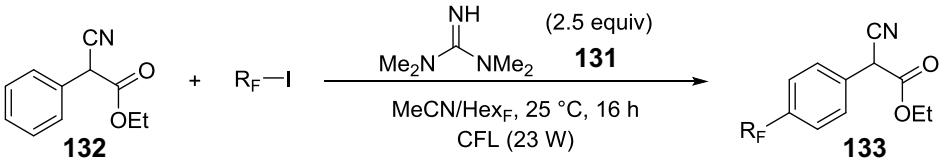

1. Initation *via* EDA complex

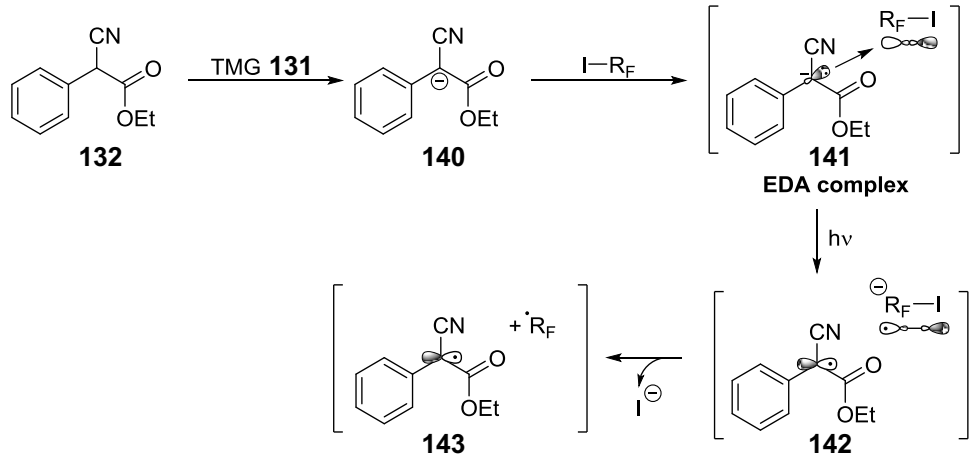

2. C−C bond through homolytic aromatic substitution (HAS)

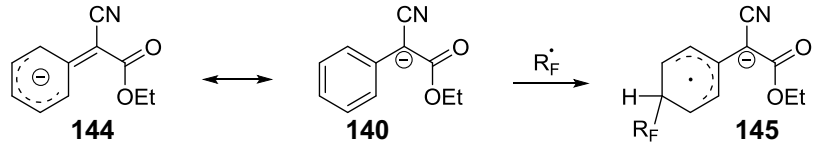

3. Propagation pathways

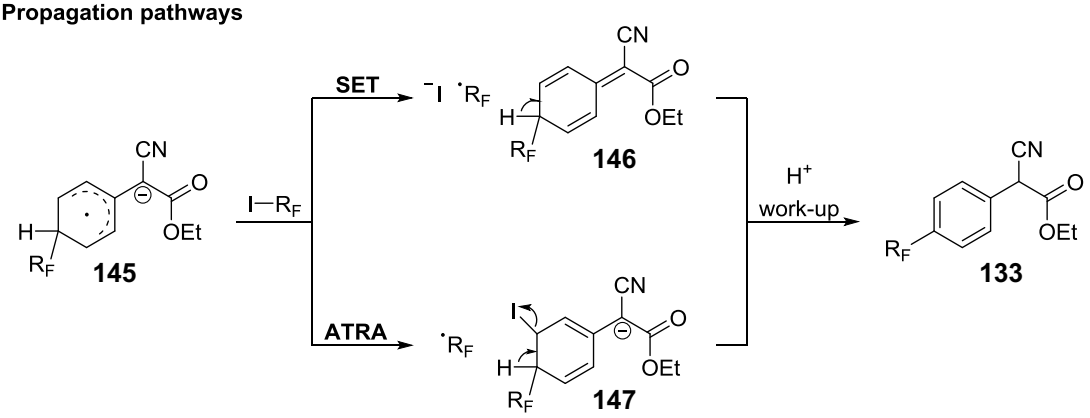

Scheme 34: Proposed mechanism of the metal-free photochemical aromatic perfluoroalkylation of α-cyano arylacetates **132** presented by Melchiorre *et al.*[53, 82]

Comparably, Melchiorre *et al.* presented the perfluoroalkylation of phenols using TMG **131** as base and a CFL (23 W) as an irradiation source (Scheme 35).[83]

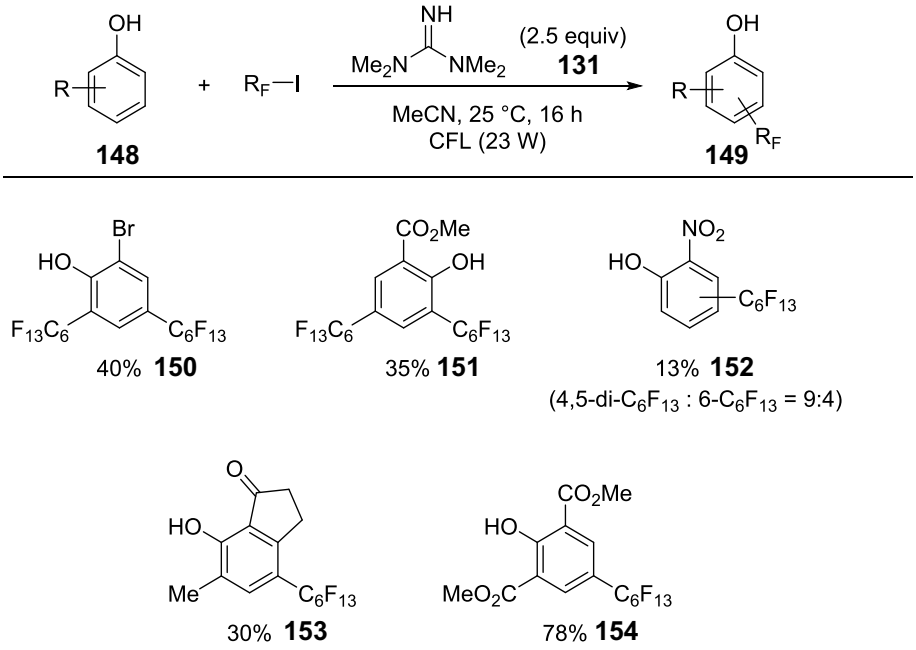

Scheme 35: Photochemical direct perfluoroalkylation of phenols **148** presented by Melchiorre *et al.*[83]

Again, TMG **131** deprotonates the used phenol derivate and the EDA complex is formed between the phenolate **155** and the used perfluoroalkyl iodide. Visible light irradiation generates perfluoroalkyl radicals and the substitution follows a homolytic aromatic substitution pathway. The perfluoroalkyl radical attacks the phenolate and the resulting cyclohexadienyl radical intermediate propagates the radical chain by oxidizing the perfluoroalkyl iodide through a SET mechanism (Scheme 36).[83]

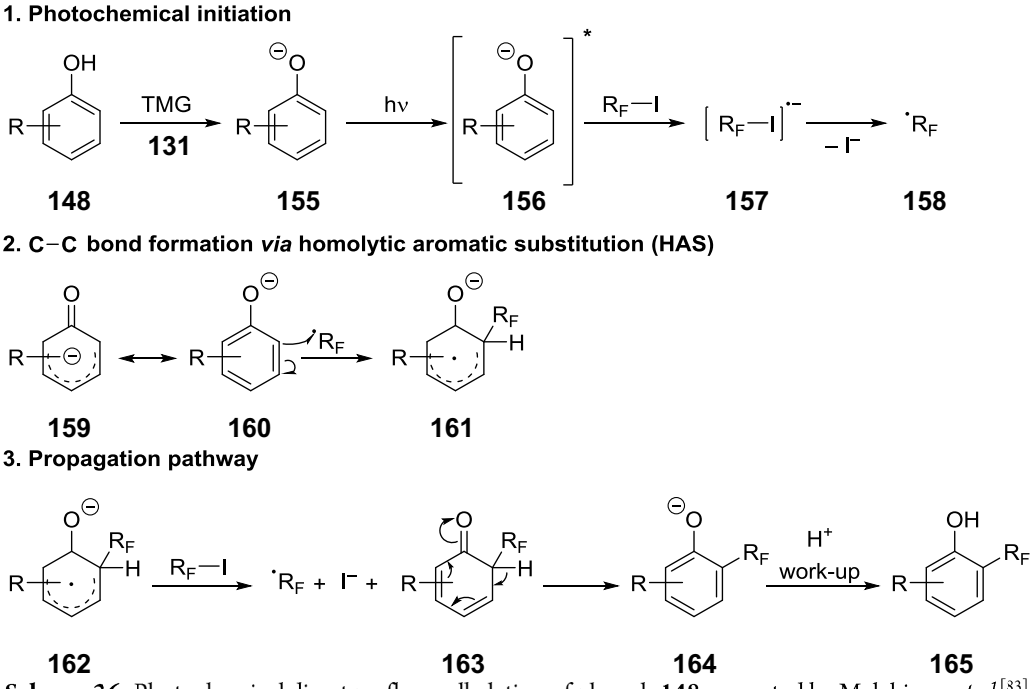

Scheme 36: Photochemical direct perfluoroalkylation of phenols **148** presented by Melchiorre *et al.*[83]

Subsequently, Melchiorre *et al.* developed a photochemical and stereoselective α-alkylation of aldehydes utilizing photo-organocatalysis.[84-85] They were able to perfluoralkylate β-ketoesters enantioselectively (Scheme 37).[86]

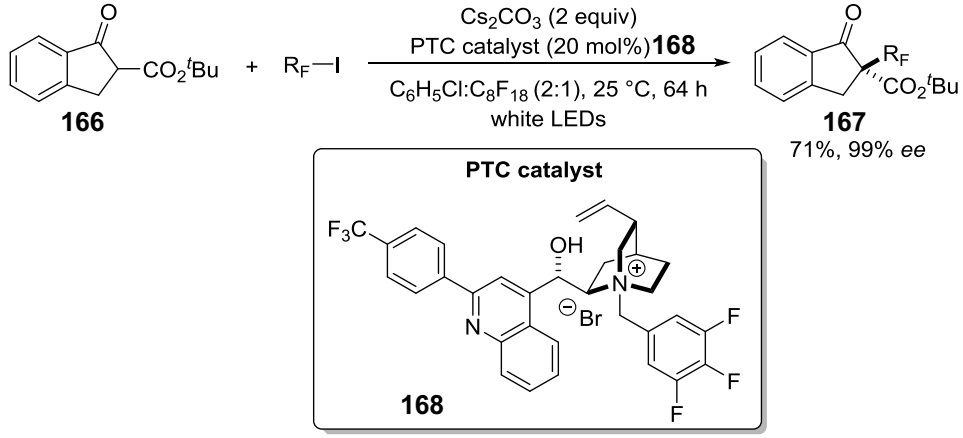

Scheme 37: Enantioselective perfluoroalkylation of β-ketoesters **166** by Melchiorre *et al.*[86]

For a successful reaction, they used a chiral quaternary ammonium salt and phase-transfer catalyst (PTC) **168**. A chiral ion-pair was formed after the deprotonation of the used β-ketoesters **166** (Scheme 38).[86]

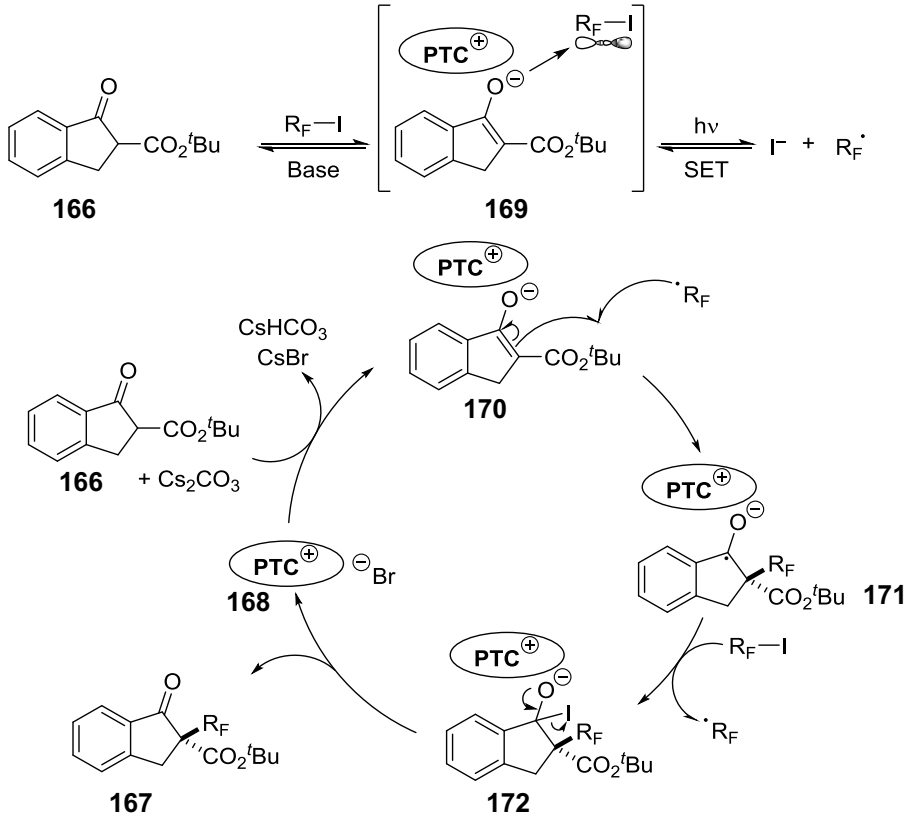

Scheme 38: Proposed reaction mechanism of the enantioselective perfluoroalkylation of β-ketoesters **166** by Melchiorre *et al.*[86]

This chiral ion pair forms the EDA complex and generates perfluoroalkyl radicals mediated by irradiation. The perfluoroalkyl radicals react with the chiral enolate **170** and the ketyl intermediate **171** is formed. After the reduction of the perfluoroalkyl iodide, the formed adduct **172** is not stable and generates the final perfluoroalkylated product **167** under the loss of iodide and the PTC catalyst **168** (Scheme 38).[86]

Phosphorus-catalyzed reactions

In 1990 Huang and Zhang published the iodoperfluoroalkylation with triphenylphosphine (**91**) (20 mol%) and other trivalent phosphorus compounds. For this purpose, they heated different unfunctionalized olefins with iodoperfluoroalkanes in acetonitrile for 4 h and isolated the products in good yields (Scheme 39).[87]

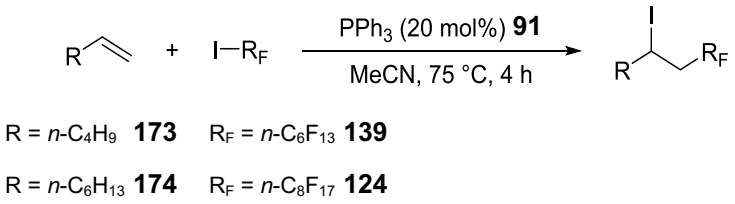

Scheme 39: Triphenylphosphine-catalyzed iodoperfluoroalkylation of unfunctionalized and linear alkenes at elevated temperatures.[87]

The suspected radical mechanism was examined by a reaction with diallyl ether (**175**) as radical clock reagent (Scheme 40). The resulting tetrahydrofuran derivative **176** supported the assumption of a free radical mechanism.[87]

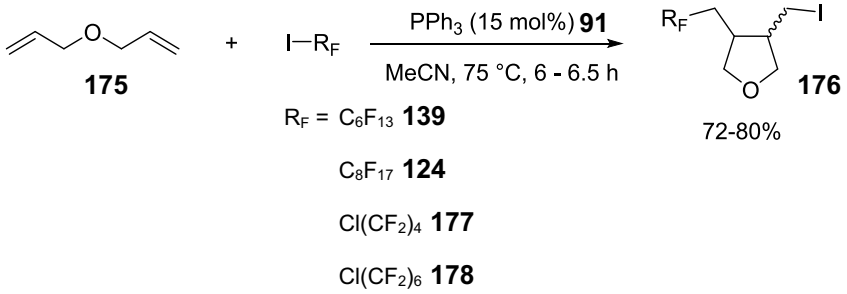

Scheme 40: Triphenylphosphine-catalyzed reaction with diallyl ether (**175**).[87]

Based on these results, Huang and Zhang proposed a radical reaction mechanism but did not consider a photoinduced process, just a single electron transfer (SET) as a starting point. The formation of a phosphonium salt in the presence of a perfluoroalkyl halide was already known.[87-88]

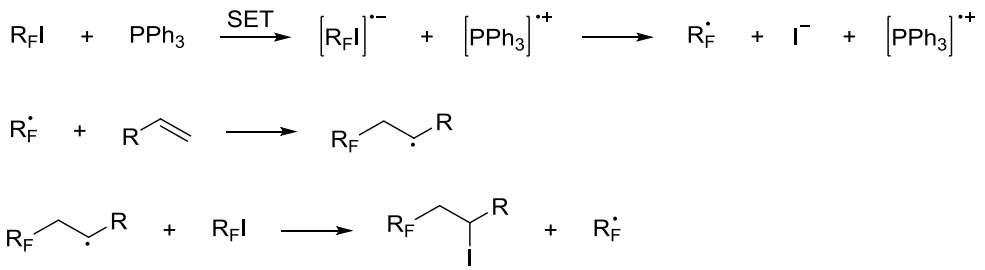

Scheme 41: Proposed radical reaction mechanism by Huang and Zhang.[87]

A publication by Moreno-Mañas *et al.* from 2002 supported that PPh_3 **91** is a suitable catalyst for iodoperfluoroalkylation. By stirring the reaction at room temperature for 48 - 70 h unfunctionalized alkenes as well as 10-undecanoic acid could be converted.[89]

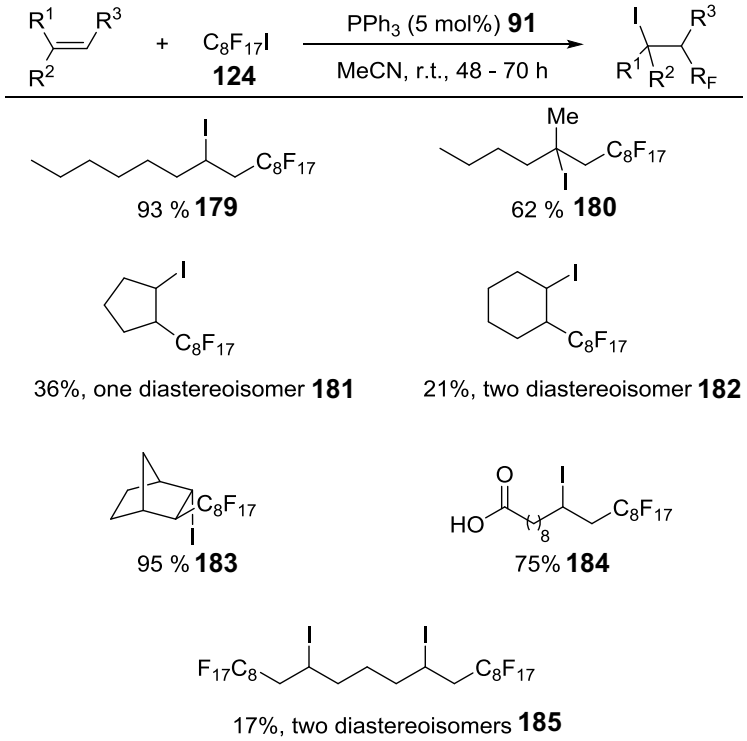

Scheme 42: Triphenylphosphine-catalyzed iodoperfluoroalkylation at room temperature.[89]

Moreno-Mañas *et al.* proposed a radical mechanism with a SET step as a starting point and a subsequent free radical mechanism.[89] This phosphine-catalyzed iodoperfluoroalkylation was not further pursued and the influence of visible light on the reaction and the catalyst was not investigated until we published the results presented later on.[4-6] Apart from investigating the best reaction conditions, the iodoperfluoroalkylation of 22 different unfunctionalized and functionalized terminal and internal alkenes using tri-*tert*-butylphosphine (**186**) as catalyst and a blue LED (461 nm) as irradiation source was presented (Scheme 43).[4]

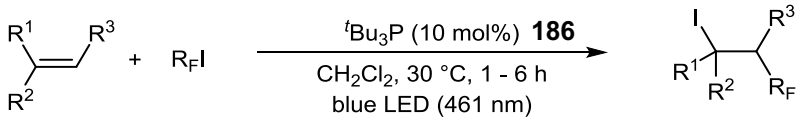

Scheme 43: Phosphine-catalyzed iodoperfluoroalkylation of alkenes.[4]

An open question after presenting this publication was the reactivity of the used catalyst and the other tested phosphorus(III) compounds. Theoretical calculations shed more light on this question and subsequently, the substrate scope was extended to alkynes at the beginning of 2020 in a further publication by us.[5-6]

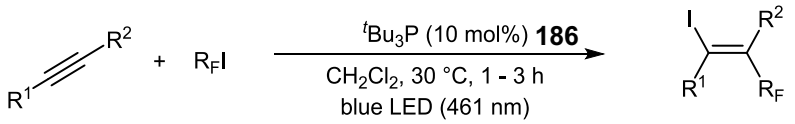

Scheme 44: Phosphine-catalyzed iodoperfluoroalkylation of alkynes.[6]

Only months after we presented the first results on the phosphine-catalyzed iodoperfluoroalkylation,[4] Zhang *et al.* published the phosphine-catalyzed difluoroalkylation of arenes and heterocycles using visible light (Scheme 45).[90]

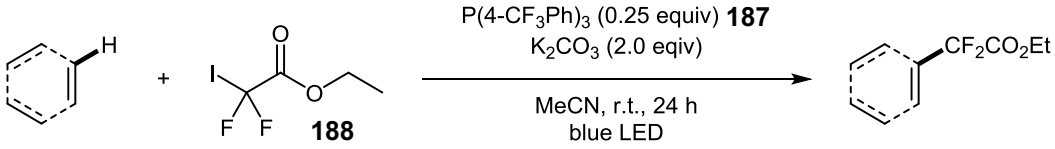

Scheme 45: Phosphine-catalyzed difluoroalkylation of arenes and heterocycles.[90]

Standard reactions were performed with 1,3,4-trimethoxybenzene (**189**) and ethyl iododifluoroacetate (**188**). By changing from triphenylphosphine (**91**) (yield: 48%) to P(4-CF_3-Ph)$_3$ (**187**) with KOAc as base, the yield could be increased to 85%. Best results were obtained when the base (K_2CO_3, yield: 90%) and the concentration in MeCN (0.2 M) were changed and led to a yield of 97% of the *gem*-difluoromethylated product **190** (Scheme 46).[90]

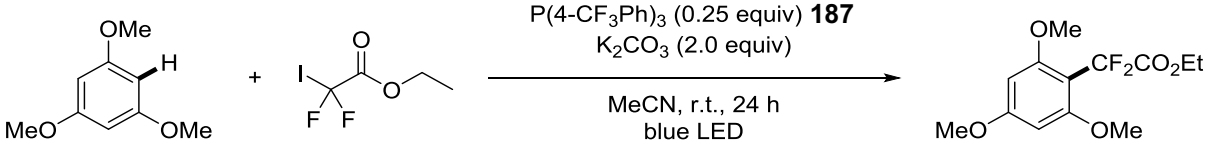

Scheme 46: Phosphine-catalyzed difluoroalkylation of 1,3,4-trimethoxybenzene (**189**).[90]

The product was not formed without either the phosphine as catalyst, a base, irradiation, or thermal initiation (80 °C). Zhang and co-workers proposed following reaction mechanism. As first step an EDA complex **A** between phosphine **187** and iododifluoroacetate **188** is formed. Visible light irradiation generates a difluoroalkyl radical **B** and is subsequently captured by the used arene or

heteroarene **C** (Scheme 47). Zhang *et al.* suggested two further reaction pathways to form the aryl cation **D**: **a**) recovery of the catalyst through SET oxidation of the intermediate **B**; **b**) a radical exchange with iododifluoroacetate **188** to generate new difluoromethyl radicals. Through deprotonation, the final difluoroalkylated product **E** is formed (Scheme 47).[90]

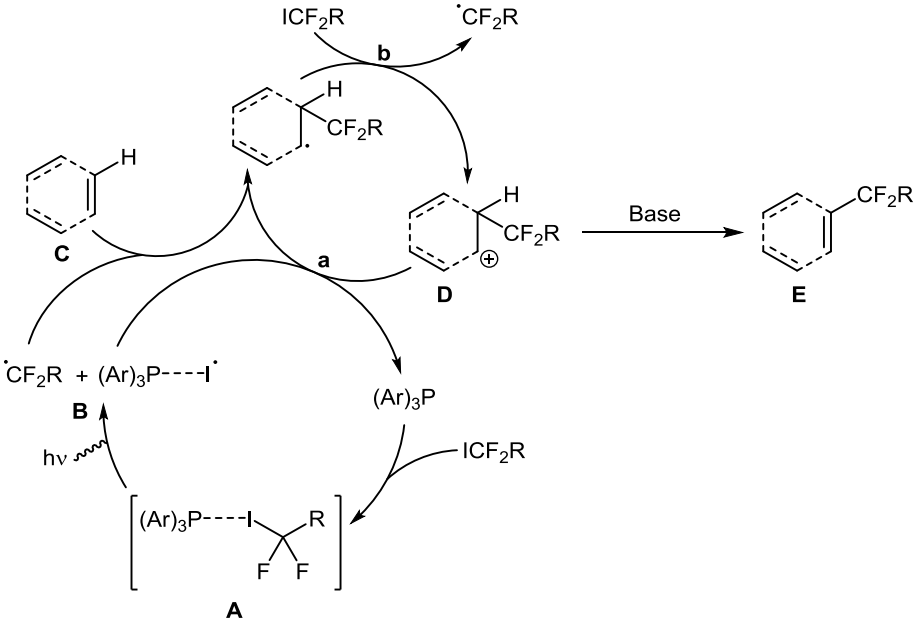

Scheme 47: Proposed reaction mechanism by Zhang *et al.*[90]

2.3. Beyond Photochemistry

Apart from photochemistry, different methods were developed to introduce a trifluoromethyl-group into an organic compound. For this purpose, nucleophilic and electrophilic trifluoromethylating reagents were developed or F_3C-radical species using radical chemistry (*via* homo or mesolysis) (Scheme 48).[81]

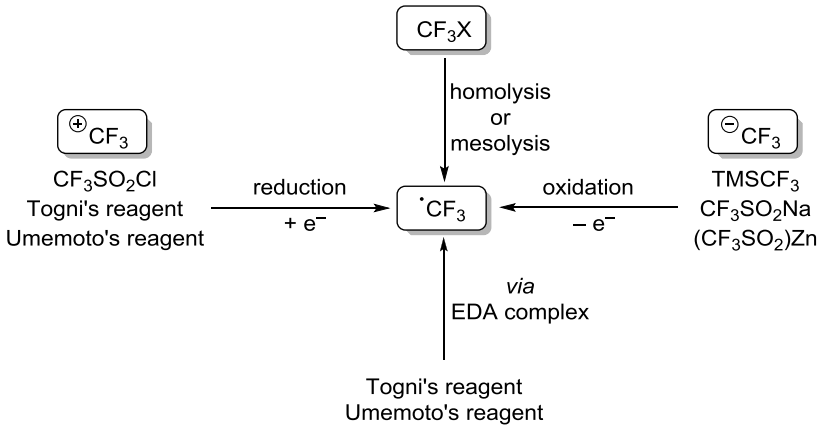

Scheme 48: Common ways to generate trifluoromethyl radicals.[81]

A radical trifluoromethylation by homolysis or mesolysis can be achieved by using a trifluoromethylation source that forms the trifluoromethyl radical like trifluoromethyl iodide,

trifluormethylacetyl or trifluoromethylsufonyl derivatives and *S*-trifluoromethyl xanthates.[81, 91-92] Radical trifluoromethylation of aromatics, heteroaromatics and unsaturated double bonds were reported by using these reagents.[18]

In the case of electrophilic trifluoromethylation, various reagents have been designed. It is challenging to generate a trifluoromethyl cation in chemical reactions (Scheme 49).[45, 91]

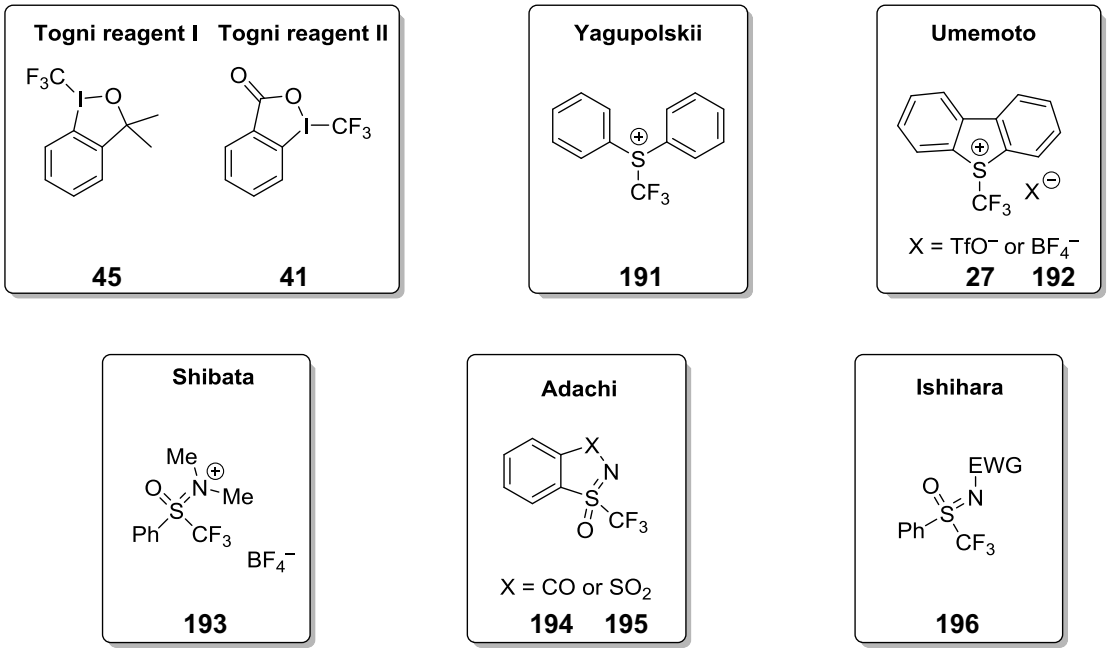

Scheme 49: Common electrophilic trifluoromethylating reagents.[45]

Through the reduction of the electrophilic trifluoromethylation reagent, the desired CF_3-radical can be generated.[81] The reaction mechanism is still a topic of debate for it remains unclear whether it its either a polar substitution mechanism (S_N) or a single electron transfer (SET mechanism) is involved.[91] Wang, Zhang and co-workers published a copper-catalyzed direct C—H trifluoromethylation of quinones, using the Togni reagent II **41** as CF_3 source. As a reaction mechanism, they proposed that the Togni reagent II **41** undergoes a SET reduction by the used copper(I) catalyst (Scheme 50).[93]

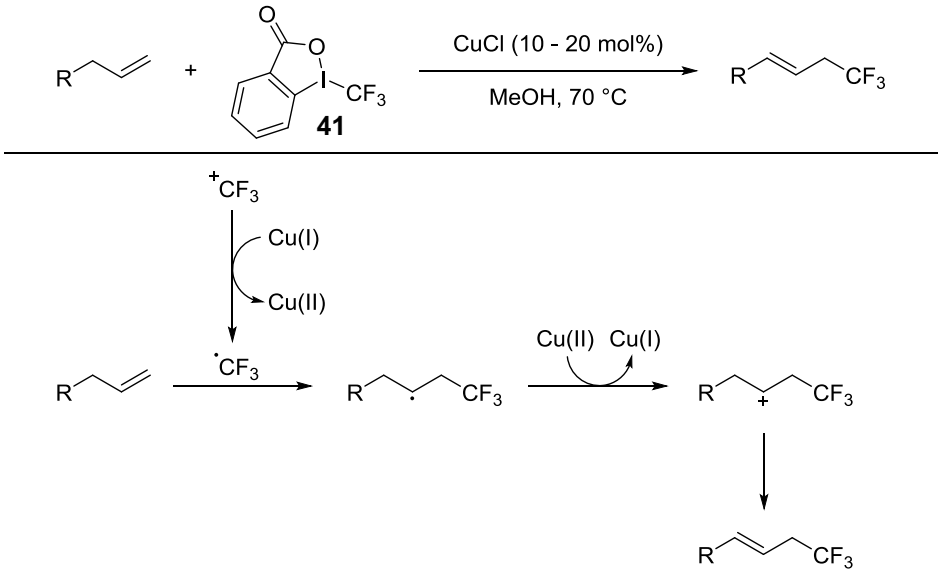

Scheme 50: Copper-catalyzed direct C—H trifluoromethylation.[93]

A following radical process and a second reverse electron transfer regenerate the copper catalyst from copper(II) to copper(I). The free radical mechanism was confirmed by trapping experiments with TEMPO as radical scavenger.[93] However, the authors also mention other works by Buchwald,[94] Liu[95] and from their group, which may point to a different mechanism.

Buchwald *et al.* presented a trifluoromethylation of unactivated olefins by using tetrakis(acetonitrile)copper(I) hexafluorophosphate $[(MeCN)_4Cu]PF_6$ as catalyst and Liu *et al.* used copper(I) thiophene-2-carboxylate (Cu(Tc)) to afford compounds containing the CF_3-group in allylic position (Scheme 51).[94-95]

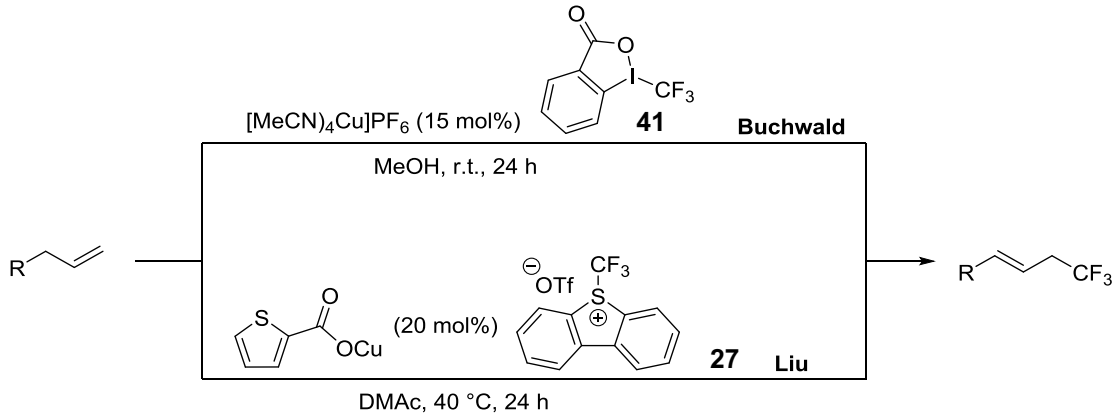

Scheme 51: Copper-catalyzed trifluoromethylation of unactivated olefins presented by Buchwald and Liu.[94-95]

Wang *et al.* used different α,α-diphenylallyl alcohols **197**, Togni reagent **41** and copper iodide as catalyst, which initiate a 1,2-aryl migration yielding different α-aryl β-trifluoromethyl ketones **226** and lead to the proposed mechanism (Scheme 52). After the generation of the CF_3 radical through reduction of the Togni's reagent with the Cu(I) catalyst, the radical adds to the double bond of the

used α,α-diphenylallyl alcohol **197**. After the formation of radical **199**, the migration of one aryl group forms a spiro[2,5]octadienyl radical **200** and leads to the intermediate **201**. Final SET leads to the formation of the α-aryl β-trifluoromethyl ketones **226** and regenerates the copper catalyst from Cu(II) to Cu(I) (Scheme 52).[96]

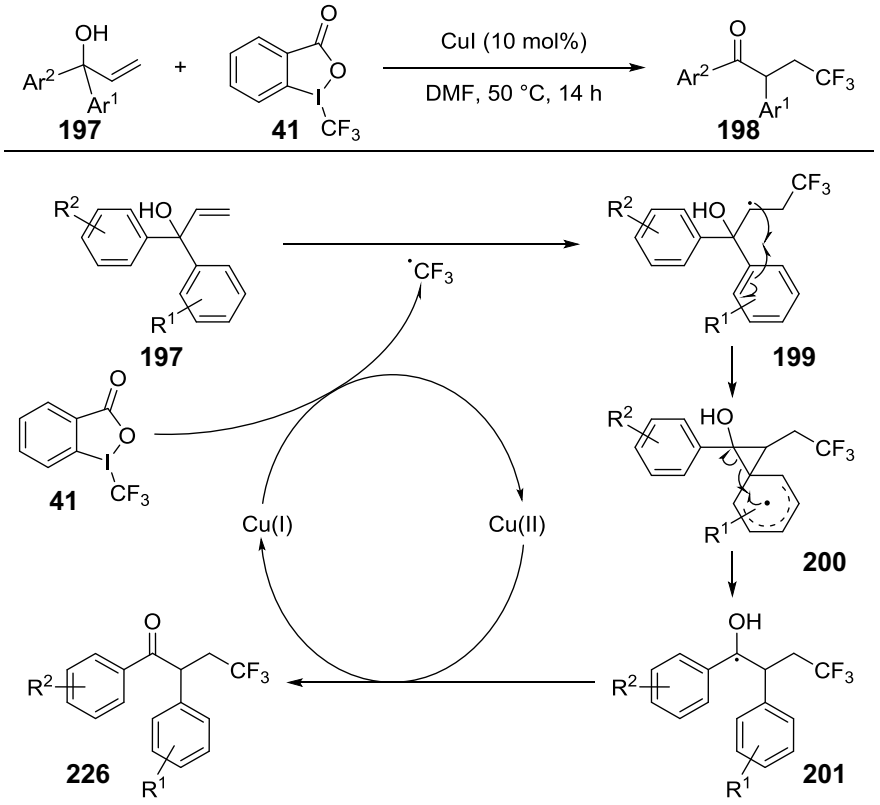

Scheme 52: Copper-mediated trifluoromethylation of diphenylallyl alcohols and the proposed mechanism.[45, 96]

Sodeoka and co-workers presented similar works but used iron(II) acetate (**202**) as a catalyst.[45, 97] Unfortunately, the group did not propose a reaction mechanism for this reaction.[97]

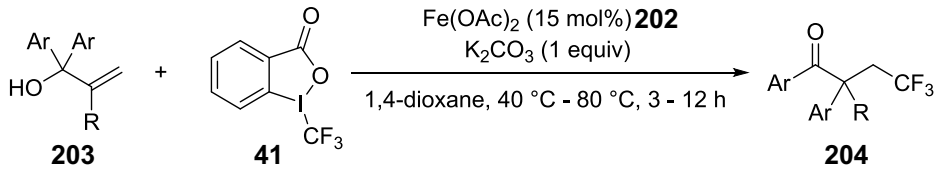

Ar =	4-Me-C_6H_4	72%
Ar =	4-OMe-C_6H_4	78%
Ar =	4-OTBS-C_6H_4	80%
Ar =	4-F-C_6H_4	80%
Ar =	4-Cl-C_6H_4	92%

Scheme 53: Iron(II) catalyst carbotrifluoromethylation.[45, 97]

Yu *et al.* published a direct aromatic C—H trifluoromethylation by forming an EDA complex between the Umemoto's reagent **192** and *N*-methylmorpholine (**205**) as metal free alternative (Scheme 54).[81] Since no irradiation was required for the reaction, this type of reaction is not mentioned in the chapter of photocatalytic activation of EDA complexes. It shall briefly be described in the following as metal-free alternative.

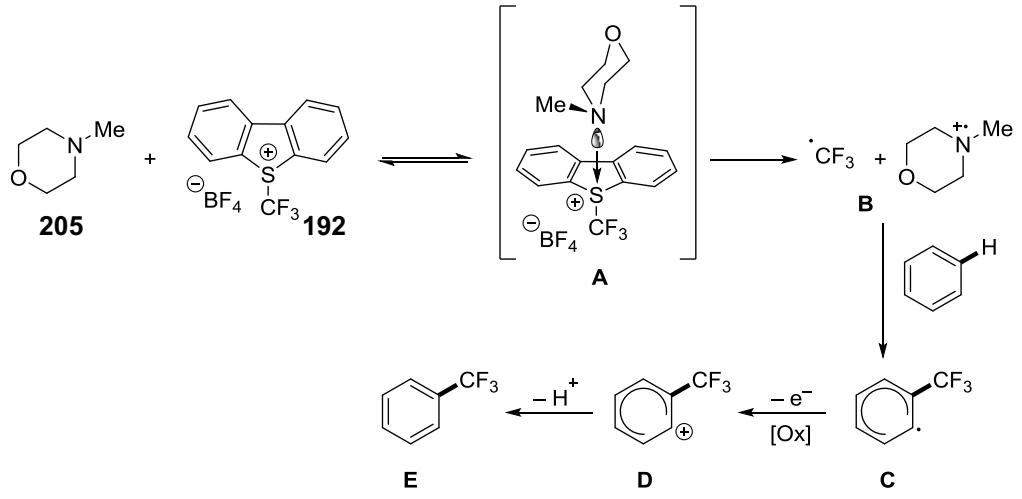

Scheme 54: Direct aromatic C-H trifluoromethylation *via* EDA complex using NMM **205** and Umemoto's reagent **192**.[81]

The EDA complex is formed between the electron-deficient Umemoto's reagent **192** and the organic base NMM **205**. After the irreversible collapse of the EDA complex (**A**), the resulting F_3C-radical (**B**) reacts with the used arene. The resulting radical intermediate (**C**) is oxidized to the cationic intermediate (**D**). The resulting trifluoromethylated arene (**E**) is formed after final deprotonation (Scheme 54).[81]

Yu and co-worker successfully transformed several tryptamine, tryptophan, and melatonin derivatives as well as other indole derivatives. For the reaction mechanism, Yu *et al.* suggested that the EDA complex thermally collapses irreversibly and the resulting trifluoromethyl radical can further react with the used educt (**B**→**C**). For the oxidation step, two considerations were suggested. Either the radical **C** is oxidized by the NMM radical cation **206** *via* path (**a**) or by the used Umemoto's reagent **192** (**b**). This step could not be completely ruled out by this publication. Assisted by *N*-methylmorpholine (**205**) the cation **D** is deprotonated to form the final product **E** (Scheme 55).[81]

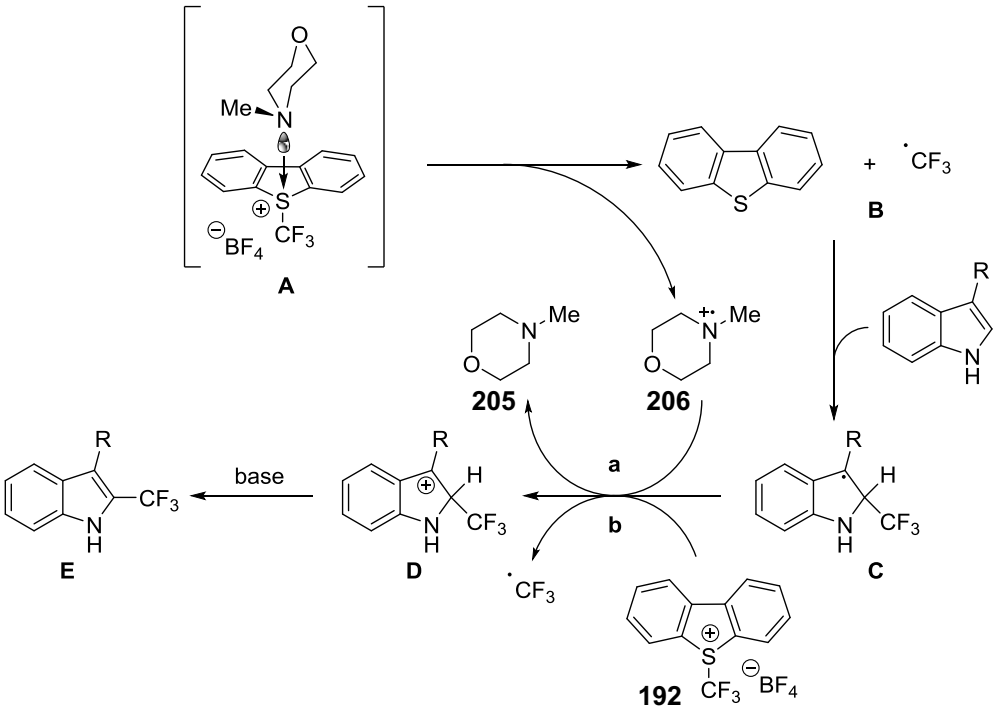

Scheme 55: The proposed mechanism by Yu *et al.* including the described oxidation step **a**/**b**.[81]

Yu *et al.* used another known CF_3 source to present a hydrotrifluoromethylation of alkenes and alkynes. By reacting Togni's reagent (II) **41** with NMM **205** and different alkenes or alkynes, the corresponding hydrotrifluoromethylated product was isolated in good yields (Scheme 56).[80]

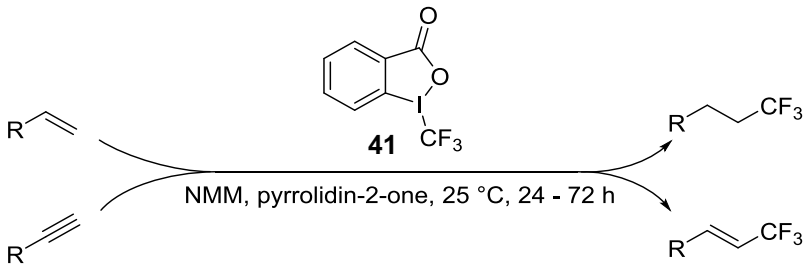

Scheme 56: Hydrotrifluoromethylation of alkenes and alkynes by Togni's reagent **41**.[80]

Similar to the aromatic C—H trifluoromethylation of arenes using the Umemoto's reagent, the EDA complex is first formed between the Togni reagent **41** and NMM **205**, which causes the radical formation in an irreversible step (Scheme 57).[80]

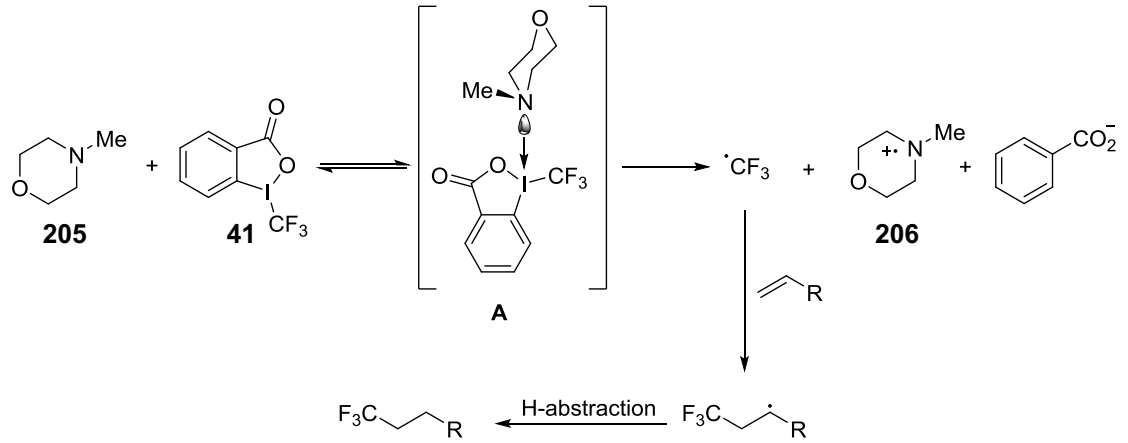

Scheme 57: Proposed mechanism for the hydrotrifluoromethylation of alkenes and alkynes using the Togni's reagent **41**.[80]

An alkene or alkyne captures the resulting trifluoromethyl radical and in a final step, the alkyl radical intermediate is formed by abstracting a hydrogen atom from the used solvent. Deuteration experiments revealed the hydrogen abstraction step.[80]

When a nucleophilic trifluoromethylation should proceed, the CF_3^--anion needs to be stabilized. Otherwise, it collapses into fluoride and a difluorocarbene. This is due to the strong destabilization by electrostatic repulsion between the anionic charge and the p-electron pairs of the fluorine atoms.[98]

Nucleophilic trifluoromethylation can be achieved by trifluoromethyl metal species, such as Hg, Cu, Zn or Cd. Nevertheless, these trifluoromethyl reagents are usually used for the substitution of aromatic iodides or bromides under thermal activation. Low yields and side products are a drawback to this method.[91] By using metals, the anionic charge is transferred to the empty orbital of the transition metal. Another approach is the transfer of charge into a fragile σ-bond, *e.g.*, C—Si bond.[98] Trifluoromethyltrimethylsilane ($TMSCF_3$), the so-called Ruppert-Prakash reagent, is such an alternative. By using an anionic initiator, for example, a fluoride anion as well as alkoxides, different aldehydes, ketones, esters and activated amines were converted.[91]

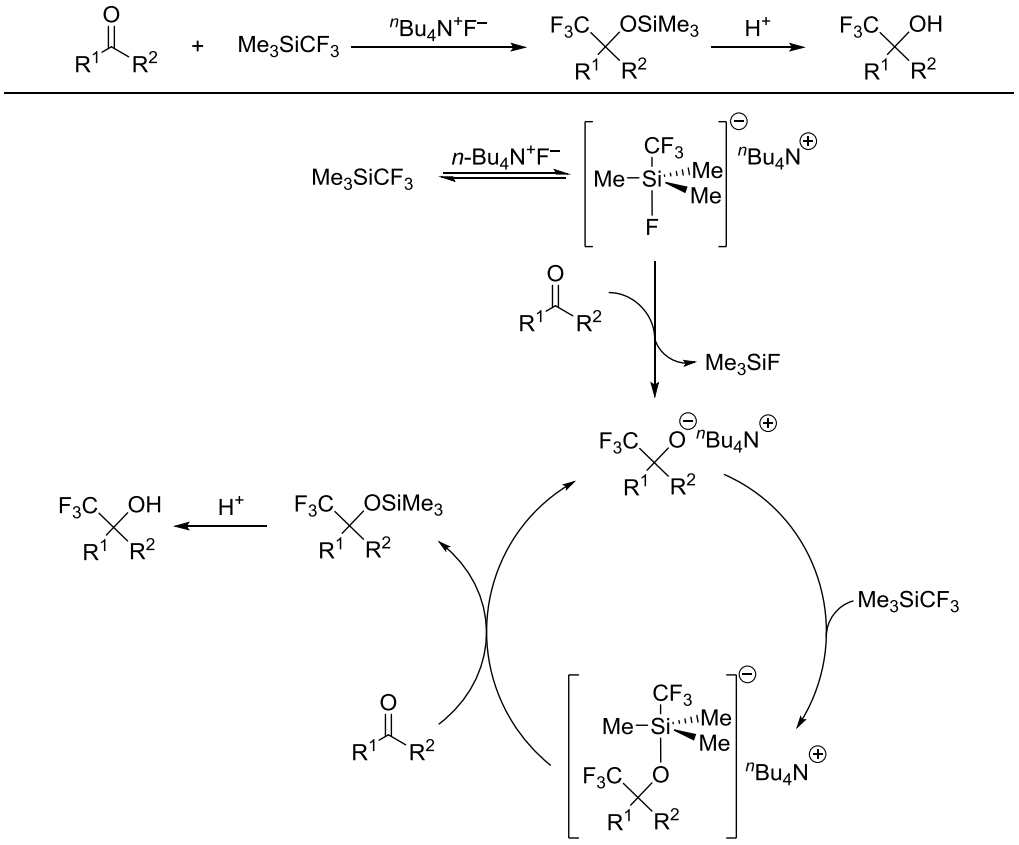

Scheme 58: Trifluoromethylation of carbonyls using the Ruppert-Prakash reagent ($TMSCF_3$) and the proposed mechanism.[99]

Through the activation of perfluoroalkyl iodides with different metals (Cu, Fe, Ni, Mg, Pd, Ag, Cd) or metal complexes ($Pd(PPh_3)_4$, $IrH(CO)(PPh_3)_3$) the addition to alkenes and alkynes is possible and gives access to perfluoroalkylated products. The metal or transition-metal complex act as an electron donor and transfers its electron the perfluoroalkyl iodide and generates perfluoroalkyl radicals and a iodine anion.[100] Another metal-free alternative is the FLP-catalyzed iodoperfluoroalkylation in 2016 that was published by Czekelilus *et al.* and that shall be discussed later on.[1]

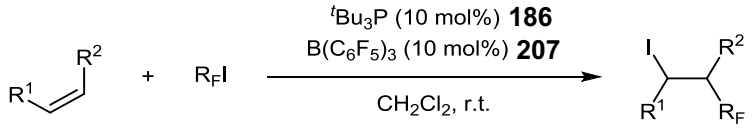

Scheme 59: FLP-catalyzed iodoperfluoroalyklation of alkenes.[1]

3. Research Question

In 2016, Czekelius *et al.* presented their findings on a FLP-catalyzed iodoperfluoroalkylation of unfunctionalized alkenes using $B(C_6F_5)_3$ **207** and $^tBu_3P$ **186** as catalyst (Scheme 60). The question arose whether the FLP-catalyzed reaction proceeds *via* a radical or ionic mechanism. First evidence for a radical reaction was presented supporting a radical mechanism.[1]

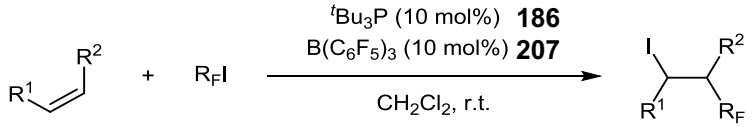

Scheme 60: FLP-catalyzed iodoperfluoroalyklation of alkenes.[1]

One goal of this doctoral dissertation was to elucidate the reaction mechanism in action and to obtain further insights regarding the mechanism. For this purpose, several test reactions were planned. First, a heteroatom-free radical clock was synthesized. Different products were to be expected following a radical in contrast to an ionic mechanism (Scheme 61).

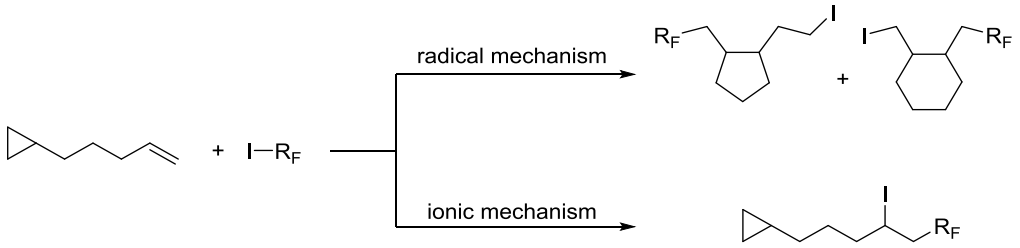

Scheme 61: Synthesized radical clock and the potential formed products.[2]

Further investigations of the mechanism were started, including reactions with 1,4-cyclohexadiene and tributyltin hydride and commercially available radical scavengers such as BHT or TEMPO. The influence of the phosphane was also investigated.

In this context, a borane-free iodoperfluoroalkylation using solely $^tBu_3P$ under the influence of light will be examined. In 2017 Chen *et al.* presented a light-mediated iodoperfluoroalkylation in the presence of an amine.[75] Consequently, a light-mediated reaction in the presence of a phosphane is highly likely. A consideration of this light-mediated reaction path is supported by two publications on a phosphorus-catalyzed iodoperfluoroalkylation, which did not address a photochemical process, but most likely irradiated the reaction solution.[87, 89] A repetition of these literature-known experiments will reveal whether irradiation is necessary or not. In case a photo-mediated reaction is present, the optimal reaction conditions and a reaction setup for the photomediated iodoperfluoroalkylation will be conducted.

Secondly, the reaction mechanism must be clarified in detail. UV-VIS measurements and NMR spectroscopic investigations should prove an EDA complex formation. The suspected radical mechanism in this reaction should be proven by the use of radical clocks and radical scavengers. Possible limitation of the reaction should be revealed by studying the substrate scope. Initially, to establish the reaction in literature, the focus should be based on the substrate spectrum of alkenes. Subsequently, an extension to the alkynes should follow (Scheme 62).

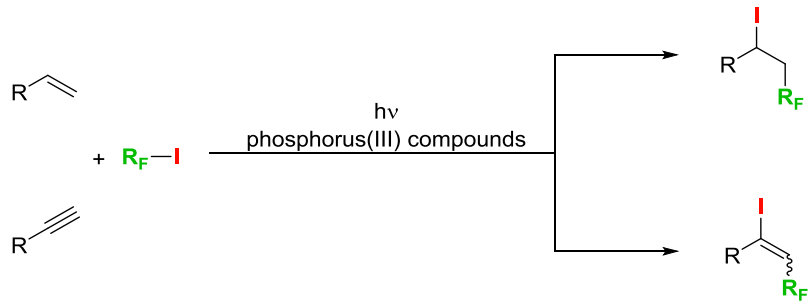

Scheme 62: Investigation of photochemical perfluoroalkylation using phosphorus(III) compounds of unsaturated hydrocarbons.

As a final evaluation, the phosphorus-catalyzed and photo-mediated iodoperfluoroalkylation should be compared with the FLP-catalyzed reaction. The advantages and disadvantages of the two reactions should be compared and elaborated.

4. Cumulative part I

In 2016 Czekelius *et al.*[1] published a frustrated Lewis pair (FLP)-catalyzed iodoperfluoroalkylation that was further investigated by Dr. Michael Spittler in his doctoral thesis.[3] The results published in 2016 shall be briefly summarized in the following, to indicate the motives of the first publication[2] in this doctoral thesis. For the investigation of the FLP-catalyzed iodoperfluoroalkylation, the already established and most prominent Lewis pair $B(C_6F_5)_3/{}^tBu_3P$ was used.[101-102] Tris(pentafluorophenyl)borane (**207**) ($B(C_6F_5)_3$), often shortened as BCF, as strong and sterically demanding Lewis acid and tri-*tert*-butylphosphine (**186**) ($^tBu_3P$), as Lewis base, became well-known by the work of Stephan *et al.* in 2006.[103] The first experiments showed that by mixing $B(C_6F_5)_3/{}^tBu_3P$ with perfluoroalkyl iodides, the iodophosphonium fluoroboroate-salt $[{}^tBu_3PI][FB(C_6F_5)_3]$ **208** was formed and isolated (Table 5).[1] Different perfluoroalkyl iodides were used and the results led to questions regarding the reaction mechanism (Scheme 66).

Table 5: Overview of the tested perfluoroalkyl iodides to form the iodophosphoium fluoroborate-salt **208**.[1]

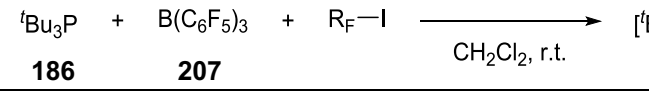

R_F—I	F_3C—I	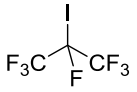	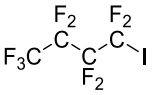	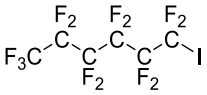	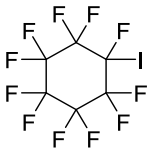	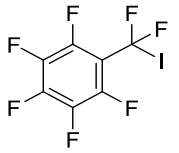
[h:min]	00:20	24:00	24:00	00:20	01:00	00:30
Yield [%]	65	62	54	85	75	70

When perfluorocyclohexyl iodide (**209**) was tested, the observation led to the idea of a formal β-elimination process for the perfluoroalkyl iodide (Scheme 63). Due to the absence of a β-fluoride in case of perfluoroalkyl iodides like CF_3I **25** or the tested perfluorobenzyl iodide, an *α*-elimination followed by carbene formation would be a possible explanation.[1]

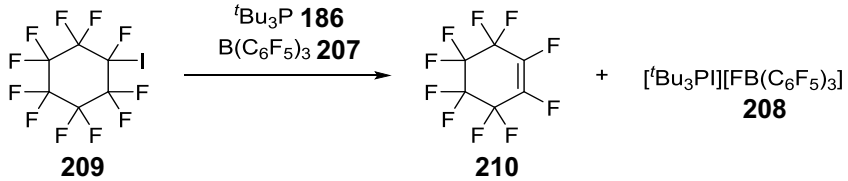

Scheme 63: Iodophosphonium fluoroborate $[{}^tBu_3PI][FB(C_6F_5)_3]$ **208** formation with perfluorocyclohexyl iodide (**209**).[1]

After isolating the formed iodophosphonium fluoroborate $[{}^tBu_3PI][FB(C_6F_5)_3]$ **208** it was tested to react with hex-1-ene or cyclohexene, but no reaction occurred. When the reaction was tested with the

individual components and nonafluoro-1-iodobutane (**101**) the iodoperfluoroalkylated product of 1-hexene was isolated in 73% yield. Under the same conditions, twelve different substrates were tested and ten products could be isolated (Scheme 65). While (*Z*)-3-hexene was successfully transformed, no conversion was detected for the (*E*)-isomer of 3-hexene. Besides, styrene was not converted into the iodoperfluoroalkylated product.[1] Later investigations showed that styrene even acts as an inhibitor in a iodoperfluoroalkylation reaction.[2] This phenomena is known and is attributed to radical quenching by formed stable radicals.[89] To get better insights into the reaction mechanism, control reactions were conducted. First, ^{19}F- and ^{31}P-NMR-spectra, of a mixture of a perfluoroalkyl iodide and $^{t}Bu_3P$ were recorded. The spectra of the mixtures revealed a shift in the NMR spectra and indicated an interaction between the halide and the phosphorus compound. No π-complex formation between the Lewis base $B(C_6F_5)_3$ **207** and 1-hexene in the ^{1}H- and ^{11}B-NMR spectra was detected. Both Lewis acid and base had to be present in the reaction; otherwise, no reaction occurred.[1] When 1,6-heptadiene (**212**) was used, the question arose if a radical or ionic mechanism was more likely for the FLP-catalyzed reaction (Scheme 64).[1]

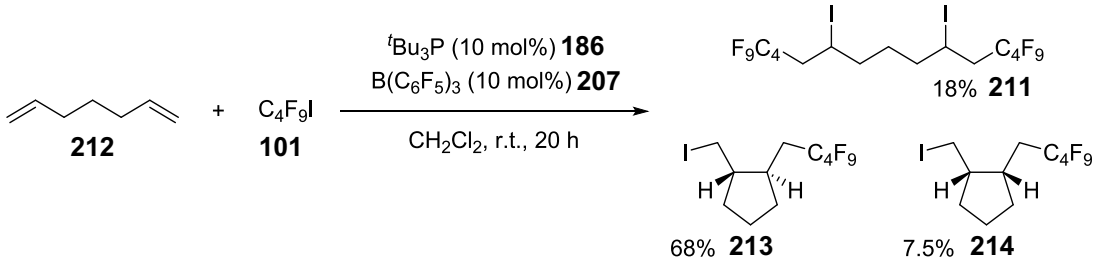

Scheme 64: FLP-catalyzed reaction of 1,6-heptadiene (**212**) with C_4F_9I **101**.[1]

The formed cyclopentane derivatives suggested a radical mechanism. EPR measurements and the addition of the radical scavenger 3,5-di-*tert*-butyl-4-hydroxytoluene (BHT) to a reaction could not prove the presence of radical intermediates.[1]

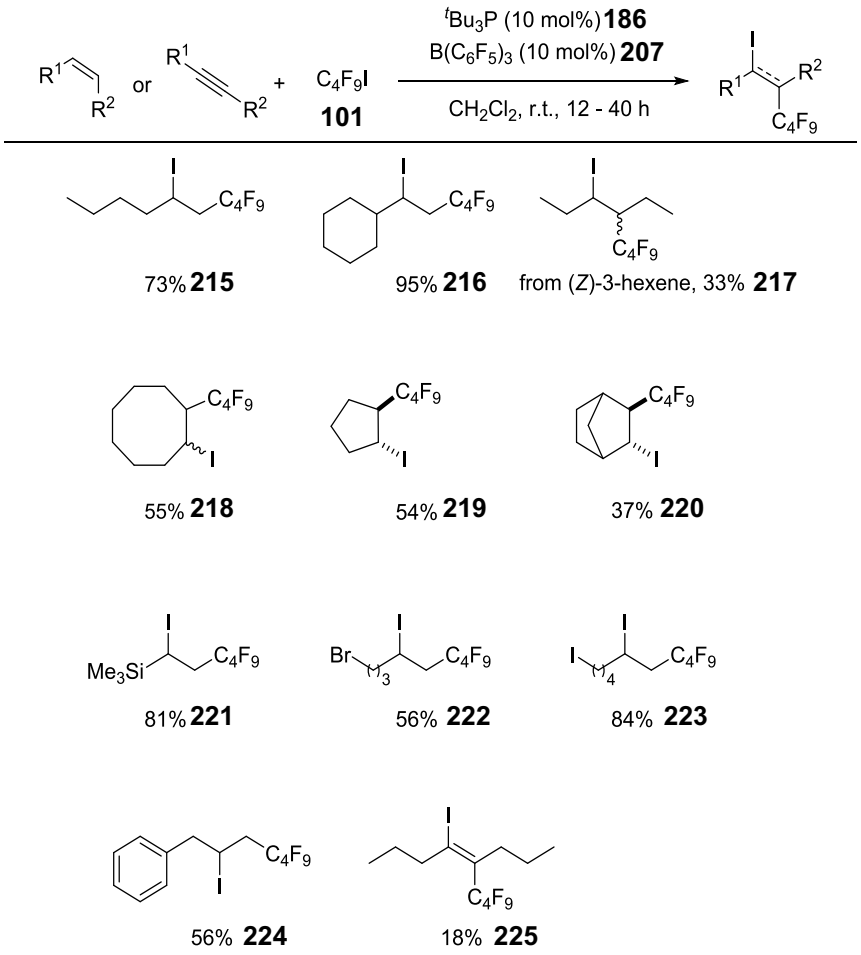

Scheme 65: FLP-catalyzed iodoperfluoroalkylation of unsaturated hydrocarbons.[1]

Since neither an ionic nor a radical mechanism could be fully proven four different reaction pathsways for the FLP-catalyzed reaction were proposed (Scheme 66). The two ionic reaction pathways are described under **a** and **b** (Scheme 66, top). First, the C—I-bond is cleaved heterolytically to form a phosphonium salt. In the case of reaction path **a**, a cyclic iodine cation is formed by halogen transfer. Ring-opening is performed by the perfluoroalkyl anion *via* the most accessible side (Scheme 66, top, **I**). In the reaction pathway **b** the electron-poor borane activates the alkene. The resulting alkyl *tris*(pentafluorophenyl)borate forms the intermediate **II**. In the third reaction path **c**, a perfluoroalkyl radical is formed reductively by the phosphine. Intermediate **II** is formed by the addition of the perfluoroalkyl radical to the alkene. Subsequently, a radical chain reaction is followed by iodine transfer from the perfluoroalkyl iodide. The fourth reaction pathway **d** suggests the formation of a perfluoroalkylborate. Intermediate **II** is formed by homolytic bond cleavage and subsequent addition to the alkene.[1]

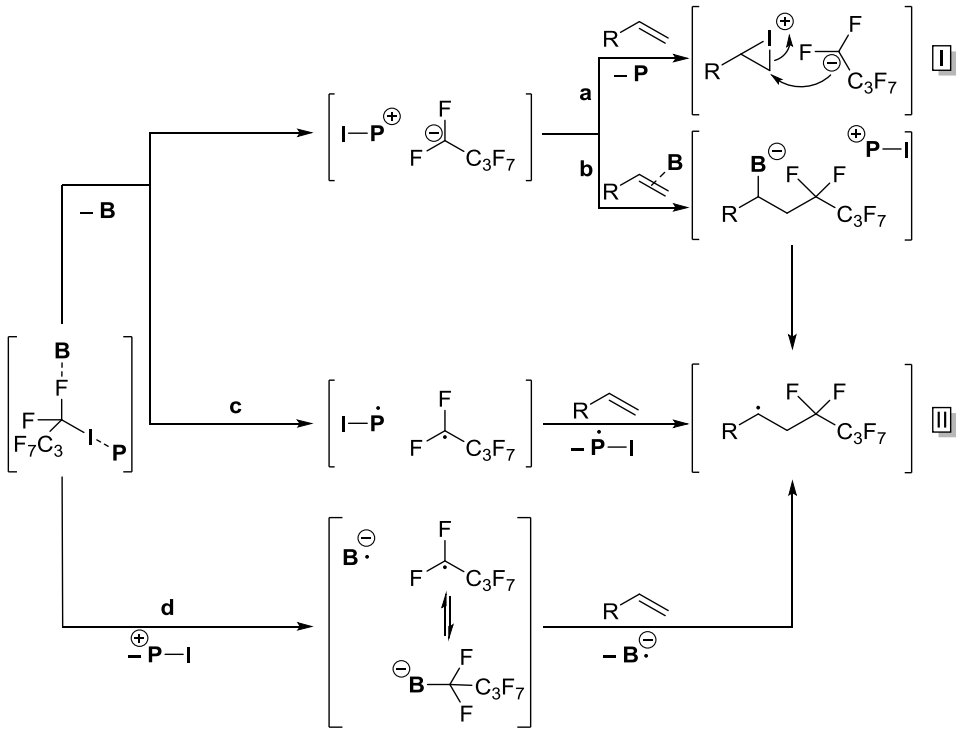

Scheme 66: Proposed reaction routes for FLP-catalyzed iodoperfluoroalkylation.[1]

4.1. Mechanistic Insights into FLP-Catalyzed Iodoperfluoroalkylations

The conducted experiments of the publication: "Mechanistic Insights into FLP-Catalyzed Iodoperfluoroalkylations"[2] and a brief discussion of the results will be summarized below. The individual contributions to this publication and the publication is presented without changes at the end of the chapter (p. 67).

The mechanism of the FLP-catalyzed iodoperfluoroalkylation could not be evaluated in the first place.[1] Therefore, a radical scavenger should be synthesized, which does not contain any heteroatoms, since borane **207** barely tolerates heteroatoms. Since mainly terminal alkenes had been investigated until then, the radical scavenger should contain a terminal alkene on the one side and a cyclopropane ring on the other (Scheme 67). A putatively formed radical causes a ring-opening of the three-membered ring **229**. Depending on the regioselectivity ring opening of the three-membered ring, a five **231** or six **227** membered ring product will be formed (Scheme 67).[2]

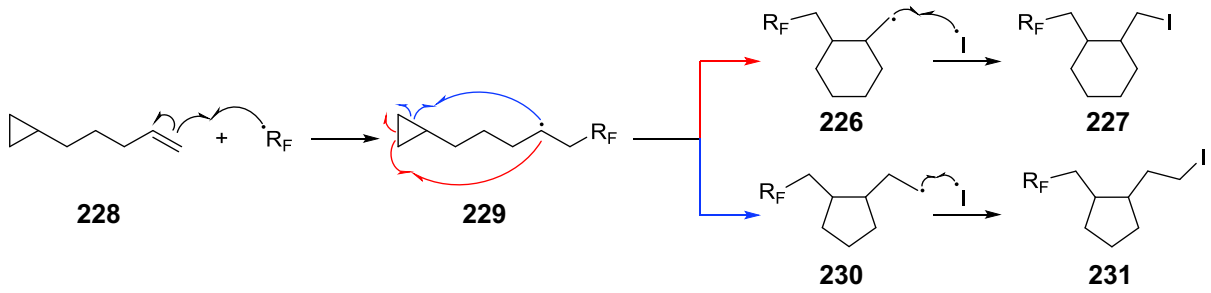

Scheme 67: Radical ring-opening of pent-4-en-1-ylcyclopropane (**228**).[2]

In case of an ionic mechanism, the iodine atom adds to the higher substituted carbon atom and the perfluoroalkyl chain to the terminal end of the alkene and the iodoperfluoroalkylated product **232** is formed (Scheme 68).[2]

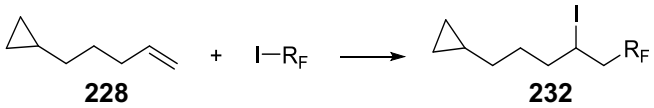

Scheme 68: Ionic iodoperfluoroalkylation of pent-4-en-1-ylcyclopropane (**228**).[2]

The synthesis of pent-4-en-1-ylcyclopropane (**228**) was started in the master thesis and completed for this publication at the beginning of the doctoral thesis.[2, 104] The synthesis is briefly summarized below (Scheme 69). Starting from 5-hexenol (**233**), the cyclopropane ring was first introduced to the alkene. The Simmons-Smith cyclopropane reactions (**I**) performed did not lead to complete conversion of 5-hexen-1-ol (**233**).

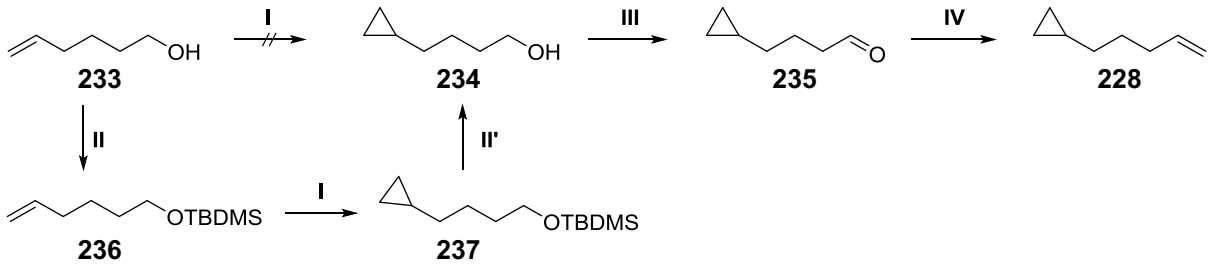

Scheme 69: Synthesis route for the preparation of pent-4-en-1-ylcyclopropanes (**228**). **I** = Cyclopropanation, **II/II'** = TBDMS-protection/-deprotection, **III** = Oxidation, **IV** = Wittig reaction.[2]

Educt **233** and the cyclopropanated product **234** could not be separated after the reaction. Furthermore, it was observed that the hydroxy group was no longer present after the cyclopropanation. Instead, a methoxy group was observed in the ^{1}H-NMR spectrum and no OH-band was detected in the IR spectra. Several literature known procedures [105-106] did not lead to complete conversion and did not avoid the formation of the methoxy group. For this reason, a protective group was introduced with TBDMSCl. The protecting group was subsequently removed with TBAF after the cyclopropanation reaction (**II'**, Scheme 69). To perform a complete cyclopropanation, different types of Simmons-Smith reactions were conducted. However, only when diethyl zinc (2.0 equiv), freshly distilled diiodomethane (2.0 equiv) and trifluoroacetic acid (2.0 equiv) were used, the reaction turned to completion and product **237** was formed.[2] After oxidation (**III**) of the alcohol **234** to aldehyde **235** with Dess-Martin periodinane and a Wittig reaction (**IV**), the final product **228** was obtained (Scheme 69).[2] The intermediate products **236 - 235** and also the final cyclopropanated product **228** appeared to be highly volatile. However, in a FLP-catalyzed iodoperfluoroalkylation, only the ionic pathway product **232** was formed and no cyclization product was detected (Scheme 70).[2]

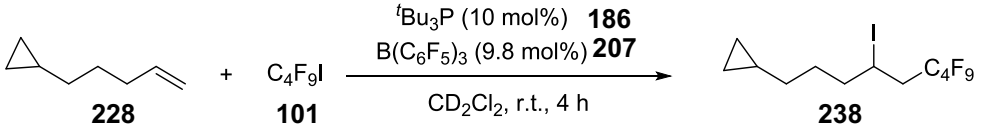

Scheme 70: Iodoperfluoroalkylation of pent-4-en-1-ylcyclopropane (**228**).[2]

Nevertheless, the formed iodoperfluoroalkylated product **238** and the absence of a cyclization product **227** or **231** did not exclude a radical mechanism. If the formation of the iodoperfluoroalkylated product **238** is faster than a cyclization product, a radical mechanism cannot be excluded. As a second radical clock, 6-bromohexene (**239**) was synthesized and a FLP-catalyzed iodoperfluoroalkylation was performed. But no cyclization product was formed either (Scheme 71).[2]

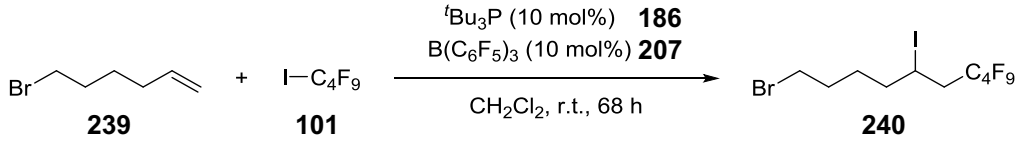

Scheme 71: FLP-catalyzed iodoperfluoroalkylation of 6-bromohexene (**239**).[2]

Since radical clock reactions could not confirm a radical mechanism, butylhydroxytoluene (**242**) (BHT) and 2,2,6,6,-tetramethylpiperidine 1-oxyl (**244**) (TEMPO) were used as radical scavengers. In 2016, BHT **242** was already tested but did not influence the conversion rate.[1] For the investigation of the reaction mechanism, BHT **242** was tested again and was added to a reaction of vinylcyclohexane (**241**) and C_4F_9I **101** (Scheme 72).[2]

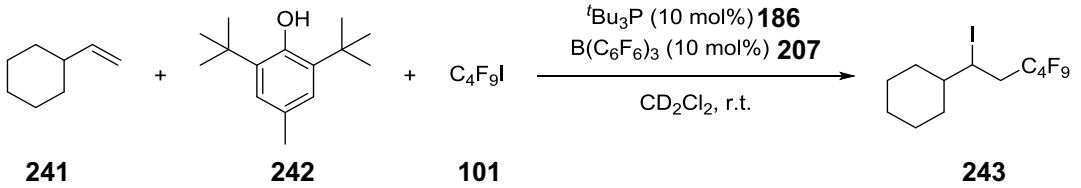

Scheme 72: FLP-catalyzed reaction of vinylcyclohexane (**241**) and C_4F_9I **101** with BHT **242**.[2]

A control NMR spectrum showed a conversion of 60% already after 1 h. No additional signals in the ^{1}H-NMR spectrum indicated a radical mechanism. It should be noted that BHT **242** is a sterically demanding radical scavenger. Sterically larger radicals may not be trapped in this case. Besides, mixtures of BHT **242** with $B(C_6F_5)_3$ **207** or with $^tBu_3P$ **186** showed no significant shift in the ^{19}F- and ^{31}P-NMR spectra (Figure 1, Figure 2).[2]

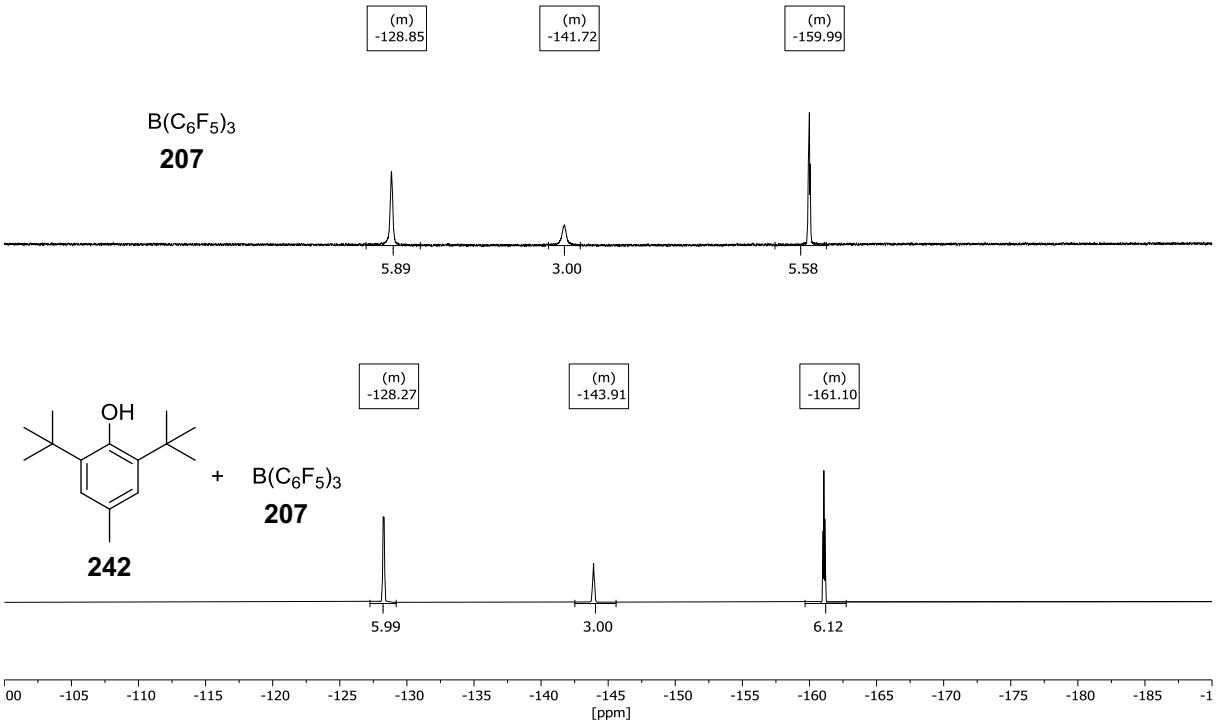

Figure 1: Stacked ^{19}F-NMR spectra (C_6D_6, 282 MHz) of $B(C_6F_5)_3$ **207** (top) and mixture $B(C_6F_5)_3$ **207** and BHT **242** (bottom) with external standard ($CFCl_3$ in C_6D_6).[2]

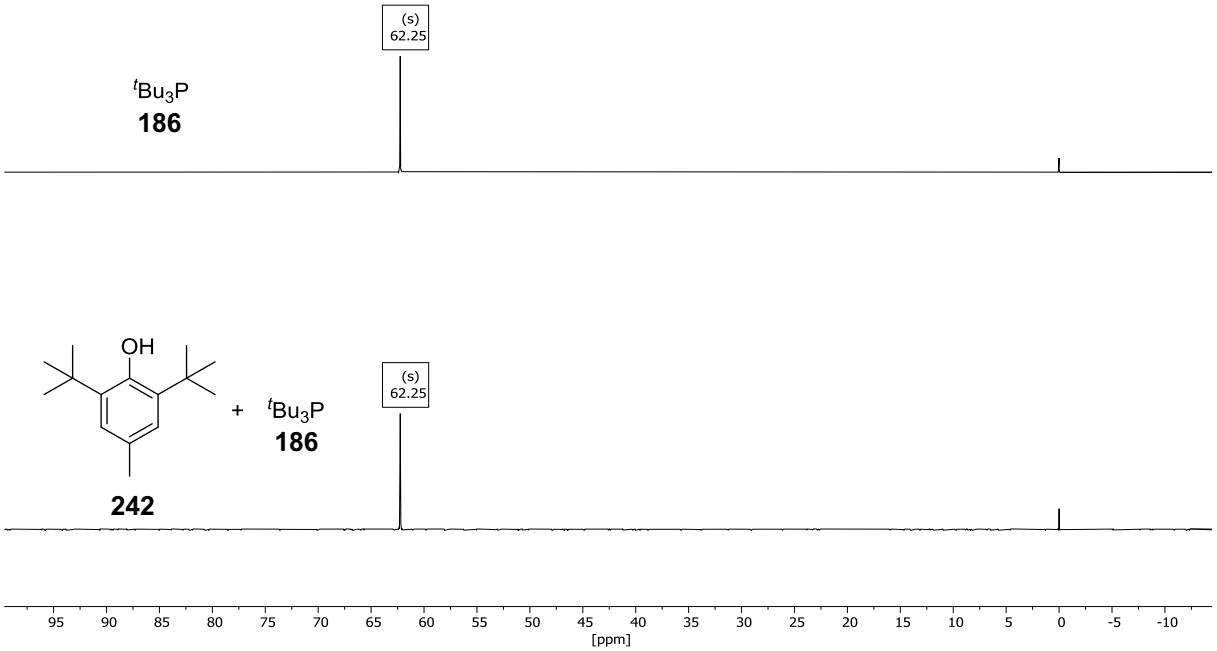

Figure 2: Stacked ^{31}P-NMR spectra (CH_2Cl_2, 121 MHz) of ^{t}Bu$_3$P **186** (top) and mixture ^{t}Bu$_3$P **186** and BHT **242** (bottom) with external standard (H_3PO_4 in D_2O).[2]

Further, TEMPO **244** was used as a second radical scavenger and was added to a reaction of vinylcyclohexane (**241**) and C_4F_9I, but no conversion was detected (Scheme 73). The addition of TEMPO **244** to an FLP-catalyzed reaction appears to completely suppress the reactivity of the borane **207** and phosphine **186** and quenched the reaction.[2]

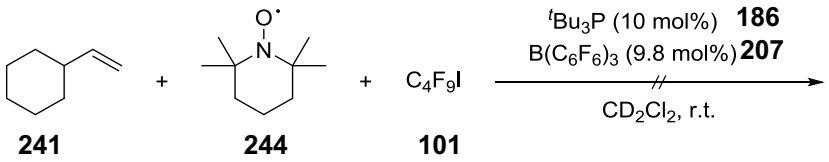

Scheme 73: FLP-catalyzed reaction of vinylcyclohexane (**241**) and C_4F_9I **101** with TEMPO **244**.[2]

The addition of TEMPO **244** to an ongoing reaction with vinylcyclohexane (**241**) and nonafluoro-1-iodobutane (**101**) even led to the termination of the reaction (Scheme 74). The radical scavenger TEMPO **244** was added 20 min after the reaction was started.[2]

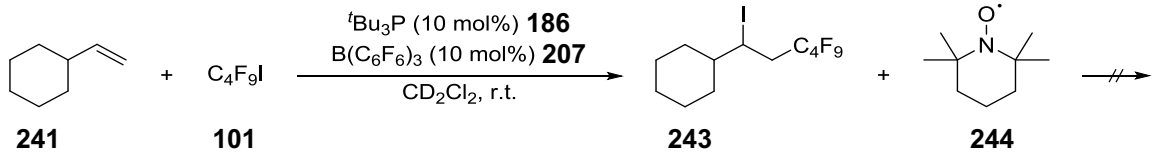

Scheme 74: Addition of TEMPO **244** to a running FLP-catalyzed reaction of vinylcyclohexane (**241**) and C_4F_9I **101**.[2]

The ^{19}F-NMR spectrum of $B(C_6F_5)_3$ **207** with TEMPO **244** showed an interaction between the borane and the radical scavenger, which is due to borate formation (Figure 3). Due to the interaction of TEMPO **244** with the empty orbital of the borane **207**, radical formation is unlikely and the determination of the mechanism is hampered.[2]

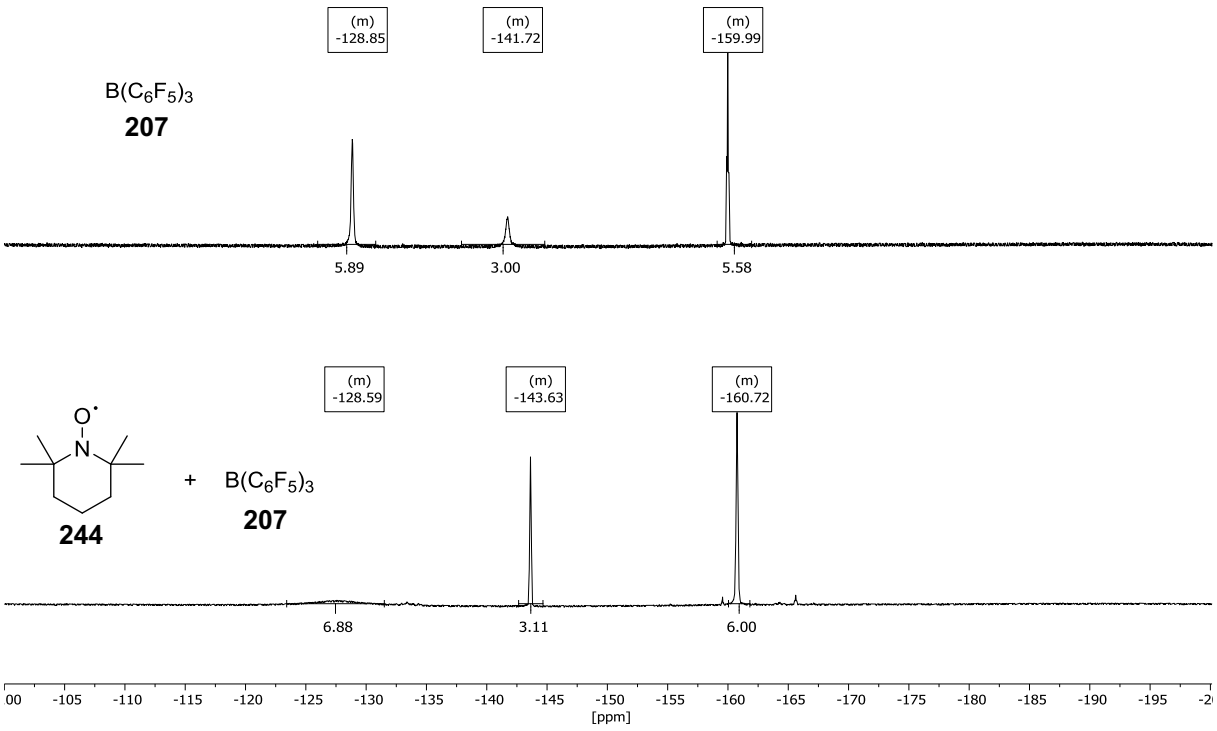

Figure 3: Stacked ^{19}F-NMR spectra (CD_2Cl_2, 282 MHz) of $B(C_6F_5)_3$ **207** (top) and mixture $B(C_6F_5)_3$ **207** and TEMPO **244** (bottom) with external standard ($CFCl_3$ in C_6D_6).[2]

In addition to the experiments to investigate the radical mechanism, the examination of the Lewis base was conducted. For this purpose, the contributions of Tolman on the field of phosphorus compounds were followed.[107] Similar electron-rich and sterically demanding phosphines as $^{t}Bu_3P$ were investigated in an ^{19}F- and ^{31}P-NMR-experiment. The phosphine $^{t}Bu_3P$ **186** showed the strongest shift in a ^{19}F- and ^{31}P-NMR spectrum with C_4F_9I **101**. Furthermore, only when $^{t}Bu_3P$ was used as phosphine in a reaction of vinylcyclohexane (**241**) and C_4F_9I **101** a full conversion was detected (Table 6).[2]

Table 6: Phosphine screening and the corresponding conversion of vinylcyclohexane with C_4F_9I **101**.[2]

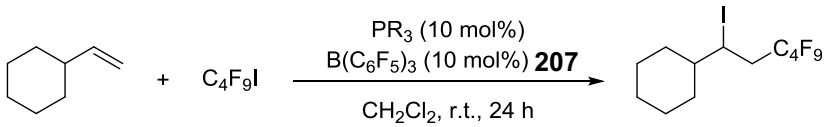

241 + C4F9I **101** → **243**

entry	phosphine		conversion [%]	
			^{1}H-NMR	**^{19}F-NMR**
1	Tri-*tert*-butylphosphine	$^{t}Bu_3P$	≥95%	≥95%
2	Tricyclohexylphosphine	PCy_3	–	–
3	Tri-*n*-butylphosphine	$^{n}Bu_3P$	–	–
4	Trimesitylphosphine	$PMes_3$	–	–
5	Tri(*o*-tolyl)phophine	$P(o\text{-tol})_3$	–	–
6	Tris(pentafluorophenyl)phosphine	$P(C_6F_5)_3$	–	–

4.2. Contributions to the publication

The publication "Mechanistic Insights into FLP-Catalyzed Iodoperfluoroalkylations" was published in collaboration with Dr. M. Spittler and Prof. C. Czekelius.[2] The publication is presented unmodified with the corresponding supporting information in this doctoral thesis. An overview of the contribution of the respective authors was already presented in the doctoral thesis of Dr. M. Spittler.[3] The summary of the individual contributions will be listed here once again. The experimental part was conducted by Dr. M. Spittler (75%) and Lucas Helmecke (25%).

Dr. M. Spittler examined the solvent screening, the kinetic investigations, and the associated calculations. Furthermore, he examined the side reactions involving $^{t}Bu_3P$ and $B(C_6F_5)_3$ alone and in combination with C_4F_9I. He isolated $[^{t}Bu_3PR][FB(C_6F_5)_3]$ (R = H or I) and conducted the related reactions. Accompanying that he conducted the test reactions involving styrene, 1,4-cyclohexadiene and tributyltin hydride. For the manuscript he prepared all chapters, the conceptualisation, the literature search and the supporting information was mainly conducted by Dr. M. Spittler.

L. Helmecke contributed the phosphane screening, NMR-shifts, the associated test reactions of the different phosphanes, the synthesis of pent-4-en-1-ylcyclopropane and the connected test reactions. Also, the reactions with the radical scavengers 3,5-di-*tert*-butyl-4-hydroxytoluene (BHT), 2,2,6,6-tetramethyl-1-piperidinyloxy (TEMPO) and the photochemical reactions with styrene. He also contributed to the literature research, a first version of the introduction, of a paragraph on phosphane screening and participated in the correction process. Lucas Helmecke contributed the results regarding the above-mentioned phosphane screening, synthesis of pent-4-en-1-ylcyclopropane, 6-bromohexene and the test reactions with the radical scavangers BHT and TEMPO in the Supporting Information. He contributed to the correction process of the Supporting information.

Prof. C. Czekelius was involved in the preparation of the introduction, the conclusion, the correction of the manuscript and the correction process of the supporting information.

ChemPubSoc Europe

DOI: 10.1002/ejoc.201800866

EurJOC European Journal of Organic Chemistry

Full Paper

Frustrated Lewis Pair Catalysis

SPECIAL ISSUE

Mechanistic Insights into FLP-Catalyzed Iodoperfluoroalkylations

Michael Spittler,[a] Lucas Helmecke,[a] and Constantin Czekelius*[a]

Dedicated to Professor Dr. Manfred Braun on the occasion of his 70th birthday

Abstract: The frustrated Lewis pair-catalyzed iodoperfluoroalkylation of olefins, its substrate activation mode, and catalyst degradation pathways are mechanistically investigated by kinetic measurements. The transformation most likely proceeds via coordination of the phosphane to the perfluoroalkyl iodide and involves radical intermediates.

Introduction

Today, fluorinated organic molecules play a key role in both science and technology.[1] Despite the negative public reputation of CFCs, which have caused a depletion of the ozone layer, the synthesis of fluorinated compounds has fostered synthetic method development[2] due to their widespread application in the fields of agrochemicals,[3] pharmaceuticals[4] and medicinal chemistry.[5] The flourishing use of fluorine is based upon its unique properties such as the high stability of the C–F bond (binding energy: 440–490 kJ/mol), its small size (1.47 Å) and its high electronegativity (4.0).[1,6] A single substitution of hydrogen by fluorine can alter the characteristics of a drug massively, for example with respect to its pharmacodynamics and pharmacokinetics.[1,6,7] Consequently, the development of selective fluorination techniques is of great importance in the pharmaceutical industry. A plethora of methods for fluorination and fluoroalkylation has been described in past years[8] involving special fluorinating reagents,[8f,9] diverse transition metal catalysts,[10] metal-free alternatives involving amines as Lewis base catalysts,[11] or photo-mediated perfluoroalkylations.[11,12] However, enantioselective methods and late stage introduction of fluorine is still a crucial goal.

In 2016, we reported the iodoperfluoroalkylation of unsaturated hydrocarbons by frustrated Lewis pairs (Scheme 1).[13] Using a catalyst system based on the seminal contributions by Piers, Stephan and Erker[14] we found that alkynes as well as terminal and internal *cis*-alkenes are perfluoroalkylated in the presence of tri-*tert*-butylphosphane (**2**) and tris(pentafluorophenyl)borane (**3**). The reaction proceeds regioselectively with iodine at the higher substituted carbon, but it is not diastereoselective in most cases. For example, the transformation of (*Z*)-3-hexene gives a mixture of the lk- and ul-isomers.

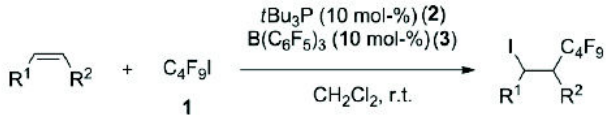

Scheme 1. FLP-catalyzed iodoperfluoroalkylation of unsaturated hydrocarbons.[13]

In the absence of alkenes the addition of various perfluoroalkyl iodides to the Lewis pair catalyst leads to the formation of the unreactive salt [*t*Bu$_3$PI][FB(C$_6$F$_5$)$_3$] (**4**) (Scheme 2). This may be explained by elimination of fluoride in either α- or β-position from an intermediately formed perfluoroalkyl borate.

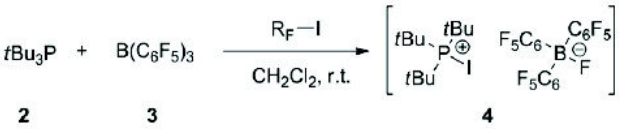

Scheme 2. Salt formation of iodophosphonium fluoroborate.

These observations raised the question whether the reaction proceeds via an ionic or radical pathway. The initial results, as reported earlier, did not allow to unequivocally provide an answer. Herein, we would like to report mechanistic investigations addressing the elucidation of this reaction mechanism.

Results and Discussion

We started our investigation with a screening of the Lewis base in order to check whether tri-*tert*-butylphosphane (**2**) can be substituted. To identify potential candidates, we screened phosphanes with comparable properties regarding their steric bulk and donor strength. As a measure for bulkiness, the ligand cone angle (θ) can be utilized. *t*Bu$_3$P, which is commonly used in FLP chemistry, has a ligand cone angle of 182°,[15] which makes it one of the bulkiest phosphanes. Additionally, the Tolman elec-

[a] *Institute for Organic Chemistry and Macromolecular Chemistry, Heinrich-Heine-Universität Düsseldorf, Universitätsstr. 1, 40225 Düsseldorf, Germany*
E-mail: constantin.czekelius@hhu.de
http://www.catalysis.hhu.de/
Supporting information and ORCID(s) from the author(s) for this article are available on the WWW under https://doi.org/10.1002/ejoc.201800866.

tronic parameter (TEP) assesses the donor strength of the Lewis base. These properties are shown in Figure 1 for the different phosphanes screened.

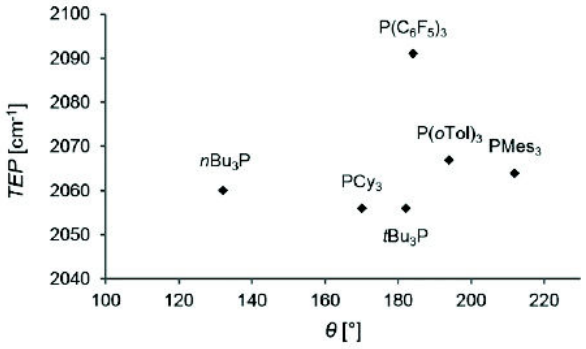

Figure 1. Tolman electronic parameter (TEP) and ligand cone angle of selected phosphanes.[15]

To scrutinize suitable phosphanes, which can interact with perfluoroalkyl iodides and thereby weaken the C–I-bond, NMR spectra of equimolar mixtures of phosphanes and nonafluoro-1-iodobutane (**1**) were recorded and compared to reference samples. A shift of the $-CF_2I$-moiety of the perfluoroalkyl iodide as well as the phosphane was observed only for tBu$_3$P and PCy$_3$. For nBu$_3$P only a slight shift of the $-CF_2I$-moiety was detected (Table 1).

Table 1. Mixtures of phosphanes and C_4F_9I, change in NMR shift.[a,b]

Phosphane	^{19}F $\Delta\delta$ [ppm]	^{31}P $\Delta\delta$ [ppm]
tBu$_3$P	11.5	4.5
nBu$_3$P	3.4	0
PCy$_3$	8.48	2.1
PMes$_3$	0	0
P(oTol)$_3$	0	0
P(C$_6$F$_5$)$_3$	0	0

[a] Equimolar mixture of phosphane and C_4F_9I in CH_2Cl_2. External standard $CFCl_3$ in C_6D_6. [b] For spectra, see Supporting Information.

As a test reaction the well-established iodoperfluoroalkylation of vinylcyclohexane (**5**) was chosen (Scheme 3). Only the use of tBu$_3$P led to formation of the corresponding product (>95 % conversion) while the other phosphanes did not promote the reaction at all. The unique combination of high basicity and bulkiness is apparently crucial for successful transformation of the perfluoroalkyl iodide.

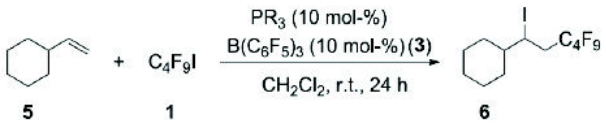

Scheme 3. Iodoperfluoroalkylation of vinylcyclohexane.

Next, we investigated the influence of the solvent in detail. Surprisingly, as shown in Table 2, no conversion was observed at all in aromatic solvents such as benzene or toluene. On the other side, electron-deficient, halogenated aromatic solvents seem to be appropriate for the perfluoroalkylation. Our data do not support the assumption that the dipole moment alone is the key property in this case, as our reaction works best in CH_2Cl_2 (1.6 D) and results in lower yields when using chlorobenzene (1.7 D) or fluorobenzene (1.6 D).

Table 2. Solvent screening in the iodoperfluoroalkylation of vinylcyclohexane.[a]

Solvent	Conversion [%]		Dipole moment[16]
	^{1}H	^{19}F	[D]
[D$_6$]Benzene	0	0	0
Toluene	0	0	0.4
CH_2Cl_2	95	≥99	1.6
Chlorobenzene	32	31	1.7
1,2-Dichlorobenzene	68	72	2.5
1,3-Dichlorobenzene	49	50	1.7
Fluorobenzene	35	35	1.6
1,2-Difluorobenzene	68	72	–
1,4-Difluorobenzene	26	25	–

[a] Vinylcyclohexane (0.41 mmol), C_4F_9I (0.41 mmol), B(C$_6$F$_5$)$_3$ (10 mol-%), tBu$_3$P (10 mol-%), solvent (1.2 mL), room temp., 24 h.

One possible explanation for these results is a π-stacking effect.[17] Due to stronger electrostatic interactions, benzene and the perfluorinated phenyl rings of B(C$_6$F$_5$)$_3$ should show a stronger interaction compared to halogenated benzene derivatives.[17] This interaction possibly causes a deactivation of the Lewis acid.

To elucidate the mechanism of this perfluoroalkylation, we started kinetic investigations. Our first results were quite promising, since we observed a clean reaction without by-product formation and seemingly simple curve progressions (Figure 2). Fitting the curve assuming zeroth, first or second order kinetics, good coefficients of determination were obtained. However, zeroth and first order fits have a significant intercept. A second order fit suits the data well, implying a second order dependency of either C_4F_9I **1**, vinylcyclohexane (**5**) or a combination of them. At this point, further reactions had to be conducted to learn more about the rate determining factors.

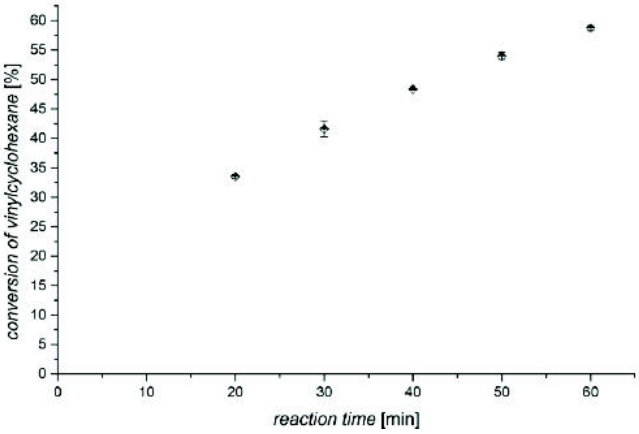

Figure 2. GC-experiments, reference procedure: vinylcyclohexane (1.0 equiv.), C_4F_9I (1.0 equiv.), tBu$_3$P (5 mol-%), B(C$_6$F$_5$)$_3$ (5 mol-%), CH_2Cl_2, 20 °C.

We envisioned that the cleavage of the C–I-bond in nonafluoro-1-iodobutane (**1**), either homo- or heterolytically, could take part in the rate-limiting step. Figure 3 depicts the strong dependency of the reaction rate on the C_4F_9I concentration.

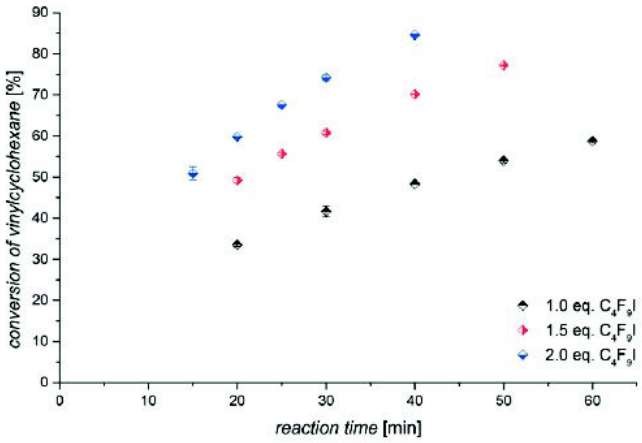

Figure 3. Influence of an excess of C_4F_9I on the reaction rate: C_4F_9I (1.0, 1.5, 2.0 equiv.), vinylcyclohexane (1.0 equiv.), tBu_3P (5 mol-%), $B(C_6F_5)_3$ (5 mol-%), CH_2Cl_2, 20 °C.

We calculated linear fits of a zeroth, first and second order dependence on the C_4F_9I concentration (see Supporting Information). A first order dependency fits the variation of the perfluoroalkyl iodide concentration best. For 1.0 equivalent a rate constant of $k_{1.0}$ = 0.012 min^{-1}, for 1.5 equivalents $k_{1.5}$ = 0.011 min^{-1} and for 2.0 equivalents $k_{2.0}$ = 0.010 min^{-1} was calculated. This suggests that the iodoperfluoroalkylation is first order regarding C_4F_9I. Still, a constant offset for a first order fit was observed, indicating a faster second process at the beginning of the reaction. To investigate this interesting effect further, we varied the ratio of both Lewis base and Lewis acid. To our surprise, a sharp increase regarding the offset was found by increasing the amount of tBu_3P (Figure 4).

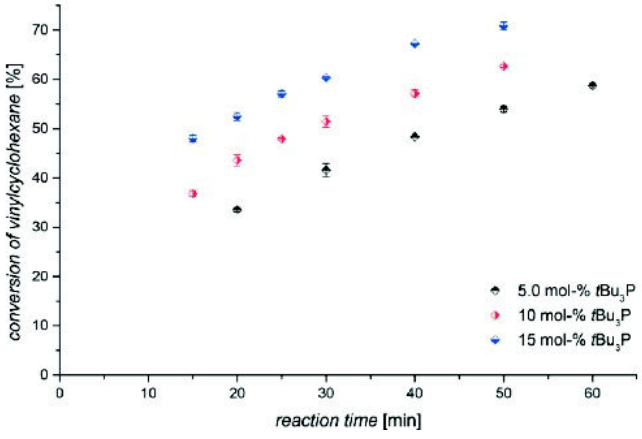

Figure 4. Influence of an excess of tBu_3P on the reaction rate: tBu_3P (5, 10 and 15 mol-%), vinylcyclohexane (1.0 equiv.), C_4F_9I (1.0 equiv.), $B(C_6F_5)_3$ (5 mol-%), CH_2Cl_2, 20 °C.

As Figure 5 shows, by tripling the amount of tBu_3P, the slope increases slightly from –0.012 min^{-1} to –0.017 min^{-1}, but the intercept is more than doubled from 0.18 to 0.41. Apparently, tBu_3P plays a key role in a fast-starting reaction, but does not seem to be determining for the subsequent reaction progress.

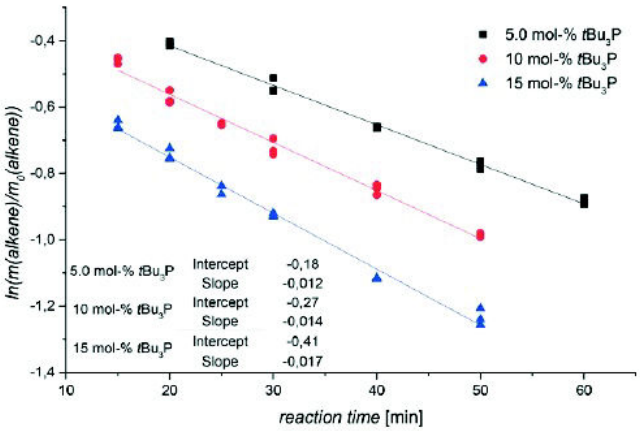

Figure 5. Calculation regarding the influence of an excess of tBu_3P on the reaction rate (see Supporting Information).

In order to follow the fast initial process involving free tBu_3P, an altered procedure using NMR analysis and 1-undecene (**13**) instead of vinylcyclohexane (**5**) was used. Herein, the first data point was obtained after 7 min reaction time (Figure 6).

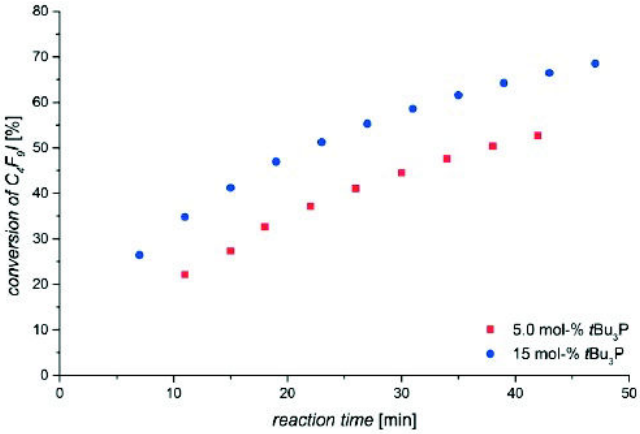

Figure 6. Influence of an excess of tBu_3P: tBu_3P (5 and 15 mol-%), 1-undecene (1.1 equiv.), C_4F_9I (1.0 equiv.), $B(C_6F_5)_3$ (10 mol-%), CH_2Cl_2, room temp.

Remarkably, 26 % conversion was detected after 7 min using 15 mol-% tBu_3P. The resulting change in rate constants ($k_{5.0}$ = 0.016 min^{-1}, k_{15} = 0.020 min^{-1}) is comparable to the GC-experiments (Figure 4). The same applies for the intercepts, since tripling the amount of tBu_3P results in an approximately doubled intercept. Throughout this experiment with an excess of tBu_3P, a very interesting observation were newly formed signals in the ^{19}F-NMR spectrum (Figure 7). These signals seem to arise from a $B(C_6F_5)_3$ derivative and the integral ratio relative to the $B(C_6F_5)_3$ signals did not shift over the monitoring period.

Therefore, we tested an excess of the Lewis acid $B(C_6F_5)_3$. Different potential ways for $B(C_6F_5)_3$ to activate substrates are described in literature. Stephan and co-worker[7c] documented an interaction between fluorine and $B(C_6F_5)_3$, which can result in fluoride abstraction under certain conditions giving hydrophosphonium fluoroborate **9** (Scheme 4). $B(C_6F_5)_3$ can also interact with alkenes.[18]

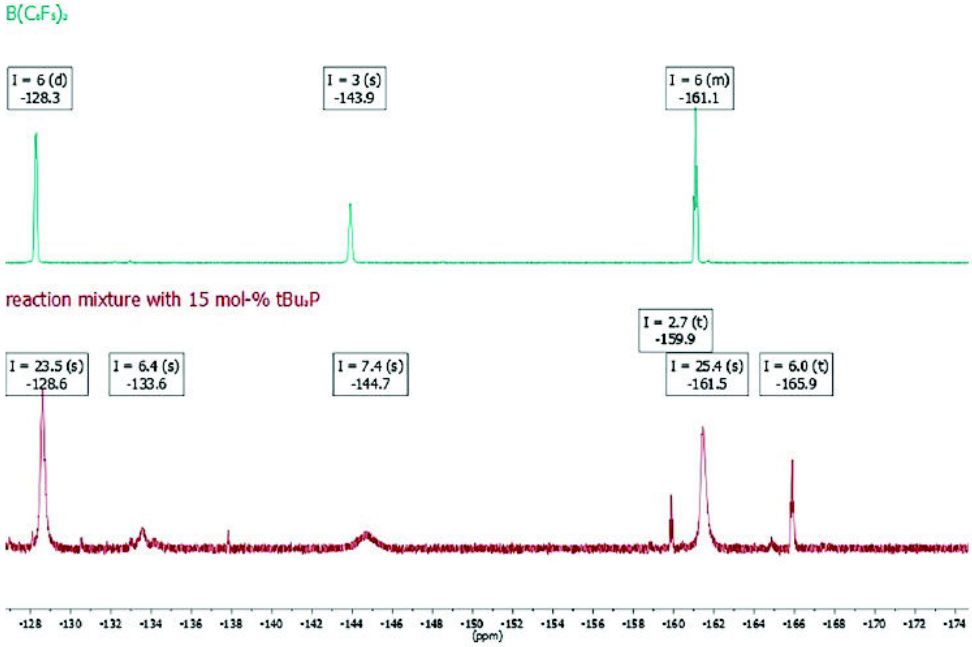

Figure 7. Comparison of ^{19}F-NMR spectra, top: $B(C_6F_5)_3$, below: reaction mixture with 15 mol-% tBu_3P.

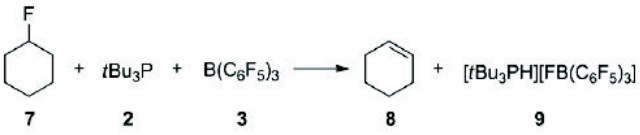

Scheme 4. Fluoride abstraction by $B(C_6F_5)_3$[7c]

Consequently, a variation of the concentration of this Lewis acid $B(C_6F_5)_3$ may have an effect on the reaction rate. As already mentioned, we observed formation of fluoroborate [tBu$_3$PI]-[FB(C_6F_5)$_3$] (**4**) after mixing $B(C_6F_5)_3$, tBu$_3$P and C_4F_9I (Scheme 2).[13] Higher $B(C_6F_5)_3$ ratios increased the rate constant notably without a change regarding the offset or altering the curve's progression (Figure 8). So it seems unlikely that $B(C_6F_5)_3$ is involved in the fast initial process. Assuming a first order dependency, doubling the concentration of $B(C_6F_5)_3$ should result in a doubled rate constant, but we did not observe such an effect (Table 3) and only a slight increase.

One interesting observation throughout our experiments was that premixing tBu$_3$P and $B(C_6F_5)_3$ in CH_2Cl_2 resulted in a yellow solution, whereas reaction mixtures to which $B(C_6F_5)_3$ was added last, showed no color. Solutions of both tBu$_3$P and $B(C_6F_5)_3$ alone are colorless. Piers et al.[19] reported the same observation after mixing tBu$_3$P (**2**) and $B(C_6F_5)_3$ (**3**) and concluded the formation of an addition product by a S_NAr reaction forming **12** after subsequent deprotonation and yielding [tBu$_3$PH][FB(C_6F_5)$_3$] (**9**) as by-product (Scheme 5).

We conducted iodoperfluoroalkylation reactions after premixing tBu$_3$P and $B(C_6F_5)_3$ for 33 and 61 min to assess a reaction between the Lewis pair. However, the reaction rate did not change substantially ($k_{standard}$ = 0.012 min^{-1}, k_{33min} = 0.011 min^{-1}, k_{61min} = 0.010 min^{-1}) (Figure 9).

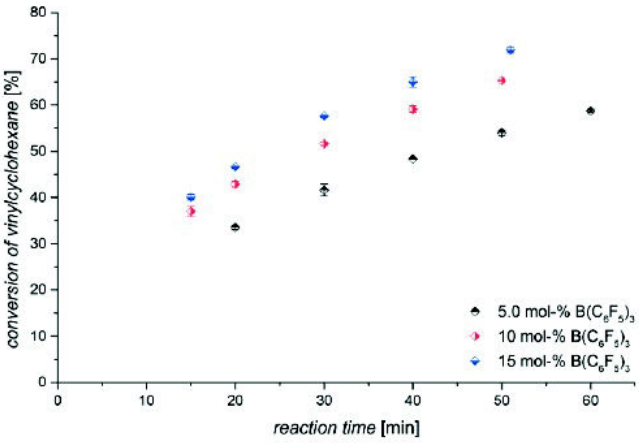

Figure 8. Influence of an excess of $B(C_6F_5)_3$ on the reaction rate: $B(C_6F_5)_3$ (5, 10 and 15 mol-%), vinylcyclohexane (1.0 equiv.), C_4F_9I (1.0 equiv.), tBu$_3$P (5 mol-%), $B(C_6F_5)_3$ (5 mol-%), CH_2Cl_2, room temp.

Table 3. GC-experiment, variation of the $B(C_6F_5)_3$ concentration.[a]

$B(C_6F_5)_3$ [mol-%]	slope [min^{-1}]	intercept
5.0	–0.012	0.18
10	–0.017	0.22
15	–0.021	0.21

[a] See Supporting Information.

To validate this observation, an analogous NMR-experiment was conducted with higher catalyst loading. tBu$_3$P and $B(C_6F_5)_3$ were premixed for 78 min. As before, only a slight drop in reaction rate was detected (k = 0.024 min^{-1} compared to k = 0.026 min^{-1}, Figure 10).

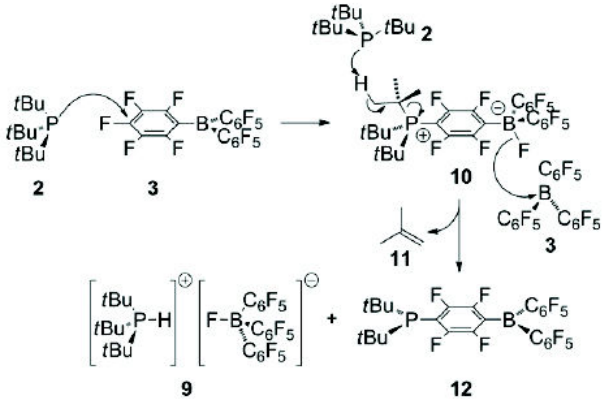

Scheme 5. Proposed mechanism for the nucleophilic aromatic substitution of tBu$_3$P at B(C$_6$F$_5$)$_3$ by Piers et al.[19]

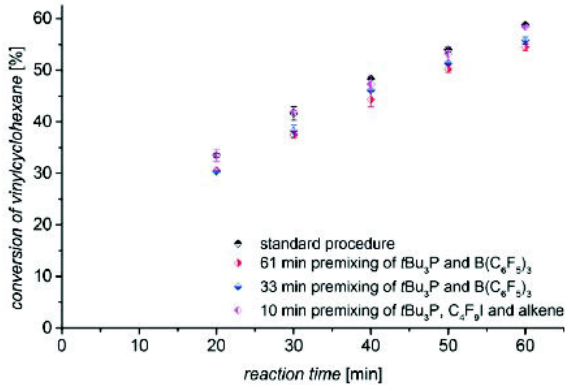

Figure 9. A comparison of different reaction procedures focusing on the premixing of tBu$_3$P and B(C$_6$F$_5$)$_3$; vinylcyclohexane (1.0 equiv.), C$_4$F$_9$I (1.0 equiv.), tBu$_3$P (5 mol-%), B(C$_6$F$_5$)$_3$ (5 mol-%), CH$_2$Cl$_2$, 20 °C.

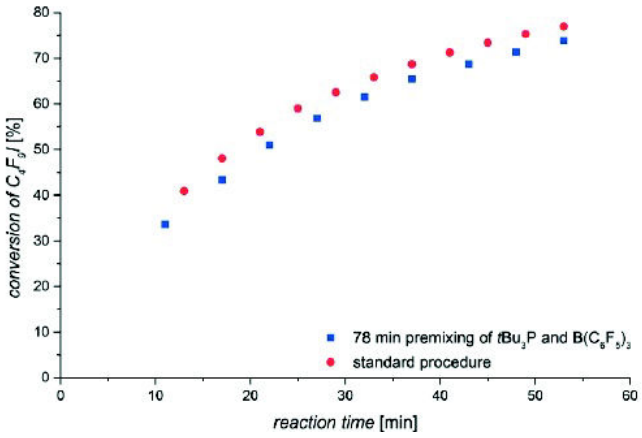

Figure 10. Iodoperfluoroalkylation after premixing of tBu$_3$P and B(C$_6$F$_5$)$_3$ for 78 min: vinylcyclohexane (1.0 equiv.) C$_4$F$_9$I (1.0 equiv.), tBu$_3$P (10 mol-%), B(C$_6$F$_5$)$_3$ (10 mol-%), CH$_2$Cl$_2$, room temp.

After premixing tBu$_3$P and B(C$_6$F$_5$)$_3$ for 78 min and subsequent addition of C$_4$F$_9$I as well, nearly no change in shift of the pentafluorophenyl-signals was detected in the ^{19}F-NMR spectrum. This supports the assumption that the reaction of tBu$_3$P and B(C$_6$F$_5$)$_3$ is slower than the perfluoroalkylation period itself. As a consequence, nucleophilic substitution of tBu$_3$P at B(C$_6$F$_5$)$_3$ does not seem to play a major role in our system.

After an extended premixing (25 hours) of tBu$_3$P and B(C$_6$F$_5$)$_3$ the reaction rate drops severely. However, the reaction still proceeds smoothly and gives 55 % conversion after 324 min (Figure 11). The first ^{19}F NMR spectrum in this kinetic investigation clearly indicated the formation of [FB(C$_6$F$_5$)$_3$]$^-$ on the basis of its diagnostic signal at –189 ppm. The amount of [FB(C$_6$F$_5$)$_3$]$^-$ was found to be constant within the observation period.

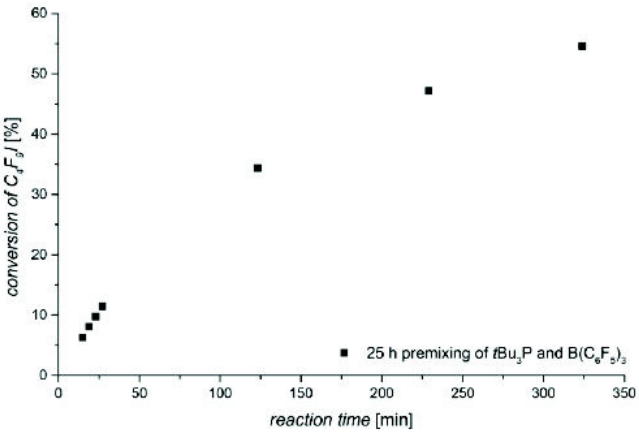

Figure 11. Reaction progress after 25 h premixing of tBu$_3$P and B(C$_6$F$_5$)$_3$.

The last component to investigate in this study was vinylcyclohexane (**5**). Since the GC method used could not be validated for an excess of this alkene (see Supporting Information), the reaction was followed by NMR (Figure 12).

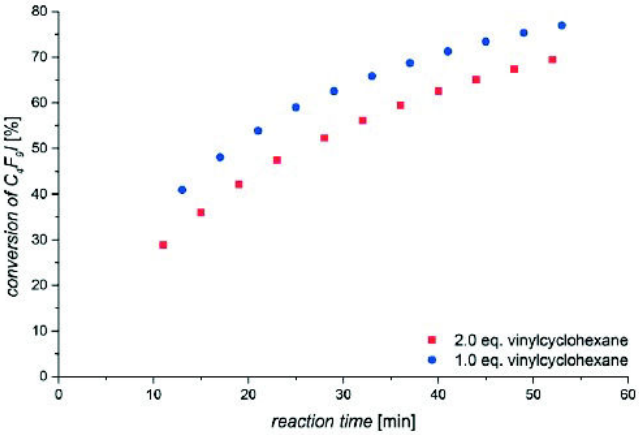

Figure 12. Influence of an excess of vinylcyclohexane: vinylcyclohexane (1.0, 2.0 equiv.) C$_4$F$_9$I (1.0 equiv.), tBu$_3$P (10 mol-%), B(C$_6$F$_5$)$_3$ (10 mol-%), CH$_2$Cl$_2$, room temp.

After linearization, a rate constant of $k_{2.0}$ = 0.022 min^{-1} was obtained for two equivalents of vinylcyclohexane (**5**), which is slightly lower than that for one equivalent ($k_{1.0}$ = 0.026 min^{-1}). We wanted to verify this observation with a linear alkene. 1-Undecene (**13**) was chosen as a high-boiling compound and we observed the same behavior (Figure 13). The rate constant also drops slightly for an excess of 1-undecene ($k_{1.1}$ = 0.015 min^{-1}, $k_{2.0}$ = 0.012 min^{-1}).

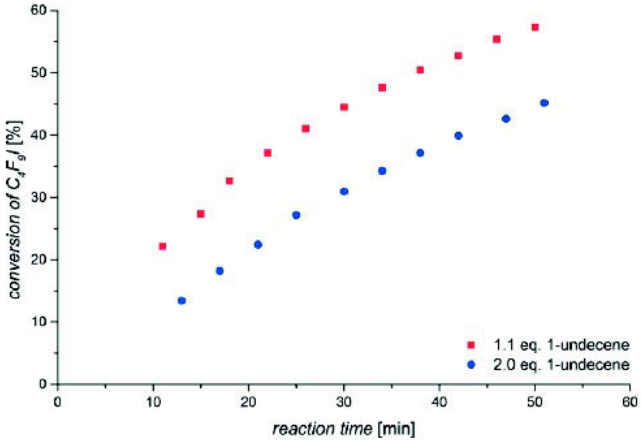

Figure 13. Influence of an excess of 1-undecene: 1-undecene (1.1, 2.0 equiv.) C_4F_9I (1.0 equiv.), tBu$_3$P (5 mol-%), $B(C_6F_5)_3$ (5 mol-%), CH_2Cl_2, room temp.

These results suggest that the alkene does not take part in the rate-limiting step. On the contrary, it slows the reaction down, presumably by its coordination to $B(C_6F_5)_3$.[18] This coordination has been proposed to potentially result in a nucleophilic attack e.g. by phosphanes forming the corresponding betaines.[18a,18b] Such process could also play a role in our reaction system, but we have no spectroscopic evidence for betaine formation.

To evaluate the loss of active catalyst by fluoroborate formation within our usual observation period, we premixed tBu$_3$P, $B(C_6F_5)_3$ and C_4F_9I and added vinylcyclohexane (**5**) after 60 min. To our surprise, this resulted in a completely different curve progression. Most noticeable, the usual offset as an indication for a fast initial process cannot be observed (Figure 14). On the contrary, the reaction showed an initial lag phase.

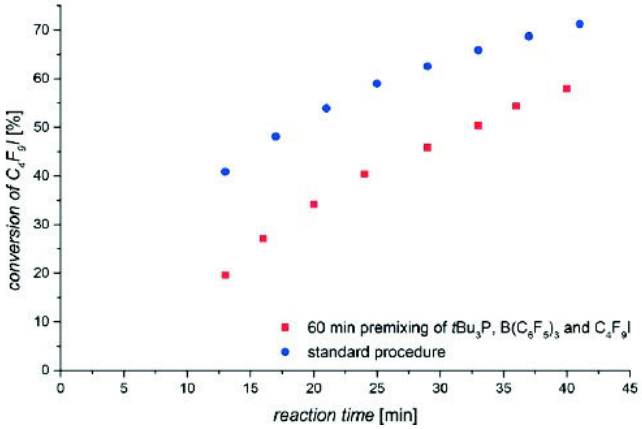

Figure 14. Reaction progress after 60 min premixing of tBu$_3$P, $B(C_6F_5)_3$ and C_4F_9I: vinylcyclohexane and C_4F_9I (1.0 equiv.), tBu$_3$P (10 mol-%), $B(C_6F_5)_3$ (10 mol-%), CH_2Cl_2, room temp.

After a short induction period, the reaction proceeds with a slightly lower rate constant (k_{60min} = 0.023 min^{-1}, $k_{standard}$ = 0.026 min^{-1}). This similar rate constant implies that the amount of catalytically active species does not seem to be reduced substantially. However, minor amounts of the diagnostic signal for $[FB(C_6F_5)_3]^-$ at –191 ppm in the ^{19}F-NMR spectra were detected. To verify an initiation phase, a similar procedure was tested in a GC-experiment (5 mol-% catalyst). tBu$_3$P, $B(C_6F_5)_3$ and C_4F_9I were mixed for 62 min before the addition of vinylcyclohexane. Like before, a lag phase is visible (Figure 15) and the rate constant drops slightly (k_{62min} = 0.0084 min^{-1}, $k_{standard}$ = 0.012 min^{-1}).

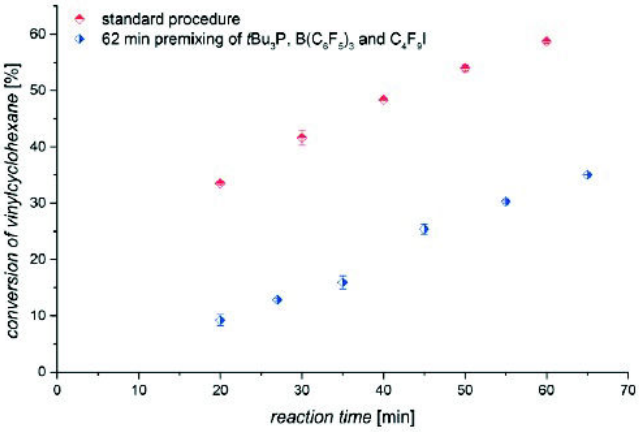

Figure 15. Reaction progress after 62 min premixing of tBu$_3$P, $B(C_6F_5)_3$ and C_4F_9I: vinylcyclohexane and C_4F_9I (1.0 equiv.), tBu$_3$P (5 mol-%), $B(C_6F_5)_3$ (5 mol-%), CH_2Cl_2, room temp.

We tried to quantify the loss of catalytically active species by salt formation. Since both $[t\text{Bu}_3\text{PR}]^+$ (R = H or I) and $[FB(C_6F_5)_3]^-$ cannot be quantified via GC, NMR experiments were conducted. After mixing tBu$_3$P, $B(C_6F_5)_3$ and C_4F_9I in CD_2Cl_2, ^{19}F-NMR spectra were measured over a period of 52 min. Unexpectedly, no new ^{19}F signal for $[FB(C_6F_5)_3]^-$ was observed, but a gradual upfield shift of the original $B(C_6F_5)_3$ (Figure 16).

Most likely, a fast interchange of fluoride between $[FB(C_6F_5)_3]^-$ and free $B(C_6F_5)_3$ occurs. Even at –30 °C no separation into two signal sets in NMR was observed. Hence, the interchange seems to be quite fast. To validate this assumption, $B(C_6F_5)_3$ **3** and $[t\text{Bu}_3\text{PH}][FB(C_6F_5)_3]$ **9** were mixed in equimolar ratio. As assumed, only one signal set was observed (Figure 17).

On a closer look, the resulting shifts of an equimolar mixture of $B(C_6F_5)_3$ (**3**) and $[t\text{Bu}_3\text{PH}][FB(C_6F_5)_3]$ (**9**) were precisely in the middle of the original shifts. This observation opened a potential possibility to quantify salt formation. With this insight at hand, we reviewed the spectra of our NMR-experiments. For our standard procedure with 1.0 equiv. vinylcyclohexane (**5**), only a slight shift (*o*,*m*-F: –0.6 ppm, *p*-F: –1.7 ppm) of the pentafluorophenyl-signals in $B(C_6F_5)_3$ can be noticed within 53 min, implying no significant loss of catalytic species.

As an alternative cause for a shift of the pentafluorophenyl signals, a mixture of iodoperfluoroalkylation product **6** and $B(C_6F_5)_3$ (**3**) was probed. No shift was observed. Additionally, iodoperfluoroalkylation product **6** and tBu$_3$P (**2**) were mixed and no shift was detected in this case, too.

In order to test for a catalyst regeneration we probed a combination of $B(C_6F_5)_3$ and phosphonium fluoroborate salts $[t\text{Bu}_3\text{PR}][FB(C_6F_5)_3]$ (R = H or I) (Scheme 6).

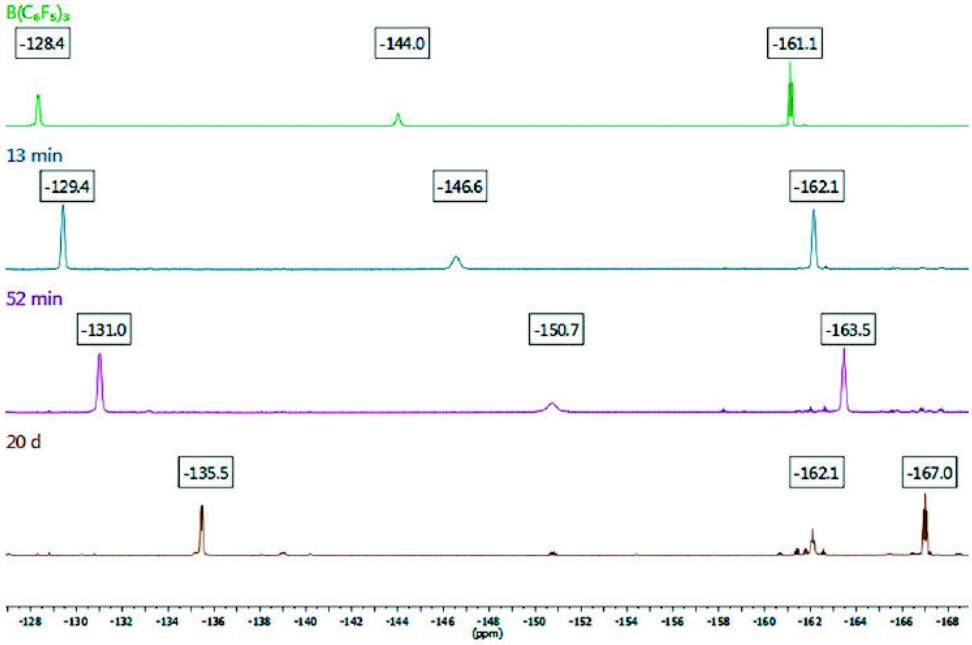

Figure 16. Comparison of ^{19}F-NMR spectra, top: $B(C_6F_5)_3$, below: reaction of tBu$_3$P, $B(C_6F_5)_3$ with C_4F_9I.

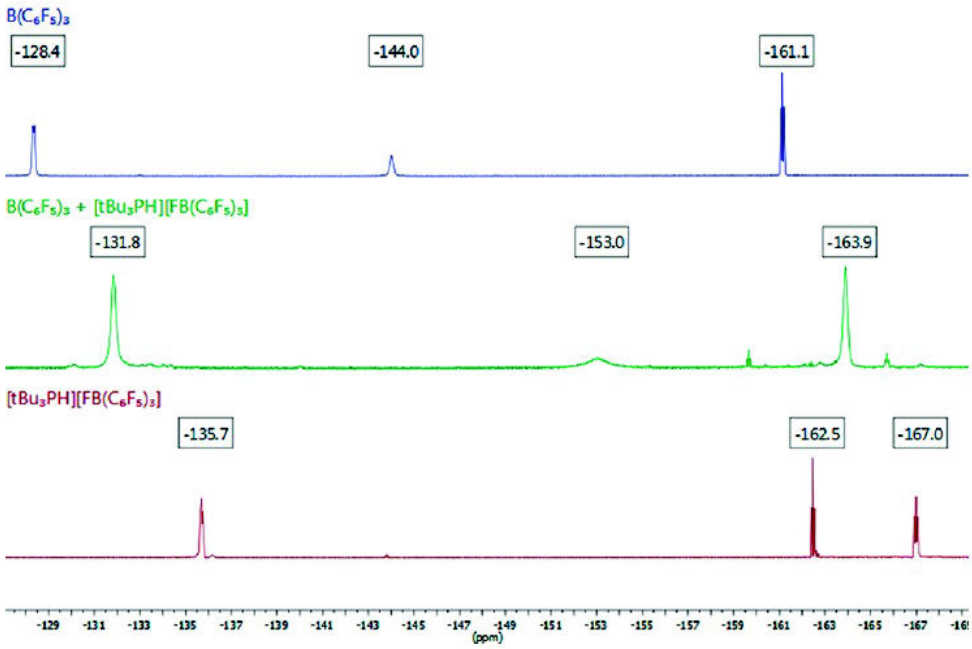

Figure 17. Comparison of ^{19}F-NMR spectra, top: $B(C_6F_5)_3$, middle: 1:1 mixture of $B(C_6F_5)_3$ and [tBu$_3$PH][FB(C_6F_5)$_3$], bottom: [tBu$_3$PH][FB(C_6F_5)$_3$].

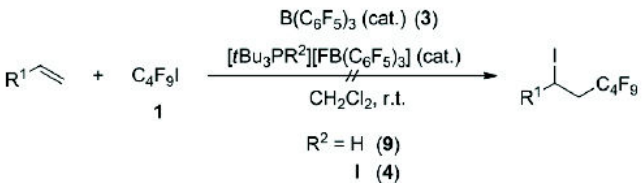

Scheme 6. Attempt to iodoperfluoroalkylate in the presence of [tBu$_3$PR]-[FB(C_6F_5)$_3$] (R = H or I) in combination with $B(C_6F_5)_3$

With both phosphonium salts we observed no reaction at all. ^{31}P-NMR spectra showed no change of the [tBu$_3$PR]-shifts and as described before, only one signal set was observed for the pentafluorophenyl rings. Consequently, no regeneration of free tBu$_3$P occurs for a combination of the salts and $B(C_6F_5)_3$.

An alternative pathway for this perfluoroalkylation is a photochemical process. Chen et al.[11] showed that Lewis bases can promote the photochemical reaction between alkenes and perfluoroalkyl iodides via halogen-bonding. For that reason we conducted all experiments under best possible exclusion of ambient light and working under red light. To probe this photomediated pathway for our system, we conducted a GC-experiment under reference conditions but used tBu$_3$P as the only catalyst.

Under these conditions we detected a conversion of 3–5 % as followed by GC and NMR, which might be caused by the sample withdrawal itself. As a comparison, we tested a photochemical reaction of vinylcyclohexane (**5**) and nonafluoro-1-iodobutane (**1**) promoted by 10 mol-% tBu_3P (**2**) under the influence of direct sunlight. Within 24 h a conversion of about 40 % was observed.

Following kinetic investigations, we addressed the question whether the reaction mechanism involves ionic or radical intermediates. While in FLP-mediated reactions commonly ionic pathways are described, Stephan et al.[20] reported single electron transfer processes in the reaction of the aromatic phosphane Mes_3P and $B(C_6F_5)_3$ with tetrachloro-1,4-benzoquinone. They were able to prove the formation of the corresponding radical cation $[Mes_3P{\bullet}]^+$. However, when aliphatic phosphane tBu_3P was used as Lewis base, the reaction seemed to follow an ionic pathway. We had found earlier[13] that 1,6-heptadiene (**14**) is transformed under the reaction conditions into the difunctionalized compound **15** and perfluoroalkylated cyclopentane derivatives **16** and **17** (Scheme 7). This finding is more consistent with a radical than the involvement of a primary carbocation. In the literature, the formation of cyclic products via a radical mechanism has already been described.[21]

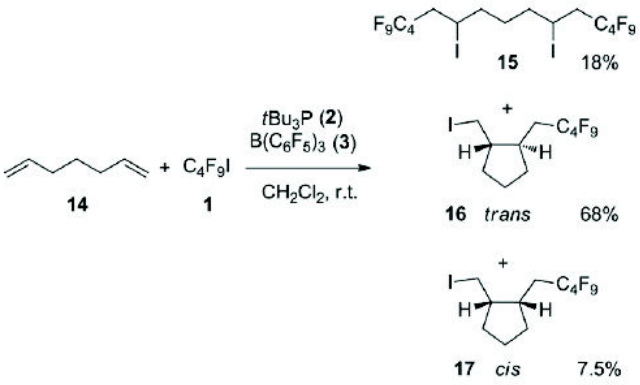

Scheme 7. Iodoperfluoroalkylation of 1,6-heptadiene.[13]

To obtain further evidence for a radical mechanism, we probed the perfluoroalkylation of two alkenes, which can cyclize under radical conditions. Studer and co-workers reported the cyclisation of 6-bromohexene (**18**) under radical conditions.[22] However, following our methodology we could only isolate the acyclic perfluoroalkylation product **19** (Scheme 8).

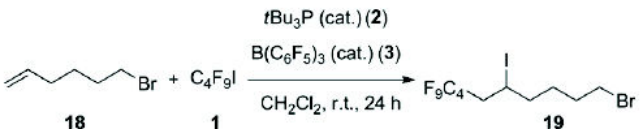

Scheme 8. Iodoperfluoroalkylation of vinylcyclohexane.

It is described in literature that the corresponding cyclic product is exclusively formed following bromine abstraction[23] and not by a terminal addition of a radical to the alkene. Subsequently, 4-penten-1-yl-cyclopropane (**20**) was synthesized and a perfluoroalkylation was conducted (Scheme 9).

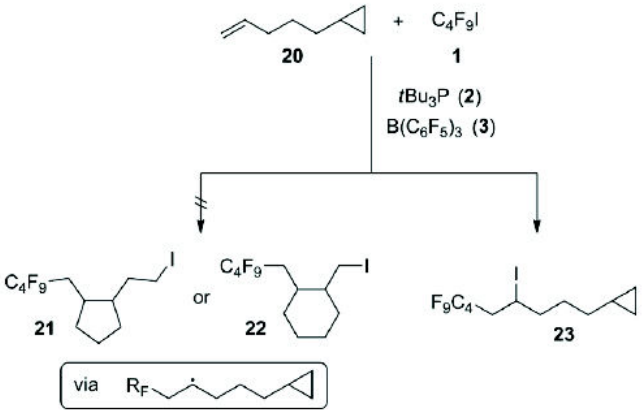

Scheme 9. Iodoperfluoroalkylation of 4-penten-1-ylcyclopropane.

After an attack of a perfluoroalkyl radical at the double bond, a secondary radical would be formed, which could open the cyclopropane ring. However, we did not observe such a process. NMR spectroscopy showed acyclic iodoperfluoroalkylation product **23** of the alkene and an unimpaired cyclopropane ring.

As described before,[13] styrene (**24**) does not react under the standard conditions at all. Moreover, one equivalent of styrene inhibits the FLP-catalyzed perfluoroalkylation of vinylcyclohexane (**5**) (Scheme 10). Since styrene may quench radicals undergoing polymerization, a mixture of styrene, tBu_3P and C_4F_9I was irradiated at 370 nm and 254 nm, respectively, as a test reaction. No conversion or polymerization was detected. Therefore, quenching of radicals by styrene (**24**) seems to be less likely. Potentially, π-stacking[24] or coordination of boron to the alkene might quench the reaction.[18]

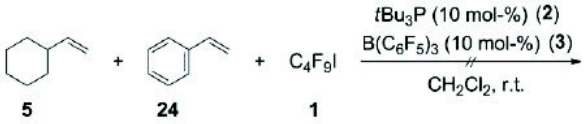

Scheme 10. Iodoperfluoroalkylation of vinylcyclohexane in the presence of styrene.

As another alternative to discriminate between radical and ionic mechanisms, 1,4-cyclohexadiene (**25**) was subjected to our catalytic system. This diene itself did not react with C_4F_9I (**1**) in presence of catalytic amounts of tBu_3P (**2**) and $B(C_6F_5)_3$ (**3**). As with styrene, it inhibited the conversion of vinylcyclohexane (**5**). NMR spectra show unreacted vinylcyclohexane and 1,4-cyclohexadiene (see Supporting Information).

After mixing equimolar amounts of 1,4-cyclohexadiene, C_4F_9I, tBu_3P and $B(C_6F_5)_3$, substantial amounts (about 30 %) of benzene (**26**) were detected, suggesting the presence of radical intermediates (Scheme 11). However, no C_4F_9H (**29**) could be detected in this case. The ^{19}F-NMR spectrum shows a nearly complete consumption of C_4F_9I (**1**) and the formation of $[tBu_3PI][FB(C_6F_5)_3]$ (**4**).

Next, we tested free radical 2,2,6,6-tetramethylpiperidine 1-oxyl (**27**, TEMPO). A perfluoroalkylation in presence of one equivalent TEMPO showed no conversion at all, the same is true for a reaction in the presence of 0.1 equivalents (Scheme 12). As an alternative procedure, TEMPO was added to an ongoing

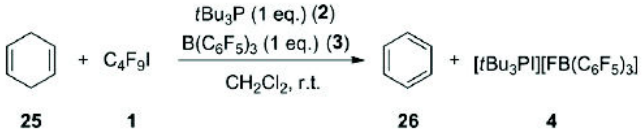

Scheme 11. Radical dehydrogenation of 1,4-cyclohexadiene in the presence of tBu$_3$P, B(C$_6$F$_5$)$_3$ and C$_4$F$_9$I.

iodoperfluoroalkylation after 20 min. Consecutive NMR-controls showed a direct stop of the reaction after the addition of TEMPO. However, B(C$_6$F$_5$)$_3$ did seem to react. ^{19}F-NMR spectra of an equimolar mixture of TEMPO and B(C$_6$F$_5$)$_3$ showed an alteration of the pentafluorophenyl-signals. Additionally, the ^{11}B-NMR spectrum indicated the presence of a tetrahedral boron center. Presumably, direct interaction between TEMPO and B(C$_6$F$_5$)$_3$ quenches the perfluoroalkylation.

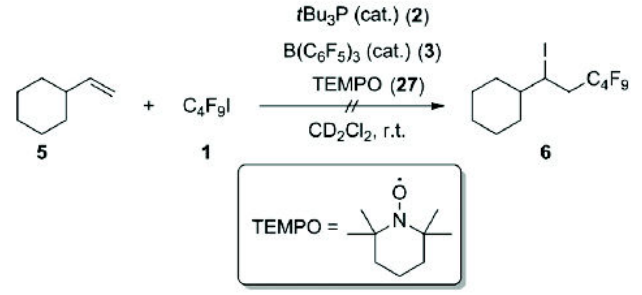

Scheme 12. Attempt for an iodoperfluoroalkylation in the presence of free radical TEMPO.

Our last experiments in the context of radical reactions addressed the addition of tributyltin hydride (**28**) as a radical hydrogen donor. As a negative control, we mixed vinylcyclohexane (**5**), C$_4$F$_9$I and Bu$_3$SnH in an amber glass NMR-tube and observed no reaction (Scheme 13). When we mixed tBu$_3$P, vinylcyclohexane, C$_4$F$_9$I and Bu$_3$SnH in a transparent NMR tube, we detected the formation of C$_4$F$_9$H (**29**). This reaction is expected for a radical reaction between perfluoroalkyl-radical (•C$_4$F$_9$) and Bu$_3$SnH. Then, we conducted an experiment under standard iodoperfluoroalkylation conditions, but added Bu$_3$SnH after

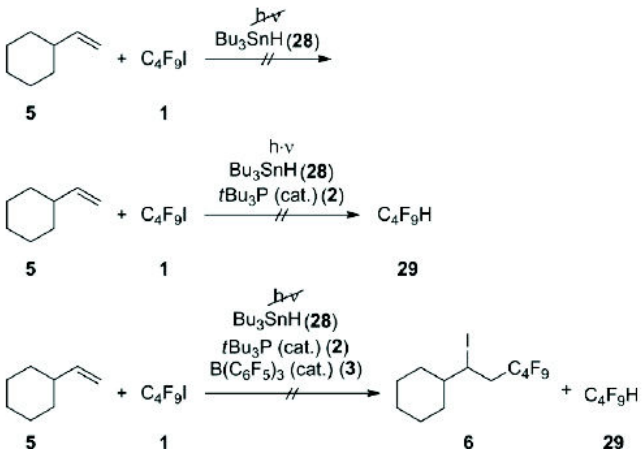

Scheme 13. Experiments involving tributyltin hydride.

20 min in the dark. Iodoperfluoroalkylation product **6**, C$_4$F$_9$H (**29**) and presumably perfluorooctane were observed.

These results suggested that radicals play an important role in the FLP-catalyzed iodoperfluoroalkylation.

Conclusions

The investigated frustrated Lewis pair-catalyzed iodoperfluoroalkylation of olefins is a highly complex reaction. Our kinetic experiments suggest a first order dependence on the perfluoroalkyl iodide, which is coordinated and activated by the phosphane. The Lewis base is involved in a fast starting reaction, which slows down rapidly. An excess of the phosphane results in a strong offset, followed by reaction rates comparable to those under standard conditions. An excess of the Lewis acid also increases the reaction rate moderately, but does not alter the curve progression. The alkene does not seem to take part in a rate-limiting step. On the contrary, an excess slows down the reaction speed, presumably by coordinating to the Lewis acid.

Two potential pathways for a deactivation of the catalyst were investigated. On the one hand, tBu$_3$P, B(C$_6$F$_5$)$_3$ and the perfluoroalkyl iodide can form a iodophosphonium fluoroborate [tBu$_3$PI][FB(C$_6$F$_5$)$_3$]. On the other hand, tBu$_3$P and B(C$_6$F$_5$)$_3$ can react in a S$_N$Ar-reaction to form a phosphino borane and hydrophosphonium fluoroborate [tBu$_3$PH][FB(C$_6$F$_5$)$_3$]. Experimental evidence shows, that the latter process does not seem to play a significant role for our system. In contrast, the formation of the iodophosphonium fluoroborate can deactivate the catalyst system more readily.

This FLP-catalyzed iodoperfluoroalkylation may follow an ionic or radical pathway. Transformations in the presence of hydrogen donors such as 1,4-cyclohexadiene or tributyltin hydride suggest the occurrence of perfluoroalkyl radicals. A radical pathway is rare for FLP-catalyzed reactions and may open new synthetic potential for the activation of small molecules.

Experimental Section

General Notes: All syntheses involving air- and moisture-sensitive compounds were carried out inside a glovebox under N$_2$ atmosphere. Reagents as well as solvents were purchased from Acros, Sigma Aldrich, abcr, TCI, J & K scientific or VWR Chemicals. Solvents were dried with the solvent purification system MP-SPS 800 from M. Braun, predistilled and if necessary degassed by freeze-pump-thaw. Reactions were monitored by thin-layer chromatography (TLC) using Macherey–Nagel silica gel plates ALUGRAM® Xtra SIL G/UV$_{254}$ (0.20 mm thickness). ^{1}H-, ^{11}B-, ^{13}C, ^{19}F-, ^{31}P-NMR spectra were recorded on Bruker Avance III 300 and 600. Chemical shifts are reported in parts per million (ppm). ^{1}H-NMR shifts are reported in reference to the corresponding solvent. ^{19}F-NMR shifts were reported in ppm and referenced to CFCl$_3$ in C$_6$D$_6$ and ^{31}P-NMR to H$_3$PO$_4$ in D$_2$O. IR spectra were recorded using a Jasco FT/IR-6200 spectrometer. Samples were measured as film on a NaCl crystal. The absorption bands were given in wave numbers (cm^{-1}). Elemental analyses were measured on an Elementar Vario Micro Cube.

6-Bromohexene (18): Triphenylphosphane (11.5 g, 43.9 mmol, 1.10 equiv.) in CH$_2$Cl$_2$ (29 mL) was cooled to 0 °C. Bromine (2.30 mL,

43.9 mmol, 1.10 equiv.) was added dropwise and the solution was stirred for 2 h at room temperature. Subsequently, pyridine (4.30 mL, 53.3 mmol, 1.10 equiv.) was added dropwise to the reaction solution and the mixture was cooled to 0 °C. 5-Hexen-1-ol (4.80 mL, 39.9 mmol, 1.00 equiv.) in CH_2Cl_2 (7 mL) was added dropwise and the solution was stirred for 20 h at room temperature. After complete conversion of the alcohol, which was controlled via TLC (hexane/ethyl acetate, 90:10), pentane (20 mL) was added to the reaction solution. The reaction flask was cooled to −78 °C and the precipitate was filtered off. The clear reaction solution was concentrated and washed with hydrochloric acid (1 M, 3 × 20 mL). The aqueous phase was extracted with pentane (3 × 20 mL). The combined organic phases were washed with saturated $NaHCO_3$ (10 mL) and dried with Na_2SO_4. The solution was again concentrated and distilled at reduced pressure (61–63 °C, 45 mbar). A clear oil was obtained (3.17 g, 19.4 mmol, 49 %). ^{1}H NMR (300 MHz, $CDCl_3$): δ = 5.88–5.72 (ddt, J = 16.9, 10.2, 6.7 Hz, 1 H, CH_2CH), 5.08–4.94 (m, 2 H, CH_2CH), 3.46–3.37 (t, J = 6.8 Hz, 2 H, CH_2Br), 2.15–2.03 (m, 2 H, CH_2CHCH_2), 1.94–1.82 (m, 2 H, CH_2CH_2Br), 1.61–1.48 (m, 2 H, $CH_2CH_2CH_2Br$) ppm.[25]

6-(*tert*-Butyldimethylsilyloxy)-1-hexene: TBDMSCl (24.5 g, 162 mmol, 1.01 equiv.) and imidazole (13.1 g, 193 mmol, 1.20 equiv.) were added to a solution of 5-hexen-1-ol (16.0 g, 160 mmol, 1.00 equiv.) in THF (80 mL). After stirring overnight desalinated water (40 mL) was added. The aqueous layer was extracted with diethyl ether (5 × 20 mL) and dried with Na_2SO_4. After evaporation of diethyl ether, the crude product was distilled under reduced pressure to obtain the desired product (99 °C, 30 mbar). (29.8 g, 139 mmol, 87 %). ^{1}H NMR (300 MHz, $CDCl_3$): δ = 5.90–5.73 (ddt, J = 16.9, 10.2, 6.7 Hz, 1 H, CH_2=CH), 5.06–4.90 (m, 2 H, CH_2=CH), 3.67–3.57 (t, J = 6.3 Hz, 2 H, CH_2OTBDMS), 2.14–1.99 (d, J = 7.1 Hz, 2 H, CH_2CH_2OTBDMS), 1.63–1.48 (m, 2 H, $CH_2CH_2CH_2$OTBDMS), 1.48–1.37 (m, 2 H, $CH_2CH_2CH_2CH_2$OTBDMS), 0.95–0.84 [s, 9 H, $OSi(CH_2)_2(CH_3)_3$], 0.09–0.01 [s, 6 H, $OSi(CH_2)_2(CH_3)_3$] ppm. IR (film on NaCl): $\tilde{\nu}$ = 3077, 2930, 1642, 1472, 1387, 1361, 1255, 1102, 910, 835, 775, 661 cm^{-1}.[26]

***tert*-Butyl(4-cyclopropylbutoxy)dimethylsilane:** Et_2Zn (1.0 M in hexane, 140 mL, 140 mmol, 2.00 equiv.) in CH_2Cl_2 (250 mL) was cooled to 0 °C and trifluoroacetic acid (11.0 mL, 142 mmol, 2.04 equiv.) in CH_2Cl_2 (250 mL) was added over 2 h. After stirring the solution for 30 min a solution of freshly distilled diiodomethane (11.3 mL, 140 mmol, 2.00 equiv.) in CH_2Cl_2 (250 mL) was added over 1 h. After stirring for another 30 min 6-(*tert*-butyldimethylsilyloxy)-1-hexene (14.9 g, 69.7 mmol) in CH_2Cl_2 (140 mL) was added. The reaction was stirred at room temperature until the alkene signals disappeared completely in the ^{1}H NMR spectra. A saturated NH_4Cl solution (200 mL) was added and the aqueous layer was extracted with diethyl ether (5 × 20 mL) and dried with Na_2SO_4. The solution was concentrated (60 mL) and used as crude product.

4-Cyclopropylbutane-1-ol: The crude product *tert*-butyl(4-cyclopropylbutoxy)dimethylsilane was added to tetra-*n*-butylammonium fluoride-trihydrate (49.1 g, 138 mmol, 1.99 equiv.) and stirred overnight. After completion, saturated NH_4Cl (150 mL) was added to the reaction and the organic phase was extracted with diethyl ether (3 × 100 mL). The combined organic phases where washed with brine (200 mL) and dried with Na_2SO_4. After evaporation (750 mbar, 40 °C) of the solvent the yellow liquid was purified by column chromatography (silica gel, pentane/diethyl ether = 3:1) to give the desired product as light yellow liquid (5.79 g, 44.5 mmol, 63 %). ^{1}H NMR (300 MHz, $CDCl_3$): 3.63 (t, J = 6.8, 2 H, CH_2OH), 1.60 (m, 2 H, CH_2CH_2OH), 1.46 (m, 2 H, $CH_2CH_2CH_2OH$), 1.23 (m, 2 H, $CH_2CH_2CH_2CH_2OH$), 0.65 (m, 1 H, $CHCH_2CH_2$); 0.39 (m, 2 H, $CHCH_2CH_2$), 0.00 (m, 2 H, $CHCH_2CH_2$) ppm.[27]

4-Cyclopropylbutanal: 4-Cyclopropylbutan-1-ol **23** (5.79 g, 44.5 mmol, 1.00 equiv.) in CH_2Cl_2 (400 mL) was cooled to 0 °C. Dess–Martin periodinane (20.7 g, 49.0 mmol, 1.10 equiv.) was added in one portion and stirred for 1 h. The reaction was then stirred for a further hour at room temperature. The reaction was diluted with cooled pentane (200 mL) and the solid was removed through a Celite pad. The product was concentrated via distillation (60 °C) and a yellow liquid was obtained. ^{1}H NMR (300 MHz, $CDCl_3$): δ = 9.77 (t, J = 1.86, 1 H, HC=O), 2.46 (td, J = 7.36, 1.86, 1 H, CH_2HC=O), 1.74 (p, J = 7.36, 2 H, CH_2CH_2HC=O), 1.24 (m, 2 H, $CH_2CH_2CH_2$HC=O), 0.64 (m, 1 H, $CHCH_2CH_2$), 0.42 (m, 2 H, $CHCH_2CH_2$), 0.01 (m, 2 H, $CHCH_2CH_2$) ppm.[28]

1-(Penten-4-yl)cyclopropane (20): Methyltriphenylphosphonium bromide (24 g, 67 mmol, 1.5 equiv.) in Et_2O (220 mL) was cooled to 0 °C and *n*-butyllithium (2.5 M, 27 mL, 67 mmol, 1.5 equiv.) was added. The yellow suspension was stirred for 1 h. 4-Cyclopropylbutanal (5.8 g, 44 mmol, 1.0 equiv.) in Et_2O (45 mL) was added at 10 °C. The suspension was stirred for 1 h at room temperature and quenched with saturated NH_4Cl (150 mL). The suspension was filtered through a Celite pad and concentrated via distillation. The crude product was purified by column chromatography (silica gel, eluent: pentane) and concentrated via distillation (oil bath = 150 °C) to get a clear liquid. Finally, it was stirred over NaH and condensed under reduced pressure (0.52 g, 4.7 mmol, 10 %). 1-(Penten-4-yl)-cyclopropane **20** is very volatile and has to be stored at −20 °C. ^{1}H NMR (300 MHz, $CDCl_3$): δ = 5.82 (ddt, J = 16.9, 10.1, 6.6 Hz, 1 H, CH_2=CH); 4.97 (m, 2 H, CH_2=CH), 2.08 (m, 2 H, CH_2=$CHCH_2$), 1.51 (m, 2 H, CH_2=$CHCH_2CH_2$), 1.21 (m, 2 H, CH_2=$CHCH_2CH_2CH_2$), 0.66 (m, 1 H, $CHCH_2CH_2$), 0.40 (m, 2 H, $CHCH_2CH_2$), 0.01 (m, 2 H, $CHCH_2CH_2$) ppm. ^{13}C{^{1}H} NMR (75 MHz, $CDCl_3$): δ = 139.3, 114.3, 34.4, 33.8, 29.1, 10.9, 4.52 ppm.

10-Bromo-1,1,1,2,2,3,3,4,4-nonafluoro-6-iododecane (23): tBu_3P (0.0153 g, 0.0756 mmol, 10 mol-%) and $B(C_6F_5)_3$ (0.0386 g, 0.0756 mmol, 10 mol-%) were weighed in an amber glass screw-top jar and dissolved in CH_2Cl_2 (2.1 mL). After addition of 6-bromohexene (**18**) (0.100 mL, 0.748 mmol, 1.00 equiv.) and nonafluoro-1-iodobutane (**1**) (0.130 mL, 0.755 mmol, 1.01 equiv.) the jar was sealed with a Teflon-insert screw cap and the solution was stirred for 68 h. After removal of the solvent the crude product was purified by column chromatography (silica gel, eluent: pentane, R_f = 0.73) to give product **23** (0.352 g, 0.692 mmol, 93 %). ^{1}H NMR (300 MHz, $CDCl_3$): δ = 4.40–4.25 (m, 1 H, CHI), 3.51–3.36 (t, J = 6.6 Hz, 2 H, CH_2Br), 3.07–2.64 (m, 2 H, CH_2CF_2), 2.08–1.46 (m, 6 H, CHI-$CH_2CH_2CH_2$-CH_2Br) ppm. ^{13}C{^{1}H} NMR (75 MHz, $CDCl_3$): δ = 42.0, 41.7, 41.4, 39.5, 33.1, 31.7, 28.5, 19.9 ppm. ^{19}F NMR (282 MHz, $CDCl_3$): δ = −80.9 to −81.1 (t, J = 9.6 Hz, 3F, CF_3), −111.1to −115.5 (m, 2 F, CF_2), −124.3 to −124.8 (m, 2 F, CF_2), −125.6to −126.2 (m, 2 F, CF_2). IR (film on NaCl): $\tilde{\nu}$ = 3215, 2942, 1455, 1433, 1350, 1232, 1134, 880, 724 cm^{-1}. $C_{10}H_{11}BrF_9I$: calcd. C 23.60, H 2.18; found C 23.61, H 2.42.

Acknowledgments

The generous support of M. Spittler by a fellowship of the Studienstiftung des deutschen Volkes is most gratefully acknowledged.

Keywords: Frustrated Lewis pairs · Perfluoroalkylation · Reaction mechanisms · Halogenation · Radicals

[1] P. Kirsch, *Modern Fluoroorganic Chemistry: Synthesis, Reactivity, Applications*, 2nd ed., Wiley-VCH, Weinheim, **2013**.

[2] H. Schofield, *J. Fluorine Chem.* **1999**, *100*, 7–11.
[3] a) T. Fujiwara, D. O'Hagan, *J. Fluorine Chem.* **2014**, *167*, 16–29; b) P. Jeschke, *ChemBioChem* **2004**, *5*, 570–589; c) P. Maienfisch, R. G. Hall, *Chimia* **2004**, *58*, 93–99.
[4] a) C. Isanbor, D. O'Hagan, *J. Fluorine Chem.* **2006**, *127*, 303–319; b) D. O'Hagan, *J. Fluorine Chem.* **2010**, *131*, 1071–1081; c) J.-P. Bégué, D. Bonnet-Delpon, *J. Fluorine Chem.* **2006**, *127*, 992–1012; d) F. M. D. Ismail, *J. Fluorine Chem.* **2002**, *118*, 27–33.
[5] a) S. Purser, P. R. Moore, S. Swallow, V. Gouverneur, *Chem. Soc. Rev.* **2008**, *37*, 320–330; b) H. J. Böhm, D. Banner, S. Bendels, M. Kansy, B. Kuhn, K. Müller, U. Obst–Sander, M. Stahl, *ChemBioChem* **2004**, *5*, 637–643; c) W. K. Hagmann, *J. Med. Chem.* **2008**, *51*, 4359–4369.
[6] L. Hunter, *Beilstein J. Org. Chem.* **2010**, *6*, 38.
[7] a) K. L. Kirk, *J. Fluorine Chem.* **2006**, *127*, 1013–1029; b) K. Müller, C. Faeh, F. Diederich, *Science* **2007**, *317*, 1881–1886; c) C. B. Caputo, D. W. Stephan, *Organometallics* **2012**, *31*, 27–30.
[8] a) T. Billard, B. R. Langlois, *Eur. J. Org. Chem.* **2007**, 891–897; b) J.-A. Ma, D. Cahard, *Chem. Rev.* **2008**, *108*, PR1–PR43; c) J.-A. Ma, D. Cahard, *J. Fluorine Chem.* **2007**, *128*, 975–996; d) R. J. Lundgren, M. Stradiotto, *Angew. Chem. Int. Ed.* **2010**, *49*, 9322–9324; *Angew. Chem.* **2010**, *122*, 9510; e) H. Erdbrink, I. Peuser, U. I. M. Gerling, D. Lentz, B. Koksch, C. Czekelius, *Org. Biomol. Chem.* **2012**, *10*, 8583–8586; f) T. Fujimoto, F. Becker, T. Ritter, *Org. Process Res. Dev.* **2014**, *18*, 1041–1044; g) J. A. Wilkinson, *Chem. Rev.* **1992**, *92*, 505–519.
[9] a) W. J. Middleton, *J. Org. Chem.* **1975**, *40*, 574–578; b) R. E. Banks, S. N. Mohialdin-Khaffaf, G. S. Lal, I. Sharif, R. G. Syvret, *J. Chem. Soc., Chem. Commun.* **1992**, 595–596.
[10] a) D. A. Nagib, M. E. Scott, D. W. C. MacMillan, *J. Am. Chem. Soc.* **2009**, *131*, 10875–10877; b) M. Khrizanforov, S. Strekalova, V. Khrizanforova, V. Grinenko, K. Kholin, M. Kadirov, T. Burganov, A. Gubaidullin, T. Gryaznova, O. Sinyashin, L. Xu, D. A. Vicic, Y. Budnikova, *Dalton Trans.* **2015**, *44*, 19674–19681; c) T. Xu, C. W. Cheung, X. Hu, *Angew. Chem. Int. Ed.* **2014**, *53*, 4910–4914; *Angew. Chem.* **2014**, *126*, 5010; d) Z. Li, A. García-Domínguez, C. Nevado, *J. Am. Chem. Soc.* **2015**, *137*, 11610–11613; e) R. N. Loy, M. S. Sanford, *Org. Lett.* **2011**, *13*, 2548–2551; f) A. Studer, *Angew. Chem. Int. Ed.* **2012**, *51*, 8950–8958; *Angew. Chem.* **2012**, *124*, 9082; g) S. Mizuta, S. Verhoog, K. M. Engle, T. Khotavivattana, M. O'Duill, K. Wheelhouse, G. Rassias, M. Médebielle, V. Gouverneur, *J. Am. Chem. Soc.* **2013**, *135*, 2505–2508; h) A. T. Herrmann, L. L. Smith, A. Zakarian, *J. Am. Chem. Soc.* **2012**, *134*, 6976–6979; i) S. Barata-Vallejo, S. M. Bonesi, A. Postigo, *Org. Biomol. Chem.* **2015**, *13*, 11153–11183; j) O. A. Tomashenko, V. V. Grushin, *Chem. Rev.* **2011**, *111*, 4475–4521.
[11] Y. Wang, J. Wang, G.-X. Li, G. He, G. Chen, *Org. Lett.* **2017**, *19*, 1442–1445.
[12] a) A. Yoshimura, A. Nomoto, M. Uchida, H. Kusano, T. Saeki, A. Ogawa, *Res. Chem. Intermed.* **2017**, *43*, 3433–3443; b) M. Slodowicz, S. Barata-Vallejo, A. Vázquez, N. S. Nudelman, A. Postigo, *J. Fluorine Chem.* **2012**, *135*, 137–143.
[13] I. Behrends, S. Bähr, C. Czekelius, *Chem. Eur. J.* **2016**, *22*, 17177–17181.
[14] a) R. Roesler, W. E. Piers, M. Parvez, *J. Organomet. Chem.* **2003**, *680*, 218–222; b) D. W. Stephan, G. Erker, *Angew. Chem. Int. Ed.* **2015**, *54*, 6400–6441; *Angew. Chem.* **2015**, *127*, 6498; c) G. Erker, D. W. Stephan (Eds.), "Frustrated Lewis Pairs, Vol. I and II", in *Top. Curr. Chem.*, Springer, Heidelberg, **2013**.
[15] C. A. Tolman, *Chem. Rev.* **1977**, *77*, 313–348.
[16] R. D. Nelson Jr., D. R. Lide Jr., A. A. Maryott, *Selected Values of Electric Dipole Moments for Molecules in the Gas Phase, Vol. 10*, U. S. National Bureau of Standards, **1967**.
[17] a) M. O. Sinnokrot, C. D. Sherrill, *J. Phys. Chem. A* **2003**, *107*, 8377–8379; b) S. E. Wheeler, K. N. Houk, *Mol. Phys.* **2009**, *107*, 749–760; c) F. Cozzi, F. Ponzini, R. Annunziata, M. Cinquini, J. S. Siegel, *Angew. Chem. Int. Ed. Engl.* **1995**, *34*, 1019–1020; *Angew. Chem.* **1995**, *107*, 1092.
[18] a) C. M. Mömming, S. Frömel, G. Kehr, R. Fröhlich, S. Grimme, G. Erker, *J. Am. Chem. Soc.* **2009**, *131*, 12280–12289; b) X. Zhao, D. W. Stephan, *Chem. Sci.* **2012**, *3*, 2123–2132; c) J. S. J. McCahill, G. C. Welch, D. W. Stephan, *Angew. Chem. Int. Ed.* **2007**, *46*, 4968–4971; *Angew. Chem.* **2007**, *119*, 5056.
[19] A. J. V. Marwitz, J. L. Dutton, L. G. Mercier, W. E. Piers, *J. Am. Chem. Soc.* **2011**, *133*, 10026–10029.
[20] L. Liu, L. L. Cao, Y. Shao, G. Ménard, D. W. Stephan, *Chem* **2017**, *3*, 259–267.
[21] a) N. O. Brace, *J. Org. Chem.* **1973**, *38*, 3167–3172; b) N. O. Brace, *J. Am. Chem. Soc.* **1964**, *86*, 523–524; c) N. O. Brace, *J. Org. Chem.* **1966**, *31*, 2879–2885.
[22] S. E. Vaillard, C. Mück-Lichtenfeld, S. Grimme, A. Studer, *Angew. Chem. Int. Ed.* **2007**, *46*, 6533–6536; *Angew. Chem.* **2007**, *119*, 6653.
[23] M. Newcomb, Radical Kinetics and Clocks, in *Encyclopedia of Radicals in Chemistry, Biology and Materials*, Wiley Online Library, **2012**.
[24] a) D. J. Parks, W. E. Piers, G. P. A. Yap, *Organometallics* **1998**, *17*, 5492–5503; b) G. W. Coates, A. R. Dunn, L. M. Henling, J. W. Ziller, E. B. Lobkovsky, R. H. Grubbs, *J. Am. Chem. Soc.* **1998**, *120*, 3641–3649.
[25] J. M. Burns, E. H. Krenske, R. P. McGeary, *Eur. J. Org. Chem.* **2017**, 252–256.
[26] a) W. A. Kinney, G. D. Crouse, L. A. Paquette, *J. Org. Chem.* **1983**, *48*, 4986–5000; b) H. Iwamoto, K. Kubota, H. Ito, *Chem. Commun.* **2016**, *52*, 5916–5919.
[27] P. Wessig, O. Mühling, *Helv. Chim. Acta* **2003**, *86*, 865–893.
[28] J. M. Janusz, P. A. Young, M. W. Scherz, K. Enzweiler, L. I. Wu, L. Gan, S. Pikul, K. L. McDow-Dunham, C. R. Johnson, C. B. Senanayake, D. E. Kellstein, S. A. Green, J. L. Tulich, T. Rosario-Jansen, I. J. Magrisso, K. R. Wehmeyer, D. L. Kuhlenbeck, T. H. Eichhold, R. L. M. Dobson, *J. Med. Chem.* **1998**, *41*, 1124–1137.

Received: June 4, 2018

5. Cumulative part II

5.1. Metal-Free Activation of C–I Bonds and Perfluoroalkylation of Alkenes with Visible Light Using Phosphine Catalysts

The conducted experiments of the publication: "Metal-Free Activation of C–I Bonds and Perfluoroalkylation of Alkenes with Visible Light Using Phosphine Catalyst"[4] and a brief discussion of the results will be summarized below. The individual contributions to this publication and the publication is presented without changes at the end of this chapter (p. 89).

The results of the investigations of the FLP-catalyzed iodoperfluoroalkylation indicated a photocatalytic radical background reaction.[2] A literature research revealed that in 2017 Chen *et al.* presented a *N,N,N′,N′*-tetraethylethylenediamine (**100**) (TEEDA)-catalyzed photocatalytic iodoperfluoroalkylation (see p. 33). Chen *et al.* referred two publications by Huang and Zhuang, as well as Moreno-Manãs.[87, 89] They already conducted reactions with PPh_3 as Lewis base in an iodoperfluoroalkylation reaction, but did not mentioned a photochemical process (see p. 44). Dr. M. Spittler conducted the first experiments on the influence of ambient light in his doctoral thesis, using tri-*tert*-butylphosphine (**186**) as Lewis base and sunlight as light source (Scheme 75).[3]

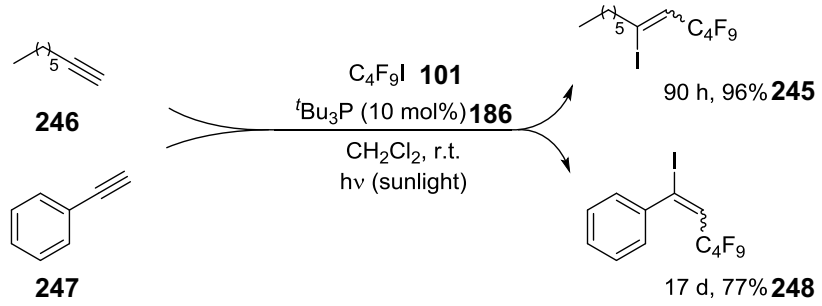

Scheme 75: Photomediated iodoperfluoroalkylation of terminal alkynes conducted by M. Spittler.[3]

The corresponding products could be isolated in good to excellent yields when $^tBu_3P$ **186** was used in catalytic amounts and C_4F_9I **101**. Nevertheless, very long reaction times were needed. In case of the FLP-catalyzed iodoperfluoroalkylation, alkynes were challenging substrates and could not be transformed.[3, 6]

Based on the results and the results already published with PPh_3,[87, 89] further investigations and establishment of a photoinduced and phosphorus-catalyzed iodoperfluoroalkylation were project of this doctoral thesis and the first corresponding publication.[4]

At the beginning of this project, a photoreactor was designed, since it was demonstrated that direct sunlight irradiation was not sufficient enough. The building and further development were carried out

by Dr. K. Baumgarten and Dr. M. Spittler. The construction was adapted to the reactions carried-out and the development of the photoreactor will be presented briefly since the reactor is one of the core elements of this project. A more detailed description of the photoreactor and its composition was described in the supporting information of the corresponding publication (p. 234).[4]

The following pictures show the used photoreactors, and the wavelengths of the used LED strips (Figure 4, Figure 6). The respective wavelength was selected *via* the LCD display or the manual control that was directly connected to the photoreactor. A LED strip (30 LED/m, 12 V, 393 nm) or a RGB LED strip (120 LED/m, 12 V, 461 nm – 630 nm) were used. Since high-intensity irradiation was used, the lid of the photoreactors was designed with curved air ducts. Moreover, ambient light was keept out of the photoreactor during the reaction. The air from the installed cooling fan could still flow through the designed air ducts (Figure 5).[4]

Figure 4: Self-designed photoreactors. With LCD display (left) and with manual light control (right).[4]

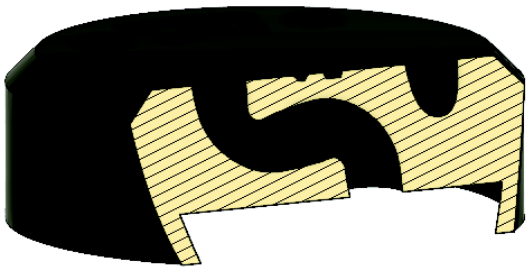

Figure 5: Cut off the modeled lid for the photoreactor.[4]

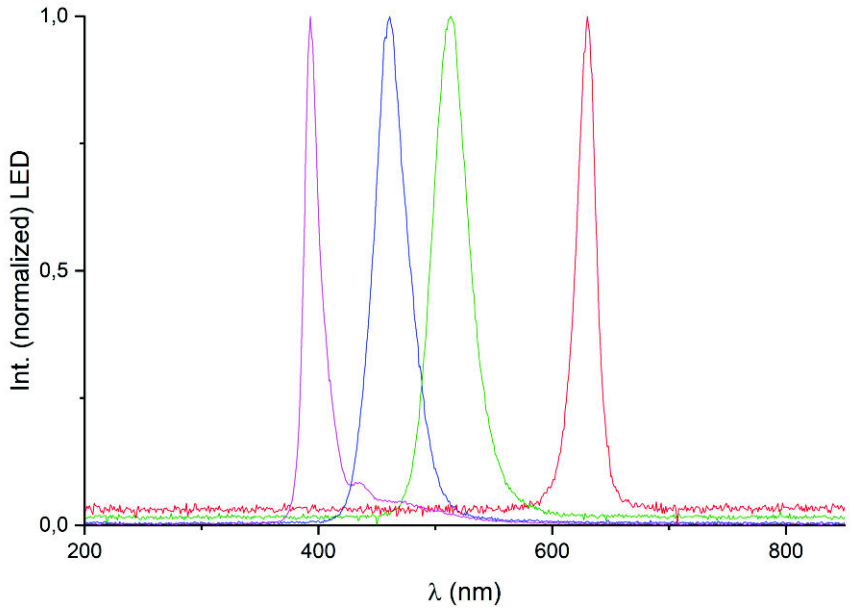

Figure 6: Wavelength of the used LEDs inside the photoreactor: λ_{max}(violet) = 393 nm, λ_{max}(blue) = 461 nm, λ_{max}(green) = 513 nm, λ_{max}(red) = 630 nm.[4]

Figure 7: Centering support for the photoreactor on top of the magnetic stir plate (left) and with the attached photoreactor (right).

The photoreactor was positioned with a centering support on top of a magnetic stir plate, to ensure that the reactions were always stirred in the same way. (Figure 8, left). Unless otherwise stated, the photoreactions were conducted inside 4 mL screw neck glass vials with a septa screw cap. To prevent the reaction vials from falling, a support was attached underneath the lid (Figure 8).

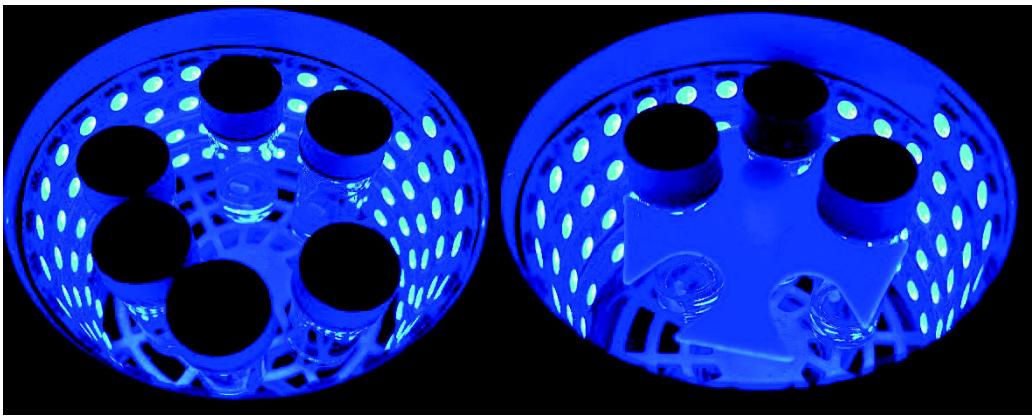

Figure 8: View of the inside of the photoreactor during a reaction. Without support of the reaction vials (left) and with support of the reaction vials (right).

In addition to the photoreactors, a device for reactions in a Schlenk tube was developed (Figure 9, top). For that purpose, a hollow rod was 3D-printed, and the LED strips were glued to the top site. Air could be blown through the hollowed rod to cool the LED strips. The LED strip was placed in a test tube inside the Schlenk tube.

Figure 9: Setup for photoreactions in a Schlenk-tube.

Reactions at reduced temperature or with a connected balloon with trifluoroiodomethane (**25**) gas could be conducted with this device. As mentioned in the introduction, Moreno-Mañas published a triphenylphosphine-catalyzed iodoperfluoroalkylation by stirring alkenes and perfluoroalkyl iodides at room temperature for 48 - 70 h (see: Phosphorus-catalyzed reactions, p. 45, Scheme 42).[89] A repetition of the published protocol of Moreno-Mañas revealed no conversion after 48 h of stirring 1-octene (**174**) and $C_8F_{17}I$ **124** in the dark, using PPh_3 **91** as catalyst.[4] Based on these results, light seemed to be an essential factor for the completion of the reaction.

The investigation of the photomediated iodoperfluoroalkylation was started with the screening of different phosphorus(III) compounds. To identify the optimal catalyst, 20 different phosphines and phosphites were tested in a reaction of 1-octene (**174**) and C_4F_9I **101** (Scheme 76).

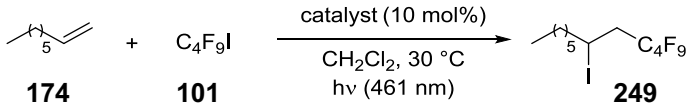

Scheme 76: Reaction with 1-octene (**174**) and C_4F_9I **101** for the screening of various phosphors compounds.[4]

Due to the experience with dichloromethane as solvent in the FLP-catalyzed iodoperfluoroalkylation, it was applied for the first test reactions. A conversion of 99% after 1 h was only achieved when $^tBu_3P$ was used catalyst and an irradiation wavelength of 461 nm (entry 11, Table 7). However, switching to longer wavelengths did not result in full conversions (entry 9 - 10, Table 7). Reactions with different solvents demonstrated that dichloromethane was the most suitable solvent (entry 9 - 10, Table 7). Following the investigated reaction conditions, 22 different non- and functionalized alkenes were converted.[4]

Table 7: Solvent and light screening with 1-octene (**174**) and C_4F_9I **101** as model substrate.[4]

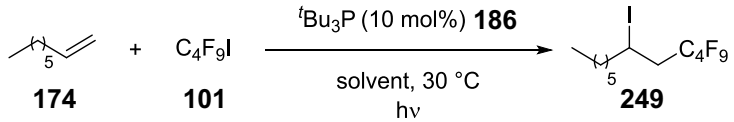

174 **101** **249**

entry	solvent	light source	time [h]	conversion [%]
1	acetonitrile	blue LED (461 nm)	2	91
2	carbon tetrachloride	blue LED (461 nm)	1	5
3	1,2-difluorobenzene	blue LED (461 nm)	2	97
4	dichloromethane	blue LED (461 nm)	1	≥99
5	tetrahydrofurane	blue LED (461 nm)	2	52
6	toluene	blue LED (461 nm)	2	58
7	dichloromethane	no light	1	12
8	dichloromethane	ambient light	1	17
9	dichloromethane	red LED (630 nm)	1	10
10	dichloromethane	green LED (513 nm)	1	29
11	dichloromethane	blue LED (461 nm)	1	≥99

Furthermore, the reaction mechanism was examined using 2,2-diallylmalonate as radical clock and TEMPO **244** as a radical scavenger. Using TEMPO **244** as radical scavenger, the perfluoroalkylation product was formed and by a 5-*exo*-trig cyclization, a cyclopentane product was formed from 2,2-diallylmalonate. The investigations of the FLP-catalyzed iodoperfluoroalkylation demonstrated the interaction of $^tBu_3P$ **186** and C_4F_9I **101**.[2] The interaction of the halogen donor and acceptor were assumed as the starting point for the reaction mechanism, followed by radical formation through the irradiation of visible light (Scheme 77).[4]

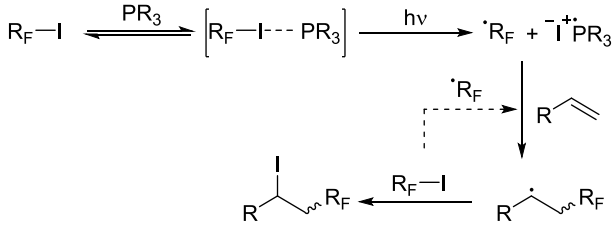

Scheme 77: Control experiments to support the evidence for a of a radical mechanism.[4]

In contrary to what is described in literature for some EDA complexes,[52] a redshift was not observed in the UV-VIS spectra by mixing the phosphorus compound and C_4F_9I **101** (Figure 10).[4] Instead, a substantial increase of the absorption was observed in the case of the mixture of $^tBu_3P$ **186**, $^nBu_3P$ and $(MeO)_3P$ with C_4F_9I **101** in the UV-VIS spectra.

Due to the increase in absorption, a longer tailing occurs in the region over 400 nm, which is most pronounced for $^{t}Bu_3P$ **186**. The longer tailing in the visible light region was attributed to the $[RCF_2—I—P^{t}Bu_3]$ complex, that facilitate normally forbidden *n*-σ* transitions.[4]

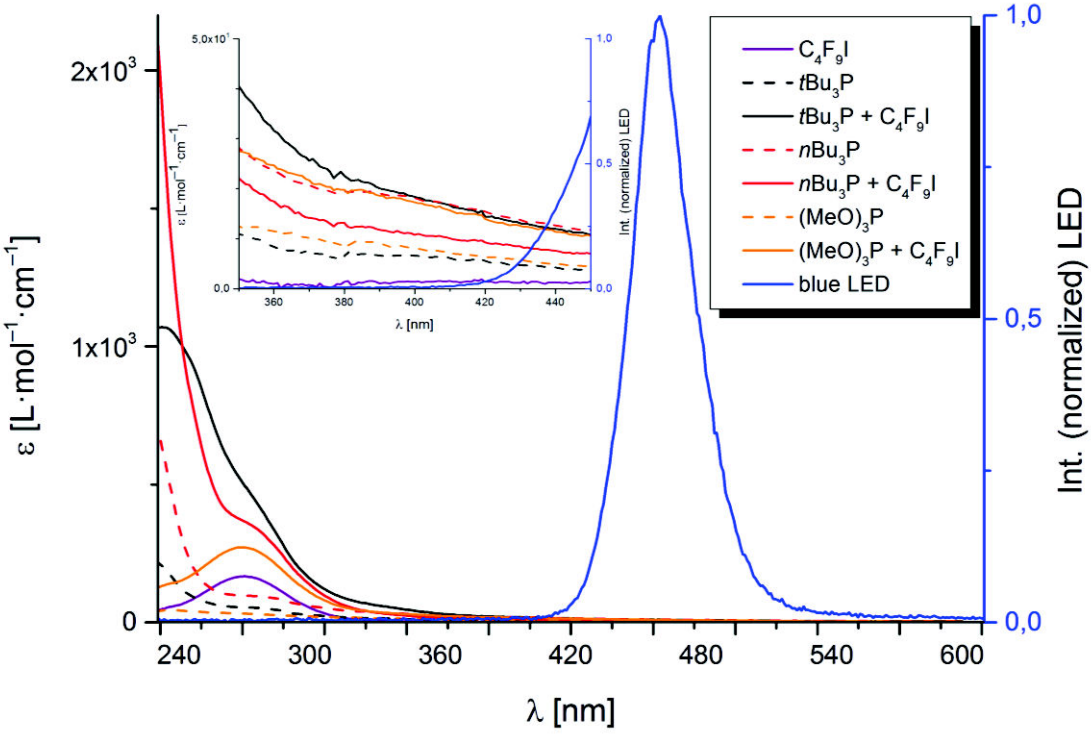

Figure 10: UV-VIS spectra of different phosphorus compounds (dotted line), mixtures of phosphorus compounds and C_4F_9I **101** (straight line), as well as the wavelength of the blue, LED. The smaller inset shows the region between 350 nm and 450 nm.[4]

5.2. Contributions to the publication

The publication "Metal-Free Activation of C–I Bonds and Perfluoroalkylation of alkenes with Visible Light Using Phosphine Catalysts" was published in collaboration with Dr. M. Spittler, Dr. K. Baumgarten and Prof. C. Czekelius.

Independently from the experimental part the work and effort of Dr. K. Baumgarten and Dr. M. Spittler, for the used photoreactor shall be presented. Dr. K. Baumgarten and Dr. M. Spittler worked on the design, the conceptual work and did the manufacturing of the photoreactor.

The experimental part was conducted by Lucas Helmecke (95%) and Dr. M. Spittler (5%).

L. Helmecke performed the catalyst, light and solvent screening, as well as the synthesis and isolation of the iodoperfluoroalkylated products. He also performed the control experiments supporting the radical mechanism and the UV-VIS measurements.

Dr. M. Spittler synthesized dec-9-en-1-yl-4-methylbenzenesulfonate, 10-azido-dec-1-ene, pent-4-enamide, pent-4-en-1-yl 4-chlorobenzoate, *N*-allyl-4-chlorobenzamide, 1-bromo-4-(hex-5-en-1-yloxy)benzene, 6-bromohexene, 1-(3-allylphenyl)ethan-1-one and 2-(hex-5-en-1-yl)isoindoline-1,3-dione as part of his doctoral thesis.[3] These were used as substrates for the publication.

The manuscript was mainly written by Lucas Helmecke. This includes the structure, the conceptualization and the literary research. Furthermore, he wrote the supporting information for the manuscript and created the blueprint for the photoreactor in the Supporting Information.

Dr. M. Spittler and Dr. K. Baumgarten corrected the manuscript and the Supporting Information. The text of the manuscript was revised by Dr. M. Spittler.

Prof. C. Czekelius extended and changed the introduction of the manuscript. Furthermore, he was significantly involved in the correction and the revision of the manuscript and the supporting information.

OL Organic Letters

Letter

Cite This: Org. Lett. 2019, 21, 7823–7827

pubs.acs.org/OrgLett

Metal-Free Activation of C–I Bonds and Perfluoroalkylation of Alkenes with Visible Light Using Phosphine Catalysts

Lucas Helmecke, Michael Spittler, Kai Baumgarten, and Constantin Czekelius*

Institute of Organic Chemistry and Macromolecular Chemistry, Heinrich-Heine-Universität Düsseldorf, Universitätsstr. 1, 40225 Düsseldorf, Germany

Supporting Information

ABSTRACT: An efficient metal-free, photomediated iodo perfluoroalkylation under mild conditions was developed. Using catalytic amounts (10 mol %) of phosphines and blue light irradiation, various olefins are transformed into the corresponding addition products within short reaction times. For this purpose, a modular and convenient 3D printed photoreactor was constructed, which is presented as an open source model. The reaction presumably proceeds upon generation of perfluoroalkyl radicals, which are formed by catalyst-induced absorption enhancement.

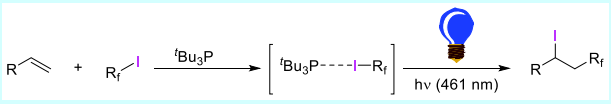

Fluoroorganic compounds have key importance in synthesis and industry. The majority of modern small molecule drugs incorporate a fluorine atom due to the beneficial pharmacodynamic and -kinetic profile.[1] Therefore, the development of efficient fluorinations and perfluoroalkylations has fueled method development in particular within the last decades.[2]

The iodo perfluoroalkylation of simple alkenes allows for straightforward incorporation of a trifluoromethyl or other perfluoroalkyl substituent into molecules. This process typically proceeds via perfluoroalkyl radicals commonly generated by radical initiators[3] or upon UV irradiation.[4] However, such conditions are often incompatible with sensitive functional groups limiting either yield or substrate scope.

Photocatalysis using visible instead of UV light has evolved quickly in recent years.[5] Transition metal complexes have been successfully employed as photocatalysts for the generation of perfluoroalkyl radicals. In a seminal contribution, MacMillan and co-workers reported the highly enantioselective α-trifluoromethylation of aldehydes using $Ru(bpy)_3$ and a chiral organocatalyst.[6] Likewise, copper complexes have been reported for atom transfer radical addition (ATRA) reactions[7] and successfully employed as catalysts for perfluoroalkylations.[8] In this process, irradiation with green LED light (530 nm) is sufficient. Difficult substrates such as styrene derivatives are successfully transformed. Recently, a copper-catalyzed asymmetric cyanofluoroalkylation of alkenes was presented.[9]

In addition to metal complexes or organic dyes absorbing visible light and acting as sensitizers,[10] metal-free photomediators such as amines have been developed activating the carbon–iodine bond. Perfluoroalkyl iodides typically show an absorption maximum below 300 nm requiring UV irradiation.[11] A charge-transfer or an electron donor–acceptor (EDA) complex absorb light of lower energy than the individual components leading to radical formation.[5a,12] Complexes from halides and Lewis bases are well-known since the 19th century[13] and were more recently investigated in computational,[14] solid state,[15] and solution studies.[16]

Recently, amines have been described as photomediators for the iodo perfluoroalkylation of unsaturated hydrocarbons,[17] diisonitriles,[18] and 2-isocyanoaryl thioesters/benzoselenazoles[19] or for α-perfluoroalkylations with accompanying vicinal β-alkenylation.[20] Furthermore, enantioselective α-perfluoroalkylations of enamine intermediates[21] or β-ketoesters[22] by amines have been presented. In a typical reaction, 3 equiv of *N*,*N*,*N*′,*N*′-tetraethylethylene diamine (TEEDA) over the course of 36 h were employed.[17] A compact fluorescent lamp, low pressure Hg lamp, or direct sun light was required.

Recently, we reported mechanistic studies addressing the frustrated Lewis pair (FLP)-catalyzed perfluoroalkylation of simple olefins in which a photoinduced radical mechanism may be operating.[23] Moreno-Mañas[24] as well as Huang and Zhang[25] reported earlier PPh_3 and related phosphorus(III) compounds as catalysts for iodo perfluoroalkylations of alkenes. They proposed a SET initiation step but did not comment on a potential light-induced radical generation.[24,25] We repeated the protocol of Moreno-Mañas (see Supporting Information) revealing that no conversion was detected after 48 h in the dark. Upon exposure with ambient light for 16 h, 8% conversion was detected in our setup. For a more detailed study, we developed a cooled photoreactor assembled from 3D-printed parts and high density RGB LED strips (120 LEDs/m) (free STL-print files are available on demand, see Supporting Information).

We began our investigations by screening phosphorus compounds as potential catalysts (see Supporting Information). As a test reaction we chose the iodo perfluoroalkylation of 1-octene (**1**) with nonafluoro-1-iodobutane (**2**) (1.1 equiv) in dichloromethane (Table 1). Using triphenylphosphine as catalyst we found 88% conversion after 2 h (Table 1, entry 11). Screening of different phosphines and phosphites revealed

Received: August 8, 2019
Published: September 18, 2019

DOI: 10.1021/acs.orglett.9b02812
Org. Lett. 2019, 21, 7823–7827

Table 1. Screening of Phosphine and Phosphite Photocatalysts (Selection)[a]

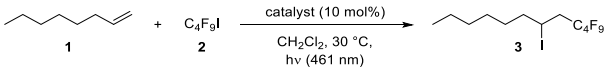

entry	catalyst	time [h]	conversion [%]
1	no catalyst	72	0
2	$^tBu_3P$	1	≥99
3	Cy_3P	1.5	84
4	$(o\text{-Tol})_3P$	4	52
5	$(C_6F_5)_3P$	6	25
6	$(p\text{-F-}C_6H_4)_3P$	24	65
7	$(C_6H_5O)_3P$	24	3
8	$(MeO)_3P$	6	94
9	$(EtO)_3P$	6	91
10	$(Ph)_2PCH_2P(Ph)_2$	4	94
11	Ph_3P	2	88

[a]Screening conditions: 1-octene (**1**), C_4F_9I **2** (1.1 equiv), and catalyst (10 mol %) in CH_2Cl_2 (1 mL), 30 °C, and irradiation at 461 nm.

tri-*tert*-butylphosphine (**4**) as superior catalyst (Table 1, entry 2). Using 10 mol % of catalyst, full conversion was already detected after 1 h. In contrast, stagnation occurred after 8 h employing less active catalysts. The dark yellow to deep red coloration of the solution suggests the emergence of free iodine, which could interact with the phosphine[26] or act as an inhibitor for the radical reaction.[27] In addition, efficient irradiation into the reaction solution becomes more difficult.

Several polar and nonpolar solvents gave useful conversions within 2 h. Dichloromethane was best suited as it leads to ≥99% conversion after 1 h (Table 2, entry 5) and shows the additional

Table 2. Screening of Solvents in the Conversion of 1-Octene (1) with C_4F_9I (2) in Different Solvents and at Different Wavelength[a]

entry	solvent	light source	time [h]	conversion [%]
1	acetonitrile	blue LED	2	91
2	carbon tetrachloride	blue LED	1	5
3	1,2-difluorobenzene	blue LED	2	97
5	dichloromethane	blue LED	1	≥99
6	tetrahydrofuran	blue LED	2	52
7	toluene	blue LED	2	58
8	dichloromethane	no light	1	12
9	dichloromethane	ambient light	1	17
10	dichloromethane	red LED (630 nm)	1	10
11	dichloromethane	green LED (531 nm)	1	29
12	dichloromethane	blue LED (461 nm)	1	≥99

[a]Screening conditions: 1-octene (**1**), C_4F_9I **2** (1.1 equiv), and $^tBu_3P$ **4** (10 mol %) were irradiated in the corresponding solvent (2 mL) for the indicated time at 30 °C. For the emission spectrum of the blue LED, see Figure 1.

advantage that the solvent can be easily removed after the reaction without loss of the eventually volatile perfluoroalkylation products. In order to investigate the influence of the light source further, we tested the irradiation of green, red, or ambient light, respectively (Table 2, entries 9−11). Red or ambient light do not promote the reaction sufficiently. While blue light of 461 nm led to full conversion after 1 h, the same outcome was found already after 15 min when a shorter wavelength LED (405 nm) under otherwise identical conditions was employed. However, in this case ^{19}F-NMR-spectroscopy showed formation of C_4F_9H in higher concentrations (see Supporting Information). In a control reaction, 1-octene (**1**) and C_4F_9I **2** were irradiated in the absence of any phosphine. No conversion was detected after 72 h (Table 1, entry 1) and only 32% after 49 d upon irradiation using a blue LED.

With the optimized reaction conditions in hand, 1-octene (**1**) was converted with perfluoroalkyl iodides of different chain length (Scheme 1). Using trifluoromethyl iodide gas, the

Scheme 1. Photocatalytic Iodo Perfluoroalkylation of Alkenes Using Tri-*tert*-butylphosphine[a]

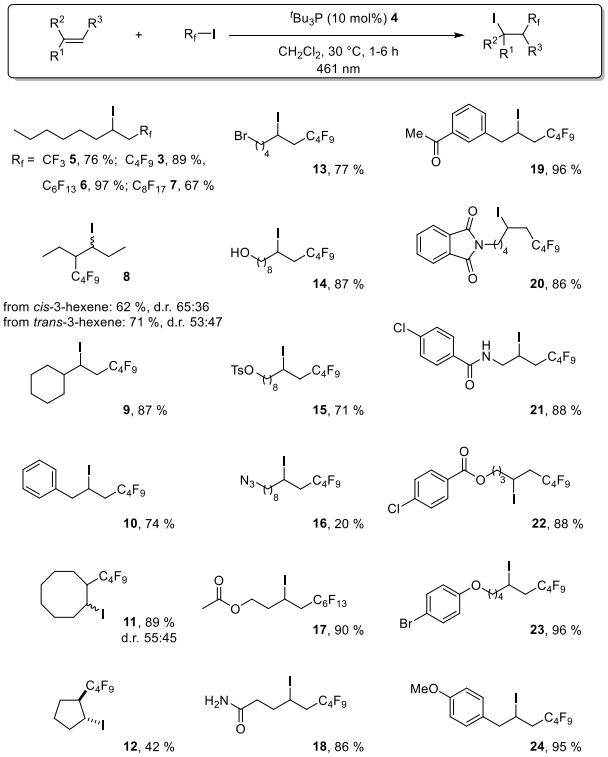

[a]Reaction conditions: $^tBu_3P$ (10 mol %), the corresponding alkene and perfluoroalkyl iodide (1.1 equiv) in CH_2Cl_2 (2 mL), irradiation at 461 nm (blue LED) for 1−6 h.

corresponding product was isolated in 76% yield. Nonafluoro-1-iodobutane (**2**) was successfully added to internal and terminal olefins as well as *cis*- and *trans*-configured starting materials. In the case of terminal alkenes, complete regioselectivity was observed. The developed perfluoroalkylation method shows a broad substrate scope. Halides, alcohols, ethers, esters, and amides were successfully transformed into the corresponding 1,2-addition products. The low yield of azide-functionalized product **16** can be explained by the difficulty in the purification and the instability of the isolated product. No formation of a side product by Staudinger reaction could be detected by ^{1}H NMR spectroscopy. In most cases, complete conversion was achieved within one to 3 h of irradiation. Only when iodo trifluoromethane gas was used, the reaction solution was stirred for a longer reaction time (6 h). In the case of electron-deficient substrates, no reaction occurs, presumably due to the electrophilic character of the perfluoroalkyl radical (see Supporting

DOI: 10.1021/acs.orglett.9b02812
Org. Lett. 2019, 21, 7823−7827

Information, reaction of compounds **35** or **36**).[4d,28] In the reaction with styrene, neither addition nor polymerization of the starting material was detected. In fact, styrene acts as inhibitor in the perfluoroalkylation of vinylcyclohexene, a generally reactive substrate. Moreno-Mañas et al. reported similar observations for the reaction of styrene or 1,3-cyclohexadiene referring to the high stability of potentially formed benzylic or allylic radicals.[24] To demonstrate the scalability of the reaction, 8.93 g (19.5 mmol) of product **3** was successfully prepared with the described setup in 98% yield (Scheme 2).

Scheme 2. Large-Scale Transformation of 1-Octene (1)[a]

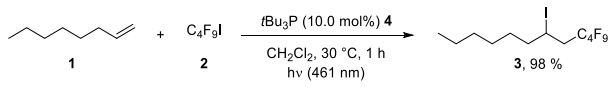

[a]Reaction conditions: 1-octene (**1**), C_4F_9I **2** (1.1 equiv), and $^tBu_3P$ **4** (10 mol %) in CH_2Cl_2 (24 mL) and irradiation at 461 nm for 1 h.

In order to study the mechanism of this efficient reaction in more detail we addressed potential intermediates and bond activation pathways. Upon mixing $^tBu_3P$ (**4**) and C_4F_9I (**2**) a substantial shift of both the $-CF_2I$ moiety and the phosphine was observed in the corresponding NMR spectrum indicating an interaction between these two compounds.[23b] As mentioned earlier, interactions of an electron-donating Lewis base and a halo-perfluoroalkane and the accompanying shifts in the NMR spectrum have already been reported in the literature.[16b,c] Fast interaction between the electron-rich phosphine and the perfluoroalkyl iodide is presumably followed by a rate-determining SET step leading to bond breakage and perfluoroalkyl radical formation. This is in line with the formation of free iodine during the reaction, in particular when less active catalysts are used. To support a radical-type mechanism, which has been proposed by concomitant occurrence of an EDA complex,[12a,b,29] we irradiated a solution of $^tBu_3P$ (**4**) and C_4F_9I (**2**) in the presence of 2,2,6,6-tetramethylpiperidine 1-oxyl (**25**, TEMPO) as radical scavenger (Scheme 3). The perfluoroalkylation product of TEMPO **26** and the $[^tBu_3PI]^+$ cation **27** were detected by mass spectrometry (Supporting Information). Likewise, the transformation of 2,2-diallylmalonate (**28**) as radical clock resulted in the formation of the five-membered ring cyclization product **29** via internal ring closure, strongly suggesting a radical intermediate.

Scheme 3. Control Experiments Supporting a Radical-Involving Mechanism[a,b]

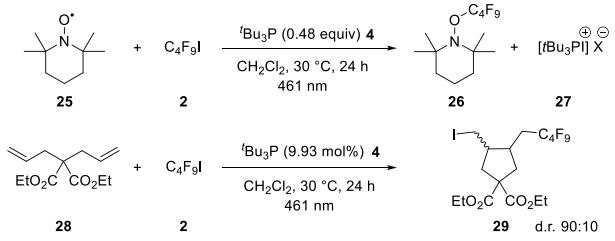

[a]Reaction conditions: $^tBu_3P$ **4** (0.48 equiv), TEMPO **25** (1.1 equiv), and C_4F_9I **2** (1.0 equiv) in CH_2Cl_2 (2.1 mL), irradiation at 461 nm (blue LED) for 24 h. [b]$^tBu_3P$ **4** (9.93 mol %), 2,2-diallylmalonate **28** (1.00 equiv), and C_4F_9I **2** (1.16 equiv) in CH_2Cl_2 (2.0 mL), irradiation at 461 nm (blue LED) for 24 h.

Based on related Lewis base-catalyzed perfluoroalkylations[12a,b,30] and on both experimental evidence for the formation of phosphine-perfluoroalkyl iodide adducts as well as C–I bond breakage forming perfluoroalkyl radicals, we propose the following mechanism (Scheme 4). Upon formation of an EDA complex, blue light irradiation leads to $R_fF_2C–I$ bond cleavage and concomitant perfluoroalkyl radical formation.

Scheme 4. Proposed Mechanism

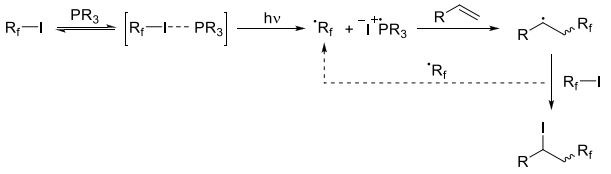

Following the proposal of a light-induced homolytic bond cleavage we became interested in the actual chromophore since the reaction mixtures were seemingly colorless at the beginning of the reaction. Therefore, we measured the UV–vis spectra of solutions of different phosphines or phosphites alone and in equimolar mixtures with C_4F_9I (**2**), respectively (Figure 1).

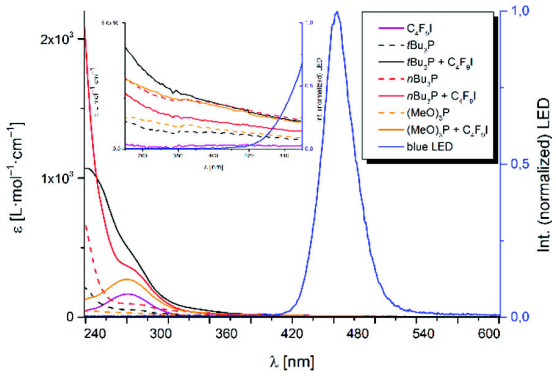

Figure 1. UV–vis spectra of C_4F_9I (**2**), $^tBu_3P$ (**4**), $^nBu_3P$, $(MeO)_3P$ (dotted lines), and mixtures of the phosphorus-compound and C_4F_9I (**2**) (continuous line). All concentrations are 1.0 mM in dichloromethane. The emission spectrum of the blue LED (λ_{max} = 461 nm) is printed in blue. The smaller inset shows the region between 350 and 450 nm.

For $^nBu_3P$, $^tBu_3P$, and $(MeO)_3P$, we noticed a substantial increase of the absorption in the presence of the perfluoroalkyl iodide. A bathochromic shift due to the presence of an EDA complex was not detected. Calculations published recently for the visible-light-mediated synthesis of aryl phosphonates showed that probably only small amounts of a weak EDA complex are formed with an absorbance in the visible region between 400 and 420 nm, which were difficult to detect.[31] In contrast, mixing of amines (Et_3N, pyrrolidine, or TEEDA) and perfluoroalkyl iodide results in only little change in the corresponding UV–vis absorption spectra. While $^nBu_3P$ shows a more pronounced absorbance, the absorption band of $^tBu_3P$ is wider and expands more into the region of visible light. This seemingly marginal tailing may explain why $^tBu_3P$ is a significantly more efficient catalyst. A potential explanation for the observed increase and broadening of the absorption bands may be given by a breaking of local symmetry upon formation of

DOI: 10.1021/acs.orglett.9b02812
Org. Lett. 2019, 21, 7823–7827

the [RCF_2−I−P^tBu_3] complex. This could facilitate normally forbidden n−σ^* transitions.

Supporting this argument, crystal structures and calculations indicate that the [R−X−LB] angle is typically close to 180°, which is more difficult to adopt for $^tBu_3P$ than for $^nBu_3P$.[13b,14b,d] However, limited structural evidence is available because only few crystal structures of phosphine complexes with iodo-organic compounds are known in the literature.[32] UV−vis absorption measurements indicate the possibility of selective bond activation not by shifting maximal absorption into the visible light region but by enhancing the corresponding absorption coefficient. This would allow for chemoselectivity even in the presence of delicate functional groups or differentiation of equal bonds with different local symmetry.

In summary, a metal-free photomediated activation of perfluoroalkyl iodides using phosphines or phosphites has been developed. Using blue LED light, efficient addition to alkenes under mild conditions occurs. The reaction requires neither an expensive metal photoredox catalyst nor UV light irradiation and involves an operationally simple workup procedure by precipitation of the catalyst after solvent removal. Control experiments and electron absorption spectra indicate that the efficiency of the catalyst is connected to a selective absorption enhancement allowing for the use of a visible light source.

■ ASSOCIATED CONTENT

Supporting Information

The Supporting Information is available free of charge on the ACS Publications website at DOI: 10.1021/acs.orglett.9b02812.

Experimental procedures, analytical data of compounds, LED-reactor setup, UV−vis spectra, ^{1}H- and ^{13}C-spectra (PDF)

■ AUTHOR INFORMATION

Corresponding Author

*E-mail: constantin.czekelius@uni-duesseldorf.de.

ORCID

Constantin Czekelius: 0000-0002-2814-8686

Notes

The authors declare no competing financial interest.

■ ACKNOWLEDGMENTS

The generous support of M.S. by a fellowship of the Studienstiftung des deutschen Volkes is most gratefully acknowledged. The authors cordially thank Prof. Dr. Peter Gilch (HHU Düsseldorf) for helpful discussions.

■ REFERENCES

(1) (a) Hunter, L. *Beilstein J. Org. Chem.* **2010**, *6*, 38. (b) Kirk, K. L. *J. Fluorine Chem.* **2006**, *127*, 1013−1029. (c) Müller, K.; Faeh, C.; Diederich, F. *Science* **2007**, *317*, 1881−1886. (d) Purser, S.; Moore, P. R.; Swallow, S.; Gouverneur, V. *Chem. Soc. Rev.* **2008**, *37*, 320−330. (e) Hagmann, W. K. *J. Med. Chem.* **2008**, *51*, 4359−4369. (f) Böhm, H. J.; Banner, D.; Bendels, S.; Kansy, M.; Kuhn, B.; Müller, K.; Obst-Sander, U.; Stahl, M. *ChemBioChem* **2004**, *5*, 637−643. (g) Ojima, I. *Fluorine in Medicinal Chemistry and Chemical Biology*; Wiley-Blackwell: Chichester, 2009. (h) Wang, J.; Sánchez-Roselló, M.; Aceña, J. L.; del Pozo, C.; Sorochinsky, A. E.; Fustero, S.; Soloshonok, V. A.; Liu, H. *Chem. Rev.* **2014**, *114*, 2432−2506.

(2) (a) Tomashenko, O. A.; Grushin, V. V. *Chem. Rev.* **2011**, *111*, 4475−4521. (b) Ma, J.-A.; Cahard, D. J. *J. Fluorine Chem.* **2007**, *128*, 975−996. (c) Ma, J.-A.; Cahard, D. *Chem. Rev.* **2008**, *108*, PR1−PR43. (d) Barata-Vallejo, S.; Postigo, A. *Coord. Chem. Rev.* **2013**, *257*, 3051−3069. (e) Barata-Vallejo, S.; Torviso, M. R.; Lantaño, B.; Bonesi, S. M.; Postigo, A. *J. Fluorine Chem.* **2014**, *161*, 134−141. (f) Kirsch, P. *Modern Fluoroorganic Chemistry: Synthesis, Reactivity, Applications*, 2nd ed.; Wiley-VCH: Weinheim, 2013. (g) Studer, A. *Angew. Chem., Int. Ed.* **2012**, *51*, 8950−8958. (h) Zheng, D.; Studer, A. *Org. Lett.* **2019**, *21*, 325−329.

(3) Liu, S. Q.; Wang, S. W.; Qing, F.-L. *J. Fluorine Chem.* **2005**, *126*, 771−778.

(4) (a) Habib, M. H.; Mallouk, T. E. *J. Fluorine Chem.* **1991**, *53*, 53−60. (b) Yoshimura, A.; Nomoto, A.; Uchida, M.; Kusano, H.; Saeki, T.; Ogawa, A. *Res. Chem. Intermed.* **2017**, *43*, 3433−3443. (c) Tsuchii, K.; Imura, M.; Kamada, N.; Hirao, T.; Ogawa, A. *J. Org. Chem.* **2004**, *69*, 6658−6665. (d) Dolbier, W. R. *Chem. Rev.* **1996**, *96*, 1557−1584. (e) Brace, N. O. *J. Org. Chem.* **1963**, *28*, 3093−3102.

(5) (a) Romero, N. A.; Nicewicz, D. A. *Chem. Rev.* **2016**, *116*, 10075−10166. (b) Wang, C.-S.; Dixneuf, P. H.; Soulé, J.-F. *Chem. Rev.* **2018**, *118*, 7532−7585.

(6) (a) Stephenson, C.; MacMillan, D. W. C.; Yoon, T. P. *Visible Light Photocatalysis in Organic Chemistry*; Wiley-VCH, 2018. (b) Prier, C. K.; Rankic, D. A.; MacMillan, D. W. C. *Chem. Rev.* **2013**, *113*, 5322−5363. (c) Nagib, D. A.; Scott, M. E.; MacMillan, D. W. C. *J. Am. Chem. Soc.* **2009**, *131*, 10875−10877.

(7) (a) Reiser, O. *Acc. Chem. Res.* **2016**, *49*, 1990−1996. (b) Tang, X.-J.; Dolbier, W. R., Jr. *Angew. Chem., Int. Ed.* **2015**, *54*, 4246−4249.

(8) Rawner, T.; Lutsker, E.; Kaiser, C. A.; Reiser, O. *ACS Catal.* **2018**, *8*, 3950−3956.

(9) Guo, Q.; Wang, M.; Peng, Q.; Huo, Y.; Liu, Q.; Wang, R.; Xu, Z. *ACS Catal.* **2019**, *9*, 4470−4476.

(10) (a) Reckenthäler, M.; Griesbeck, A. G. *Adv. Synth. Catal.* **2013**, *355*, 2727−2744. (b) Hari, D. P.; König, B. *Chem. Commun.* **2014**, *50* (51), 6688−6699.

(11) Kavita, K.; Das, P. K. *Chem. Phys. Lett.* **2001**, *338*, 118−122.

(12) (a) Lima, C. G. S.; Lima, T. M.; Lima, T.; Duarte, M.; Jurberg, I. D.; Paixão, M. W. *ACS Catal.* **2016**, *6*, 1389−1407. (b) Postigo, A. *Eur. J. Org. Chem.* **2018**, *2018*, 6391−6404. (c) Vaillard, S. E.; Postigo, A.; Rossi, R. A. *Organometallics* **2004**, *23*, 3003−3007. (d) Marzo, L.; Pagire, S. K.; Reiser, O.; König, B. *Angew. Chem., Int. Ed.* **2018**, *57*, 10034−10072.

(13) (a) Guthrie, F. *J. Chem. Soc.* **1863**, *16*, 239−244. (b) Politzer, P.; Lane, P.; Concha, M. C.; Ma, Y.; Murray, J. S. *J. Mol. Model.* **2007**, *13*, 305−311.

(14) (a) Lommerse, J. P. M.; Stone, A. J.; Taylor, R.; Allen, F. H. *J. Am. Chem. Soc.* **1996**, *118*, 3108−3116. (b) Clark, T.; Hennemann, M.; Murray, J. S.; Politzer, P. *J. Mol. Model.* **2007**, *13*, 291−296. (c) Murray, J. S.; Lane, P.; Politzer, P. *J. Mol. Model.* **2009**, *15*, 723−729. (d) Bulfield, D.; Huber, S. M. *Chem. - Eur. J.* **2016**, *22*, 14434−14450.

(15) (a) Metrangolo, P.; Neukirch, H.; Pilati, T.; Resnati, G. *Acc. Chem. Res.* **2005**, *38*, 386−395. (b) Lisac, K.; Topić, F.; Arhangelskis, M.; Cepić, S.; Julien, P. A.; Nickels, C. W.; Morris, A. J.; Friščić, T.; Cinčić, D. *Nat. Commun.* **2019**, *10*, 61.

(16) (a) Messina, M. T.; Metrangolo, P.; Panzeri, W.; Ragg, E.; Resnati, G. *Tetrahedron Lett.* **1998**, *39*, 9069−9072. (b) Metrangolo, P.; Panzeri, W.; Recupero, F.; Resnati, G. *J. Fluorine Chem.* **2002**, *114*, 27−33. (c) Sarwar, M. G.; Dragisic, B.; Salsberg, L. J.; Gouliaras, C.; Taylor, M. S. *J. Am. Chem. Soc.* **2010**, *132* (5), 1646−1653. (d) Erdelyi, M. *Chem. Soc. Rev.* **2012**, *41*, 3547−3557. (e) Hakkert, S. B.; Gräfenstein, J.; Erdelyi, M. *Faraday Discuss.* **2017**, *203*, 333−346.

(17) Wang, Y.; Wang, J.; Li, G.-X.; He, G.; Chen, G. *Org. Lett.* **2017**, *19*, 1442−1445.

(18) Sun, X.; Wang, W.; Li, Y.; Ma, J.; Yu, S. *Org. Lett.* **2016**, *18*, 4638−4641.

(19) Liu, Y.; Chen, X.-L.; Sun, K.; Li, X.-Y.; Zeng, F.-L.; Liu, X.-C.; Qu, L.-B.; Zhao, Y.-F.; Yu, B. *Org. Lett.* **2019**, *21*, 4019−4024.

(20) Tang, X.; Studer, A. *Angew. Chem., Int. Ed.* **2018**, *57*, 814−817.

DOI: 10.1021/acs.orglett.9b02812
Org. Lett. 2019, 21, 7823−7827

(21) Yajima, T.; Ikegami, M. *Eur. J. Org. Chem.* **2017**, *2017*, 2126−2129.
(22) Woźniak, Ł.; Murphy, J. J.; Melchiorre, P. *J. Am. Chem. Soc.* **2015**, *137*, 5678−5681.
(23) (a) Behrends, I.; Bähr, S.; Czekelius, C. *Chem. - Eur. J.* **2016**, *22*, 17177−17181. (b) Spittler, M.; Helmecke, L.; Czekelius, C. *Eur. J. Org. Chem.* **2019**, *2019*, 458−468.
(24) Lumbierres, M.; Moreno-Mañas, M.; Vallribera, A. *Tetrahedron* **2002**, *58*, 4061−4065.
(25) Huang, W.-Y.; Zhang, H.-Z. *J. Fluorine Chem.* **1990**, *50*, 133−140.
(26) Du Mont, W.-W.; Bätcher, M.; Pohl, S.; Saak, W. *Angew. Chem., Int. Ed. Engl.* **1987**, *26*, 912−913.
(27) (a) Filippini, G.; Silvi, M.; Melchiorre, P. *Angew. Chem., Int. Ed.* **2017**, *56*, 4447−4451. (b) Studer, A.; Curran, D. P. *Angew. Chem., Int. Ed.* **2016**, *55*, 58−102.
(28) Erdbrink, H.; Peuser, I.; Gerling, U. I. M.; Lentz, D.; Koksch, B.; Czekelius, C. *Org. Biomol. Chem.* **2012**, *10*, 8583−8586.
(29) Rosokha, S. V.; Kochi, J. K. *Acc. Chem. Res.* **2008**, *41*, 641−653.
(30) Sun, X.; He, Y.; Yu, S. *J. Photochem. Photobiol., A* **2018**, *355*, 326−331.
(31) Lecroq, W.; Bazille, P.; Morlet-Savary, F.; Breugst, M.; Lalevée, J.; Gaumont, A.-C.; Lakhdar, S. *Org. Lett.* **2018**, *20*, 4164−4167.
(32) Xu, Y.; Huang, J.; Gabidullin, B.; Bryce, D. L. *Chem. Commun.* **2018**, *54*, 11041−11043.

DOI: 10.1021/acs.orglett.9b02812
Org. Lett. 2019, 21, 7823−7827

6. Cumulative part III

6.1. Visible Light-Induced Homolytic Cleavage of Perfluoroalkyl Iodides Mediated by Phosphines

The experiments described in the publication: "Visible Light-Induced Homolytic Cleavage of Perfluoroalkyl Iodides Mediated by Phosphines"[5] and a brief discussion of the results will be summarized below. The individual contributions to this publication and the publication is presented without changes at the end of this chapter (p. 99).

In 2019 the iodoperfluoroalkylation of alkenes performed by using light and a phosphorus(III) compound as catalyst (10 mol%) was presented.[4] Unanswered questions resulted from this publication. It should be clarified why tri-*tert*-butylphosphine (**186**) achieved the best results as a catalyst while using blue light (461 nm) irradiation. Furthermore, it shall be clarified why tri-*n*-butylphosphine and trimethylphosphite are also suitable catalysts for this type of reaction. Moreover, the proposed mechanism in the previous publication[4] should be validated by the theoretical calculations.

Based on the already measured UV-VIS spectra,[4] theoretical calculations were performed by Mario Bracker.[5] The calculations revealed the interaction of the $^{t}Bu_3P$ and dichloromethane as solvent (Figure 11).

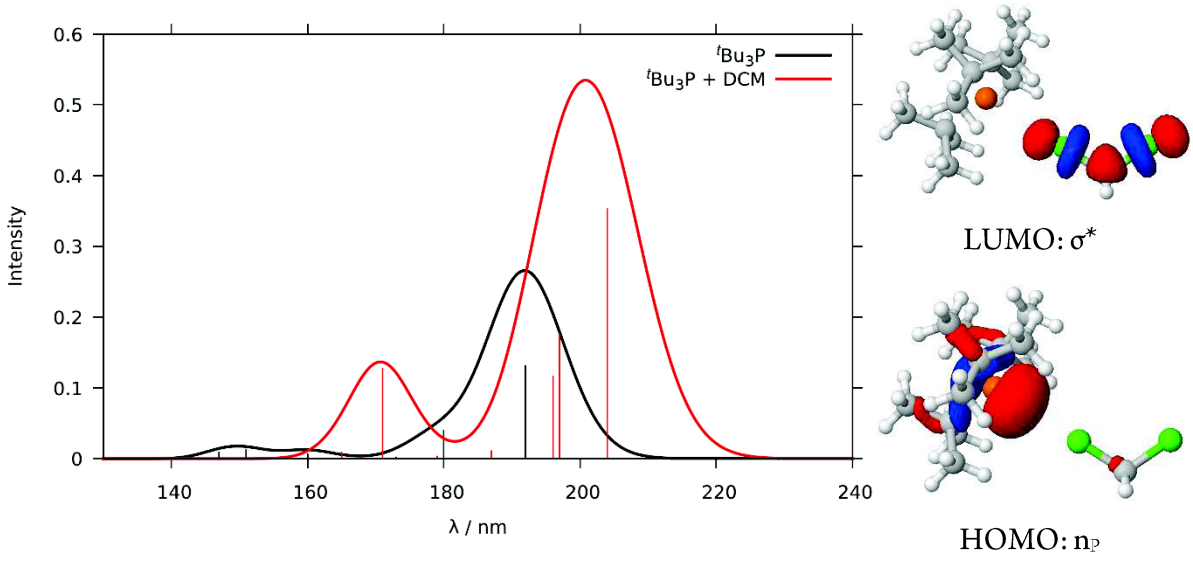

Figure 11: Calculated absorption spectra of $^{t}Bu_3P$ **186** in CH_2Cl_2 (black line: continuum solvent model; red line: $^{t}Bu_3P$-CH_2Cl_2 adduct sourrounded by a continuum solvent model of CH_2Cl_2) and frontier molecular orbitals of the adduct.[5]

Experimental UV-VIS measurements in pentane as a non-coordinating solvent were conducted to prove the calculations. In comparison to the measurements in pentane, the absorption was higher when dichloromethane was used as solvent (Figure 12).[5]

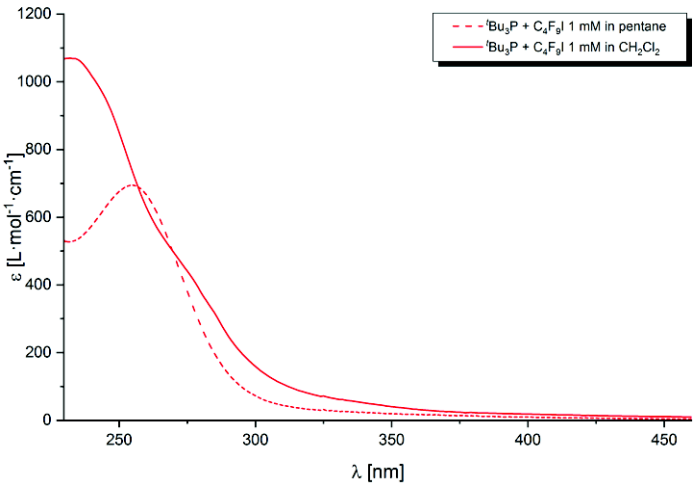

Figure 12: UV-VIS spectrum of ^{t}Bu$_3$P **186** and C$_4$F$_9$I **101** in pentane (dotted line) and in CH_2Cl_2 (straight line).[5]

Further calculations, based on relativistic density functional theory and multireference configuration interaction methods, clarified the occurrence of an increasing of the absorption coefficient and the wide tailing into the visible light region. For this reason, it is possible to cleave the C—I-bond with visible light instead of UV radiation by using ^{t}Bu$_3$P **186** as Lewis base.

Another open question was the difference between the catalytic activation of ^{t}Bu$_3$P **186** and the related phosphine ^{n}Bu$_3$P. Besides, the phosphite $(MeO)_3P$ was included in these calculations since it already showed good results in the catalyst screening experiments.[4] Experimentally the calculations were provided by two conformationally locked phosphites. By freezing the conformation, the influence of the oxygen orbitals to the reaction should be prevented.

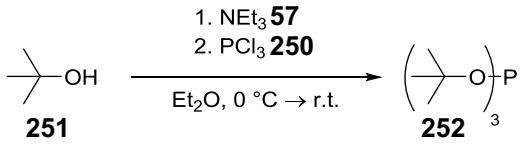

Scheme 78: Synthesis of tri-*tert*-butylphosphite (**252**).[5]

Tri-*tert*-butylphosphite (**252**) was synthesized from *tert*-butyl alcohol (**251**) using triethylamine (**57**) and phosphorus trichloride (**250**) (Scheme 78).[5] The second phosphite was synthezised from 2-(hydroxymethyl)-3-methylpropane-1,3-diol (**253**) to get a so called "caged posphite" **254** (Scheme 79).[5]

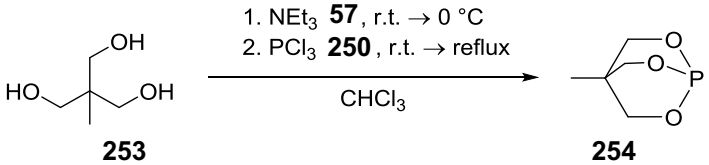

Scheme 79: Synthesis of the "caged phosphite" **254**.[5]

Both conformationally locked phosphites were tested in a reaction with 1-octene (**174**) and C_4F_9I **101**, but were not as reactive as trimethyl phosphite (Scheme 80). In case of the "caged phosphite" **254** no product formation was detected *via* ^1H- and ^{19}F-NMR spectroscopy.[5]

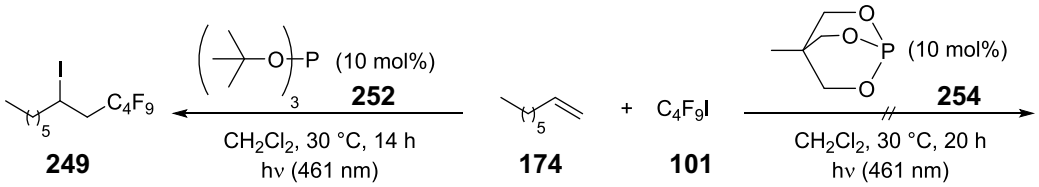

Scheme 80: Reaction with 1-octene (**174**) and C_4F_9I **101** using "caged phosphite" **254** and tri-*tert*-butylphosphite (**252**).[5]

By using tri-*tert*-butylphosphite (**252**) a conversion of 56% was detected after 14 h of irradiation. Due to the instability of tri-*tert*-butylphosphite (**252**),[108] the Lewis base as catalyst degrades with the reaction time. At least, a UV-VIS spectra of the synthesized phosphites with C_4F_9I **101** was measured. In the case of the "caged phosphite" **254** the tailing into the visible light region was weaker than for tri-*tert*-butylphosphite (**252**) and trimethyl phosphite (Figure 13).[5]

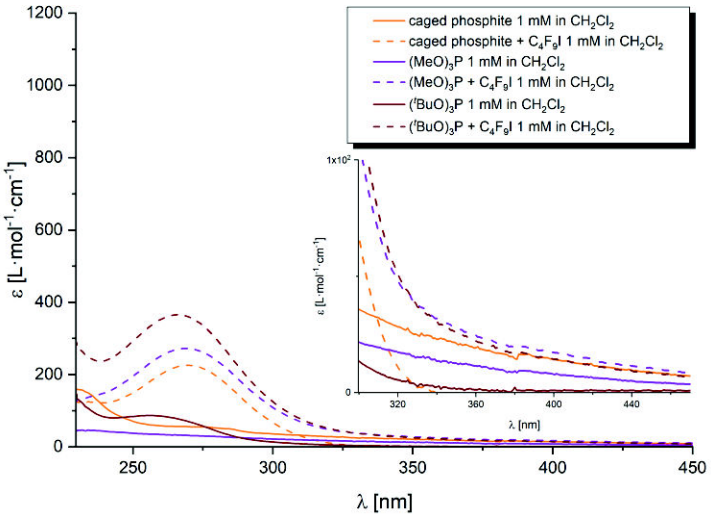

Figure 13: Experimental UV-VIS spectra of the "caged phosphite" **254**, trimethyl phosphite and tri-*tert*-butylphosphite (**252**).[5]

These results confirmed the theoretical assumption that in one conformation of the flexible trimethyl phosphite the oxygen lone pairs interact with the HOMO of the formed [$(RO)_3$-P—I-R_F] complex.[5]

6.2. Contributions to the publication

The publication "Visible Light-Induced Homolytic Cleavage of Perfluoroalkyl Iodides Mediated by Phosphines" was published in collaboration with Mario Bracker, Dr. M. Kleinschmidt, Prof. C. Czekelius und Prof. C. M. Marian.[5] The individual author contribution is listed as part of the publication.

L. Helmecke carried out the experimental investigations. This included the synthesis of the required phosphites (4-methyl-2,6,7-trioxa-1-phosphabicyclo-[2,2,2]-octane (**254**) ("caged phosphite") and tri-*tert*-butyl phosphite (**252**)) as well as the UV-VIS spectra. In addition, the experimental results were visualized.

M. Braker carried out the theoretical investigations and the corresponding visualization.

Dr. M. Kleinschmidt contributed to the conceptualisation, the supervision and the funding acquisition.

Prof. C. M. Marian contributed to the conceptualisation, the supervision, the funding acquisition and writing and preparation of the manuscript.

Prof. C. Czekelius was significantly involved in writing the manuscript, correction process and the revision of the manuscript and the supporting information.

molecules

MDPI

Article

Visible Light-Induced Homolytic Cleavage of Perfluoroalkyl Iodides Mediated by Phosphines

Mario Bracker [1], Lucas Helmecke [2], Martin Kleinschmidt [1,*], Constantin Czekelius [2,*] and Christel M. Marian [1,*]

[1] Institute of Theoretical and Computational Chemistry, Heinrich-Heine-University Düsseldorf, 40204 Düsseldorf, Germany; mario.bracker@hhu.de

[2] Institute of Organic and Macromolecular Chemistry, Heinrich-Heine-University Düsseldorf, 40204 Düsseldorf, Germany; lucas.helmecke@hhu.de

* Correspondence: Martin.Kleinschmidt@hhu.de (M.K.); Constantin.Czekelius@hhu.de (C.C.); Christel.Marian@hhu.de (C.M.M.); Tel.: +49-211-8113212 (M.K.); +49-211-8115362 (C.C.); +49-211-8113210 (C.M.M.)

Academic Editors: Paulo Jorge Costa and Fabrizio Santoro
Received: 14 February 2020; Accepted: 25 March 2020; Published: 1 April 2020

Abstract: In an effort to explain the experimentally observed variation of the photocatalytic activity of $^{t}Bu_3P$, $^{n}Bu_3P$ and $(MeO)_3P$ in the blue-light regime [Helmecke et al., Org. Lett. 21 (2019) 7823], we have explored the absorption characteristics of several phosphine– and phosphite–IC_4F_9 adducts by means of relativistic density functional theory and multireference configuration interaction methods. Based on the results of these computational and complementary experimental studies, we offer an explanation for the broad tailing of the absorption of $^{t}Bu_3P$-IC_4F_9 and $(MeO)_3P$-IC_4F_9 into the visible-light region. Larger coordinate displacements of the ground and excited singlet potential energy wells in $^{n}Bu_3P$-IC_4F_9, in particular with regard to the P–I–C bending angle, reduce the Franck–Condon factors and thus the absorption probability compared to $^{t}Bu_3P$-IC_4F_9. Spectroscopic and computational evaluation of conformationally flexible and locked phosphites suggests that the reactivity of $(MeO)_3P$ may be the result of oxygen lone-pair participation and concomitant broadening of absorption. The proposed mechanism for the phosphine-catalyzed homolytic C–I cleavage of perfluorobutane iodide involves $S_1 \leftarrow S_0$ absorption of the adduct followed by intersystem crossing to the photochemically active T_1 state.

Keywords: halogen bond; iodoperfluoroalkylation; radical; absorption spectra; adiabatic transition; intersystem crossing; density functional thory; multireference configuration interaction; spin–orbit coupling

1. Introduction

Organic compounds incorporating fluorine substituents or a perfluoroalkyl group show unique properties and are therefore very important synthetic targets in pharmaceutical research and industry [1–4]. The introduction of fluorine as the most electronegative element results in a different polarization profile of the molecule associated with improved pharmacodynamic and -kinetic properties. It is therefore not surprising that the development of a synthetic methodology for the efficient, safe, and environmentally benign preparation of these compounds by transition metal catalysis or photocatalysis has found increasing interest in the last decades [5–10].

The introduction of perfluoroalkyl groups or perfluoroalkanoates by addition of the corresponding perfluoroalkyl iodide to unsaturated hydrocarbons such as alkenes or alkynes is synthetically highly

valuable since a plethora of such starting materials are easily accessible and commercially available. In addition, subsequent displacement of the iodine substituent by nucleophilic substitution or metalation allows for further functionalization of the fluorinated molecule. The iodoperfluoroalkylations of double bonds can be initiated by homolytic C–I bond cleavage using radical initiators [11,12] or UV irradiation [13,14]. In cases where such conditions are not advisable for delicate substrates, photocatalytic methods [15–17] using visible light irradiation offers advantages. Herein, transition metal complexes based on iridium or ruthenium [18,19], as well as copper [20–22], have been successfully employed for atom transfer radical addition (ATRA) reactions.

In addition to metal complexes, organic photocatalysts have also been reported for iodoperfluoroalkylation reactions of unsaturated hydrocarbons, either by using them as triplet sensitizers [23,24] or by activation via the corresponding electron donor–acceptor (EDA) complexes [25–27]. In the latter case, the formation of a halogen bond between the electron-deficient perfluoroalkyl iodide and a suitable Lewis base results in homolytic bond cleavage upon irradiation of visible light. Amines [28–33], phenols [34], ketones [35,36], as well as phosphines [37–41] have been reported for this purpose in either stoichiometric or catalytic quantities.

In our studies addressing the Lewis-base-mediated iodoperfluoroalkylation of simple alkenes [40,42,43] we found that catalytic amounts of phosphines and phosphites effectively catalyze this process with complete regioselectivity upon irradiation with visible light (461 nm) (Scheme 1). Mechanistic investigations involving ^{19}F-NMR analysis suggested the intermediate formation of an EDA complex $F(CF_2)_n$–I $\cdots$ PR_3 by halogen bond formation to the phosphorus atom [44,45]. In addition, the reaction was shown to proceed via free perfluoroalkyl radicals. It is therefore assumed that visible light absorption of the EDA complex formation leads to homolytic bond cleavage and subsequent radical chain reaction.

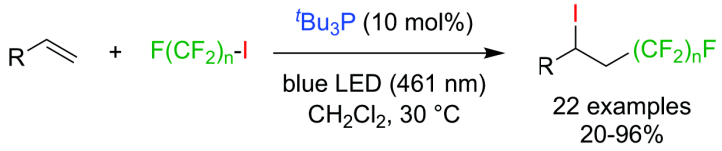

Scheme 1. Phosphine-catalyzed iodoperfluoroalkylation of simple alkenes.

Two observations called for a more detailed analysis, however. First, among the numerous tested phosphorus compounds, tri(*tert*-butyl)phosphine (^{t}Bu$_3$P) showed the fastest conversion, while tri(*n*-butyl)phosphine (^{n}Bu$_3$P) with comparable lone pair donor properties was much less efficient. In contrast, electron-deficient trimethylphosphite ((MeO)$_3$P) performed very well. Second, the UV-vis spectra of EDA complexes formed upon mixing perfluorobutyl iodide (C_4F_9I) with the above-mentioned phosphorus (III) compounds—without an alkene present—showed increased absorption but substantially different peak tailing into the visible light region [46]. In addition, in all cases the overlap of the EDA complex absorption with the emission spectrum of the blue LED employed in the reaction (λ_{max} = 461 nm) was very small (Figure 1). As a result, the different catalyst performances cannot be attributed exclusively to the absorption profile or the donor properties, but additional factors such as the geometry-dependency of the corresponding singlet–triplet transitions need to be taken into account. Therefore, we aimed at an improved understanding of the photochemical, homolytic bond cleavage process by calculation of the excited-state geometries of the perfluorobutyl iodide adducts [47–49] as well as a modeling of the intersystem crossing (ISC) process.

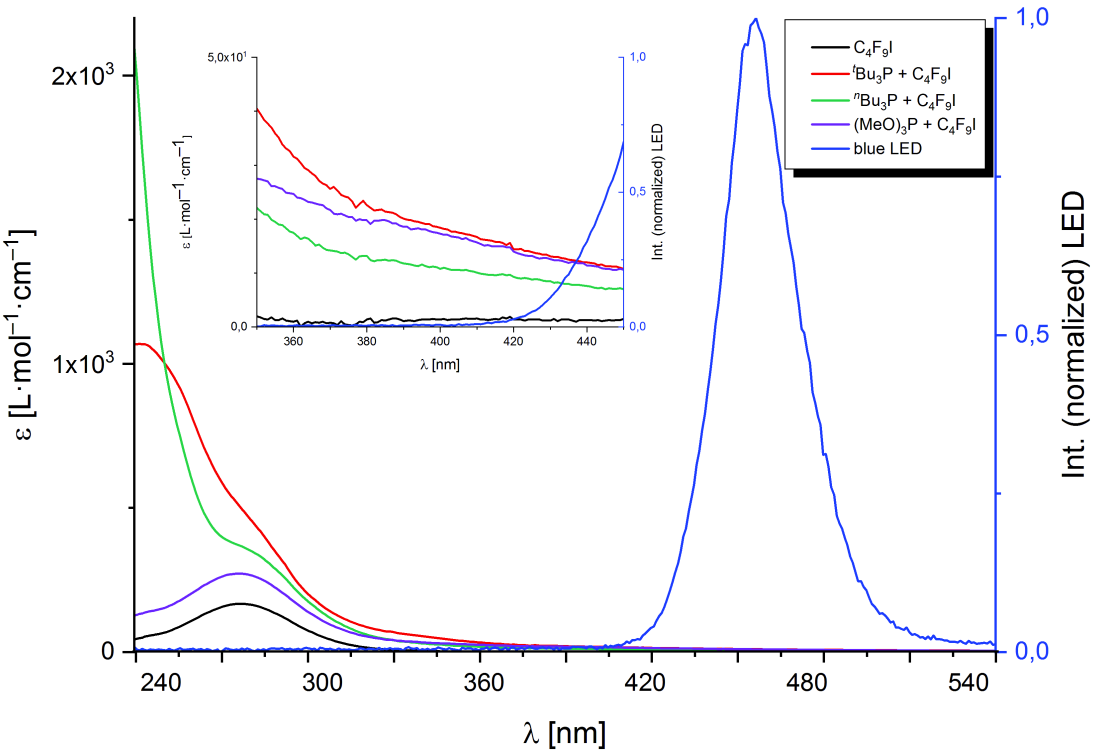

Figure 1. UV-vis spectra of C_4F_9I, $^tBu_3P$, $^nBu_3P$, $(MeO)_3P$ and mixtures of the phosphorus compounds with C_4F_9I.

2. Results

2.1. Quantum Chemical Characterization of the Compounds in the Franck–Condon Region

2.1.1. Perfluorobutyl Iodide

Due to the presence of the heavy iodine atom, relativistic calculations have to be performed for modeling the photophysics and photochemistry of the compounds. Spin selection rules are therefore not strictly obeyed. Spin–orbit interaction is particularly pronounced between electronic states involving differently oriented *p*-type orbitals, located at the iodine center, such as the lone-pair n_I orbitals that represent the nearly degenerate highest occupied molecular orbital (HOMO) and HOMO-1 in the C_4F_9I ground-state geometry. The C–I σ bonding (HOMO-2) and σ^* antibonding (lowest unoccupied molecular orbital, LUMO) involve iodine *p* atomic orbitals as well (Figure 2).

The vertical absorption spectrum of the non-coordinated perfluorobutyl iodide molecule is characterized by weak $(n_I \rightarrow \sigma^*)$ transitions in the middle-UV region and a strong $(\sigma \rightarrow \sigma^*)$ transition in the far UV (Figure S1). With regard to the current experiments, only the weak first absorption band is of interest. The spectral broadening and the enhancement of that band, which are observed when spin–orbit coupling (SOC) is switched on (Figure 2a), can be traced back to intensity borrowing of the spin-forbidden $^3(n_I\sigma^*)$ transitions from the optically bright $^1(\sigma\sigma^*)$ transition at 167 nm. Comparison between theory and experiment (Figures 2a and S2) reveals excellent agreement of the spectral shapes and absorption maxima λ_{max} (theory: 268 nm, experiment: 270 nm).

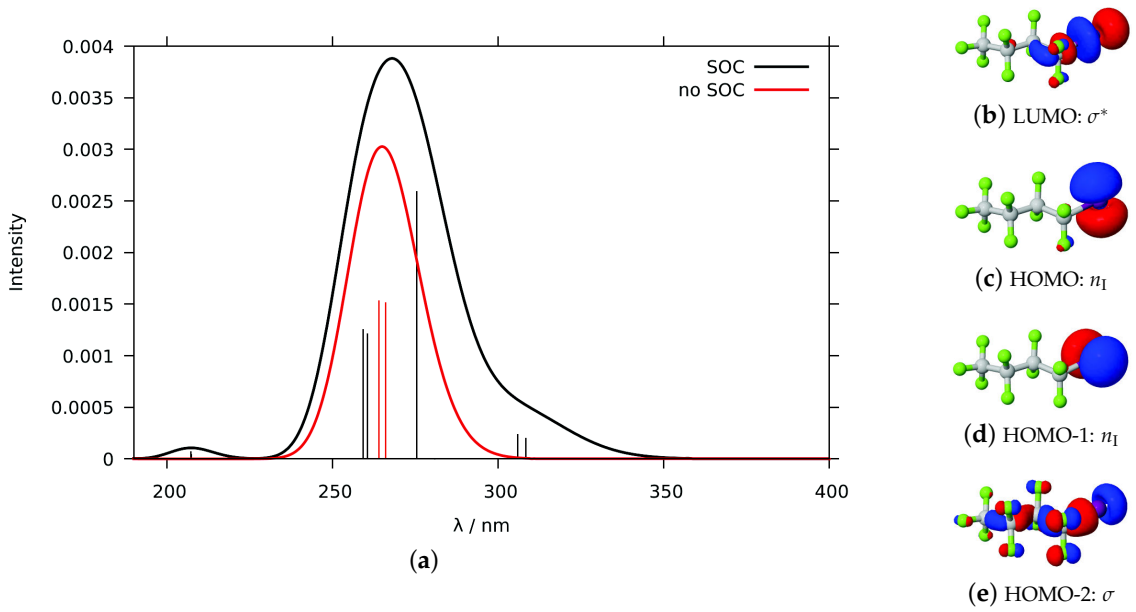

Figure 2. Calculated first absorption band of C_4F_9I (red: no spin–orbit coupling, only singlet transitions, black: including spin–orbit coupling, singlet as well as triplet transitions) and molecular orbitals involved in the transitions. The spectral envelope was obtained by broadening the line spectrum by Gaussians with standard deviation $\sigma = 1500$ cm^{-1}. HOMO denotes the highest occupied molecular orbital, LUMO the lowest unoccupied molecular orbital.

We observe a small red shift of the absorption maximum by 6 nm when basis sets of higher quality are employed, i.e., triple zeta plus polarization functions on all atoms (cf. Figure S3).

2.1.2. Phosphines

The first absorption band of the isolated ^{t}Bu$_3$P, ^{n}Bu$_3$P, and (MeO)$_3$P molecules peak at wavelengths shorter than 200 nm (Figure S4). Only their tails can be seen in the experimental observation window. They involve the respective lone-pair orbital on phosphorus, n_P, and a pair of nearly degenerate σ^* orbitals of the trialkylphosphine. In dichloromethane (DCM) solution, phophine–DCM adducts can be formed, with a marked impact on the photophysics (Figure 3a) [47–49]. The first excited singlet state of the adduct is an optically bright charge transfer (CT) state originating from the excitation of an n_P electron on the electron-rich phosphine to a σ^* orbital on DCM (Figure 3). This CT excitation is somewhat red-shifted with regard to the local phosphine excitations ($\lambda_{max} = 205$ nm in ^{t}Bu$_3$P–DCM compared to $\lambda_{max} = 192$ nm in ^{t}Bu$_3$P) but much stronger (oscillator strength $f = 0.353$ in ^{t}Bu$_3$P–DCM compared to $f = 0.132$ in ^{t}Bu$_3$P). The adduct complex is therefore expected to dominate the residual intensity of the ^{t}Bu$_3$P absorption in the low-energy regime. This assumption is supported by the experimental observation of a lower absorbance of ^{t}Bu$_3$P in non-coordinating solvents such as pentane in the wave length region > 250 nm (cf. Figure S5).

2.1.3. Phosphine–Perfluorobutyl Iodide Adducts

^{t}Bu$_3$P, ^{n}Bu$_3$P, and (MeO)$_3$P form perfluorobutyl iodide adducts with nearly linear C–I–P coordination in the electronic ground state. In line with the donor capabilities of these phosphines, the elongation of the I–C bond is most pronounced in the ^{t}Bu$_3$P–IC_4F_9 adduct and smallest in (MeO)$_3$P–IC_4F_9. (For details, see Table 1.)

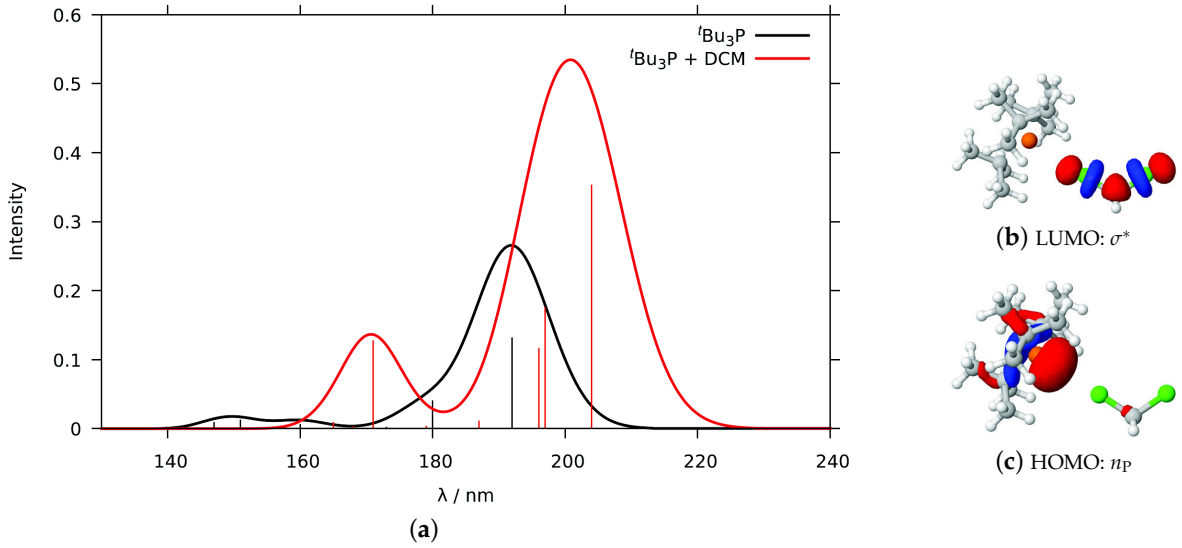

Figure 3. Calculated absorption spectra of $^{t}Bu_3P$ in DCM (black: continuum solvent model, red: $^{t}Bu_3P$-DCM adduct surrounded by a continuum solvent model of DCM) and frontier molecular orbitals of the $^{t}Bu_3P$-DCM monoadduct.

Table 1. Selected geometry parameters of perfluorobutyl iodide and its phosphine and phosphite adducts in the electronic ground state (S_0), the first excited triplet (T_1), and singlet (S_1) state.

Compound	P–I Bond Length/pm			I–C Bond Length/pm			P–I–C Bond Angle/°		
	S_0	T_1	S_1	S_0	T_1	S_1	S_0	T_1	S_1
C_4F_9I				216					
$^{t}Bu_3P$-IC_4F_9	297	303	343	225	309	270	179	110	104
$^{n}Bu_3P$-IC_4F_9	297	308	331[a]	224	292	281[a]	177	76	96[a]
$(MeO)_3P$-IC_4F_9	316	294	320[a]	220	318	294[a]	179	78	96[a]

[a] S_1/S_0 conical intersection.

In all phosphine adducts, the HOMO is predominantly composed of the lone-pair orbital on phosphorus (n_P), whereas the LUMO is a σ^*-type orbital. MO plots are shown for $^{t}Bu_3P$-IC_4F_9 in Figure 4, whereas those of the other adduct compounds may be found in Figures S6 and S7.

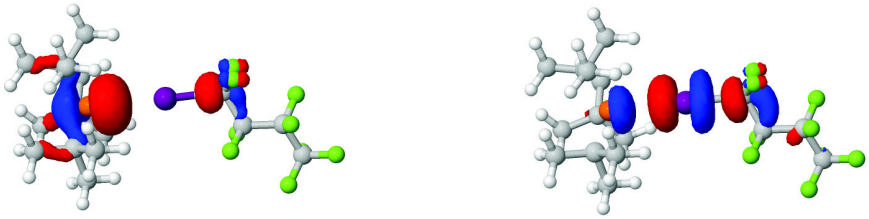

Figure 4. Frontier molecular orbitals of the $^{t}Bu_3P$-IC_4F_9 adduct at the S_0 geometry.

The direct $T_1 \leftarrow S_0$ transitions of all phosphine adducts have negligible oscillator strengths in the Franck–Condon (FC) region. The strongly absorbing $^{1}(n_P\sigma^*)$ CT state forms the first excited singlet state of $^{t}Bu_3P$-IC_4F_9. The triplet excitations from the two lone-pair orbitals on the iodine center (n_I) to the

σ^*-orbital are close in energy but SOC between these states is not very pronounced. For this reason, the first $S_1 \leftarrow S_0$ absorption maxima computed in the absence and presence of SOC are nearly identical (cf. Figure S8). A qualitatively similar energy scheme is obtained in the case of ^{n}Bu$_3$P-IC$_4$F$_9$ whose calculated absorption maximum is somewhat blue-shifted. In (MeO)$_3$P-IC$_4$F$_9$, the much weaker $^1(n_I\sigma^*)$ transitions are energetically favored over the $^1(n_P\sigma^*)$ CT transition, but the states are close in energy. In line with the lower electron donor capabilities of (MeO)$_3$P, the peak maximum is even more blue-shifted.

While the trends among the phosphine adducts are reproduced correctly, the computed absorption bands of the CT transitions (Figure 5) are red-shifted with respect to the corresponding experimental data (Figure 1) by about 20 nm. Note, however, that the transparency of the dichloromethane solvent quickly degrades for wavelengths shorter than 240 nm. To check the influence of the solvent on the absorption characteristics, the experiment was repeated for ^{t}Bu$_3$P-IC$_4$F$_9$ in pentane solution (transparency $\geq$ 90% up to 220 nm). And indeed, the first absorption band peaks at 255 nm in that solvent before the cut-off is reached (cf. Figures S2, S9 and S10).

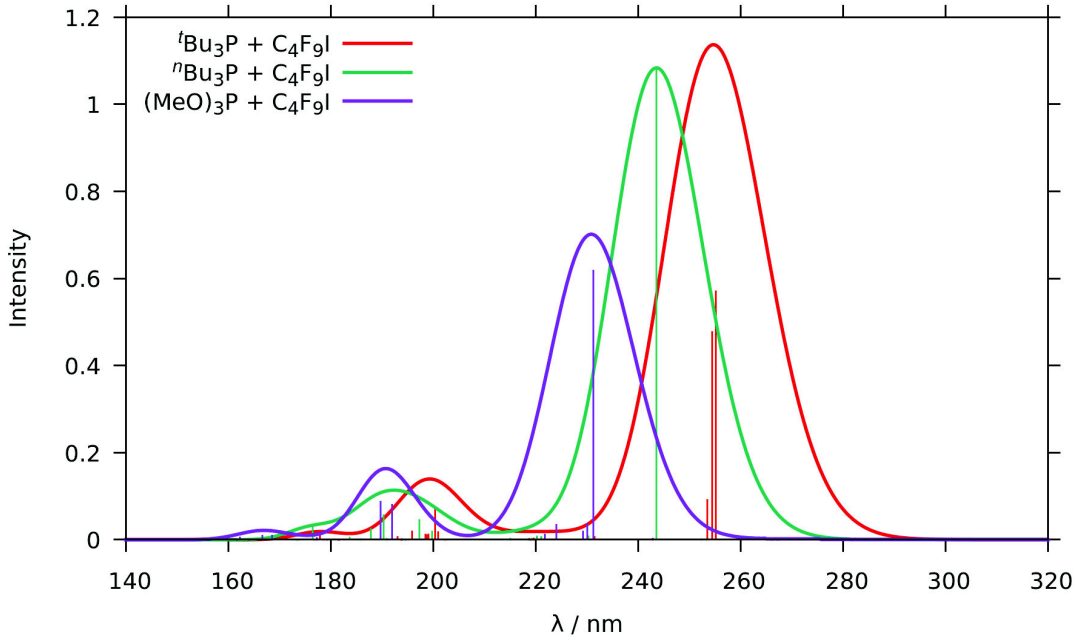

Figure 5. Calculated absorption spectra of the phosphine and phosphite adducts in DCM including spin–orbit coupling (SOC).

Despite the good agreement between theory and experiment with regard to absorption maxima, quantum chemical calculations, performed at the respective ground-state geometries of the adducts, are not sufficient to explain the blue-light excitation of the compounds and their photochemistry. To this end, adiabatic excitation energies and minimum geometries of the lowest excited singlet and triplet states have to be known.

Similar to the basis set dependence of the C$_4$F$_9$I absorption, we observe a small red shift (4 nm) and a slight increase of the intensity of the first absorption band of the ^{t}Bu$_3$P-IC$_4$F$_9$ adduct when using a better atomic orbital basis set (cf. Figure S11). In view of the small changes and the markedly higher computational cost, we refrain from carrying out the elaborate excited-state geometry optimizations using the TZVP basis sets.

2.2. Relaxed Excited-State Geometries of the Phosphine–Perfluorobutyl Iodide Adducts

2.2.1. The First Excited Triplet State

The T_1 states form very shallow basins in the I–C dissociative region of the respective potential energy surfaces (PESs) (cf. heatmaps in Figure 6a–c).

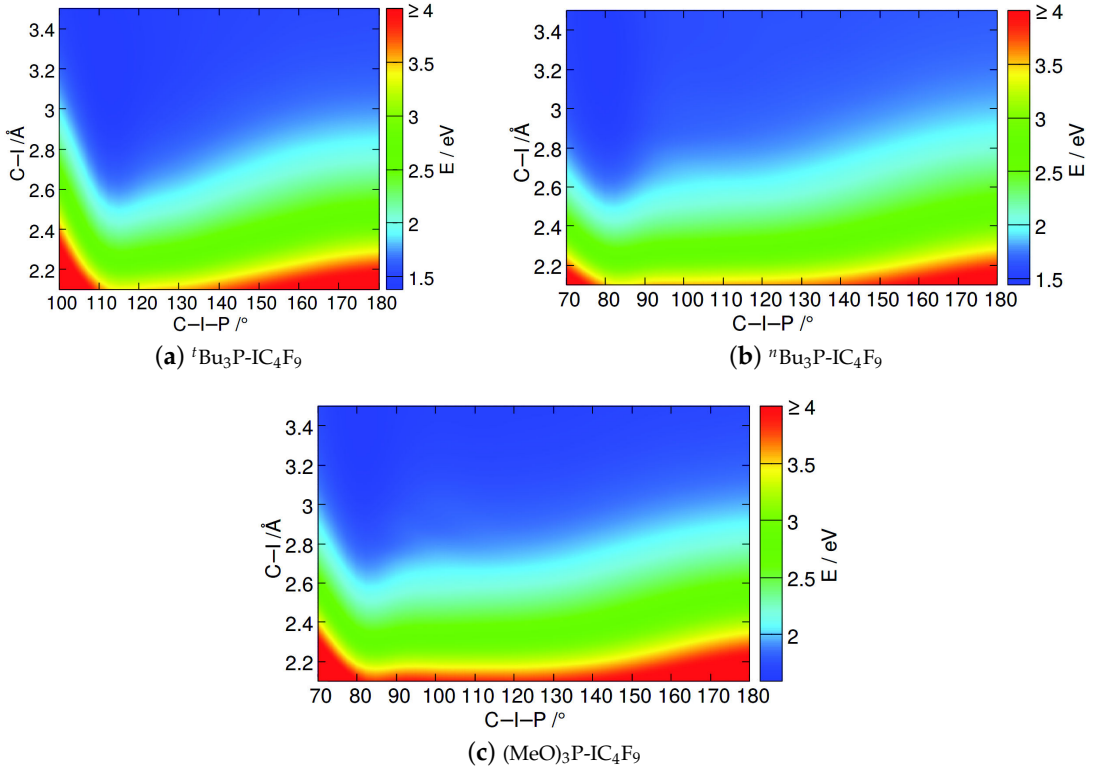

(**a**) $^{t}Bu_3P\text{-}IC_4F_9$ (**b**) $^{n}Bu_3P\text{-}IC_4F_9$

(**c**) $(MeO)_3P\text{-}IC_4F_9$

Figure 6. Heatmaps of the T_1 potential energy surfaces of the phosphine and phosphite adducts as functions of the C–I bond length and the C–I–P angle. All other internal coordinates were kept fixed to the minimum geometry parameters of the respective T_1 state. The energy scales on the right refer to DFT and multireference configuration interaction (DFT/MRCI) energies relative to the ground-state minimum. Note the different scales of the *x*-axes.

Here, the biradicalic triplet is the lowest-energy state, and I–C bond cleavage can proceed nearly without any barrier. In addition to the markedly increased I–C bond length, we notice significant changes of the P–I–C bond angle with respect to the diamagnetic species (cf. Table 1). The P–I–C bond angle varies among the three adducts from approximately 110° in $^{t}Bu_3P\text{-}IC_4F_9$ for the phosphine with the largest steric demand to less than 80° in $^{n}Bu_3P\text{-}IC_4F_9$ and $(MeO)_3P\text{-}IC_4F_9$ (Figure 7). The electronic structures of the T_1 states (cf. Figure S12 for the singly occupied molecular orbitals, SOMOs) are in qualitative agreement with the picture of a perfluoroakyl radical attached to a negatively charged iodine and a phosphine radical cation ($F_9C_4^{\bullet} \cdots {}^{\ominus}I^{\bullet\oplus}PR_3$).

Adiabatically, the T_1 minima are located between 1.42 and 1.62 eV (Table 2) above the corresponding S_0 minima—too high in energy to be reached by thermal activation. Direct light activation is doomed to fail as well because the singlet–triplet mixing is too low in this CT state for making direct $T_1 \leftarrow S_0$ absorption

feasible (vide infra). The most probable activation pathway of the triplet channel is photoexcitation of the S_1 state followed by ISC to the T_1 PES.

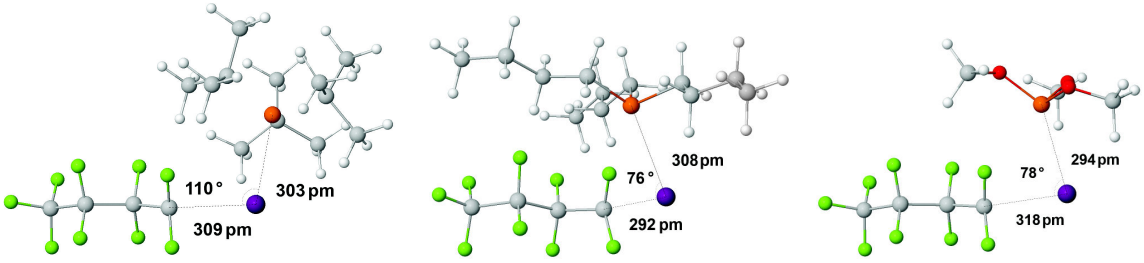

(**a**) $^{t}Bu_3P$-IC_4F_9 (**b**) $^{n}Bu_3P$-IC_4F_9 (**c**) $(MeO)_3P$-IC_4F_9

Figure 7. Nuclear arrangement of the phosphine–IC_4F_9 adducts at the optimized T_1 minima.

Table 2. Vertical and adiabatic excitation energies (ΔE_{vert} and ΔE_{adia}/eV) and corresponding transition wavelengths (λ_{vert} and λ_{adia}/nm) including SOC at the DFT/multireference spin–orbit configuration interaction (MRSOCI) level of theory. Triplet energies have been averaged over the three states with largest T_1 contributions.

Compound	**T_1**				**S_1**			
	ΔE_{vert}	**λ_{vert}**	**ΔE_{adia}**	**λ_{adia}**	**ΔE_{vert}**	**λ_{vert}**	**ΔE_{adia}**	**λ_{adia}**
$^{t}Bu_3P$-IC_4F_9	3.70	335	1.42	870	4.84	256	1.70	729
$^{n}Bu_3P$-IC_4F_9	3.91	317	1.46	850	5.07	245	1.82[a]	681[a]
$(MeO)_3P$-IC_4F_9	4.48	276	1.62	765	5.34	232	1.87[a]	663[a]

[a] S_1/S_0 conical intersection.

2.2.2. The First Excited Singlet State

Unfortunately, minima on the S_1 PESs of the phosphine-IC_4F_9 adducts could not be determined using the same computational protocol as for the T_1 states. Upon relaxation of the S_1 geometry at the time-dependent density functional theory (TDDFT)-Tamm–Dancoff approximation (TDA) level, the S_1 and S_0 states of all adducts undergo conical intersections where the calculation stops. Subsequent multireference configuration interaction (MRCI) single-point calculations revealed substantial double excitation contributions to the S_o and S_1 wave functions at these geometries. We therefore preformed minimum searches based on numerical MRCI gradients to locate the lowest points on the S_1 PESs. The nuclear arrangements at these minima are displayed in Figure 8 together with the course of the S_0 and S_1 potential energies along linearly interpolated paths connecting the singlet ground and excited state minima.

While the S_0 and S_1 potentials of $^{t}Bu_3P$-IC_4F_9 still exhibit a small energy gap of about 0.20 eV at the S_1 minimum, S_0 and S_1 are practically degenerate at the relaxed S_1 geometries of $^{n}Bu_3P$-IC_4F_9 and $(MeO)_3P$-IC_4F_9 and underdo conical intersections. In any case, the S_0 and S_1 wave functions are strongly mixed in the neighborhood, and non-adiabatic coupling is large. On the one hand, we therefore expect non-radiative deactivation by internal conversion (IC) to the electronic ground state to be fast in all phosphine adducts. On the other hand, the T_1-dominated states lie energetically close as well ($\Delta E_{S_1-T_1} \leq 0.20$ eV) and their mutual spin–orbit couplings (Figure 9a) should suffice to transfer substantial population from S_1 to T_1 by ISC. Whether the photochemically active triplet channels can be reached depends on subtle differences between the competing IC and ISC dynamics.

The entries in Table 2 show that the origins of the $S_1 \leftarrow S_0$ transitions of all phosphine adducts can, in principle, be reached by irradiation with the blue LED ($\lambda_{max} = 461$ nm) used in the experiment. Despite

the higher vertical excitation energy of $(MeO)_3P–IC_4F_9$ in the FC region compared to $^tBu_3P–IC_4F_9$, we find nearly equal adiabatic S_1-S_0 energies in all adduct complexes. Moreover, while the computed oscillator strength of the $S_1 \leftarrow S_0$ absorption of the $^nBu_3P$-IC_4F_9 adduct is somewhat smaller than in the $^tBu_3P–IC_4F_9$ adduct (Figure 9b), it is substantially larger than the corresponding quantity in the $(MeO)_3P–IC_4F_9$ adduct. One may therefore wonder why the experimentally observed absorption intensity of the $^nBu_3P$-IC_4F_9 adduct is so much weaker than that of the two other compounds in the blue-light regime.

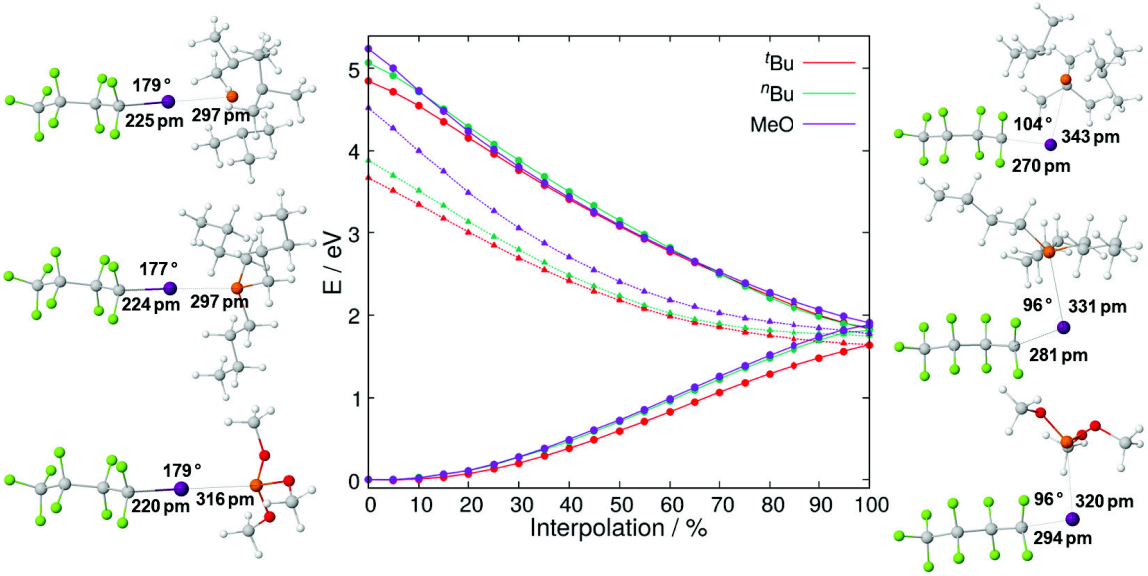

Figure 8. Energy profiles of the ground and first excited singlet states (solid lines) and the first excited triplet states (dotted lines) of the phosphine–IC_4F_9 adducts along linearly interpolated paths connecting the S_0 minimum (left, 0%) and the optimized S_1 geometry (right, 100%).

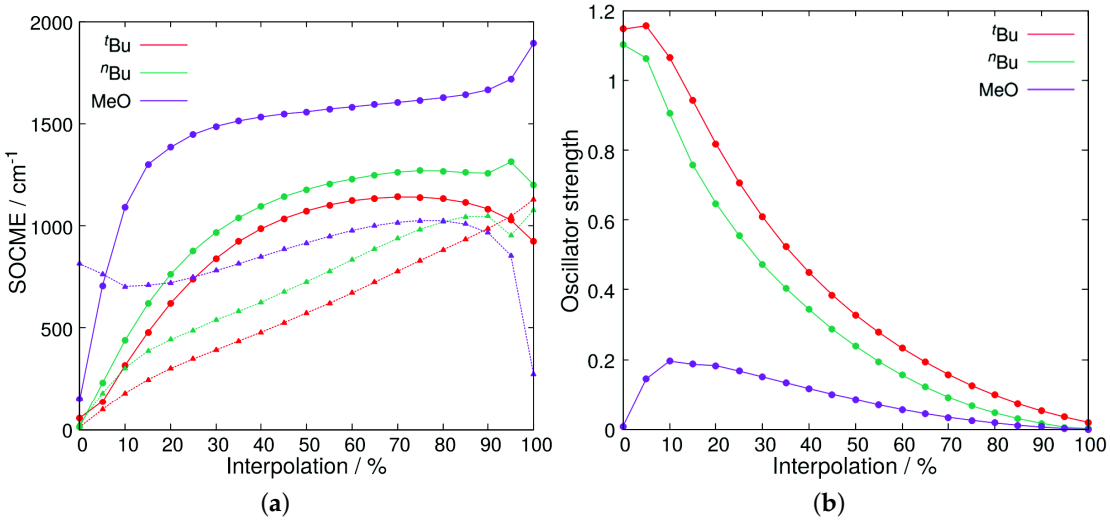

Figure 9. (**a**) Spin–orbit coupling matrix elements $|\langle T_1|\hat{\mathcal{H}}_{so}|S_0\rangle|$ (dotted lines) and $|\langle T_1|\hat{\mathcal{H}}_{so}|S_1\rangle|$ (solid lines) and (**b**) oscillator strengths of the $S_1 \leftarrow S_0$ transitions along linearly interpolated paths connecting the S_0 minimum (0%) and the optimized S_1 geometry (100%).

On a related note, the high efficiency of $(MeO)_3P$ as catalyst in the iodoperfluoroalkylation contrasts with both the smaller maximal absorption and its weaker Lewis basicity. Moreover, it seems to be correlated with the broad tailing of the absorption into the visible light region. The HOMO of the $(MeO)_3P$–IC_4F_9 adduct shows a substantial participation of the oxygen lone pairs (Figure 10a). This suggests a strong influence of the conformational flexibility of the alkoxide substituents upon the HOMO energy. This should lead to absorption band broadening due to a large ensemble of different conformers. Since a complete analysis of the conformational space and its corresponding excited states of $F(CF_2)_n$-I$\cdots$P$(OMe)_3$ was out of reach, we aimed at the spectroscopic and computational evaluation of different, conformationally locked phosphites, such as the "caged" phosphite 4-methyl-2,6,7-trioxa-1-phosphabicyclo[2.2.2]octane and tri(*tert*-butyl)phosphite (^{t}BuO)$_3$P [50–52]. In the case of the caged phosphite, the oxygen lone pairs point in the same direction as the phosphorus lone pair. Accordingly, substantial participation was not found in the HOMO but only in the HOMO-2 orbital (Figure 10b). In contrast, the highly rigid (^{t}BuO)$_3$P with the oxygen lone pairs pointing backwards shows their strong participation in the HOMO of the adduct with (I-P-O-C) dihedral angles of 62–64° (Figure 10c).

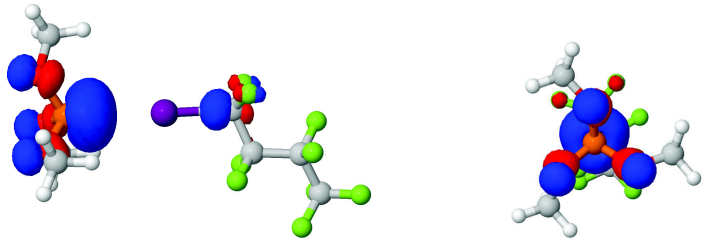

(**a**) $(MeO)_3P$-IC_4F_9: HOMO, side and rear view

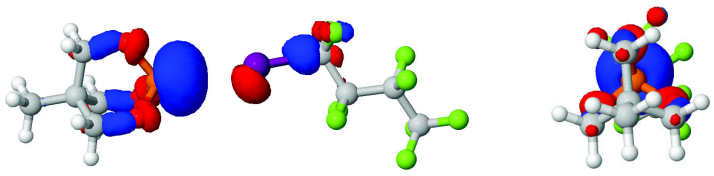

(**b**) $C_5H_9O_3P$-IC_4F_9: HOMO-2, side and rear view

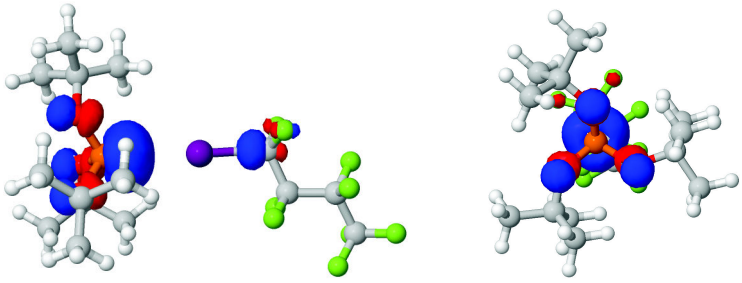

(**c**) (^{t}BuO)$_3$P-IC_4F_9: HOMO, side and rear view

Figure 10. Frontier molecular orbitals of the phosphite–IC_4F_9 adducts at the S_0 geometry.

The corresponding calculated absorption spectra (Figure 11a) for the three phosphite adducts show a substantial difference in excitation energies supporting this assumption further. These findings correlate with the experimental, spectroscopic analysis of the corresponding perfluoroalkyl iodide–phosphite complexes (Figure 11b). Complex formation in solution is less pronounced than in the case of phosphines. Therefore, absorption in the region of 240–320 nm is dominated by free perfluoroalkyl iodide. The caged

phosphite shows very small broadening in absorption and was also completely inactive as catalysts; (^{t}BuO)$_3$P showed increased absorption and substantial tailing into the visible light region. It should be noted, however, that tailing was even more pronounced for (MeO)$_3$P and a stronger absorption above 440 nm correlates with higher activity as catalyst.

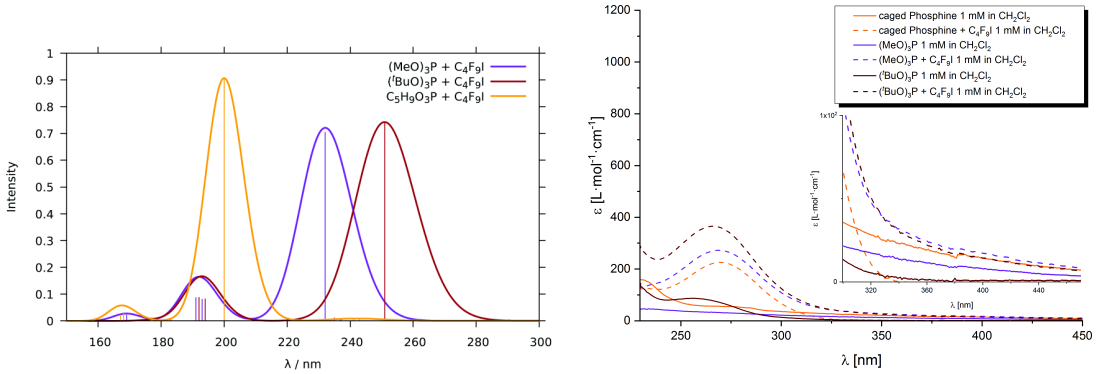

(**a**) (**b**)

Figure 11. (**a**) Calculated and (**b**) measured absorption spectra of the three phosphite–IC$_4$F$_9$ adducts. In addition, experimental absorption spectra of the pure phosphites in DCM solution are shown.

3. Discussion

To understand the different photochemical behaviors of the adducts, we note that the probability $W_{\mathrm{rad}}^{\mathrm{FC}}(f-i)$ of a radiative transition from an initial electronic state i to a final electronic state f,

$$W_{\mathrm{rad}}^{\mathrm{FC}}(f-i) = \frac{4e^2}{3c^3\hbar^4}\sum_b\sum_a (E_{f,b}-E_{i,a})^3 \left|\langle\Psi_f|\hat{\mu}|\Psi_i\rangle\right|^2 \left|\langle v_{f,b}|v_{i,a}\rangle\right|^2, \quad (1)$$

does not depend solely on the electric transition dipole moment $\left|\langle\Psi_f|\hat{\mu}|\Psi_i\rangle\right|$ and the energy difference $(E_f - E_i)$ of the two states. Through the Franck–Condon factors $\left|\langle v_{f,b}|v_{i,a}\rangle\right|^2$, i.e., the squared overlaps of the vibrational wave functions, it depends on the coordinate displacements of the two potential minima as well. In Equation (1), e denotes the charge of the electron, c the velocity of light, and $\hbar$ the Planck constant h divided by 2π.

Inspection of the molecular structures in Figure 8 reveals that the S$_1$ minimum of the ^{t}Bu$_3$P-IC$_4$F$_9$ adduct lies geometrically somewhat closer to the corresponding ground-state equilibrium than the ^{n}Bu$_3$P-IC$_4$F$_9$ and (MeO)$_3$P-IC$_4$F$_9$ adducts. The closer geometrical distance between the S$_0$ and S$_1$ minima is also reflected in the slightly shallower slope of the ground-state energy profile in Figure 8. In particular, the small overlap of the ground- and excited-state vibrational wave functions in the C–I–P angle bending coordinate of ^{n}Bu$_3$P-IC$_4$F$_9$ hampers the transition from the nearly linear ground-state equilibrium structure to the bent structure in the S$_1$ potential well. This overlap is not large in ^{t}Bu$_3$P-IC$_4$F$_9$ either, but it appears sufficient to explain the stronger residual absorption of the S$_1$ state in the blue wavelength region (cf. Figure 1). We note further that the oscillator strength of the S$_1$ ←S$_0$ transition is the largest one among the three complexes (Table 2).

In all three cases, the S$_1$ minimum lies geometrically in the exit channel of the T$_1$ state toward C–I dissociation. The mutual SOC of the S$_1$ and T$_1$ states in this region implies that S$_1$ ⇝T$_1$ ISC is possible in competition with S$_1$ ⇝S$_0$ internal conversion back to the S$_0$ minimum. Based on these data, we propose

the following mechanism for the blue-light-initiated phosphine-catalyzed homolytic C–I cleavage of perfluorobutane iodide:

$$\begin{array}{rcl} {}^1(R_3P + IC_4F_9) & \rightarrow & {}^1(R_3P - IC_4F_9) \overset{\text{blue LED}}{\rightleftharpoons} {}^1(R_3P - IC_4F_9)^* \\ & \overset{\text{ISC}}{\rightsquigarrow} & {}^3(R_3P^{\oplus\bullet} - I^{\ominus} \cdots C_4F_9)^* \rightarrow R_3PI^{\rceil\bullet} + {}^\bullet C_4F_9. \end{array} \quad (2)$$

While the different behavior of the phosphines ^{t}Bu$_3$P and ^{n}Bu$_3$P can be correlated primarily by their absorption profile, the surprisingly high reactivity of (some) phosphites may be the result of oxygen lone-pair participation and concomitant broadening of absorption. The strong tailing in the case of (MeO)$_3$P and the associated relatively high absorption above 440 nm may be explained by its high conformational flexibility. Due to rotation about the P–O bond, energetically disfavored conformers are accessible in small fractions that show optimal orbital alignment for excitation. In the case of the conformationally locked (^{t}BuO)$_3$P, the oxygen lone pairs are already in a suitable position but the associated energy barriers are higher and the optimal geometry for excitation may be out of reach.

4. Materials and Methods

4.1. Computational Methods

Closed-shell ground-state geometries were optimized with resricted Kohn–Sham (KS) density functional theory (DFT) using Turbomole [53–55] in conjunction with the B3-LYP functional [56,57], Grimme D3-BJ dispersion corrections [58,59] and the continuum solvent model COSMO [60,61] for mimicking a DCM solvent environment. Unless stated otherwise, the def2-SVP atomic orbital basis sets [62] from the Turbomole library were utilized for all atoms, save for iodine, which was represented by a relativistic small-core effective core potential and the corresponding def2-TZVPD basis [63]. To check the sensitivity of the results with respect to the choice of atomic orbital basis set, additional test calculations on the absorption properties of C_4F_9I and its ^{t}Bu$_3$P adduct were performed employing the larger def2-TZVP basis sets for H, C, F, and P [64,65], while keeping the iodine basis set unmodified. Triplet geometry optimizations were performed with the corresponding time-dependent DFT (TDDFT) [66] module using the Tamm–Dancoff approximation [67] (TDA) to TDDFT. In (MeO)$_3$P-IC$_4$F$_9$, where TDDFT-TDA did not converge, we employed unrestricted KS DFT instead for the geometry optimization of the triplet state. Numerical second derivatives for vibrational analyses were computed with SNF [68].

Minimum searches at the TDDFT level were not successful for the excited singlet states of the adducts. In these cases, we employed a computational protocol based on numerical DFT/MRCI gradients [69]. The combined DFT and multireference configuration interaction (DFT/MRCI) [70,71] approach was used in conjunction with the semiempirical R2018 Hamiltonian [72] and the standard configuration selection threshold of 1.0 E_h to determine spin–orbit free excitation energies and oscillator strengths. The KS orbitals and orbital energies for the DFT/MRCI calculations were optimized utilizing the BH-LYP [57,73] density functional, empirical dispersion corrections [58,59], and an implicit DCM solvent environment [60,61]. Auxiliary basis sets for the resolution-of-the-identity approximation of the two-electron integrals [70,74] were taken from the Turbomole library [55], i.e., we chose the def2-TZVPD auxiliary basis set [75] on iodine and the def2-SVP sets [64] on all other atoms.

Interstate spin–orbit coupling matrix elements (SOCMEs) for determining the probability of ISC were computed by the SPOCK program [76–78] using a spin–orbit effective core potential for iodine [63] and an effective one-center mean-field approximation to the Breit–Pauli SOC operator [79,80] for the lighter elements. For efficiency reasons, vertical excitation energies and oscillator strengths of multiplicity-mixed wave functions were determined by quasi-degenerate perturbation theory (QDPT) in the basis of

DFT/MRCI wave functions. Adiabatic excitation energies including SOC were obtained by means of multireference spin–orbit configuration interaction (MRSOCI) [81] calculations.

4.2. Experimental Procedures

All preparations involving air- and moisture-sensitive compounds were carried out inside a glove box (*Vacuum Atmospheres* model OMNI-LAB) under N_2 atmosphere (*Air Liquide ALPHAGAZ*^{TM} 5.0). Glassware was dried for 2 h at 120 °C and cooled down in vacuo.

Nonafluoro-1-iodobutane was purchased from TCI and was filtered through a column packed with aluminum oxide 90 basic 0.063–0.200 mm (activity stage I) and an activated molecular sieve (4 Å) under N_2 atmosphere. The clear and colorless liquid was stored in amber glass vials under N_2 atmosphere. Tri-tert-butylphosphine was purchased from Sigma Aldrich. 4-Methyl-2,6,7-trioxa-1-phosphabicyclo[2.2.2]octane [82] and tri(*tert*-butyl)phosphite [50,83] were prepared according to the literature.

Pentane and dichloromethane were dried with the solvent purification system MP-SPS 800 from M. Braun and degassed with freeze-pump-thaw. UV-vis measurements were performed on a Perkin Elmer Lamda 2 UV-vis spectrometer in Hellma cuvettes (10 × 10 mm, Suprasil quartz glass).

5. Conclusions

The results of the present computational chemistry study support the mechanism of a phosphine-assisted light-induced homolytic C–I bond cleavage, proposed earlier by some of us [40] on the basis of experimental observations. In addition, they provide an explanation for the fact that $^{t}Bu_3P$ is a much better photocatalyst in the blue-light regime than $^{n}Bu_3P$. While the origin of the $S_1 \leftarrow S_0$ absorption band should be energetically accessible to blue-light radiation in both butylphosphine–IC_4F_9 adducts, the larger coordinate displacements of the ground and excited singlet potential energy wells in $^{n}Bu_3P$-IC_4F_9 reduce the overlaps of the vibrational wave functions and thus the absorption probability compared to $^{t}Bu_3P$-IC_4F_9. Due to the presence of iodine and its involvement in the electronic transitions, spin–orbit coupling is strong enough to enable intersystem crossing and to facilitate the population of the biradicalic triplet state, which is the photochemically active state.

The fact that both $^{t}Bu_3P$ and $(MeO)_3P$ are active catalysts for the iodoperfluoroalkylation can be rationalized by two different factors. In the case of the bulky phosphine as strong Lewis base donor, the overall increase in absorption results in a tailing into the visible light region sufficient for radical generation. In the case of the electron-deficient, conformationally flexible phosphite, the overall increase of absorption is only small, but efficient oxygen lone-pair participation in the HOMO, found in a small fraction of conformers, may be the reason for the observed broad tailing into the longer wavelength region and concomitant catalytic activity.

Supplementary Materials: The following are available online. Description of general experimental procedures, synthesis of phosphites, reactions, NMR spectra, UV-vis measurements and further computational details, Figure S1: Calculated absorption spectra of C_4F_9I in CH_2Cl_2 with and without SOC, Figure S2: Experimental UV-vis spectra of C_4F_9I, $^{t}Bu_3P$, and $^{t}Bu_3P$ + C_4F_9I in CH_2Cl_2, Figure S3: Atomic orbital basis set dependence of the calculated absorption spectrum of C_4F_9I (190–400 nm) in CH_2Cl_2, Figure S4: Computed absorption spectra of the phosphines ($^{t}Bu_3P$, $^{n}Bu_3P$) and the phosphite $(MeO)_3P$ in CH_2Cl_2 with SOC, Figure S5: Comparison of the experimental UV-vis spectra of $^{t}Bu_3P$ in pentane and in CH_2Cl_2, Figure S6: Frontier molecular orbitals of the $^{n}Bu_3P$-IC_4F_9 adduct, Figure S7: Frontier molecular orbitals of the $(MeO)_3P$-IC_4F_9 adduct, Figure S8: Calculated absorption spectra of $^{t}Bu_3P$–C_4F_9I in CH_2Cl_2 with and without SOC, Figure S9: Experimental UV-vis spectra of C_4F_9I, $^{t}Bu_3P$, and $^{t}Bu_3P$ + C_4F_9I in pentane, Figure S10: Comparison of the experimental UV-vis spectra of $^{t}Bu_3P$ + C_4F_9I in pentane and in CH_2Cl_2, Figure S11: Atomic orbital basis set dependence of the calculated DFT/MRCI singlet absorption spectrum of the $^{t}Bu_3P$–C_4F_9I adduct complex, Figure S12: Singly occupied MOs (SOMOs) of the phosphine and phosphite adducts in the relaxed T_1 state, Figures S13–S18: Solvent influence on the measured absorption spectra, Figures S19–S23: Impact

of spin–orbit coupling on the calculated spectra, Figures S24–S39: Minimum nuclear arrangements with selected geometry parameters

Author Contributions: Conceptualization, M.K., C.C., and C.M.M.; theoretical investigation, M.B.; experimental investigation, L.H.; writing—original draft preparation, C.C. and C.M.M.; visualization, M.B. and L.H.; supervision, M.K., C.C., and C.M.M.; funding acquisition, M.K., C.C., and C.M.M. All authors have read and agreed to the published version of the manuscript.

Funding: This research was funded by the Deutsche Forschungsgemeinschaft (DFG, German Research Foundation)—396890929/GRK 2482.

Conflicts of Interest: The authors declare no conflict of interest. The funders had no role in the design of the study; in the collection, analyses, or interpretation of data; in the writing of the manuscript, or in the decision to publish the results.

Abbreviations

The following abbreviations are used in this manuscript:

ATRA	atom transfer radical addition
CT	charge transfer
DCM	dichloromethane
DFT	density functional theory
EDA	electron donor–acceptor
HOMO	highest occupied molecular orbital
IC	internal conversion
ISC	intersystem crossing
KS	Kohn–Sham
LED	light-emitting diode
LUMO	lowest unoccupied molecular orbital
MRCI	multi-reference configuration interaction
MRSOCI	multi-reference spin–orbit configuration interaction
PES	potential energy surface
QDPT	quasi-degenerate perturbation theory
SOC	spin–orbit coupling
SOCME	spin–orbit coupling matrix element
SOMO	singly occupied molecular orbital
TDDFT	time-dependent density functional theory
TDA	Tamm–Dancoff approximation

References

1. Müller, K.; Faeh, C.; Diederich, F. Fluorine in Pharmaceuticals: Looking Beyond Intuition. *Science* **2007**, *317*, 1881–1886. [CrossRef]
2. Purser, S.; Moore, P.R.; Swallow, S.; Gouverneur, V. Fluorine in medicinal chemistry. *Chem. Soc. Rev.* **2008**, *37*, 320–330. [CrossRef]
3. Wang, J.; Sánchez-Roselló, M.; Aceña, J.L.; del Pozo, C.; Sorochinsky, A.E.; Fustero, S.; Soloshonok, V.A.; Liu, H. Fluorine in Pharmaceutical Industry: Fluorine-Containing Drugs Introduced to the Market in the Last Decade (2001–2011). *Chem. Rev.* **2014**, *114*, 2432–2506. [CrossRef]
4. Ojima, I. *Fluorine in Medicinal Chemistry and Chemical Biology*; Wiley-Blackwell: Chichester, UK, 2009. [CrossRef]
5. Ma, J.A.; Cahard, D. Strategies for nucleophilic, electrophilic, and radical trifluoromethylations. *J. Fluor. Chem.* **2007**, *128*, 975–996. [CrossRef]
6. Ma, J.A.; Cahard, D. Update 1 of: Asymmetric Fluorination, Trifluoromethylation, and Perfluoroalkylation Reactions. *Chem. Rev.* **2008**, *108*, PR1–PR43. [CrossRef] [PubMed]

7. Tomashenko, O.A.; Grushin, V.V. Aromatic Trifluoromethylation with Metal Complexes. *Chem. Rev.* **2011**, *111*, 4475–4521. [CrossRef] [PubMed]
8. Barata-Vallejo, S.; Postigo, A. Metal-mediated radical perfluoroalkylation of organic compounds. *Coord. Chem. Rev.* **2013**, *257*, 3051–3069. [CrossRef]
9. Studer, A. A "Renaissance" in Radical Trifluoromethylation. *Angew. Chem. Int. Ed.* **2012**, *51*, 8950–8958. [CrossRef]
10. Kirsch, P. *Modern Fluoroorganic Chemistry: Synthesis, Reactivity, Applications*, 2nd ed.; Wiley-VCH: Weinheim, Germany, 2013. [CrossRef]
11. Liu, S.Q.; Wang, S.W.; Qing, F.L. The perfluoroallylation of alkynes and transformation of the products. *J. Fluor. Chem.* **2005**, *126*, 771–778. [CrossRef]
12. Erdbrink, H.; Peuser, I.; Gerling, U.I.M.; Lentz, D.; Koksch, B.; Czekelius, C. Conjugate hydrotrifluoromethylation of α,β-unsaturated acyl-oxazolidinones: Synthesis of chiral fluorinated amino acids. *Org. Biomol. Chem.* **2012**, *10*, 8583–8586. [CrossRef]
13. Brace, N.O. l-Iodo-2-(perfluoroalkyl)cycloalkanes by the Free Radical Addition of Iodoperfluoroalkanes to Cyclohexane and Cyclopentene. *J. Org. Chem.* **1963**, *28*, 3093–3102. [CrossRef]
14. Dolbier, W.R. Structure, Reactivity, and Chemistry of Fluoroalkyl Radicals. *Chem. Rev.* **1996**, *96*, 1557–1584. [CrossRef] [PubMed]
15. Romero, N.A.; Nicewicz, D.A. Organic Photoredox Catalysis. *Chem. Rev.* **2016**, *116*, 10075–10166. [CrossRef] [PubMed]
16. Wang, C.S.; Dixneuf, P.H.; Soulé, J.F. Photoredox Catalysis for Building C–C Bonds from C(sp^2)–H Bonds. *Chem. Rev.* **2018**, *118*, 7532–7585. [CrossRef] [PubMed]
17. Stephenson, C.; Yoon, T.; MacMillan, D.W.C. *Visible Light Photocatalysis in Organic Chemistry*; Wiley-VCH: Weinheim, Germany, 2018; doi:10.1002/9783527674145. [CrossRef]
18. Nagib, D.A.; Scott, M.E.; MacMillan, D.W.C. Enantioselective α-Trifluoromethylation of Aldehydes via Photoredox Organocatalysis. *J. Am. Chem. Soc.* **2009**, *131*, 10875–10877. [CrossRef]
19. Prier, C.K.; Rankic, D.A.; MacMillan, D.W.C. Visible Light Photoredox Catalysis with Transition Metal Complexes: Applications in Organic Synthesis. *Chem. Rev.* **2013**, *113*, 5322–5363. [CrossRef]
20. Rawner, T.; Lutsker, E.; Kaiser, C.A.; Reiser, O. The Different Faces of Photoredox Catalysts: Visible-Light-Mediated Atom Transfer Radical Addition (ATRA) Reactions of Perfluoroalkyl Iodides with Styrenes and Phenylacetylenes. *ACS Catal.* **2018**, *8*, 3950–3956. [CrossRef]
21. Guo, Q.; Wang, M.; Peng, Q.; Huo, Y.; Liu, Q.; Wang, R.; Xu, Z. Dual-Functional Chiral Cu-Catalyst- Induced Photoredox Asymmetric Cyanofluoroalkylation of Alkenes. *ACS Catal.* **2019**, *9*, 4470–4476. [CrossRef]
22. Li, Z.L.; Fang, G.C.; Gu, Q.S.; Liu, X.Y. Recent advances in copper-catalysed radical-involved asymmetric 1,2-difunctionalization of alkenes. *Chem. Soc. Rev.* **2020**, *49*, 32–48. [CrossRef]
23. Reckenthäler, M.; Griesbeck, A.G. Photoredox Catalysis for Organic Syntheses. *Adv. Synth. Catal.* **2013**, *355*, 2727–2744. [CrossRef]
24. Hari, D.P.; König, B. Synthetic applications of eosin Y in photoredox catalysis. *Chem. Commun.* **2014**, *50*, 6688–6699. [CrossRef] [PubMed]
25. Postigo, A. Electron Donor-Acceptor Complexes in Perfluoroalkylation Reactions. *Eur. J. Org. Chem.* **2018**, *2018*, 6391–6404. [CrossRef]
26. Lima, C.G.S.; d. M. Lima, T.; Duarte, M.; jurberg, I.D.; Paixão, M.W. Organic Synthesis Enabled by Light-Irradiation of EDA Complexes: Theoretical Background and Synthetic Applications. *ACS Catal.* **2016**, *6*, 1389–1407. [CrossRef]
27. Marzo, L.; Pagire, S.K.; Reiser, O.; König, O. Visible-Light Photocatalysis: Does It Make a Difference in Organic Synthesis? *Angew. Chem. Int. Ed.* **2018**, *57*, 10034–10072. [CrossRef] [PubMed]
28. Sun, X.; Wang, W.; Li, Y.; Ma, J.; Yu, S. Halogen-Bond-Promoted Double Radical Isocyanide Insertion under Visible-Light Irradiation: Synthesis of 2-Fluoroalkylated Quinoxalines. *Org. Lett.* **2016**, *18*, 4638–4641. [CrossRef]
29. Sun, X.; He, Y.; Yu, S. Halogen-bond-mediated atom transfer radical addition of perfluoroalkyl iodides to alkynes under visible light irradiation. *J. Photochem. Photobiol. A* **2018**, *355*, 326–331. [CrossRef]

30. Wang, Y.; Wang, J.; Li, G.X.; He, G.; Chen, G. Halogen-Bond-Promoted Photoactivation of Perfluoroalkyl Iodides: A Photochemical Protocol for Perfluoroalkylation Reactions. *Org. Lett.* **2017**, *19*, 1442–1445. [CrossRef]
31. Tang, X.; Studer, A. Alkene 1,2-Difunctionalization by Radical Alkenyl Migration. *Angew. Chem. Int. Ed.* **2018**, *57*, 814–817. [CrossRef]
32. Yajima, T.; Ikegami, M. Metal-Free Visible-Light Radical Iodoperfluoroalkylation of Terminal Alkenes and Alkynes. *Eur. J. Org. Chem.* **2017**, 2126–2129. [CrossRef]
33. Rosso, C.; Williams, J.D.; Filippini, G.; Prato, M.; Kappe, C.O. Visible-Light-Mediated Iodoperfluoroalkylation of Alkenes in Flow and Its Application to the Synthesis of a Key Fulvestrant Intermediate. *Org. Lett.* **2019**, *21*, 5341–5345. [CrossRef]
34. Zhu, E.; Liu, X.X.; Wang, A.J.; Mao, T.; Zhao, L.; Zhang, X.; He, C.Y. Visible light promoted fluoroalkylation of alkenes and alkynes using 2-bromophenol as a catalyst. *Chem. Commun.* **2019**, *55*, 12259–12262. [CrossRef] [PubMed]
35. Wozniak, Ł.; Murphy, J.J.; Melchiorre, P. Photo-organocatalytic Enantioselective Perfluoroalkylation of β-Ketoesters. *J. Am. Chem. Soc.* **2015**, *137*, 5678–5681. [CrossRef] [PubMed]
36. Mao, T.; Ma, M.J.; Zhao, L.; Xue, D.P.; Yu, Y.; Gu, J.; He, C.Y. A general and green fluoroalkylation reaction promoted via noncovalent interactions between acetone and fluoroalkyl iodides. *Chem. Commun.* **2020**. [CrossRef] [PubMed]
37. Huang, W.Y.; Zhang, H.Z. Reaction of perfluoroalkyl iodides with alkenes initiated by organophosphine and related compounds. *J. Fluor. Chem.* **1990**, *50*, 133–140. [CrossRef]
38. Lumbierres, M.; Moreno-Mañas, M.; Vallribera, A. Addition of perfluorooctyl iodide to alkenes. Catalysis by triphenylphosphane. *Tetrahedron* **2002**, *58*, 4061–4065. [CrossRef]
39. Zhao, L.; Huang, Y.; Wang, Z.; Zhu, E.; Mao, T.; Jia, J.; Gu, J.; Li, X.F.; He, C.Y. Organophosphine-Catalyzed Difluoroalkylation of Alkenes. *Org. Lett.* **2019**, *21*, 6705–6709. [CrossRef]
40. Helmecke, L.; Spittler, M.; Baumgarten, K.; Czekelius, C. Metal-Free Activation of C–I Bonds and Perfluoroalkylation of Alkenes with Visible Light Using Phosphine Catalysts. *Org. Lett.* **2019**, *21*, 7823–7827. [CrossRef]
41. Lu, H.; Wang, D.; Zhang, A. Visible Light-Promoted Phosphine-Catalyzed Difluoroalkylation of Arenes and Heterocycles. *J. Org. Chem.* **2020**, *85*, 942–951. [CrossRef]
42. Behrends, I.; Bähr, S.; Czekelius, C. Perfluoroalkylation of Alkenes by Frustrated Lewis Pairs. *Chem. Eur. J.* **2016**, *22*, 17177–17181. [CrossRef]
43. Spittler, M.; Helmecke, L.; Czekelius, C. Mechanistic Insights into FLP-Catalyzed Iodoperfluoroalkylations. *Eur. J. Org. Chem.* **2019**, pp. 458–468. [CrossRef]
44. Bulfield, D.; Huber, S.M. Halogen Bonding in Organic Synthesis and Organocatalysis. *Chem. Eur. J.* **2016**, *22*, 14434–14450. [CrossRef] [PubMed]
45. Cavallo, G.; Metrangolo, P.; Milani, R.; Pilati, T.; Priimagi, A.; Resnati, G.; Terraneo, G. The Halogen Bond. *Chem. Rev.* **2016**, *116*, 2478–2601. [CrossRef] [PubMed]
46. Rabie, U.M.A. A review on electronic spectral studies of charge transfer complexes. *J. Mol. Struct.* **2013**, *1034*, 393–403. [CrossRef]
47. Clark, T.; Hennemann, M.; Murray, J.S.; Politzer, P. Halogen bonding: The σ-hole. *J. Mol. Model.* **2007**, *13*, 291–296. [CrossRef] [PubMed]
48. Chudzinski, M.G.; Taylor, M.S. Correlations between Computation and Experimental Thermodynamics of Halogen Bonding. *J. Org. Chem.* **2012**, *77*, 3483–3491. [CrossRef] [PubMed]
49. Angarov, V.; Kozuch, S. On the σ, π and δ hole interactions: A molecular orbital overview. *New J. Chem.* **2018**, *42*, 1413–1422. [CrossRef]
50. Manning, H.C.; Bai, M.; Anderson, B.M.; Lisiak, R.; Samuelson, L.E.; Bornhop, D.J. Expeditious synthesis of 'P'-protected macrocycles en route to lanthanide chelate metal complexes. *Tetrahedron Lett.* **2005**, *46*, 4707–4710. [CrossRef]
51. Bietti, M.; Calcagni, A.; Salamone, M. The Role of Structural Effects on the Reactions of Alkoxyl Radicals with Trialkyl and Triaryl Phosphites. A Time-Resolved Kinetic Study. *J. Org. Chem.* **2010**, *75*, 4514–4520. [CrossRef]

52. Mark, V.; Wazer, J.R.V. Tri-*t*-butyl Phosphite and Some of Its Reactions. *J. Org. Chem.* **1964**, *29*, 1006–1008. [CrossRef]
53. Treutler, O.; Ahlrichs, R. Efficient molecular numerical integration schemes. *J. Chem. Phys.* **1995**, *102*, 346–354. [CrossRef]
54. von Arnim, M.; Ahlrichs, R. Performance of Parallel TURBOMOLE for Density Functional Calculations. *J. Comput. Chem.* **1998**, *19*, 1746–1757. [CrossRef]
55. TURBOMOLE, a Development of University of Karlsruhe and Forschungszentrum Karlsruhe GmbH, 1989–2007, TURBOMOLE GmbH, Since 2007. Available online: http://www.turbomole.com (accessed on 30 March 2020).
56. Becke, A.D. Density-functional thermochemistry. 3. The role of exact exchange. *J. Chem. Phys.* **1993**, *98*, 5648–5652. [CrossRef]
57. Lee, C.; Yang, W.; Parr, R.G. Development of the Colle-Salvetti Correlation-Energy Formula into a Functional of the Electron Density. *Phys. Rev. B* **1988**, *37*, 785–789. [CrossRef]
58. Grimme, S.; Antony, J.; Ehrlich, S.; Krieg, H. A consistent and accurate ab initio parametrization of density functional dispersion correction (DFT-D) for the 94 elements H-Pu. *J. Chem. Phys.* **2010**, *132*, 154104. [CrossRef]
59. Grimme, S. Density functional theory with London dispersion corrections. *WIREs Comput. Mol. Sci.* **2011**, *1*, 211–228. [CrossRef]
60. Klamt, A.; Schüürmann, G. COSMO: A New Approach to Dielectric Screening in Solvents with Explicit Expressions for the Screening Energy and its Gradient. *J. Chem. Soc. Perkin Trans. 2* **1993**, *5*, 799–805. [CrossRef]
61. Schäfer, A.; Klamt, A.; Sattel, D.; Lohrenz, J.C.W.; Eckert, F. COSMO Implementation in TURBOMOLE: Extension of an Efficient Quantum Chemical Code Towards Liquid Systems. *Phys. Chem. Chem. Phys.* **2000**, *2*, 2187–2193. [CrossRef]
62. Schäfer, A.; Horn, H.; Ahlrichs, R. Fully optimized contracted Gaussian basis sets for atoms Li to Kr. *J. Chem. Phys.* **1992**, *97*, 2571–2577. [CrossRef]
63. Peterson, K.A.; Figgen, D.; Goll, E.; Stoll, H.; Dolg, M. Systematically convergent basis sets with relativistic pseudopotentials. II. Small-core pseudopotentials and correlation consistent basis sets for the post-d group 16–18 elements. *J. Chem. Phys.* **2003**, *119*, 11113. [CrossRef]
64. Weigend, F.; Häser, M.; Patzelt, H.; Ahlrichs, R. RI-MP2: Optimized auxiliary basis sets and demonstration of efficiency. *Chem. Phys. Lett.* **1998**, *294*, 143–152. [CrossRef]
65. Weigend, F.; Ahlrichs, R. Balanced basis sets of split valence, triple zeta valence and quadruple zeta valence quality for H to Rn: Design and assessment of accuracy. *Phys. Chem. Chem. Phys.* **2005**, *7*, 3297–3305. [CrossRef] [PubMed]
66. Furche, F.; Ahlrichs, R. Adiabatic Time-Dependent Density Functional Methods for Excited State Properties. *J. Chem. Phys.* **2002**, *117*, 7433–7447. [CrossRef]
67. Hirata, S.; Head-Gordon, M. Time-dependent density functional theory within the Tamm–Dancoff approximation. *Chem. Phys. Lett.* **1999**, *314*, 291–299. [CrossRef]
68. Weymuth, T.; Haag, M.P.; Kiewisch, K.; Luber, S.; Schenk, S.; Jacob, C.R.; Herrmann, C.; Neugebauer, J.; Reiher, M. MOVIPAC: Vibrational Spectroscopy with a Robust Meta-Program for Massively Parallel Standard and Inverse Calculations. *J. Comput. Chem.* **2012**, *33*, 2186–2198. [CrossRef]
69. Pohler, L.; Kleinschmidt, M.; Etinski, M.; Marian, C.M. In search of the dark state of 5-methyl-2-hydroxypyrimidine using a numerical DFT/MRCI gradient. *Mol. Phys.* **2012**, *110*, 2429–2438. [CrossRef]
70. Grimme, S.; Waletzke, M. A combination of Kohn–Sham density functional theory and multi-reference configuration interaction methods. *J. Chem. Phys.* **1999**, *111*, 5645–5655. [CrossRef]
71. Marian, C.M.; Heil, A.; Kleinschmidt, M. The DFT/MRCI Method. *WIREs Comp. Mol. Sci.* **2019**, *9*, e1394. [CrossRef]
72. Heil, A.; Kleinschmidt, M.; Marian, C.M. On the performance of DFT/MRCI Hamiltonians for electronic excitations in transition metal complexes: The role of the damping function. *J. Chem. Phys.* **2018**, *149*, 164106. [CrossRef]
73. Becke, A.D. A new mixing of Hartree–Fock and local density-functional theories. *J. Chem. Phys.* **1993**, *98*, 1372–1377. [CrossRef]

74. Vahtras, O.; Almlöf, J.; Feyereisen, M. Integral approximations for LCAO-SCF calculations. *Chem. Phys. Lett.* **1993**, *213*, 514 – 518. [CrossRef]
75. Hellweg, A.; Hättig, C.; Höfener, S.; Klopper, W. Optimized accurate auxiliary basis sets for RI-MP2 and RI-CC2 calculations for the atoms Rb to Rn. *Theoret. Chem. Acc.* **2007**, *117*, 587–597. [CrossRef]
76. Kleinschmidt, M.; Tatchen, J.; Marian, C.M. Spin-Orbit Coupling of DFT/MRCI Wavefunctions: Method, Test Calculations, and Application to Thiophene. *J. Comput. Chem.* **2002**, *23*, 824–833. [CrossRef] [PubMed]
77. Kleinschmidt, M.; Marian, C.M. Efficient Generation of Matrix Elements for One-Electron Spin–Orbit Operators. *Chem. Phys.* **2005**, *311*, 71–79. [CrossRef]
78. Kleinschmidt, M.; van Wüllen, C.; Marian, C.M. Intersystem-crossing and phosphorescence rates in *Fac*-$Ir^{III}(ppy)_3$: A Theor. Study Involv. Multi-Ref. Interact. Wavefunct. *J. Chem. Phys.* **2015**, *142*, 094301. [CrossRef] [PubMed]
79. Hess, B.A.; Marian, C.M.; Wahlgren, U.; Gropen, O. A Mean-Field Spin-orbit Method Applicable to Correlated Wavefunctions. *Chem. Phys. Lett.* **1996**, *251*, 365–371. [CrossRef]
80. AMFI is an atomic spin–orbit integral program written by B. Schimmelpfennig, University of Stockholm, 1996.
81. Kleinschmidt, M.; Tatchen, J.; Marian, C.M. SPOCK.CI: A Multireference Spin–Orbit Configuration Interaction Method for Large Molecules. *J. Chem. Phys.* **2006**, *124*, 124101. [CrossRef]
82. Cole, J.R.; Dellinger, M.E.; Johnson, T.J.; Reinecke, B.A.; Pike, R.D.; Pennington, W.T.; Krawiec, M.; Rheingold, A.L. Caged phosphite complexes of copper(I) halides. *J. Chem. Crystallogr.* **2003**, *33*, 341–347. [CrossRef]
83. Taira, K.; Mock, W.L.; Gorenstein, D.G. Experimental Tests of the Stereoelectronic Effect at Phosphorus: Nucleophilic Reactivity of Phosphite Esters. *J. Am. Chem. Soc.* **1984**, *106*, 7831–7835. [CrossRef]

7. Cumulative part IV

7.1. Metal-free Iodoperfluoroalkylation: Photocatalysis vs. Frustrated Lewis Pair Catalysis

The conducted experiments of the publication: "Metal-free Iodoperfluoroalkylation: Photocatalysis vs. Frustrated Lewis Pair Catalysis"[6] and a brief discussion of the results will be summarized below. The manuscript and the Supporting Information are not attached to this doctoral thesis. Helmecke, L.; Spittler, M.; Schmidt, B. M.; Czekelius, C. *Synthesis* **2020**, 6; DOI: 10.1055/s-0040-1707232.[6]

In 2019, the iodoperfluoroalkylation of alkenes, performed by using visible light and phosphorus(III) compounds were presented.[4] In the following publication, the substrate spectrum should be extended to alkynes and further insights into the reaction should be given. Furthermore, results of the FLP-catalyzed iodoperfluoroalkylation were presented and both methods were compared. The investigation of the photomediated iodoperfluoroalkylation was expanded by reactions with different alkynes using internal, terminal and phenylacetylenes (Scheme 81).[6]

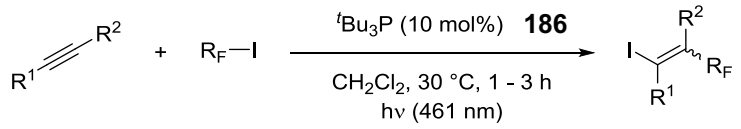

Scheme 81: Photocatalytic iodoperfluoroalkylation of alkynes using $^{t}Bu_3P$ **186**.[6]

In comparison to the FLP-catalyzed iodoperfluoroalkylation it was verified that the photomediated and phosphorus-catalyzed iodoperfluoroalkylation is capable of reacting with alkynes. The FLP-catalyzed reaction did not tolerate alkynes as substrates and low or no conversions were achieved.[3, 6] In addition to the expanded substrate scope, the perfluoroalkyl iodide was changed to 2,2,-difluoro-1-iodoacetate (**188**) and was successfully reacted with 1-octene (**174**) and 1-octyne (**246**) (Scheme 82).

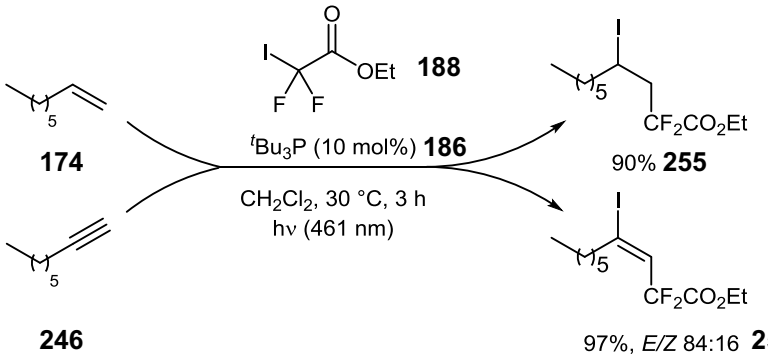

Scheme 82: Reaction of 2,2-difluoro-1-iodoacetate (**188**) with 1-octene (**174**) and 1-octyne (**246**).[6]

In order to exclude the influence of heat radiation of the LEDs, an experiment with 1-octene (**174**) and C_4F_9I **101** was conducted at elevated temperatures. The ambient light was excluded entirely by covering the reaction vial with aluminum foil (Scheme 83).

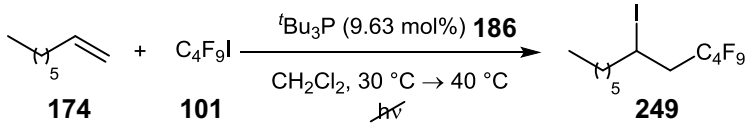

Scheme 83: Reaction of 1-octene (**174**) and C_4F_9I **101** at elevated temperature.[6]

Even after the reaction solution was heated up to reflux of the solvent, no complete conversion was achieved after 1 h. Secondly, a reaction with 1-octene (**174**) and C_4F_9I **101** was performed to demonstrate the necessity of permanent irradiation. For this purpose, an interval irradiation experiment was conducted. During the irradiation times, a permanent reaction conversion was detected. The reaction became significantly slower but did not stop entirely in periods of no irradiation. This was attributed to the fact that the remaining radicals still react with the educts in the dark phases.[6] Screening of various phosphorus(III) compounds as catalysts already demonstrated that PPh_3 **91** and $(MeO)_3P$ are capable catalysts.[4] Determination of the binding constant indicated the strongest interaction between $^tBu_3P$ **186** ($14.15\ M^{-1}$) followed by significant smaller binding constants for PPh_3 **91** ($0.96\ M^{-1}$) and $(MeO)_3P$ ($0.46\ M^{-1}$).[6]

7.2. Contributions to the publication

The publication "Metal-free Iodoperfluoroalkylation: Photocatalysis vs. Frustrated Lewis Pair Catalysis" was published in collaboration with Dr. M. Spittler, Dr. B. M. Schmidt and Prof. C. Czekelius.

The experimental part was conducted by L. Helmecke (75%) and Dr. M. Spittler (25%).

L. Helmecke carried out the photomediated iodoperfluoroalkylations, reactions with ethyldifluoroiodoacetate and reactions with iodide salts (NaI, TBAI). Furthermore, he performed the interveral irradiation, the experiments under elevated temperature and the determination of the association constant as well as the visualization of the results. As educts *N*-(*tert*-butoxycarbonyl)-*N*-(prop-2-ynyl)aniline and 2-(prop-2-yn-1-yl)isoindoline-1,3-dione were synthesized and the reactions with ethynylcyclopropane were carried out. Compilation, writing and visualization of the manuscript and the supporting information was done by Lucas Helmecke.

The described FLP-catalyzed iodoperfluoroalkylation were already presented in the doctoral thesis of Dr. M. Spittler.[3] This includes the FLP-catalyzed iodoperfluoroalkylations, the borane synthesis and parts of the educt synthesis (pent-4-en-1-yl 4-chlorobenzoates, (hex-5-en-1-yl)-4-bromophenylether). Dr. M. Spittler was significantly involved in the correction of the manuscript and the supporting information.

Dr. B. M. Schmidt measured the grown crystals of (*Z*)-(3,3,4,4,5,5,6,6-nonafluoro-1-iodo-2-methylhex-1-en-1-yl)benzene and described the crystallographic details.

Prof. C. Czekelius was significantly involved in writing the manuscript, correction process and the revision of the manuscript and the supporting information.

8. Unpublished Results

In this chapter of the doctoral thesis, unpublished results are presented. This includes further experiments to determine the capabilities of the photomediated and phosphorus-catalyzed iodoperfluoroalkylation and whether it can be applied to other halogen-containing compounds.

8.1. Iodoperfluoroalkylation using (*R*)-BINAP as catalyst

When different phosphorus(III) compounds were tested as a catalyst, it was also examined whether chiral phosphines can catalyze the reaction and whether the resulting product was enantiomerically enriched. For this purpose a reaction solution containing vinylcyclohexane (**241**), C_4F_9I **101** and (*R*)-BINAP **257** was irradiated at –78 °C (Scheme 84).

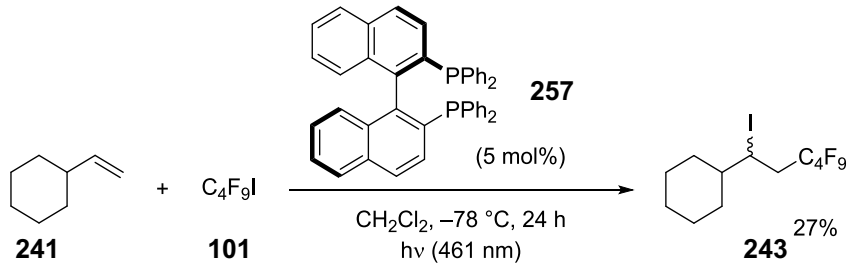

Scheme 84: (*R*)-BINAP-catalyzed reaction of vinylcyclohexane (**241**) and C_4F_9I **101**.

The already shown Schlenk-tube (see Figure 9, p. 85) was used as a reaction setup to be able to perform the reaction at –78 °C. The LED was inside a test tube and illuminated the reaction solution inside the Schlenk tube (Figure 14).

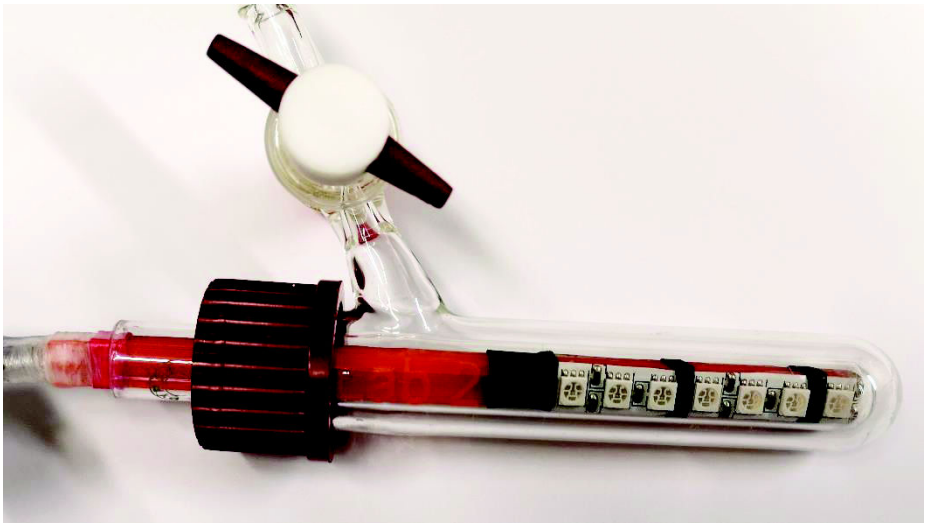

Figure 14: Setup for photoreactions in a Schlenk-tube.

No reaction control was performed to determine the conversion. After 24 h irradiation, only 27 % of the iodoperfluoroalkylated product **243** were yielded. Since the solvent was evaporated under a stream of nitrogen to transfer it to a column the product, parts of the iodoperfluoroalkylation product might

have got lost. However, the chromatogram of the iodoperfluoroalkylated product **243** on a chiral GC indicated that only a racemic product mixture was isolated (Figure 15).

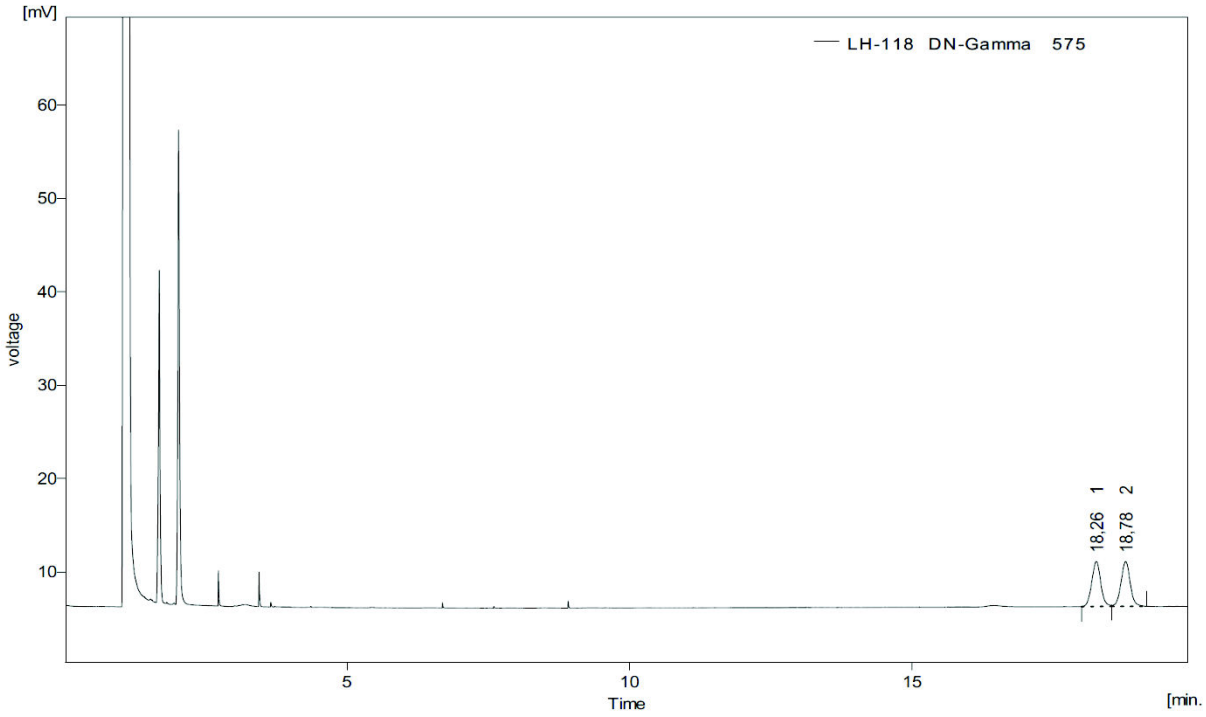

Result Table (Uncal - LH-118 DN-Gamma 575)

	Reten. Time [min]	Area [mV.s]	Height [mV]	Height [%]	W05 [min]	Area [%]
1	18,257	53,098	4,812	50,1	0,17	49,6
2	18,777	54,036	4,800	49,9	0,17	50,4
	Total	107,133	9,612	100,0		100,0

Figure 15: Chiral GC chromatogram of the isolated iodoperfluoroalkylated product **243** of vinylcyclohexane (**241**).

The experiment showed that the reaction can also be carried out at low temperatures. The use of (*R*)-BINAP **257** demonstrated that other phosphorus compounds can be used. However, based on this result no further experiments with other chiral phosphanes were perfomed.

8.2. Reactions with electron-deficient alkenes and alkynes

As already demonstrated, electron-rich alkenes and alkynes were successfully converted with different iodoperfluoroalkanes.[4, 6] Experiments with 2,3-dichloro-1-propene (**258**), (*E*)-stilbene (**259**) and styrene (**261**) demonstrated a limitation of the photomediated iodoperfluoroalkylation reaction.[4] Accordingly, diphenylacetylene (**260**) could not be converted during the investigations of the substrate spectrum of the alkynes (Scheme 85).

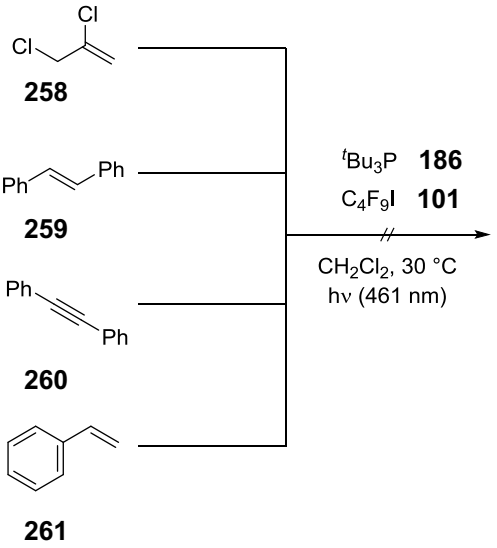

Scheme 85: Unsuccessful reactions with electron poor alkenes and alkynes.

These compounds have also been tested as substrates in the study of FLP-catalyzed iodoperfluroalkylation but none of these compounds could be converted. When styrene (**261**) was added to a reaction of vinylcyclohexane (**241**) no reaction occurs.[4]

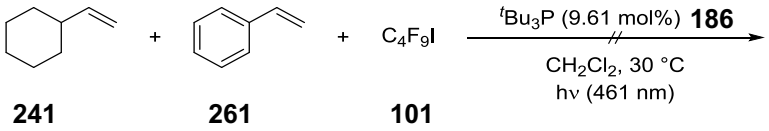

Scheme 86: Reaction of vinylcyclohexane (**241**) and C_4F_9I **101** in presence of styrene (**261**).[4]

The problem of implementing styrene (**261**) as an educt was already described in literature. A lack of reaction product formation has been attributed to stable benzylic and allylic intermediate radicals forming throughout the reaction.[89] In addition, various acrylic derivates were tested, but none of these derivatives could be converted (Scheme 87).

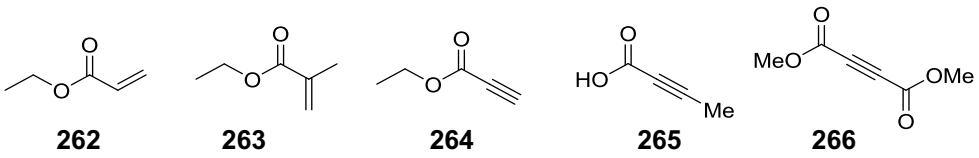

Scheme 87: Various tested acrylic derivatives.

When nonafluoro-1-iodobutane (**101**) was added to the acrylic derivatives, the reaction solutions turned brown to dark black within one hour. After 2 h up to 24 h of irradiation, a sample was withdrawn of each reaction solution to measure a ^{19}F-NMR spectrum. The ^{19}F-NMR spectra of the corresponding reactions indicated no product formation. The ^{19}F-NMR spectra were similar to a spectrum of nonafluoro-1-iodobutane (**101**) (Figure 16).

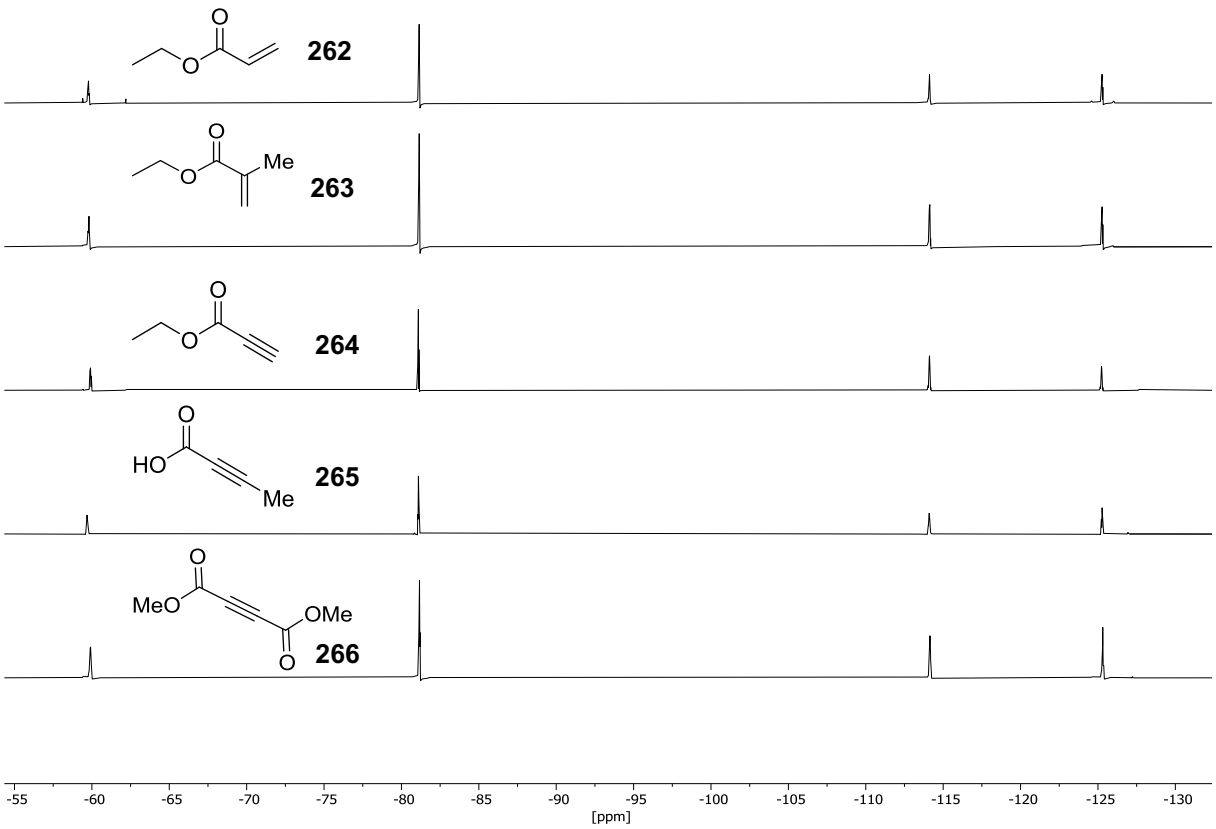

Figure 16: Stacked ^{19}F-NMR spectra (300 MHz, $CDCl_3$) of the reaction solutions with different acrylic derivatives and C_4F_9I **101**.

Melchiorre *et al.* published a photochemical aromatic perfluoroalkylation of α-cyano arylacetates[82] and a photo-organocatalytic, enantioselective perfluoroalkylation of β-ketoesters[86] and added perfluorhexane (C_6F_{14}) or perfluorooctane (C_6F_{18}) as second solvent to the reaction. By adding the perfluoroalkylated solvent which forms a second phase the resulting perfluorinated product was transferred to the perfluoroalkylated solvent phase and could not inhibit the reaction process.[82] The addition of perfluorooctane to a reaction of ethyl propiolate (**264**) with C_4F_9I **101** was tested and the reaction solution was irradiated at 395 nm (Scheme 88).

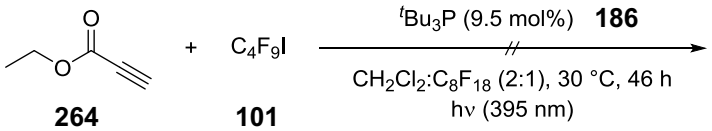

Scheme 88: Reaction of ethyl propiolate (**264**) with C_4F_9I **101** and CH_2Cl_2:C_8F_{18} as solvent.

When ethyl propiolate (**264**) was added to the solution of ^{t}Bu$_3$P **186**, C_4F_9I **101** and the two phasic solvent system of CH_2Cl_2:C_8F_{18}, the upper CH_2Cl_2 phase turned instantly dark brown. After the irradiation, the C_8F_{18} phase was still colorless and the upper CH_2Cl_2 phase turned darker (Figure 17).

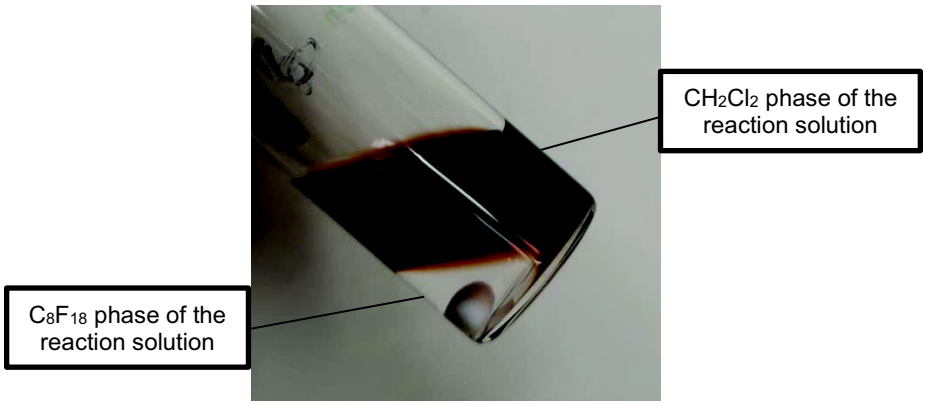

Figure 17: Picture of the vial after the reaction of ethyl propiolate (**264**) with C_4F_9I **101** and CH_2Cl_2:C_8F_{18} as solvent.

After the irradiation a sample of the CH_2Cl_2 phase and the C_8F_{18} phase was withdrawn for the ^{1}H- and ^{19}F-NMR spectroscopy (Figure 18 and Figure 19). The C_8F_{18} phase did not dissolve in $CDCl_3$ and was therefore was shaken thoroughly before the sample was measured.

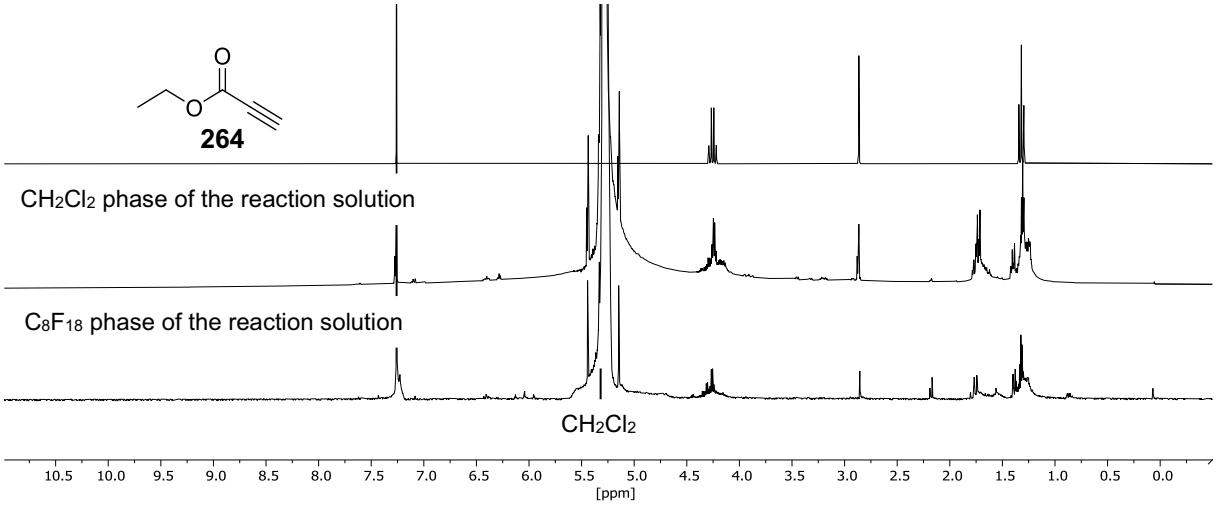

Figure 18: Stacked ^{1}H-NMR spectra (600 MHz, $CDCl_3$) of ethyl propiolate (**264**) (top), the upper CH_2Cl_2 phase of the reaction solution (middle) and the C_8F_{18} bottom phase (bottom) of reaction solution.

In the ^{1}H- as well as in ^{19}F-NMR spectrum no signal could be detected, that would indicate a product formation. In the ^{1}H-NMR spectrum the educt signals were still detectable in both phases (Figure 18). By withdrawing the sample of the lower phase the cannula might be contaminated with the reaction solution of the top phase. That might be the reason, why the educt signals are also visible in the ^{1}H-NMR spectrum. In the ^{19}F-NMR spectrum, the superposition of the signals due to the high number of fluorine atoms was a problem (Figure 19). However, in both spectra, the IC*F*$_2$-group is still present at approximately 60 ppm. This indicates at least an incomplete reaction. Even by irradiating with a 395 nm light source, no product formation could be achieved.

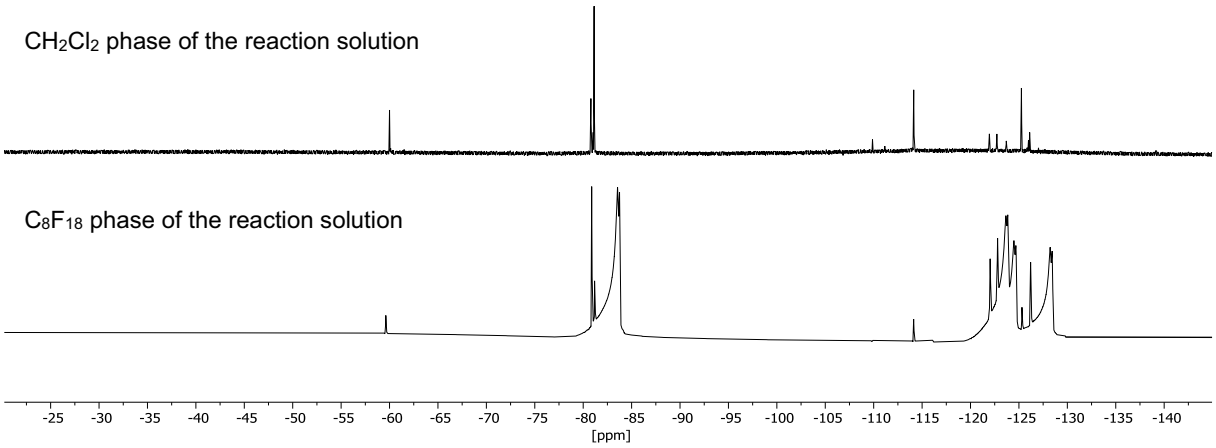

Figure 19: Stacked ^{19}F-NMR spectra (600 MHz, $CDCl_3$) of the upper CH_2Cl_2 phase of the reaction solution (top) and the C_8F_{18} bottom phase (bottom) of reaction solution.

8.3. Reactions with 1-bromoperfluorohexane (267)

It has already been demonstrated that different iodoperfluoroalkanes and 2,2,-difluoro-1-iodoacetate (**188**) react with alkenes and alkynes by using ^{t}Bu$_3$P **186** as catalyst and irradiation with visible light.[4, 6] In addition, it was shown that the Lewis base and the fluorinated iodine compound interact by forming an EDA complex. Therefore, it should be examined whether not only iodinated compounds, but also other halogenated compounds can be activated by phosphorus(III) compounds. Due to the good results with fully perfluoroalkylated halogenated compounds, the experiments were performed with 1-bromoperfluorohexane (**267**) under standard conditions. 1-Bromoperfluorohexane (**267**) was mixed with 1-octene (**174**) and in another reaction with 1-octyne (**246**) (Scheme 89).

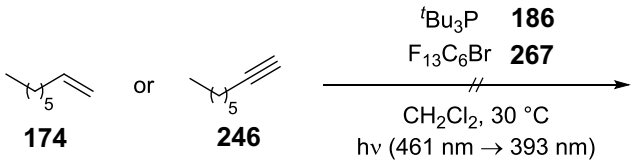

Scheme 89: Reaction with 1-octene (**174**) or 1-octyne (**246**) with $C_6F_{13}Br$ **267**.

The reaction solution was first irradiated for 2 h and 20 h at 461 nm and a sample was withdrawn for the ^{19}F-NMR spectroscopy. Afterward, the reaction solution was irradiated at 395 nm. The ^{19}F-NMR spectrum of the individual samples showed that none of the irradiation types showed a change compared to the $F_{13}C_6Br$ **267** spectrum (Figure 20).

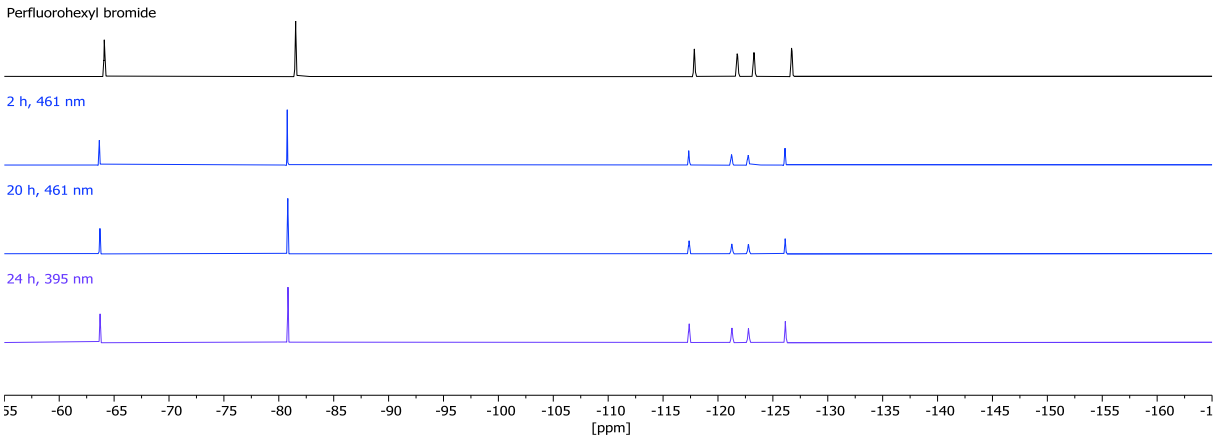

Figure 20: Stacked ^{19}F-NMR spectra (300 MHz, $CDCl_3$) of the reaction solution of 1-octene (**106**) with $F_{13}C_6Br$ **267** after 2 h, 20 h at 461 nm, 24 h at 395 nm and a spectrum of $C_6F_{13}Br$ **267**.

By changing the educt to 1-octyne (**246**), the ^{19}F-NMR spectra showed no changes either, compared to the used educt (Figure 21). When a sample of $C_6F_{13}Br$ in $CDCl_3$ was prepared for the ^{19}F-NMR spectroscopy, it was noticed that two phases were formed and $C_6F_{13}Br$ was not dissolved in the solvent.

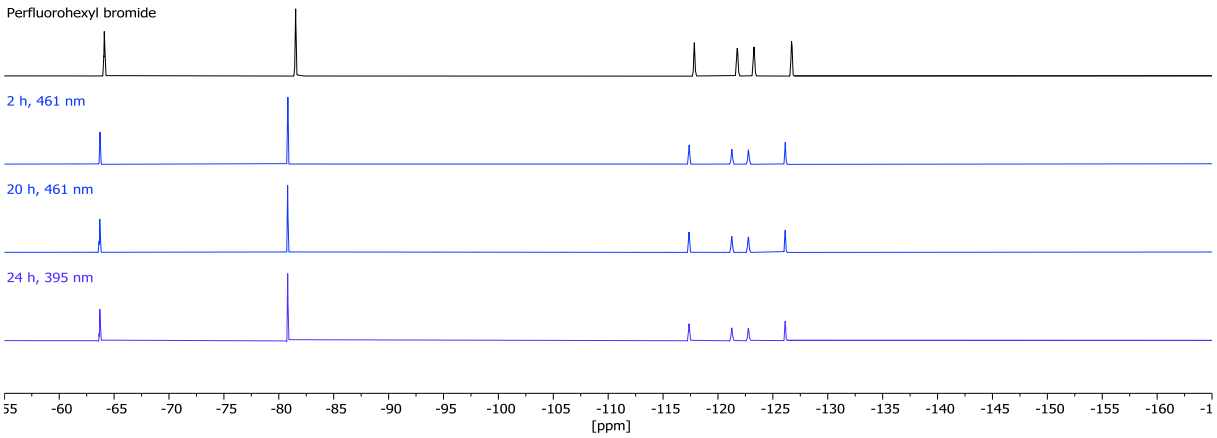

Figure 21: Stacked ^{19}F NMR spectra (300 MHz, $CDCl_3$) of the reaction solution of 1-octyne (**246**) with $C_6F_{13}Br$ **267** after 2 h, 20 h at 461 nm, 24 h at 395 nm and a spectrum of $C_6F_{13}Br$ **267**.

Hence, it was considered that $C_6F_{13}Br$ **267** was not dissolved in dichloromethane throughout the performed reaction. However, reactions in Et_2O or MeCN did not show any conversion either. Based on these results, the reactions with $C_6F_{13}Br$ **267** were not pursued any further, since an activation of fluorinated bromine compound with ^{t}Bu$_3$P **186** did not seem to be possible.

8.4. Crystallization experiments

To visualize potential unusual phenomena and to give further insights into the emerging EDA complex between ^{t}Bu$_3$P **186** and C_4F_9I **101**, it was attempted to crystallize the donor-acceptor pair (Scheme 90). In initial experiments, the two starting materials were mixed and it was noticed that the mainly crystalline ^{t}Bu$_3$P **186** (m.p. 27 - 29 °C)[109] dissolved in C_4F_9I **101**.

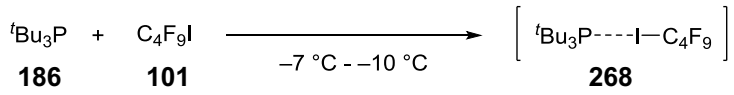

Scheme 90: Crystallization experiment of $^{t}Bu_3P$ **186** and C_4F_9I **101**.

At room temperature the two educts did not crystallize and only a clear colorless liquid was formed (Figure 22, left). When the liquid was cooled to –20 °C in the glovebox, only amorphous crystals were formed. For this reason, $^{t}Bu_3P$ **186** and C_4F_9I **101** were mixed in a small vial and this mixture was slowly cooled to –7 to –10 °C in a screw-cap glass with Teflon™ inlet (Figure 22, right). Only one half of the outer vail was placed in the cooling liquid, resulting in the formation of needle-like colorless crystals (Figure 22, right).

Figure 22: Sealed vial of $^{t}Bu_3P$ **186** and C_4F_9I **101** inside a closed bottle under N_2-atmosphere (left) and cooled to –7 °C - –10 °C inside a cooling bath (right).

An attempt was made to measure these crystals by X-ray diffraction. One measurement was carried out, but no single crystal was displayed. The unit cell was too large and contained several halogen-bridged adducts. A second crystallization was conducted and various solvents were added, in the expectation to obtain a better crystal for the next measurement (Table 8). No crystals could be obtained when MeOH, MeCN or Et_2O were used (entry 1 - 3, Table 8). However, when a mixture of MeOH and Et_2O or MeCN was used, small light-yellow crystals grew inside the solvent at a lower temperature.

Table 8: Crystallization experiment of $^{t}Bu_3P$ **186** and C_4F_9I **101** with different solvents.

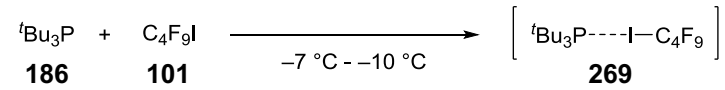

entry	solvent	
1	MeOH	no crystals
2	MeCN	dark brown solution
3	Et_2O	amorphous crystals
4	MeOH + Et_2O	light yellow crystals
5	MeOH + MeCN	light yellow crystals

To ensure the absence of oxygen inside the used vials and to evaporate the solvent, a small stream of nitrogen was injected *via* a cannula into the vial through the attached septum (Figure 23). The crystals were also measured in the X-ray structure analysis, but the unit cell could not be represented to give a correct statement about the formed adduct, too.

Figure 23: Sealed vials of $^{t}Bu_3P$ **186**, C_4F_9I **101** and a solvent inside a closed bottle under N_2-atmosphere and cooled to –7 °C - –10 °C inside a cooling bath.

Bryce and co-workers published the characterization of a cocrystal of triphenylphosphine (**91**) as an electron acceptor and a halogen bond donor (*e.g.* 1,3,5-trifluoro-2,4,6-triiodobenzene (*sym*-$C_6F_3I_3$)). However, Bryce *et al.* also described that, to their knowledge, no further reports of similar cocrystallizations are known in literature.[110] In addition, the handling of the very oxidation-sensitive $^{t}Bu_3P$ **186** probably also plays a key role, why no good crystal or measurement of the crystal could be obtained. Nonafluoro-1-butane (**101**) might not be stable as well since a colorless solution of C_4F_9I **101** turns violet under ambient light irradiation over a more extended period of time.

8.5. Synthesis and reactions of iodoethynyl derivatives

It should be investigated if the established method for the activation of perfluoroalkyl iodides with phosphorus compounds can be applied to the reaction with iodoethynyl-derivatives **270** (Scheme 91).

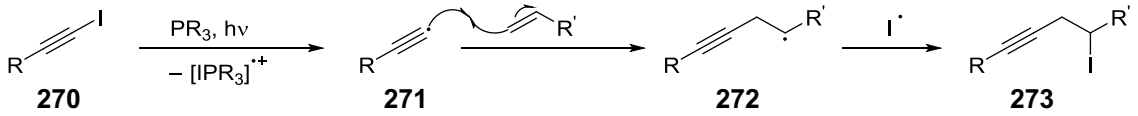

Scheme 91: Activation of iodoethynyl derivatives withs subsequent reaction of alkenes.

For this purpose, an iodine atom should be introduced at the terminal end of an alkyne. By adding a phosphorus compound as Lewis base to interact with the iodine, and by irradiation with visible light, radicals should be generated to form the terminal alkyne radical **271**. An alkene should react with radical **271** to form the radical **272**. Subsequently, the previously formed iodine radical should lead to the combined product **273**. At first, five different iodoethynyl derivatives were synthesized starting from the corresponding alkynes (Scheme 92).

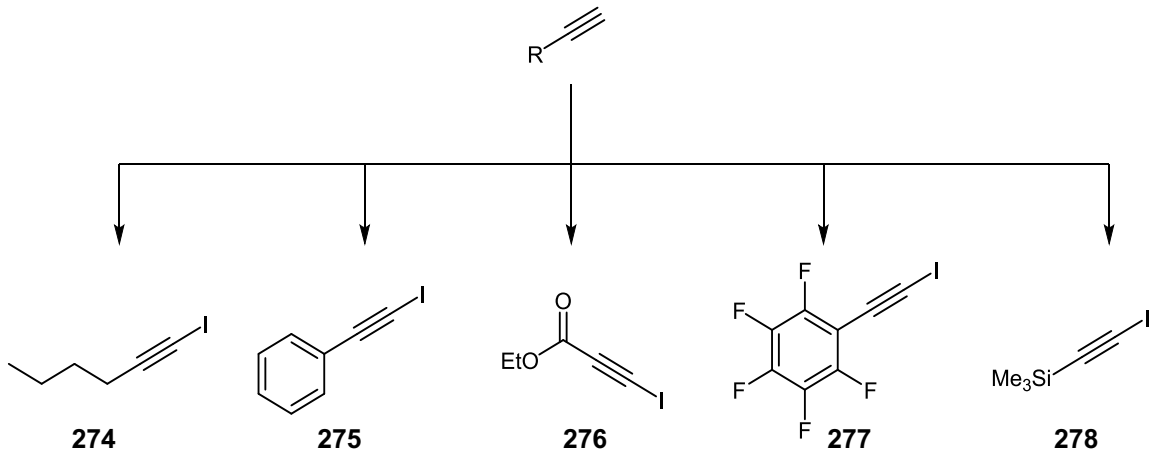

Scheme 92: Overview of the synthesized iodoethynyl derivatives.

All syntheses were performed with *N*-iodosuccinimide (**279**). However, when phenylacetylene was used the product was not formed and only the educt was re-isolated. Thus, a reaction of iodine (**282**) with morpholine (**281**) was performed and (iodoethynyl)benzene (**275**) was isolated in moderate yield.

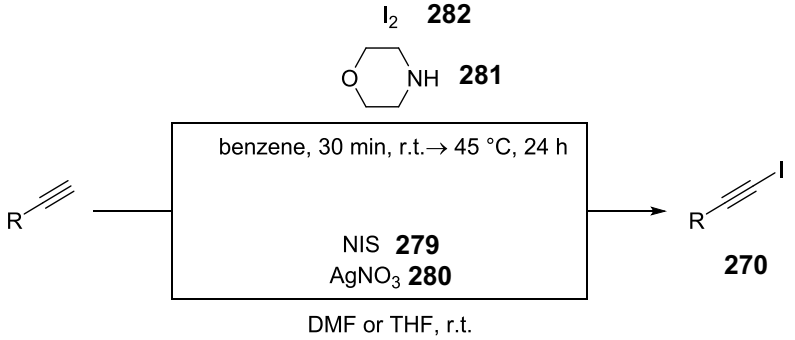

Scheme 93: Methods for the synthesis of iodoethynyl derivatives **270**.

All alkynes except 1-ethynyl-2,3,4,5,6-pentafluorobenzene (**286**) were available and could be converted to the corresponding iodoethynyl compounds. 1-Ethynyl-2,3,4,5,6-pentafluorobenzene (**286**) was synthesized from the literature known procedure[111] *via* a Sonogashira coupling and was provided after the deprotection to synthesis the iodoethynyl-derivatives **277**.

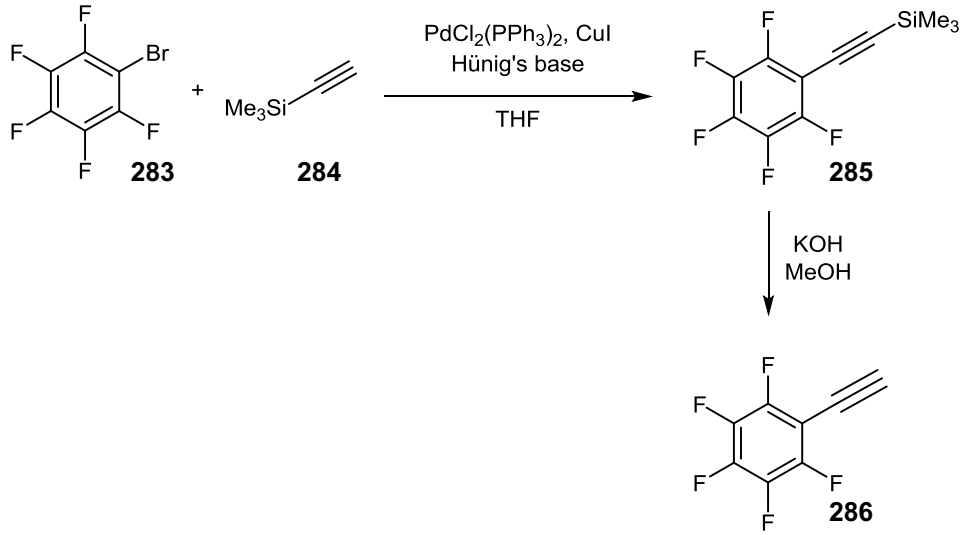

Scheme 94: Synthesis of 1-ethynyl-2,3,4,5,6-pentafluorobenzene **286**.[111]

A ^{19}F-NMR spectrum of the alkyne **286** showed that it contained bromopentafluorobenzene (**283**) (approx. 69%), which could not be removed (Figure 24). Pentafluorophenylacetylene (**286**) was therefore used with the impurity, as the iodoethynyl product **277** could be purified *via* column chromatography.

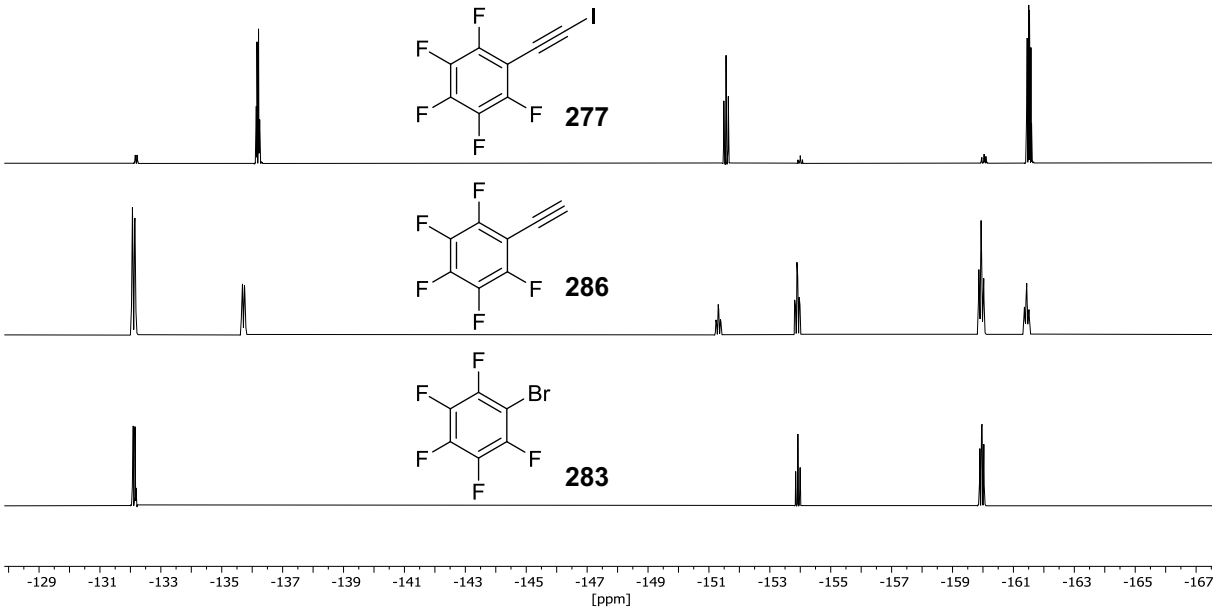

Figure 24: Stacked ^{19}F-NMR spectra ($CDCl_3$, 282 MHz) of the iodoethynyl derivative **277** (top), 1-ethynyl-2,3,4,5,6-pentafluorobenzene (**286**) (middle) and bromopentafluorobenzene (**283**) (bottom).

After the reaction of 1-ethynyl-2,3,4,5,6-pentafluorobenzene (**286**) with NIS **279** and a purification by column chromatography using silica gel, the resulting liquid was slightly purple. Therefore it was purified over aluminum oxide once more to remove iodine from the final iodoethynyl derivative **277**. A colorless liquid was obtained which was stored at –20 °C. Diederich *et al.* describe the iodoethynyl compound **277** as air-stable for days.[112] While working with the previously almost colorless liquid, it turned more and more purple again. A ^{19}F-NMR spectrum of the iodoethynyl product **277** showed additional signals to the product signals (Figure 24). A comparison with the educt spectrum of bromopentafluorobenzene (**283**) proved that it could not be removed entirely from the iodoethynyl product **277**.

8.6. Photoreactions with iodoethynyl derivatives

For the first reactions with alkenes and the synthesized iodoethenyl derivatives, vinylcyclohexane (**241**) and 1-octene (**174**) were selected. Both alkenes were successfully tested in the field of FLP-catalyzed[1] and photomediated iodoperfluoroalkylation reactions.[4] 3-Iodopropiolate (**276**) was reacted with vinylcyclohexane (**241**) and catalytic amounts of ^{t}Bu$_3$P **186** (Scheme 95).

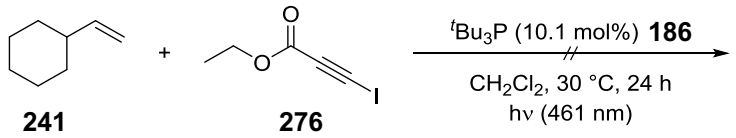

Scheme 95: Photoreaction of ethyl 3-iodopropiolate (**276**) with vinylcyclohexane (**241**).

Tri-*tert*-butylphosphine (**186**) and vinylcyclohexane (**241**) were weighed into a reaction vial. Ethyl 3-iodopropiolate (**276**) was dissolved in dichloromethane in a separate vial and added to the reaction solution. The solution immediately turned dark black. The reaction solution was irradiated for 24 h at 461 nm, and a sample for the ^{1}H- and ^{19}F-NMR spectroscopy was withdrawn (Figure 25).

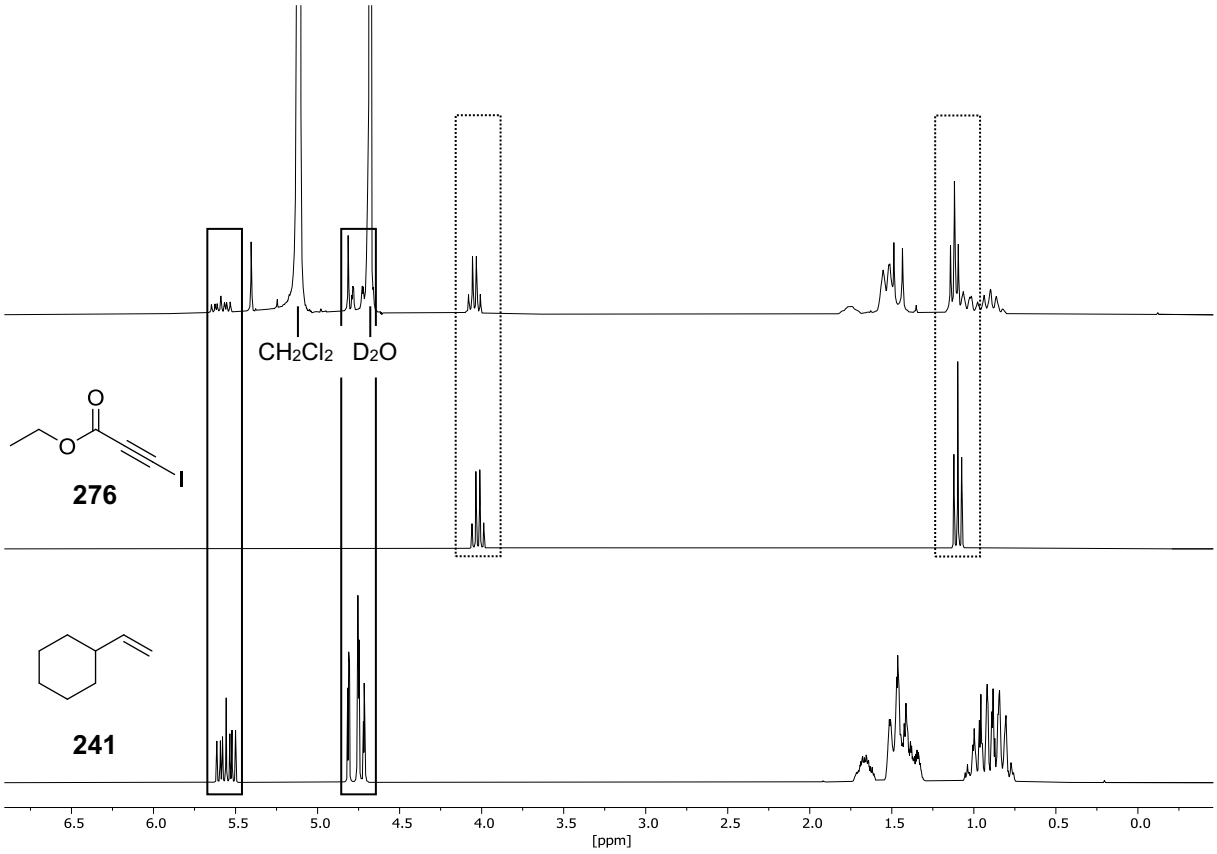

Figure 25: Stacked ^{1}H-NMR spectra ($CDCl_3$, 300 MHz) of the reaction solution after 24 h of irradiation (top), ethyl 3-iodopropiolate (**276**) (middle) and vinylcyclohexane (**241**) (bottom).

The ^{1}H-NMR spectra showed no new signals, and the alkene signals of vinylcyclohexane (**241**) were still present after 24 h of irradiation (Figure 25, straight box). The ethyl group signals of ethyl 3-iodopropiolate (**276**) were unaffected as well (Figure 25, dotted box). An external standard (H_3PO_4 in D_2O) was added to the NMR tube to compare the phosphorus spectra. Several phosphorus spectra with different concentrations showed no signals. The second test reaction with ethyl 3-iodopropiolate (**276**) was conducted with 1-octene (**174**) (Scheme 96).

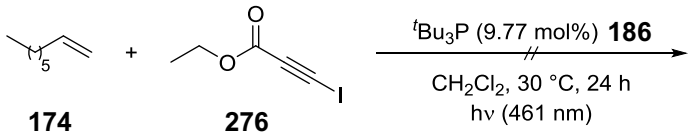

Scheme 96: Photoreaction of ethyl 3-iodopropiolate (**276**) with 1-octene (**174**).

The ^{1}H-NMR spectrum of the reaction solution showed no new signals after 24 h of irradiation. The alkene signals of 1-octene (**174**) (Figure 26, straight box) and the CH_2-signals of the ethyl group of the iodoethynl derivative **276** (Figure 26, dotted box) were still present.

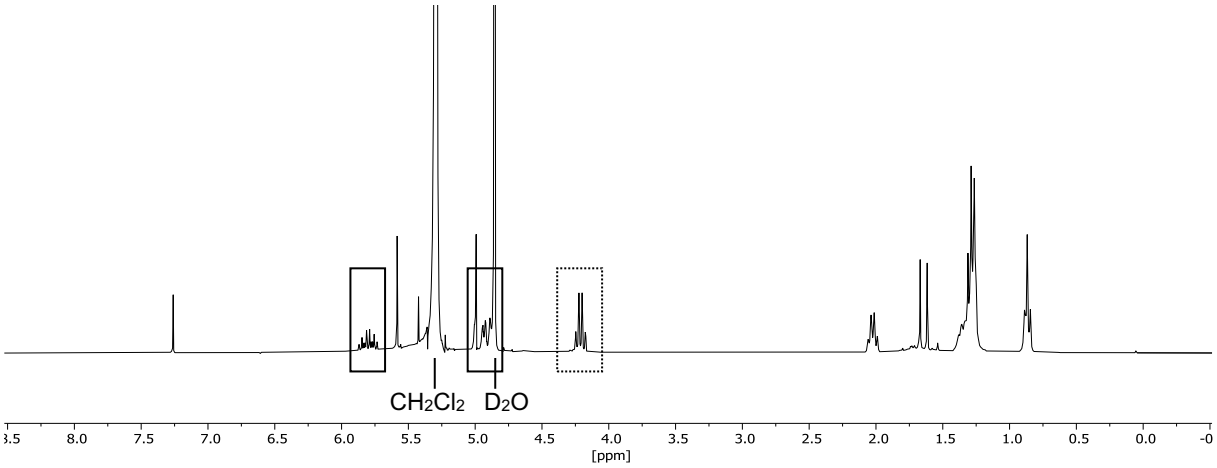

Figure 26: ^{1}H-NMR spectrum ($CDCl_3$, 300 MHz) of the reaction solution of ethyl 3-iodopropiolate (**276**) with 1-octene (174) after 24 h of irradiation.

As soon as $^{t}Bu_3P$ **186** and the iodoethynyl compound **276** were mixed into one vial both solids turned black immediately. The two solids were transferred with CH_2Cl_2 into a Young NMR tube. For a ^{1}H- and ^{31}P-NMR measurement, one external standard was added (H_3PO_4 in D_2O). The solution was dark black inside the Young NMR tube. The ^{1}H-NMR spectrum showed that the signals of the ethyl group of ethyl 3-iodopropiolate (**276**) completely disappeared (Figure 27).

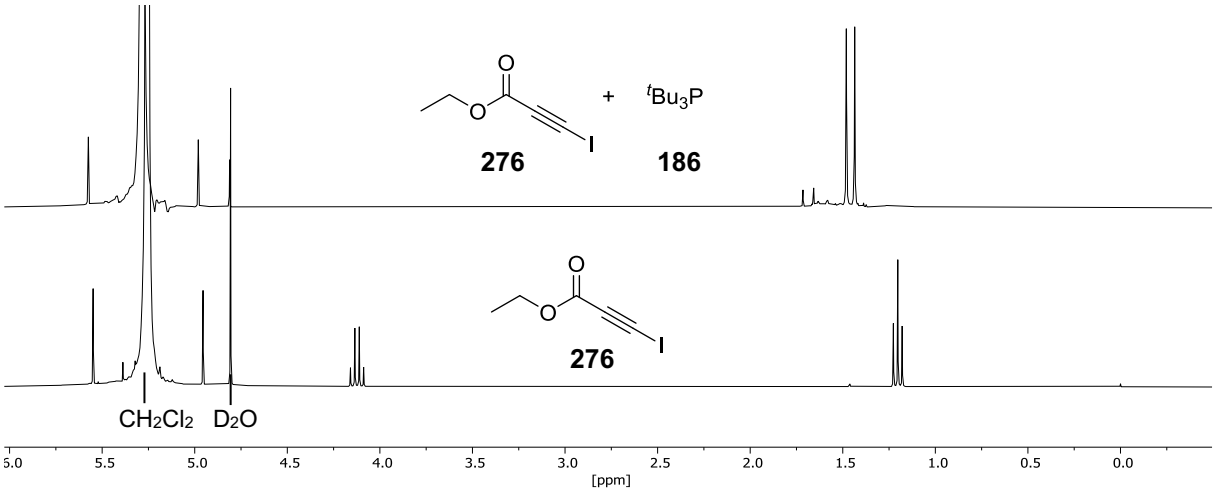

Figure 27: Stacked ^{1}H-NMR spectra (D_2O, 300 MHz) of ethyl 3-iodopropiolate (**276**) with $^{t}Bu_3P$ **186** in CH_2Cl_2 (top) and ethyl 3-iodopropiolate (**276**) in CH_2Cl_2 (bottom).

In contrast to the ^{1}H-NMR spectrum, the ^{31}P-NMR spectrum showed additional signals (Figure 28). As an external standard H_3PO_4 in D_2O was added to the NMR tube. The spectrum was locked to the H_3PO_4 signal ($\delta = 0$ ppm). The $^{t}Bu_3P$ **186** signal completely disappeared, and additional signals appeared. The ^{31}P-NMR spectrum of pure $^{t}Bu_3P$ **186** was only recorded from 100 ppm to −15 ppm.

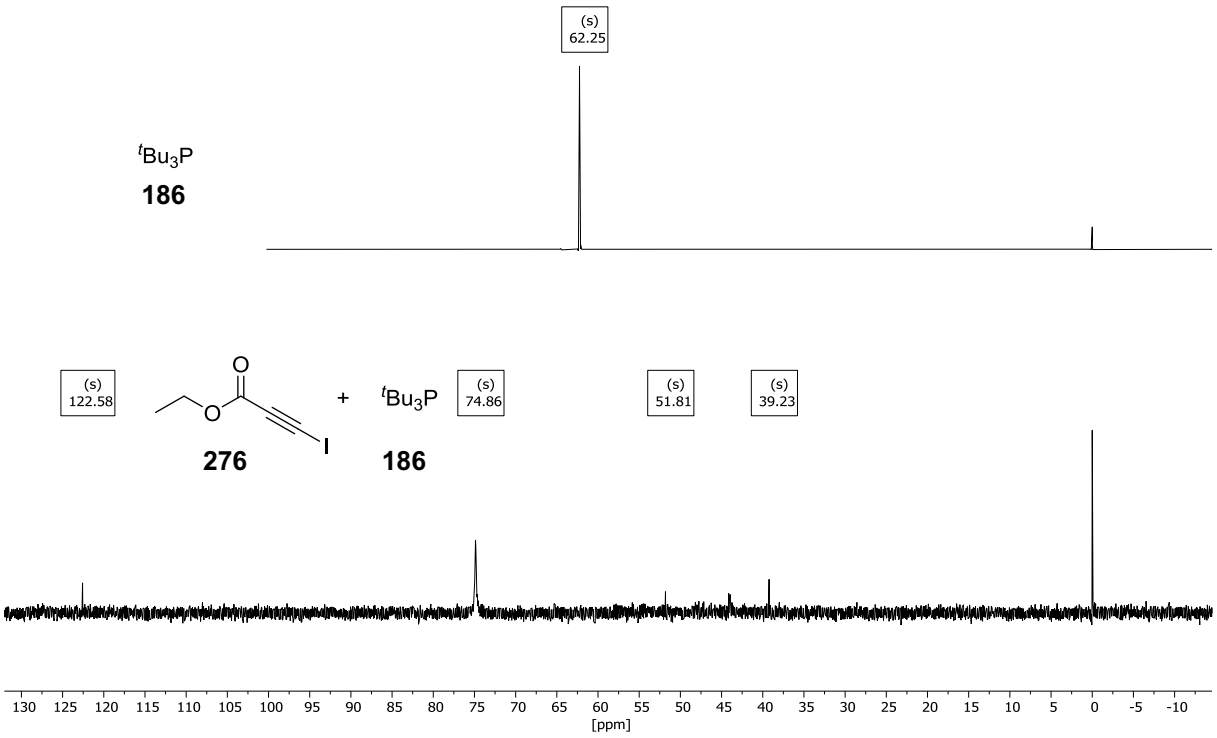

Figure 28: Stacked ^{31}P-NMR spectra (121 MHz) of $^{t}Bu_3P$ **186** in CH_2Cl_2 and ethyl 3-iodopropiolate (**276**) with $^{t}Bu_3P$ **186** in CH_2Cl_2 (bottom) with external standard (H_3PO_4 in D_2O).

The disappearance of the signals in the ^{1}H-NMR spectrum could indicate that radicals were formed, and polymerization occurs. A similar observation was made when acrylate derivatives were tested in the photomediated iodoperfluoroalkylaton. Ethyl propiolate (**264**), as well as ethyl acrylate, could not be converted.[4, 6] In the FLP-catalyzed iodoperfluoroalkylation, acrylic derivatives could not be converted either, due to the radicals that were formed and the presumed occurrence of polymerization.[3]

Since ethyl 3-iodopropiolate (**276**) could not be converted, 1,2,3,4,5-pentafluoro-6-(iodoethynyl)benzene (**277**) was tested with 1-octene (**174**) and vinylcyclohexane (**241**). While working with 1,2,3,4,5-pentafluoro-6-(iodoethynyl)benzene (**277**) it turned slightly violet. It was added directly to the reaction solution of vinylcyclohexane(**241**) and $^{t}Bu_3P$ **186** (Scheme 97).

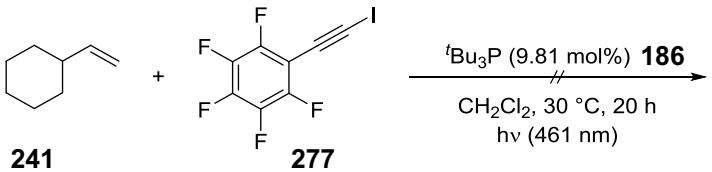

Scheme 97: Photoreaction of 2,3,4,5-pentafluoro-6-(iodoethynyl)benzene (**277**) with vinylcyclohexane (**241**).

After 20 h of irradiation, the reaction solution was dark brown. A ^{1}H-NMR spectrum after 2 h and 20 h of irradiation showed no new signals. The alkene signals were still present (solid box, Figure 29). The ^{19}F-NMR spectra showed no new signals, too.

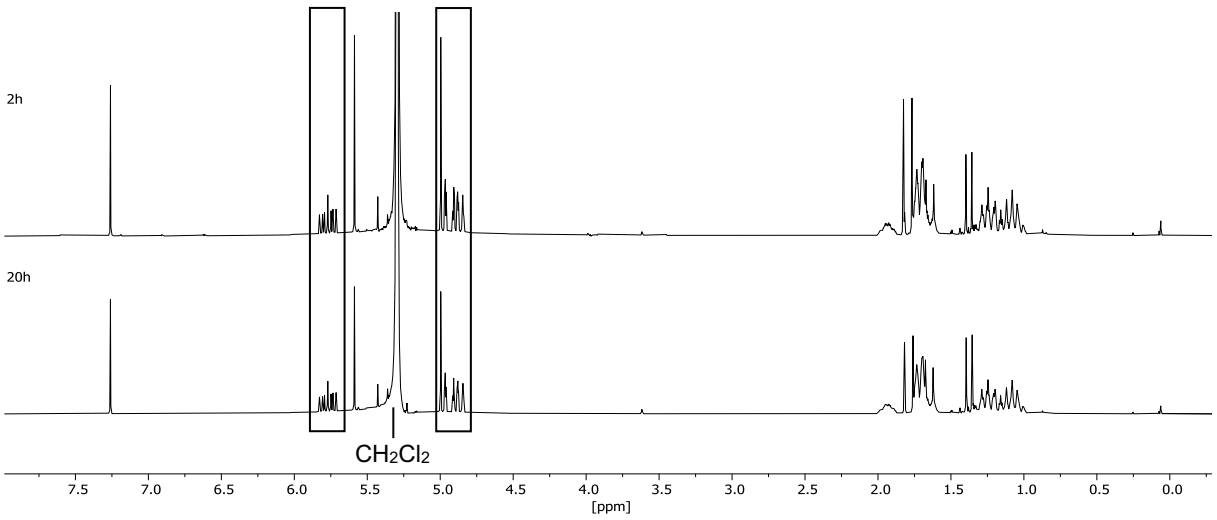

Figure 29: Stacked ^{1}H-NMR spectra ($CDCl_3$, 300 MHz) of the reaction solution after 2 h (top) and 20 h (bottom) of irradiation.

A comparison of the spectrum of the reaction solution after 20 h of irradiation and the spectrum of the used iodoethynyl-educt **277** revealed that the signals of the impurity were shifted (Figure 30). The impurity was the starting material bromopentafluorobenzene (**283**), which could not be removed.

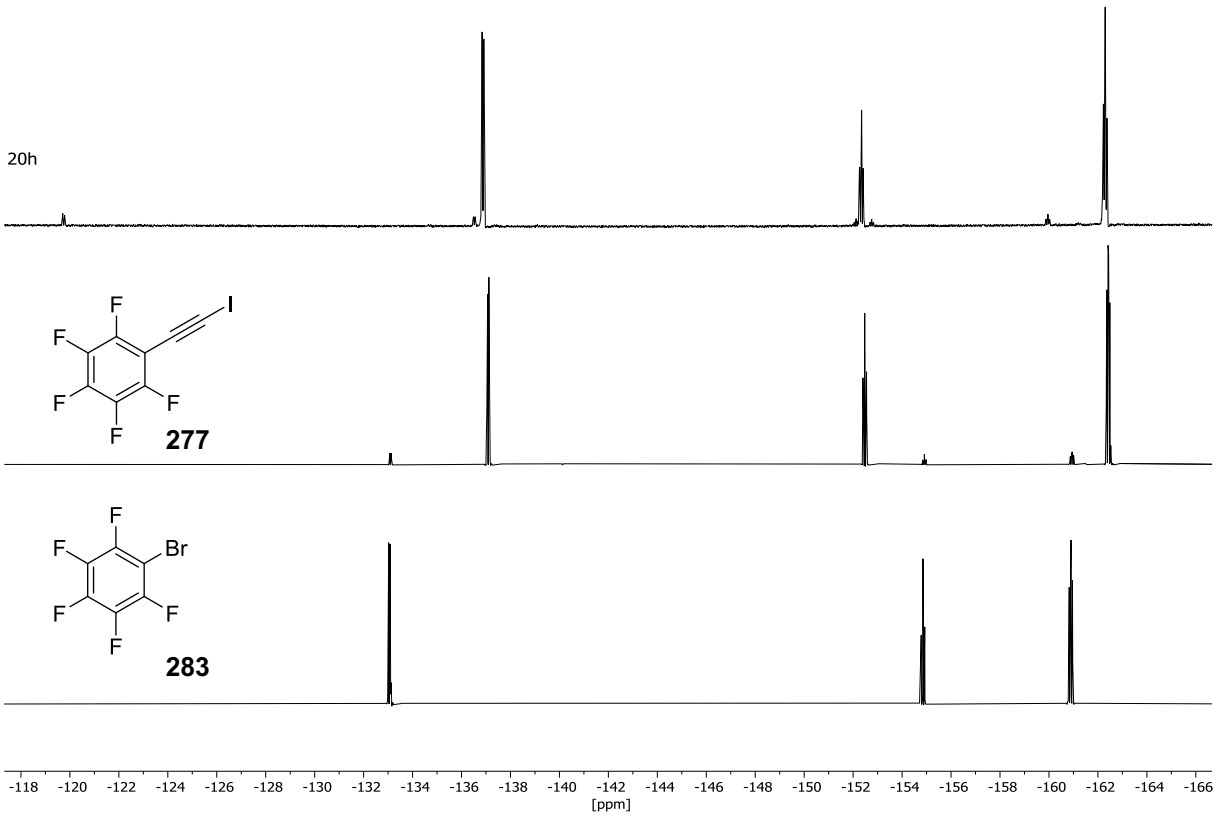

Figure 30: Stacked ^{19}F-NMR spectra ($CDCl_3$, 282 MHz) of the reaction solution after 20 h (top), 1,2,3,4,5-pentafluoro-6-(iodoethynyl)benezen (**277**) (middle) and bromopentafluorobenzene (**283**) (bottom).

The same experiment was conducted with 1-octene (**174**) and 1,2,3,4,5-pentafluoro-6-(iodoethynyl)benzene (**277**) (Scheme 98). After 2 h and 20 h of irradiation at 461 nm, a sample for

the ^{1}H- and ^{19}F-NMR spectroscopy was withdrawn. The alkene signals were still present in both spectra (solid box, Figure 31).

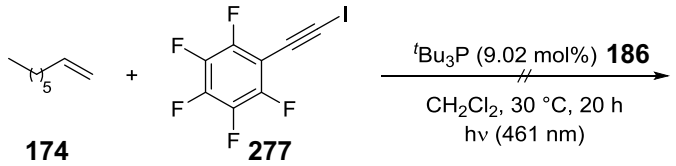

Scheme 98: Photoreaction of 2,3,4,5-pentafluoro-6-(iodoethynyl)benzene (**277**) with 1-octene (**174**).

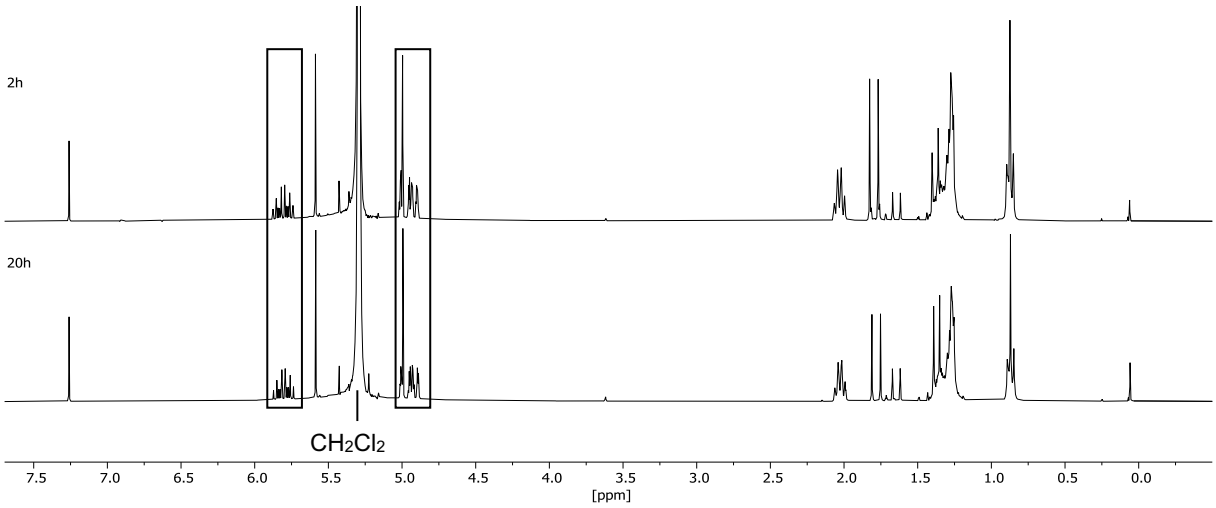

Figure 31: Stacked ^{1}H-NMR spectra ($CDCl_3$, 300 MHz) of the reaction solution after 2 h (top) and 20 h (bottom) of irradiation.

Both used alkenes, vinylcyclohexane (**241**) and 1-octene (**174**), showed no conversion after the irradiation with 2,3,4,5-pentafluoro-6-(iodoethynyl)benzene (**277**). Tri-*tert*-butylphosphine (**186**) and 2,3,4,5-pentafluoro-6-(iodoethynyl)benzene (**277**) were added to a Young NMR tube with dichloromethane and external standards ($CFCl_3$ in C_6D_6, H_3PO_4 in D_2O) to investigate the shift in the corresponding NMR spectrum. The ^{19}F-NMR spectrum of the mixture with ^{t}Bu$_3$P **186** showed a slightly more significant shift of the signals compared to the spectrum of the reaction solution (Figure 30 and Figure 32). The impurities were shifted here, too. However, new signals appeared in the ^{19}F-NMR spectrum (Figure 32).

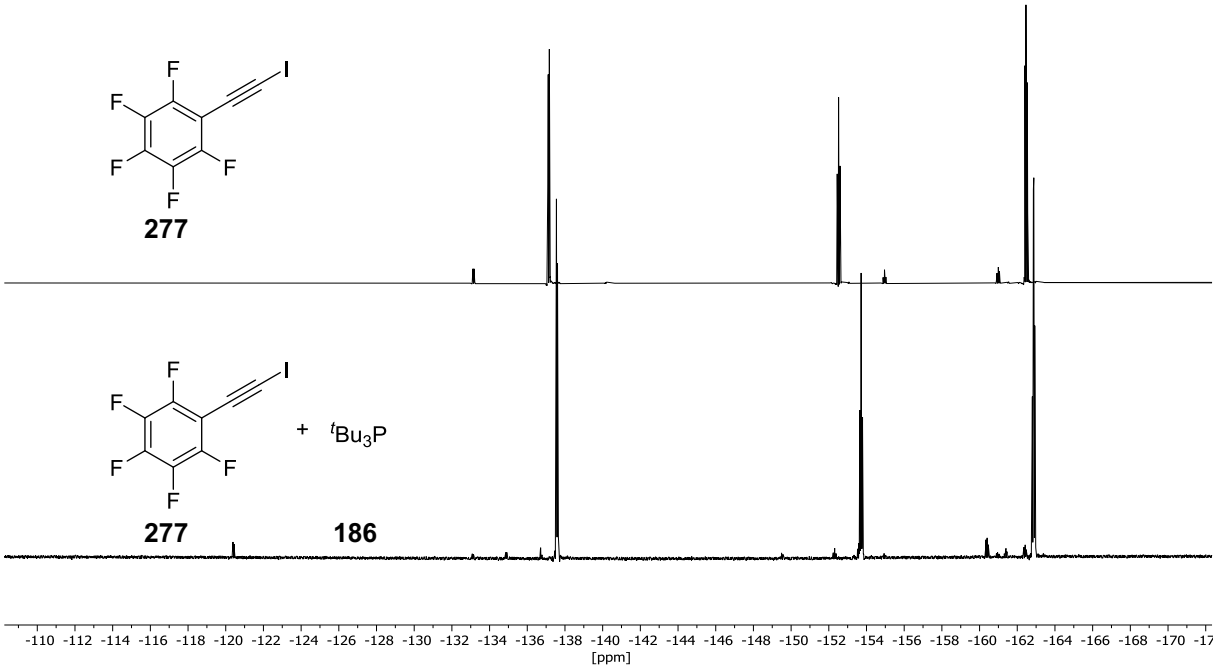

Figure 32: Stacked ^{19}F-NMR spectra (CH_2Cl_2, 282 MHz) of 2,3,4,5-pentafluoro-6-(iodoethynyl)benzene (**277**) (top) and 2,3,4,5-pentafluoro-6-(iodoethynyl)benzene (**277**) with $^{t}Bu_3P$ **186** (bottom).

In contrast, the ^{31}P-NMR spectrum showed no new signals (Figure 33). On the other hand, the $^{t}Bu_3P$ **186** signal is strongly shifted. When $^{t}Bu_3P$ **186** is mixed with nonafluoro-1-iodobutane (**101**) a similar shift is observed (4.5 ppm).[2]

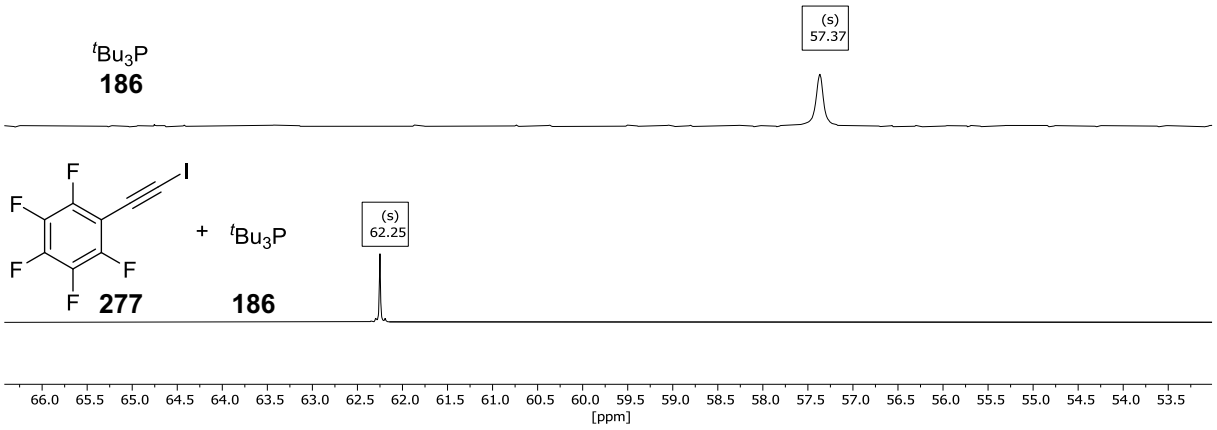

Figure 33: Stacked ^{31}P-NMR spectra (CH_2Cl_2, 282 MHz) of 2,3,4,5-pentafluoro-6-(iodoethynyl)benzene (**277**) with $^{t}Bu_3P$ **186** (top) and $^{t}Bu_3P$ **186** (bottom) with external standard (H_3PO_4 in D_2O).

Despite the shift in the ^{31}P-NMR spectrum, which indicates an interaction between the phosphine **186** and iodoethynyl-compound **277**, no reaction occurred when the alkene was added. Ethyl 3-iodopropiolate (**276**) was not suitable as an educt. In the reaction solution, no reaction was observed after the irradiation, and when phosphine **186** and iodoethynyl-compound **276** were added, the

disappearance of the signals in the ^{1}H-NMR spectrum indicated polymerization or side reaction (Figure 27). In comparison, 2,3,4,5-pentafluoro-6-(iodoethynyl)benzene (**277**) showed a substantial shift in the ^{31}P-NMR spectrum when ^{t}Bu$_3$P **186** was added (Figure 33). However, again no reaction occurred when an alkene was added. The gradual violet coloration of the starting material **277** indicated the formation of iodine. Free iodine decreases the quality of the educt **277** and inhibits radical reactions.[113-114] Since this iodoethynyl-compound **277** had to be synthesized in a three-step preparation, this type of reaction was repeated with more easily accessible starting materials. But when the reaction was tested with 1-iodohex-1-yne (**274**), (iodoethynyl)benzene (**275**) or 1-iodo-2-(trimethyl)silylacetylene (**278**) in the presence of 1-octene (**174**) and catalytic amounts of ^{t}Bu$_3$P **186** (Scheme 102).

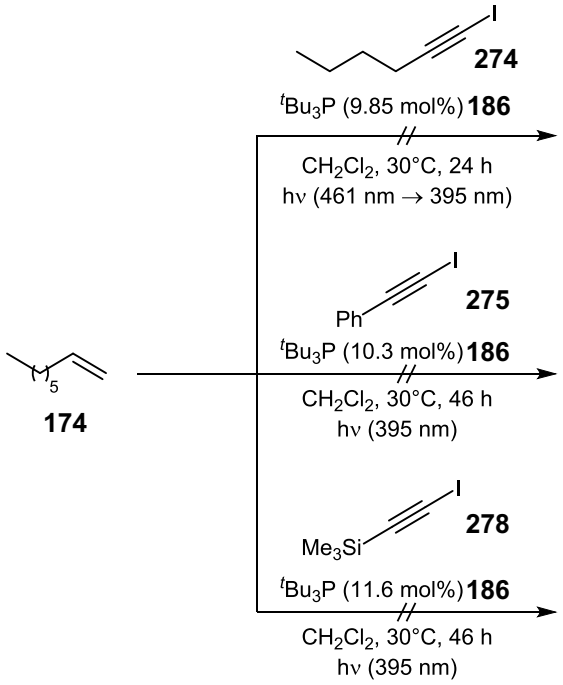

Scheme 99: Photoreactions of 1-iodohex-1-yne (**274**), (iodoethynyl)benzene (**275**) and 1-iodo-2-(trimethyl)silylacetylene (**278**) in the presence of 1-octene with catalytic amounts of ^{t}Bu$_3$P **186**.

Even the change of the irradiation from 461 nm to 395 nm did not lead to product formation. Moreover, even the change from catalytic quantities ^{t}Bu$_3$P **186** to stoichiometric quantities of phosphine **186** did not lead to a product formation after the indicated irradiation time (Scheme 100).

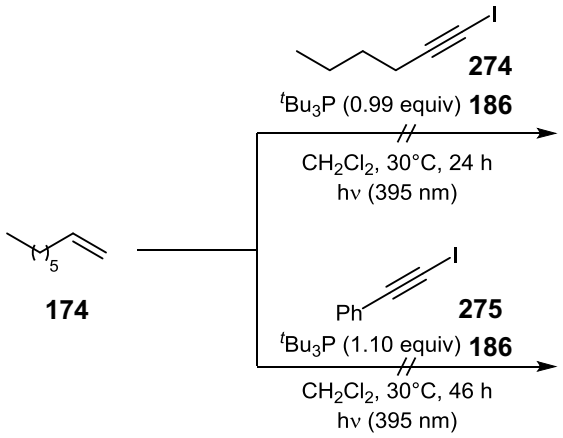

Scheme 100: Photoreactions of 1-iodohex-1-yne (**274**), (iodoethynyl)benzene (**275**) in the presence of 1-octene with stoichiometric amounts of $^{t}Bu_3P$ **186**.

In a final experiment, the addition of C_8F_{18}, which has already been described (p. 125), was tested as a solvent additive to remove the resulting product or by-products from the reaction solution. Neither the addition of catalytic or stoichiometric amounts of $^{t}Bu_3P$ **186** nor a change of the solvent from CH_2Cl_2 to MeCN resulted in product formation (Scheme 101).

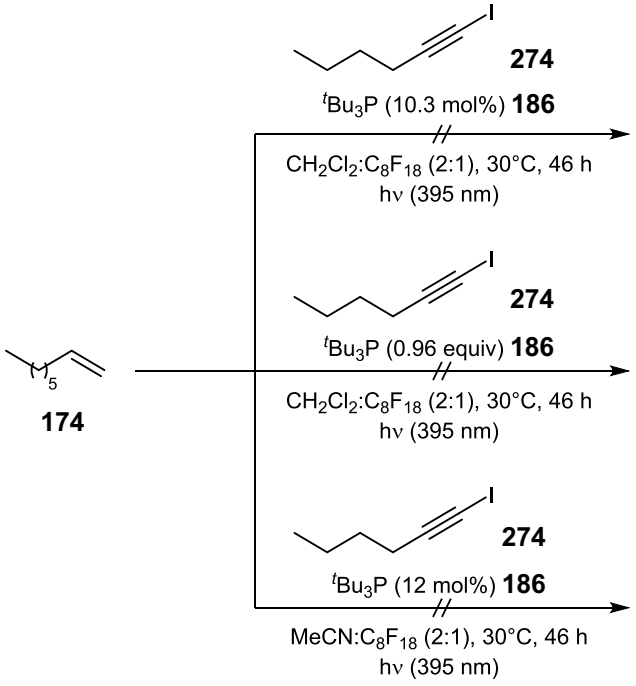

Scheme 101: Photoreactions of 1-iodohex-1-yne (**274**)in the presence of 1-octene (**174**) with different solvent systems.

9. Summary

By examining the mechanism of FLP-catalyzed iodooperfluoroalkylation in more detail, it was shown that the reaction can also be carried out exclusively with a phosphane and the irradiation of visible light.[2-4] A review of the literature showed only two other examples of phosphorus-catalyzed iodoperfluoroalkylations. Both did not mentioned a photomediated process.[87, 89] This point was taken as an motivation for this work. By repeating the literature-known experiments, the starting point for further investigation was set. It was shown that a permanent light irradiation was necessary to achieve complete conversion of the iodoperfluoroalkylation.[4]

The screening of different phosphorus(III) compounds revealed, that tri-*tert*-buylphosphine (**186**) was the most effective catalyst for this reaction. By irradiation, with blue light, various alkenes and alkynes were successfully transformed into the corresponding perfluoroalkylated products (Scheme 102).[4, 6]

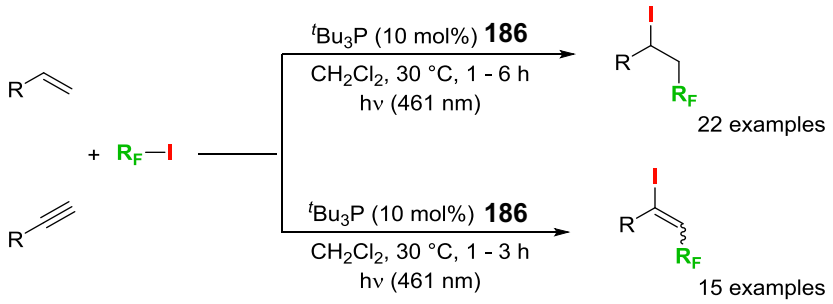

Scheme 102: Investigation of photochemical perfluoroalkylation using ^{t}Bu$_3$P **186** as catalyst.[4, 6]

The photomediated iodoperfluoroalkylation is advantageous to the FLP-catalyzed reaction due to a higher functional group tolerance and the shorter reaction time. This could be demonstrated in the investigation of the superstrate spectrum of the alkynes.[6] Switching from perfluoroalkyl iodides to ethyl difluoroiodoacetate demonstrated, that the reaction is not limited to the perfluoroalkyl iodides. However, theoretical calculations give more profound insights into the reactivity. The theoretical calculations confirmed a more accurate picture of the absorption characteristics and supported the experimentally measured UV-VIS spectra.[5]

The conducted experiments and the establishment of the method of the photoinduced and phosphorus-catalyzed iodoperfluoroalkylation resulted in four publications of the results.[2, 4-6]

10. Experimental Section

All syntheses involving air- and moisture-sensitive compounds were carried out inside a glove box (Vacuum Atmospheres Company, OMNI-LAB) under N_2 atmosphere (Air Liquide ALPHAGAZ™ 5.0). Glassware was dried for 2 hours at 120 °C and cooled down *in vacuo*.

Reagents, as well as solvents, were purchased from abcr, Acros, Fluorochem, J & K scientific, Sigma Aldrich, TCI, and VWR chemicals. Chemicals were used without further purification or purified according to laboratory methods.[115] Solvents (dichloromethane, toluene, *n*-pentane, tetrahydrofurane, and diethyl ether) were dried with the solvent purification system (MP-SPS 800 M.Braun), distilled and degassed with freeze-pump-thaw if necessary.

Nonafluoro-1-iodobutane was filtered through a column packed with aluminum oxide 90 basic 0.063-0.200 mm (activity stage I) and activated molecular sieve (4 Å) under N_2 atmosphere. The clear liquid was stored in amber glass vials under N_2 atmosphere and molecular sieve (4 Å)

Reactions were monitored by thin-layer chromatography (TLC) using Macherey-Nagel silica gel plates ALUGRAM® Xtra SIL G/UV254 (0.20 mm thickness) and visualized by UV light or staining reagents if necessary. As staining reagents self-prepared potassium permanganate solution ($KMnO_4$ (3.0 g), K_2CO_3 (20 g), NaOH (5.0 mL 5.0%), H_2O (300 mL)) or cerium molybdophosphoric acid (molybdophosphoric acid (0.5 g), H_2O (250 mL), conc. H_2SO_4 (16 mL), Ce(IV)sulphate (2.0 g)) were used. Chromatographic purification of products was performed on silica gel (Macherey-Nagel 60 M (0.04 - 0.063 mm)).

^{1}H-, ^{13}C-, ^{19}F-, ^{31}P-NMR spectra were recorded on Bruker Avance III 300 and 600. Chemical shifts are reported in parts per million (ppm) to the corresponding solvent. The order of citation in parentheses is a) multiplicity (s = singlet, d = doublet, t = triplet, q = quartet, ddd = doublet of doublet of doublet, td = triplet of doublet, m = multiplet), b) coupling constants, c) number of protons and d) assignment. Coupling constants (*J*) were reported in Hertz (Hz). If not described differently, the NMR-spectra were measured at 298 K. When it is mentioned, ^{19}F-NMR shifts were referenced to $CFCl_3$ in C_6D_6 and ^{31}P-NMR to H_3PO_4 in D_2O as an external standard.

IR spectra were recorded using a Jasco FT/IR-6200 spectrometer. Samples were measured as film on a NaCl single crystal. The absorption bands were given in wavenumbers (cm^{-1}).

Melting points were recorded on a Büchi B-540.

UV-VIS-measurements were measured on a Perkin Elmer Lamda 2 UV-VIS spectrometer in Hellma cuvettes (10 x 10 mm, Suprasil quartz glass).

High-resolution mass spectra (HRMS) were measured with a Bruker Daltonics UHR-QTOF maXis 4G.

Elemental analysis were measured on an elementar Vario Micro Cube.

As chiral GC a Dani Master GC was used with a chiral column (DN-GAMMA, 25 m x 0.25 mm x 0.25µm). The sample was injected with a Hamilton CR-700-20. Hydrogen was generated with a UHP-40H from the company WGA. Nitrogen, Helium (both 99.999%) and synthetic air (20.5 ± 0.5 % O_2 in N_2) were purchased from Air Liquide ALPHAGAZ™.

Inside the fume hood, all reactions were conducted under red light (Jedi Lightning E27 ID60, 806 lm, 11W) and best possible light exclusion. Inside the glovebox, all reactions were prepared with an RGB LED-strip as light source. The emission spectra of the LED-strip were measured with a RED Tide USB650UV-spectrometer. Unless otherwise stated, all photoreactions were conducted inside 4 mL screw neck glass vials with a septa screw cap. The used photoreactor is self-assembled and is described in the literature.[4]

Structural formulas were prepared with Chemdraw Professional 16.0 from CambridgeSoft. NMR-spectra were analyzed with MestReNova (version 11.0.0 and 14.1.1) from Mestrelab Research. Images of the 3D modeled objects were visualized with Autodesk Fusion 360 (version 2.0.8176).

Eur. J. Org. Chem. · ISSN 1099–0690

https://doi.org/10.1002/ejoc.201800866

SUPPORTING INFORMATION

Title: Mechanistic Insights into FLP-Catalyzed Iodoperfluoroalkylations
Author(s): Michael Spittler, Lucas Helmecke, Constantin Czekelius*

Contents

1 General Experimental Procedures

All syntheses involving air- and moisture-sensitive compounds were carried out inside a glove box (*Vacuum Atmospheres Company* model OMNI-LAB) under N_2 atmosphere (*Air Liquide ALPHAGAZ*™ 5.0). Glassware was dried for 2 hours at 120 °C and cooled down in vacuo.

Reagents as well as solvents were purchased from Acros, Sigma Aldrich, abcr, TCI, J & K scientific or VWR Chemicals. Chemicals were used without further purification or purified according to laboratory methods.[1] Vinylcyclohexane was purified by distillation at ambient pressure after refluxing over CaH_2 for 2 h. Solvents were dried with the solvent purification system MP-SPS 800 from *M.Braun*, predistilled and if necessary degassed with freeze-pump-thaw.

Reactions were monitored by thin-layer chromatography (TLC) using *Macherey-Nagel* silica gel plates ALUGRAM® Xtra SIL G/UV_{254} (0.20 mm thickness) and visualised by UV light or staining reagents if necessary. As staining reagents self-prepared potassium permanganate solution ($KMnO_4$ (3.0 g), K_2CO_3 (20 g), NaOH (5.0 ml 5.0%), H_2O (300 ml)) or cerium molybdophosphoric acid (molybdophosphoric acid (0.5 g), H_2O (250 ml), conc. H_2SO_4 (16 ml), Ce(IV)sulphate (2.0 g)) were used. Chromatographic purification of products was performed on *Macherey-Nagel* 60 M (0.04 - 0.063 mm) silica gel.

^{1}H-, ^{11}B-, ^{13}C, ^{19}F-, ^{31}P-NMR spectra were recorded on *Bruker* Avance III 300 and 600. Chemical shifts are reported in parts per million (ppm). ^{1}H-NMR shifts are reported in reference to the corresponding solvent. ^{19}F-NMR shifts were reported in ppm and referenced to $CFCl_3$ in C_6D_6 and ^{31}P-NMR to H_3PO_4 in D_2O. The order of citation in parentheses is a) multiplicity (s = singlet, d = doublet, t = triplet, q = quartet, ddd = doublet of doublet of doublet, td = triplet of doublet, m = multiplet), b) coupling constants, c) number of protons, and d) assignment. Coupling constants (*J*) were reported in Hertz (Hz). The attributions of the chemical shifts were determined by means of COSY, HSQC, and HMQC experiments. If not described differently the NMR-spectra were measured at 298 K. For inert additions to an NMR sample outsight the glovebox, a Kontes® NMR tube sealing manifold was used.

IR spectra were recorded using a *Jasco* FT/IR-6200 spectrometer. Samples were measured as film on a NaCl crystal. The absorption bands were given in wave numbers (cm^{-1}). High resolution mass spectra (HRMS) were measured with a *Bruker Daltonics* UHR-QTOF maXis 4G. Elemental analysis were measured on an *elementar* Vario Micro Cube.

Due to the volatility of 4-pentenyl-1-cyclopropane it was obtained as mixture with solvent and small amounts of impurities, whereby an elemental analysis was not possible.

Tris(pentafluorophenyl)borane ($B(C_6F_5)_3$[2] and [$^tBu_3PI$][$FB(C_6F_5)_3$][3] were synthesised according to a literature procedure. GC setup and experiments are described in the respective chapter.

2 Screenings

2.1 Phosphane screening

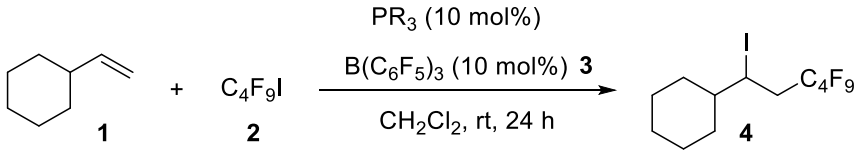

Phosphane (10 mol%) and tris(pentafluorophenyl)borane (**2**) (10 mol%) were weighed into a small glass vial and dissolved in CH_2Cl_2 (1.2 ml). After placing the glass vial in an amber glass screw-top jar vinylcyclohexane (**1**) (56 µl, 0.41 mmol, 1.0 eq.) was added. Under light exclusion using red light, nonafluoro-1-iodobutane (**2**) (70 µl, 0.41 mmol, 1.0 eq.) was added and the jar was sealed with a Teflon-insert screw cap. After stirring for 24 h conversion was determined *via* ^{1}H- and ^{19}F-NMR-spectroscopy (Table 1).

Table 1: Phosphane screening, calculated conversions.

		conversion [%]	
		^{1}H-NMR	^{19}F-NMR
Tri-*tert*-butylphosphane	$^tBu_3P$	≥95%	≥95%
Tricyclohexylphosphane	PCy_3	–	–
Tri-*n*-butylphosphane	$^nBu_3P$	–	–
Trimesitylphosphane	$PMes_3$	–	–
Tri(*o*-tolyl)phosphane	$P(o\text{-tol})_3$	–	–
Tris(pentafluorophenyl)phosphane	$P(C_6F_5)_3$	–	–

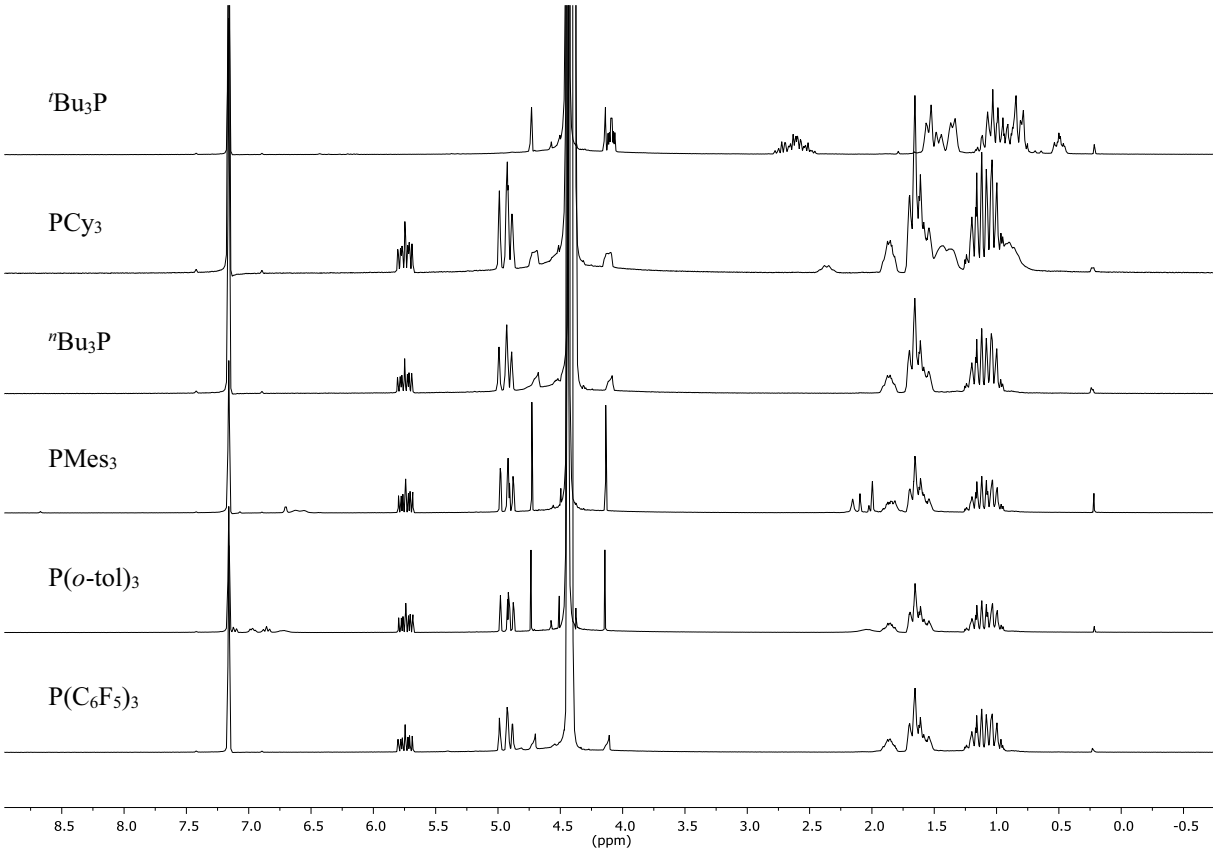

NMR-spectrum 1: ^{1}H-NMR-spectra (300 MHz, C_6D_6) of reaction solution after 24 h in CH_2Cl_2.

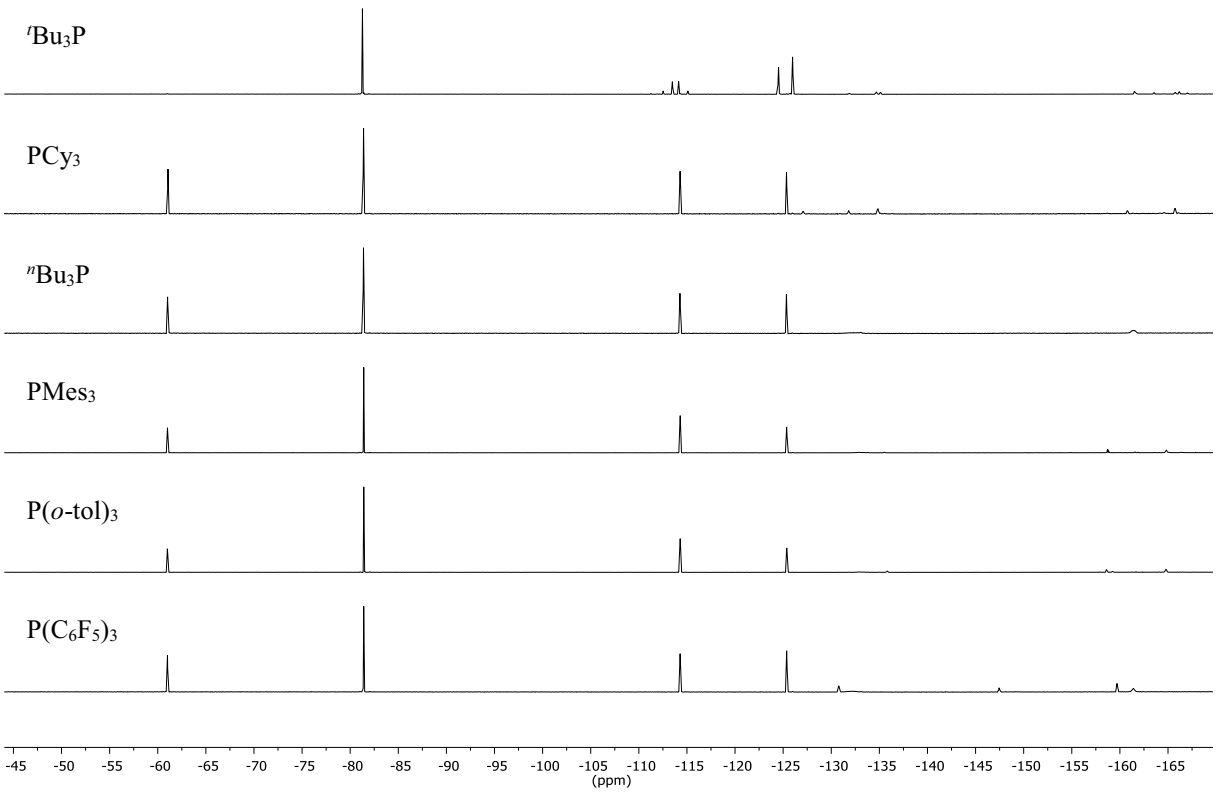

NMR-spectrum 2: ^{19}F-NMR-spectra (282 MHz, C_6D_6) of reaction solution after 24 h in CH_2Cl_2.

2.2 Determination of the NMR-shifts of the phosphanes in the presence of nonafluoro-1-iodobutane

The individual phosphane was weighed into a small glass vial, dissolved in CH_2Cl_2 (0.5 ml) and transferred into a Young valve NMR tube equipped with H_3PO_4 in D_2O and $CFCl_3$ in C_6D_6 as external standards. After measuring ^{31}P-NMR-spectra, nonafluoro-1-iodobutane (**2**) was added inside the glovebox and the ^{31}P-NMR- as well as ^{19}F-NMR-spectra were measured (Table 2).

Table 2: Shifts of the different phosphanes without and with nonafluoro-1-iodobutane and the corresponding Tolman electronic parameter as well as ligand cone angle.[4]

					Δδ			
		^{31}P-NMR without C_4F_9I [ppm]	^{31}P-NMR with C_4F_9I [ppm]	^{19}F-NMR [ppm]	^{31}P-NMR [ppm]	^{19}F-NMR [ppm]	ν (CO)[4] [cm^{-1}]	θ[4] [degree]
Nonafluoro-1-iodobutane				–60.5 –81.6 –114.5 –125.6				
Tri-*tert*-butylphosphane	$^{t}Bu_3P$	62.3	57.8	–72.0 –81.6 –115.7 –125.7	4.48	11.5 0.01 1.25 0.10	2056.1	182
Tricyclohexylphosphane	PCy_3	10.4	8.34	–69.0 –81.6 –115.5 –125.7	2.06	8.48 0.01 1.04 0.10	2056.4	170
Tri-*n*-butylphosphane	$^{n}Bu_3P$	–31.4	–31.4	–63.9 –81.6 –114.9 –125.7	–	3.40 0.02 0.40 0.06	2060.3	132
Trimesitylphosphane	$PMes_3$	–36.9	–36.9	–60.6 –81.6 –114.5 –125.6	–	0.06 0.00 0.02 0.01	2064.1	212
Tri(*o*-tolyl)phosphane	$P(o\text{-tol})_3$	–30.4	–30.4	–60.6 –81.6 –114.5 –125.6	–	0.11 0.01 0.04 0.01	2066.6	194
Tris(pentafluorophenyl)phosphane	$(C_6F_5)_3P$	–74.7	–74.7	–60.6 –81.7 –114.5 –125.7	–	0.10 0.10 0.01 0.05	2090.9	184

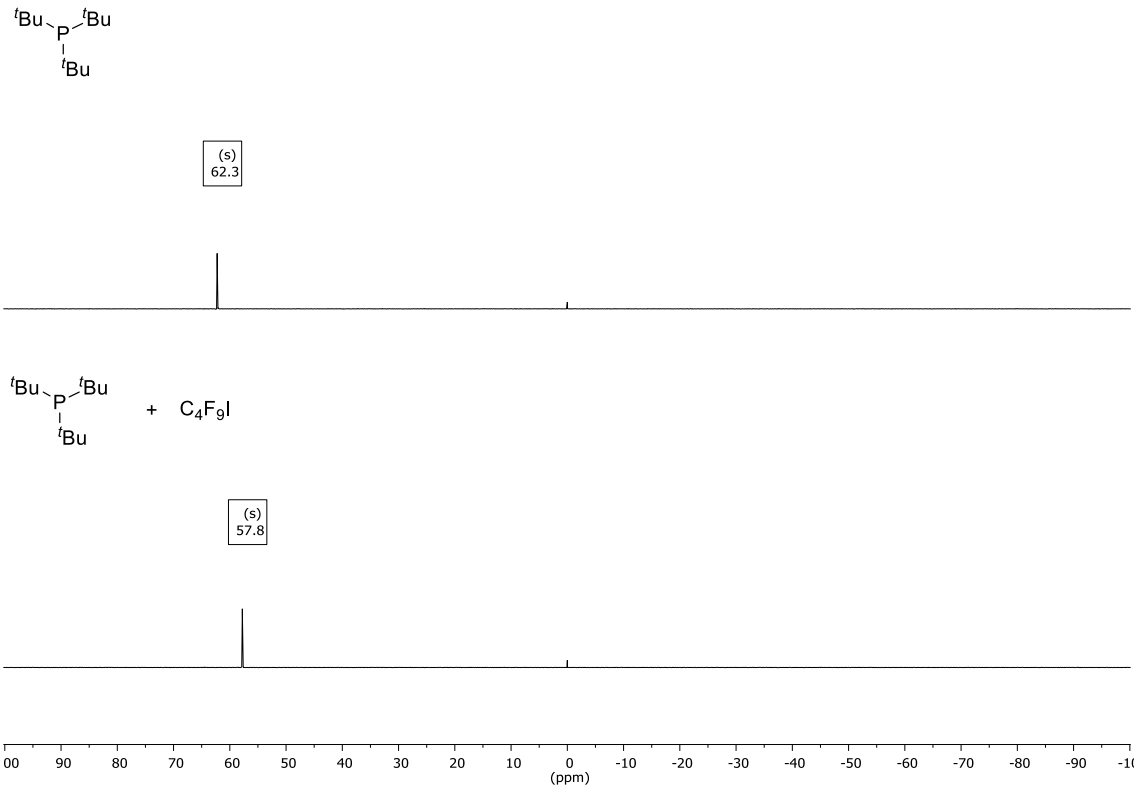

NMR-spectrum 3: ^{31}P-NMR-spectra (121 MHz, D_2O) in CH_2Cl_2.

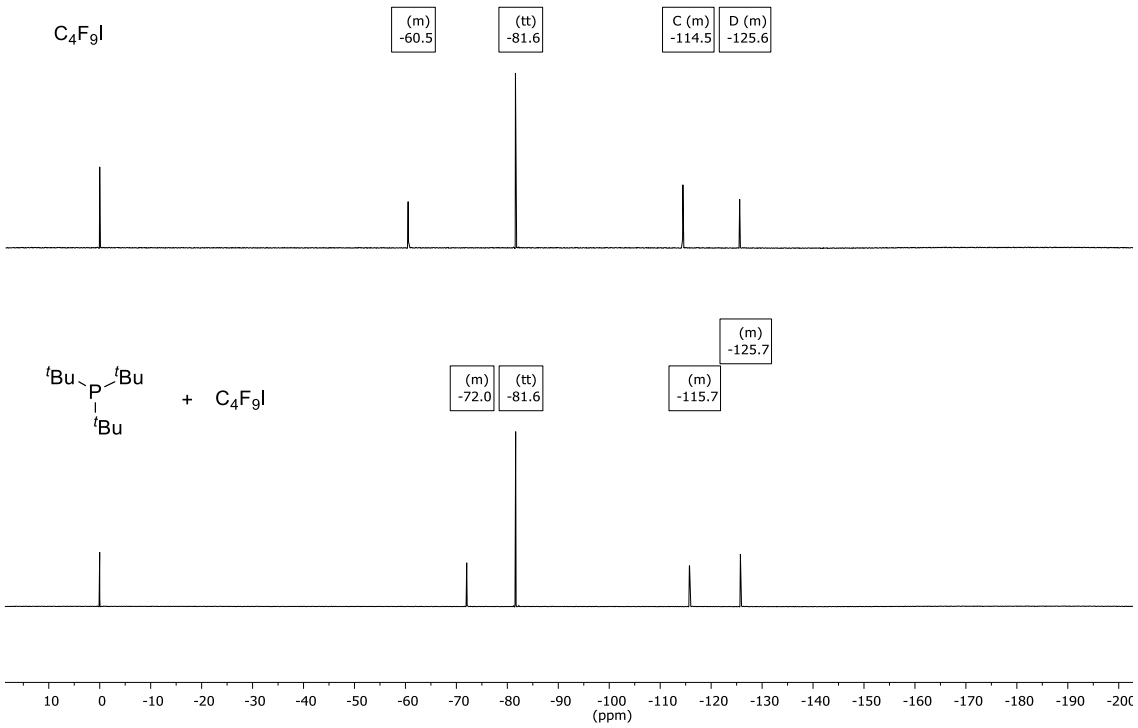

NMR-spectrum 4: ^{19}F-NMR-spectra (282 MHz, C_6D_6) in CH_2Cl_2.

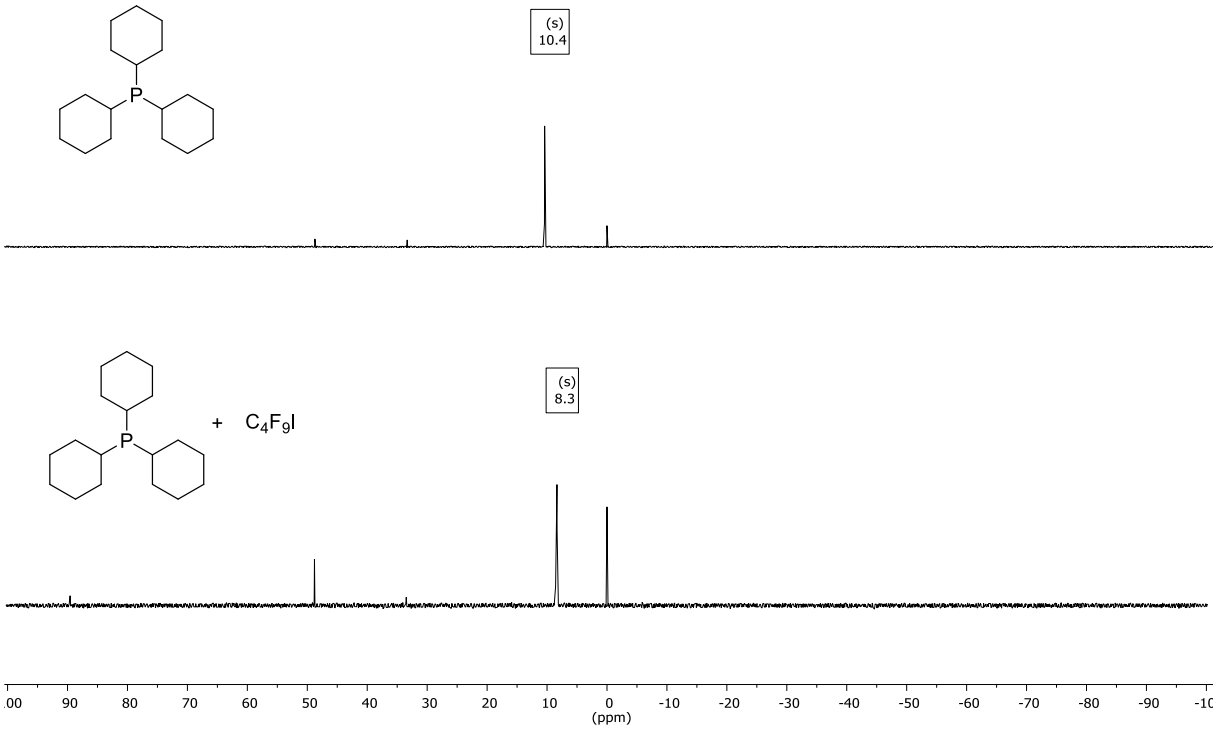

NMR-spectrum 5: ^{31}P-NMR-spectra (121 MHz, D_2O) in CH_2Cl_2.

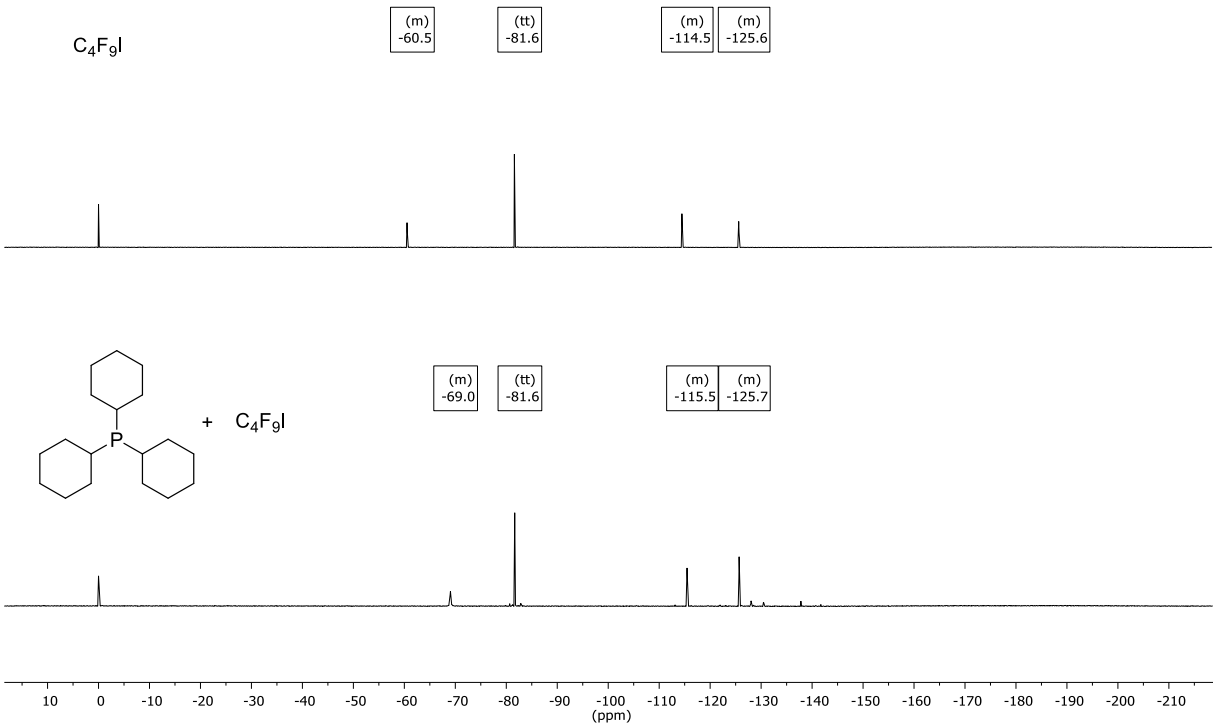

NMR-spectrum 6: ^{19}F-NMR-spectra (282 MHz, C_6D_6) in CH_2Cl_2.

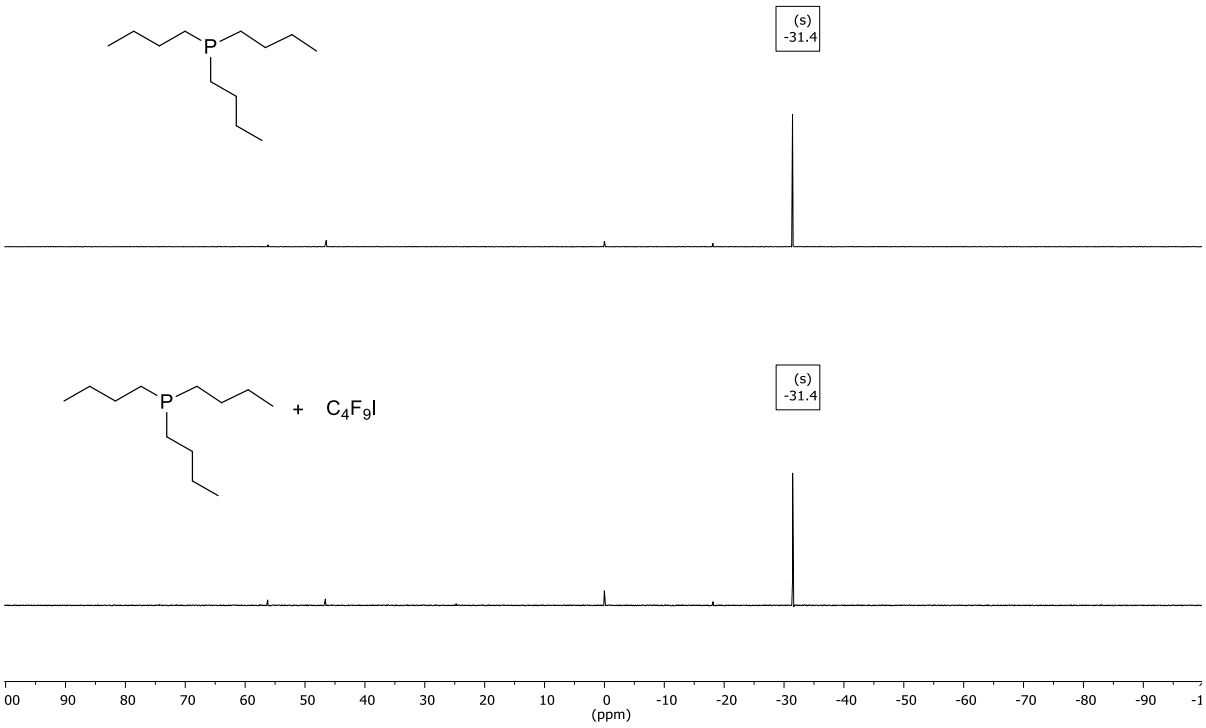

NMR-spectrum 7: ^{31}P-NMR-spectra (121 MHz, D_2O) in CH_2Cl_2.

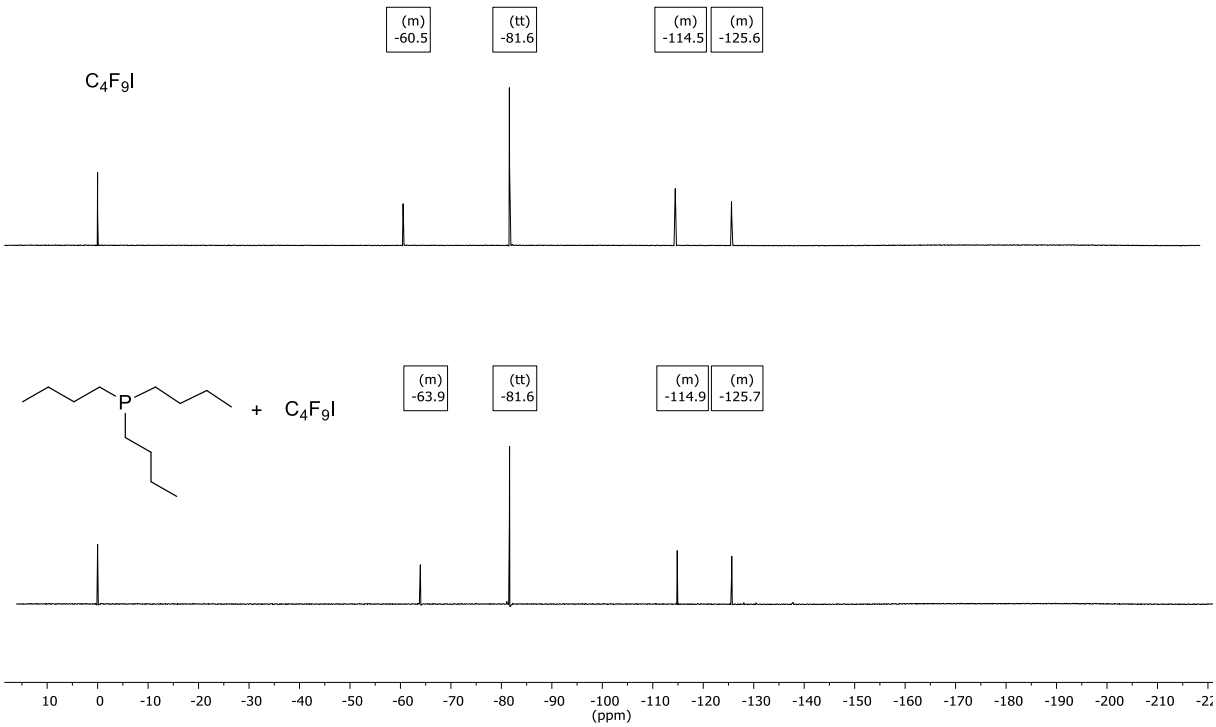

NMR-spectrum 8: ^{19}F-NMR-spectra (282 MHz, C_6D_6) in CH_2Cl_2.

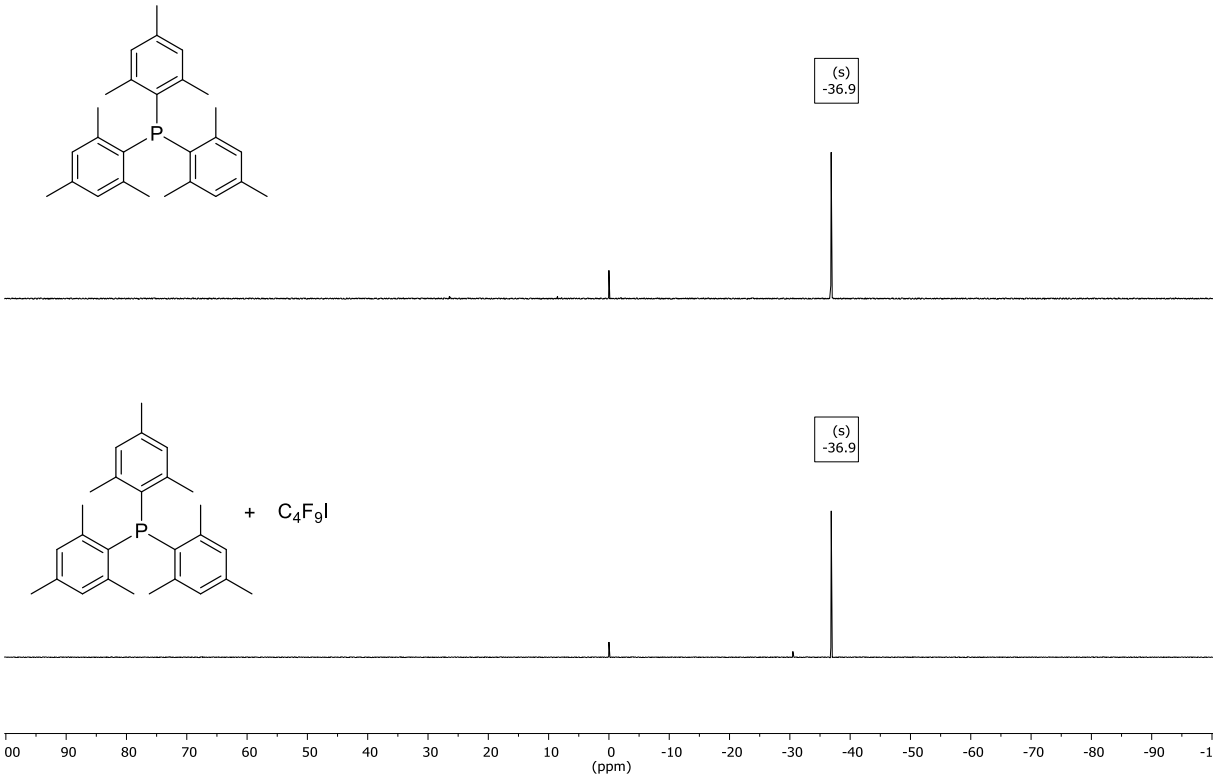

NMR-spectrum 9: ^{31}P-NMR-spectra (121 MHz, D_2O) in CH_2Cl_2.

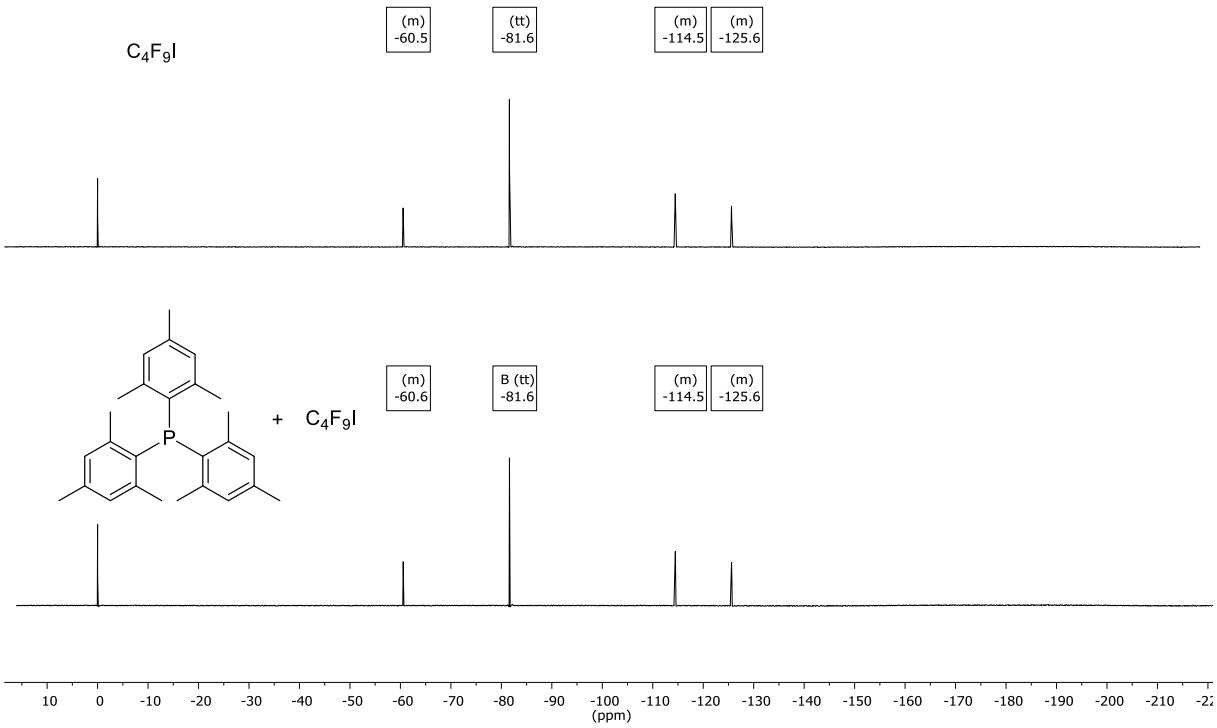

NMR-spectrum 10: ^{19}F-NMR-spectra (282 MHz, C_6D_6) in CH_2Cl_2.

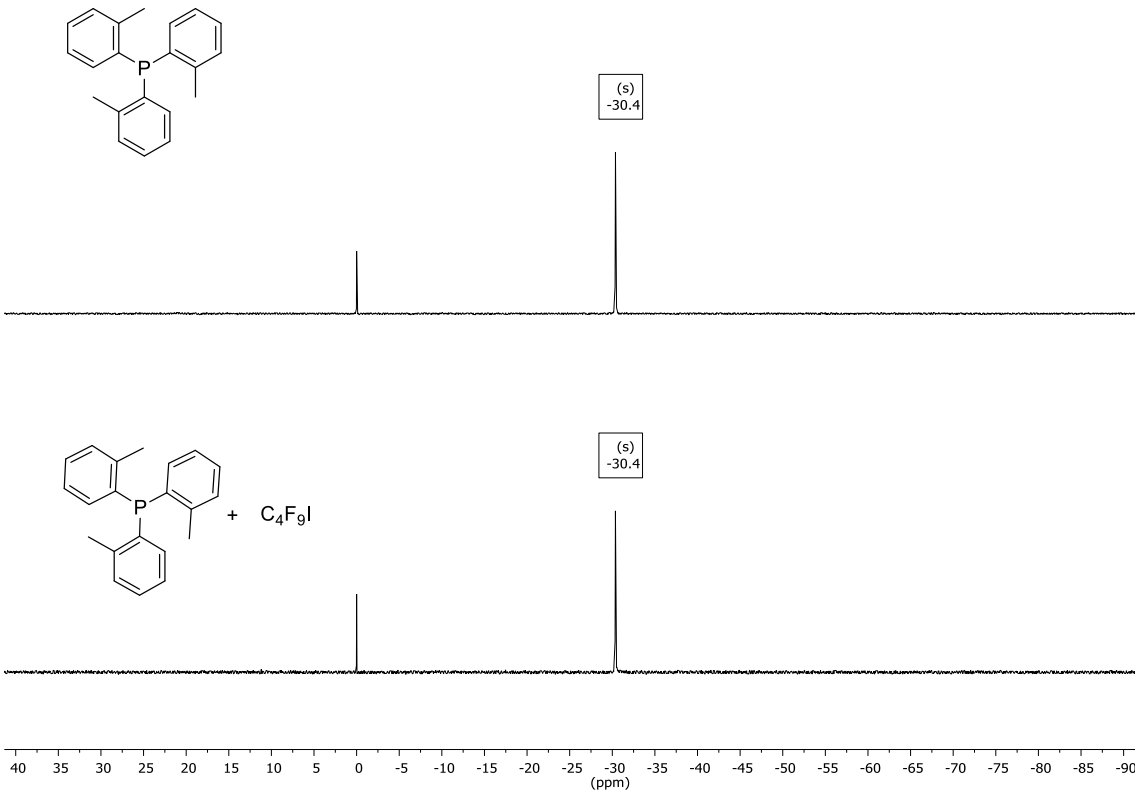

NMR-spectrum 11: ^{31}P-NMR-spectra (121 MHz, D_2O) in CH_2Cl_2.

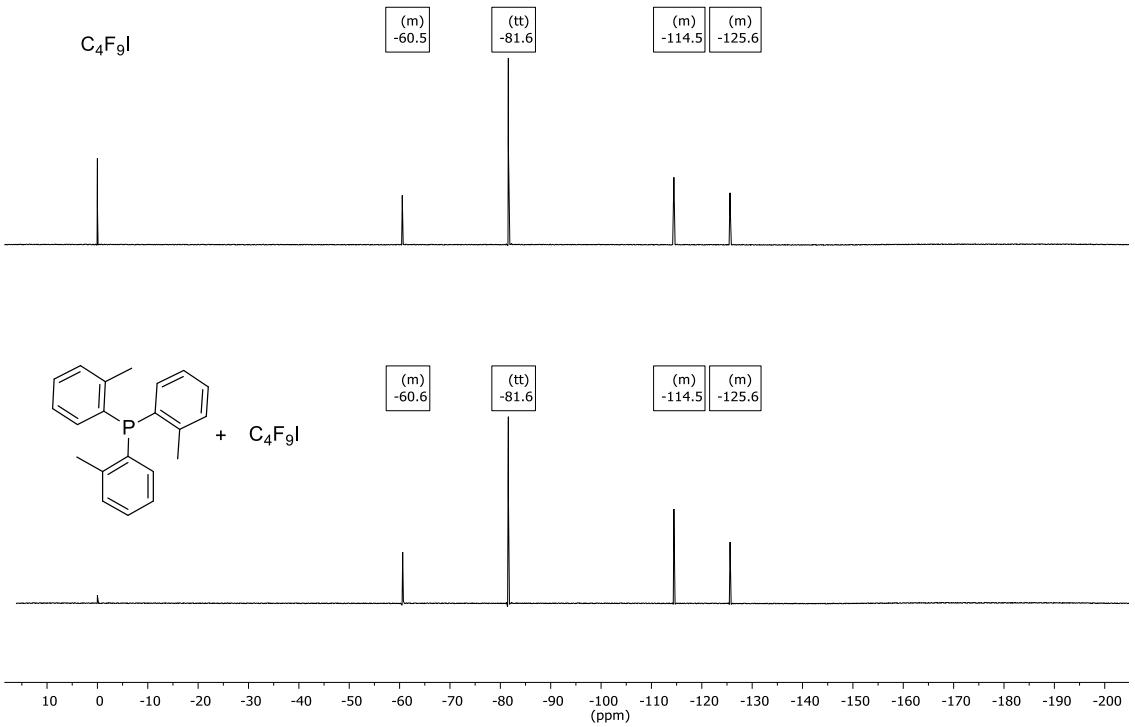

NMR-spectrum 12: ^{19}F-NMR-spectra (282 MHz, C_6D_6) in CH_2Cl_2.

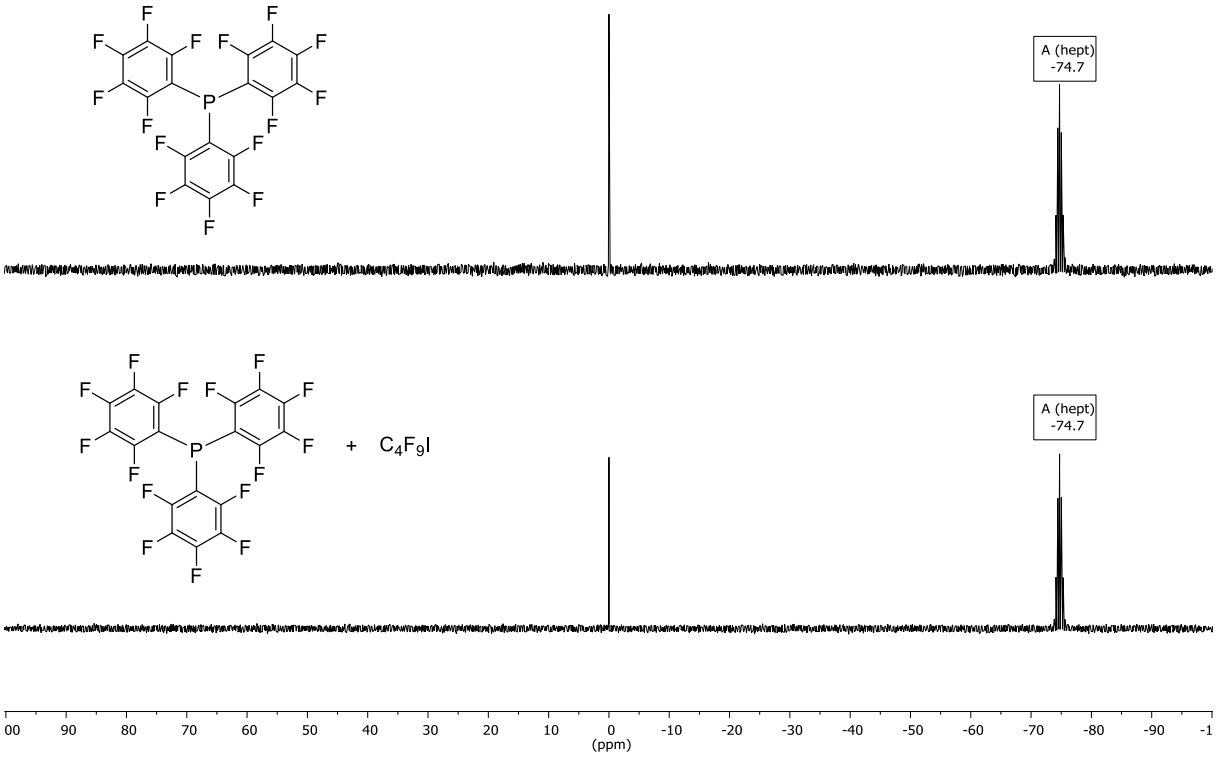

NMR-spectrum 13: ^{31}P-NMR-spectra (121 MHz, D_2O) in CH_2Cl_2.

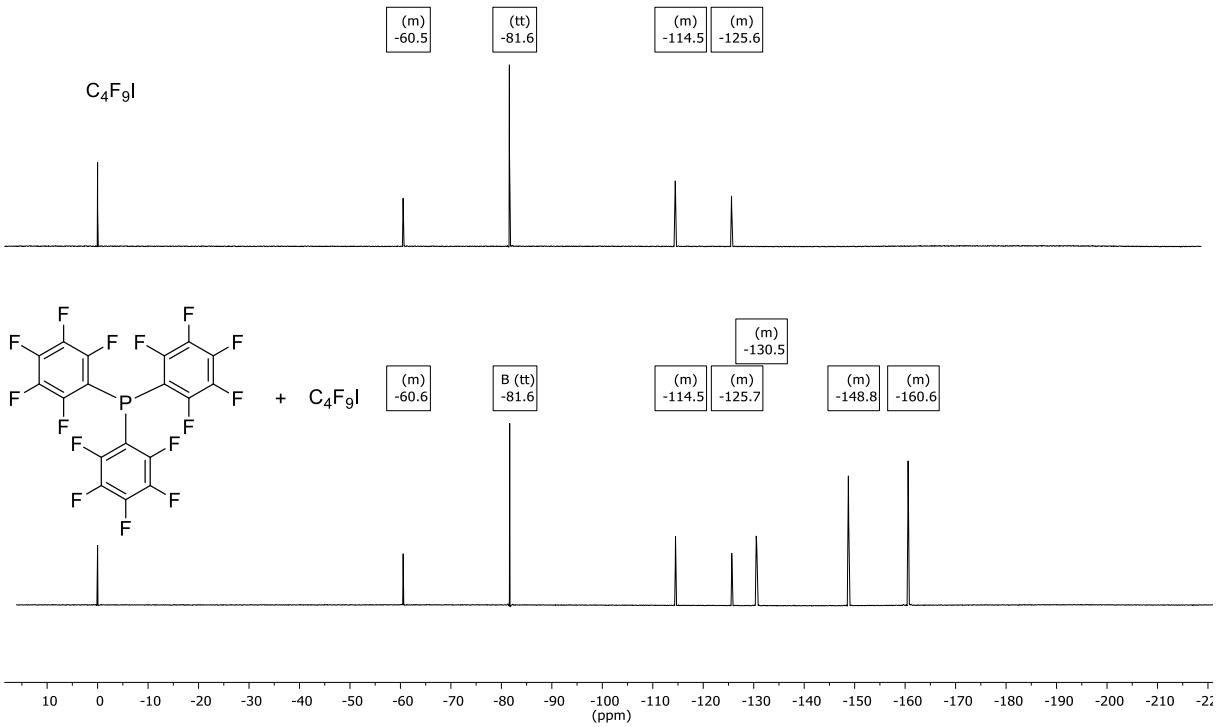

NMR-spectrum 14: ^{19}F-NMR-spectra (282 MHz, C_6D_6) in CH_2Cl_2.

2.3 Solvent screening

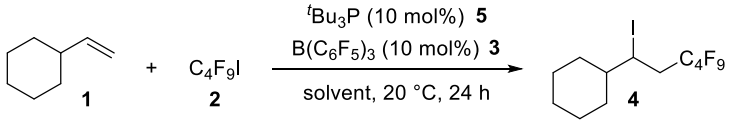

$^{t}Bu_3P$ (**5**) (10 mol%) and $B(C_6F_5)_3$ (**3**) (10 mol%) were weighed into a small glass vial and dissolved in the denoted solvent (1.2 ml). After placing the glass vial in an amber glass screw-top jar, vinylcyclohexane (**1**) (56 µl, 0.41 mmol, 1.0 eq.) was added. Under light exclusion using red light nonafluoro-1-iodobutane (**2**) (70 µl, 0.41 mmol, 1.0 eq.) was added and the jar was sealed with a Teflon-insert screw cap. After stirring for 24 h at 20 °C, a sample was taken (0.10 ml) and diluted with C_6D_6 (0.50 ml). Conversion was determined *via* ^{1}H- and ^{19}F-NMR-spectroscopy (Table 3).

Table 3: Overview of the result of the solvent screening.

	conversion [%]		dipole moment
	^{1}H-NMR	^{19}F-NMR	[debye][5]
benzene-d_6	–	–	0
toluene	–	–	0.4
CH_2Cl_2	95	≥99	1.6
chlorobenzene	32	31	1.7
1,2-dichlorobenzene	68	72	2.5
1,3-dichlorobenzene	49	50	1.7
fluorobenzene	35	35	1.6
1,2-difluorobenzene	68	72	–
1,4-difluorobenzene	26	25	–

3 Iodoperfluoroalkylation reactions

3.1 Reaction of 6-bromohexene with nonafluoro-1-iodobutane

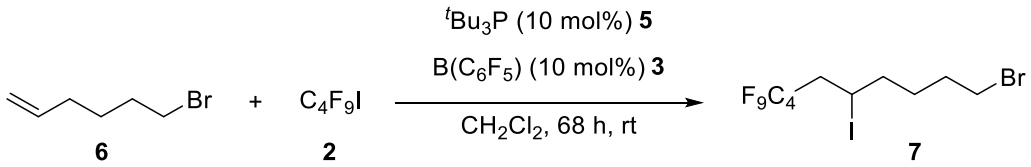

^{t}Bu$_3$P (**5**) (0.0153 g, 0.0756 mmol, 10 mol%) and B(C_6F_5)$_3$ (**3**) (0.0386 g, 0.0756 mmol, 10 mol%) were weighed in an amber glass screw-top jar and dissolved in CH_2Cl_2 (2.1 ml). After addition of 6-bromohexene (**6**) (100 µl, 0.748 mmol, 1.00 eq.) and nonafluoro-1-iodobutane (**2**) (130 µl, 0.755 mmol, 1.01 eq.) the jar was sealed with a Teflon-insert screw cap and the solution was stirred for 68 h. After removal of the solvent the crude product was purified by column chromatography (silica gel, eluent: pentane, $R_f = 0.73$) to give product **7** (0.352 g, 0.692 mmol, 93%).

^{1}H-NMR (300 MHz, $CDCl_3$) δ [ppm] 4.40 - 4.25 (m, 1H, C*H*I), 3.51 - 3.36 (t, J = 6.6 Hz, 2H, CH_2Br), 3.07 - 2.64 (m, 2H, CH_2CF$_2$), 2.08 - 1.46 (m, 6H, CHI-CH_2CH_2CH_2-CH$_2$Br). **^{13}C{^{1}H}-NMR** (75.5 MHz, $CDCl_3$) δ [ppm] 41.7 (−H$_2$*C*CF$_2$R$_F$, t, $^2J_{CF}$ = 21.0 Hz), 39.5, 33.1, 31.7, 28.5, 19.9. **^{19}F-NMR** (282 MHz, $CDCl_3$) δ [ppm] –80.9 - –81.1 (t, J = 9.6 Hz, 3F, CF_3), –111.1 - −115.5 (m, 2F, CF_2), –124.3 - –124.8 (m, 2F, CF_2), –125.6 - –126.2 (m, 2F, CF_2). **IR** (film on NaCl), $\tilde{\nu}$ [cm^{-1}] 3215, 2942, 1455, 1433, 1350, 1232, 1134, 880, 724. **Elemental analysis** for $C_{10}H_{11}BrF_9I$: calculated: C: 23.60 %, H: 2.18 %, measured: C: 23.61%, H: 2.42%.

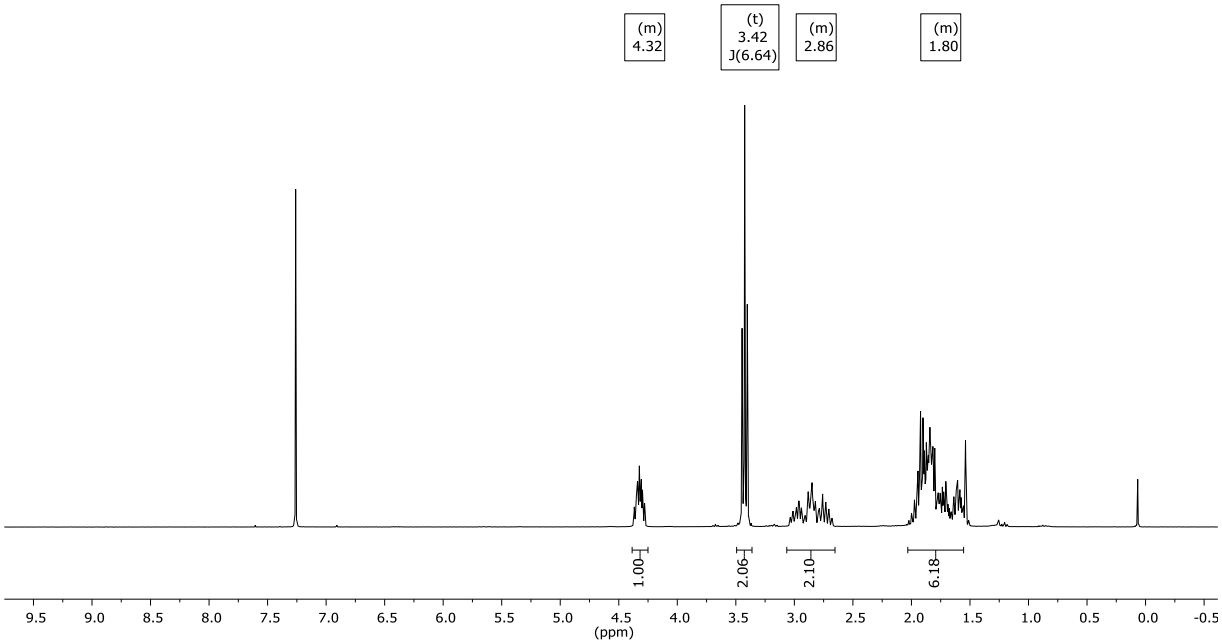

NMR-spectrum 15: ^{1}H-NMR-spectrum (300 MHz, $CDCl_3$) of 10-bromo-1,1,1,2,2,3,3,4,4-nonafluoro-6-iododecane.

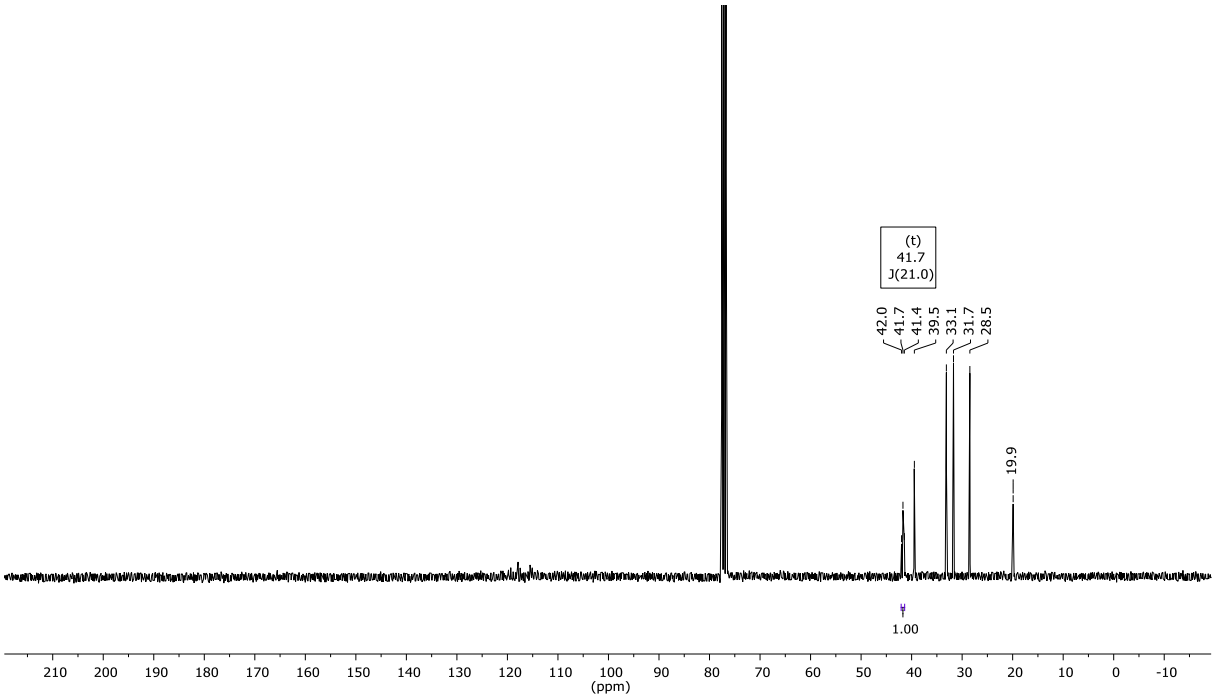

NMR-spectrum 16: ^{13}C-NMR-spectrum (75.5 MHz, $CDCl_3$) of 10-bromo-1,1,1,2,2,3,3,4,4-nonafluoro-6-iododecane.

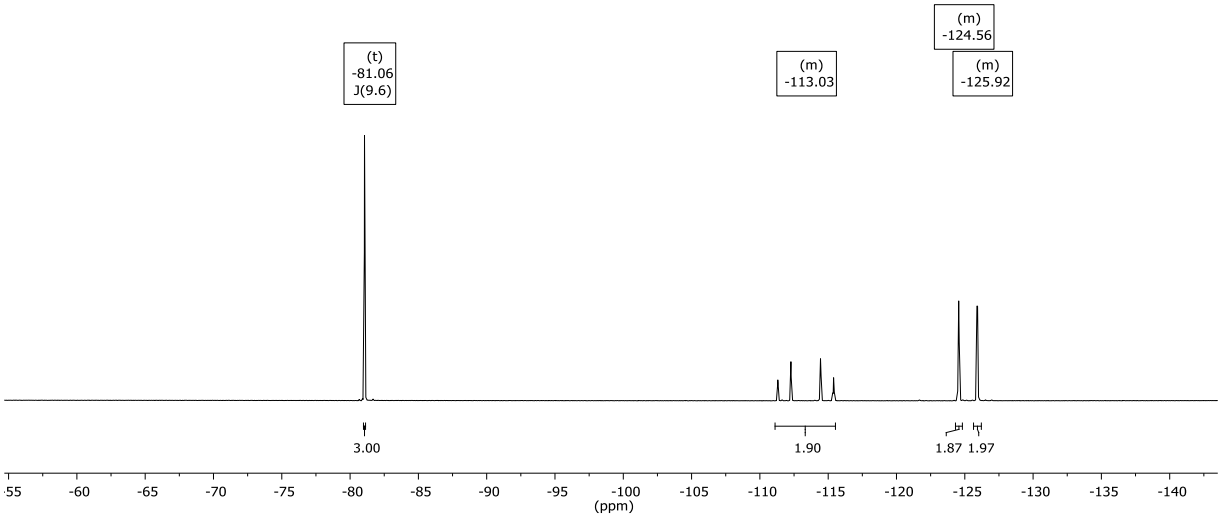

NMR-spectrum 17: ^{13}F-NMR-spectrum (282 MHz, $CDCl_3$) of 10-bromo-1,1,1,2,2,3,3,4,4-nonafluoro-6-iododecane.

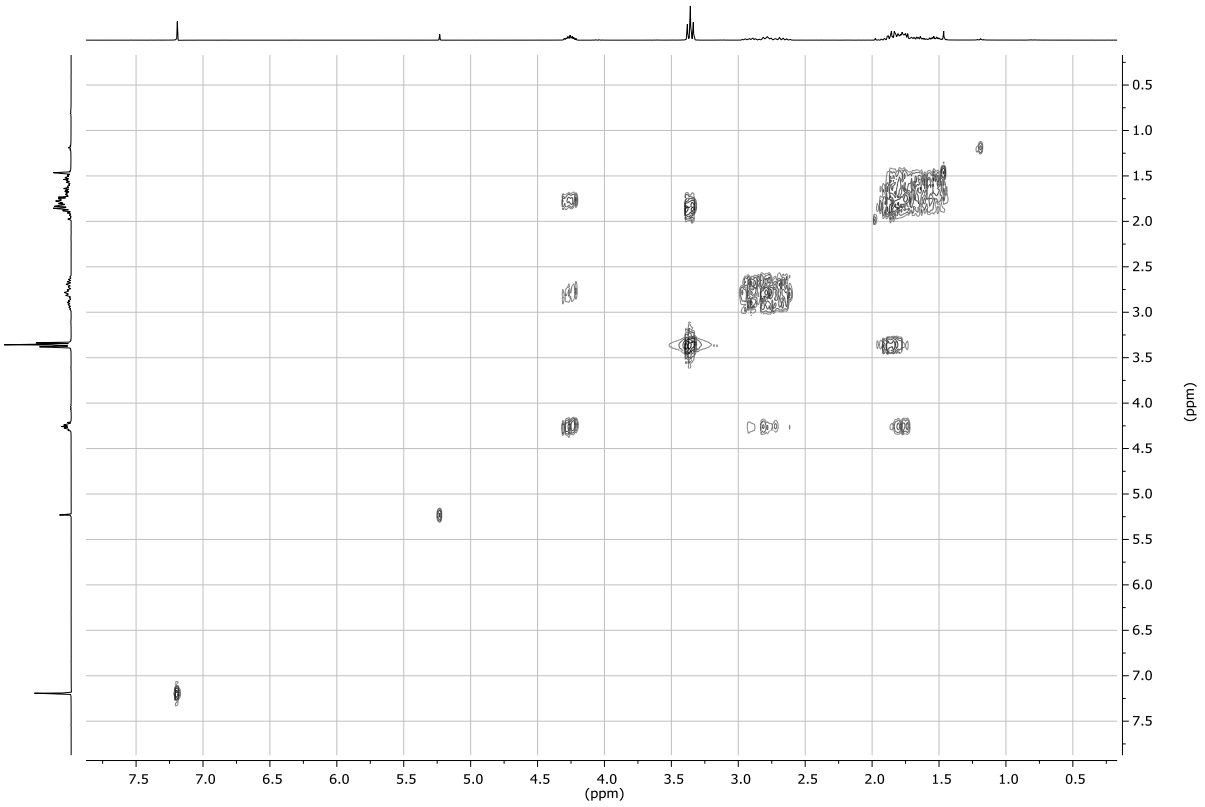

NMR-spectrum 18: COSY-spectrum (300 MHz, $CDCl_3$) of 10-bromo-1,1,1,2,2,3,3,4,4-nonafluoro-6-iododecane.

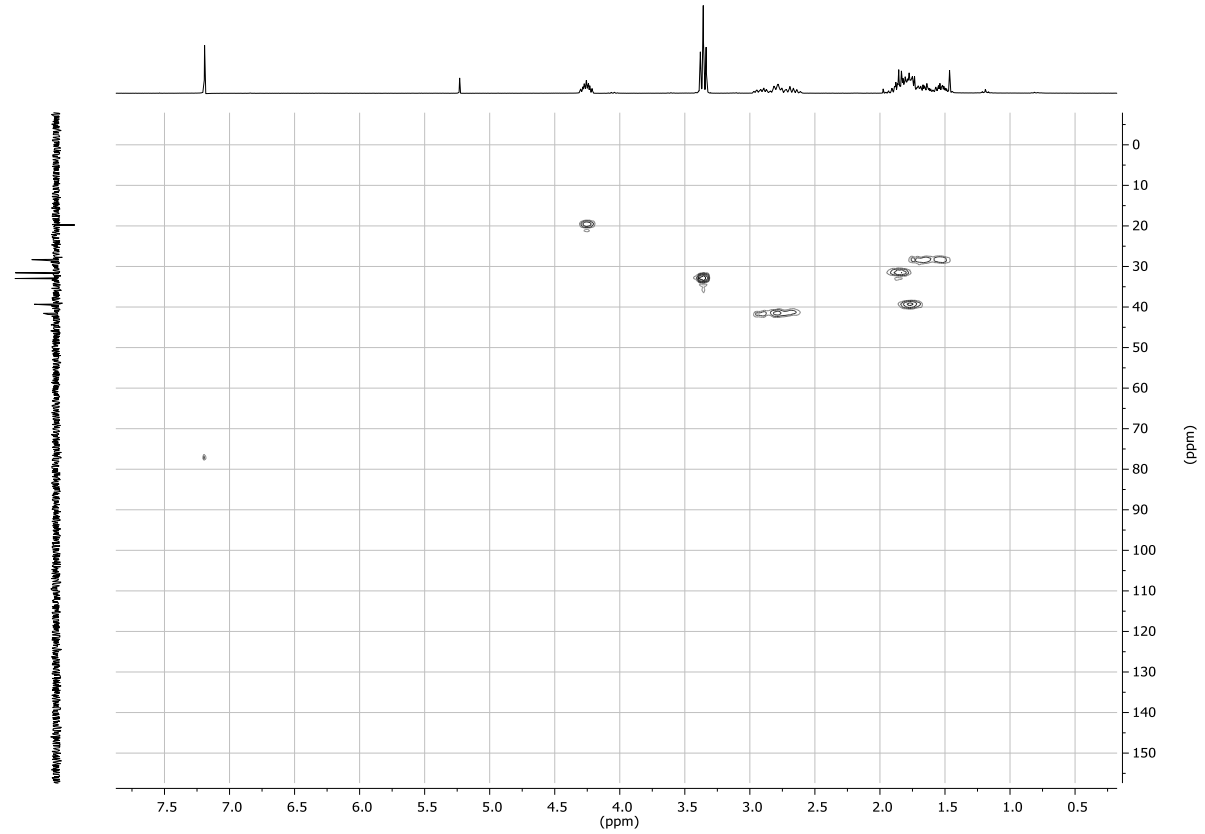

NMR-spectrum 19: HSQC-spectrum (300, 75.5 MHz, $CDCl_3$) of 10-bromo-1,1,1,2,2,3,3,4,4-nonafluoro-6-iododecane.

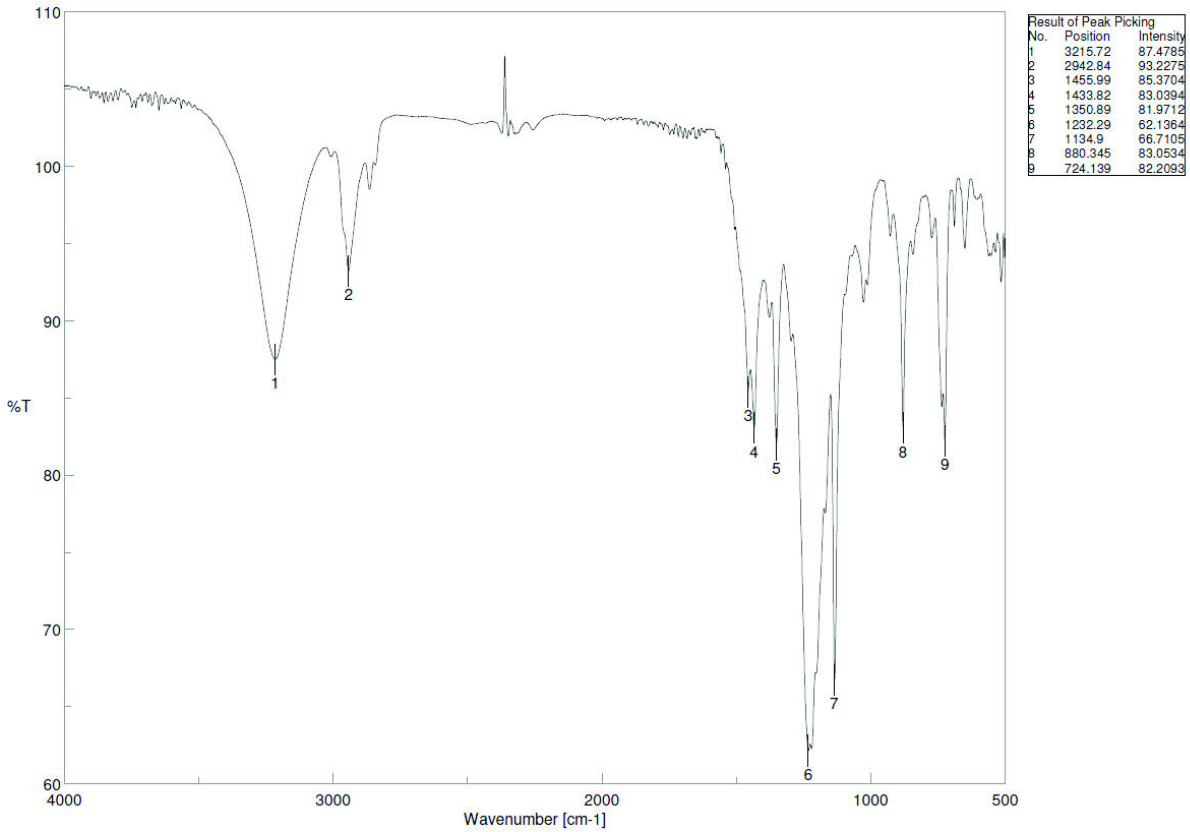

IR-spectrum (film on NaCl) 1: 10-bromo-1,1,1,2,2,3,3,4,4-nonafluoro-6-iododecane.

3.2 Reaction of 4-penten-1-ylcyclopropane, NMR-experiment

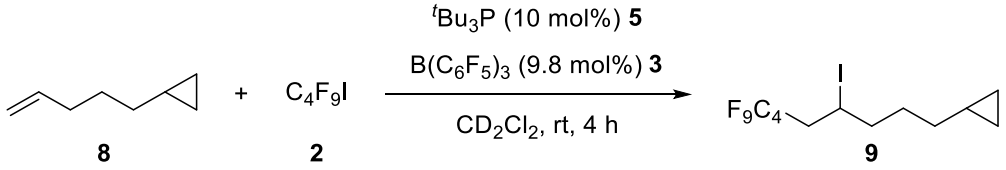

Inside the glovebox, $^{t}Bu_3P$ (**5**) (5.6 mg, 0.0277 mmol, 10 mol%) and $B(C_6F_5)_3$ (**3**) (13.8 mg, 0.0270 mmol, 9.8 mol%) were weighed into a small glass vial, dissolved in CD_2Cl_2 (0.6 ml) and transferred into an amber NMR tube. Outside the glovebox, 4-penten-1-ylcyclopropane (**8**) (30.3 mg, 0.275 mmol, 1.00 eq.) and nonafluoro-1-iodobutane (**2**) (35.0 µl, 0.206 mmol, 1.15 eq.) was added with a syringe under argon atmosphere. The NMR tube was sealed with a black cap, wrapped with aluminum foil and measured after 4 h.

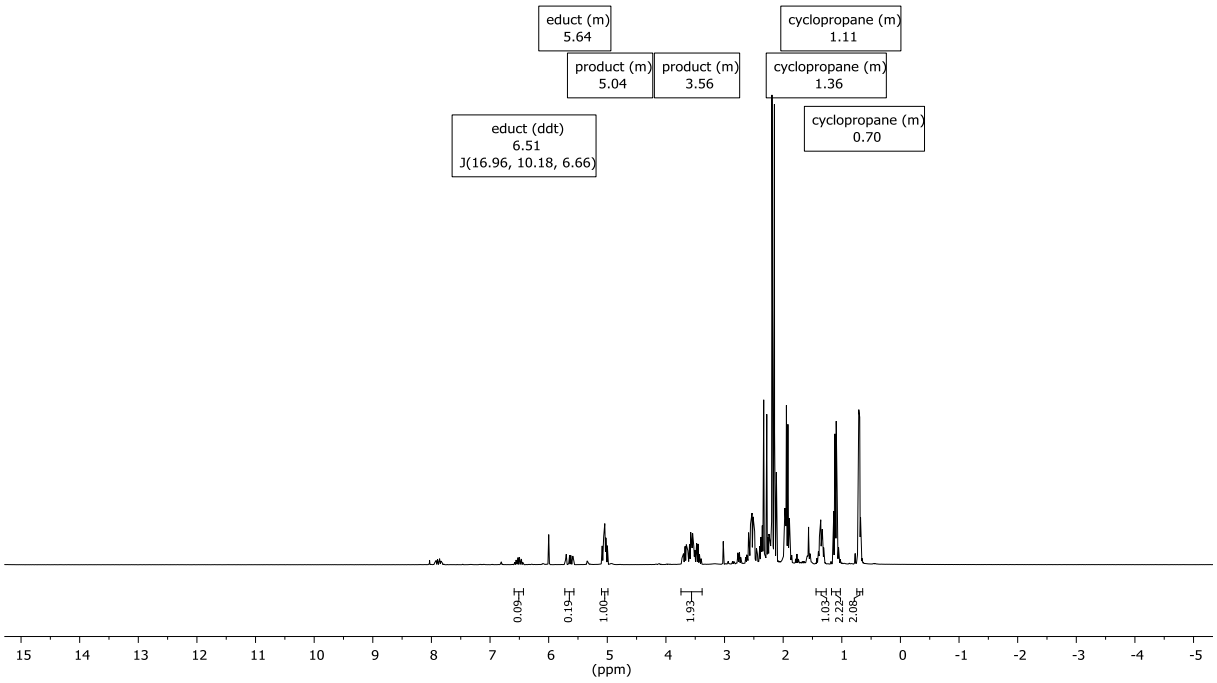

NMR-spectrum 20: ^{1}H-NMR-spectra (300 MHz, CD_2Cl_2) of the reaction with 4-penten-1-ylcyclopropane.

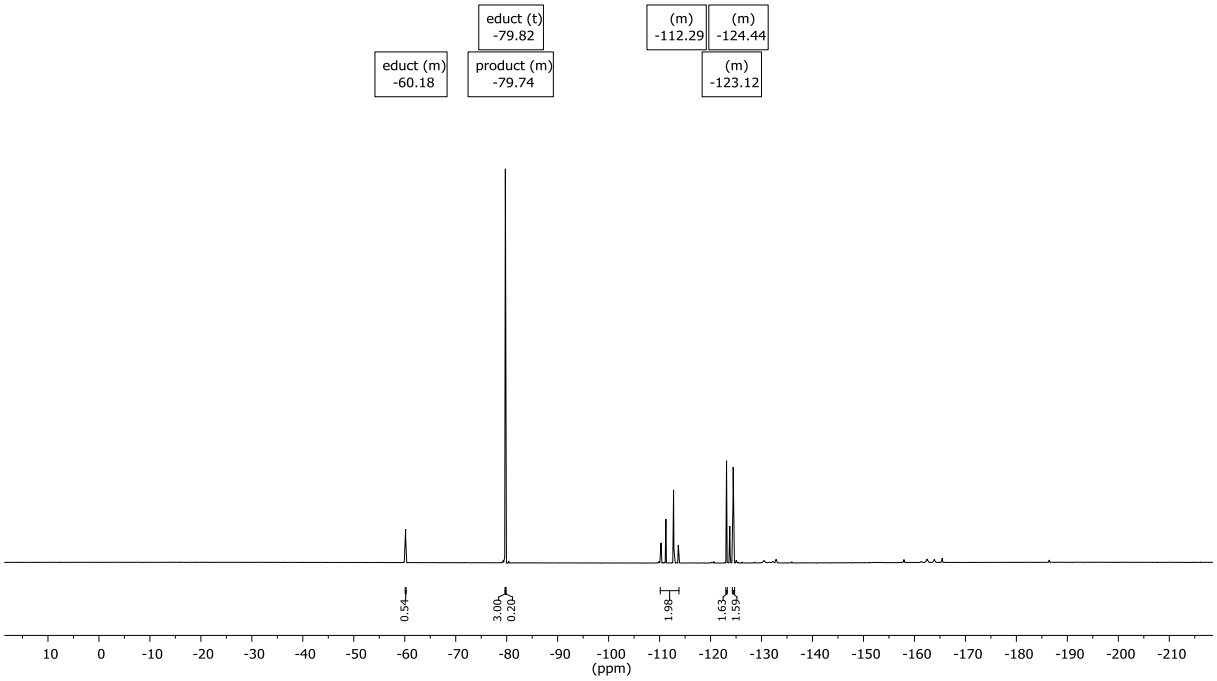

NMR-spectrum 21: ^{19}F-NMR-spectra (282 MHz, CD_2Cl_2) of the reaction with 4-penten-1-ylcyclopropane.

3.3 Reactions involving 1,4-cyclohexadiene

3.3.1 Iodoperfluoroalkylation of 1,4-cyclohexadiene

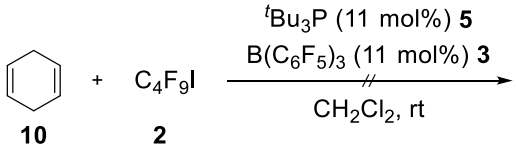

1,4-Cyclohexadiene (**10**) (56.3 mg, 0.703 mmol, 1.00 eq.) and nonafluoro-1-iodobutane (**2**) (255 mg, 0.737 mmol, 1.05 eq.) were weighed into an amber glass jar and dissolved in CH_2Cl_2 (0.5 ml). A solution of $^tBu_3P$ (**5**) (15.6 mg, 0.0771 mmol, 11 mol%) and $B(C_6F_5)_3$ (**3**) (39.4 mg, 0.0770 mmol, 11 mol%) in CH_2Cl_2 (1.6 ml) was added. The jar was sealed with a Teflon-insert screw cap. After 2 and 9 days NMR samples were withdrawn.

3.3.2 Iodoperfluoroalkylation of vinylcyclohexane in the presence of 1,4-cyclohexadiene

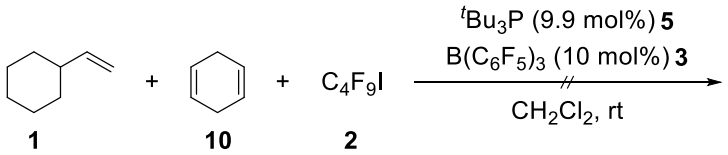

1,4-Cyclohexadiene (**10**) (56.5 mg, 0.705 mmol, 1.04 eq.) was weighed into an amber glass jar and dissolved in CH_2Cl_2 (1.0 ml). After addition of vinylcyclohexane (**1**) (100 µl, 0.730 mmol, 1.00 eq.) and nonafluoro-1-iodobutane (**2**) (125 µl, 0.726 mmol, 0.994 eq.), a solution of $^tBu_3P$ (**5**) (14.6 mg, 0.0722 mmol, 9.9 mol%) and $B(C_6F_5)_3$ (**3**) (37.6 mg, 0.0734 mmol, 10 mol%) in CH_2Cl_2 (1.1 ml) was added. The jar was sealed with a Teflon-insert screw cap. After 1 and 8 days NMR samples were withdrawn.

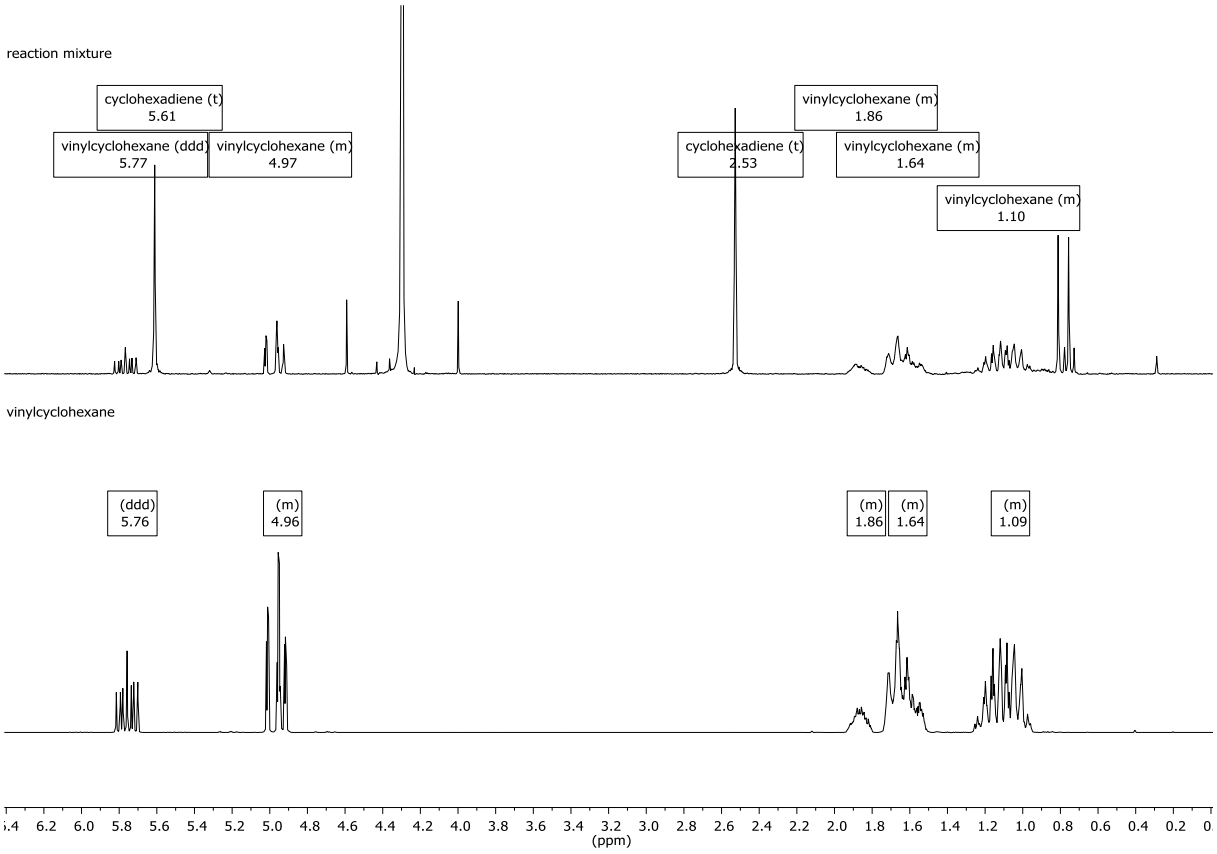

NMR-spectrum 22: Stacked ^{1}H-NMR-spectra (300 MHz, C_6D_6) of the reaction solution after 24 h (top) and vinylcyclohexane (bottom).

3.3.3 Stoichiometric reaction of 1,4-cyclohexadiene, ^{t}Bu$_3$P and B(C$_6$F$_5$)$_3$

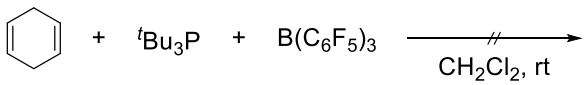

10 **5** **3**

^{t}Bu$_3$P (**5**) (53.9 mg, 0.266 mmol, 1.0 eq.) and B(C$_6$F$_5$)$_3$ (**3**) (133 mg, 0.260 mmol, 0.98 eq.) were weighed into an amber glass jar and dissolved in CH_2Cl_2 (1.0 ml). 1,4-Cyclohexadiene (**10**) (21 mg, 0.26 mmol, 1.0 eq.) was added and the jar was sealed with a Teflon-insert screw cap. After 6 and 13 days NMR samples were withdrawn.

3.3.4 Stoichiometric reaction of 1,4-cyclohexadiene, ^{t}Bu$_3$P, B(C$_6$F$_5$)$_3$ and C$_4$F$_9$I

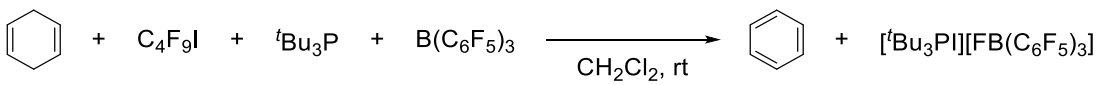

10 **2** **5** **3** **11** **12**

^{t}Bu$_3$P (**5**) (137 mg, 0.265 mmol, 1.0 eq.) and B(C$_6$F$_5$)$_3$ (**3**) (53.6 mg, 0.268 mmol, 0.98 eq.) were weighed into an amber glass jar and dissolved in CH_2Cl_2 (1.0 ml). 1,4-Cyclohexadiene (**10**) (25 µl, 0.26 mmol, 1.0 eq.) and nonafluoro-1-iodobutane (**2**) (45 µl, 0.26 mmol, 1.0 eq.) were added and the jar was sealed with a Teflon-insert screw cap. After 13 days an NMR samples was withdrawn.

By column chromatography, undefined fluorinated products were obtained.

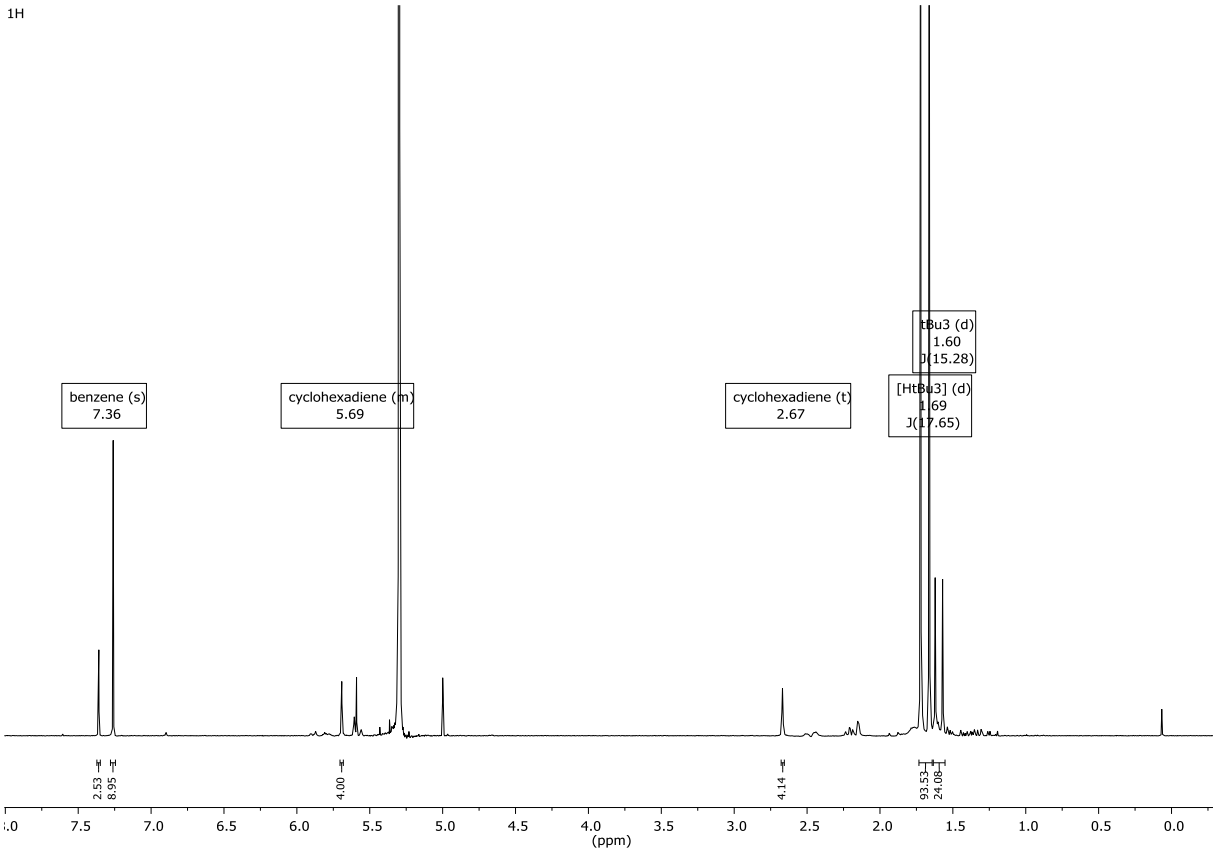

NMR-spectrum 23: ^{1}H-NMR-spectrum (300 MHz, $CDCl_3$) after 13 days reaction time.

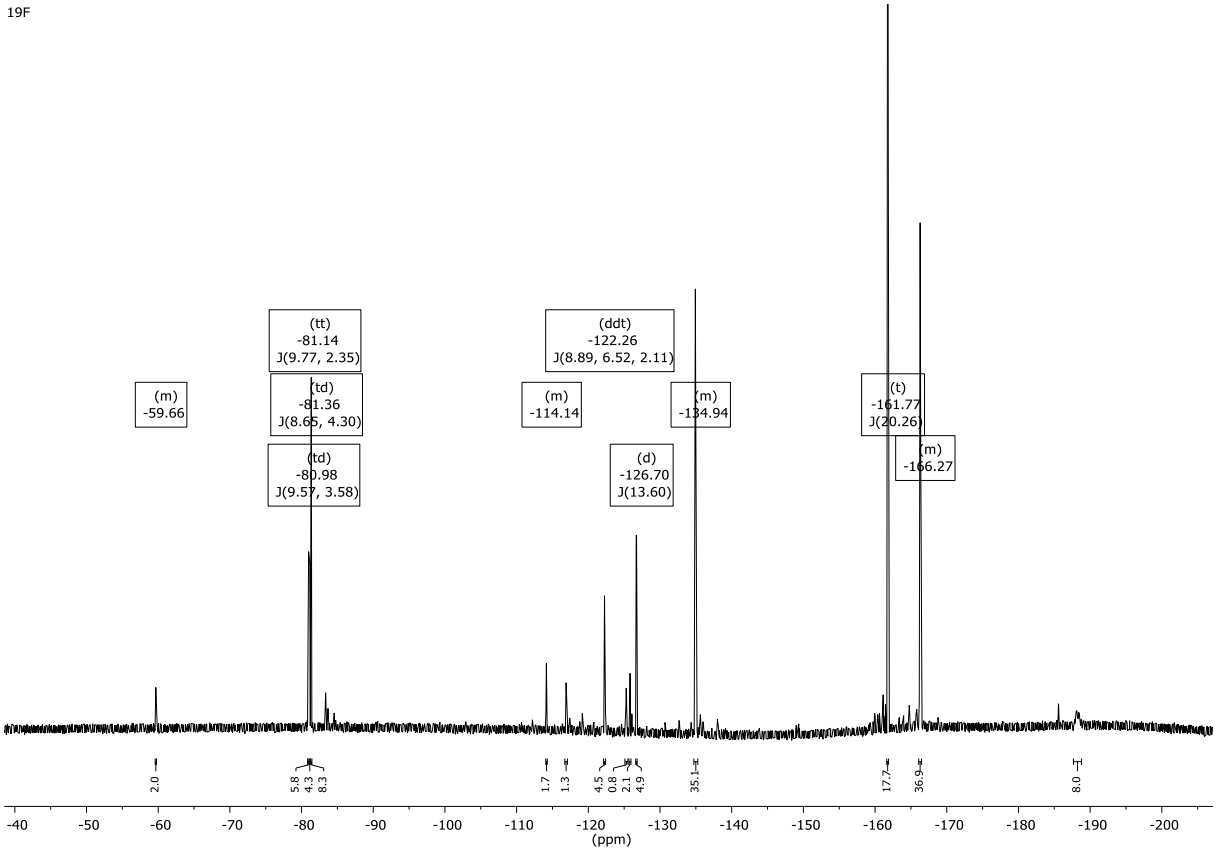

NMR-spectrum 24: ^{19}F-NMR-spectrum (282 MHz, $CDCl_3$) after 13 days reaction time.

3.4 Reactions involving styrene

3.4.1 Iodoperfluoroalkylation of styrene

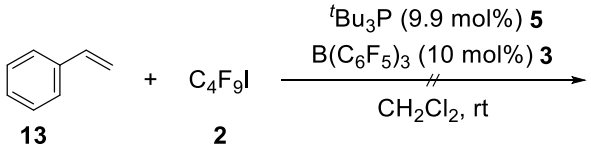

Freshly distilled styrene (**13**) (77.6 mg, 0.745 mmol, 1.00 eq.) was weighed into an amber glass jar and dissolved in CH_2Cl_2 (0.5 ml). Nonafluoro-1-iodobutane (**2**) (125 µl, 0.726 mmol, 0.974 eq.) as well as a solution of $^tBu_3P$ (**5**) (14.9 mg, 0.0736 mmol, 9.9 mol%) and $B(C_6F_5)_3$ (**3**) (39.0 mg, 0.0762 mmol, 10 mol%) in CH_2Cl_2 (1.6 ml) was added. The jar was sealed with a Teflon-insert screw cap. After 1 and 9 days NMR samples were withdrawn.

3.4.2 Iodoperfluoroalkylation of vinylcyclohexane in the presence of styrene

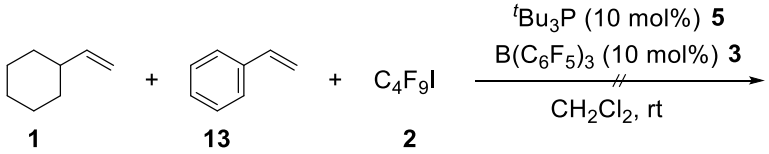

Freshly distilled styrene (**13**) (76.0 mg, 0.730 mmol, 1.00 eq.) was weighed into an amber glass jar and dissolved in CH_2Cl_2 (0.5 ml). Vinylcyclohexane (**1**) (100 µl, 0.730 mmol, 1.00 eq.) and nonafluoro-1-iodobutane (**2**) (125 µl, 0.726 mmol, 0.994 eq.) as well as a solution of $^tBu_3P$ (**5**) (14.7 mg, 0.0727 mmol, 10 mol%) and $B(C_6F_5)_3$ (**3**) (38.5 mg, 0.0752 mmol, 10 mol%) in CH_2Cl_2 (1.6 ml) was added. The jar was sealed with a Teflon-insert screw cap. After 1 and 9 days NMR samples were withdrawn.

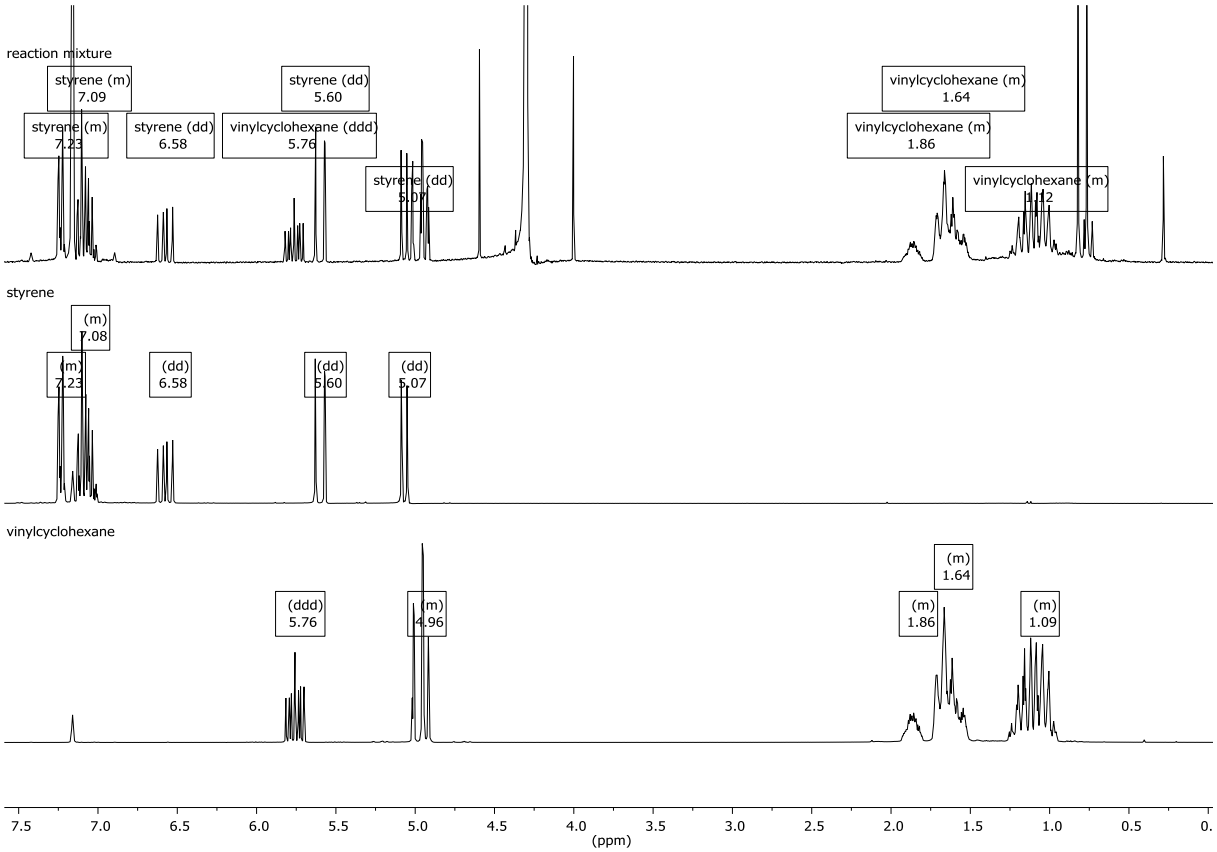

NMR-spectrum 25: Stacked ^{1}H-NMR-spectra (300 MHz, C_6D_6) of the reaction solution after 24 h (top), styrene (middle) and vinylcyclohexane (bottom).

3.4.3 Test reaction for a styrene polymerisation

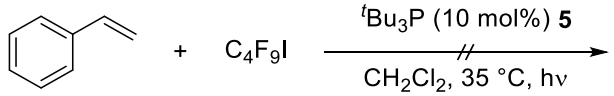

13 **2**

$^{t}Bu_3P$ (**5**) (3.7 mg, 0.018 mmol, 10 mol%) was weighed into a small glass vial, dissolved in CH_2Cl_2 (0.5 ml) and styrene (**13**) (70.4 mg, 0.177 mmol, 1.00 eq.) was added. The solution was transferred into a Young valve NMR tube. Under light exclusion using red light nonafluoro-1-iodobutane (**2**) (35.0 µl, 0.206 mmol, 1.15 eq.) was added. The Young valve NMR tube was sealed and irradiated for 2 h (blue LED (370 nm). After the first NMR spectra measurement the sample was irradiated for further 2 h (254 nm).

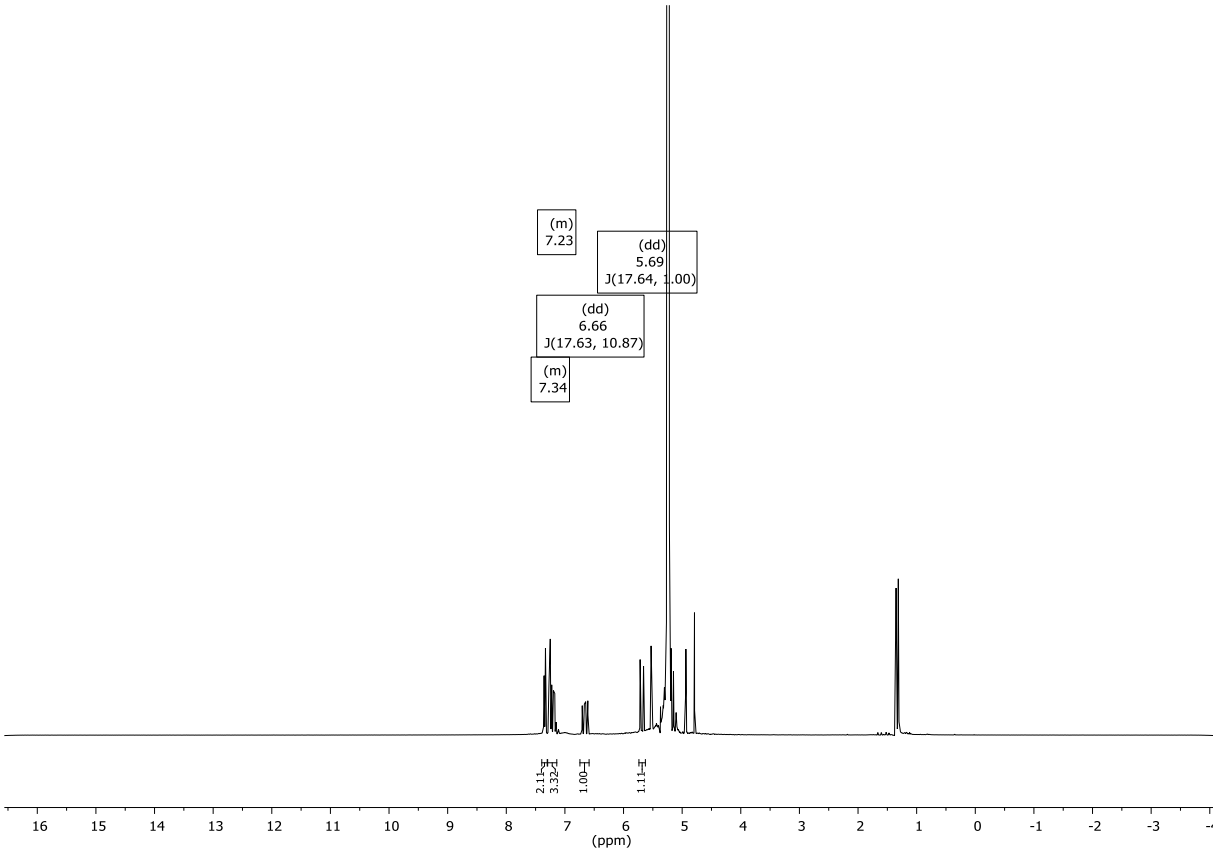

NMR-spectrum 26: ^{1}H-NMR-spectra (300 MHz, D_2O) in CH_2Cl_2 after irradiation (370 nm).

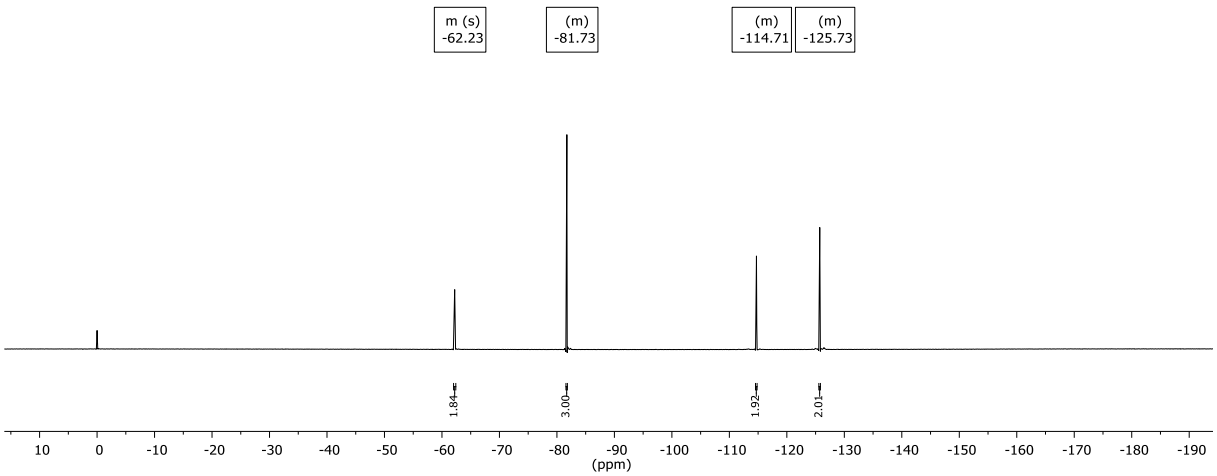

NMR-spectrum 27: ^{19}F-NMR-spectra (282 MHz, D_2O) in CH_2Cl_2 after irradiation (370 nm).

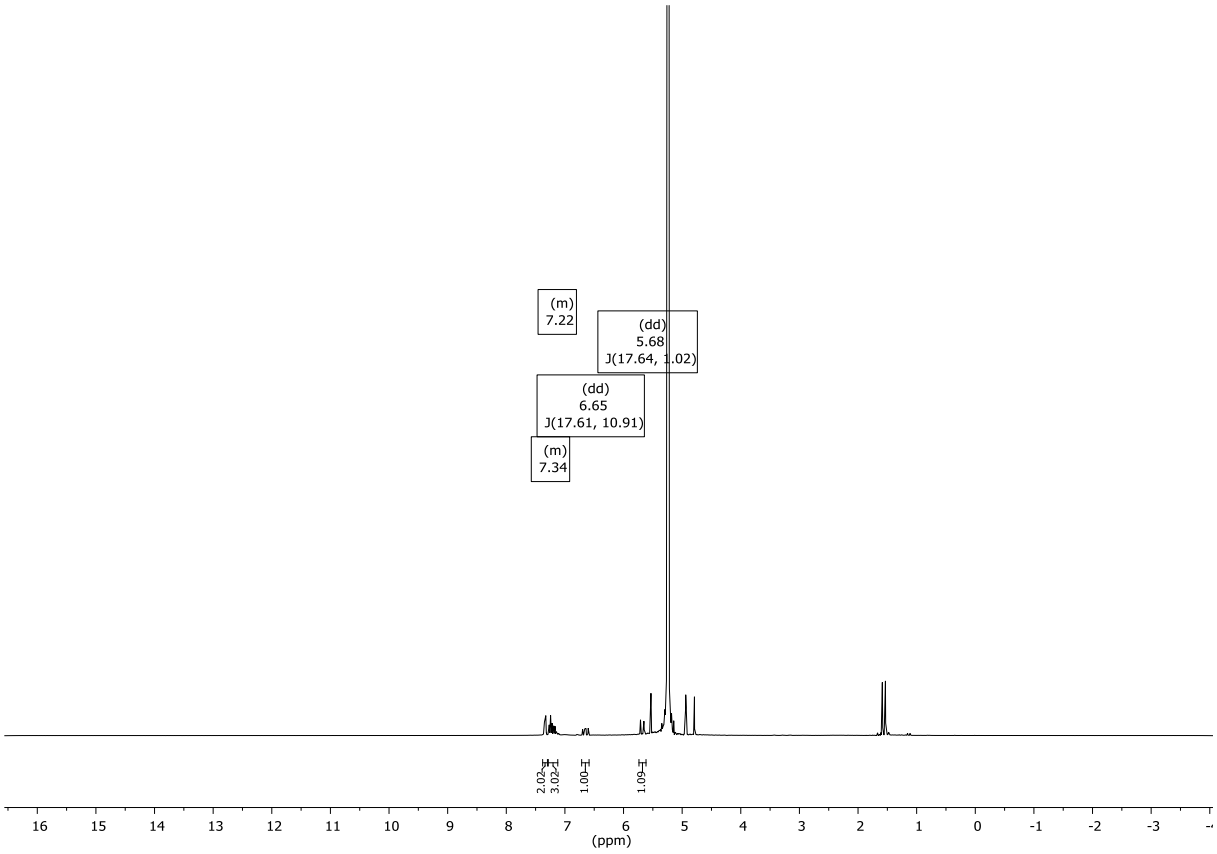

NMR-spectrum 28: ^{1}H-NMR-spectra (300 MHz, D_2O) in CH_2Cl_2 after irradiation (254 nm).

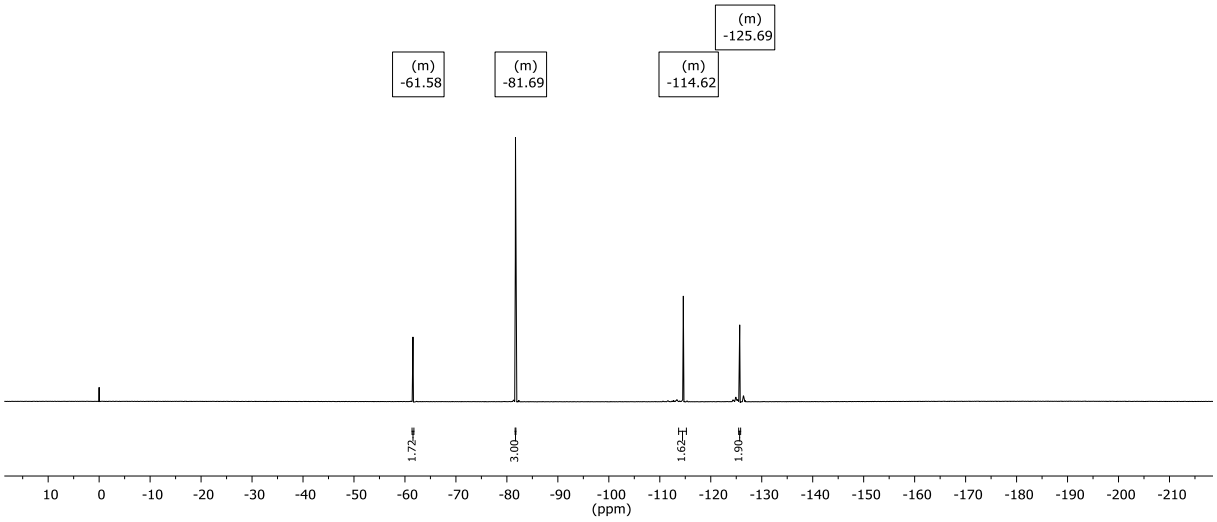

NMR-spectrum 29: ^{19}F-NMR-spectra (282 MHz, D_2O) in CH_2Cl_2 after irradiation (254 nm).

3.5 Reaction in the presence of 2,2,6,6-tetramethylpiperidine 1-oxyl (TEMPO)

3.5.1 Equimolar amounts of TEMPO

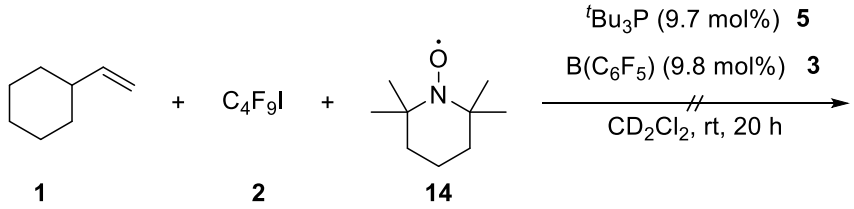

^{t}Bu$_3$P (**5**) (3.5 mg, 0.017 mmol, 9.7 mol%) and B(C_6F_5)$_3$ (**3**) (9.0 mg, 0.018 mmol, 9.7 mol%) were weighed into a small glass vial, dissolved in CD_2Cl_2 (0.3 ml) and vinylcyclohexane (**1**) (25.0 µl, 0.179 mmol, 1.00 eq.) was added. The solution was transferred into a Young valve NMR tube. Separately TEMPO (**14**) (31.0 mg, 0.198 mmol, 1.10 eq.) was weighed in another glass vial, dissolved in CD_2Cl_2 (0.2 ml) and transferred into the same Young valve NMR tube. Under light exclusion using red light nonafluoro-1-iodobutane (**2**) (35.0 µl, 0.206 mmol, 1.15 eq.) was added. The Young valve NMR tube was sealed and an NMR measurement was conducted after 20 h.

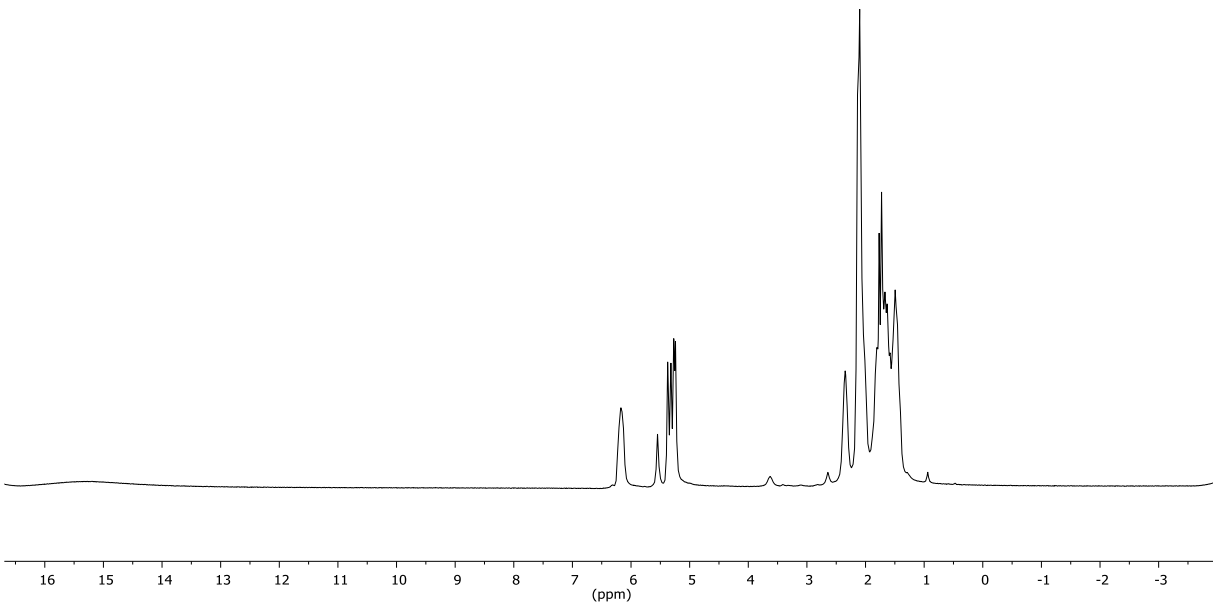

NMR-spectrum 30: ^{1}H-NMR-spectra (300 MHz, CD_2Cl_2) of the reaction with 1.10 eq. TEMPO.

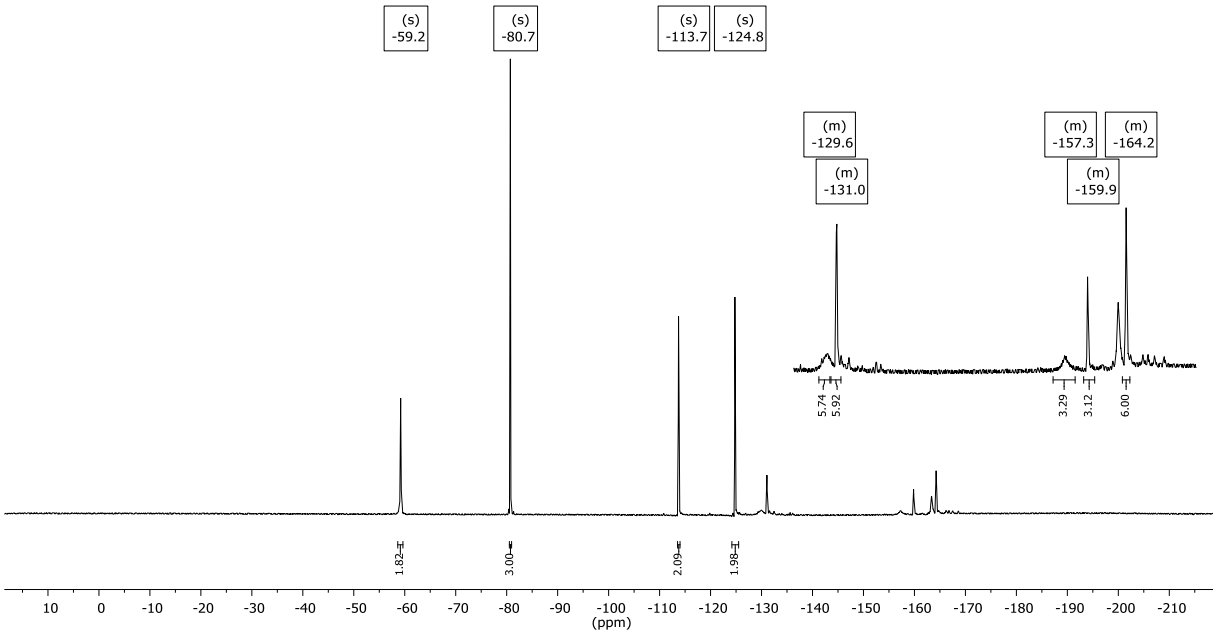

NMR-spectrum 31: ^{19}F-NMR-spectra (282 MHz, CD_2Cl_2) of the reaction with 1.10 eq. TEMPO.

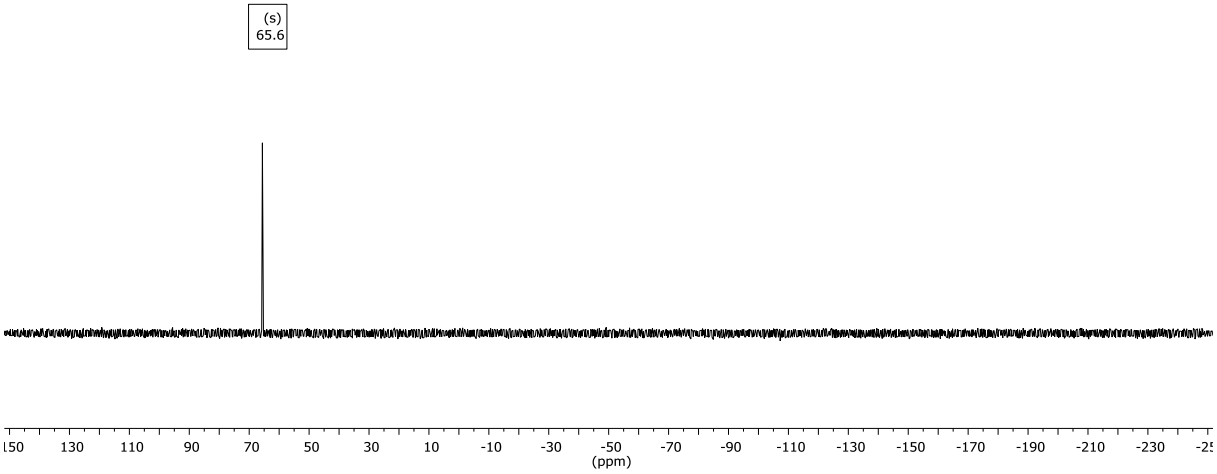

NMR-spectrum 32: ^{31}P-NMR-spectra (121 MHz, CD_2Cl_2) of the reaction with 1.10 eq. TEMPO.

3.5.2 12.8 mol% TEMPO

$^{t}Bu_3P$ (**5**) (3.6 mg, 0.018 mmol, 9.9 mol%) and $B(C_6F_5)_3$ (**3**) (9.2 mg, 0.018 mmol, 10 mol%) were weighed into a small glass vial, dissolved in CD_2Cl_2 (0.2 ml) and vinylcyclohexane (**1**) (25.0 µl, 0.179 mmol, 1.00 eq.) was added. The solution was transferred into a Young valve NMR tube. Separately TEMPO (**14**) (3.6 mg, 0.023 mmol, 13 mol%) was weighed in another glass vial, dissolved in CD_2Cl_2 (0.2 ml) and transferred into the same Young valve NMR tube. Under light exclusion using red light nonafluoro-1-iodobutane (**2**) (35.0 µl, 0.206 mmol, 1.15 eq.) was added. The Young valve NMR tube was sealed and the solution was measured after 24 h.

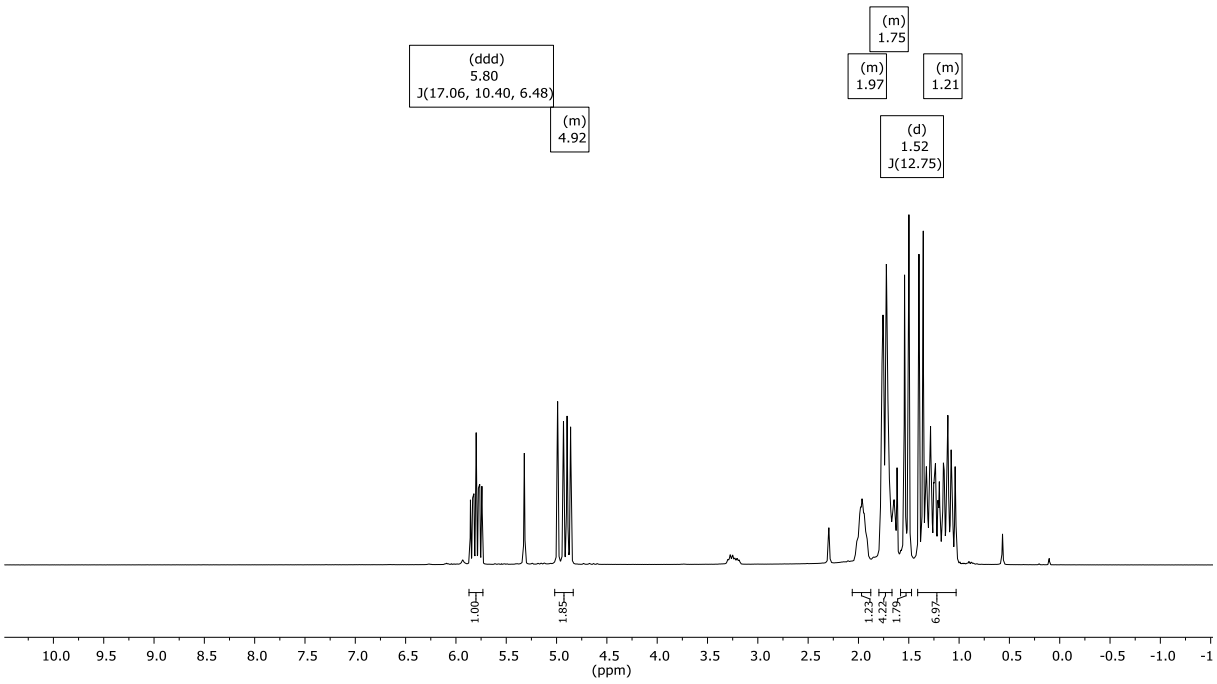

NMR-spectrum 33: ^{1}H-NMR-spectra (300 MHz, CD_2Cl_2) of the reaction with TEMPO, 12.8 mol%.

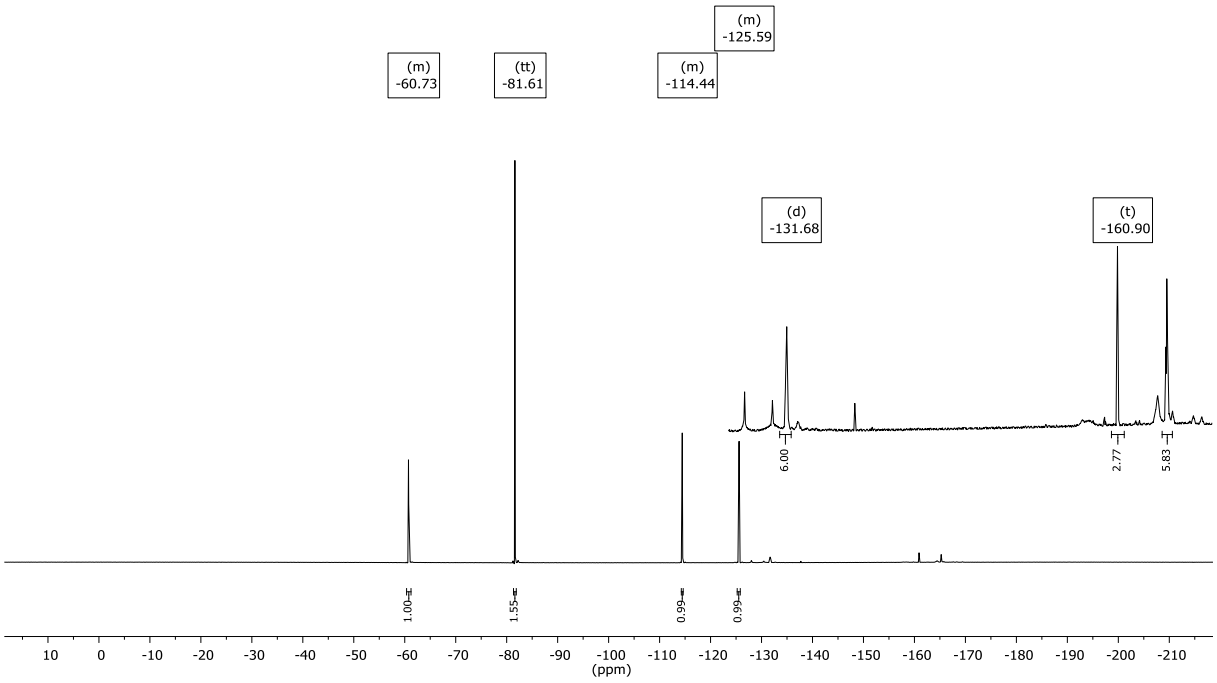

NMR-spectrum 34: ^{19}F-NMR-spectra (282 MHz, CD_2Cl_2) of the reaction with TEMPO, 12.8 mol%.

3.5.3 Delayed addition of TEMPO

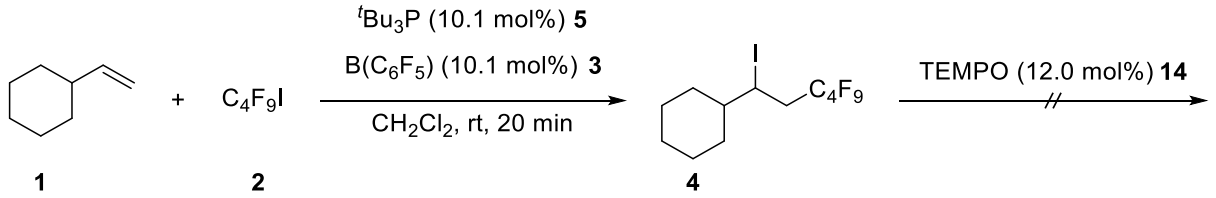

^{t}Bu$_3$P (**5**) (3.6 mg, 0.018 mmol, 10 mol%) and B(C_6F_5)$_3$ (**3**) (9.1 mg, 0.018 mmol, 10 mol%) were weighed into a small glass vial, dissolved in CH_2Cl_2 (0.45 ml). Under light exclusion using red light vinylcyclohexane (**1**) (24.0 µl, 0.175 mmol, 1.00 eq.) and nonafluoro-1-iodobutane (**2**) (30.0 µl, 0.175 mmol, 1.00 eq.) were added and stirred for 20 min. The solution was transferred into an amber NMR tube. Separately weighed TEMPO (**14**) (3.3 mg, 0.021 mmol, 12 mol%) was dissolved in CH_2Cl_2 (0.1 ml) and transferred into the same amber NMR tube. The NMR tube was sealed and the solution was measured after 1 h.

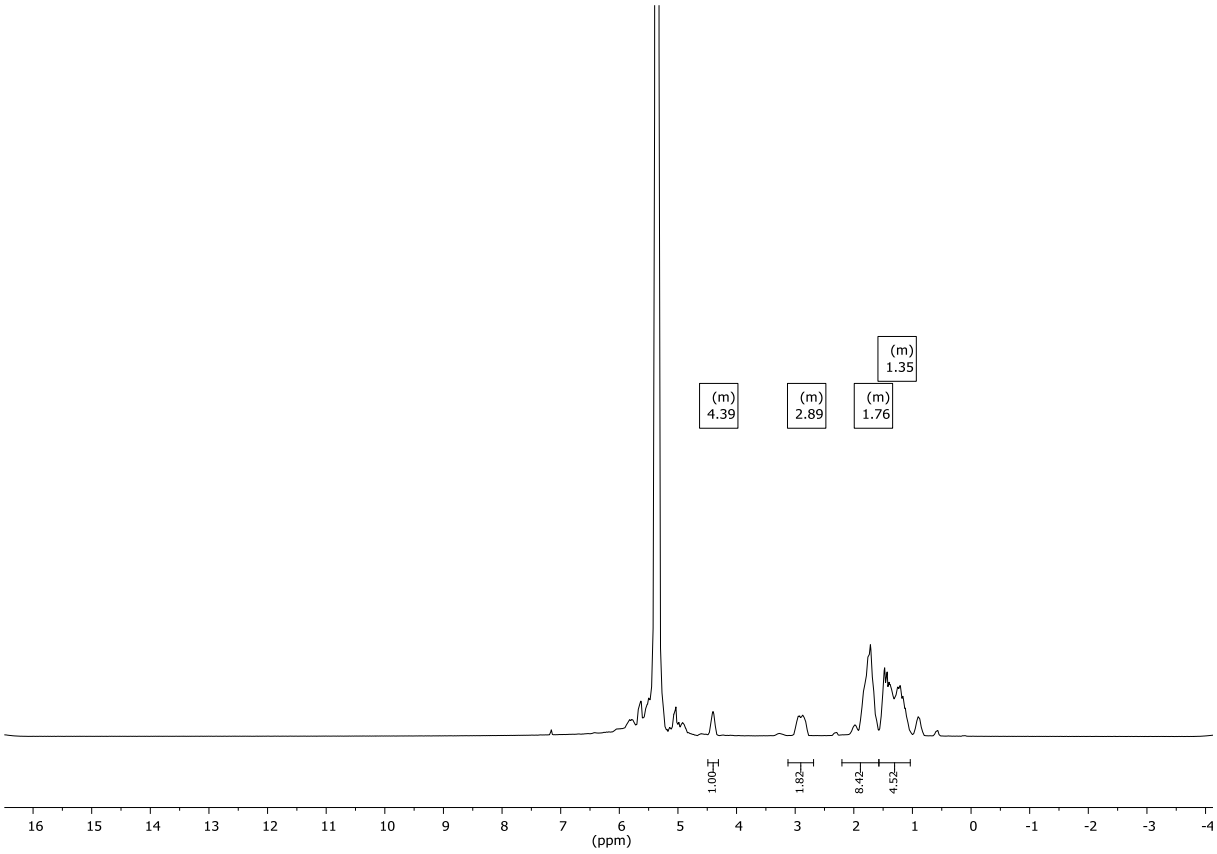

NMR-spectrum 35: ^{1}H-NMR-spectra (300 MHz, C_6D_6) in CH_2Cl_2 of the reaction with subsequent addition of TEMPO.

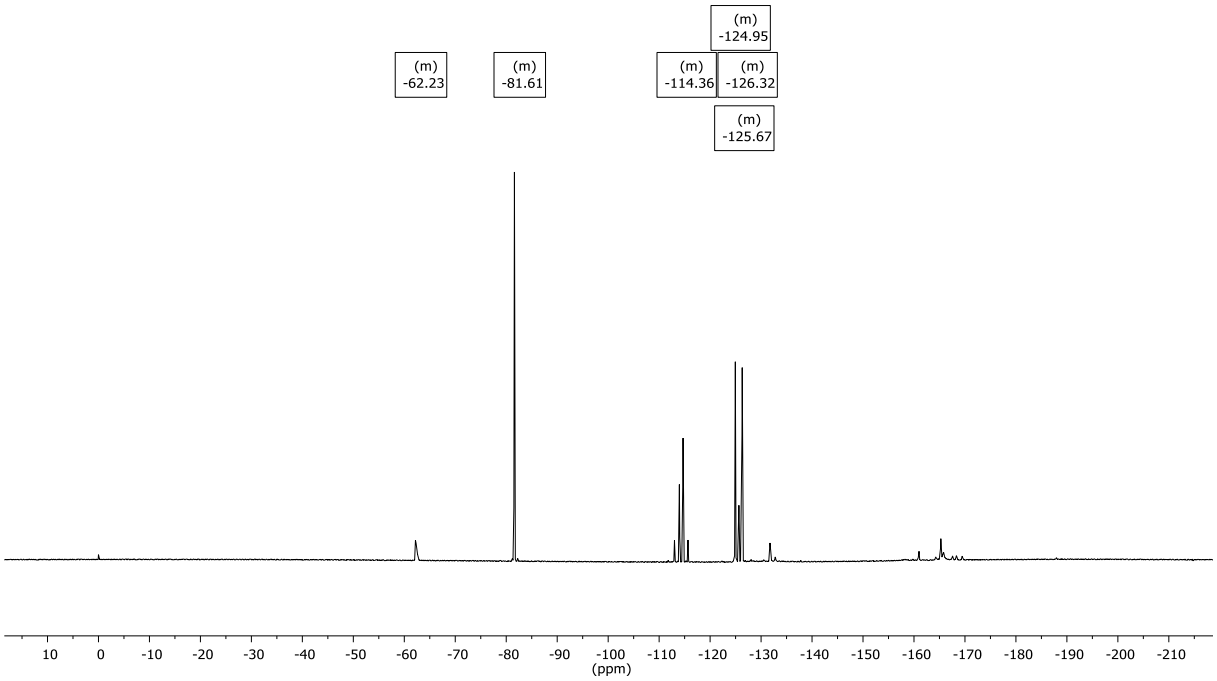

NMR-spectrum 36: ^{19}F-NMR-spectra (282 MHz, C_6D_6) in CH_2Cl_2 of the reaction with subsequent addition of TEMPO.

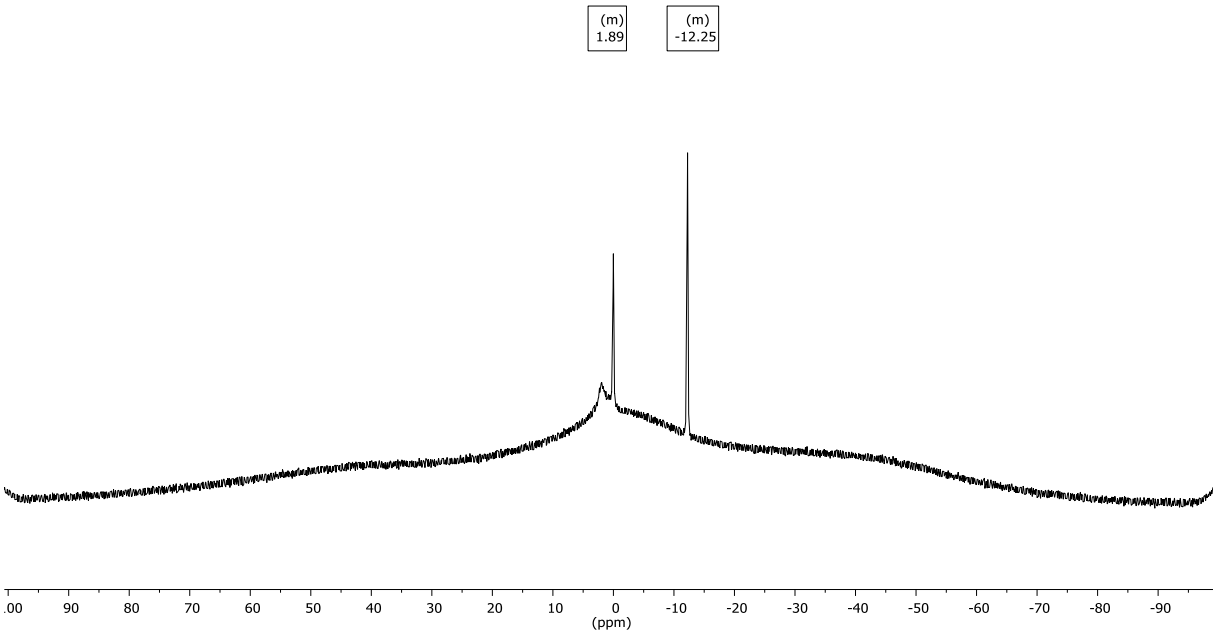

NMR-spectrum 37: ^{11}B-NMR-spectrum (282 MHz, C_6D_6) in CH_2Cl_2 of the reaction with subsequent addition of TEMPO.

3.6 Reactions involving tributyltin hydride

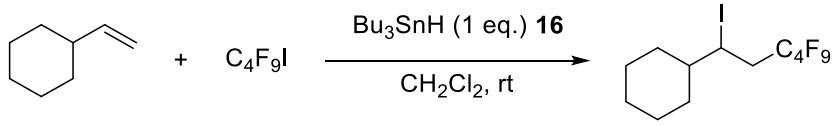

1 **2** **4**

3.6.1 Control reaction with vinylcyclohexane and nonafluoro-1-iodobutane

Under light exclusion using red light, vinylcyclohexane (**1**) (25.0 µl, 0.183 mmol, 1.00 eq.) and nonafluoro-1-iodobutane (**2**) (32.0 µl, 0.186 mmol, 1.02 eq.) were injected into an amber glass NMR-tube, equipped with $CFCl_3$ in C_6D_6 as an external standard. The reactants were dissolved in CH_2Cl_2 (0.80 ml). Outside the glovebox, tributyltin hydride (**16**) (20 µl, 0.076 mmol, 0.42 eq.) was added under inert conditions.

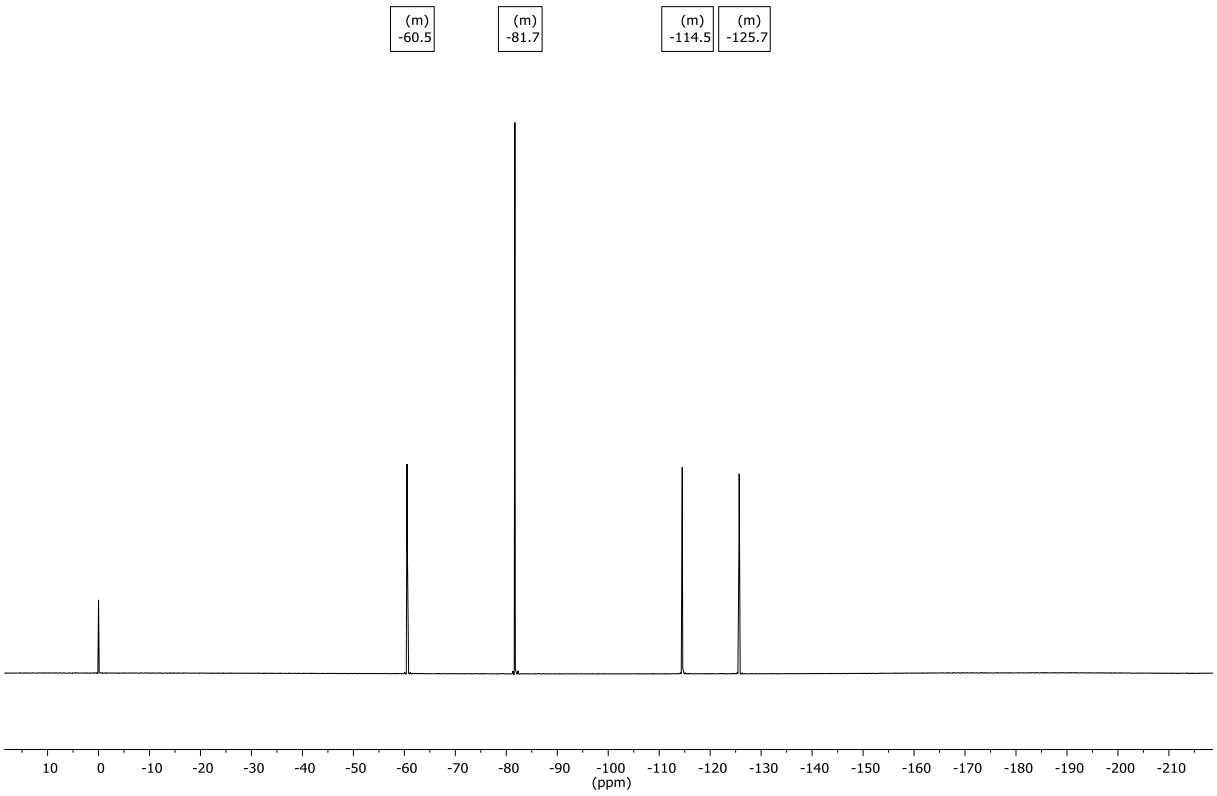

NMR-spectrum 38: ^{19}F-NMR-spectrum (282 MHz, C_6D_6) in CH_2Cl_2 of the reaction solution after 1.5 h.

3.6.2 Control reaction with ^{t}Bu$_3$P, vinylcyclohexane and nonafluoro-1-iodobutane

Vinylcyclohexane (**1**) (25.0 µl, 0.183 mmol, 1.00 eq.) and nonafluoro-1-iodobutane (**2**) (32.0 µl, 0.186 mmol, 1.02 eq.) were added to a solution of ^{t}Bu$_3$P (**5**) (3.8 mg, 0.019 mmol, 10 mol%) in CH_2Cl_2 (0.55 ml) in transparent NMR-tube, equipped with $CFCl_3$ in C_6D_6 as an external standard. Outside the glovebox, tributyltin hydride (**16**) (50 µl, 0.076 mmol, 0.42 eq.) was added under inert conditions.

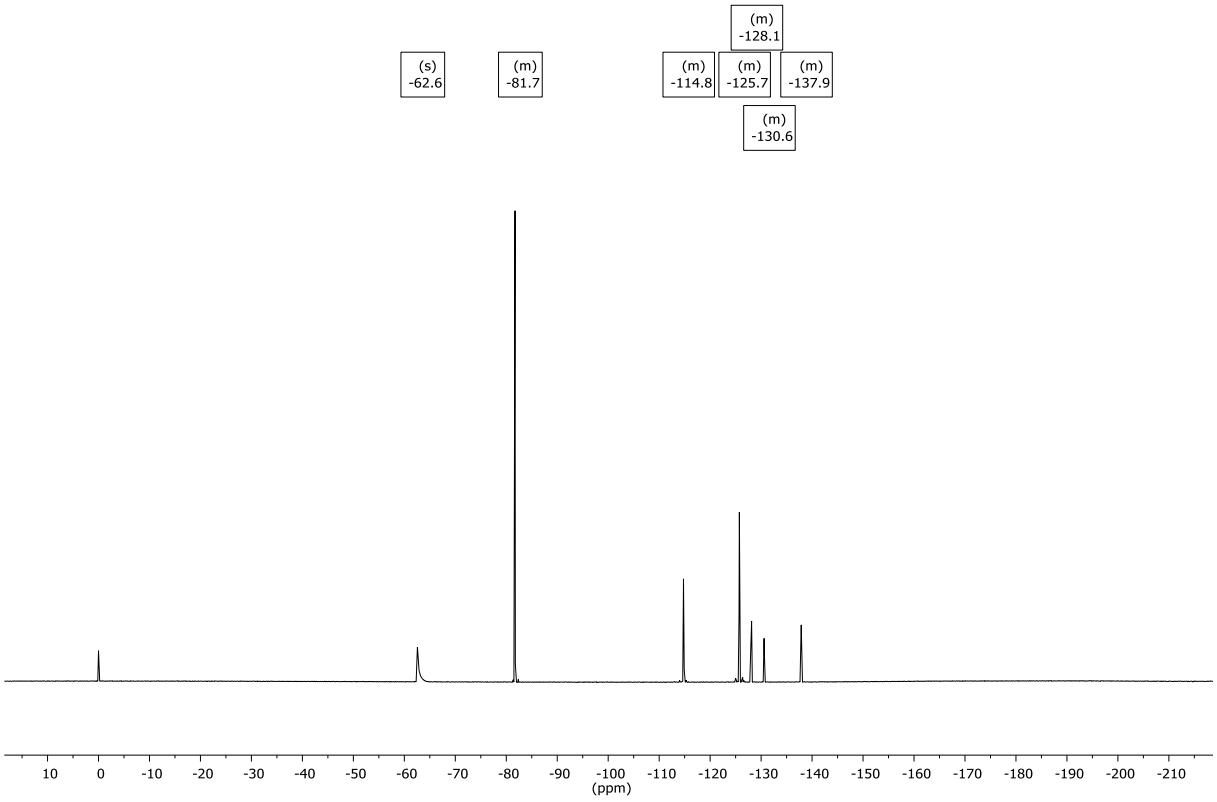

NMR-spectrum 39: ^{19}F-NMR-spectrum (282 MHz, C_6D_6) in CH_2Cl_2 of the reaction solution after 1 h. Reference for C_4F_9H.[6]

3.6.3 Reaction in the presence of ^{t}Bu$_3$P, B(C$_6$F$_5$)$_3$, vinylcyclohexane and nonafluoro-1-iodobutane

Under light exclusion using red light, vinylcyclohexane (**1**) (25.0 µl, 0.183 mmol, 1.00 eq.) and nonafluoro-1-iodobutane (**2**) (32.0 µl, 0.186 mmol, 1.02 eq.) were added to a solution of ^{t}Bu$_3$P (**5**) (3.6 mg, 0.018 mmol, 9.7 mol%) in combination with B(C$_6$F$_5$)$_3$ (**3**) (9.3 mg, 0.018 mmol, 9.9 mol%) in CH_2Cl_2 (0.55 ml) in transparent NMR-tube, equipped with $CFCl_3$ in C_6D_6 as an external standard. Outside the glovebox, tributyltin hydride (**16**) (50 µl, 0.076 mmol, 0.42 eq.) was added under inert conditions.

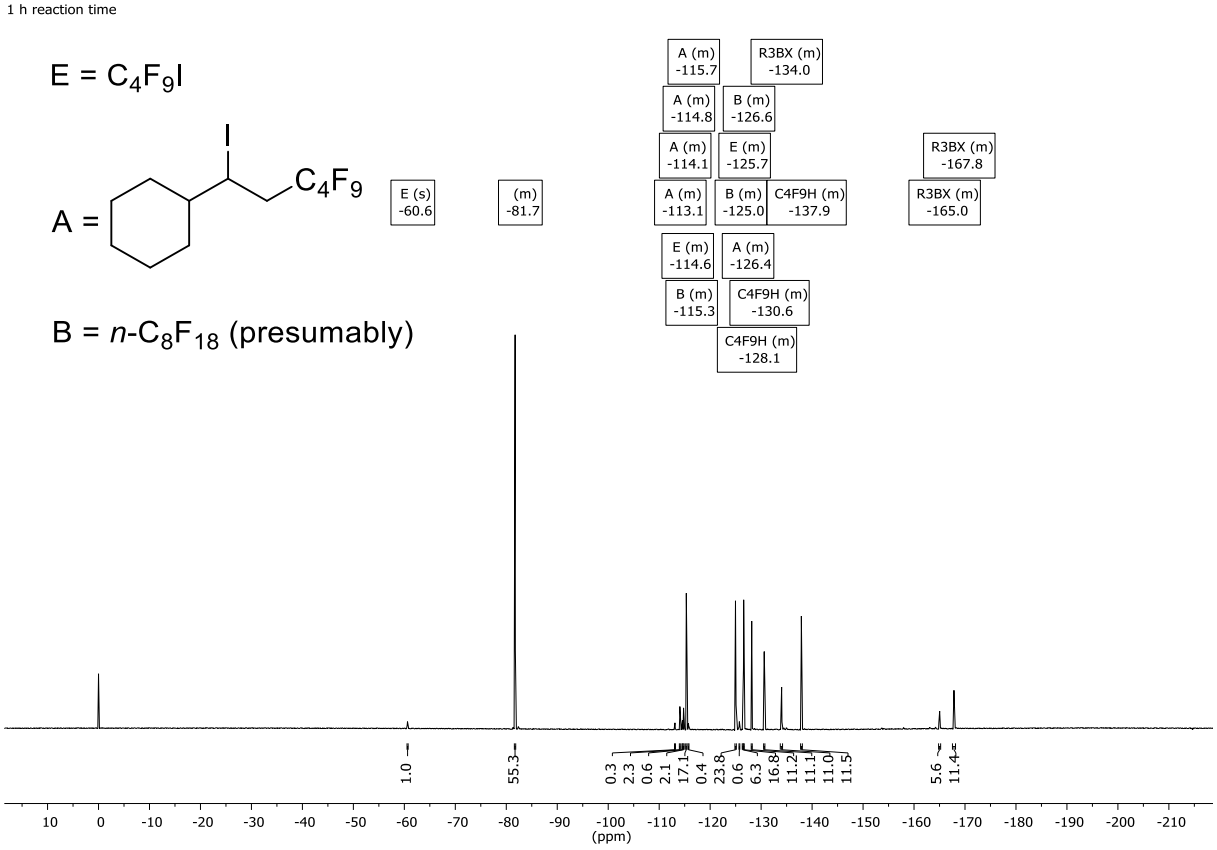

NMR-spectrum 40: ^{19}F-NMR-spectrum (282 MHz, C_6D_6) in CH_2Cl_2 of the reaction solution after 1 h. Reference for C_4F_9H.[6]

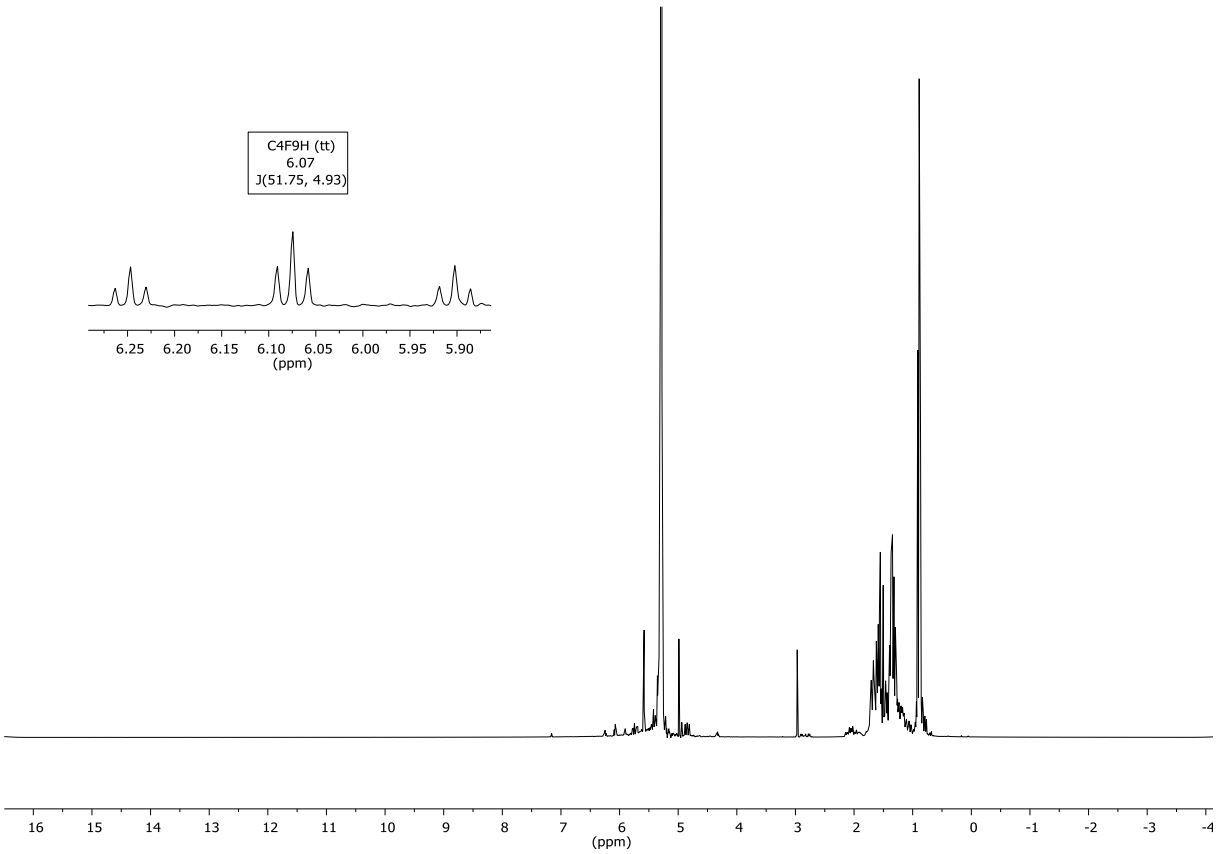

NMR-spectrum 41: ^{1}H-NMR-spectrum (300 MHz, C_6D_6) in CH_2Cl_2 of the reaction solution after 7 h. Reference for C_4F_9H.[6]

3.7 Reaction in the presence of [^{t}Bu$_3$PI][FB(C$_6$F$_5$)$_3$] and B(C$_6$F$_5$)$_3$

[^{t}Bu$_3$PI][FB(C$_6$F$_5$)$_3$] (**12**) (13.2 mg, 0.015 mmol, 8.4 mol%) and B(C$_6$F$_5$)$_3$ (**3**) (9.2 mg, 0.018 mmol, 9.8 mol%) were weighed into a glass vial and dissolved in CH_2Cl_2 (0.80 ml). Under light exclusion using red light, vinylcyclohexane (**1**) (25.0 µl, 0.183 mmol, 1.00 eq.) as well as nonafluoro-1-iodobutane (**2**) (32.0 µl, 0.186 mmol, 1.02 eq.) were added. The solution was transferred into a Young valve NMR tube equipped with $CFCl_3$ in C_6D_6 as an external standard.

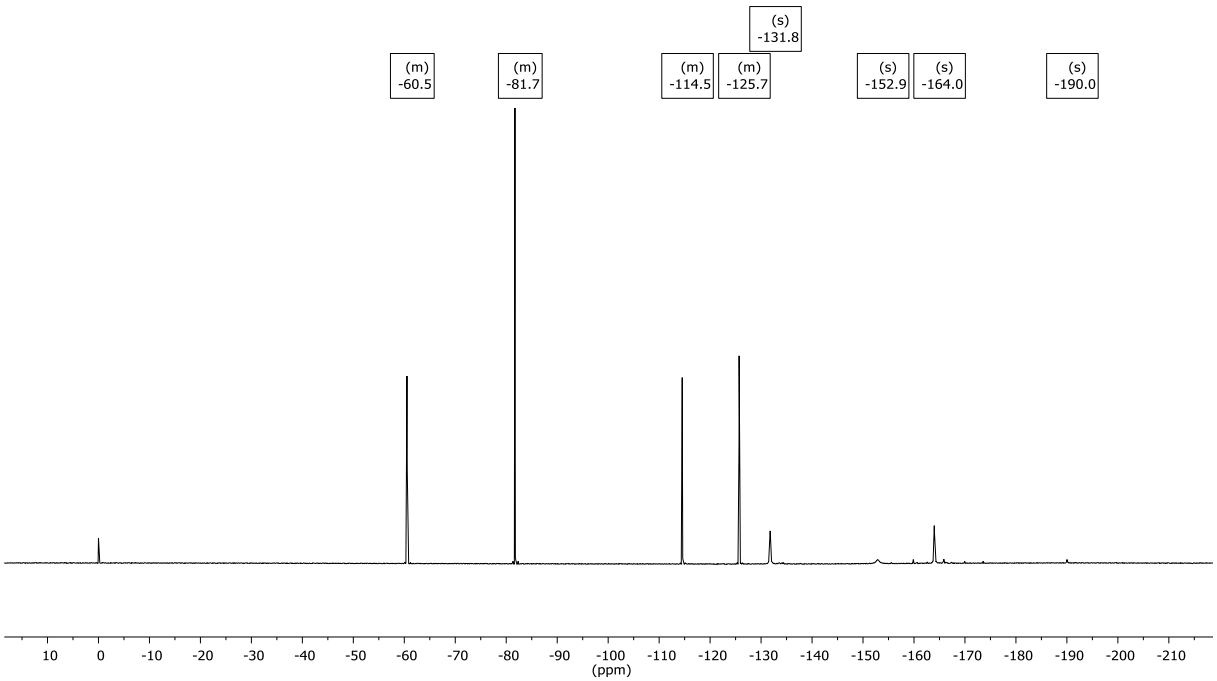

NMR-spectrum 42: ^{19}F-NMR-spectrum (282 MHz, C$_6$D$_6$) in CH_2Cl_2, iodoperfluoroalkylation in the presence of [^{t}Bu$_3$PI][FB(C$_6$F$_5$)$_3$] and B(C$_6$F$_5$)$_3$, 7.5 h reaction time.

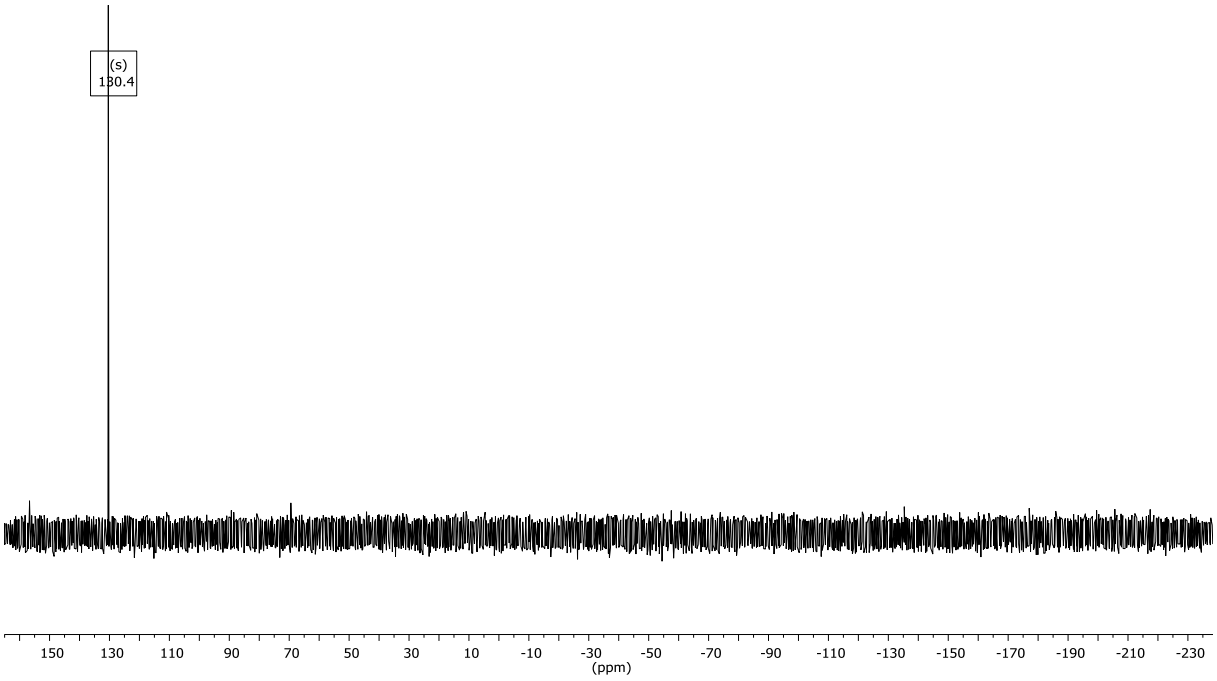

NMR-spectrum 43: ^{31}P-NMR-spectrum (121 MHz, C_6D_6) in CH_2Cl_2, iodoperfluoroalkylation in the presence of [^{t}Bu$_3$PI][FB(C_6F_5)$_3$] and B(C_6F_5)$_3$, 7.5 h reaction time.

3.8 Reaction in the presence of [^{t}Bu$_3$PH][FB(C_6F_5)$_3$] and B(C_6F_5)$_3$

[^{t}Bu$_3$PH][FB(C_6F_5)$_3$] (**17**) (10.1 mg, 0.014 mmol, 10 mol%) and B(C_6F_5)$_3$ (**3**) (7.4 mg, 0.014 mmol, 11 mol%) were weighed into a glass vial, dissolved in CH_2Cl_2 (0.40 ml) and transferred into an amber glass NMR tube equipped with $CFCl_3$ in C_6D_6 as an external standard. Under light exclusion using red light, a solution of 1-undecene (**18**) (20.8 mg, 0.135 mmol, 1.00 eq.) as well as nonafluoro-1-iodobutane (**2**) (46.6 mg, 0.135 mmol, 0.999 eq.) in CH_2Cl_2 (0.40 ml) was added.

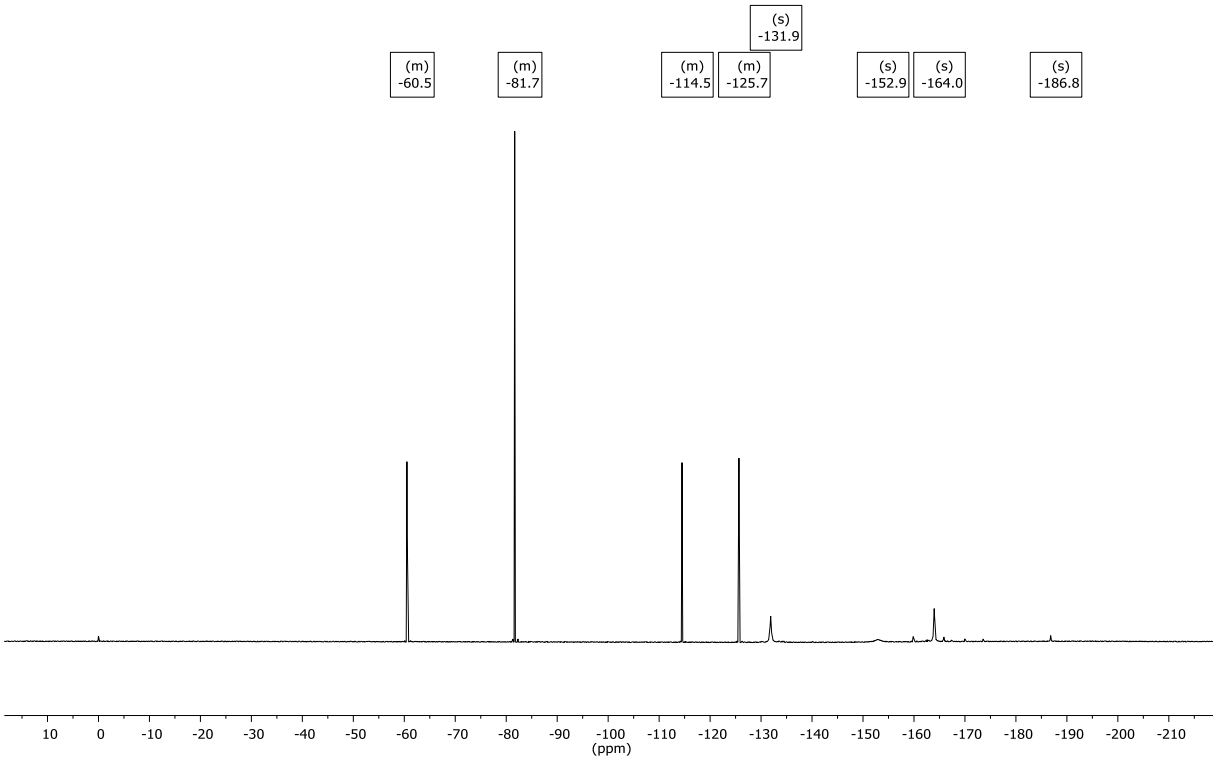

NMR-spectrum 44: ^{19}F-NMR-spectrum (282 MHz, C_6D_6) in CH_2Cl_2, iodoperfluoroalkylation in the presence of [^{t}Bu$_3$PH][FB(C$_6$F$_5$)$_3$] and B(C$_6$F$_5$)$_3$, 27 h reaction time.

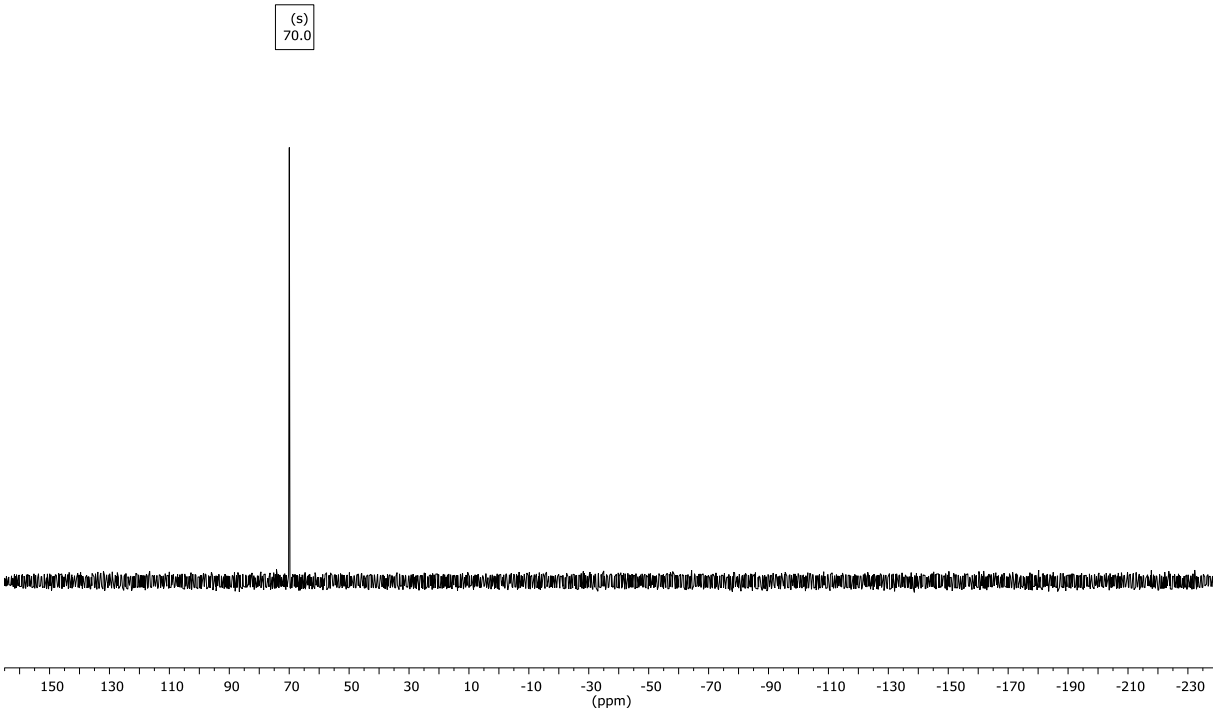

NMR-spectrum 45: ^{31}P-NMR-spectrum (121 MHz, C_6D_6) in CH_2Cl_2, iodoperfluoroalkylation in the presence of [^{t}Bu$_3$PH][FB(C$_6$F$_5$)$_3$] and B(C$_6$F$_5$)$_3$, 27 h reaction time.

3.9 $^{t}Bu_3P$ mediated photochemical background reaction

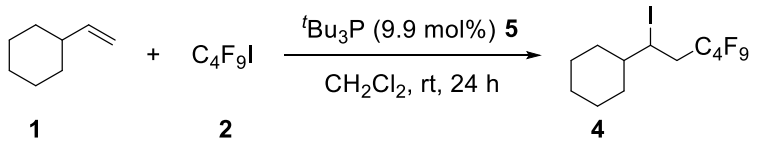

3.9.1 Reaction under light exclusion

Inside the glovebox, $^{t}Bu_3P$ (**5**) (7.3 mg, 0.036 mmol, 9.9 mol%) was weighed into a glass vial, dissolved in CH_2Cl_2 (0.60 ml) and transferred into a pointed flask. All following work steps were conducted under red light and best possible light exclusion. A round-bottom flask, enwrapped with aluminium foil, was filled with *n*-decane (**19**) (40.0 µl), vinylcyclohexane (**1**) (40.3 mg. 0.365 mmol, 1.00 eq.) and nonafluoro-1-iodobutane (**2**) (131 mg, 0.378 mmol, 1.03 eq.) dissolved in CH_2Cl_2 (0.70 ml). Outside the glovebox, the $^{t}Bu_3P$ solution was transferred into the educt solution. After stirring for 64 minutes, aqueous H_2O_2 (30%, 0.10 ml) was added to quench the reaction. A sample was withdrawn for both NMR and GC measurements.

3.9.2 Reaction under irradiation

Inside the glovebox, $^{t}Bu_3P$ (**5**) (14.8 mg, 0.0736 mmol, 10 mol%) was weighed into a transparent glass jar, dissolved in CH_2Cl_2 (2.5 ml) and vinylcyclohexane (**1**) (100 µl, 0.730 mmol, 1.00 eq.) as well as nonafluoro-1-iodobutane (**2**) (125 µl, 0.726 mmol, 0.995 eq.) were added. After 24 h an NMR-sample was withdrawn.

4 Radical clock synthesis

4.1 Synthesis of 6-bromohexene

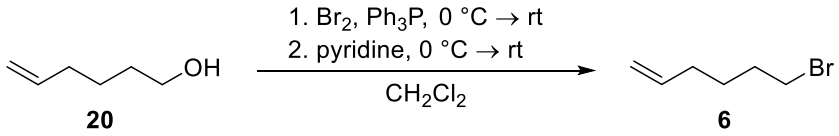

Triphenylphosphane (11.5 g, 43.9 mmol, 1.10 eq.) in CH_2Cl_2 (29 ml) was cooled to 0 °C. Bromine (2.30 ml, 43.9 mmol, 1.10 eq.) was added dropwise and the solution was stirred for 2 h at room temperature. Subsequently, pyridine (4.30 ml, 43.9 mmol, 1.10 eq.) was added dropwise to the reaction solution and the mixture was cooled again to 0 °C. 5-Hexen-1-ol (**20**) (4.80 ml, 39.9 mmol, 1.00 eq.) in CH_2Cl_2 (7 ml) was added dropwise and the solution was stirred for 20 h at room temperature. After complete conversion of the alcohol, which was controlled *via* TLC (hexane: ethyl acetate 90:10), pentane (20 ml) was added to the reaction solution. The reaction flask was cooled to −78°C and the precipitate was filtered off. The clear reaction solution was concentrated and washed with hydrochloric acid (1 M, 3 x 20 ml). The aqueous phase was extracted with pentane (3 x 20 ml). The combined organic phases were washed with saturated $NaHCO_3$ (10 ml) and dried over Na_2SO_4. The solution was again concentrated and distillated at reduced pressure (61-63 °C, 45 mbar). A clear oil was obtained (3.17 g, 19.4 mmol, 49%).

^{1}H-NMR (300 MHz, $CDCl_3$) δ [ppm] 5.88 – 5.72 (ddt, *J* = 16.9, 10.2, 6.7 Hz, 1H, CH_2CH), 5.08 – 4.94 (m, 2H, CH_2CH), 3.46 – 3.37 (t, *J* = 6.8 Hz, 2H, CH_2Br), 2.15 – 2.03 (m, 2H, CH_2CHCH_2), 1.94 – 1.82 (m, 2H, CH_2CH_2Br), 1.61 – 1.48 (m, 2H, $CH_2CH_2CH_2Br$).

Spectroscopic data are consistent with literature values.[7]

4.2 1-(Penten-4-yl)cyclopropane

4.2.1 Synthesis of 6-(*tert*-butyldimethylsilyloxy)-1-hexene

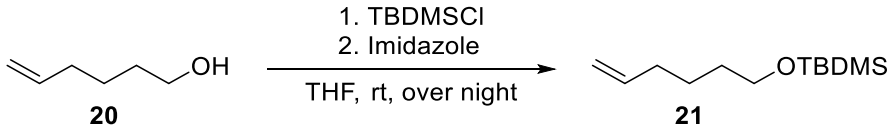

To a solution of 5-hexen-1-ol (**20**) (16.0 g, 160 mmol, 1.00 eq.) in THF (80 ml), TBDMSCl (24.5 g, 162 mmol, 1.01 eq.) and imidazole (13.1 g, 193 mmol, 1.20 eq.) were added. After stirring overnight desalinated water (40 ml) was added and the aqueous layer was extracted with diethyl ether (5 x 20 ml) and dried over Na_2SO_4. After evaporation of diethyl ether, the crude product was distilled under reduced pressure to obtain the desired product **21** (130 °C, 99 °C, 30 mbar). (29.8 g, 139 mmol, 87 %).

^{1}H-NMR (300 MHz, $CDCl_3$) δ [ppm] 5.90 – 5.73 (ddt, *J* = 16.9, 10.2, 6.7 Hz, 1H, CH_2=C*H*), 5.06 – 4.90 (m, 2H, C*H*$_2$=CH), 3.67 - 3.57 (t, *J* = 6.3 Hz, 2H, C*H*$_2$OTBDMS), 2.14 – 1.99 (d, *J* = 7.1 Hz, 2H, C*H*$_2$$CH_2$OTBDMS), 1.63 – 1.48 (m, 2H, C*H*$_2$$CH_2$$CH_2$OTBDMS), 1.48 – 1.37 (m, 2H, C*H*$_2$$CH_2$$CH_2$$CH_2$OTBDMS), 0.95 – 0.84 (s, 9H, OSi(CH_2)$_2$(C*H*$_3$)$_3$), 0.09 – 0.01 (s, 6H, OSi(C*H*$_2$)$_2$(CH_3)$_3$). **IR** (film on NaCl), $\tilde{\nu}$ [cm^{-1}] 3077, 2930, 1642, 1472, 1387, 1361, 1255, 1102, 910, 835, 775, 661.

Spectroscopic data are consistent with literature values.[8]

4.2.2 Synthesis of *tert*-butyl(4-cyclopropylbutoxy)dimethylsilane

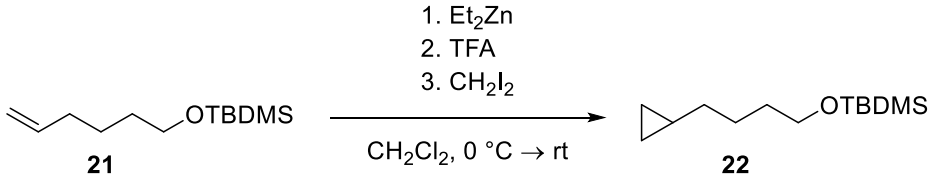

21 **22**

Et_2Zn (1.0 M in hexane, 140 ml, 140 mmol, 2.00 eq.) in CH_2Cl_2 (250 ml) was cooled to 0 °C and trifluoroacetic acid (11.0 ml, 142 mmol, 2.04 eq.) in CH_2Cl_2 (250 ml) was added over 2 h. After stirring the solution for 30 min a solution of freshly distilled diiodomethane (11.3 ml, 140 mmol, 2.00 eq.) in CH_2Cl_2 (250 ml) was added over 1 h. After stirring for another 30 min 6-(*tert*-butyldimethylsilyloxy)-1-hexene (**21**) (14.9 g, 69.7 mmol) in CH_2Cl_2 (140 ml) was added. The reaction solution was stirred at rt until a complete consumption of the alkene was detected by NMR-spectroscopy. A saturated NH_4Cl solution (200 ml) was added and the aqueous layer was extracted with diethyl ether (5 x 20 ml) and dried over Na_2SO_4. The solution was concentrated (60 ml) and used as crude product for the next reaction.

4.2.3 Synthesis of 4-cyclopropylbutane-1-ol

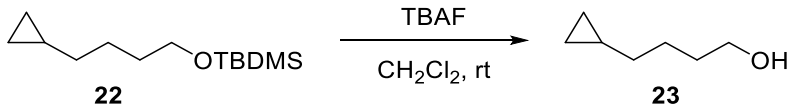

22 **23**

The crude product **22** of **4.2.2** was added to tetra-*n*-butylammonium fluoride -trihydrate (49.1 g, 138 mmol, 1.99 eq.) and stirred overnight. After completion, saturated NH_4Cl (150 ml) was added to the reaction and the organic phase was extracted with diethyl ether (3 x 100 ml). The combined organic phases where washed with brine (200 ml) and dried over Na_2SO_4. After evaporation (750 mbar, 40 °C) of the solvent the yellow liquid was purified by column chromatography (silica gel, pentane:diethyl ether = 3:1) to give the desired product as light yellow liquid (5.79 g, 44.5 mmol, 63 %).

^{1}H-NMR (300 MHz, $CDCl_3$) δ [ppm] 3.63 (t, *J* = 6.8, 2H, C*H*$_2$OH), 1.60 (m, 2H, C*H*$_2$$CH_2$OH), 1.46 (m, 2H, C*H*$_2$$CH_2$$CH_2$OH), 1.23 (m, 2H, C*H*$_2$$CH_2$$CH_2$$CH_2$OH), 0.65 (m, 1H, C*H*$CH_2$$CH_2$); 0.39 (m, 2H, $CHCH_2$C*H*$_2$), 0.00 (m, 2H, $CHCH_2$C*H*$_2$).

Spectroscopic data are consistent with literature values.[9]

4.2.4 4-Cyclopropylbutanal

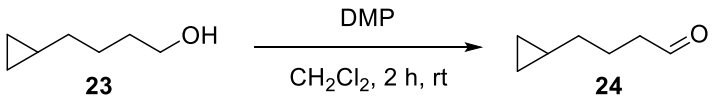

4-Cyclopropylbutan-1-ol (**23**) (5.79 g, 44.5 mmol, 1.00 eq.) in CH_2Cl_2 (400 ml) was cooled to 0 °C. Dess-Martin periodinane (20.7 g, 49.0 mmol, 1.10 eq.) was added in one portion and stirred for 1 h. The reaction was then stirred for a further hour at room temperature. The reaction was diluted with cooled pentane (200 ml) and the solid was removed through a celite pad. The product was concentrated *via* distillation (60 °C) and a yellow liquid was obtained.

^{1}H-NMR (300 MHz, $CDCl_3$) δ [ppm] 9.77 (t, *J* =1.86, 1H, *H*C=O), 2.46 (td, *J* = 7.36, 1.86, 1H, C*H*$_2$HC=O), 1.74 (p, *J* = 7.36, 2H; C*H*$_2$CH$_2$HC=O), 1.24 (m, 2H, C*H*$_2$CH$_2$CH$_2$HC=O), 0.64 (m, 1H, C*H*CH$_2$CH$_2$), 0.42 (m, 2H, CHC*H*$_2$CH$_2$), 0.01 (m, 2H, CHCH$_2$C*H*$_2$).

Spectroscopic data are consistent with literature values.[10]

4.2.5 1-(Penten-4-yl)cyclopropane

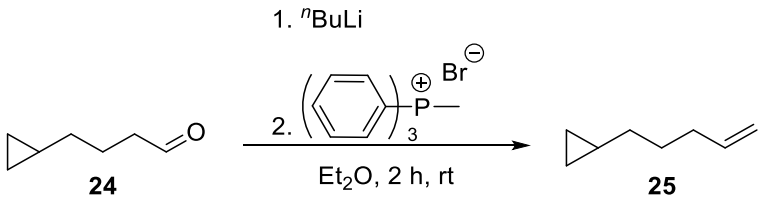

Methyltriphenylphosphonium bromide (23.9 g, 66.8 mmol, 1.50 eq.) in Et_2O (220 ml) was cooled to 0 °C and *n*-butyllithium (2.50 M, 26.8 ml, 66.7 mmol, 1.50 eq.) was added. The yellow suspension was stirred for 1 h. 4-Cyclopropylbutanal (**24**) (5.8 g, 44 mmol, 1.0 eq.) in Et_2O (45 ml) was added at 10 °C. The suspension was stirred for 1 h at room temperature and quenched with saturated NH_4Cl (150 ml). The suspension was filtered through a celite pad and concentrated *via* distillation. The crude product was purified by column chromatography (silica gel, eluent: pentane) and concentrated *via* distillation (oil bath = 150 °C) to get a clear liquid. Finally, it was stirred over NaH and condensed under reduced pressure (0.516 g, 4.68 mmol, 10 %). 1-(Penten-4-yl)cyclopropane (**25**) is very volatile and has to be stored at −20 °C.

^{1}H-NMR (300 MHz, $CDCl_3$) δ [ppm] 5.82 (ddt, J = 16.9, 10.1, 6.6, 1H, CH_2=C*H*); 4.97 (m, 2H, C*H*$_2$=CH), 2.08 (m, 2H, CH$_2$=CHC*H*$_2$), 1.51 (m, 2H, CH$_2$=CHCH$_2$C*H*$_2$), 1.21 (m, 2H, CH$_2$=CHCH$_2$CH$_2$C*H*$_2$), 0.66 (m, 1H, C*H*CH$_2$CH$_2$), 0.40 (m, 2H, CHCH$_2$C*H*$_2$), 0.01 (m, 2H, CHC*H*$_2$CH$_2$). **^{13}C{^{1}H}-NMR** (75.5 MHz, $CDCl_3$) δ [ppm] 139.3, 114.3, 34.4, 33.8, 29.1, 10.9, 4.52.

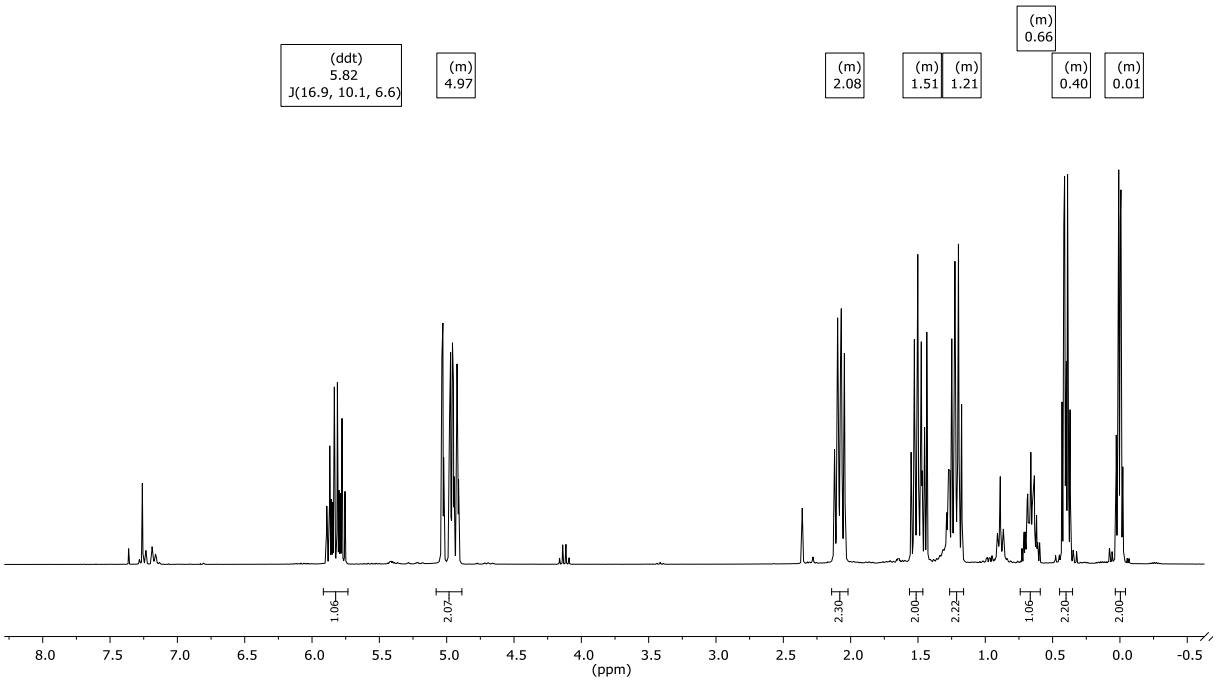

NMR-spectrum 46: ^{1}H-NMR-spectrum (300 MHz, $CDCl_3$) of 1-(penten-4-yl)cyclopropane.

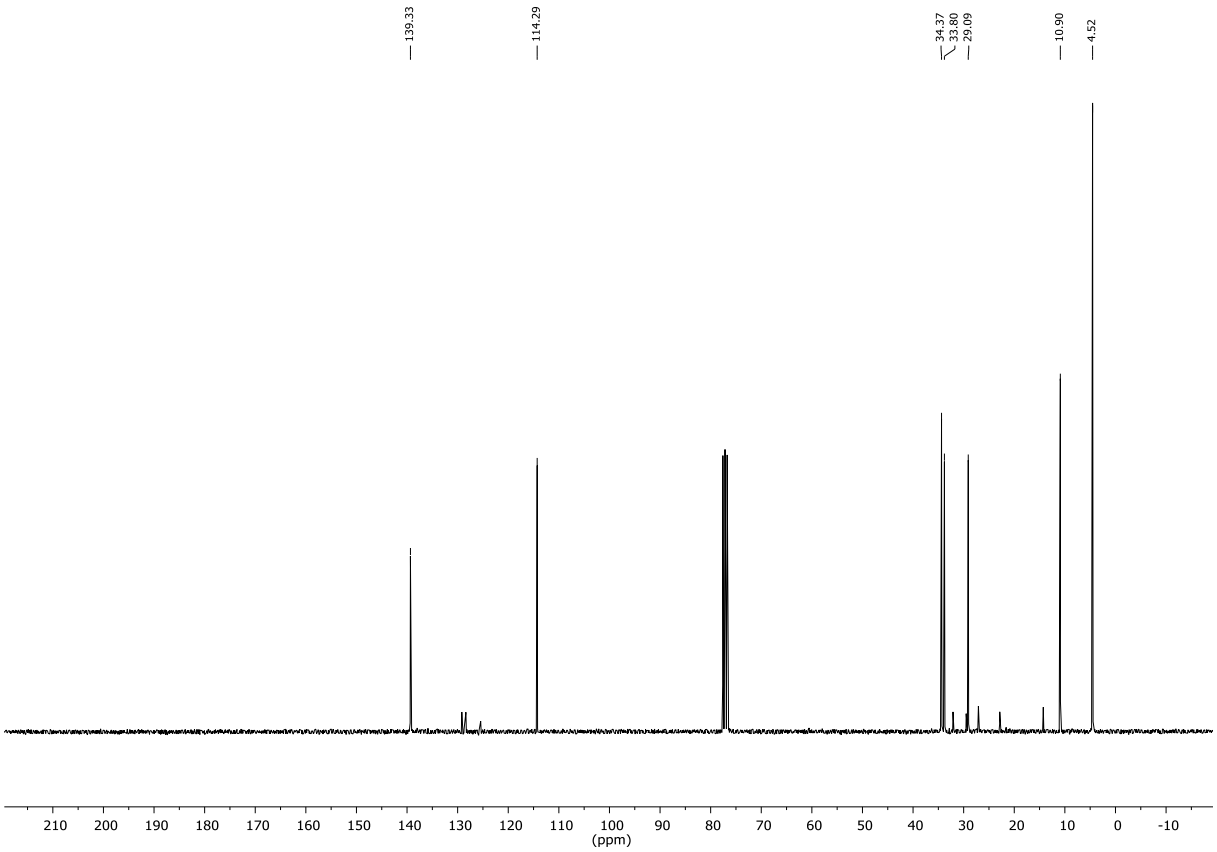

NMR-spectrum 47: ^{13}C-NMR-spectrum (75.5 MHz, $CDCl_3$) of 1-(penten-4-yl)cyclopropane.

5 [^{t}Bu$_3$PI][FB(C$_6$F$_5$)$_3$] formation, NMR-experiments

5.1 Room temperature measurement

Inside the glovebox, ^{t}Bu$_3$P (**5**) (8.2 mg, 0.041 mmol, 0.28 eq.) and B(C$_6$F$_5$)$_3$ (**3**) (22 mg, 0.042 mmol, 0.29 eq.) were weighed into a glass, dissolved in CD_2Cl_2 (overall 0.62 ml) and transferred into a Young valve NMR tube. Fluorobenzene (10 µl, 0.11 mmol) was added as an internal standard, followed by addition of nonafluoro-1-iodobutane (**2**) (50 mg, 0.14 mmol, 1.0 eq.). The NMR tube was sealed and NMR-measurements were conducted.

5.2 Low temperature measurement

Inside the glovebox, ^{t}Bu$_3$P (**5**) (7.5 mg, 0.037 mmol, 0.26 eq.) was dissolved in CD_2Cl_2 and transferred into a Young valve NMR tube, which was filled with trifluoromethylcyclohexane (3.5 µl, 0.025 mmol) as internal standard. A solution B(C$_6$F$_5$)$_3$ (**3**) (19 mg, 0.036 mmol, 0.25 eq.) in combination with nonafluoro-1-iodobutane (**2**) (50 mg, 0.15 mmol, 1.0 eq.) was added. Several spectra were measured at 25 °C up to −30 °C.

6 Synthesis of [^{t}Bu$_3$PH][FB(C$_6$F$_5$)$_3$]

^{t}Bu$_3$P (**5**) (198 mg, 0.979 mmol, 1.00 eq.) and B(C$_6$F$_5$)$_3$ (**3**) (538 mg, 1.05 mmol, 1.07 eq.) were dissolved in toluene (20 ml) in a transparent screw-cap jar. After 2 d the reaction solution was transferred into a reactor bomb and heated up to 100 °C for 5 d. The resulting two-phase system was transferred into a flask and layered with pentane. After 1 d at −20 °C crystals (95.3 mg) were obtained.

^{1}H-NMR (300 MHz, CD_2Cl_2) δ [ppm] 5.45 (d, *J* = 443 Hz, 1H), 1.61 (d, *J* = 15.7 Hz, 27H). **^{19}F-NMR** (282 MHz, CD_2Cl_2) δ [ppm] −135.4 - −135.9 (m), −162.5 (t, *J* = 20.1 Hz), −166.8 - −167.3 (m), −187.7. ^{31}P NMR (121 MHz, CD_2Cl_2) δ [ppm] 56.69. **^{11}B NMR** (96 MHz, CD_2Cl_2) δ [ppm] −0.50 (d, *J* = 71.2 Hz).

Piers et al.[11] described slightly different shifts for [^{t}Bu$_3$PH][FB(C$_6$F$_5$)$_3$] (**17**). However, ^{1}H- and ^{31}P-NMR-spectra show the determining signals for [^{t}Bu$_3$PH]$^+$ and ^{19}F- as well as ^{11}B-NMR-spectra show the determining signals for [FB(C$_6$F$_5$)$_3$]$^-$.

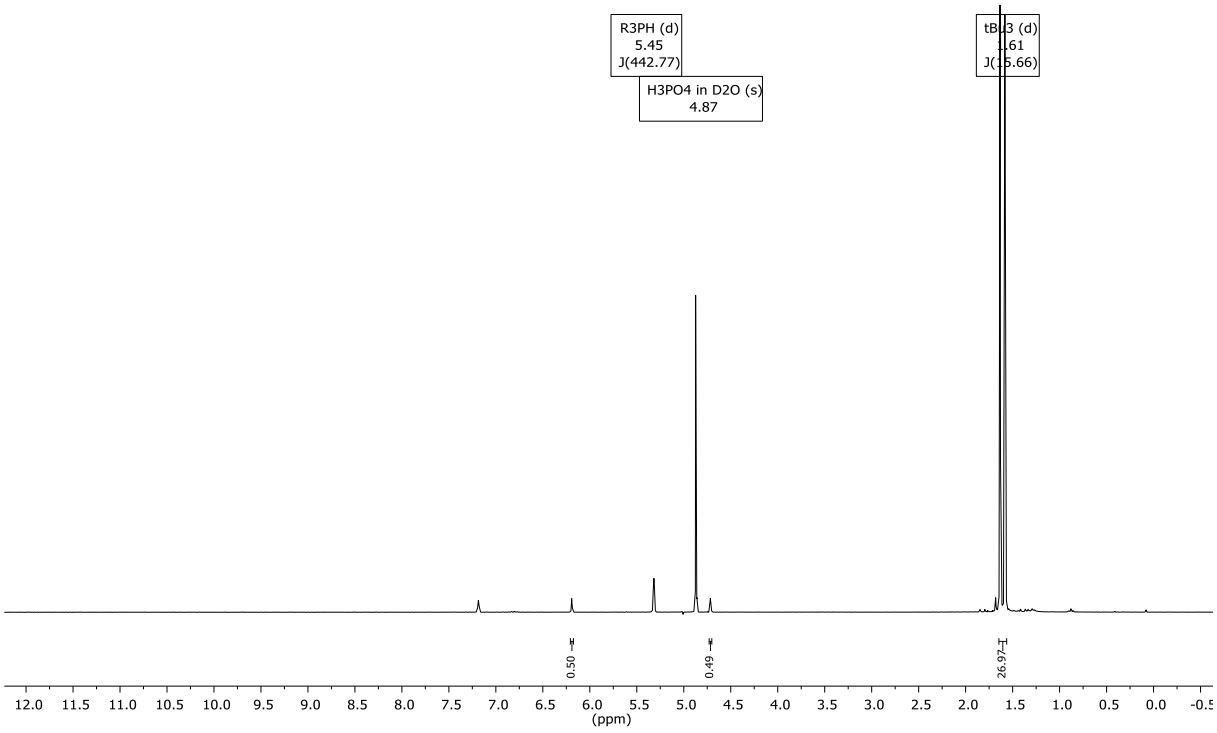

NMR-spectrum 48: ^{1}H-NMR-spectrum (300 MHz, CD_2Cl_2) of [^{t}Bu$_3$PH][FB(C_6F_5)$_3$].

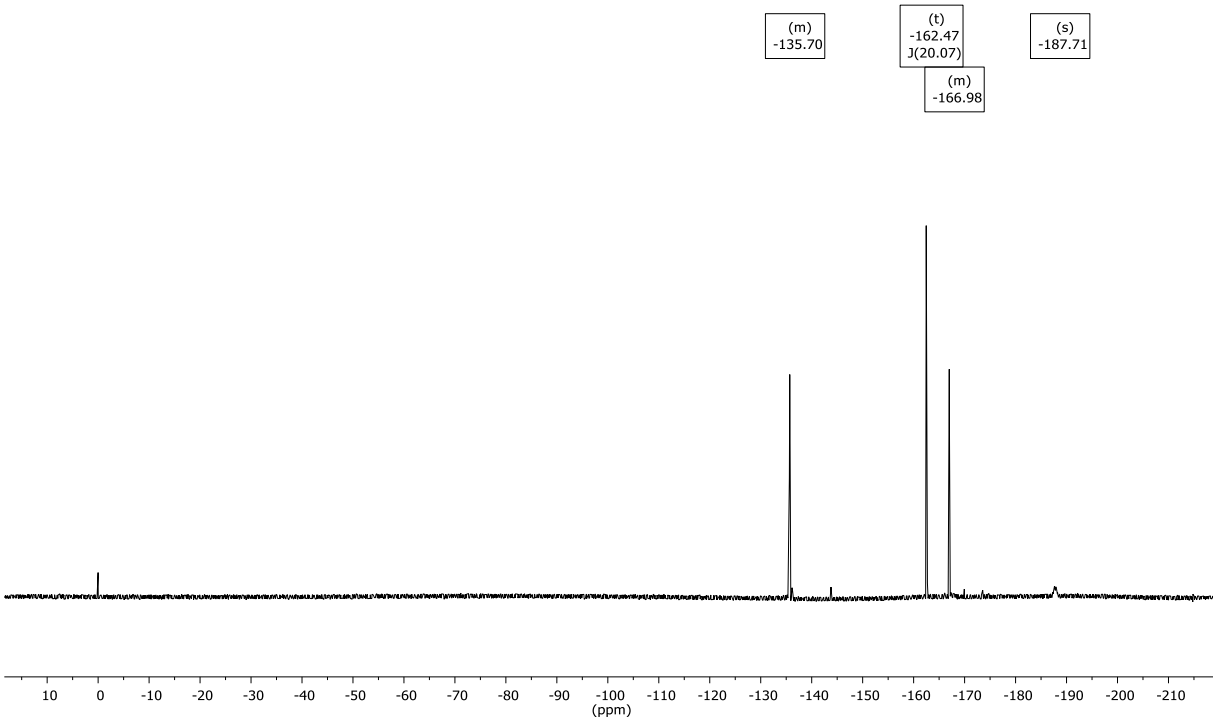

NMR-spectrum 49: ^{19}F-NMR-spectrum (282 MHz, CD_2Cl_2) of [^{t}Bu$_3$PH][FB(C_6F_5)$_3$].

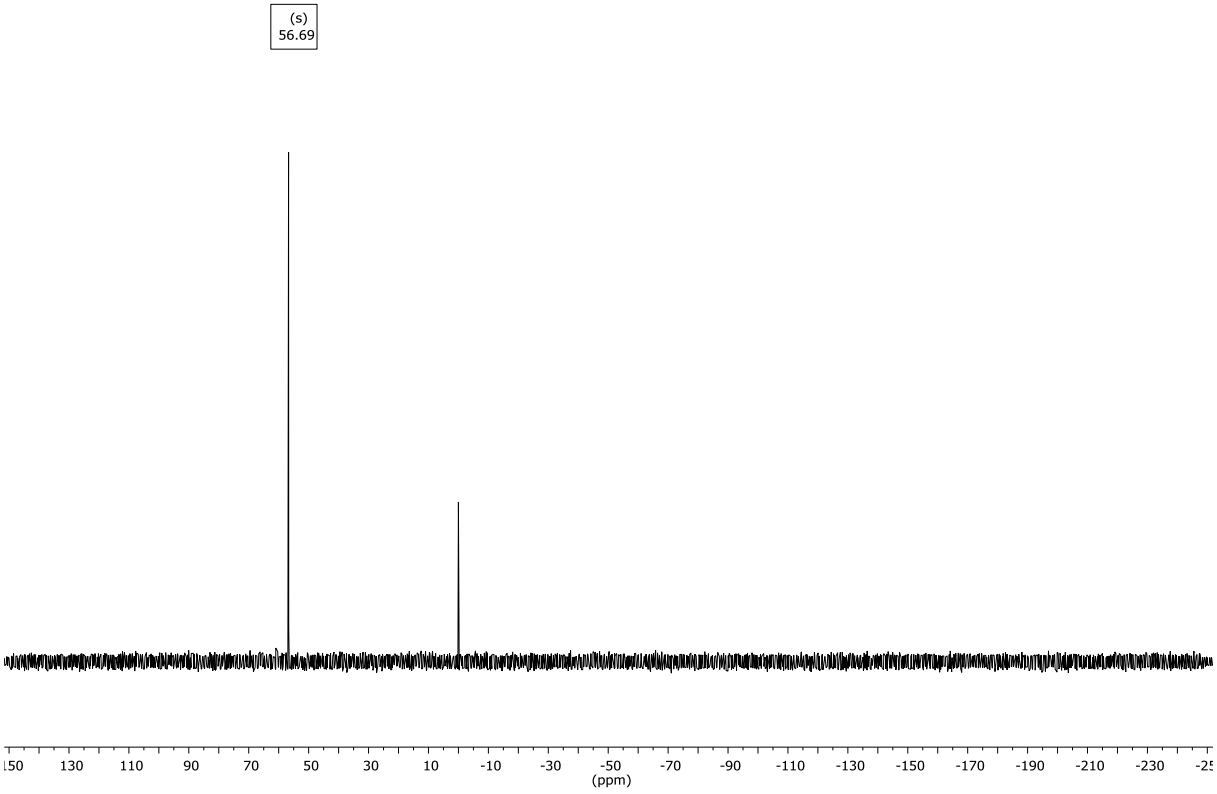

NMR-spectrum 50: ^{31}P-NMR-spectrum (121 MHz, CD_2Cl_2) of [^{t}Bu$_3$PH][FB(C$_6$F$_5$)$_3$].

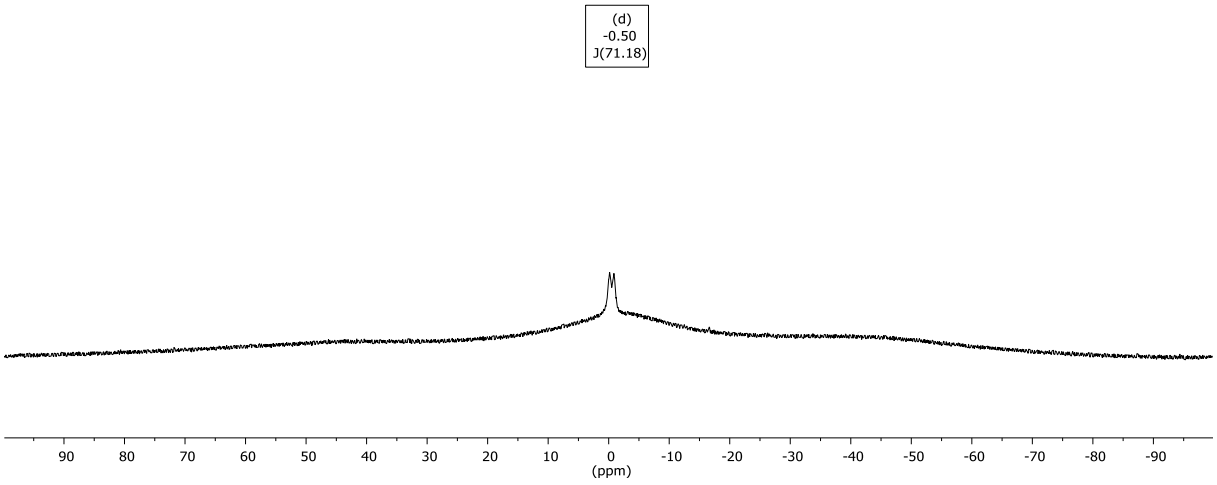

NMR-spectrum 51: ^{11}B-NMR-spectrum (96 MHz, CD_2Cl_2) of [^{t}Bu$_3$PH][FB(C$_6$F$_5$)$_3$].

7 GC-experiments

Preface

To monitor the reaction progress, we used *n*-decane (TCI, purity ≥99.5%, product number: S0282, stored over 4 Å molecular sieve) as an internal standard. For the calibration curve, we prepared solutions of vinylcyclohexane (**1**) and *n*-decane (**19**) in CH_2Cl_2 in volumetric flasks inside the glovebox. GC measurements were conducted with a Perkin Elmer Clarus 500 GC without an autosampler equipped with a SUPELCO SLB-5ms column (30 m x 0.25 mm x 0.25 µm).

We validated our GC method in a range of about 15 - 90% conversion, because of higher standard deviations outside this range. As a result, we could not measure data for an excess of vinylcyclohexane (**1**) and had to use NMR measurements. These higher standard deviations apart from our calibration range can be understood in the light of a substantial boiling point difference between vinylcyclohexane (b.p. = 128 °C) and *n*-decane (b.p. = 174 °C), resulting in mass discrimination by the split stream.

Standard procedure A for GC experiments

A 10 ml round-bottom flask was wrapped in aluminum foil and then equipped with a Teflon stir bar (6 x 2 mm) as well as *n*-decane (**19**) (80.0 µl) as internal standard. $^t Bu_3P$ (**5**) and $B(C_6F_5)_3$ (**3**) were weighed into separate glass vials. After these first preparations, all work steps were conducted under red light and best possible light exclusion. $^t Bu_3P$ (**5**) was dissolved, transferred into the round-bottom flask and the vial was rinsed twice (in total 1.3 ml CH_2Cl_2). Vinylcyclohexane (**1**) as well as nonafluoro-1-iodobutane (**2**) were added. One minute after adding C_4F_9I, a solution of freshly dissolved $B(C_6F_5)_3$ (**3**) was added and the vial was rinsed twice (in total 1.3 ml CH_2Cl_2). The flask was sealed with a rubber septum and then unloaded from the glovebox. It was attached to an N_2 stream and stirred at 20 °C (thermostat). Samples were withdrawn as follows: A 1.0 ml syringe (Braun) was flushed with N_2 at a separate flask three times, then 0.10 ml of the reaction solution were withdrawn and diluted with 0.10 ml CH_2Cl_2 (saturated with water). This solution was used for injection into the GC.

Table 4: Calibration curve for vinylcyclohexane with *n*-decane as internal standard.

c(vinylcyclohexane) [mg·ml^{-1}]	c(*n*-decane) [mg·ml^{-1}]	c(V)/c(D)	area(vinylcyclohexane) [µV·s]	area(*n*-decane) [µV·s]	area(V)/area(D)
29.8	25.6	1.17	23719	20258	1.17
			24777	21176	1.17
			19991	17224	1.16
			22081	19054	1.16
			33018	27379	1.21
			32540	27473	1.18
24.2	25.6	0.945	20462	20064	1.02
			22055	22322	0.99
			19807	19843	1.00
			20709	20565	1.01
			11616	12086	0.96
18.1	25.6	0.709	8542	16889	0.506
			10845	21615	0.502
			5197	10812	0.481
			10151	20200	0.503
			10353	20386	0.508
12.1	25.6	0.473	8542	16889	0.506
			10845	21615	0.502
			5197	10812	0.481
			10151	20200	0.503
			10353	20386	0.508
4.03	25.6	0.158	3308	20089	0.165
			3303	19792	0.167
			3218	19732	0.163
			1860	11827	0.157
			3117	18840	0.165

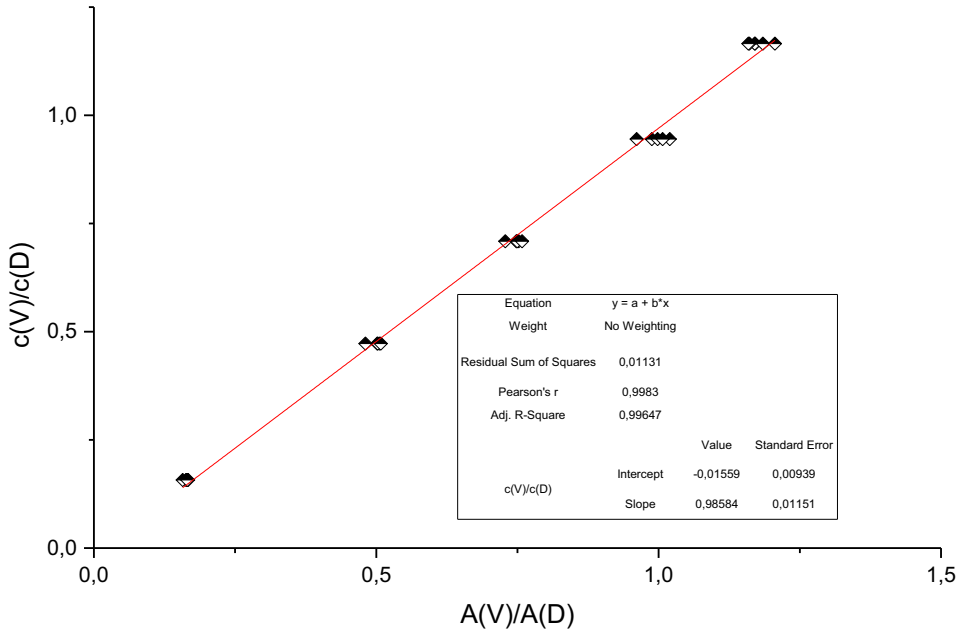

Figure 1: Calibration curve for vinylcyclohexane.

The following datasets contain calculated values. The mass of vinylcyclohexane is calculated with the following equation:

$$\mathrm{m(V)} = (0{,}98584 \cdot \mathrm{A(V)(A(D)} - 0{,}01559) \cdot \mathrm{m(D)}$$

Subsequently, the conversion is calculated as follows:

$$\mathrm{conversion} = (\mathrm{m_0(V)} - \mathrm{m(V)})/\mathrm{m_0(V)}$$

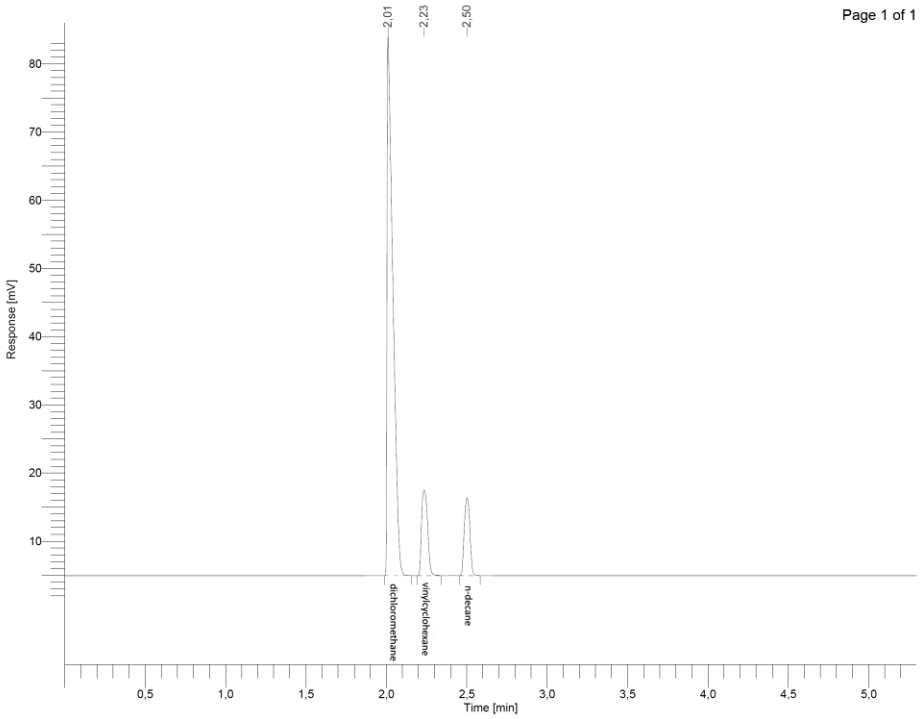

Figure 2: Exemplary chromatogram of the calibration.

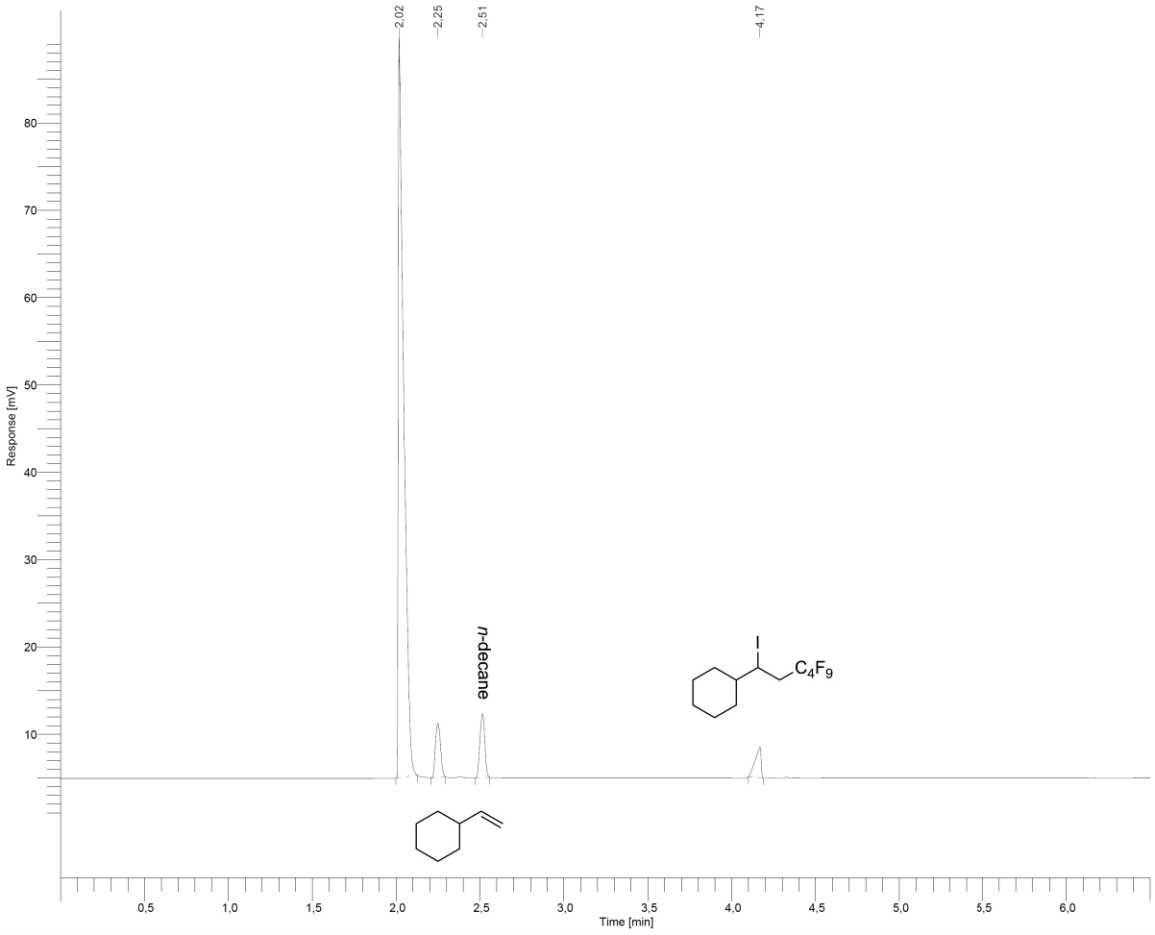

Figure 3: Exemplary chromatogram of a reaction solution.

7.1 GC-experiment, standard conditions

$^{t}Bu_3P$ (**5**) (7.5 mg, 0.037 mmol, 5.0 mol%), vinylcyclohexane (**1**) (100 µl, 0.730 mmol, 1.00 eq.), nonafluoro-1-iodobutane (**2**) (125 µl, 0.726 mmol, 0.994 eq.) and $B(C_6F_5)_3$ (**3**) (18.7 mg, 0.0365 mmol, 5.0 mol%) were reacted as described in Standard procedure A for GC experiments.

Table 5: Standard conditions.

reaction time [min]	area(vinylcyclohexane) [µV·s]	area(*n*-decane) [µV·s]	A(V)/A(D)[a]	m(V)[a] [mg]	conversion[a] [%]	m(V)/m(V_0)[a]	ln([V]/[V_0])[a]
20	14089	14830	0.950	53.8	33	0.67	-0.403
20	15586	16463	0.947	53.6	33	0.67	-0.407
20	15914	16944	0.939	53.2	34	0.66	-0.415
30	17161	20105	0.854	48.2	40	0.60	-0.512
30	12145	14755	0.823	46.5	42	0.58	-0.549
30	12310	14998	0.821	46.3	42	0.58	-0.552
40	10447	14134	0.739	41.6	48	0.52	-0.659
40	10817	14655	0.738	41.6	48	0.52	-0.661
40	11384	15463	0.736	41.5	48	0.52	-0.663
50	9730	14576	0.668	37.5	53	0.47	-0.763
50	9073	13916	0.652	36.6	55	0.45	-0.787
50	9639	14644	0.658	37.0	54	0.46	-0.778
60	9054	15329	0.591	33.1	59	0.41	-0.889
60	8843	15023	0.589	33.0	59	0.41	-0.892
60	9621	16060	0.599	33.6	58	0.42	-0.874

[a] Calculated values; V = vinylcyclohexane, D = *n*-decane.

Table 6: Basis for depicted graphs, standard conditions.

Δt [min]	average conversion [%]	standard deviation [%]
20	34	0.40
30	42	1.31
40	48	0.11
50	54	0.56
60	59	0.40

7.2 GC-experiments, 10 mol% $^{t}Bu_3P$

$^{t}Bu_3P$ (**5**) (14.8 mg, 0.0732 mmol, 10 mol%), vinylcyclohexane (**1**) (100 µl, 0.730 mmol, 1.00 eq.), nonafluoro-1-iodobutane (**2**) (125 µl, 0.726 mmol, 0.994 eq.) and $B(C_6F_5)_3$ (**3**) (18.6 mg, 0.0363 mmol, 5.0 mol%) were reacted as described in Standard procedure A for GC experiments.

Table 7: Standard procedure, 10 mol% $^{t}Bu_3P$.

reaction time [min]	area(vinylcyclohexane) [µV·s]	area(*n*-decane) [µV·s]	A(V)/A(D)[a]	m(V)[a] [mg]	conversion[a] [%]	m(V)/m(V_0)[a]	ln([V]/[V_0])[a]
15	12930	14535	0.890	50.3	38	0.62	-0.470
15	16766	18496	0.906	51.3	36	0.64	-0.451
15	15529	17195	0.903	51.1	37	0.63	-0.455
20	14601	17740	0.823	46.5	42	0.58	-0.549
20	12729	16041	0.794	44.8	44	0.56	-0.587
20	12308	15436	0.797	45.0	44	0.56	-0.582
25	11059	14895	0.742	41.8	48	0.52	-0.655
25	11534	15450	0.747	42.1	48	0.52	-0.649
25	11938	16089	0.742	41.8	48	0.52	-0.655
30	14415	20194	0.714	40.2	50	0.50	-0.695
30	11905	17463	0.682	38.3	52	0.48	-0.742
30	13381	19449	0.688	38.7	52	0.48	-0.732
40	9306	15394	0.605	33.9	58	0.42	-0.865
40	12123	19455	0.623	35.0	57	0.43	-0.834
40	12210	19805	0.617	34.6	57	0.43	-0.845
50	8912	16491	0.540	30.2	62	0.38	-0.980
50	8707	16167	0.539	30.1	63	0.37	-0.984
50	8739	16354	0.534	29.9	63	0.37	-0.992

[a] Calculated values; V = vinylcyclohexane, D = *n*-decane.

Table 8: Basis for depicted graphs, standard procedure, 10 mol% $^{t}Bu_3P$.

Δt [min]	average conversion [%]	standard deviation [%]
15	37	0.64
20	44	1.15
25	48	0.18
30	51	1.22
40	57	0.67
60	59	0.40

7.3 GC-experiments, 15 mol% $^{t}Bu_3P$

$^{t}Bu_3P$ (**5**) (22.2 mg, 0.110 mmol, 15 mol%), vinylcyclohexane (**1**) (100 µl, 0.730 mmol, 1.00 eq.), nonafluoro-1-iodobutane (**2**) (125 µl, 0.726 mmol, 0.994 eq.) and $B(C_6F_5)_3$ (**3**) (18.8 mg, 0.0367 mmol, 5.0 mol%) were reacted as described in Standard procedure A for GC experiments.

Table 9: Standard procedure, 15 mol% $^{t}Bu_3P$.

reaction time [min]	area(vinylcyclohexane) [µV·s]	area(*n*-decane) [µV·s]	A(V)/A(D)[a]	m(V)[a] [mg]	conversion[a] [%]	m(V)/m(V_0)[a]	ln([V]/[V_0])[a]
15	11378	15412	0.738	41.6	48	0.52	-0.660
15	11473	15589	0.736	41.5	48	0.52	-0.663
15	15038	19956	0.754	42.5	47	0.53	-0.639
20	10695	15919	0.672	37.8	53	0.47	-0.757
20	10442	15479	0.675	37.9	53	0.47	-0.753
20	13653	19683	0.694	39.0	52	0.48	-0.724
25	9388	15499	0.606	34.0	58	0.42	-0.863
25	12908	20787	0.621	34.8	57	0.43	-0.837
25	13226	21298	0.621	34.8	57	0.43	-0.837
30	10794	18831	0.573	32.1	60	0.40	-0.920
30	11291	19813	0.570	31.9	60	0.40	-0.926
30	10472	18441	0.568	31.8	61	0.39	-0.929
40	7243	15265	0.474	26.4	67	0.33	-1.115
40	7664	16163	0.474	26.4	67	0.33	-1.115
40	7695	16278	0.473	26.3	67	0.33	-1.118
50	6787	16133	0.421	23.3	71	0.29	-1.239
50	6382	15412	0.414	22.9	72	0.28	-1.256
50	8808	20279	0.434	24.1	70	0.30	-1.206

[a] Calculated values; V = vinylcyclohexane, D = *n*-decane.

Table 10: Basis for depicted graphs, standard procedure, 15 mol% $^{t}Bu_3P$.

Δt [min]	average conversion [%]	standard deviation [%]
15	48	0.68
20	52	0.85
25	57	0.63
30	60	0.19
40	67	0.07
50	71	0.74

7.4 GC-experiments, 1.5 eq. C_4F_9I

$^tBu_3P$ (**5**) (7.5 mg, 0.037 mmol, 5.1 mol%), vinylcyclohexane (**1**) (100 µl, 0.730 mmol, 1.00 eq.), nonafluoro-1-iodobutane (**2**) (190 µl, 1.10 mmol, 1.51 eq.) and $B(C_6F_5)_3$ (**3**) (18.6 mg, 0.0363 mmol, 5.0 mol%) were reacted as described in Standard procedure A for GC experiments.

Table 11: Standard procedure, 1.5 eq. C_4F_9I.

reaction time [min]	area(vinylcyclohexane) [µV·s]	area(*n*-decane) [µV·s]	A(V)/A(D)[a]	m(V)[a] [mg]	conversion[a] [%]	m(V)/m(V_0)[a]	ln([V]/[V_0])[a]
20	10270	14013	0.733	41.3	49	0.51	-0.668
20	10538	14437	0.730	41.1	49	0.51	-0.672
20	9530	13326	0.715	40.3	50	0.50	-0.693
25	8883	13878	0.640	35.9	55	0.45	-0.806
25	9775	15399	0.635	35.6	56	0.44	-0.815
25	9673	15298	0.632	35.5	56	0.44	-0.819
30	8051	14152	0.569	31.8	60	0.40	-0.927
30	7863	13916	0.565	31.6	61	0.39	-0.934
30	7423	13316	0.557	31.2	61	0.39	-0.948
40	6199	14268	0.434	24.1	70	0.30	-1.206
40	6632	15350	0.432	24.0	70	0.30	-1.212
40	6902	15915	0.434	24.1	70	0.30	-1.208
50	4822	14400	0.335	18.4	77	0.23	-1.478
50	4947	14856	0.333	18.3	77	0.23	-1.483

[a] Calculated values; V = vinylcyclohexane, D = *n*-decane.

Table 12: Basis for depicted graphs, standard conditions, 1.5 eq. C_4F_9I.

Δt [min]	average conversion [%]	standard deviation [%]
20	49	0.68
25	56	0.28
30	61	0.42
40	70	0.09
50	77	0.09

7.5 GC-experiments, 2.0 eq. C_4F_9I

$^tBu_3P$ (**5**) (7.4 mg, 0.037 mmol, 5.0 mol%), vinylcyclohexane (**1**) (100 µl, 0.730 mmol, 1.00 eq.), nonafluoro-1-iodobutane (**2**) (250 µl, 1.45 mmol, 1.99 eq.) and $B(C_6F_5)_3$ (**3**) (18.8 mg, 0.0367 mmol, 5.0 mol%) were reacted as described in Standard procedure A for GC experiments.

Table 13: Standard procedure, 2.0 eq. C_4F_9I.

reaction time [min]	area(vinylcyclohexane) [µV·s]	area(*n*-decane) [µV·s]	A(V)/A(D)[a]	m(V)[a] [mg]	conversion[a] [%]	m(V)/m(V_0)[a]	ln([V]/[V_0])[a]
15	9771	14076	0.694	39.1	51	0.49	-0.723
15	12372	16999	0.728	41.0	49	0.51	-0.675
15	9887	14430	0.685	38.5	52	0.48	-0.737
20	7906	13714	0.576	32.3	60	0.40	-0.914
20	8186	14117	0.580	32.5	60	0.40	-0.908
20	7985	13812	0.578	32.4	60	0.40	-0.911
25	6902	14681	0.470	26.2	68	0.32	-1.124
25	7287	15551	0.469	26.1	68	0.32	-1.128
25	7232	15434	0.469	26.1	68	0.32	-1.128
30	5425	14484	0.375	20.7	74	0.26	-1.360
30	7436	19157	0.388	21.4	73	0.27	-1.323
30	5578	15175	0.368	20.3	75	0.25	-1.380
40	3887	16675	0.233	12.5	84	0.16	-1.862
40	4224	18451	0.229	12.3	85	0.15	-1.881
40	5224	22534	0.232	12.4	85	0.15	-1.868

[a] Calculated values; V = vinylcyclohexane, D = *n*-decane.

Table 14: Basis for depicted graphs, standard procedure, 2.0 eq. C_4F_9I.

Δt [min]	average conversion [%]	standard deviation [%]
15	51	1.61
20	60	0.12
25	68	0.06
30	74	0.75
40	85	0.15

7.6 GC-experiments, 10 mol% $B(C_6F_5)_3$

$^tBu_3P$ (**5**) (7.5 mg, 0.037 mmol, 5.1 mol%), vinylcyclohexane (**1**) (100 µl, 0.730 mmol, 1.00 eq.), nonafluoro-1-iodobutane (**2**) (125 µl, 0.726 mmol, 0.994 eq.) and $B(C_6F_5)_3$ (**3**) (37.5 mg, 0.0732 mmol, 10 mol%) were reacted as described in Standard procedure A for GC experiments.

Table 15: Standard procedure, 10 mol% $B(C_6F_5)_3$.

reaction time [min]	area(vinylcyclohexane) [µV·s]	area(*n*-decane) [µV·s]	A(V)/A(D)[a]	m(V)[a] [mg]	conversion[a] [%]	m(V)/m(V_0)[a]	ln([V]/[V_0])[a]
15	12208	13865	0.880	49.8	38	0.62	-0.481
15	13745	15145	0.908	51.3	36	0.64	-0.450
15	13598	15074	0.902	51.0	37	0.63	-0.456
20	11615	14433	0.805	45.4	44	0.56	-0.572
20	12293	14946	0.822	46.4	42	0.58	-0.550
20	12299	15076	0.816	46.1	43	0.57	-0.558
30	13200	18880	0.699	39.3	51	0.49	-0.716
30	10082	14629	0.689	38.8	52	0.48	-0.731
30	10212	14831	0.689	38.7	52	0.48	-0.732
40	10542	17605	0.599	33.6	58	0.42	-0.875
40	9378	16046	0.584	32.7	59	0.41	-0.900
40	9227	15929	0.579	32.4	60	0.40	-0.909
50	7400	14797	0.500	27.9	65	0.35	-1.060
50	8122	16157	0.503	28.0	65	0.35	-1.055
50	7847	15682	0.500	27.9	65	0.35	-1.060

[a] Calculated values; V = vinylcyclohexane, D = *n*-decane.

Table 16: Basis for depicted graphs, standard procedure, 10 mol% $B(C_6F_5)_3$.

Δt [min]	average conversion [%]	standard deviation [%]
15	37	1.02
20	43	0.64
30	52	0.43
40	59	0.72
50	65	0.10

7.7 GC-experiments, 15 mol% $B(C_6F_5)_3$

$^tBu_3P$ (**5**) (7.5 mg, 0.037 mmol, 5.1 mol%), vinylcyclohexane (**1**) (100 µl, 0.730 mmol, 1.00 eq.), nonafluoro-1-iodobutane (**2**) (125 µl, 0.726 mmol, 0.994 eq.) and $B(C_6F_5)_3$ (**3**) (56.1 mg, 0.110 mmol, 15 mol%) were reacted as described in Standard procedure A for GC experiments.

Table 17: Standard procedure, 15 mol% $B(C_6F_5)_3$.

reaction time [min]	area(vinylcyclohexane) [µV·s]	area(*n*-decane) [µV·s]	A(V)/A(D)[a]	m(V)[a] [mg]	conversion[a] [%]	m(V)/m(V_0)[a]	ln([V]/[V_0])[a]
15	13787	15999	0.862	48.7	39	0.61	-0.503
15	12653	14765	0.857	48.4	40	0.60	-0.508
15	13288	15743	0.844	47.7	41	0.59	-0.524
20	11702	15277	0.766	43.2	46	0.54	-0.623
20	11178	14668	0.762	43.0	47	0.53	-0.628
20	12047	15906	0.757	42.7	47	0.53	-0.634
30	9442	15414	0.613	34.4	57	0.43	-0.851
30	9344	15414	0.606	34.0	58	0.42	-0.862
30	9572	15808	0.606	34.0	58	0.42	-0.863
40	9377	17941	0.523	29.2	64	0.36	-1.015
40	7311	14858	0.492	27.4	66	0.34	-1.077
40	9465	18876	0.501	28.0	65	0.35	-1.058
51	6167	15145	0.407	22.5	72	0.28	-1.273
51	6161	15393	0.400	22.1	73	0.27	-1.291
51	7387	17686	0.418	23.1	71	0.29	-1.247

[a] Calculated values; V = vinylcyclohexane, D = *n*-decane.

Table 18: Basis for depicted graphs, standard procedure, 15 mol% $B(C_6F_5)_3$.

Δt [min]	average conversion [%]	standard deviation [%]
15	40	0.65
20	47	0.31
30	58	0.28
40	65	1.12
51	72	0.63

7.8 GC-experiment, 33 min premixing of $^{t}Bu_3P$ and $B(C_6F_5)_3$

Analogous to Standard procedure A for GC experiments, $^{t}Bu_3P$ (**5**) (7.4 mg, 0.037 mmol, 5.0 mol%) as well as $B(C_6F_5)_3$ (**3**) (18.5 mg, 0.361 mmol, 4.9 mol%) were dissolved in CH_2Cl_2 (1.0 ml + 0.5 ml for rinsing) and filled into a pointed flask. After 33 min this solution was added to a solution of vinylcyclohexane (**1**) (100 µl, 0.730 mmol, 1.00 eq.) and nonafluoro-1-iodobutane (**2**) (125 µl, 0.726 mmol, 0.994 eq.) in CH_2Cl_2 (1.0 ml) outside the glovebox.

Table 19: Varied procedure, 33 min premixing of $^{t}Bu_3P$ and $B(C_6F_5)_3$.

reaction time [min]	area(vinylcyclohexane) [µV·s]	area(*n*-decane) [µV·s]	A(V)/A(D)[a]	m(V)[a] [mg]	conversion[a] [%]	m(V)/m(V$_0$)[a]	ln([V]/[V$_0$])[a]
20	15646	15848	0.987	55.9	31	0.69	-0.364
20	15870	16021	0.991	56.1	30	0.70	-0.361
20	16158	16285	0.992	56.2	30	0.70	-0.359
30	13508	15629	0.864	48.8	39	0.61	-0.500
30	15121	16887	0.895	50.6	37	0.63	-0.463
30	13056	14871	0.878	49.6	38	0.62	-0.484
40	13833	17912	0.772	43.6	46	0.54	-0.614
40	13741	17930	0.766	43.2	46	0.54	-0.622
40	14774	19187	0.770	43.4	46	0.54	-0.617
50	12489	17902	0.698	39.3	51	0.49	-0.718
50	14860	21306	0.697	39.2	51	0.49	-0.718
50	15125	21829	0.693	39.0	52	0.48	-0.725
60	10742	16659	0.645	36.2	55	0.45	-0.799
60	11091	17560	0.632	35.5	56	0.44	-0.820
60	10970	17520	0.626	35.1	56	0.44	-0.829

[a] Calculated values; V = vinylcyclohexane, D = *n*-decane.

Table 20: Basis for depicted graphs, varied procedure, 33 min premixing of $^{t}Bu_3P$ and $B(C_6F_5)_3$.

Δt [min]	average conversion [%]	standard deviation [%]
20	30	0.18
30	38	1.12
40	46	0.21
50	51	0.19
60	56	0.69

7.9 GC-experiment, 61 min premixing of $^{t}Bu_3P$ and $B(C_6F_5)_3$

Analogous to Standard procedure A for GC experiments, $^{t}Bu_3P$ (**5**) (7.4 mg, 0.037 mmol, 5.0 mol%) as well as $B(C_6F_5)_3$ (**3**) (18.6 mg, 0.363 mmol, 5.0 mol%) were premixed and stirred for 61 min inside the glovebox. Vinylcyclohexane (**1**) (100 µl, 0.730 mmol, 1.00 eq.) and nonafluoro-1-iodobutane (**2**) (125 µl, 0.726 mmol, 0.994 eq.) were added inside the glovebox.

Table 21: Varied procedure, 61 min premixing of $^{t}Bu_3P$ and $B(C_6F_5)_3$.

reaction time [min]	area(vinylcyclohexane) [µV·s]	area(*n*-decane) [µV·s]	A(V)/A(D)[a]	m(V)[a] [mg]	conversion[a] [%]	m(V)/m(V_0)[a]	ln([V]/[V_0])[a]
20	15428	15646	0.986	55.9	31	0.69	-0.365
20	14717	14914	0.987	55.9	31	0.69	-0.365
20	15067	15274	0.986	55.9	31	0.69	-0.365
30	12891	14320	0.900	50.9	37	0.63	-0.458
30	12696	14374	0.883	49.9	38	0.62	-0.477
30	13229	14929	0.886	50.1	38	0.62	-0.474
40	15683	19208	0.816	46.1	43	0.57	-0.558
40	12518	15854	0.790	44.5	45	0.55	-0.592
40	12041	15500	0.777	43.8	46	0.54	-0.608
50	11819	16350	0.723	40.7	49	0.51	-0.682
50	11429	16197	0.706	39.7	51	0.49	-0.707
50	11593	16374	0.708	39.9	50	0.50	-0.703
60	10787	16278	0.663	37.2	54	0.46	-0.771
60	9816	15237	0.644	36.2	55	0.45	-0.800
60	10025	15432	0.650	36.5	55	0.45	-0.791

[a] Calculated values; V = vinylcyclohexane, D = *n*-decane.

Table 22: Basis for depicted graphs, varied procedure, 61 min premixing of $^{t}Bu_3P$ and $B(C_6F_5)_3$.

Δt [min]	average conversion [%]	standard deviation [%]
20	31	0.03
30	37	0.65
40	44	1.45
50	50	0.67
60	54	0.68

7.10 GC-experiment, 10 min premixing of $^{t}Bu_3P$, C_4F_9I and alkene

Analogous to Standard procedure A for GC experiments, to a solution of $^{t}Bu_3P$ (**5**) (7.5 mg, 0.037 mmol, 5.1 mol%) in CH_2Cl_2 (1.3 ml), vinylcyclohexane (**1**) (100 µl, 0.730 mmol, 1.00 eq.) as well as nonafluoro-1-iodobutane (**2**) (125 µl, 0.726 mmol, 0.994 eq.) were added. After 10 min a solution of $B(C_6F_5)_3$ (**3**) (18.8 mg, 0.367 mmol, 5.0 mol%) was added inside the glovebox.

Table 23: Varied procedure, 10 min premixing of $^{t}Bu_3P$, C_4F_9I and alkene.

reaction time [min]	area(vinylcyclohexane) [µV·s]	area(*n*-decane) [µV·s]	A(V)/A(D)[a]	m(V)[a] [mg]	conversion[a] [%]	m(V)/m(V_0)[a]	ln([V]/[V_0])[a]
20	12998	13773	0.944	53.4	34	0.66	-0.410
20	13803	14834	0.930	52.7	35	0.65	-0.424
20	18937	19641	0.964	54.6	32	0.68	-0.388
30	12199	14739	0.828	46.7	42	0.58	-0.544
30	13098	15764	0.831	46.9	42	0.58	-0.540
30	12603	15287	0.824	46.6	42	0.58	-0.548
40	13742	17735	0.775	43.7	46	0.54	-0.611
40	10479	14336	0.731	41.2	49	0.51	-0.670
40	14717	19571	0.752	42.4	47	0.53	-0.642
50	11826	17048	0.694	39.0	52	0.48	-0.724
50	9412	14276	0.659	37.0	54	0.46	-0.776
50	9995	15156	0.659	37.1	54	0.46	-0.776
60	8321	14001	0.594	33.3	59	0.41	-0.883
60	9206	15392	0.598	33.5	58	0.42	-0.876
60	9114	15267	0.597	33.5	58	0.42	-0.878

[a] Calculated values; V = vinylcyclohexane, D = *n*-decane.

Table 24: Basis for depicted graphs, varied procedure, 10 min premixing of $^{t}Bu_3P$, C_4F_9I and alkene.

Δt [min]	average conversion [%]	standard deviation [%]
20	33	1.21
30	42	0.23
40	47	1.57
50	53	1.42
60	58	0.14

7.11 GC-experiment, 62 min premixing of $^{t}Bu_3P$, $B(C_6F_5)_3$ and C_4F_9I

Analogous to Standard procedure A for GC experiments, a solution of $^{t}Bu_3P$ (**5**) (7.4 mg, 0.037 mmol, 5.0 mol%), $B(C_6F_5)_3$ (**3**) (18.6 mg, 0.363 mmol, 5.0 mol%) and nonafluoro-1-iodobutane (**2**) (125 µl, 0.726 mmol, 0.994 eq.) in CH_2Cl_2 (2.5 ml) was stirred for 62 min inside the glovebox. Vinylcyclohexane (**1**) (100 µl, 0.730 mmol, 1.00 eq.) was added.

Table 25: Varied procedure, 62 min premixing of $^{t}Bu_3P$, $B(C_6F_5)_3$ and C_4F_9I.

reaction time [min]	area(vinylcyclohexane) [µV·s]	area(*n*-decane) [µV·s]	A(V)/A(D)[a]	m(V)[a] [mg]	conversion[a] [%]	m(V)/m(V_0)[a]	ln([V]/[V_0])[a,b]
20	17206	13523	1.272	72.3	10	0.90	–
20	18466	14204	1.300	73.9	8	0.92	–
20	18917	14744	1.283	73.0	9	0.91	–
27	16049	13050	1.230	69.9	13	0.87	–
27	17178	13877	1.238	70.4	13	0.87	–
27	18167	14690	1.237	70.3	13	0.87	–
35	16877	14392	1.173	66.6	17	0.83	-0.190
35	20751	17227	1.205	68.4	15	0.85	-0.162
35	21488	17966	1.196	67.9	16	0.84	-0.169
45	13383	12794	1.046	59.3	26	0.74	-0.305
45	15209	14198	1.071	60.8	25	0.75	-0.281
45	15103	14251	1.060	60.1	25	0.75	-0.292
55	14656	14736	0.995	56.4	30	0.70	-0.357
55	15867	16034	0.990	56.1	30	0.70	-0.362
55	15772	15971	0.988	55.9	31	0.69	-0.364
65	12288	13306	0.923	52.3	35	0.65	-0.432
65	13273	14348	0.925	52.3	35	0.65	-0.430
65	13407	14512	0.924	52.3	35	0.65	-0.432

[a] Calculated values; V = vinylcyclohexane, D = *n*-decane. [b] Several data points were not used for further calculations, since they are not within the calibration range.

Table 26: Basis for depicted graphs, varied procedure, 62 min premixing of $^{t}Bu_3P$, $B(C_6F_5)_3$ and C_4F_9I.

Δt [min]	average conversion [%]	standard deviation [%]
20	9	1.00
27	13	0.31
35	16	1.18
45	25	0.90
55	30	0.26
65	35	0.06

8 NMR-experiments

Preface to NMR-experiments

At first we used trifluoromethylcyclohexane as an internal standard, but this seemed to result in an interference with our catalytic system. Hence, we were forced to perform this reaction without an internal standard, but used an external standard ($CFCl_3$ in C_6D_6) for signal referencing. We chose CH_2Cl_2 as the solvent after tests in CD_2Cl_2 due to a better comparability to our GC experiments and doubts regarding a constant quality of CD_2Cl_2.

Subsequent datasets show a first data point after 10 - 13 minutes. This time gap is caused by 1) a preparation inside the glovebox, resulting in a gap between addition $B(C_6F_5)_3$ (**3**) and introduction into the NMR 2) automated insertion into the NMR spectrometer (contrary to manually).

Standard procedure B

Inside the glovebox, $^tBu_3P$ (**5**) was dissolved in CH_2Cl_2 and transferred into a Young valve NMR tube, which was enwrapped in aluminium foil and equipped with $CFCl_3$ in C_6D_6 as an external standard. Under red light, vinylcyclohexane (**1**) followed by nonafluoro-1-iodobutane (**2**) was injected directly into the NMR tube. About one minute later, a solution of $B(C_6F_5)_3$ (**3**) in CH_2Cl_2 was added. Overall 0.90 ml CH_2Cl_2 were used. The tube was sealed with a Young valve and NMR-measurements were conducted.

For the kinetic analysis, ^{19}F-NMR-spectra (relaxation delay = 8 s) were analysed. Four signals, two of educt and product each, were used for the calculation of its substance amount fraction. The signal of the internal standard was set to an integral of 1.0.

8.1 NMR-experiment, standard procedure

$^{t}Bu_3P$ (**5**) (3.6 mg, 0.018 mmol, 10 mol%), vinylcyclohexane (**1**) (24.0 µl, 0.175 mmol, 1.00 eq.), nonafluoro-1-iodobutane (**2**) (30.0 µl, 0.174 mmol, 0.994 eq.) and $B(C_6F_5)_3$ (**3**) (9.0 mg, 0.018 mmol, 10 mol%) were reacted as described in Standard procedure B.

Table 27: Standard procedure, 1.0 equivalents of vinylcyclohexane.

shift [ppm]	0 (ES)	−62.3 (E)[a]	−124.9 (P)[b]	−125.6 (E)[a]	−126.2 (P)[b]	Δt [min]	χ(product)[c]	χ(educt)[c]	ln(χ(educt))[c]
	1	7.95	5.44	7.64	5.34	13	0.409	0.591	-0.526
	1	6.97	6.43	6.75	6.28	17	0.481	0.519	-0.656
	1	6.25	7.27	6.04	7.10	21	0.539	0.461	-0.774
	1	5.70	7.99	5.24	7.75	25	0.590	0.410	-0.891
	1	5.11	8.49	4.95	8.30	29	0.625	0.375	-0.982
integral	1	4.67	8.92	4.49	8.75	33	0.659	0.341	-1.075
	1	4.32	9.42	4.15	9.18	37	0.687	0.313	-1.162
	1	4.00	9.82	3.83	9.61	41	0.713	0.287	-1.247
	1	3.67	10.01	3.51	9.84	45	0.734	0.266	-1.326
	1	3.43	10.40	3.29	10.10	49	0.753	0.247	-1.399
	1	3.20	10.56	3.04	10.33	53	0.770	0.230	-1.470

[a] Educt signal C_4F_9I. [b] Product signal, $C_{12}H_{14}F_9I$. [c] Calculated values.

8.2 NMR-experiment, 2.0 eq. vinylcyclohexane

^{t}Bu$_3$P (**5**) (3.6 mg, 0.018 mmol, 10 mol%), vinylcyclohexane (**1**) (38.6 mg, 0.351 mmol, 2.01 eq.), nonafluoro-1-iodobutane (**2**) (30.0 µl, 0.174 mmol, 1.00 eq.) and B(C_6F_5)$_3$ (**3**) (9.0 mg, 0.018 mmol, 10 mol%) were reacted as described in Standard procedure B.

Table 28: Standard procedure, 2.0 equivalents of vinylcyclohexane.

shift [ppm]	0 (ES)	−62.3 (E)[a]	−124.9 (P)[b]	−125.6 (E)[a]	−126.2 (P)[b]	Δt [min]	χ(product)[c]	χ(educt)[c]	ln(χ(educt))[c]
integral	1	14.29	5.93	14.54	5.75	11	0.288	0.712	-0.340
	1	13.51	7.69	13.58	7.54	15	0.360	0.640	-0.446
	1	11.84	8.76	11.95	8.57	19	0.421	0.579	-0.547
	1	11.05	10.20	11.31	9.99	23	0.475	0.525	-0.643
	1	10.12	11.26	10.33	11.15	28	0.523	0.477	-0.740
	1	9.29	12.26	9.60	11.94	32	0.562	0.438	-0.825
	1	8.55	12.94	8.87	12.61	36	0.595	0.405	-0.903
	1	8.08	13.91	8.39	13.55	40	0.625	0.375	-0.981
	1	7.18	13.90	7.51	13.53	44	0.651	0.349	-1.053
	1	7.04	15.11	7.38	14.74	48	0.674	0.326	-1.122
	1	6.61	15.65	6.95	15.23	52	0.695	0.305	-1.187
	1	6.25	16.07	6.42	15.55	56	0.714	0.286	-1.252

[a] Educt signal, C_4F_9I. [b] Product signal, $C_{12}H_{14}F_9I$. [c] Calculated values.

8.3 NMR-experiment, 78 min premixing of $^{t}Bu_3P$ and $B(C_6F_5)_3$

Analogous to Standard procedure B, $^{t}Bu_3P$ (**5**) (3.7 mg, 0.018 mmol, 10 mol%) and $B(C_6F_5)_3$ (**3**) (9.0 mg, 0.018 mmol, 10 mol%) were weighed into a glass vial, dissolved in CH_2Cl_2 (0.80 ml) and transferred into an NMR tube. After 78 min vinylcyclohexane (**1**) (24.0 µl, 0.175 mmol, 1.00 eq.) as well as nonafluoro-1-iodobutane (**2**) (30.0 µl, 0.174 mmol, 0.994 eq.) were injected, it was rinsed with CH_2Cl_2 (0.10 ml) and NMR measurements were conducted.

Table 29: Varied procedure, 78 min premixing of $^{t}Bu_3P$ and $B(C_6F_5)_3$.

shift [ppm]	0 (ES)	−62.3 (E)[a]	−124.9 (P)[b]	−125.6 (E)[a]	−126.2 (P)[b]	Δt [min]	χ(product)[c]	χ(educt)[c]	ln(χ(educt))[c]
integral	1	9.14	4.58	8.91	4.56	11	0.336	0.664	-0.410
	1	7.74	5.92	7.49	5.75	17	0.434	0.566	-0.569
	1	6.79	7.03	6.59	6.89	22	0.510	0.490	-0.713
	1	6.06	7.92	5.88	7.79	27	0.568	0.432	-0.840
	1	5.41	8.63	5.24	8.41	32	0.615	0.385	-0.956
	1	4.91	9.24	4.73	9.02	37	0.654	0.346	-1.063
	1	4.50	9.81	4.32	9.57	43	0.687	0.313	-1.162
	1	4.07	10.05	3.90	9.80	48	0.714	0.286	-1.250
	1	3.73	10.43	3.57	10.15	53	0.738	0.262	-1.340

[a] Educt signal, C_4F_9I. [b] Product signal, $C_{12}H_{14}F_9I$. [c] Calculated values.

8.4 NMR-experiment, 25 h premixing of $^{t}Bu_3P$ and $B(C_6F_5)_3$.

Analogous to Standard procedure B, $^{t}Bu_3P$ (**5**) (3.6 mg, 0.018 mmol, 10 mol%) and $B(C_6F_5)_3$ (**3**) (8.9 mg, 0.017 mmol, 9.9 mol%) were weighed into a glass vial, dissolved in CD_2Cl_2 (0.45 ml) and transferred into an NMR tube. The NMR tube was sealed with a Young valve and an NMR measurement was conducted. After 25 h nonafluoro-1-iodobutane (**2**) (30.0 µl, 0.174 mmol, 0.994 eq.) as well as vinylcyclohexane (**1**) (24.0 µl, 0.175 mmol, 1.00 eq.) were injected, it was rinsed with CD_2Cl_2 (0.45 ml) and NMR measurements were conducted.

Table 30: Varied procedure, 25 h premixing of $^{t}Bu_3P$ and $B(C_6F_5)_3$.

shift [ppm]	−62.3 (E)[a]	−124.9 (P)[b]	−125.6 (E)[a]	−126.2 (P)[b]	Δt [min]	χ(product)[c]	χ(educt)[c]	ln(χ(educt))[c]
	6.00	0.41	5.77	0.38	15	0.063	0.937	-0.065
	6.00	0.52	5.81	0.52	19	0.081	0.919	-0.084
	6.00	0.65	5.81	0.63	23	0.098	0.902	-0.103
integral	6.00	0.75	5.81	0.78	27	0.115	0.885	-0.122
	6.00	3.11	5.79	3.07	123	0.344	0.656	-0.421
	6.00	5.38	5.78	5.15	229	0.472	0.528	-0.639
	6.00	7.21	5.76	6.93	324	0.546	0.454	-0.790

[a] Educt signal, C_4F_9I. [b] Product signal, $C_{12}H_{14}F_9I$. [c] Calculated values.

8.5 NMR-experiment, 60 min premixing of $^{t}Bu_3P$, $B(C_6F_5)_3$ and C_4F_9I

Analogous to Standard procedure B, $^{t}Bu_3P$ (**5**) (3.6 mg, 0.018 mmol, 10 mol%) and $B(C_6F_5)_3$ (**3**) (8.9 mg, 0.017 mmol, 9.9 mol%) were weighed into a glass vial, dissolved in CH_2Cl_2 (0.80 ml) and transferred into an NMR tube. Nonafluoro-1-iodobutane (**2**) (30.0 µl, 0.174 mmol, 0.994 eq.) was injected directly into the NMR tube and the tube was sealed with a Young valve. After 60 min, vinylcyclohexane (**1**) (24.0 µl, 0.175 mmol, 1.00 eq.) was injected, it was rinsed with CH_2Cl_2 (0.10 ml) and NMR measurements were conducted.

Table 31: Varied procedure, 60 min premixing of $^{t}Bu_3P$, $B(C_6F_5)_3$ and C_4F_9I.

shift [ppm]	0 (ES)	−62.3 (E)[a]	−124.9 (P)[b]	−125.6 (E)[a]	−126.2 (P)[b]	Δt [min]	χ(product)[c]	χ(educt)[c]	ln(χ(educt))[c]
integral	1	14.66	3.54	14.26	3.49	13	0.196	0.804	-0.218
	1	13.47	4.98	13.11	4.92	16	0.271	0.729	-0.317
	1	12.33	6.42	12.02	6.23	20	0.342	0.658	-0.418
	1	11.10	7.46	10.82	7.36	24	0.403	0.597	-0.516
	1	10.27	8.64	9.95	8.46	29	0.458	0.542	-0.613
	1	9.39	9.46	9.08	9.30	33	0.504	0.496	-0.701
	1	8.67	10.28	8.40	10.07	36	0.544	0.456	-0.785
	1	8.15	11.22	7.89	10.90	40	0.580	0.420	-0.867

[a] Educt signal, C_4F_9I. [b] Product signal, $C_{12}H_{14}F_9I$. [c] Calculated values.

Standard procedure C

Inside the glovebox, $^{t}Bu_3P$ (**5**) was dissolved in CH_2Cl_2 (0.80 ml) and one half (0.40 ml) of this solution was transferred into an NMR tube, which was enwrapped in aluminium foil and equipped with $CFCl_3$ in C_6D_6 as an external standard. Under red light, nonafluoro-1-iodobutane (**2**) was injected directly into the NMR tube. About one minute later, a solution of $B(C_6F_5)_3$ (**3**) mixed with 1-undecene (**18**) in CH_2Cl_2 was added. Overall 0.90 ml CH_2Cl_2 were injected into the NMR tube. The tube was sealed with a Young valve and NMR-measurements were conducted.

For the kinetic analysis, ^{19}F-NMR-spectra (relaxation delay = 8 s) were analysed. Four signals, two of educt and product each, were used for the calculation of its substance amount fraction.

8.6 NMR-experiment, 1.1 eq. 1-undecene

$^{t}Bu_3P$ (**5**) (1.8 mg, 0.0089 mmol, 5.1 mol%), 1-undecene (**18**) (29.8 mg, 0.193 mmol, 1.11 eq.), nonafluoro-1-iodobutane (**2**) (30.0 µl, 0.174 mmol, 1.00 eq.) and $B(C_6F_5)_3$ (**3**) (4.5 mg, 0.0088 mmol, 5.1 mol%) were reacted as described in Standard procedure C.

Table 32: Standard procedure, 1.1 equivalents of 1-undecene.

shift [ppm]	0 (ES)	−62.3 (E)[a]	−124.1 (P)[b]	−125.7 (E)[a]	−126.4 (P)[b]	Δt [min]	χ(product)[c]	χ(educt)[c]	ln(χ(educt))[c]
	1	188.31	52.21	183.28	53.48	11	0.221	0.779	-0.250
	1	162.51	60.84	157.21	59.46	15	0.273	0.727	-0.319
	1	154.76	73.44	149.61	74.23	18	0.327	0.673	-0.396
	1	141.75	82.84	137.51	82.17	22	0.371	0.629	-0.464
	1	139.04	96.15	134.54	94.38	26	0.411	0.589	-0.529
integral	1	127.75	101.30	123.59	100.37	30	0.445	0.555	-0.589
	1	114.06	103.07	109.76	100.35	34	0.476	0.524	-0.647
	1	119.14	120.53	115.29	117.99	38	0.504	0.496	-0.702
	1	109.27	120.76	105.03	118.13	42	0.527	0.473	-0.749
	1	104.54	126.68	98.91	125.53	46	0.554	0.446	-0.806
	1	97.25	129.27	93.95	127.74	50	0.573	0.427	-0.852

[a] Educt signal, C_4F_9I. [b] Product signal, $C_{12}H_{14}F_9I$. [c] Calculated values.

8.7 NMR-experiment, 2.0 eq. 1-undecene

$^{t}Bu_3P$ (**5**) (1.8 mg, 0.0086 mmol, 5.0 mol%), 1-undecene (**18**) (54.1 mg, 0.351 mmol, 2.02 eq.), nonafluoro-1-iodobutane (**2**) (30.0 µl, 0.174 mmol, 1.00 eq.) and $B(C_6F_5)_3$ (**3**) (4.5 mg, 0.0088 mmol, 5.1 mol%) were reacted as described in Standard procedure C.

Table 33: Standard procedure, 2.0 equivalents of 1-undecene.

shift [ppm]	0 (ES)	−62.3 (E)[a]	−124.1 (P)[b]	−125.7 (E)[a]	−126.4 (P)[b]	Δt [min]	χ(product)[c]	χ(educt)[c]	ln(χ(educt))[c]
integral	1	11.87	1.82	11.48	1.80	13	0.134	0.866	-0.144
	1	10.44	2.28	10.11	2.29	17	0.182	0.818	-0.201
	1	10.29	3.00	9.92	2.84	21	0.224	0.776	-0.254
	1	9.77	3.57	9.48	3.61	25	0.272	0.728	-0.317
	1	9.05	4.03	8.74	3.94	30	0.309	0.691	-0.370
	1	8.74	4.48	8.45	4.49	34	0.343	0.657	-0.420
	1	8.24	4.92	7.97	4.66	38	0.371	0.629	-0.464
	1	8.18	5.38	7.92	5.32	42	0.399	0.601	-0.510
	1	7.67	5.66	7.44	5.57	47	0.426	0.574	-0.556
	1	7.46	6.10	7.21	5.99	51	0.452	0.548	-0.601

[a] Educt signal, C_4F_9I. [b] Product signal, $C_{12}H_{14}F_9I$. [c] Calculated values.

8.8 NMR-experiment, 1.1 eq. 1-undecene, 15 mol% $^{t}Bu_3P$

Analogous to Standard procedure C, $^{t}Bu_3P$ (**5**) (5.3 mg, 0.026 mmol, 15 mol%) was dissolved in CH_2Cl_2 (0.50 ml) and transferred into a pointed bottom flask. $B(C_6F_5)_3$ (**3**) (4.5 mg, 0.0088 mmol, 5.1 mol%) and 1-undecene (**18**) (30.1 mg, 0.195 mmol, 1.12 eq.) were dissolved in CH_2Cl_2 and transferred into an amber glass NMR tube. Nonafluoro-1-iodobutane (**2**) (30.0 µl, 0.174 mmol, 1.00 eq.) was added. Outside the glovebox, the $^{t}Bu_3P$ solution was added inertly under argon. NMR measurements were conducted.

Table 34: Varied procedure, 1.1 eq. 1-undecene, 15 mol% $^{t}Bu_3P$.

shift [ppm]	0 (ES)	−62.3 (E)[a]	−124.1 (P)[b]	−125.7 (E)[a]	−126.4 (P)[b]	Δt [min]	χ(product)[c]	χ(educt)[c]	ln(χ(educt))[c]
	1	144.67	52.70	148.79	52.78	7	0.264	0.736	-0.307
	1	142.17	77.68	146.52	76.44	11	0.348	0.652	-0.428
	1	121.82	88.10	127.28	86.60	15	0.412	0.588	-0.531
	1	112.52	102.89	117.42	100.67	19	0.470	0.530	-0.634
	1	104.25	114.05	109.79	110.96	23	0.512	0.488	-0.718
	1	95.58	122.86	102.43	121.85	27	0.553	0.447	-0.805
integral	1	87.31	128.89	93.02	126.21	31	0.586	0.414	-0.882
	1	77.23	130.81	84.47	128.35	35	0.616	0.384	-0.957
	1	77.34	147.11	84.90	144.21	39	0.642	0.358	-1.028
	1	70.17	147.27	77.14	145.03	43	0.665	0.335	-1.093
	1	69.22	160.21	76.47	156.70	47	0.685	0.315	-1.155
	1	61.59	157.65	68.42	153.58	51	0.705	0.295	-1.222
	1	61.53	169.36	69.04	167.42	55	0.721	0.279	-1.275

[a] Educt signal, C_4F_9I. [b] Product signal, $C_{12}H_{14}F_9I$. [c] Calculated values.

Spectroscopic data for iodoperfluoroalkylation product of 1-undecene (1,1,1,2,2,3,3,4,4-nonafluoro-6-iodopentadecane) (**26**) are as follows:

^{1}H-NMR (300 MHz, C_6D_6) δ [ppm] 4.07 - 3.91 (m, 1H), 2.76 - 2.48 (m, 1H), 2.52 - 2.25 (m, 1H), 1.53 - 1.00 (m, 17H), 0.99 - 0.87 (m, 2H).**^{19}F-NMR** (282 MHz, C_6D_6) δ [ppm] −81.2 (tt, J = 9.6, 3.5 Hz), −111.4 - −112.7 (m), −113.8 - −115.0 (m), −124.3 - −124.6 (m), −125.8 - −126.0 (m). **^{13}C-NMR** (75 MHz, C_6D_6) δ [ppm] 41.6 (−$H_2C$$CF_2R_F$, t, $^{2}J_{CF}$ = 20.8 Hz), 40.51, 40.49, 32.31, 29.93, 29.81, 29.73, 28.81, 23.13, 20.34, 14.37. **IR** (film on NaCl), ṽ [cm^{-1}] 2927, 2857, 1467, 1351, 1235, 1136, 1016, 880, 724, 553.

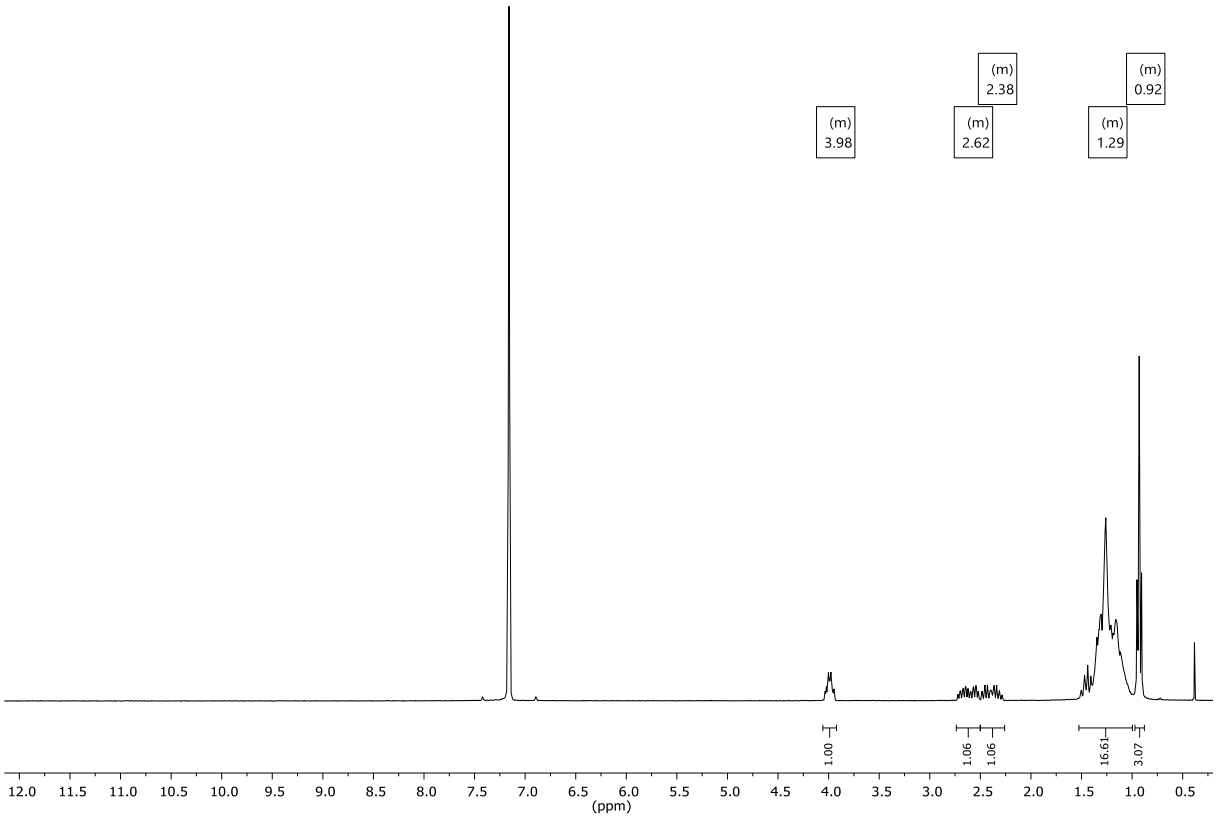

NMR-spectrum 52: ^{1}H (300 MHz, C_6D_6) of 1,1,1,2,2,3,3,4,4-nonafluoro-6-iodopentadecane.

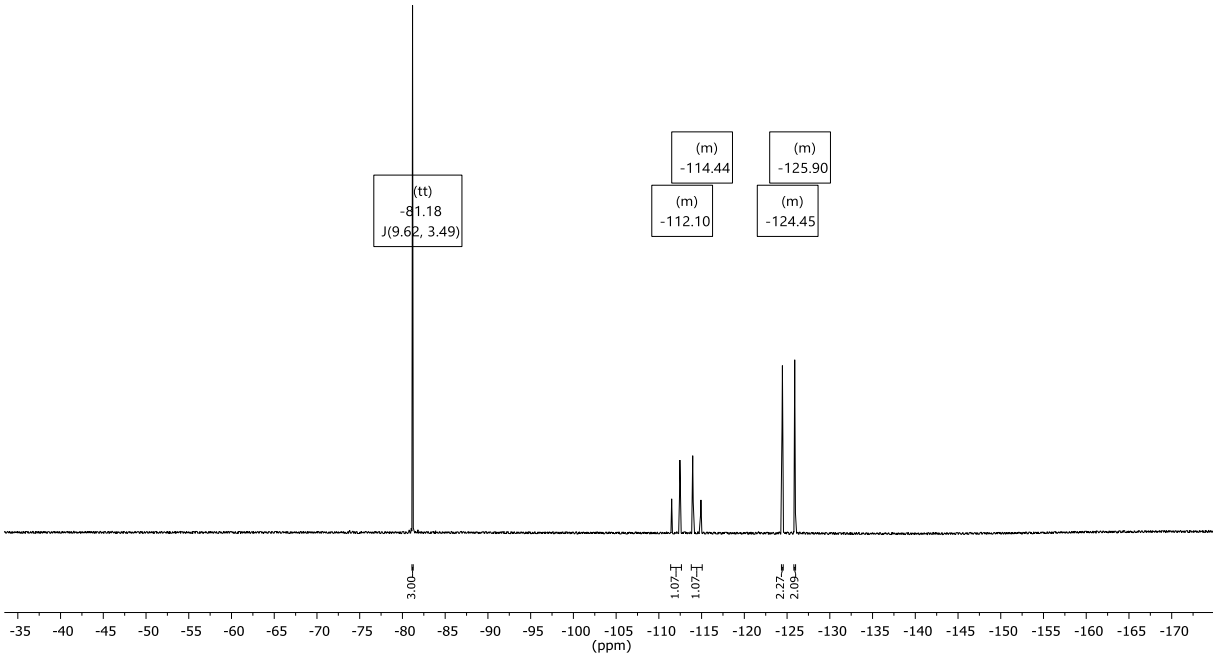

NMR-spectrum 53: ^{19}F (282 MHz, C_6D_6) of 1,1,1,2,2,3,3,4,4-nonafluoro-6-iodopentadecane.

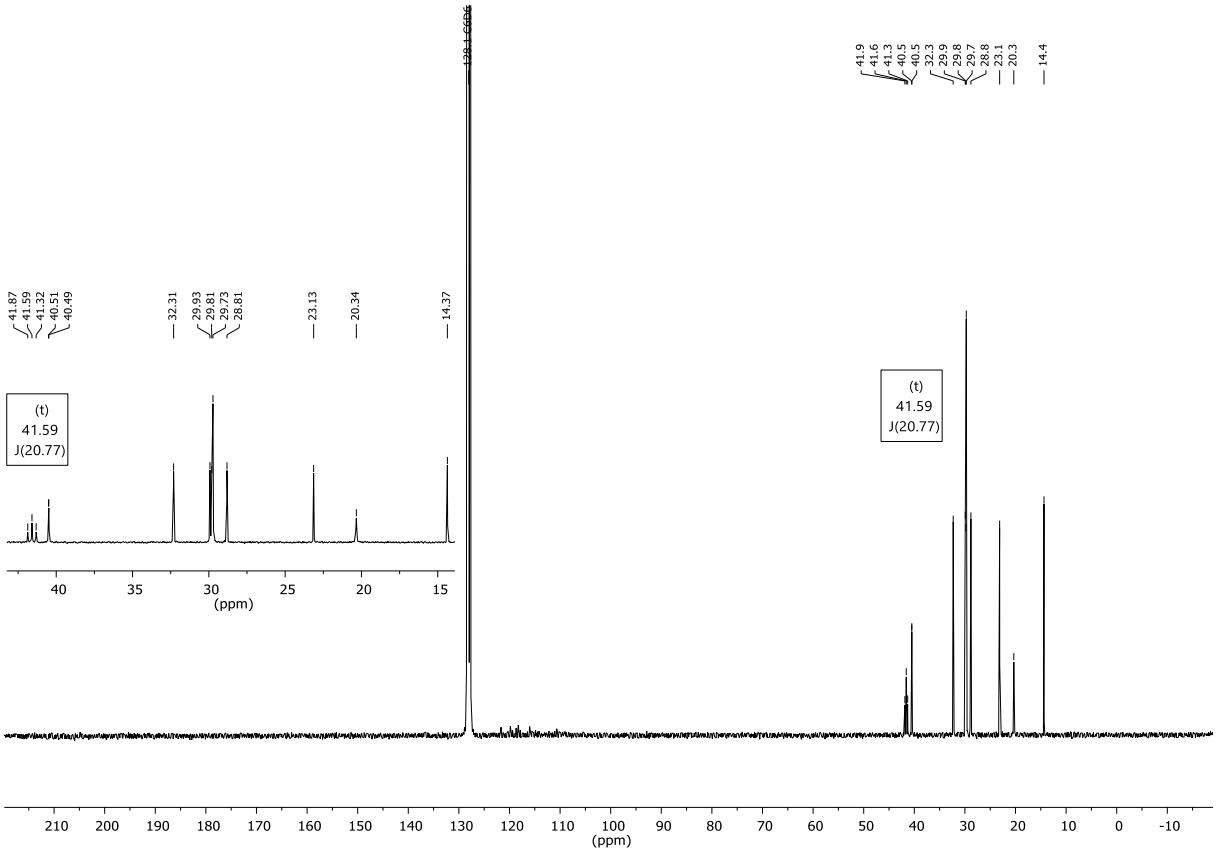

NMR-spectrum 54: ^{13}C (75 MHz, C_6D_6) of 1,1,1,2,2,3,3,4,4-nonafluoro-6-iodopentadecane.

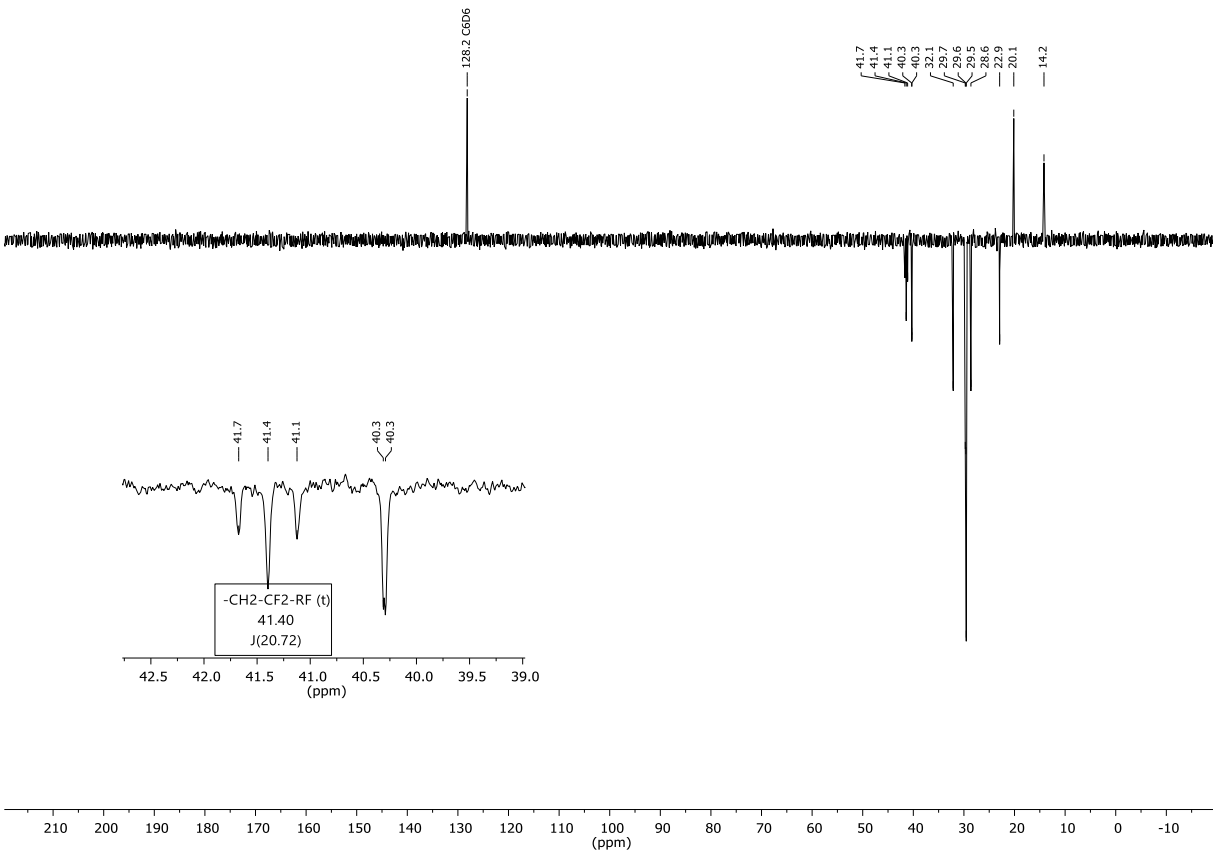

NMR-spectrum 55: DEPT (75 MHz, C_6D_6) of 1,1,1,2,2,3,3,4,4-nonafluoro-6-iodopentadecane.

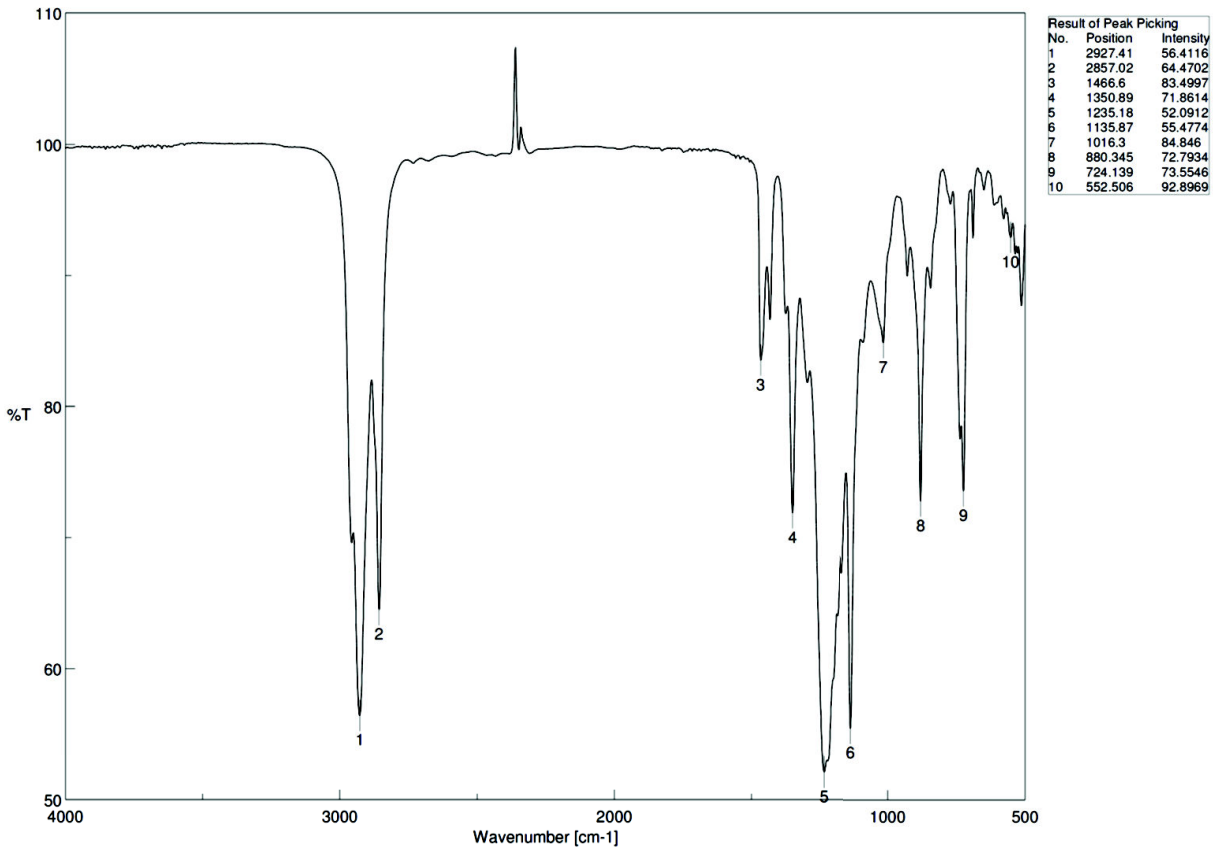

IR-spectrum (film on NaCl) 2: 1,1,1,2,2,3,3,4,4-nonafluoro-6-iodopentadecane.

8.9 Calculations

For our calculations we used the presented values

To examine zeroth order behaviour, we used the corresponding integrated rate law.

$$[A]_t=[A]_0 - k\cdot t \text{ or } [A]_t - [A]_0 = - k\cdot t$$

To examine first order behaviour, we used the corresponding integrated rate law.

$$\frac{[A]_t}{[A]_0} = e^{-k\cdot t} \text{ or } \ln\left(\frac{[A]_t}{[A]_0}\right) = - k\cdot t$$

To examine second order behaviour, we used the corresponding integrated rate law.

$$\frac{1}{[A]_0} - \frac{1}{[A]_t} = - k\cdot t$$

Throughout GC experiments we measured the conversion of vinylcyclohexane, hence we had to extrapolate from the values calculated for vinylcyclohexane to nonafluoro-1-iodobutane concentrations. For this purpose, the consumed amount of substance of vinylcyclohexane was offset with the initial amount of nonafluoro-1-iodobutane. For a better comparability, similar time spans should be incorporated.

8.9.1 GC experiment, different fits for standard curve

Table 35: Calculated values for the depicted fits.

reaction time [min]	$[C_4F_9I]_0$ [mol/l]	$[C_4F_9I]$ [mol/l]	$[C_4F_9I]-[C_4F_9I]_0$ [mol/l]	$\ln([C_4F_9I]/[C_4F_9I]_0)$	$1/[C_4F_9I]_0-1/[C_4F_9I]$ [l/mol]
20	0.25893	0.17201	-0.08692	-0.40901	-1.95156
20	0.25893	0.17139	-0.08754	-0.41261	-1.97256
20	0.25893	0.16998	-0.08895	-0.42086	-2.02089
30	0.25893	0.15394	-0.10499	-0.52	-2.63399
30	0.25893	0.14823	-0.1107	-0.55777	-2.88403
30	0.25893	0.1478	-0.11113	-0.56072	-2.90399
40	0.25893	0.1325	-0.12643	-0.66995	-3.68488
40	0.25893	0.13231	-0.12662	-0.6714	-3.69588
40	0.25893	0.13196	-0.12698	-0.6741	-3.71627
50	0.25893	0.11909	-0.13984	-0.77667	-4.53489
50	0.25893	0.11618	-0.14275	-0.80144	-4.74546
50	0.25893	0.11735	-0.14158	-0.79143	-4.65974
60	0.25893	0.10469	-0.15424	-0.90558	-5.6902
60	0.25893	0.10431	-0.15462	-0.90919	-5.72476
60	0.25893	0.10627	-0.15267	-0.89063	-5.5484

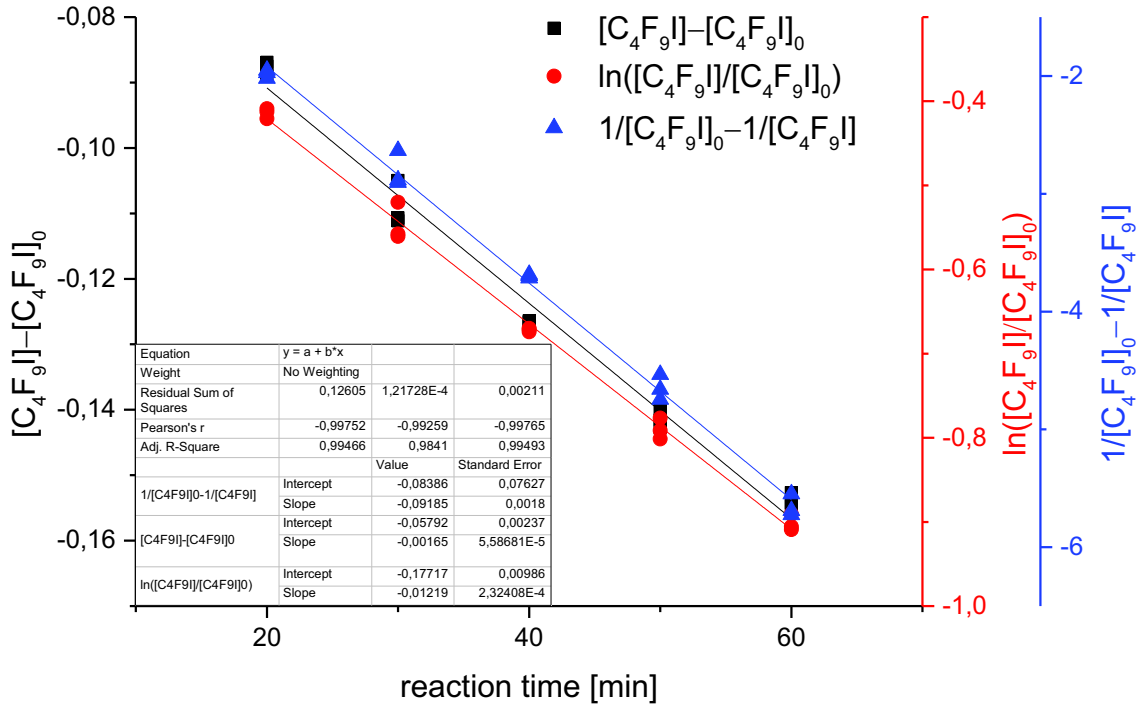

Figure 4: GC experiment, zeroth, first and second order fit for standard curve.

8.9.2 GC-experiments, variation of C_4F_9I

Table 36: Calculated values for a zeroth, first and second order fit.

reaction time [min]	$[C_4F_9I]_0$ [mol/l]	$[C_4F_9I]$ [mol/l]	$[C_4F_9I]-[C_4F_9I]_0$ [mol/l]	$\ln([C_4F_9I]/[C_4F_9I]_0)$	$1/[C_4F_9I]_0-1/[C_4F_9I]$ [l/mol]
1.0 eq. C_4F_9I					
20	0.25893	0.17201	-0.08692	-0.40901	-1.95156
20	0.25893	0.17139	-0.08754	-0.41261	-1.97256
20	0.25893	0.16998	-0.08895	-0.42086	-2.02089
30	0.25893	0.15394	-0.10499	-0.52	-2.63399
30	0.25893	0.14823	-0.1107	-0.55777	-2.88403
30	0.25893	0.1478	-0.11113	-0.56072	-2.90399
40	0.25893	0.1325	-0.12643	-0.66995	-3.68488
40	0.25893	0.13231	-0.12662	-0.6714	-3.69588
40	0.25893	0.13196	-0.12698	-0.6741	-3.71627
50	0.25893	0.11909	-0.13984	-0.77667	-4.53489
50	0.25893	0.11618	-0.14275	-0.80144	-4.74546
50	0.25893	0.11735	-0.14158	-0.79143	-4.65974
60	0.25893	0.10469	-0.15424	-0.90558	-5.6902
60	0.25893	0.10431	-0.15462	-0.90919	-5.72476
60	0.25893	0.10627	-0.15267	-0.89063	-5.5484
1.5 eq. C_4F_9I					
20	0.38466	0.26067	-0.12399	-0.38911	-1.23659
20	0.38466	0.26013	-0.12453	-0.39118	-1.24454
20	0.38466	0.25744	-0.12722	-0.40158	-1.28474
25	0.38466	0.24377	-0.14089	-0.45612	-1.50247
25	0.38466	0.24281	-0.14185	-0.46009	-1.51876
25	0.38466	0.24236	-0.1423	-0.46194	-1.52642
30	0.38466	0.23082	-0.15385	-0.51074	-1.73276
30	0.38466	0.23011	-0.15455	-0.51379	-1.746
30	0.38466	0.22873	-0.15593	-0.51981	-1.77223
40	0.38466	0.20635	-0.17832	-0.62281	-2.24654
40	0.38466	0.20591	-0.17876	-0.62495	-2.2569
40	0.38466	0.2062	-0.17846	-0.62351	-2.24992
50	0.38466	0.18834	-0.19632	-0.71413	-2.70991
50	0.38466	0.18821	-0.19645	-0.71479	-2.71342
50	0.38466	0.18787	-0.19679	-0.71659	-2.72302
2.0 eq. C_4F_9I					
15	0.49577	0.36741	-0.12836	-0.29963	-0.70469
15	0.49577	0.37341	-0.12236	-0.28344	-0.66096
15	0.49577	0.36581	-0.12996	-0.30401	-0.71662
20	0.49577	0.34643	-0.14934	-0.35843	-0.86953
20	0.49577	0.34703	-0.14874	-0.3567	-0.86452
20	0.49577	0.34672	-0.14905	-0.3576	-0.86711
25	0.49577	0.32746	-0.16831	-0.41473	-1.0367
25	0.49577	0.32719	-0.16858	-0.41557	-1.03927
25	0.49577	0.32719	-0.16858	-0.41558	-1.03929
30	0.49577	0.31042	-0.18535	-0.46818	-1.20436
30	0.49577	0.31285	-0.18292	-0.46039	-1.17937
30	0.49577	0.30918	-0.18659	-0.47219	-1.21732
40	0.49577	0.2852	-0.21057	-0.55292	-1.48924
40	0.49577	0.28446	-0.21131	-0.55553	-1.49841
40	0.49577	0.28497	-0.2108	-0.55372	-1.49204

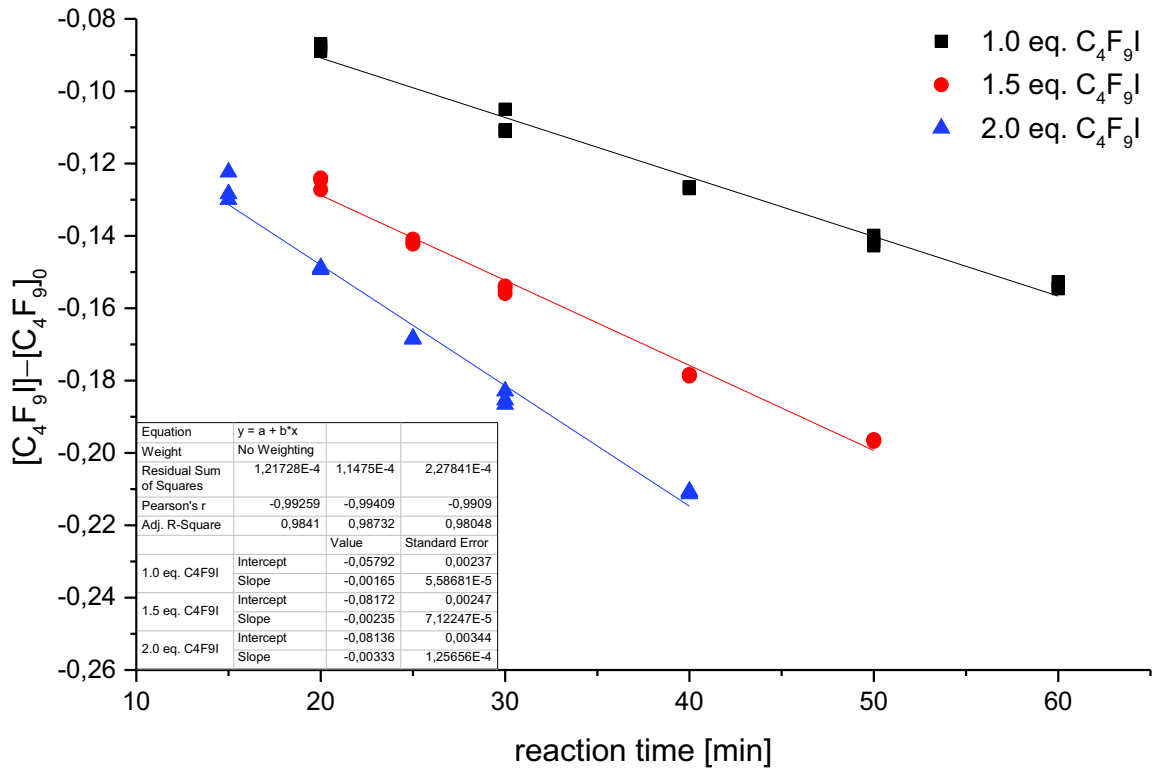

Equation	y = a + b*x		
Weight	No Weighting		
Residual Sum of Squares	1,21728E-4	1,1475E-4	2,27841E-4
Pearson's r	-0,99259	-0,99409	-0,9909
Adj. R-Square	0,9841	0,98732	0,98048
		Value	Standard Error
1.0 eq. C4F9I	Intercept	-0,05792	0,00237
	Slope	-0,00165	5,58681E-5
1.5 eq. C4F9I	Intercept	-0,08172	0,00247
	Slope	-0,00235	7,12247E-5
2.0 eq. C4F9I	Intercept	-0,08136	0,00344
	Slope	-0,00333	1,25656E-4

Figure 5: GC experiment, zeroth order fit for a variation of C_4F_9I.

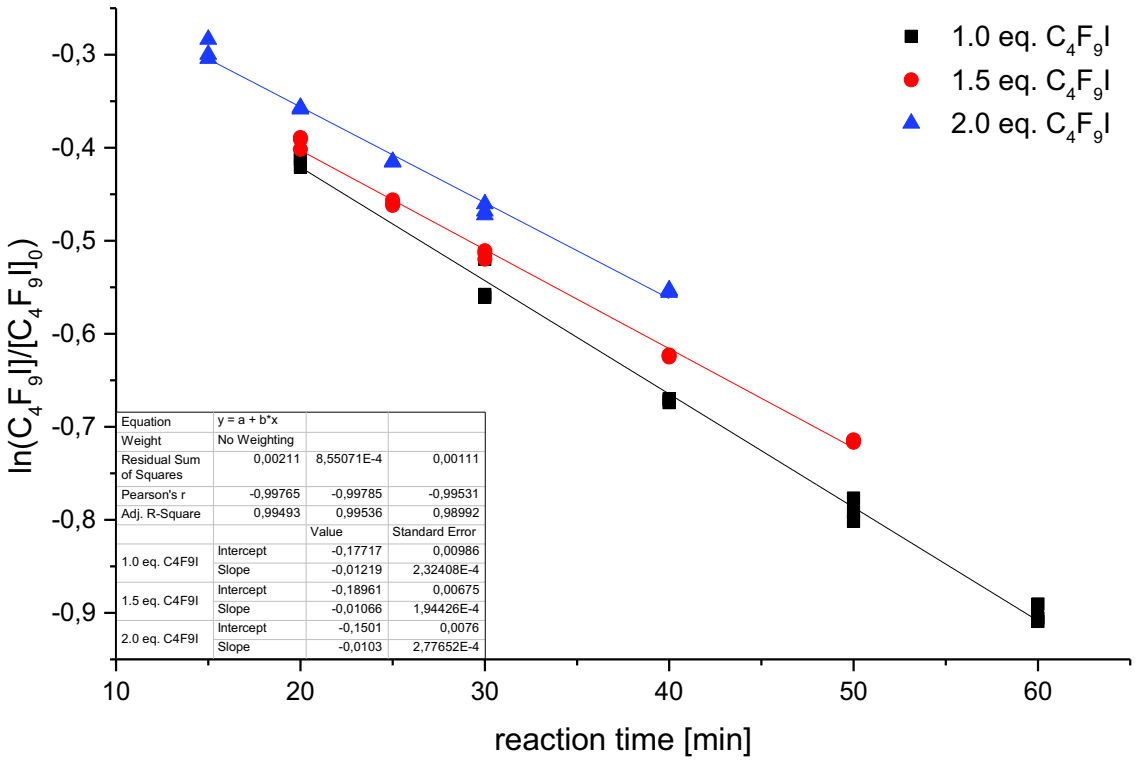

Equation	y = a + b*x		
Weight	No Weighting		
Residual Sum of Squares	0,00211	8,55071E-4	0,00111
Pearson's r	-0,99765	-0,99785	-0,99531
Adj. R-Square	0,99493	0,99536	0,98992
		Value	Standard Error
1.0 eq. C4F9I	Intercept	-0,17717	0,00986
	Slope	-0,01219	2,32408E-4
1.5 eq. C4F9I	Intercept	-0,18961	0,00675
	Slope	-0,01066	1,94426E-4
2.0 eq. C4F9I	Intercept	-0,1501	0,0076
	Slope	-0,0103	2,77652E-4

Figure 6: GC experiment, first order fit for a variation of C_4F_9I.

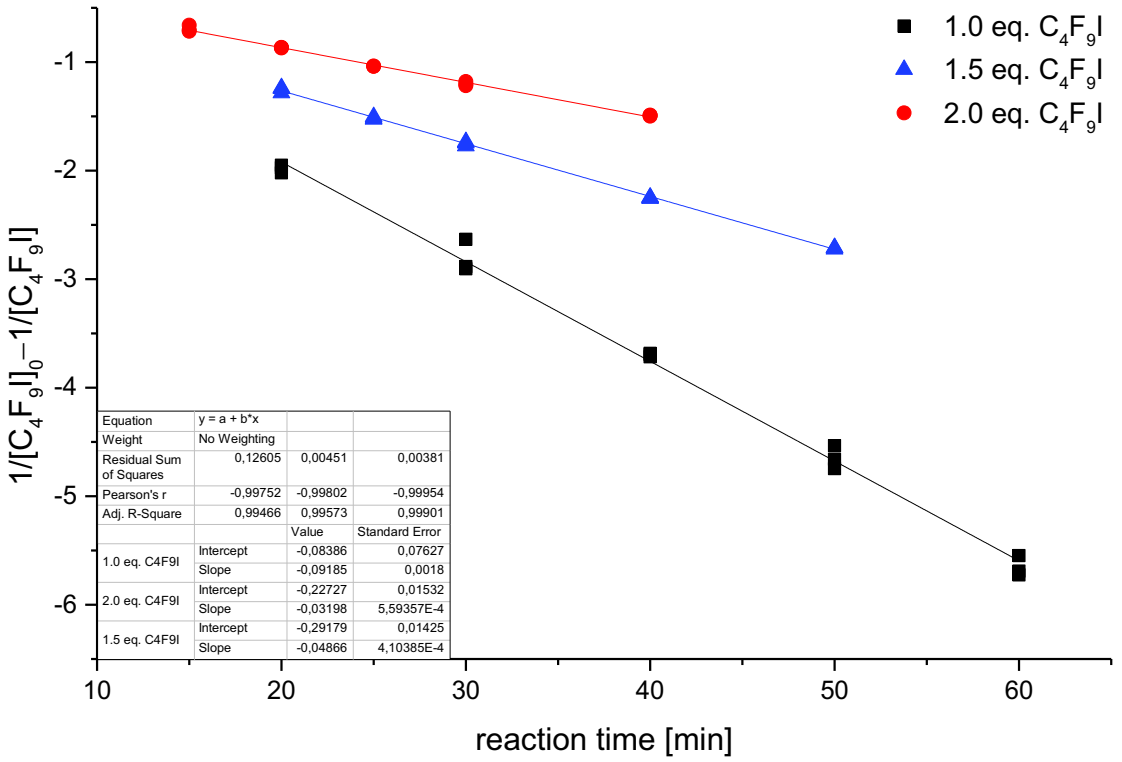

Equation	y = a + b*x		
Weight	No Weighting		
Residual Sum of Squares	0,12605	0,00451	0,00381
Pearson's r	-0,99752	-0,99802	-0,99954
Adj. R-Square	0,99466	0,99573	0,99901
		Value	Standard Error
1.0 eq. C4F9I	Intercept	-0,08386	0,07627
	Slope	-0,09185	0,0018
2.0 eq. C4F9I	Intercept	-0,22727	0,01532
	Slope	-0,03198	5,59357E-4
1.5 eq. C4F9I	Intercept	-0,29179	0,01425
	Slope	-0,04866	4,10385E-4

Figure 7: GC experiment, second order fit for a variation of C_4F_9I.

8.9.3 GC-experiments, variation of $^tBu_3P$

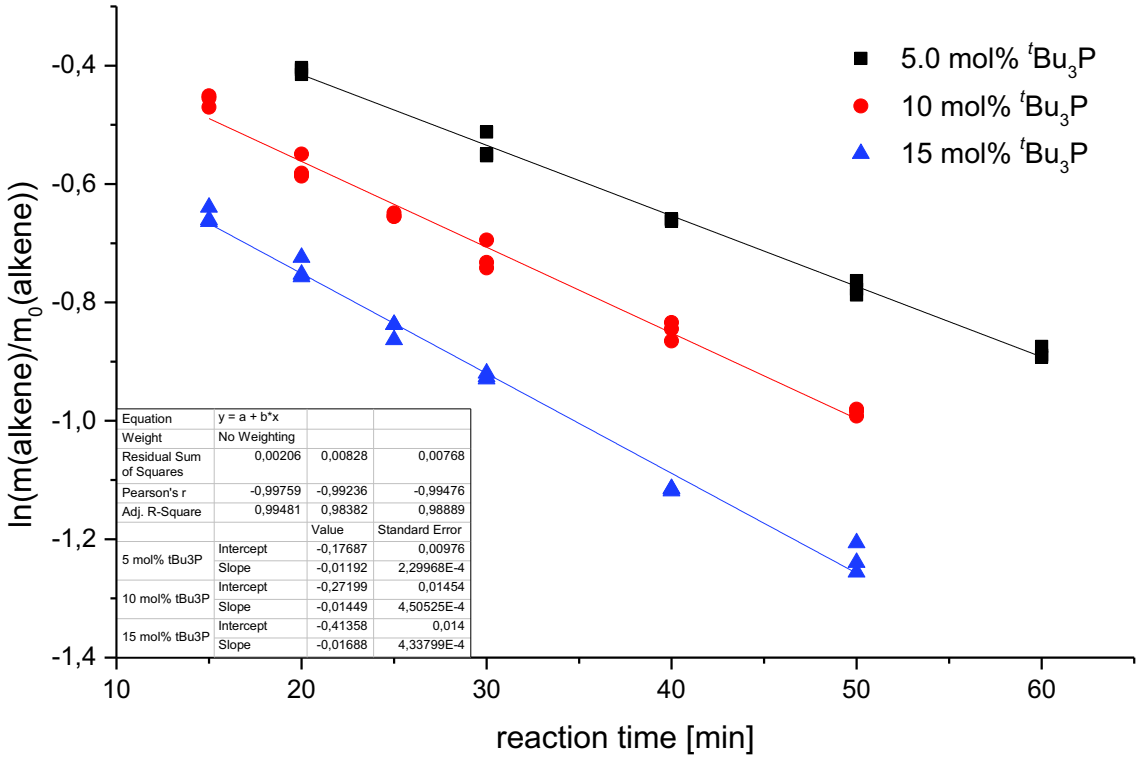

Equation	y = a + b*x		
Weight	No Weighting		
Residual Sum of Squares	0,00206	0,00828	0,00768
Pearson's r	-0,99759	-0,99236	-0,99476
Adj. R-Square	0,99481	0,98382	0,98889
		Value	Standard Error
5 mol% tBu3P	Intercept	-0,17687	0,00976
	Slope	-0,01192	2,29968E-4
10 mol% tBu3P	Intercept	-0,27199	0,01454
	Slope	-0,01449	4,50525E-4
15 mol% tBu3P	Intercept	-0,41358	0,014
	Slope	-0,01688	4,33799E-4

Figure 8: GC experiment, first order fit for a variation of $^tBu_3P$.

8.9.4 GC-experiments, variation of $B(C_6F_5)_3$

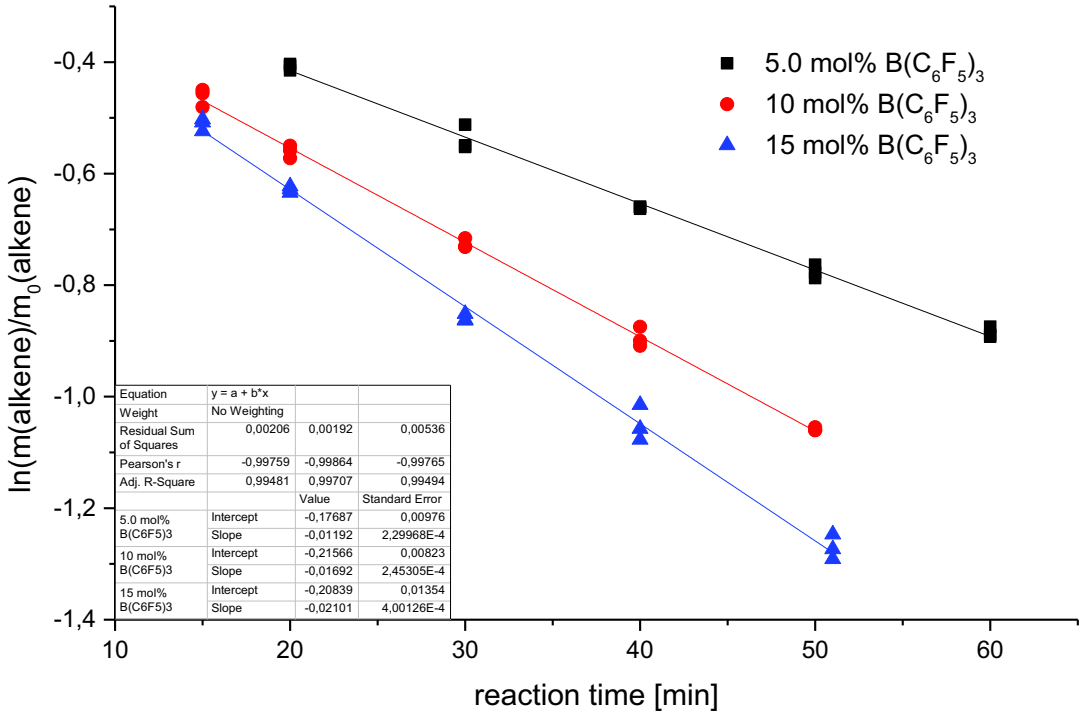

Equation	y = a + b*x		
Weight	No Weighting		
Residual Sum of Squares	0,00206	0,00192	0,00536
Pearson's r	-0,99759	-0,99864	-0,99765
Adj. R-Square	0,99481	0,99707	0,99494
		Value	Standard Error
5.0 mol% B(C6F5)3	Intercept	-0,17687	0,00976
	Slope	-0,01192	2,29968E-4
10 mol% B(C6F5)3	Intercept	-0,21566	0,00823
	Slope	-0,01692	2,45305E-4
15 mol% B(C6F5)3	Intercept	-0,20839	0,01354
	Slope	-0,02101	4,00126E-4

Figure 9: GC experiment, first order fit for a variation of $B(C_6F_5)_3$.

8.9.5 GC-experiments, varied procedures

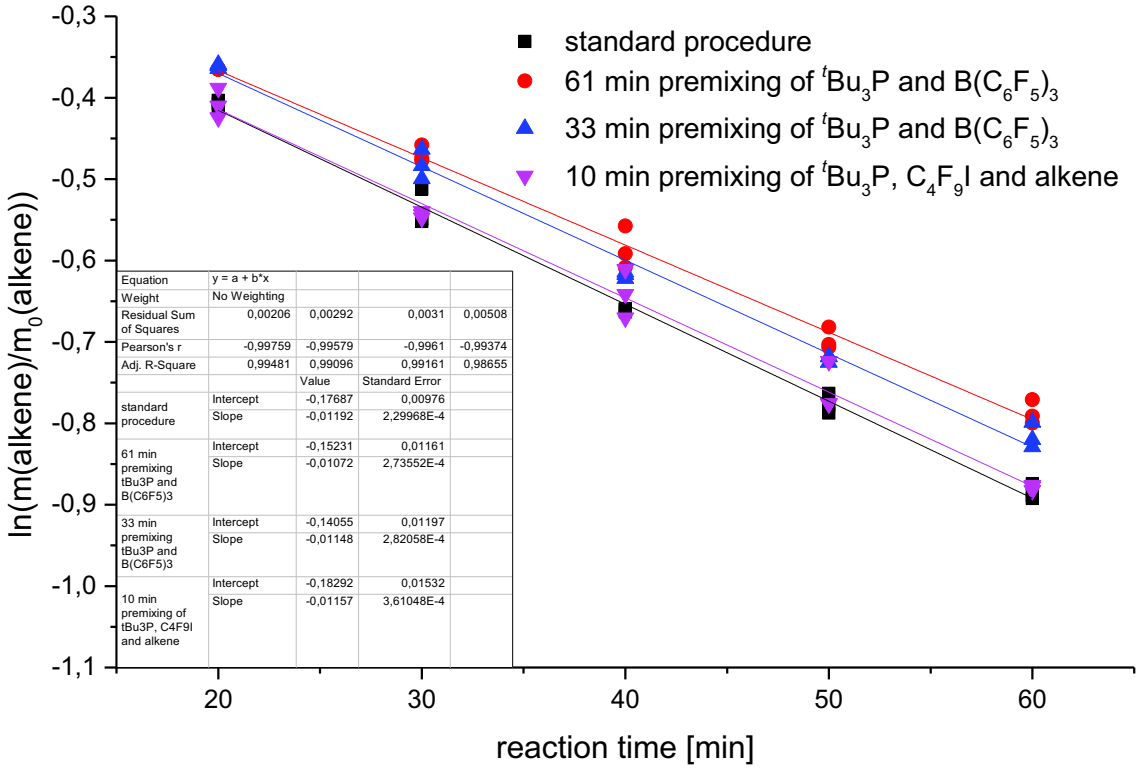

Equation	y = a + b*x			
Weight	No Weighting			
Residual Sum of Squares	0,00206	0,00292	0,0031	0,00508
Pearson's r	-0,99759	-0,99579	-0,9961	-0,99374
Adj. R-Square	0,99481	0,99096	0,99161	0,98655
		Value	Standard Error	
standard procedure	Intercept	-0,17687	0,00976	
	Slope	-0,01192	2,29968E-4	
61 min premixing tBu3P and B(C6F5)3	Intercept	-0,15231	0,01161	
	Slope	-0,01072	2,73552E-4	
33 min premixing tBu3P and B(C6F5)3	Intercept	-0,14055	0,01197	
	Slope	-0,01148	2,82058E-4	
10 min premixing of tBu3P, C4F9I and alkene	Intercept	-0,18292	0,01532	
	Slope	-0,01157	3,61048E-4	

Figure 10: GC experiment, first order fit for a variation of $B(C_6F_5)_3$.

8.9.6 GC-experiments, 62 min premixing of $^{t}Bu_3P$, $B(C_6F_5)_3$ and C_4F_9I

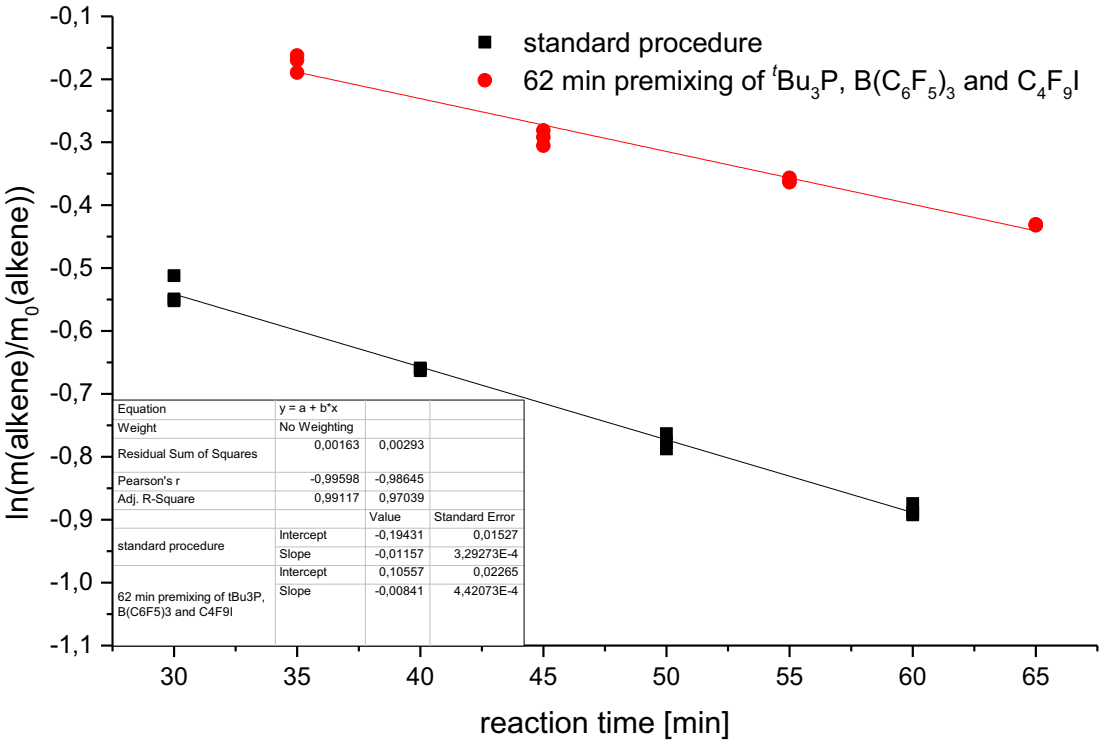

Equation	y = a + b*x		
Weight	No Weighting		
Residual Sum of Squares	0,00163	0,00293	
Pearson's r	-0,99598	-0,98645	
Adj. R-Square	0,99117	0,97039	
		Value	Standard Error
standard procedure	Intercept	-0,19431	0,01527
	Slope	-0,01157	3,29273E-4
62 min premixing of tBu3P, B(C6F5)3 and C4F9I	Intercept	0,10557	0,02265
	Slope	-0,00841	4,42073E-4

Figure 11: GC experiment, 62 min premixing of $^{t}Bu_3P$, $B(C_6F_5)_3$ and C_4F_9I.

8.9.7 NMR-experiments, variation of vinylcyclohexane

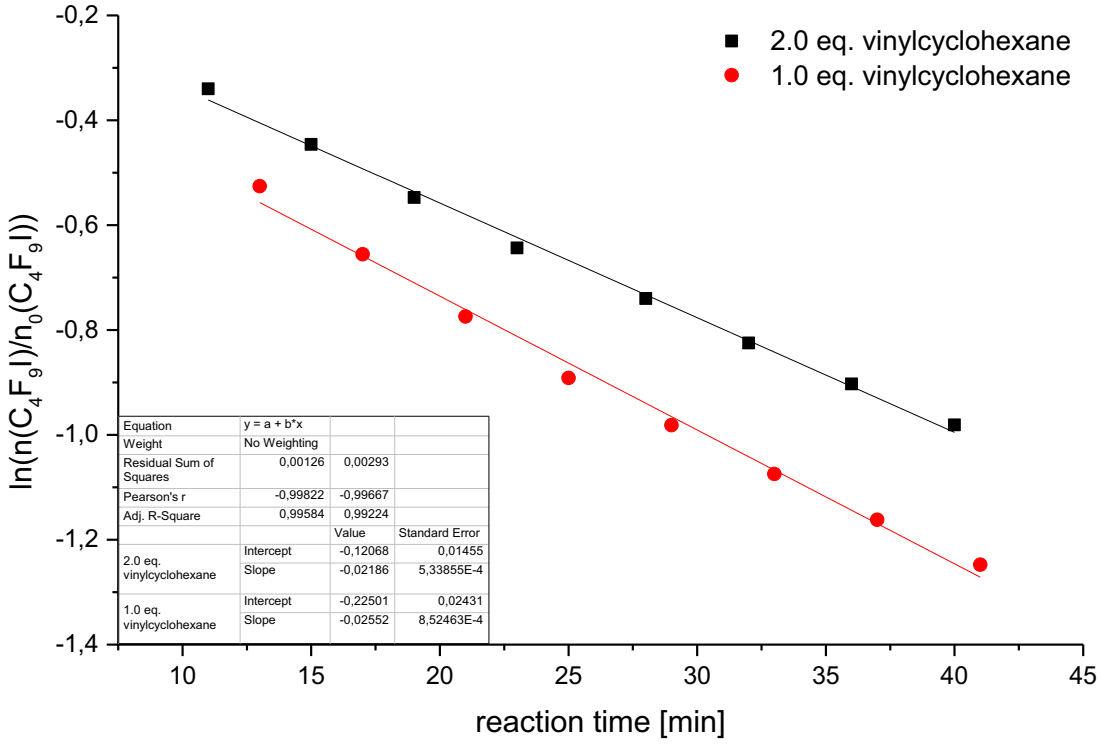

Equation	y = a + b*x		
Weight	No Weighting		
Residual Sum of Squares	0,00126	0,00293	
Pearson's r	-0,99822	-0,99667	
Adj. R-Square	0,99584	0,99224	
		Value	Standard Error
2.0 eq. vinylcyclohexane	Intercept	-0,12068	0,01455
	Slope	-0,02186	5,33855E-4
1.0 eq. vinylcyclohexane	Intercept	-0,22501	0,02431
	Slope	-0,02552	8,52463E-4

Figure 12: NMR-experiments, variation of vinylcyclohexane, C_4F_9I fit.

8.9.8 NMR-experiments, 78 min premixing of $^{t}Bu_3P$ and $B(C_6F_5)_3$

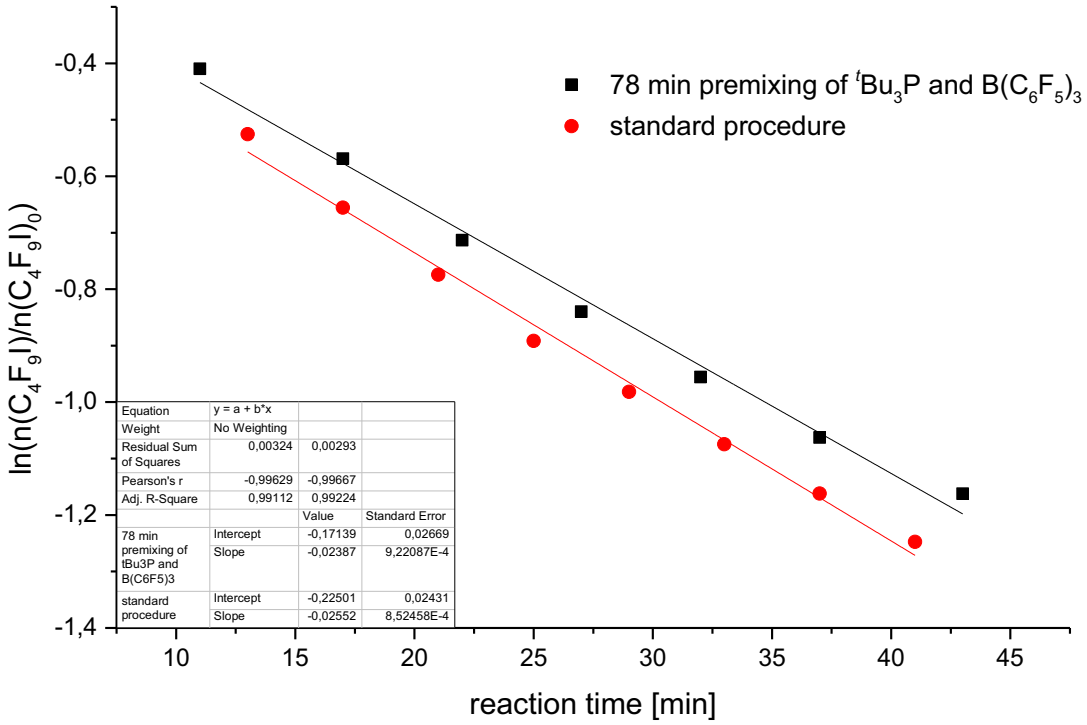

Equation	y = a + b*x		
Weight	No Weighting		
Residual Sum of Squares	0,00324	0,00293	
Pearson's r	-0,99629	-0,99667	
Adj. R-Square	0,99112	0,99224	
		Value	Standard Error
78 min premixing of tBu3P and B(C6F5)3	Intercept	-0,17139	0,02669
	Slope	-0,02387	9,22087E-4
standard procedure	Intercept	-0,22501	0,02431
	Slope	-0,02552	8,52458E-4

Figure 13: NMR-experiments, 78 min premixing of $^{t}Bu_3P$ and $B(C_6F_5)_3$. Substrate: vinylcyclohexane.

8.9.9 NMR-experiments, 60 min premixing of $^{t}Bu_3P$, $B(C_6F_5)_3$ and C_4F_9I

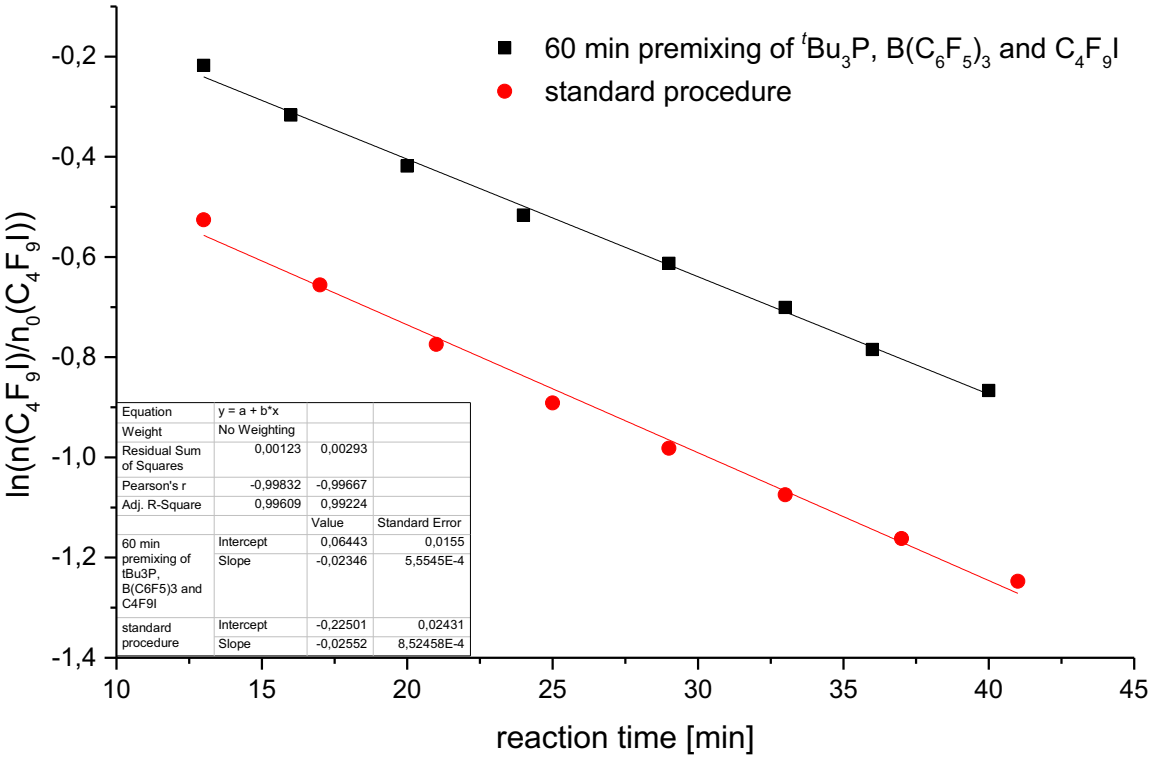

Equation	y = a + b*x		
Weight	No Weighting		
Residual Sum of Squares	0,00123	0,00293	
Pearson's r	-0,99832	-0,99667	
Adj. R-Square	0,99609	0,99224	
		Value	Standard Error
60 min premixing of tBu3P, B(C6F5)3 and C4F9I	Intercept	0,06443	0,0155
	Slope	-0,02346	5,5545E-4
standard procedure	Intercept	-0,22501	0,02431
	Slope	-0,02552	8,52458E-4

Figure 14: NMR-experiments, 60 min premixing of $^{t}Bu_3P$, $B(C_6F_5)_3$ and C_4F_9I. Substrate: vinylcyclohexane.

8.9.10 NMR-experiments, variation of $^{t}Bu_3P$

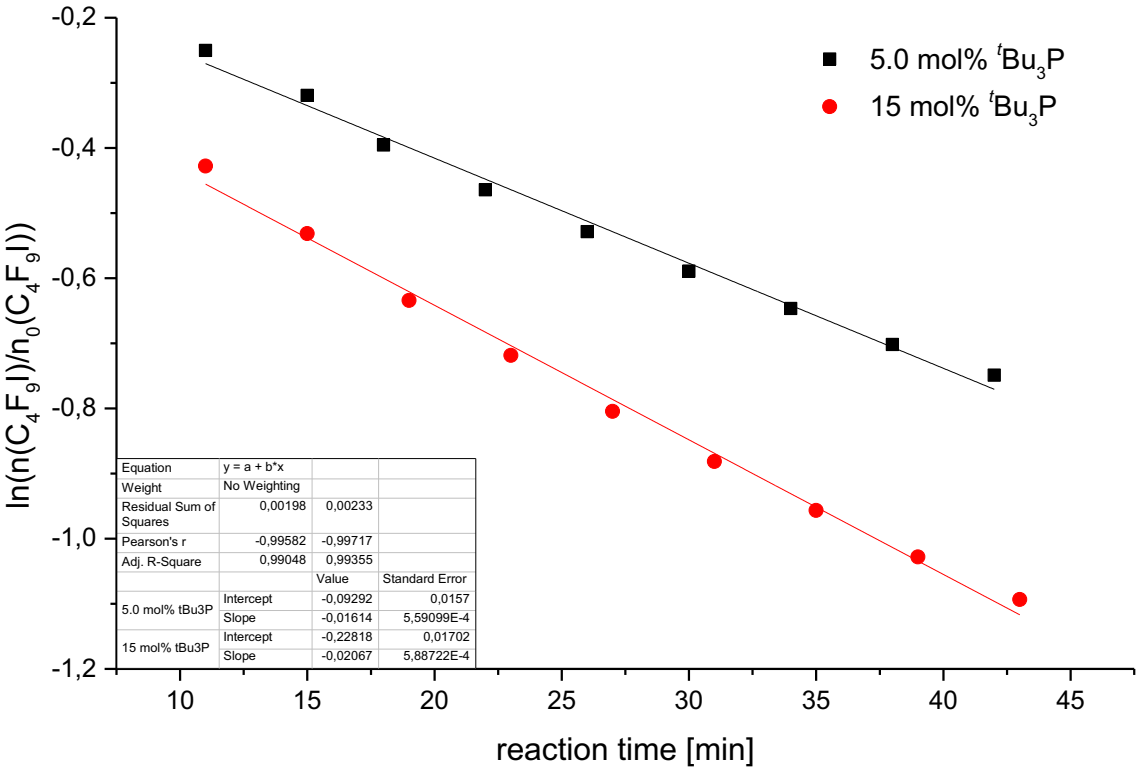

Equation	y = a + b*x		
Weight	No Weighting		
Residual Sum of Squares	0,00198	0,00233	
Pearson's r	-0,99582	-0,99717	
Adj. R-Square	0,99048	0,99355	
		Value	Standard Error
5.0 mol% tBu3P	Intercept	-0,09292	0,0157
	Slope	-0,01614	5,59099E-4
15 mol% tBu3P	Intercept	-0,22818	0,01702
	Slope	-0,02067	5,88722E-4

Figure 15: NMR-experiments, variation of $^{t}Bu_3P$. Substrate: vinylcyclohexane.

8.9.11 NMR-experiments, variation of 1-undecene

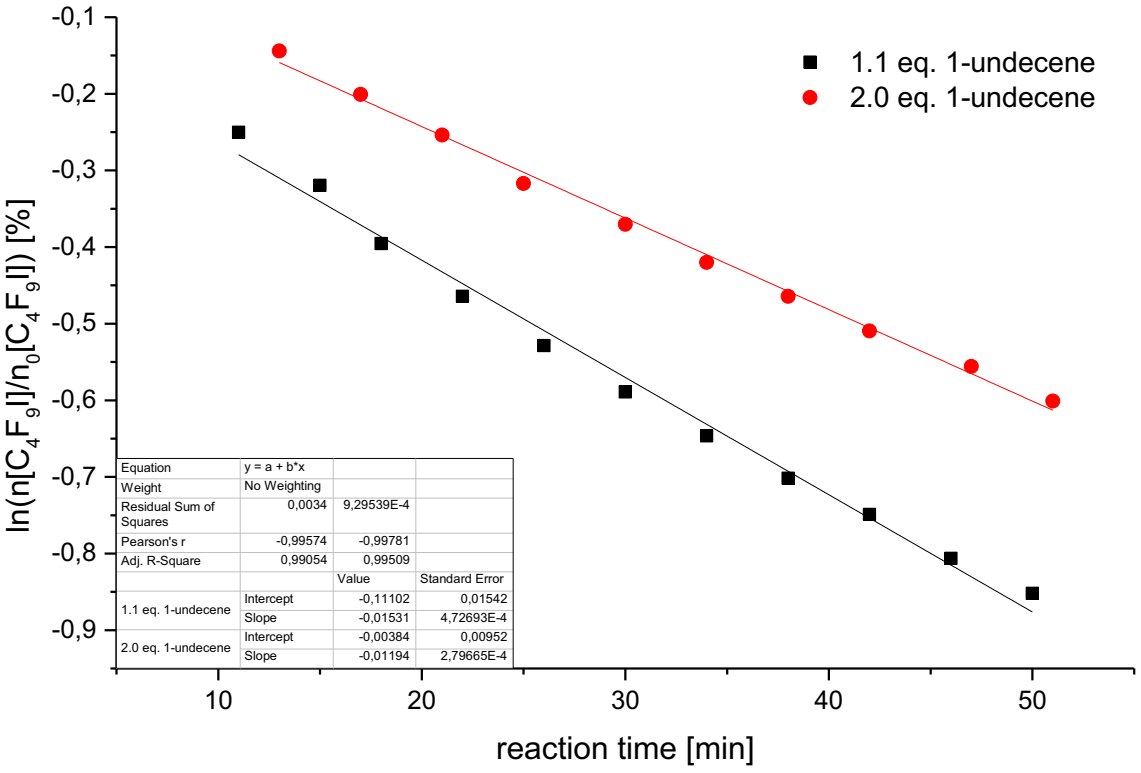

Equation	y = a + b*x		
Weight	No Weighting		
Residual Sum of Squares	0,0034	9,29539E-4	
Pearson's r	-0,99574	-0,99781	
Adj. R-Square	0,99054	0,99509	
		Value	Standard Error
1.1 eq. 1-undecene	Intercept	-0,11102	0,01542
	Slope	-0,01531	4,72693E-4
2.0 eq. 1-undecene	Intercept	-0,00384	0,00952
	Slope	-0,01194	2,79665E-4

Figure 16: NMR-experiments, variation of 1-undecene.

9 NMR examination of substance mixtures

9.1 $B(C_6F_5)_3$, C_4F_9I and vinylcyclohexane

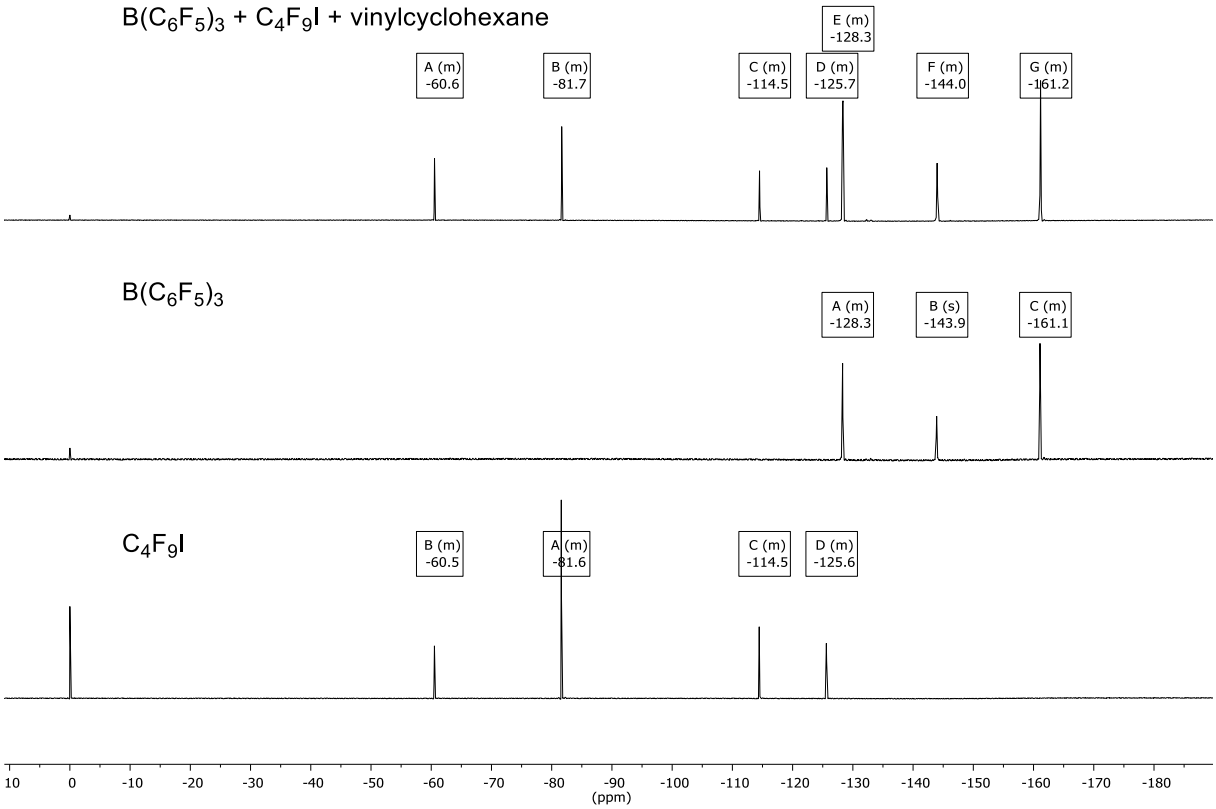

NMR-spectrum 56: ^{17}F-NMR-spectra (282 MHz in CH_2Cl_2, C_6D_6) of a mixture of $B(C_6F_5)_3$, C_4F_9I and vinylcyclohexane.

9.2 $B(C_6F_5)_3$ and 2,2,6,6-Tetramethyl-1-piperidinyloxy

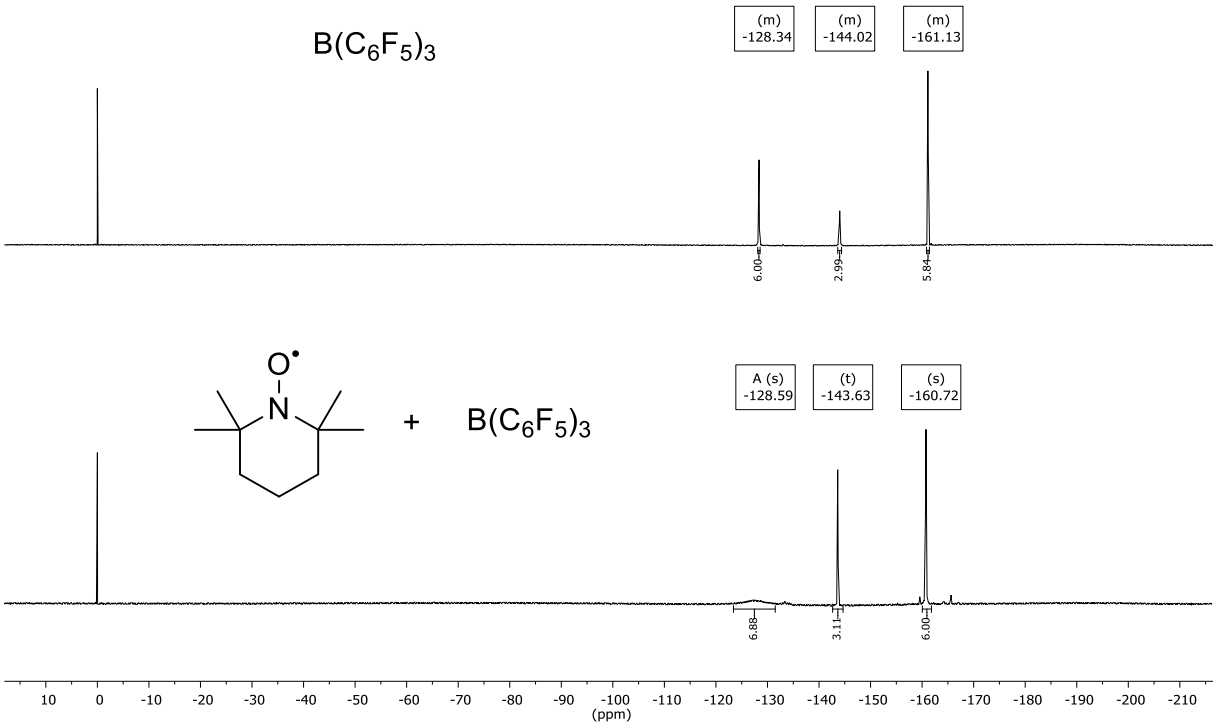

NMR-spectrum 57: ^{19}F-NMR-spectra (282 MHz, CD_2Cl_2) of $B(C_6F_5)_3$ (top), $B(C_6F_5)_3$ and TEMPO (bottom).

9.3 $^{t}Bu_3P$ and (3,3,4,4,5,5,6,6,6-nonafluoro-1-iodohexyl)cyclohexane

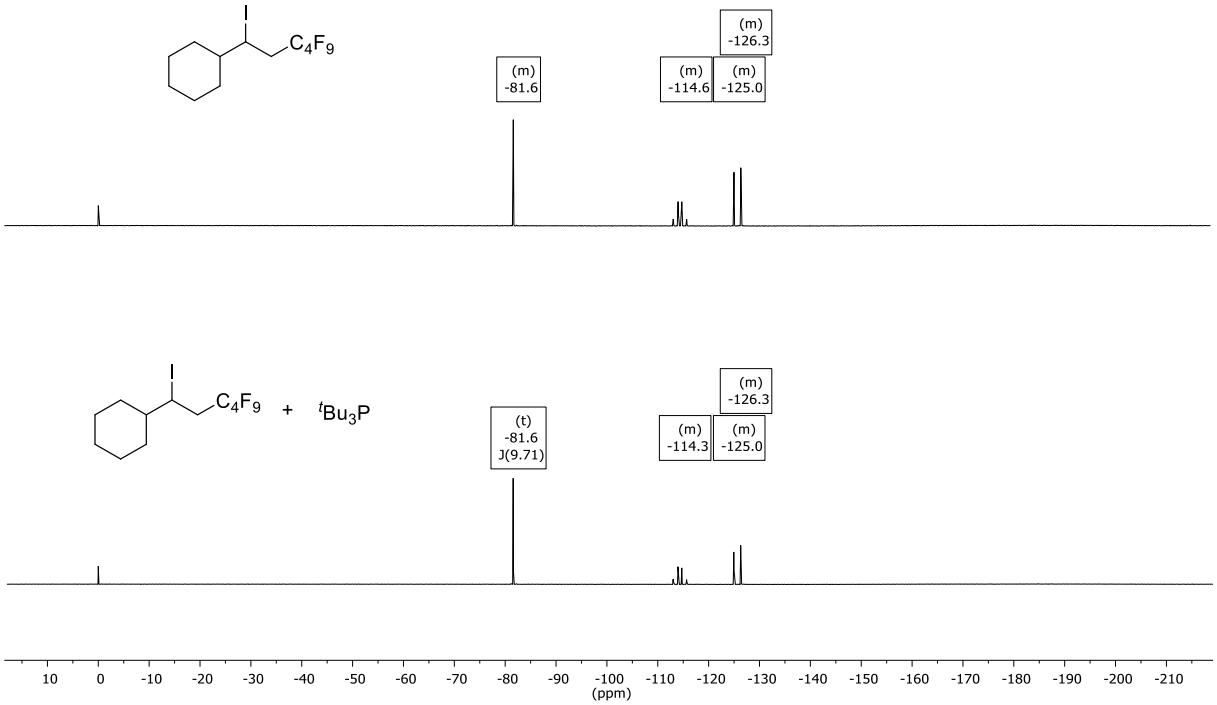

NMR-spectrum 58: ^{19}F-NMR-spectra (282 MHz, C_6D_6) in CH_2Cl_2.

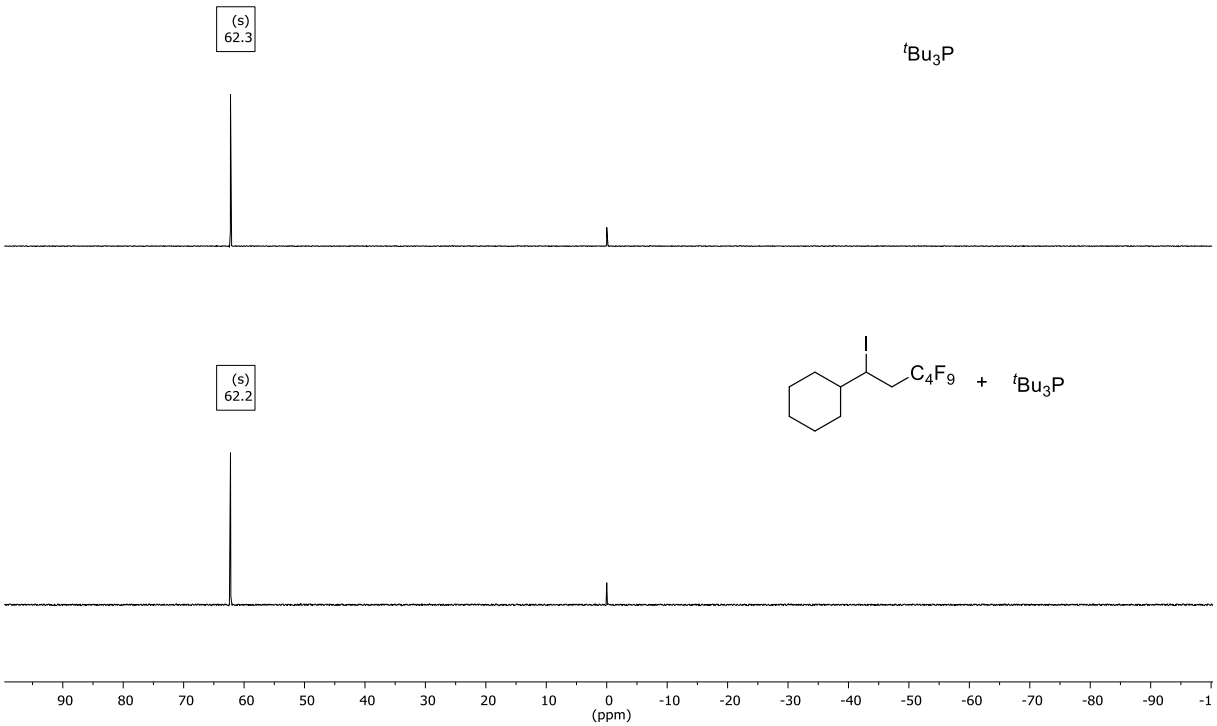

NMR-spectrum 59: ^{31}P-NMR-spectra (121 MHz, D_2O,) in CH_2Cl_2.

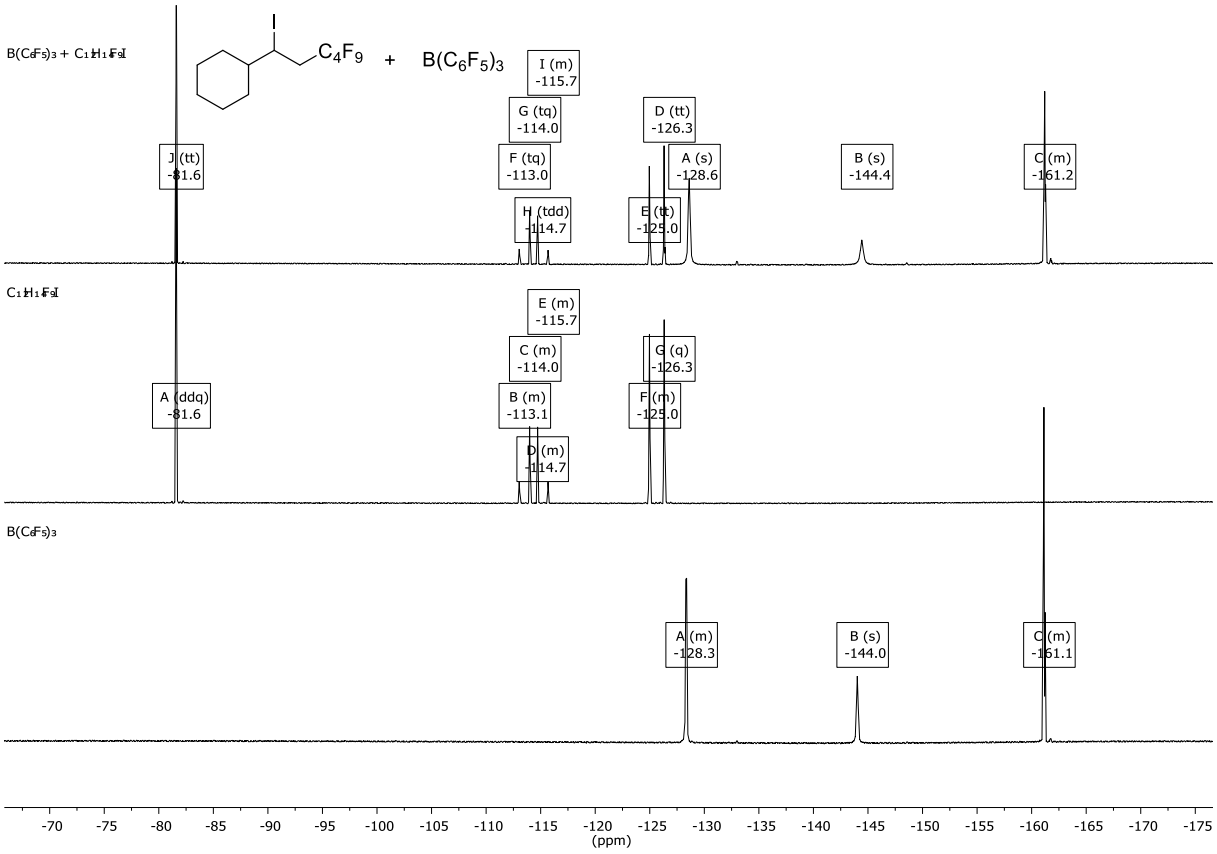

NMR-spectrum 60: ^{19}F-NMR-spectra (282 MHz, C_6D_6) in CH_2Cl_2.

9.4 $B(C_6F_5)_3$ and [^{t}Bu$_3$PH][FB(C_6F_5)$_3$]

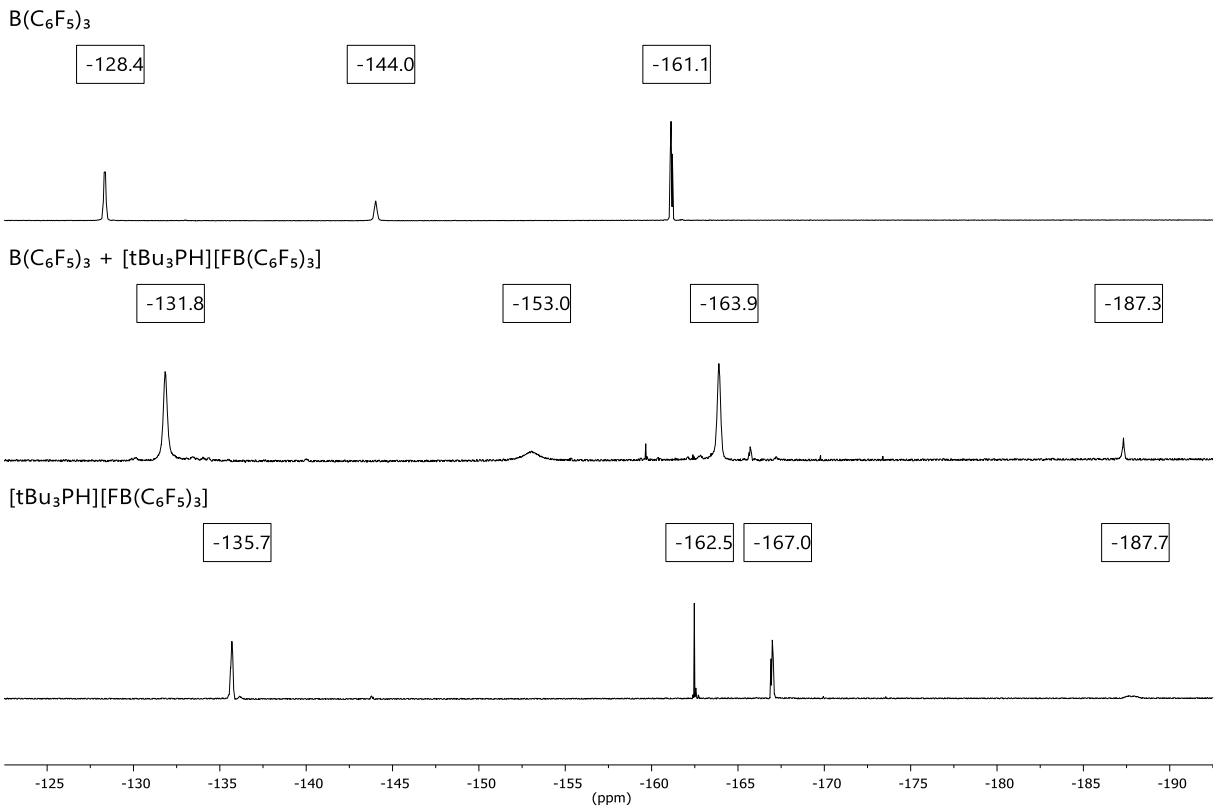

NMR-spectrum 61: ^{19}F-NMR-spectra (282 MHz, C_6D_6) in CH_2Cl_2.

10 Literature

[1] a) W. L. F. Armarego, C. L. L. Chai, Chapter 4 - Purification of Organic Chemicals, in *Purification of Laboratory Chemicals (Sixth Edition)*, Butterworth-Heinemann, Oxford, **2009**, pp. 88-444; b) W. L. F. Armarego, C. L. L. Chai, Chapter 5 - Purification of Inorganic and Metal-Organic Chemicals: (Including Organic compounds of B, Bi, P, Se, Si, and ammonium and metal salts of organic acids), in *Purification of Laboratory Chemicals (Sixth Edition)*, Butterworth-Heinemann, Oxford, **2009**, pp. 445-576.

[2] A. G. Massey, A. J. Park, *J. Organomet. Chem.* **1964**, *2*, 245-250.

[3] I. Behrends, S. Bähr, C. Czekelius, *Chem. Eur. J.* **2016**, *22*, 17177-17181.

[4] C. A. Tolman, *Chem. Rev.* **1977**, *77*, 313-348.

[5] R. D. Nelson, D. R. Lide, A. A. Maryott, *Selected Values of Electric Dipole Moments for Molecules in the Gas Phase*, U.S. National Bureau of Standards, **1967**.

[6] A. Foris, *Magn. Reson. Chem.* **2004**, *42*, 534-555.

[7] J. M. Burns, E. H. Krenske, R. P. McGeary, *Eur. J. Org. Chem.* **2017**, *2017*, 252-256.

[8] a) W. A. Kinney, G. D. Crouse, L. A. Paquette, *J. Org. Chem.* **1983**, *48*, 4986-5000; b) H. Iwamoto, K. Kubota, H. Ito, *Chem. Commun.* **2016**, *52*, 5916-5919.

[9] P. Wessig, O. Mühling, *Helv. Chim. Acta* **2003**, *86*, 865-893.

[10] J. M. Janusz, P. A. Young, M. W. Scherz, K. Enzweiler, L. I. Wu, L. Gan, S. Pikul, K. L. McDow-Dunham, C. R. Johnson, C. B. Senanayake, D. E. Kellstein, S. A. Green, J. L. Tulich, T. Rosario-Jansen, I. J. Magrisso, K. R. Wehmeyer, D. L. Kuhlenbeck, T. H. Eichhold, R. L. M. Dobson, *J. Med. Chem.* **1998**, *41*, 1112-1123.

[11] A. J. V. Marwitz, J. L. Dutton, L. G. Mercier, W. E. Piers, *J. Am. Chem. Soc.* **2011**, *133*, 10026-10029.

Supporting Information

Metal-free Activation of C-I Bonds and Perfluoroalkylation of Alkenes with Visible Light Using Phosphine Catalysts

Lucas Helmecke, Michael Spittler, Kai Baumgarten and Constantin Czekelius*

Institute for Organic Chemistry and Macromolecular Chemistry, Universität Düsseldorf, Universitätsstr. 1, D-40225 Düsseldorf, Germany

Corresponding Author

Constantin Czekelius

Fax: +49 211 81 11501

E-mail: constantin.czekelius@hhu.de

Contents

General Experimental Procedures

All syntheses involving air- and moisture-sensitive compounds were carried out inside a glove box (*Vacuum Atmospheres* model OMNI-LAB) under N_2 atmosphere (*Air Liquide ALPHAGAZ*™ 5.0). Glassware was dried for 2 hours at 120 °C and cooled down in vacuo.

Reagents as well as solvents were purchased from Acros, Sigma Aldrich, abcr, TCI, J & K scientific or VWR Chemicals. Chemicals were used without further purification or purified according to laboratory methods.[1] Nonafluoro-1-iodobutane (**2**) was filtered through a column packed with aluminum oxide 90 basic 0.063 - 0.200 mm (activity stage I) and activated molecular sieve (4 Å) under N_2 atmosphere. The clear liquid was stored in amber glass vials under N_2 atmosphere. Solvents were dried with the solvent purification system MP-SPS 800 from *M.Braun*, distilled and if necessary degassed with freeze-pump-thaw.

Reactions were monitored by thin-layer chromatography (TLC) using *Macherey-Nagel* silica gel plates ALUGRAM® Xtra SIL G/UV_{254} (0.20 mm thickness) and visualised by UV light or staining reagents if necessary. As staining reagents self-prepared potassium permanganate solution ($KMnO_4$ (3.0 g), K_2CO_3 (20 g), NaOH (5.0 ml 5.0%), H_2O (300 ml)) or cerium molybdophosphoric acid (molybdophosphoric acid (0.5 g), H_2O (250 ml), conc. H_2SO_4 (16 ml), Ce(IV)sulphate (2.0 g)) were used. Chromatographic purification of products was performed on *Macherey-Nagel* 60 M (0.04 - 0.063 mm) silica gel.

^{1}H-, ^{13}C, ^{19}F-, ^{31}P-NMR spectra were recorded on *Bruker* Avance III 300 and 600. Chemical shifts are reported in parts per million (ppm) to the corresponding solvent. The order of citation in parantheses is a) multiplicity (s = singlet, d = doublet, t = triplet, q = quartet, ddd = doublet of doublet of doublet, td = triplet of doublet, m = multiplet), b) coupling constants, c) number of protons, and d) assignment. Coupling constants (*J*) were reported in Hertz (Hz). The attributions of the chemical shifts were determined by means of COSY and HSQC experiments. If not described differently the NMR-spectra were measured at 298 K.

IR spectra were recorded using a *Jasco* FT/IR-6200 spectrometer. Samples were measured as film on a NaCl single crystal. The absorption bands were given in wave numbers (cm^{-1}). UV-VIS-measurements were measured on a Perkin Elmer Lamda 2 UV-VIS spectrometer in Hellma cuvettes (10 x 10 mm, Suprasil quartz glass)

High resolution mass spectra (HRMS) were measured with a *Bruker Daltonics* UHR-QTOF maXis 4G.

Elemental analysis were measured on an *elementar* Vario Micro Cube.

Inside the fume hood all reactions were conducted under red light (Jedi Lightning E27 ID60, 806 lm, 11W) and best possible light exclusion. Inside the glove box all reactions were prepared with an RGB LED-strip as light source. For irradiation at 405 nm a THORLABS M405L3 was used. Addition of the

individual perfluoroalkyl iodide was conducted under red light by a LED-strip. The emission spectra of the LED-strip were measured with a RED Tide USB650UV-spectrometer.

Unless otherwise stated all perfluoroalkylation reactions were conducted inside 4 ml screw neck glass vials with a septa screw cap.

General procedure A (GP-A)

Inside the glovebox the air and moisture sensitive phosphorous compound was weighed into a 4 ml reaction glass vial wrapped up in aluminum foil. Subsequently, *n*-decane and 1-octene (**1**) were weighed and added to the vial. CH_2Cl_2 (1 ml) and a Teflon stirring bar were added.

Under red light and best possible light exclusion nonafluoro-1-iodobutane (**2**) (100 µl, 0.583 mmol, 1.10 eq.) was added. Outside the glovebox the reaction vial was transferred into the photoreactor, the aluminum foil was removed, and the irradiation was started.

General procedure B (GP-B)

The phosphorous compound, *n*-decane and 1-octene (**1**) were weighed into the 4 ml reaction glass vial. CH_2Cl_2 (1 ml) and a Teflon stirring bar were added.

Under red light and best possible light exclusion nonafluoro-1-iodobutane (**2**) (100 µl, 0.583 mmol, 1.10 eq.) was added. The reaction vial was transferred into the photoreactor and the irradiation was started.

General procedure C (GP-C)

Inside the glovebox tri-*tert*-butylphosphine (**4**) was weighed into the reaction glass vial wrapped in aluminum foil. Subsequently, the alkene, CH_2Cl_2 and a Teflon stirring bar were added. The reaction vial was sealed with the septa screw cap. Outside the glovebox under a stream of nitrogen and under red light the corresponding perfluoroalkyl iodide was added. The reaction vial was sealed again with the septa screw cap and irradiation was started for the indicated time at the specified wavelength. Samples for NMR-spectroscopy were withdrawn under red light and a stream of nitrogen. After the stated reaction time the irradiation was stopped, and the solvent was evaporated under a stream of nitrogen. Purification was conducted by chromatography.

General procedure D (GP-D)

Inside the glovebox tri-*tert*-butylphosphine (**4**) was weighed into the reaction glass vial wrapped in aluminum foil. Subsequenly, the alkene, CH_2Cl_2 and a Teflon stirring bar were added. The reaction vial was sealed with the septa screw cap. Outside the glovebox, under a stream of nitrogen and under red light the corresponding perfluoroalkyl iodide was added. The reaction vial was transferred into the photoreactor, the aluminum foil was removed and irradiation was started for the indicated time at the specified wavelength. Samples for the NMR-spectroscopy were withdrawn under red light and a stream of nitrogen. After the stated reaction time the irradiation was stopped, and the solvent was evaporated under a stream of nitrogen. Purification was conducted by chromatography.

General procedure E (GP-E)

Inside the glovebox tri-*tert*-butylphosphine (**4**) was weighed into the reaction glass vial. A Teflon stirring bar was added and the vial was sealed with a septa screw cap. Outside the glovebox under a stream of nitrogen the alkene and CH_2Cl_2 were added. Under red light and best possible light exclusion the corresponding perfluoroalkyl iodide was added. The reaction vial was sealed with the septa screw cap and irradiation was started for the indicated time at the specified wavelength. Samples for NMR-spectroscopy were withdrawn under red light and a stream of nitrogen. After the stated reaction time the irradiation was stopped, and the solvent was evaporated under a stream of nitrogen. Purification was conducted by chromatography.

1. Catalyst screening

To monitor the reaction progress over a longer period of time for each individual phosphorous compound, a Shimadzu GC-2010 equipped with an auto injector AOC-20i (syringe code:10R-S-0.63C) was used. A ZB-Wax Plus column (30 m x 0.25 mm x 0.25 μm) was used. As internal standard *n*-decane (Acros Organics, purity 99+%, LOT: 1283567) was added to every reaction solution. All reactions were performed in 4 ml screw neck vials with a septa screw cap. 1-Octene (**1**) was filtered through a column packed with aluminum oxide 90 basic 0.063-0.200 mm (activity stage I) and activated molecular sieve (4 Å) and stored over activated molecular sieve (4 Å). Nonafluoro-1-iodobutane (**2**) was purified and used as described in the general experimental procedures.

Samples were always withdrawn under red light and best possible light exclusion and under a stream of nitrogen. With a 1.0 ml syringe (Braun) flushed with N_2 0.10 ml of the reaction solution were withdrawn and diluted with 0.4 ml CH_2Cl_2 in a short thread vial. The vial was sealed with a black screw cap and to exclude ambient light, covered with light-impermeable black tape.

Table 1: Screening different phosphorous compounds for the conversion of 1-octene (**1**) with C_4F_9I (**2**).

phosphorous compound			1-octene (1)	*n*-decane	time [h]	conversion [%]
Triphenyl phosphite (General procedere B)	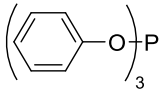	16.4 mg, 0.0528 mmol, 9.89 mol%	60.0 mg, 0.535 mmol	28.9 mg, 0.203 mmol	2	3
					4	3
					6	3
					8	3
					24	3
Chlorodiphenylphosphine (General procedere B)	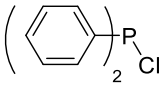	13.9 mg, 0.0630 mmol, 11.8 mol%	60.0 mg, 0.534 mmol	28.9 mg, 0.203 mmol	2	12
					4	13
					6	14
					8	15
					24	21
Diethyl benzylphosphonate (General procedere B)	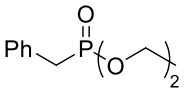	11.9 mg, 0.0521 mmol, 9.90 mol%	59.2 mg, 0.527 mmol	27.1 mg, 0.190 mmol	2	12
					4	13
					6	14
					8	15
					24	21

Table 2: Screening of the conversion of 1-octene (**1**) with C_4F_9I (**2**) and different phosphorous compounds.

phosphorous compound		1-octene (1)	*n*-decane	time [h]	conversion [%]
Trimethyl phosphite (Following general procedure B)	 9.1 mg, 0.064 mmol, 12 mol%	59.8 mg, 0.532 mmol.	28.8 mg, 0.202 mmol	2	71
				3	72
				6	94
Triethylphosphite (Following general procedure B)	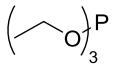 9.4 mg, 0.056 mmol, 11 mol%	59.9 mg, 0.534 mmol	28.6 mg, 0.201 mmol	2	72
				4	72
				5	91
				6	91
				7	91
				8	91
				24	94
4,6-Bis-(diphenylphosphino) dibenzofuran (Following general procedure B)	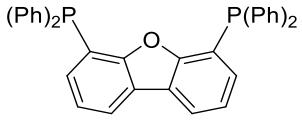 28.6, 0.0533 mmol, 9.96 mol%	60.1 mg, 0.535 mmol	28.7 mg, 0.201 mmol	2	85
				4	85
				5	85
				8	86

Table 3: Screening of the conversion of 1-octene (**1**) with C_4F_9I (**2**) and different phosphorous compounds.

phosphorous compound			1-octene (1)	*n*-decane	time [h]	conversion [%]
Triphenylphosphine (Following general procedure B)	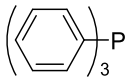	14.0, 0.0533 mmol, 10.1 mol%	59.0 mg, 0.526 mmol	28.9 mg, 0.203 mmol	1	62
					02:38	89
		27.9 mg, 0.106 mmol, 19.9 mol%	59.9 mg, 0.533 mmol	28.7 mg, 0.202 mmol	1	60
					2	88
Tri(o-tolyl)phosphine (Following general procedure B)	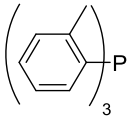	16.2 mg, 0.0532 mmol, 10.2 mol%	58.3 mg, 0.520 mmol	29.0 mg, 0.204 mmol	1	48
					2	52
					4	52
Tris(pentafluorophenyl)phosphine (Following general procedure A)	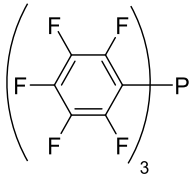	28.3 mg, 0.0532 mmol, 10.2 mol%	58.4 mg, 0.521 mmol	28.5 mg, 0.200 mmol	2	23
					4	25
					6	25
Bis(dimethylamino)phosphoryl chloride (Following general procedure A)	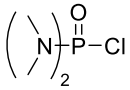	9.0 mg, 0.038 mmol, 7.2 mol%	59.7 mg, 0.532 mmol	28.9 mg, 0.203 mmol	2	4
					4	4
					6	4
					8	5
					24	8

Table 4: Screening of the conversion of 1-octene (**1**) with C_4F_9I (**2**) and different phosphorous compounds.

phosphorous compound			1-octene (1)	*n*-decane	time [h]	conversion [%]
Tris(4-fluorophenyl)phosphine (Following general procedure A)	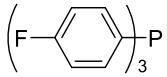	16.8, 0.0531 mmol, 9.95 mol%	60.0 mg, 0.534 mmol	28.6 mg, 0.201 mmol	2	59
					4	60
					6	60
					8	60
					24	65
2-(Diphenylphosphino) ethyltriethoxysilane (Following general procedure B)	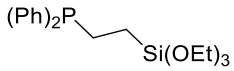	20.2 mg, 0.0536 mmol, 10.0 mol%	59.9 mg, 0.534 mmol	29.0 mg, 0.204 mmol	2	82
					4	98
					6	98
					8	98
Bis(diphenylphosphino)methane (Following general procedure B)		20.5 mg, 0.0533 mmol, 10.0 mol%	59.6 mg, 0.531 mmol	28.9 mg, 0.203 mmol	2	79
					4	94
					6	94
					8	94
		10 mg, 0.027 mmol, 5.0 mol%	59.9, 0.534 mmol	28.7 mg, 0.201 mmol	1	17
					2	59
Methyldiphenylphosphine oxide (Following general procedure B)	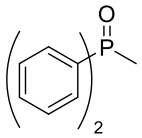	11.5 mg, 0.0532 mmol, 9.90 mol%	60.3 mg, 0.537 mmol	28.8 mg, 0.202 mmol	2	3
					4	4
					6	5
					8	6
Triphenylphosphine sulfide (Following general procedure B)	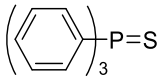	15.5 mg, 0.0526 mmol, 9.91 mol%	59.6 mg, 0.531 mmol	28.8 mg, 0.202 mmol	2	3
					4	4
					6	5
					8	5

Table 5: Screening of the conversion of 1-octene (**1**) with C_4F_9I (**2**) and different phosphorous compounds.

phosphorous compound			1-octene (1)	decane	time [h]	conversion [%]
Tricyclohexylphosphine (Following general procedure A)	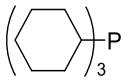	14.9 mg, 0.0531 mmol, 9.92 mol%	60.0 mg, 0.535 mmol	29.6 mg, 0.208 mmol	0:37	77
					1:26	84
					2:34	84
Tri-*n*-butylphosphine (Following general procedure A)	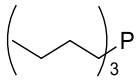	10.9 mg, 0.0539 mmol, 10.1 mol%	60.0 mg, 0.535 mmol	29.1 mg, 0.204 mmol	0:38	48
					1	64
					2	65
Tri-*tert*-butylphosphine (Following general procedure A)		10.6 mg, 0.0524 mmol, 10.0 mol%	59.0 mg, 0.526 mmol	28.6 mg, 0.201 mmol	0:24	59
					1	99
		5.5 mg, 0.027 mmol, 5.2 mol%	58.7 mg, 0.524 mmol	29.0 mg, 0.204 mmol	2	99
Tris(2,4,6-trimethylphenyl) phosphine (Following general procedure A)	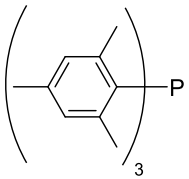	20.6 mg, 0.0530 mmol, 10.1 mol%	58.7 mg, 0.524 mmol	29.2 mg, 0.205 mmol	1	4
					2	4
					19	8
Methyldiphenylphosphine (Following general procedure A)	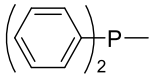	10.6 mg, 0.0529 mmol, 10.0 mol%	59.1 mg, 0.527 mmol	29.1 mg, 0,204 mmol	0:45	72
					6	72
					19	73

2. Iodo perfluoroalkylations

2.1. 1,1,1,2,2,3,3,4,4-Nonafluoro-6-iodododecane (3)

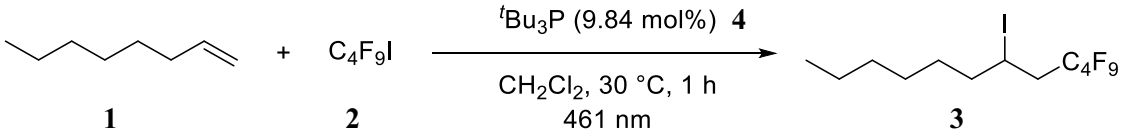

1 **2** **3**

Following **GP-C**, tri-*tert*-butylphosphine (**4**) (10.6 mg, 0.0524 mmol, 9.84 mol%), 1-octene (**1**) (59.7 mg, 0.532 mmol) and nonafluoro-1-iodobutane (**2**) (100 µl, 0.583 mmol, 1.10 eq.) were irradiated in CH_2Cl_2 (2 ml) for 1 h. Purification was conducted by chromatography on SiO_2 (pentane) yielded pure product **3** as colorless oil.

yield (458.15 g·mol^{-1}) 217 mg (0.474 mmol, 89%)

^{1}H-NMR (300 MHz, Chloroform-*d*) δ [ppm] 4.43 – 4.24 (m, 1H, C*H*I), 3.09 – 2.62 (m, 2H, CH_2R$_F$), 1.92 – 1.67 (m, 2H, CH_2CHICH), 1.50 – 1.23 (m, 8H, 4 x CH_2), 0.98 – 0.80 (m, 3H, CH_3).

^{19}F-NMR (565 MHz, Chloroform-*d*) δ [ppm] -80.64 – -81.40 (m, 3F, CF_3), -111.13 – -112.76 (m, 1F, CF_2), -114.15 – -115.42 (m, 1F, CF_2), -124.33 – -125.14 (m, 2F, CF_2), -125.43 – -126.34 (m, 2F, CF_2).

Analytic data are consistent with literature-known values.[14]

Large scale preparation of 1,1,1,2,2,3,3,4,4-Nonafluoro-6-iodododecane (3)

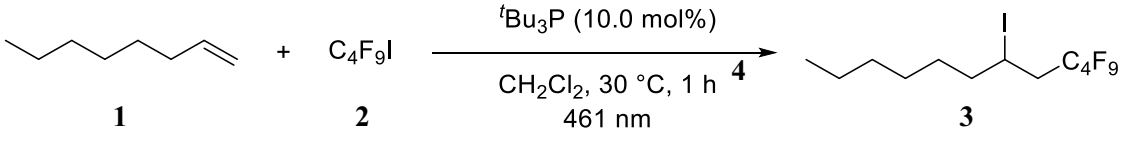

1 **2** **3**

Inside the glovebox tri-*tert*-butylphosphine (**4**) (401 mg, 1.98 mmol, 10.0 mol%) were weight into a two-necked round-bottom flask with stopcock, a stirring bar was added and sealed with a septum. Outside the glovebox CH_2Cl_2 (24 ml), 1-octene (**1**) (3.13 ml, 19.8 mmol) and nonafluoro-1-iodobutane (**2**) (3.73 ml, 27.8 mmol, 1.10 eq.) under red light. The reaction was stirred under irradiation for 1 h. Purification of the yellow reaction solution by column chromatography on SiO_2 (pentane) yielded pure product **3** as colorless oil.

yield (458.15 g·mol^{-1}) 8.93 g (19.5 mmol, 98%)

Analytic data are consistent with literature-known values.[14]

2.2. 1,1,1-Trifluoro-3-iodononane (5)

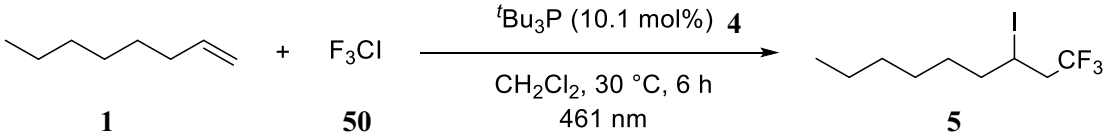

1 **50** **5**

Inside the glovebox tri-*tert*-butylphosphine (**4**) (10.8 mg, 0.0534 mmol, 10.1 mol%) and 1-octene (**1**) (59.3 mg, 0.528 mmol) were weight into an aluminum foil wrapped two-necked round-bottom flask with stopcock and dissolved with CH_2Cl_2 (2 ml). A stirring bar was added, and the flask was sealed with a septum. Outside the glovebox a balloon with CF_3I **50** was connected to the reaction flask and under red light the aluminum foil was removed inside the photoreactor. The reaction was stirred vigorously under irradiation for 6 h. Purification of the yellow reaction solution by column chromatography on SiO_2 (pentane) yielded pure product 5 as colorless liquid.

yield (308.13 $g \cdot mol^{-1}$) 123 mg (400 mmol, 76%)

^{1}H-NMR (600 MHz, Chloroform-*d*) δ [ppm] 4.26 – 4.12 (m, 1H, C*H*I), 3.00 – 2.84 (m, 1H, CH_2R_F), 2.84 – 2.73 (m, 1H, CH_2R_F), 1.87 – 1.68 (m, 2H, CH_2CHICH), 1.59 – 1.24 (m, 8H, 4 x CH_2), 0.90 (t, *J* = 6.8 Hz, 3H, CH_3).

^{19}F-NMR (565 MHz, Chloroform-*d*) δ [ppm] -63.95. (s, 3F, CF_3)

Analytic data are consistent with literature-known values.[13]

2.3. 1,1,1,2,2,3,3,4,4,5,5,6,6-Tridecafluoro-8-iodotetradecane (6)

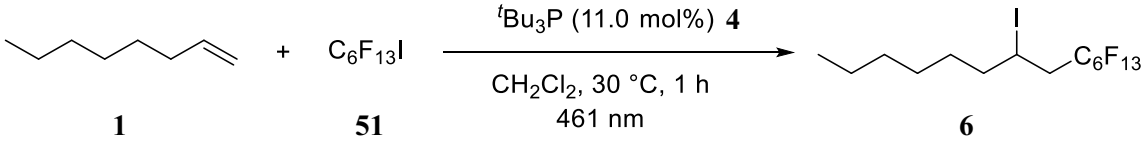

1 **51** **6**

Following **GP-C**, tri-*tert*-butylphosphine (**4**) (10.9 mg, 0.0583 mmol, 11.0 mol%), 1-octene (**1**) (59.1 mg, 0.526 mmol) and perfluoro-1-iodohexane **51** (126 µl, 0.583 mmol, 1.10 eq.) were irradiated in CH_2Cl_2 (2 ml) for 1 h. Purification was conducted by chromatography on SiO_2 (pentane) yielded pure product **6** as colorless oil.

yield (558.17 g·mol^{-1}) 287 mg (0.513 mmol, 97%)

^{1}H-NMR (600 MHz, Chloroform-*d*) δ [ppm] 4.34 (m, 1H), 3.02 – 2.85 (m, 1H), 2.85 – 2.71 (m, 1H), 1.90 – 1.69 (m, 2H), 1.60 – 1.50 (m, 1H), 1.47 – 1.23 (m, 6H), 0.90 (t, *J* = 13.9 Hz, 3H).

^{19}F-NMR (565 MHz, Chloroform-*d*) δ [ppm] -80.80 (t, *J* = 10.4 Hz, 3F, CF_3), -111.35 – -112.21 (m, 1F, CF_2), -114.21 – -115.01 (m, 1F, CF_2), -121.41 – -122.35 (m, 2F, CF_2), -122.35 – -123.21 (m, 2F, CF_2), -123.27 – -123.88 (m, 2F, CF_2), -125.60 – -126.80 (m, 2F, CF_2).

Analytic data are consistent with literature-known values.[15]

2.4. 1,1,1,2,2,3,3,4,5,5,6,7,7,8,8-Pentadecafluoro-10-iodo-4,6-dimethylhexadecane (7)

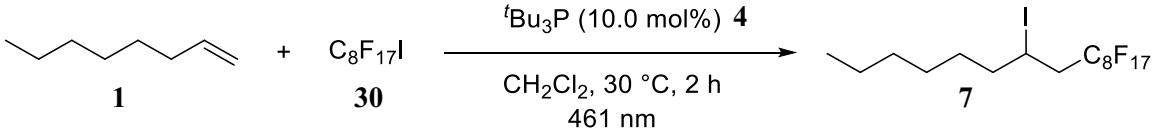

1 **30** **7**

Following **GP-D**, tri-*tert*-butylphosphine (**4**) (10.6 mg, 0.0524 mmol, 10.0 mol%), 1-octene (**1**) (58.4 mg, 0.520 mmol) and perfluorooctyl iodide **30** (321 mg, 0.588 mmol, 1.13 eq.) were irradiated in CH_2Cl_2 (2 ml) for 2 h. Purification was conducted by chromatography on SiO_2 (pentane) yielded pure product.

yield (658.18 g·mol^{-1}) 229 mg (0.348 mmol, 67%)

^{1}H-NMR (600 MHz, Chloroform-*d*) δ [ppm] 4.45 – 4.25 (m, 1H), 2.99 – 2.85 (m, 1H), 2.85 – 2.71 (m, 1H), 1.91 – 1.72 (m, 2H), 1.66 – 1.47 (m, 1H), 1.47 – 1.13 (m, 6H), 0.90 (t, J = 6.8 Hz, 3H).

^{19}F-NMR (565 MHz, Chloroform-*d*) δ [ppm] -80.62 – -80.99 (m, 3F, CF_3), -111.40 – -112.19 (m, 1F, CF_2), -114.15 – -114.98 (m, 1F, CF_2), -121.44 – -121.72 (m, 4F, 2 x CF_2), -121.73 – -122.13 (m, 2F, CF_2), -122.52 – -122.94 (m, 2F, CF_2), -123.37 – -123.80 (m, 2F, CF_2), -125.86 – -126.40 (m, 2F, CF_2).

Analytic data are consistent with literature-known values.[16]

2.5. 5-Ethyl-1,1,1,2,2,3,3,4,4-nonafluoro-6-iodooctane (8) from (*E*)-3-hexene

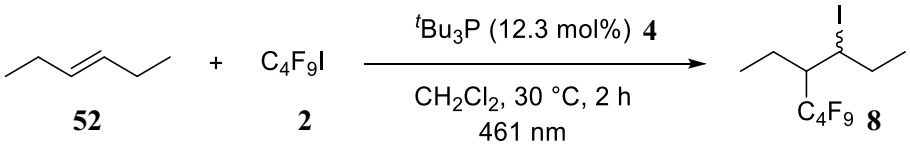

52 **2** **8**

Following **GP-C**, tri-*tert*-butylphosphine (**4**) (10.6 mg, 0.0524 mmol, 12.3 mol%), *trans*-3-hexene (**52**) (42.5 mg, 0.424 mmol) and nonafluoro-1-iodobutane (**2**) (100 µl, 0.583 mmol, 1.37 eq.) were irradiated in CH_2Cl_2 (2 ml) for 2 h. Purification was conducted by chromatography on SiO_2 (hexane (R_f = 0.75) yielded pure product **8** as coloruless liquid and mixture of diastereomers (*d.r.* 53:47).

yield (430,10 g·mol−1) 130 mg (0.303 mmol, 71 %)

^{1}H-NMR (600 MHz, Chloroform-*d*) δ [ppm] 4.41 – 4.36 (m, 1H, C*H*I, diastereomer 1), 4.30 – 4.25 (m, 1H, C*H*I, diastereomer 2), 2.69 – 2.58 (m, 1H, C*H*CF_2, diastereomer 1), 2.15 – 1.97, 1.94 – 1.84, 1.84 – 1.64, 1.61 – 1.52, 1.21 – 0.95 (each m, 20H, CH_3, CH_2).

^{19}F-NMR (298 MHz, Chloroform-*d*) δ [ppm] -80.93 (m, 6F, CF_3), -109.86 – -110.54 (m, 1F, CF_2, diastereomer 1), -112.91 – -115.43 (m, 2F, CF_2, diastereomer 1, diastereomer 2), -120.72 – -123.33 (m, 4F, CF_2), -125.06 – -126.90 (m, 4F, CF_2).

Analytic data are consistent with literature-known values.[17]

2.6. 5-Ethyl-1,1,1,2,2,3,3,4,4-nonafluoro-6-iodooctane (8) from (*Z*)-3-hexene

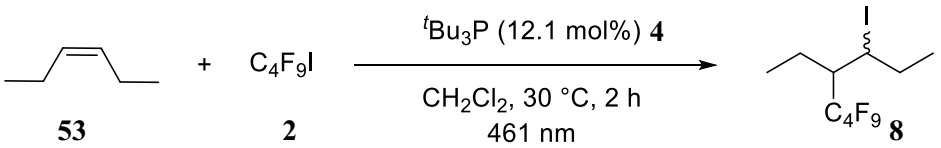

53 **2** **8**

Following **GP-C**, tri-*tert*-butylphosphine (**4**) (10.6 mg, 0.0524 mmol, 12.1 mol%), *cis*-3-hexene (**53**) (43.3 mg, 0.432 mmol) and nonafluoro-1-iodobutane (**2**) (100 µl, 0.583 mmol, 1.35 eq.) were irradiated in CH_2Cl_2 (2 ml) for 2 h. Purification was conducted by chromatography on SiO_2 (hexane) yielded pure product **8** as colorless liquid and mixture of diastereomers (*d.r.* 65:35)

yield (430,10 g·mol−1) 170 mg (0.271 mmol, 62 %)

^{1}H-NMR (600 MHz, Chloroform-*d*) δ [ppm] 4.46 – 4.37 (m, 1H, C*H*I, diastereomer 1), 4.34 – 4.27 (m, 1H, C*H*I, diastereomer 2), 2.72 – 2.61 (m, 1H, C*H*CF_2, diastereomer 1), 2.13 (m, 1H, C*H*CF_2, diastereomer 2), 2.17 – 2.02, 1.96 – 1.88, 1.86 – 1.70, 1.60 – 1.56, 1.15, 1.08 - 1.04 (each m, 20H, CH_3, CH_2).

^{19}F-NMR (565 MHz, Chloroform-*d*) δ [ppm] -80.92 (m, 6F, CF_3), -109.79 – -110.55 (m, 1F, CF_2, diastereomer 1), -112.98 – -115.23 (m; 2F, CF_2, diastereomer 1, diastereomer 2), -120.64 – -123.36 (m, 4F, CF_2), -125.10 – -126.79 (m, m; 4F, CF_2).

Analytic data are consistent with literature-known values.[17]

2.7. (3,3,4,4,5,5,6,6,6-Nonafluoro-1-iodohexyl)cyclohexane (9)

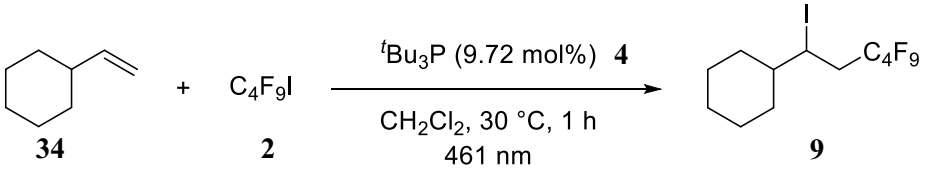

Following **GP-C**, tri-*tert*-butylphosphine (**4**) (10.6 mg, 0.0524 mmol, 9.72 mol%), vinylcyclohexane (**34**) (59.4 mg, 0.539 mmol) and nonafluoro-1-iodobutane (**2**) (100 µl, 0.583 mmol, 1.08 eq.) were irradiated in CH_2Cl_2 (2 ml) for 1 h. Purification was conducted by chromatography on SiO_2 (pentane).

yield (M = 456,13 g·mol^{-1}) 215 mg (0.471 mmol, 87%)

^{1}H-NMR (600 MHz, Chloroform-*d*) δ [ppm] 4.35 (td, *J* = 6.7, 3.0 Hz, 1H), 2.92 – 2.77 (m, 2H), 1.85 – 1.75 (m, 2H), 1.75 – 1.64 (m, 3H), 1.45 – 1.27 (m, 2H), 1.26 – 1.09 (m, 3H), 0.86 – 0.79 (m, 1H).

^{19}F-NMR (565 MHz, Chloroform-*d*) δ [ppm] -80.94 – -81.15 (m), -112.58 – -113.22 (m), -114.52 – -115.26 (m), -124.24 – -124.74 (m), -125.68 – -126.14 (m).

Analytic data are consistent with literature-known values.[17]

2.8. (4,4,5,5,6,6,7,7,7-Nonafluoro-2-iodoheptyl)benzene (10)

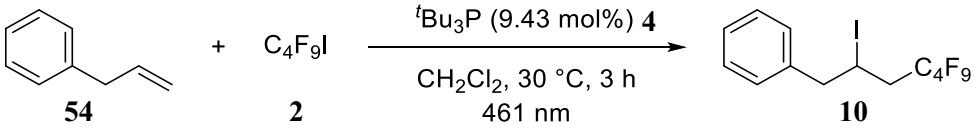

Following **GP-C**, tri-*tert*-butylphosphine (**4**) (10.7 mg, 0.0528 mmol, 9.43 mol%), allylbenzol (**54**) (66.3 mg, 0.583 mmol) and nonafluoro-1-iodobutane (**2**) (100 µl, 0.583 mmol, 1.04 eq.) were irradiated in CH_2Cl_2 (2 ml) for 3 h. Purification was conducted by chromatography on SiO_2 (pentane) yielded pure product.

yield (464,11 g·mol−1) g (mmol,)

^{1}H-NMR (600 MHz, Chloroform-*d*) δ [ppm] 7.40 – 7.28 (m, 3H, Ph-H), 7.25 – 7.16 (m, 2H, Ph-H), 4.51 – 4.43 (m, 1H, C*H*I), 3.30 (dd, J = 14.6, 5.7 Hz, 1H, PhCH_2), 3.21 (dd, *J* = 14.6, 8.9 Hz, 1H, PhCH_2), 3.04 – 2.77 (m, 2H, CH_2R_F).

^{19}F-NMR (565 MHz, Chloroform-*d*) δ [ppm] -81.02 (t, J = 9.6 Hz, 3F, CF_3), -111.92 – -112.55 (m, 1F, CF_2), -113.67 – -114.31 (m, 1F, CF_2), -124.30 – -124.70 (m, 2F, CF_2), -125.79 – -126.01 (m, 2F, CF_2).

Analytic data are consistent with literature-known values.[17]

2.9. 1-Iodo-2-(1,1,2,2,3,3,4,4,4-nonafluorobutyl)cyclooctane (11)

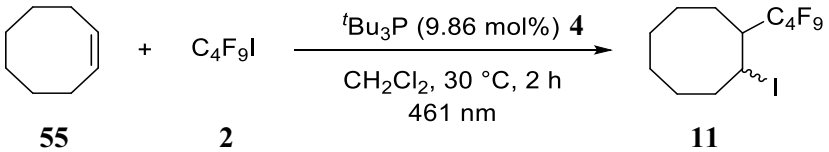

55 **2** **11**

Following **GP-E**, tri-*tert*-butylphosphine (**4**) (10.8 mg, 0.0533 mmol, 9.86 mol%), cyclooctene (**55**) (59.6 mg, 0.541 mmol) and nonafluoro-1-iodobutane (**2**) (100 µl, 0.583 mmol, 1.07 eq.) were irradiated in CH_2Cl_2 (2 ml) for 2 h. Purification was conducted by chromatography on SiO_2 (Cyclohexane) yielded pure product **11** as a mixture of diastereomers (*d.r.* 55:45).

yield (464,11 g·mol−1) 220 mg (0.481 mmol, 89%)

^{1}H-NMR (300 MHz, Chloroform-*d*) δ [ppm] 4.65 – 4.58 (m, 1H, C*H*CF_2 diastereomer 1), 4.56 – 4.49 (m, 1H, C*H*CF_2 diasteriomer 2), 2.50 – 2.33 (m), 2.32 – 2.21 (m), 2.18 – 1.96 (m), 1.96 – 1.78 (m), 1.78 – 1.38 (m).

^{19}F-NMR (298 MHz, Chloroform-*d*) δ [ppm] -80.80 – -80.96 (m, 6F, CF_3), -115.29 – -117.51 (m, 4F, CF_2), -119.79 – -121.85 (m, 4F, CF_2), -125.19 – -126.44 (m, 4F, CF_2).

Analytic data are consistent with literature-known values.[17]

2.10. 1-Iodo-2-(1,1,2,2,3,3,4,4,4-nonafluorobutyl)cyclopentane (12)

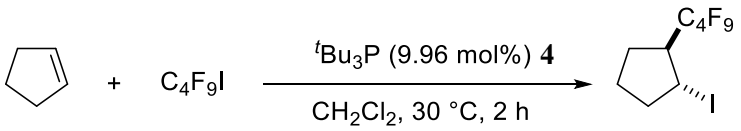

56 **2** **12**

Following **GP-E**, tri-*tert*-butylphosphine (**4**) (10.8 mg, 0.0534 mmol, 9.96 mol%), cyclopentane (**56**) (36.5 mg, 0.536 mmol) and nonafluoro-1-iodobutane (**2**) (100 µl, 0.583 mmol, 1.08 eq.) were irradiated in CH_2Cl_2 (2 ml) for 2 h. Purification was conducted by chromatography on SiO_2 (pentane) yielded pure product **12**.

yield (464,11 g·mol−1) 92.9 mg (0.224 mmol, 42%)

^{1}H-NMR (300 MHz, Chloroform-*d*) δ [ppm] 4.50 – 4.34 (ddd, *J*= 6.75, 4.52, 1H, C*HI*), 3.29 – 2.95 (m, 1H, C*H*CF_2), 2.23 – 2.03 (m, 2H, 5-H), 2.02 – 1.77 (m, 2H, CH_2), 1.77 – 1.65 (m, 2H, CH_2).

^{19}F-NMR (298 MHz, Chloroform-*d*) δ [ppm] -80.96 (t, *J* = 9.8 Hz, 3F, CF_3), -114.19 – -115.54 (m, 1F, CF_2), -119.91 – -121.06 (m, 1F, CF_2), -121.70 – -122.09 (m, 2F, CF_2), -125.14 – -127.22 (m, 2F, CF_2).

Analytic data are consistent with literature-known values.[17]

2.11. 10-Bromo-1,1,1,2,2,3,3,4,4-nonafluoro-6-iododecane (13)

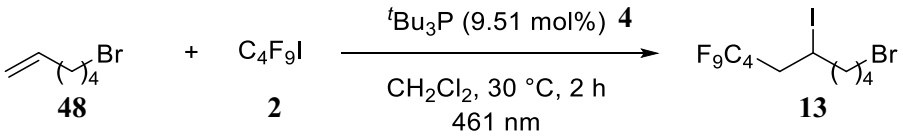

Following **GP-C**, tri-*tert*-butylphosphine (**4**) (10.7 mg, 0.529 mmol, 9.51 mol%), 6-bromohexene (**48**) (90.7 mg, 0.556 mmol) and nonafluoro-1-iodobutane (**2**) (100 µl, 0.583 mmol, 1.05 eq.) were irradiated in CH_2Cl_2 (2 ml) for 2 h. Purification was conducted by chromatography on SiO_2 (pentane) yielded pure product **13**.

yield (508.99 g·mol−1) 218.7 mg (0.430 mmol, 77 %)

^{1}H-NMR (600 MHz, Chloroform-*d*) δ [pmm] 4.40 – 4.25 (m, 1H, C*H*I), 3.51 – 3.36 (m, 2H, CH_2Br), 3.00 – 2.87 (m, 1H, C$H_2$$CF_2$), 2.84 – 2.71 (m, 1H, C$H_2$$CF_2$), 2.01 – 1.77 (m, 4H, CHI-CH_2CH_2CH_2-CH_2Br), 1.77 – 1.67 (m, 1H, CHI-CH_2CH_2CH_2-CH_2Br), 1.67 – 1.55 (m, 1H, CHI-CH_2CH_2CH_2-CH_2Br).

^{19}F-NMR (298 MHz, Chloroform-*d*) δ [ppm] -81.02 (t, *J* = 9.5 Hz, 3F, CF_3), -111.48 – -112.17 (m, 1F, CF_2), -114.52 – -115.15 (m, 1F, CF_2), -124.34 – -124.64 (m, 2F, CF_2), -125.72 – -125.99 (m, 2F, CF_2).

Analytic data are consistent with literature-known values.[18]

2.12. 11,11,12,12,13,13,14,14,14-Nonafluoro-9-iodotetradecan-1-ol (14)

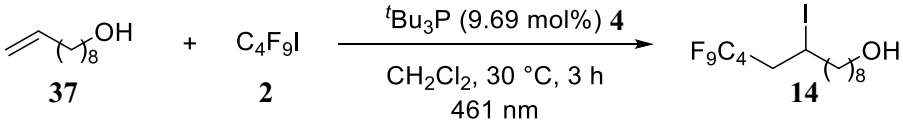

Following **GP-C**, tri-*tert*-butylphosphine (**4**) (10.9 mg, 0.0538 mmol, 9.69 mol%), dec-9-en-1-ol (**37**) (87.0 mg, 0.556 mmol) and nonafluoro-1-iodobutane (**2**) (100 µl, 0.583 mmol, 1.05 eq.) were irradiated in CH_2Cl_2 (2 ml) for 3 h. Purification was conducted by chromatography on SiO_2 (Hexan:EtOAc 90:10) yielded pure product as light yellow oil **14**.

yield (516,23 g·mol−1) 227.1 g (0.440 mmol, 79 %)

^{1}H-NMR (600 MHz, Chloroform-*d*) δ [ppm] 4.38 – 4.28 (m, 1H, C*H*I), 3.64 (t, J = 6.6 Hz, 2H, CH_2OH), 2.99 – 2.85 (m, 1H, R_FCH_2CHICH_2), 2.84 – 2.69 (m, 1H, R_FCH_2CHI), 1.87 – 1.70 (m, 2H, $R_F$$CH_2$CHIC$H_2$), 1.64 – 1.50 (m, 3H), 1.46 – 1.25 (m, 10H).

[19]F-NMR (565 MHz, Chloroform-*d*) δ [ppm] -81.04 (t, *J* = 9.1 Hz, 3F, CF_3), -111.59 – -112.66 (m, 1F, CF_2), -114.23 – -115.43 (m, 1F, CF_2), -123.96 – -125.11 (m, 2F, CF_2), -125.55 – -126.11 (m, 2F, CF_2).

Analytic data are consistent with literature-known values.[19]

2.13. 11,11,12,12,13,13,14,14,14-Nonafluoro-9-iodotetradecyl 4-methylbenzenesulfonate (15)

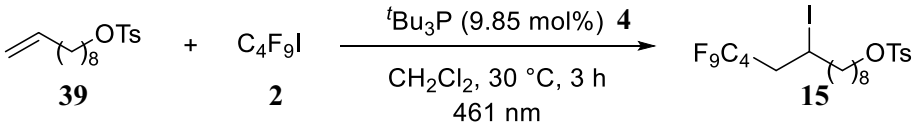

39 **2** **15**

Following **GP-C**, tri-*tert*-butylphosphine (**4**) (10.8 mg, 0.0534 mmol, 9.85 mol%), dec-9-en-1-yl 4-methylbenzenesulfonate (**39**) (168.5 mg, 0.542 mmol) and nonafluoro-1-iodobutane (**2**) (100 µl, 0.583 mmol, 1.07 eq.) were irradiated in CH_2Cl_2 (2 ml) for 3 h. Purification was conducted by chromatography on SiO_2 (Hexan:EtOAc 90:10) yielded pure product **15** as colorless oil.

yield (656,39 g·mol−1) 258.6 mg (0.394 mmol, 72%)

[1]H-NMR (300 MHz, Chloroform-*d*) δ [ppm] 7.79 (d, *J* = 8.3 Hz, 2H, Aryl), 7.34 (t, *J* = 8.0 Hz, 2H, Aryl), 4.39 – 4.24 (m, 1H, C*H*I), 4.02 (t, *J* = 6.5 Hz, 2H, Tosyl-OC*H*$_2$-), 3.06 – 2.61 (m, 2H, R_FCH_2CHI), 2.45 (s, 3H, C*H*$_3$-Aryl), 1.92 – 1.71 (m, 2H, R_FCH_2CHIC*H*$_2$-), 1.71 – 1.58 (m, 2H), 1.44 – 1.17 (m, 10H, CHICH_2-C_5H_{10}- CH_2O-).

[13]C-NMR (75.5 MHz, Chloroform-*d*) δ [ppm] 144.8, 133.4, 129.9, 128.0, 121.3, 119.3, 117.9, 119.1, 70.7, 41.7 (t, *J* = 20.9 Hz), 40.4 (d, *J* = 2.20), 29.6, 29.2, 28.9, 28.5, 25.4, 21.7, 20.9

[19]F-NMR (565 MHz, Chloroform-*d*) δ [ppm] -80.95 – -81.13 (t, *J* = 9.9 Hz, 3F), -111.65 – -112.35 (m, 1F), -114.45 – -115.15 (m, 1F), -124.37 – -124.67 (m, 2F), -125.73 – -126.11 (m, 2F).

IR (film on NaCl), ν [cm^{-1}] 2931, 2858, 1599, 1496, 1465, 1434, 1362, 1230, 1174, 1140, 1098, 1020, 942, 880, 816, 723, 688, 665, 577, 555.

Elemental analysis for $C_{21}H_{26}F_9IO_3S$ calculated: C: 38.43 %, H: 3.99 %, S: 4.88 %

measured: C: 38.73 %, H: 3.92 %, S: 5.17 %

2.14. 14-Azido-1,1,1,2,2,3,3,4,4-nonafluoro-6-iodotetradecane (16)

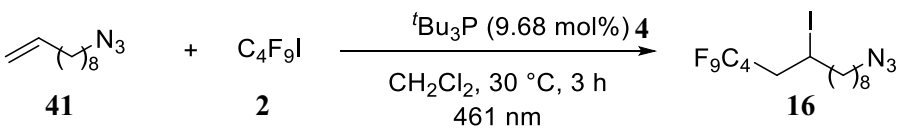

41 **2** **16**

Following **GP-C**, tri-*tert*-butylphosphine (**4**) (10.7 mg, 0.0529 mmol, 9.86 mol%), 10-azidodec-1-ene (**41**) (99 mg, 0.546 mmol) and nonafluoro-1-iodobutane (**2**) (100 µl, 0.583 mmol, 1.06 eq.) were

irradiated in CH_2Cl_2 (2 ml) for 3 h. Purification was conducted by chromatography on SiO_2 (Hexane:EtOAc 98:2) followed by a second column (*n*-hexane) yielded pure product **16** as colorless oil.

yield (527,22 g·mol−1) 58 mg (110 mmol, 20 %)

^{1}H-NMR (600 MHz, Chloroform-*d*) δ [ppm] 4.42 – 4.24 (m, 1H, C*H*I), 3.26 (t, J = 6.9 Hz, 2H, $N_3CH_2(CH_2)_8CHI$), 3.02 – 2.70 (m, 2H, CH_2R_F), 1.91 – 1.71 (m, 2H, $N_3CH_2(CH_2)_8CHI$), 1.66 – 1.51 (m, 3H, $N_3CH_2(CH_2)_8CHI$), 1.48 – 1.24 (m, 11H, $N_3CH_2(CH_2)_8CHI$).

^{13}C-NMR (75.5 MHz, Chloroform-*d*) δ [ppm] 51.7, 41.9 (t, J = 20.9 Hz), 40.5 (d, J = 2.93), 29.7, 29.3, 29.2, 29.0, 28.5, 26.8, 20.7

^{19}F-NMR (565 MHz, Chloroform-*d*) δ [ppm] -81.02 (t, J = 9.5 Hz, 3F, CF_3), -111.63 – -112.40 (m, 1F, CF_2), -114.47 – -115.18 (m, 1F, CF_2), -124.30 – -124.74 (m, 2F, CF_2), -125.51 – -126.12 (m, 2F, CF_2).

IR (film on NaCl), ν [cm^{-1}] 2932, 2859, 2097, 1464, 1434, 1351, 1135, 1015, 913, 879, 742, 554, 513

Elemental analysis for $C_{14}H_{19}F_9IN_3$ calculated: C: 31.89 %, H: 3.63 %, N: 7.97 %

measured: C: 31.74 %, H: 3.54 %, N: 7.84 %

2.15. 5,5,6,6,7,7,8,8,9,9,10,10,10-tridecafluoro-3-iododecyl acetate (17)

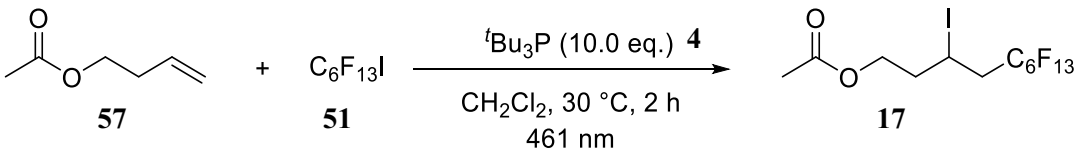

Following **GP-C**, tri-*tert*-butylphosphine (**4**) (10.8 mg, 0.0534 mmol, 10.0 mol%), but-3-en-1-yl acetate (**57**) (61.0 mg, 0.534 mmol) and perfluorohexyl iodide (**51**) (126 µl, 0.583 mmol, 1.10 eq.) were irradiated in CH_2Cl_2 (2 ml) for 2 h. Purification was conducted by chromatography on SiO_2 (Cyclohexane:CH_2Cl_2 65:35) yielded pure product **17**.

yield (560,09 g·mol−1) 270.6 g (0.483 mmol, 90 %)

^{1}H-NMR (600 MHz, Chloroform-*d*) δ [ppm] 4.45 – 4.36 (m, 1H,−CH_2CO_2−), 4.35 – 4.27 (m, 1H, −CHI−), 4.21 – 4.10 (m, 1H,−CH_2CO_2−), 3.03 – 2.90 (m, 1H, R_FCH_2−), 2.90 – 2.76 (m, 1H, R_FCH_2−), 2.22 – 2.14 (m, 1H,−CH_2CH_2−), 2.14 – 2.07 (m, 1H,−CH_2CH_2−), 2.08 – 2.02 (−CH_3, m, 3H,−CH_3).

^{13}C-NMR (151 MHz, $CDCl_3$) δ [ppm] 170.8, 119.7, 118.0, 116.3, 112.7, 111.1, 108.7, 64.2, 42.0 (−$H_2CCF_2R_F$, t, $^2J_{CF}$ = 20.9 Hz), 39.0, 20.9, 15.3.

[19]F-NMR (282 MHz, Chloroform-*d*) δ [ppm] −80.8 (tt, *J* = 10.1, 2.6 Hz, 3F), −110.9 – −115.1 (m, 2F), −121.6 – −122.0 (m, 2F), −122.7 – −123.1 (m, 2F), −123.5 – −123.9 (m, 2F), −126.0 – −126.4 (m, 2F).

IR (film on NaCl), ν [cm^{-1}] 2962, 1747, 1433, 1366, 1237, 1042, 845, 812, 733, 699, 657, 606, 553, 530.

m/z calculated for $C_{12}H_{11}F_{13}IO_2$ [M + H^+] = 560.9591, found 560.9593.

2.16. 6,6,7,7,8,8,9,9,9-Nonafluoro-4-iodononanamide (18)

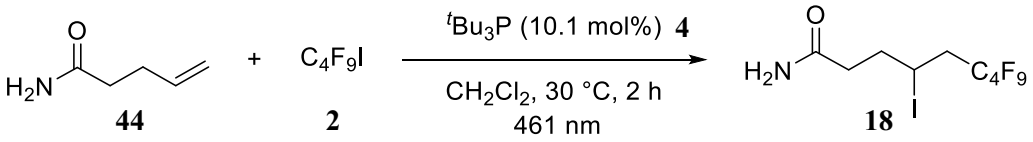

Following **GP-C**, tri-*tert*-butylphosphine (**4**) (10.8 mg, 0.0534 mmol, 10.1 mol%), Pent-4-enamide (**44**) (52.1 mg, 0.526 mg) and nonafluoro-1-iodobutane (**2**) (100 µl, 0.583 mmol, 1.10 eq.) were irradiated in CH_2Cl_2 (2 ml) for 2 h. The reaction solution was light yellow. Purification was conducted by chromatography on SiO_2 (CH_2Cl_2:MeOH 20:1) yielded a colourless solid.

yield (445,1 g·mol−1)	202.9 mg (0.456 mmol, 86%)

[1]H-NMR (600 MHz, Chloroform-*d*) δ [ppm] 5.84 (s, 1H, N*H*$_2$), 5.59 (s, 1H, N*H*$_2$), 4.43 – 4.34 (m, 1H, C*H*I), 3.00 – 2.87 (m, 1H, C*H*$_2$R$_F$), 2.86 – 2.73 (m, 1H, C*H*$_2$R$_F$), 2.57 – 2.48 (m, 1H, C(O)C*H*$_2$CH$_2$), 2.44 – 2.36 (m, 1H, C(O)C*H*$_2$CH$_2$), 2.26 – 2.15 (m, 1H, C*H*$_2$CHI), 2.11 – 2.02 (m, 1H, C*H*$_2$CHI), 1.38 (d, J = 12.4 Hz, 1H).

[13]C-NMR (75.5 MHz, Chloroform-*d*) δ [ppm] 173.8, 120.2-108.4, 42.8 (t, *J* = 20.8 Hz), 35.89, 35.81 (d, *J* = 2.14), 29.2, 19.7

[19]F-NMR (565 MHz, Chloroform-*d*) δ [ppm] -79.5 – -82.7 (t, *J* = 9.66 Hz, 3F), -111.4 – -112.6 (m, 1F), -114.1 – -115.0 (m, 1F), -124.4 – -124.7 (m, 2F), -125.8 – -126.0 (m, 2F).

IR (film on NaCl), ν [cm^{-1}] 3526, 3412, 3020, 2401, 1683, 1593, 1521, 1220, 1015, 879, 772.

Mp: 97.0-97.8 °C

Elemental analysis for $C_9H_9F_9INO$	calculated: C: 24.29 %, H: 2.04 %, N: 3.15 %
	measured: C: 24.57 %, H: 2.02 %, N: 3.07 %

2.17. 1-(3-(4,4,5,5,6,6,7,7,7-Nonafluoro-2-iodoheptyl)phenyl)ethan-1-one (19)

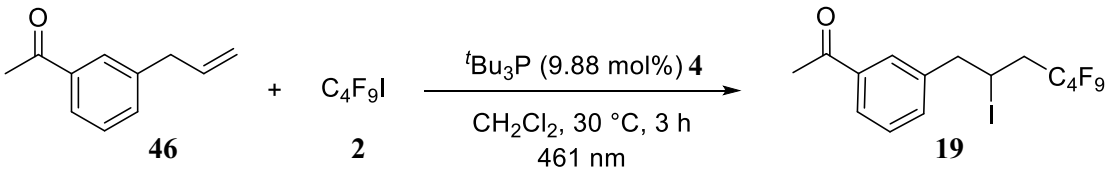

46 **2** **19**

Following **GP-C**, tri-*tert*-butylphosphine (**4**) (10.6 mg, 0.0524 mmol, 9.88 mol%), 1-(3-allylphenyl)ethan-1-one (**46**) (84.8 mg, 0.530 mmol) and nonafluoro-1-iodobutane (**2**) (100 µl, 0.583 mmol, 1.10 eq.) were irradiated in CH_2Cl_2 (2 ml) for 3 h. Purification was conducted by chromatography on SiO2 (Hexane:EtOAc 90:10) yielded pure product **19** as colorless oil.

yield (506,15 g·mol−1) 258.4 mg (0.510 mmol, 96 %)

^{1}H-NMR (600 MHz, Chloroform-*d*) δ [ppm] 7.93 – 7.86 (m, 1H, Ar-*H*), 7.83 – 7.79 (m, 1H, Ar-*H*), 7.50 – 7.44 (m, 1H, Ar-*H*), 7.43 – 7.40 (m, 1H, Ar-*H*), 4.53 – 4.43 (m, 1H, C*H*I), 3.38 (dd, J = 14.7, 4.9 Hz, 1H, Ar-CH_2-CHI), 3.21 (dd, J = 14.7, 9.6 Hz, 1H, Ar-CH_2-CHI), 3.04 – 2.81 (m, 2H, CH_2R_F), 2.62 (s, 3H, ArC(O)CH_3).

^{13}C-NMR (75.5 MHz, Chloroform-*d*) δ [ppm] 139.3, 137.8, 133.7, 129.0, 128.8, 127.7, 121.3, 119.4, 117.9, 115.6, 46.71, 41.4 (t, *J* = 21.0), 26.7, 19.1.

^{19}F-NMR (298 MHz, Chloroform-*d*) δ [ppm] -80.91 – -81.08 (m, 3F, CF_3), -111.42 – -111.99 (m, 1F, CF_2), -113.79 – -114.40 (m, 1F, CF_2), -124.30 – -124.59 (m, 2F, CF_2), -125.71 – -126.00 (m, 2F, CF_2).

IR (film on NaCl) ν [cm^{-1}] 3357, 3006, 2928, 1686, 1604, 1586, 1487, 1434, 1359, 1271, 1222, 1134, 1020, 877, 795, 738, 693, 600, 588, 535, 511.

Elemental analysis for $C_{15}H_{12}F_9IO$ calculated: C: 35.60 %, H: 2.39 %

measured: C:35.88 %, H:2.27 %

2.18. 2-(7,7,8,8,9,9,10,10,10-Nonafluoro-5-iododecyl)isoindoline-1,3-dione (20)

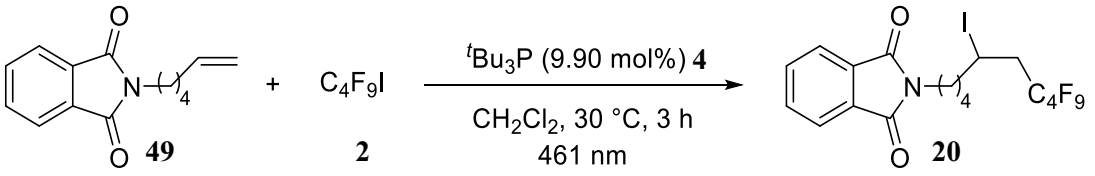

49 **2** **20**

Following **GP-C**, tri-*tert*-butylphosphine (**4**) (10.8 mg, 0.534 mmol, 9.90 mol%), 2-(hex-5-en-1-yl)isoindoline-1,3-dione (**49**) (123.6 mg, 0.539 mmol) and nonafluoro-1-iodobutane (**2**) (100 µl, 0.583 mmol, 1.08 eq.) were irradiated in CH_2Cl_2 (2 ml) for 3 h. Purification was conducted by chromatography on SiO_2 (Hexane:EtOAc 93:7) yielded pure product **20** as light brown oil.

yield (575,21 g·mol−1) 268.4 mg (0.467 mmol, 86 %)

^{1}H-NMR (300 MHz, Chloroform-*d*) δ [ppm] 7.90 – 7.77 (m, 2H, Ar-*H*), 7.77 – 7.67 (m, 2H, Ar-*H*), 4.30 (tt, J = 8.1, 5.3 Hz, 1H, C*H*I), 3.71 (t, J = 7.1 Hz, 2H, NCH_2(C_3H_6)CHI), 3.06 – 2.64 (m, 2H, CHICH_2R_F), 1.93 – 1.48 (m, 4H, NCH_2(C_3H_6)CHI).

^{19}F-NMR (282 MHz, Chloroform-*d*) δ [ppm] -81.01 (tt, *J* = 9.7, 3.3 Hz, 3F, CF_3), -111.01 – -112.75 (m, 1F, CF_2), -114.04 – -115.89 (m, 1F, CF_2), -124.23 – -124.79 (m, 2F, CF_2), -125.40 – -126.64 (m, 2F, CF_2).

Analytic data are consistent with literature-known values.[20]

2.19. 4-Chloro-N-(4,4,5,5,6,6,7,7,7-nonafluoro-2-iodoheptyl)benzamide (21)

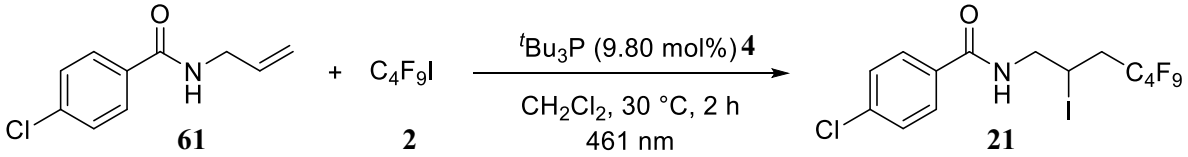

Following **GP-C**, tri-*tert*-butylphosphine (**4**) (10.7 mg, 0.0528 mmol, 9.80 mol%), *N*-allyl-4-chlorobenzamide (**61**) (105.1 mg, 0.539 mmol) and nonafluoro-1-iodobutane (**4**) (100 µl, 0.583 mmol, 1.08 eq.) were irradiated in CH_2Cl_2 (2 ml) for 2 h. Purification was conducted by chromatography on SiO_2 (Hexane:EtOAc 80:20) yielded pure product **21** as colorless crystals.

yield (541,58 g·mol−1) 257.4 mg (0.475 mmol, 88 %)

^{1}H-NMR (600 MHz, Chloroform-*d*) δ [ppm] 7.81 – 7.65 (m, 2H,), 7.54 – 7.33 (m, 2H), 6.85 – 6.48 (m, 1H), 4.65 – 4.44 (m, 1H), 4.05 – 3.85 (m, 1H), 3.80 – 3.57 (m, 1H), 2.99 – 2.75 (m, 2H).

^{13}C-NMR (75.5 MHz, Chloroform-*d*) δ [ppm] 166.6, 138.5, 132.2, 129.2, 128.6, 121.0-119.5, 48.5, 39.8 (t, *J* = 21.2), 18.9.

^{19}F-NMR (298 MHz, Chloroform-*d*) δ [ppm] -80.88 – -81.13 (t, *J* = 9.80 Hz, 3F, CF_3), -112.15 – -112.78 (m, 1F, CF_2), -113.62 – -114.26 (m, 1F, CF_2), -124.27 – -124.51 (m, 2F, CF_2), -125.73 – -125.97 (m, 2F, CF_2).

IR (film on NaCl) ν [cm^{-1}] 3303, 3075, 1643, 1598, 1539, 1488, 1433, 1353, 1303, 1234, 1135, 1095, 1016, 879, 847, 738, 689, 626, 526, 507.

Mp: 87.0-87.9 °C

Elemental analysis for $C_{14}H_{10}ClF_9INO$ calculated: C: 31.05 %, H: 1.86 %, N: 2.59 %

measured: C: 30.92 %, H: 1.73 %, N: 2.53 %

2.20. 6,6,7,7,8,8,9,9,9-Nonafluoro-4-iodononyl 4-chlorobenzoate (22)

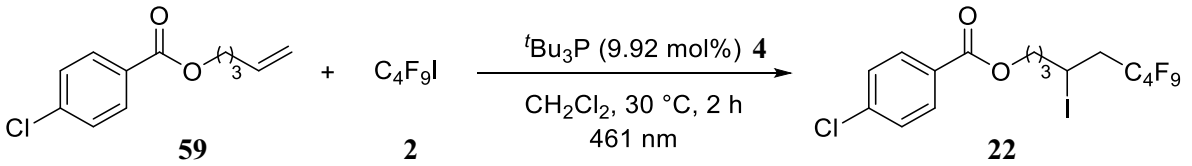

Following **GP-C**, tri-*tert*-butylphosphine (**4**) (10.7 mg, 0.0528 mmol, 9.92 mol%), pent-4-en-1-yl 4-chlorobenzoate (**59**) (119.5 mg, 0.532 mmol) and nonafluoro-1-iodobutane (**4**) (100 µl, 0.583 mmol, 1.10 eq.) were irradiated in CH_2Cl_2 (2 ml) for 2 h. Purification was conducted by chromatography on SiO_2 (pentane: Et_2O 98:2) yielded pure product **22** colorless oil.

yield (570.62 g·mol−1) 266.9 mg (0.467 mmol, 88 %)

^{1}H-NMR (600 MHz, Chloroform-*d*) δ [ppm] 8.01 – 7.93 (m, 2H, Aryl), 7.46 – 7.37 (m, 2H, Aryl), 4.44 – 4.34 (m, 3H, C*H*I, Aryl-C(O)OC*H*$_2$), 3.04 – 2.73 (m, 2H, CHIC*H*$_2$R$_f$), 2.12 – 1.84 (m, 3H, OCH$_2$(C*H*$_2$)$_2$CHI).

^{19}F-NMR (282 MHz, Chloroform-*d*) δ [ppm] -80.93 – -81.08 (t, *J*=9.73 Hz, 3F, CF_3), -111.31 – -112.03 (m, 1F, CF_2), -114.43 – -115.12 (m, 1F, CF_2), -124.31 – -124.64 (m, 2F, CF_2), -125.68 – -126.09 (m, 2F, CF_2).

Analytic data are consistent with literature-known values.[20]

2.21. 1-Bromo-4-((7,7,8,8,9,9,10,10,10-nonafluoro-5-iododecyl)oxy)benzene (23)

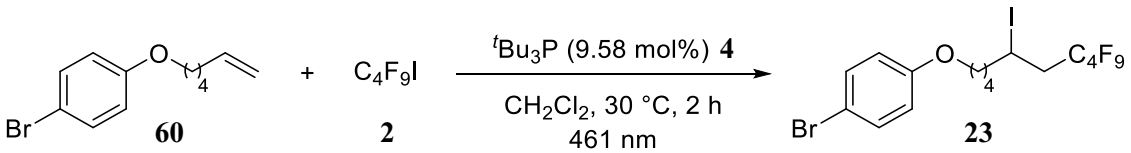

Following **GP-C**, tri-*tert*-butylphosphine (**4**) (10.8 mg, 0.0534 mmol, 9.58 mol%), 1-bromo-4-(hex-5-en-1-yloxy)benzene (**60**) (142.1 mg, 0.557 mmol) and nonafluoro-1-iodobutane (**4**) (100 µl, 0.583 mmol, 1.04 eq.) were irradiated in CH_2Cl_2 (2 ml) for 2 h. Purification was conducted by chromatography on SiO_2 (Hexane:EtOAc 99:1) followed by a second column on SiO_2 (pentane:Et_2O 99:1) yielded pure product **23** as a colorless oil.

yield (601,09 g·mol−1) 321.4 mg (0.534 mmol, 96 %)

^{1}H-NMR (300 MHz, Chloroform-*d*) δ [ppm] 7.46 – 7.31 (m, 2H), 6.85 – 6.72 (m, 2H), 4.42 – 4.29 (m, 1H), 3.95 (t, *J* = 6.0 Hz, 2H), 3.07 – 2.62 (m, 2H), 2.04 – 1.69 (m, 2H), 1.69 – 1.55 (m, 1H).

^{19}F-NMR (282 MHz, Chloroform-*d*) δ [ppm]-81.01 (tt, J = 9.7, 3.3 Hz, 3F, CF_3), -111.20 – -112.38 (m, 1F, CF_2), -114.24 – -115.45 (m, 1F, CF_2), -124.39 – -124.72 (m, 2F, CF_2), -125.65 – -126.02 (m, 2F, CF_2).

Analytic data are consistent with literature-known values.[20]

2.22. 1-Methoxy-4-(4,4,5,5,6,6,7,7,7-nonafluoro-2-iodoheptyl)benzene (24)

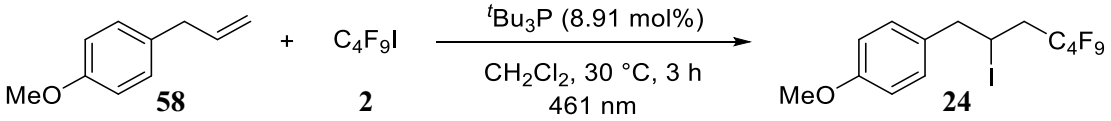

Following **GP-C**, tri-*tert*-butylphosphine (**4**) (10.6 mg, 0.0524 mmol, 8.91 mol%), 1-allyl-4-methoxybenzene (**58**) (87.2 mg, 0.588 mmol) and nonafluoro-1-iodobutane (**4**) (100 µl, 0.583 mmol, 1.00 eq.) were irradiated in CH_2Cl_2 (2 ml) for 3 h. Purification was conducted by chromatography on SiO_2 (Hexane:EtOAc 98:2) yielded pure product **24**.

yield (494,14 g·mol−1) 275.5 mg (0.557 mmol, 95 %)

^{1}H-NMR (600 MHz, Chloroform-*d*) δ [ppm] 7.18 – 7.07 (m, 2H, Ar*H*), 6.94 – 6.82 (m, 2H, Ar*H*), 4.43 (dq, *J* = 8.4, 6.4 Hz, 1H, C*H*I), 3.81 (s, 3H, OCH_3), 3.28 – 3.08 (m, 2H, ArCH_2), 3.01 – 2.73 (m, 2H, CH_2R_F).

^{19}F-NMR (282 MHz, Chloroform-*d*) δ [ppm] -81.06 (tt, *J* = 9.7, 3.2 Hz, 3F, CF_3), -111.63 – -114.70 (m, 2F, CF_2), -124.47 – -124.68 (m, 2F, CF_2), -125.82 – -126.02 (m, 2F, CF_2).

Analytic data are consistent with literature-known values.[20]

3. Screening and control reactions

3.1. Irradiating with different light sources and wavelengths

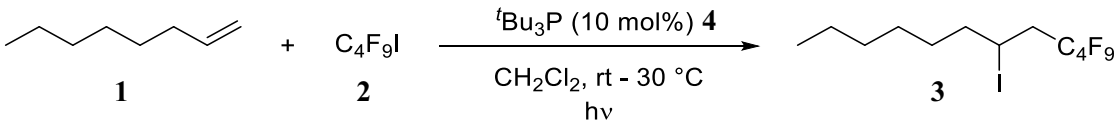

Following **GP-D**, tri-*tert*-butylphosphine (**4**) (10.6 mg, 0.0525 mmol, 10.6 mol%), 1-octene (**1**) (83 µl, 0.52 mmol) and nonafluoro-1-iodobutane (**2**) (100 µl, 0.583 mmol, 1.10 eq.) were irradiated in CH_2Cl_2 (2 ml). A sample for the NMR-spectroscopy was withdrawn under red light. Up until the measurement the NMR tube was wrapped up in aluminum foil and sealed with a black cap.

Table 6: Irradiating with different light sources for the reaction of 1-octene (**1**) with C_4F_9I **2**.

	time [h]	**conversion [%]**
without light	1	12
ambient light	1	17
red LED (630 nm)	1	10
green LED (513 nm)	1	26
blue LED (461 nm)	1	≥99
blue LED (405 nm)	0:15	≥99

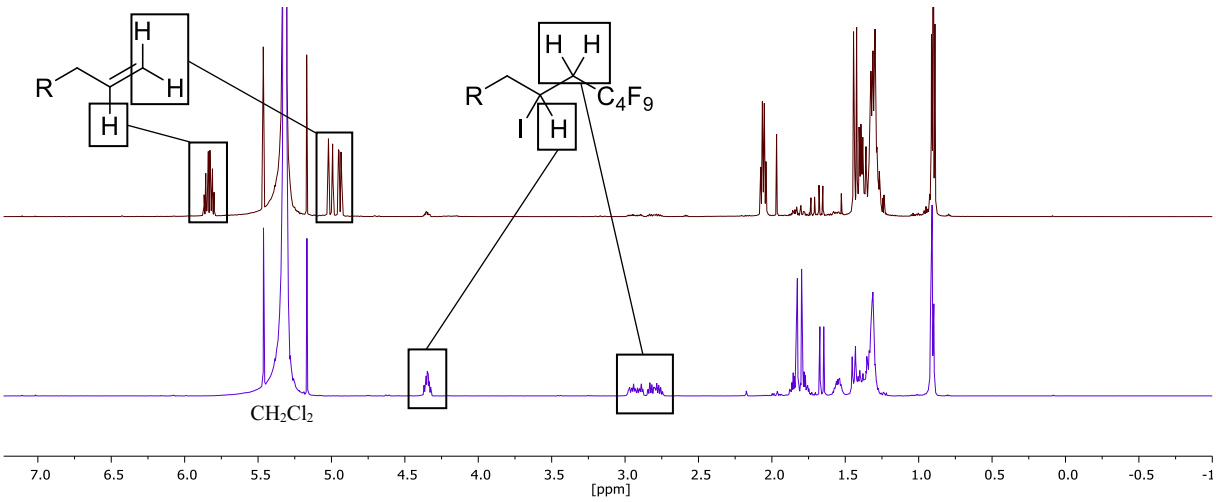

^{1}H-NMR-spectra (600 MHz, $CDCl_3$) of the reaction solution of 1-octene (1) and nonafluoro-1-iodobutane (2) irradiated at 630 nm (top) and 405 nm (bottom).

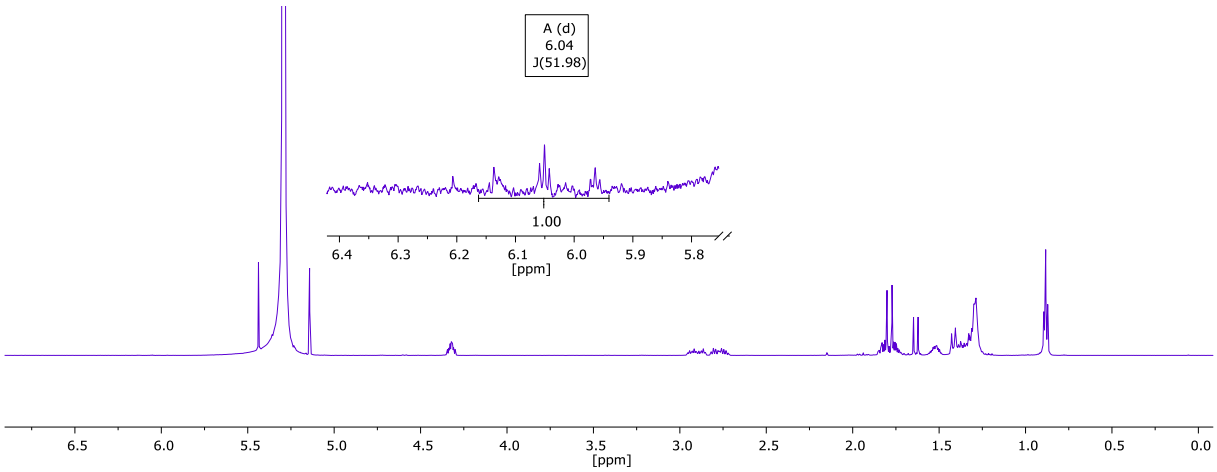

^{1}H-NMR-spectrum (600 MHz, $CDCl_3$) of the reaction solution of 1-octene (1) and nonafluoro-1-iodobutane (2) irradiated at 405 nm.

Signal at –6.04 ppm is consistent with literature known values for C_4F_9H.[2]

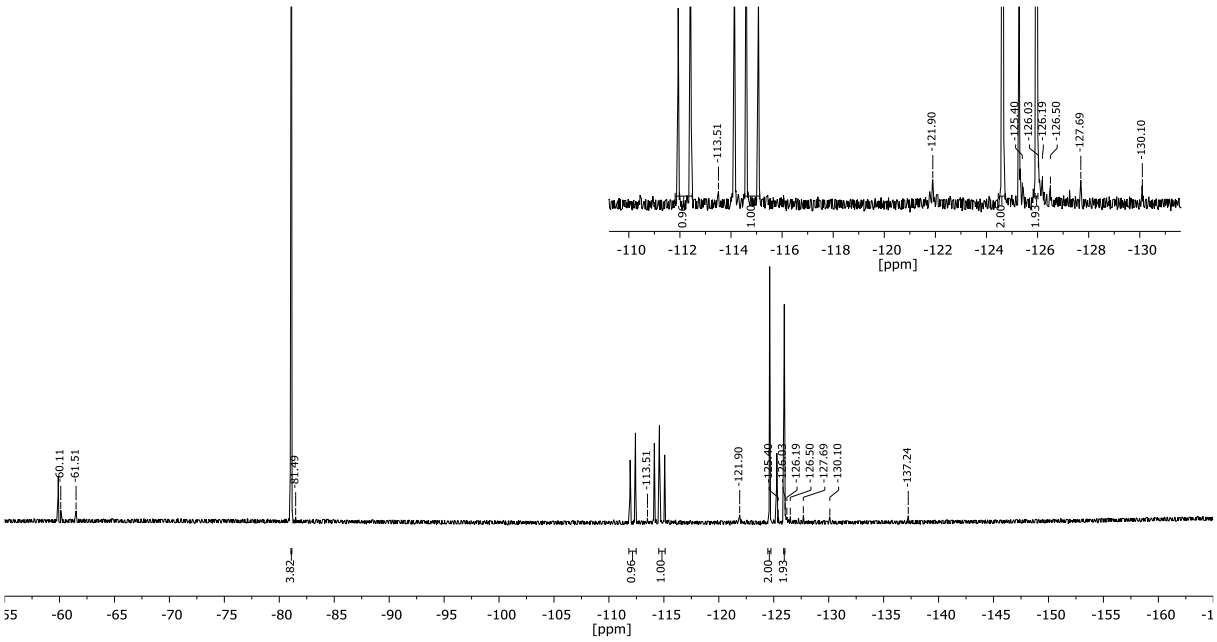

^{19}F-NMR-spectrum (564 MHz, $CDCl_3$) of the reaction solution of 1-octene (1) and nonafluoro-1-iodobutane (2) irradiated at 405 nm.

Signals at –81.49, –172.69, –130.10 and –137.24 ppm are consistent with literature known values for C_4F_9H.[2]

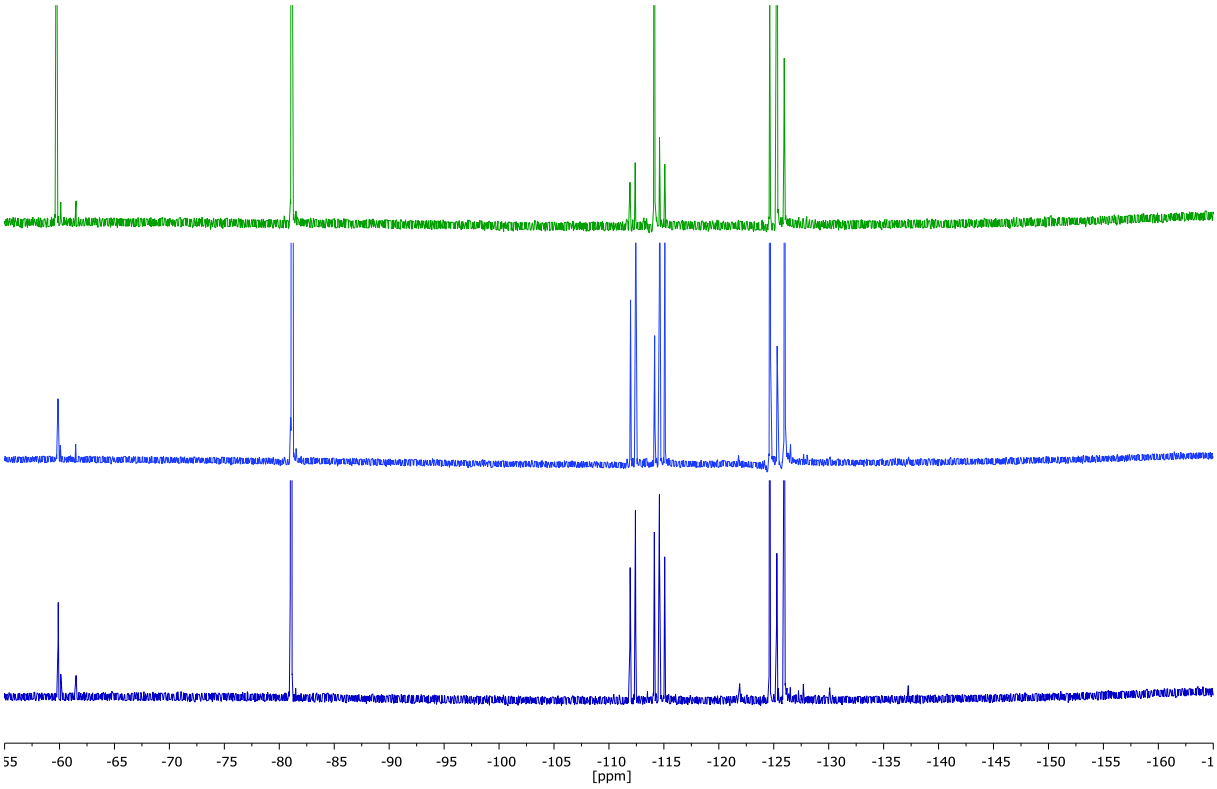

Comparison of the ^{19}F-NMR-spectra (564 MHz, $CDCl_3$) of the reaction solution of 1-octene (1) and nonafluoro-1-iodobutane (2) irradiated at 513 nm (top), 461 nm (middle) and 405 (bottom).

3.2. Solvent screening

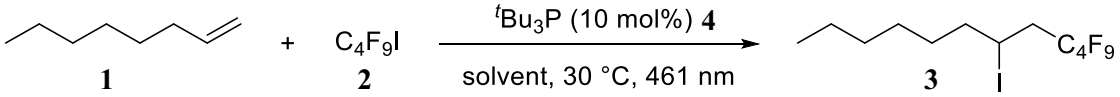

1 **2** **3**

Tri-*tert*-butylphosphine (**4**) (10.6 mg, 0.0525 mmol, 10.6 mol%), 1-octene (**1**) (83 µl, 0.52 mmol) and nonafluoro-1-iodobutane (**2**) (100 µl, 0.583 mmol, 1.10 eq.) were irradiated in the corresponding solvent (2 ml) for the indicated time.

Table 7: Solvent screening for the reaction of 1-octene (**1**) with different solvents.

solvent	time [h]	conversion [%]
Toluene[a]	2	58
Tetrahydrofuran[a]	2	52
Acetonitrile[a]	2	93
Dichloromethane[b]	1	≥99
1,2-Dichloroethane[a]	2	97
1,2-Difluorobenzene[a]	2	81
Carbon tetrachloride	1	5

a) Determination by NMR-spectroscopy

b) Determination by GC-experiment, following GP-A

3.3. Control reaction without phosphine catalyst

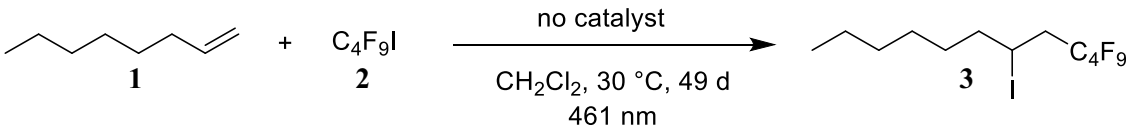

Following **GP-D**, 1-octene (**1**) (62.3 mg, 0.552 mmol) and nonafluoro-1-iodobutane (**2**) (211 mg, 0.609 mmol, 1.10 eq.) were irradiated in CH_2Cl_2 (2.1 ml) for 4 d. A sample for NMR-spectroscopy was withdrawn under red light (conversion: 0%). The reaction solution was irradiated for additional 49 d. Another sample for NMR-spectroscopy was withdrawn under red light (conversion: 32%).

3.4. Control reaction by exclusion of light

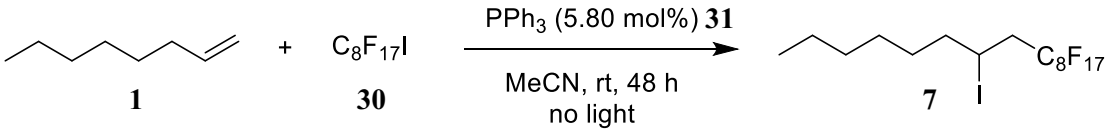

According to literature[3] in a two-neck round bottom flask, wrapped up in aluminum foil, triphenylphosphine (**31**) (47 mg, 0.18 mmol, 5.80 mol%), 1-octene (**1**) (1.23 ml, 7.78 mmol, 1.00 eq.) and heptadecafluoro-1-iodooctane (**30**) (0.82 ml, 3.1 mmol, 0.40 eq.) were stirred at rt in dry MeCN (0.93 ml) for 48 h under argon atmosphere. A sample for NMR-spectroscopy was withdrawn under red light and measured in an amber NMR-tube (no conversion). Until the measurement the NMR-tube was wrapped up in aluminum foil and sealed with a black cap. After 48 h the aluminum foil was removed from the two-neck round-bottom flask and the solution was exposed to ambient light and the fume hood lamps (fluorescent tubes). After 16 h the solution turned from a clear solution to a yellow-brownish solution (conversion: 8%).

3.5. Reaction with 2,2-diallylmalonate (28)

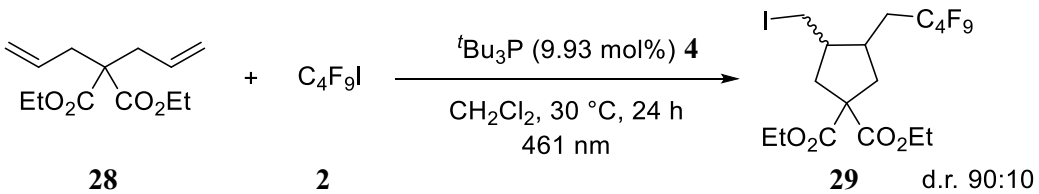

Following **GP-C**, tri-*tert*-butylphosphine (**4**) (20.1 mg, 0.0993 mmol, 9.93 mol%), 2,2-diallylmalonate (**28**) (241 mg, 1.00 mmol) and nonafluoro-1-iodobutane (**2**) (200 µl, 1.16 mmol, 1.16 eq.) were irradiated in CH_2Cl_2 (2 ml) for 24 h. Purification was conducted by column chromatography on SiO_2 (Hexane:EtOAc = 80:20).

yield (M = 586,23 g·mol^{-1}) 552 mg (0.941 mmol, 94 %)

^{1}H-NMR (300 MHz, Chloroform-*d*) δ [ppm] 4.27 – 4.16 (m, 4H), 3.15 (dd, J = 9.9, 4.4 Hz, 1H), 3.04 (t, J = 9.8 Hz, 1H), 2.66 – 2.47 (m, 4H), 2.39 – 1.96 (m, 3H), 1.25 (q, J = 7.1 Hz, 6H).

^{19}F-NMR (565 MHz, Chloroform-*d*) δ [ppm] -81.05 (t, J = 10.1 Hz), -112.56 (dt, J = 271.4, 13.9 Hz), -114.60 (dt, J = 270.8, 13.3 Hz), -124.39 (p, J = 11.9, 11.2 Hz), -125.90 (dt, J = 26.3, 13.5 Hz).

Analytic data are consistent with literature-known values.[4]

3.6. Reaction with (2,2,6,6-Tetramethylpiperidin-1-yl)oxyl (25) (TEMPO)

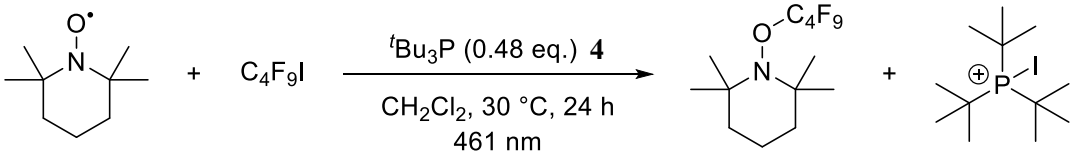

25 **2** **26** **32**

Following **GP-C** and according to literature[5], tri-*tert*-butylphosphine (**4**) (11.3 mg, 0.0558 mmol, 0.48 eq.), TEMPO **25** (20.1 mg, 0.128 mmol, 1.10 eq.) and nonafluoro-1-iodobutane (**2**) (20 µl, 0.116 mmol, 1.00 eq.) in CH_2Cl_2 (2.1 ml) were irradiated for 24 h. Purification was conducted by chromatography on SiO_2 (CH_2Cl_2:MeOH = 9:1)

ESI for $C_{13}H_{19}F_9NO$ ($M + H^+$): 376.3

ESI for $C_{12}H_{27}PI^+$ (M^+): 329.1

Comparing literature for compound **26**.[5]

3.7. Reaction with styrene (33)

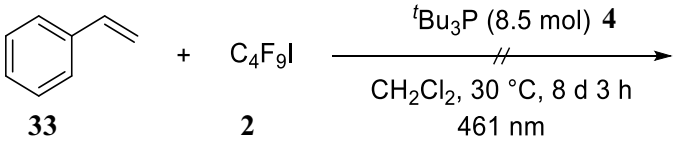

33 **2**

Following **GP-C**, tri-*tert*-butylphosphine (**4**) (5.7 mg, 0.028 mmol, 8.5 mol), styrene (**33**) (34.7 mg, 0.531 mmol) and nonafluoro-1-iodobutane (**2**) (50 µl, 0.30 mmol, 1.0 eq.) were irradiated in CH_2Cl_2 (1 ml) for 8 d 3 h. A sample for the NMR-spectroscopy was withdrawn from the dark red solution showing no conversion.

3.8. Reaction with styrene (33) and vinylcyclohexane (34)

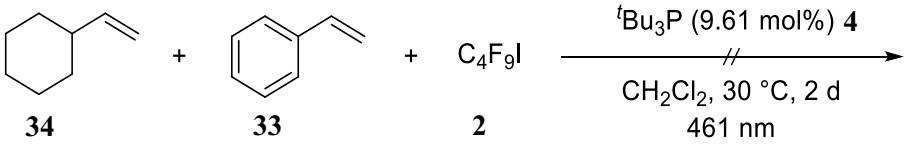

34 **33** **2**

Following **GP-C**, tri-*tert*-butylphosphine (**4**) (10.7 mg, 0.0530 mmol, 9.61 mol%), vinylcyclohexane (**34**) (60.5 mg, 0.550 mmol) styrene (**33**) (64.9 mg, 0.623 mmol, 1.13 eq.) and nonafluoro-1-iodobutane (**2**) (200 µl, 1.16 mmol, 2.12 eq.) were irradiated in CH_2Cl_2 (2 ml) for 2 d. A sample for the NMR-spectroscopy was withdrawn from the dark brown solution showing no conversion.

3.9. Reaction with *trans*-stilbene (35)

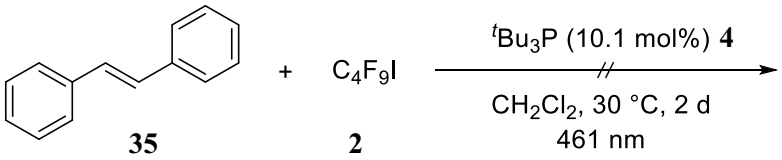

Following **GP-D**, tri-*tert*-butylphosphine (**4**) (10.9 mg, 0.0538 mmol, 10.1 mol%), *trans*-stilbene (**35**) (95.8 mg, 0.531 mmol) and nonafluoro-1-iodobutane (**2**) (200 µl, 1.16 mmol, 2.18 eq.) were irradiated in CH_2Cl_2 (2 ml) for 42 h. A sample for the NMR-spectroscopy was withdrawn from the orange-brown solution showing no conversion.

3.10. Reaction with 2,3-dichloroprop-1-ene (36)

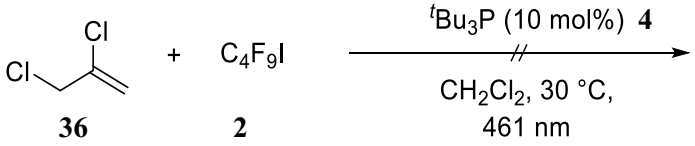

Following **GP-C**, tri-*tert*-butylphosphine (**4**) (10.7 mg, 0.0528 mmol, 8.81 mol%), 2,3-dichloroprop-1-ene (**36**) (66.5 mg, 0.600 mmol) and nonafluoro-1-iodobutane (**2**) (100 µl, 0.583 mmol, 0.972 eq.) were irradiated in CH_2Cl_2 (2 ml) for 2 h 53min. A sample for the NMR-spectroscopy was withdrawn from the redish solution showing no conversion.

4. Educt synthesis

4.1. Dec-9-en-1-yl-4-methylbenzenesulfonate (39)

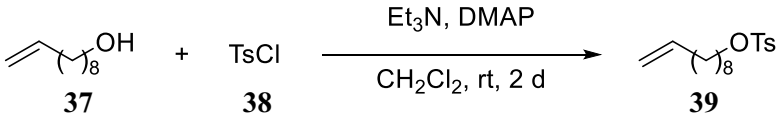

37 **38** **39**

The synthesis of dec-9-en-1-yl 4-methylbenzenesulfonate (**39**) was conducted according to a literature known procedure.[6] 9-Decen-1-ol (**37**) (3.07 g, 19.6 mmol, 1.00 eq.) was dissolved in dry CH_2Cl_2 (30 ml). Subsequently, dry triethylamine (3.50 ml, 25.1 mmol, 1.28 eq.) was added via syringe and DMAP (84 mg, 0.69 mmol, 3.5 mol%) as well as tosyl chloride (**38**) (3.75 g, 19.7 mmol, 1.01 eq.) were added in N_2 counterflow. After 2 d, H_2O (10 ml) was added, phases were separated and the aqueous phase was extracted with $CHCl_3$ (3 x 10 ml). Combined organic phases were washed with saturated NH_4Cl solution (10 ml), dried with $MgSO_4$, filtered and evaporated. Purification was conducted by chromatography on SiO_2 (*n*-hexane:EtOAc = 78:22) gave pure product **39**.

yield (M = 310.45 g·mol^{-1}) 4.97 g (16.0 mmol, 82%)

^{1}H-NMR (300 MHz, Chloroform-*d*) δ [ppm] 7.79 (d, *J* = 8.3 Hz, 2H), 7.34 (d, *J* = 7.8 Hz, 1H), 5.80 (ddt, *J* = 16.9, 10.2, 6.7 Hz, 1H), 5.04 – 4.88 (m, 2H), 4.02 (t, *J* = 6.5 Hz, 2H), 2.45 (s, 3H), 2.10 – 1.94 (m, 2H), 1.69 – 1.53 (m, 2H), 1.44 – 1.14 (m, 10H).

Analytic data are consistent with literature known values.[7]

4.2. 10-Azido-dec-1-ene (41)

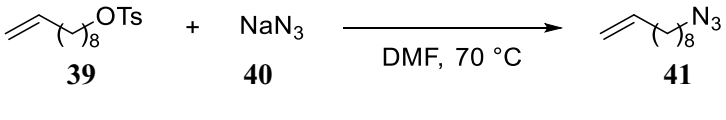

39 **40** **41**

The synthesis of 10-azidodec-1-ene (**41**) was conducted similar to a literature known procedure.[8] Dec-9-en-1-yl 4-methylbenzenesulfonate (**39**) (7.16 g, 23.1 mmol, 1.00 eq.) was dissolved in dry DMF (35 ml) and sodium azide (**40**) (2.25 g, 34.6 mmol, 1.50 eq.) was added in N_2 counterflow. The solution was heated to 70 °C overnight. H_2O (30 ml) was added, phases were separated and the aqueous layer was extracted with hexane (4 x 30 ml). Combined organic phases were washed with brine (2 x 15 ml), dried with $MgSO_4$, filtered and then evaporated. Purification was conducted by chromatography on SiO_2 (Hexane:EtOAc = 98:2) yielded a transparent liquid.

yield (M = 181.28 g·mol^{-1}) 4.02 g (22.2 mmol, 96%)

^{1}H-NMR (300 MHz, Chloroform-*d*) δ [ppm] 5.81 (ddt, *J* = 16.6, 9.8, 6.6 Hz, 1H), 5.09 – 4.87 (m, 2H), 3.26 (t, *J* = 6.9 Hz, 2H), 2.05 (q, *J* = 6.9 Hz, 2H), 1.59 (h, *J* = 6.5, 6.0 Hz, 2H), 1.46 – 1.23 (m, 10H).

Analytic data are consistent with literature known values.[8]

4.3. Pent-4-enamide (44)

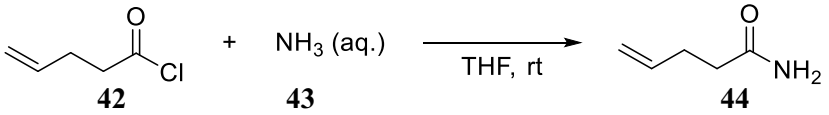

42 **43** **44**

The synthesis of pent-4-enamide (**44**) was conducted similar to a literature-known procedure.[9] A mixture of THF (64 ml) and aqueous ammonia **43** (25 w%, 63 ml, 0.82 mol, 26 eq.) was cooled with an ice bath. To this solution pent-4-enoyl chloride (**42**) (3.70 g, 31.2 mmol, 1.00 eq.) was added and the cooling bath was removed. The resulting two phase system was stirred vigorously for 18 h. THF was removed at a rotary evaporator, giving a single-phase system. This was diluted with desalinated water (20 ml), extracted with EtOAc (3 x 60 ml) and the organic phase was washed with brine. Due to an incomplete extraction (TLC), the combined aqueous layers were extracted with EtOAc (2 x 40 ml) once more. After removal of all volatiles from the combined aqueous layers, the resulting solid was dissolved in desalinated water (60 ml) and then an extraction with EtOAc (3 x 30 ml) was conducted. Combined organic layers were washed with brine (30 ml) and then dried with $MgSO_4$. After removal of all volatiles, the colorless residue was dissolved in EtOAc (50 ml), the resulting suspension washed with brine (15 ml) and then $MgSO_4$ was used to dry the organic phase. After removal of all volatiles, a colorless solid was obtained.

yield (M = 99.13 g·mol^{-1}) 2.76 g (27.8 mmol, 89%)

^{1}H-NMR (300 MHz, Chloroform-*d*) δ [ppm] 5.85 (ddt, *J* = 17.2, 10.2, 6.3 Hz, 1H), 5.59 (s, 2H), 5.10 (dq, *J* = 17.3, 1.7 Hz, 1H), 5.06 – 5.01 (m, 1H), 2.47 – 2.29 (m, 4H).

Analytic data are consistent with literature known values.[10]

4.4. 1-(3-Allylphenyl)ethan-1-one (46)

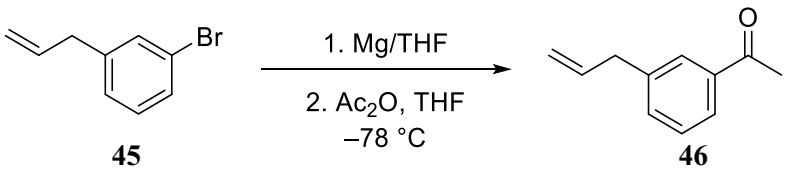

45 **46**

The synthesis of 1-(3-allylphenyl)ethan-1-one (**46**) was conducted according to a literature known procedure.[11] Activated magnesium (0.888 g, 36.5 mmol, 3.00 eq.) was suspended in dry THF (3 ml). A few drops 1-allyl-3-bromobenzene (**45**) were added to the suspended magnesium. Then, a solution of 1-allyl-3-bromobenzene (**45**) (overall 2.40 g, 12.2 mmol, 1.00 eq.) in dry THF (12 ml) was transferred into a dropping funnel and slowly added within 1 h avoiding reflux. A solution of freshly distilled acetic anhydride (3.73 g, 36.5 mmol, 3.00 eq.) in dry THF (30 ml) was cooled to −78 °C and the Grignard solution was slowly added within 25 min. After 30 min, saturated NH_4Cl solution (15 ml) was added to quench the reaction and the solution was allowed to warm up. Phases were separated and the aqueous layer was extracted with Et_2O (3 x 10 ml). Combined organic layers were washed with brine (15 ml),

dried with $MgSO_4$, filtered and then evaporated. Purification was conducted by chromatography on SiO_2 (Hexane:EtOAc = 95:5) gave pure product **46**.

yield (M = 160.22 g·mol^{-1}) 1.57 g (9.80 mmol, 80%)

^{1}H-NMR (300 MHz, Chloroform-*d*) δ [ppm] 7.83 – 7.76 (m, 2H), 7.42 – 7.36 (m, 2H), 5.97 (ddt, *J* = 18.3, 9.3, 6.7 Hz, 1H), 5.15 – 5.03 (m, 2H), 3.45 (d, *J* = 6.8 Hz, 2H), 2.60 (s, 3H).

Analytic data are consistent with literature known values.[11]

4.5. 2-(Hex-5-en-1-yl)isoindoline-1,3-dione (49)

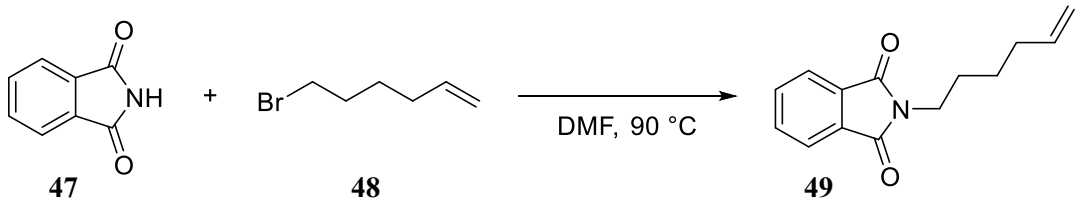

47 **48** **49**

The synthesis of 2-(hex-5-en-1-yl)isoindoline-1,3-dione (**49**) was conducted similar to a literature known procedure. 6-Bromohexene (**48**) (3.45 g, 21.2 mmol, 1.00 eq.) was dissolved in dry DMF (23 ml). Phthalimide potassium salt (**47**) (4.34 g, 23.4 mmol, 1.11 eq) was added in N_2 counterflow and the solution was heated to 90 °C for 21 h. The reaction solution was rinsed into desalinated water (75 ml), followed by rinsing with CH_2Cl_2 (50 ml). The phases were separated and the aqueous phase was extracted with CH_2Cl_2 (1 x 50 ml, 2 x 30 ml). Combined organic layers were washed with aq. KOH (0.2 M, 100 ml) as well as a mixture of brine and desalinated water (1:1, 50 ml) and then dried with Na_2SO_4. After removal of all volatiles. Purification was conducted by chromatography on SiO_2 (Hexane:EtOAc = 90:10) yielded pure product **49**.

yield (229.28 g·mol^{-1}) 3.08 g (13.4 mmol, 63%)

^{1}H-NMR (600 MHz, $CDCl_3$) δ [ppm] 7.83 – 7.78 (m, 2H), 7.72 – 7.64 (m, 2H), 5.75 (ddt, *J* = 16.9, 10.2, 6.7 Hz, 1H), 4.98 (dq, *J* = 17.1, 1.7 Hz, 1H), 4.95 – 4.88 (m, 1H), 3.67 (t, *J* = 7.3 Hz, 2H), 2.12 – 2.02 (m, 2H), 1.72 – 1.62 (m, 2H), 1.47 – 1.37 (m, 2H).

Analytic data are consistent with literature-known values.[12]

5. UV-Vis-Measurements

All samples with air- and moisture-sensitive phosphines were prepared inside the glovebox and were measured in dried and degassed CH_2Cl_2. Nonafluoro-1-iodobutane (**2**) was purified as described in the general experimental procedure and was used as colorless liquid.

5.1. Nonafluoro-1-iodobutane (2)

C_4F_9I **2** (34.6 mg, 0.100 mmol) was dissolved in CH_2Cl_2 (10.0 ml) inside the glovebox in a volumetric flask. This solution was diluted in a volumetric flask (200 µL in 2.00 ml). The following concentration was present: $[C_4F_9I]$ = 1.0 mM.

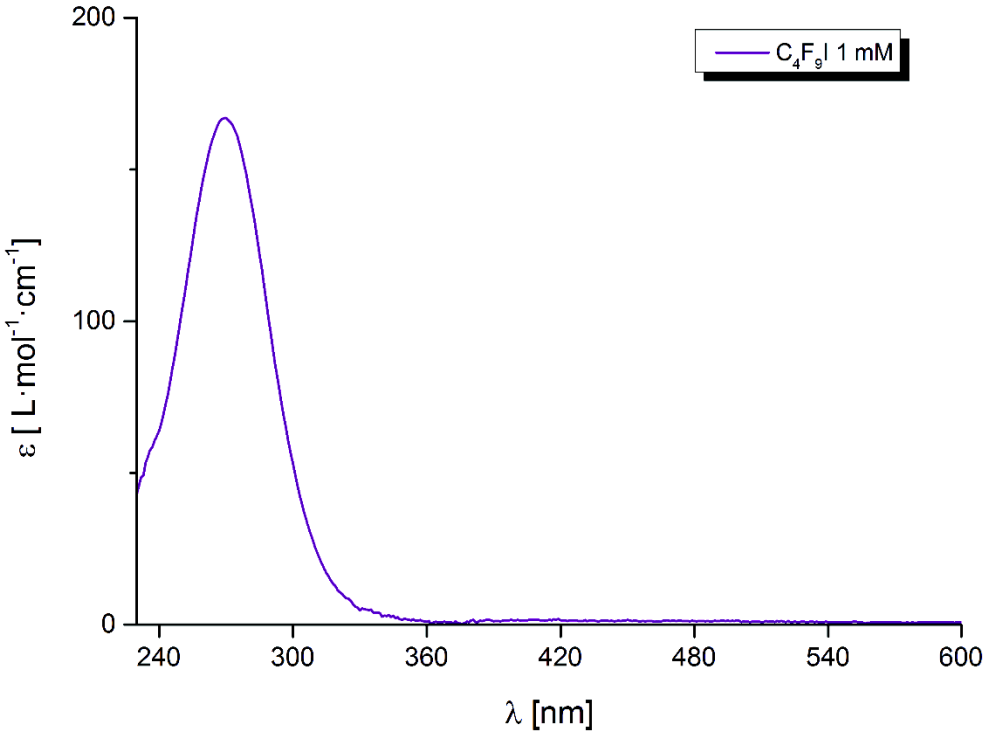

Figure 1: UV-VIS-spectra of C_4F_9I **2** (λ_{max} = 270 nm)

5.2. Tri-*tert*-butylphosphine (4) and mixture of $^{t}Bu_3P$ (4) and C_4F_9I 2

$^{t}Bu_3P$ **4** (20.2 mg, 0.100 mmol) was dissolved in CH_2Cl_2 (10.0 ml) in a volumetric flask inside the glovebox. This solution was diluted in a volumetric flask (200 µL in 2.00 ml). The following concentration was present: [$^{t}Bu_3P$] = 1 mM

$^{t}Bu_3P$ **4** (20.2 mg, 0.100 mmol) and C_4F_9I **2** (34.6 mg, 0.100 mmol) were dissolved in CH_2Cl_2 (10.0 ml) in a volumetric flask inside the glovebox. This solution was diluted in a volumetric flask (200 µL in 2.00 ml). The following concentration was present: [$^{t}Bu_3P$] = 1 mM, [C_4F_9I] = 1 mM.

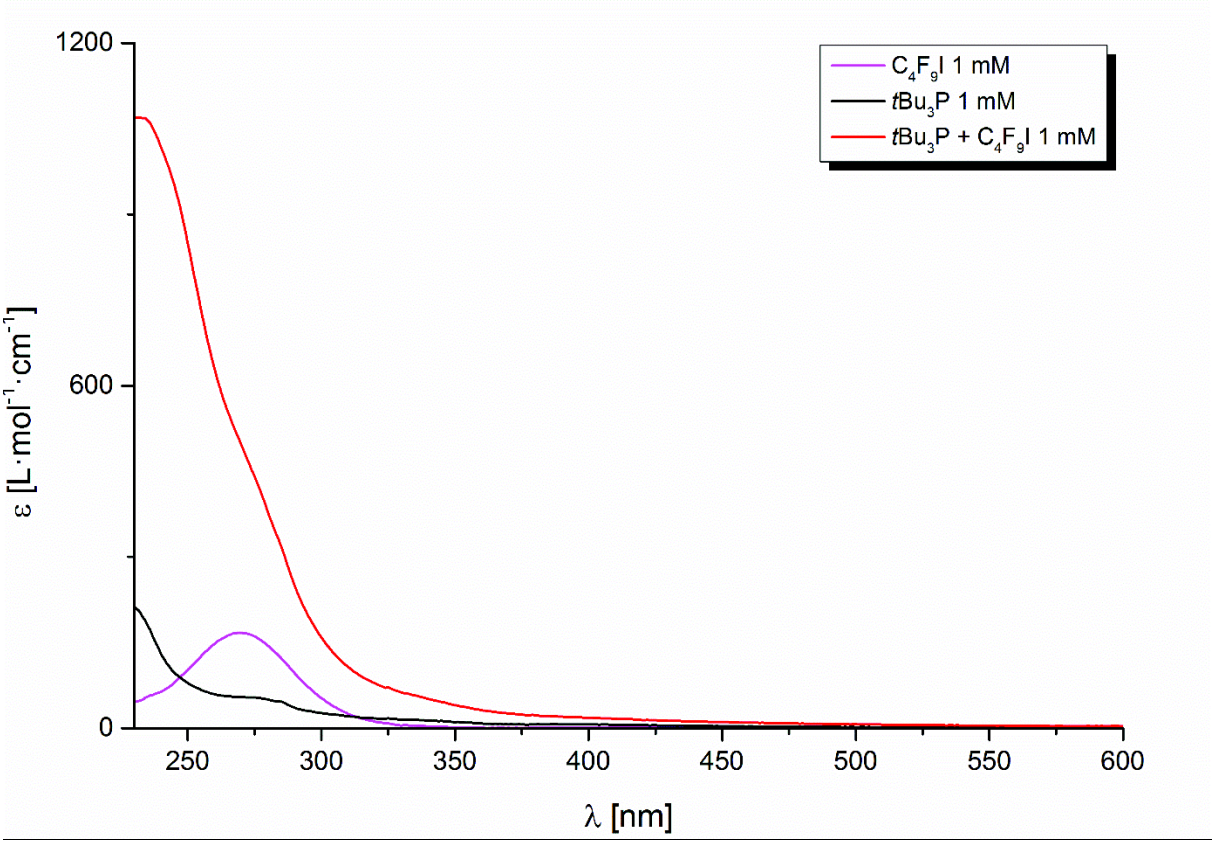

Figure 2: UV-VIS-spectra of C_4F_9I **2** (λ_{max} = 270 nm), $^{t}Bu_3P$ **4** (λ_{max} = 227 nm) and a mixture of $^{t}Bu_3P$ **4** and C_4F_9I **2** (λ_{max} = 232 nm)

5.3. Tri-*n*-butylphosphine and mixture of $^{n}Bu_3P$ and C_4F_9I 2

$^{n}Bu_3P$ (20.2 mg, 0.100 mmol) was dissolved in CH_2Cl_2 (10.0 ml) in a volumetric flask inside the glovebox. This solution was diluted in a volumetric flask (200 µL in 2.00 ml). The following concentration was present: [$^{n}Bu_3P$] = 1 mM

$^{n}Bu_3P$ (20.2 mg, 0.100 mmol) and C_4F_9I **2** (34.6 mg, 0.100 mmol) were dissolved in CH_2Cl_2 (10.0 ml) in a volumetric flask inside the glovebox. This solution was diluted in a volumetric flask (200 µL in 2.00 ml). The following concentration was present: [$^{n}Bu_3P$] = 1 mM, [C_4F_9I] = 1 mM.

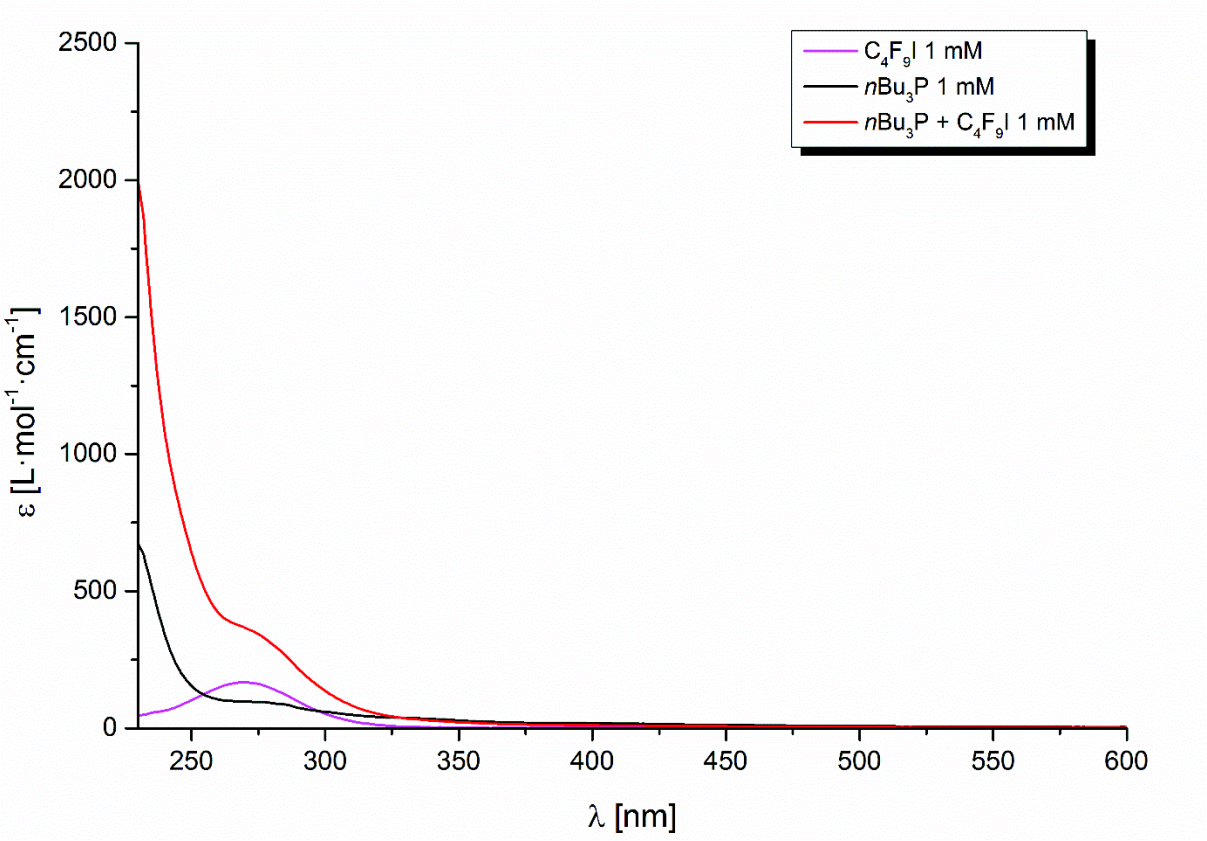

Figure 3: UV-VIS-spectra of C_4F_9I **2** (λ_{max} = 270 nm), $^{n}Bu_3P$ (λ_{max} = 227 nm) and a mixture of $^{n}Bu_3P$ and C_4F_9I **2** (λ_{max} = 229 nm)

5.4. Trimethylphosphite and mixture of $(MeO)_3P$ and C_4F_9I 2

$(MeO)_3P$ (12.4 mg, 0.100 mmol) was dissolved in CH_2Cl_2 (10.0 ml) in a volumetric flask. This solution was diluted in a volumetric flask (200 µL in 2.00 ml). The following concentration was present: $[(MeO)_3P]$ = 1 mM

$(MeO)_3P$ (12.4 mg, 0.100 mmol) and C_4F_9I **2** (34.6 mg, 0.100 mmol) were dissolved in CH_2Cl_2 (10.0 ml) in a volumetric flask inside the glovebox. This solution was diluted in a volumetric flask (200 µL in 2.00 ml). The following concentration was present: $[(MeO)_3P]$ = 1 mM, $[C_4F_9I]$ = 1 mM.

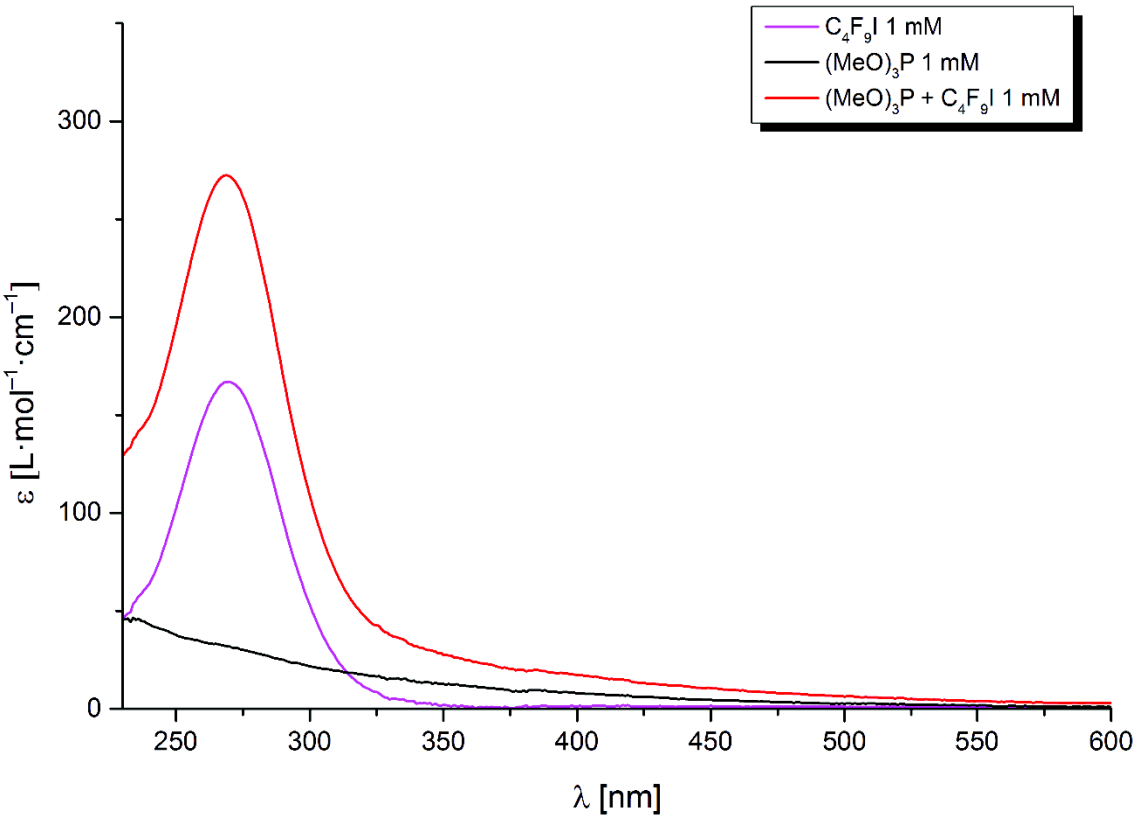

Figure 4: UV-VIS-spectra of C_4F_9I **2** (λ_{max} = 270 nm), $(MeO)_3P$ (λ_{max} = 234 nm) and a mixture of $(MeO)_3P$ and C_4F_9I **2** (λ_{max} = 269 nm)

5.5. Tricyclohexylphosphite and mixture of Cy_3P and C_4F_9I 2

Cy_3P (28.1 mg, 0.100 mmol) was dissolved in CH_2Cl_2 (10.0 ml) in a volumetric flask inside the glovebox. This solution was diluted in a volumetric flask (200 µL in 2.00 ml). The following concentration was present: [Cy_3P] = 1 mM

Cy_3P (28.1 mg, 0.100 mmol) and C_4F_9I **2** (34.6 mg, 0.100 mmol) were dissolved in CH_2Cl_2 (10.0 ml) in a volumetric flask inside the glovebox. This solution was diluted in a volumetric flask (200 µL in 2.00 ml). The following concentration was present: [Cy_3P] = 1 mM, [C_4F_9I] = 1 mM.

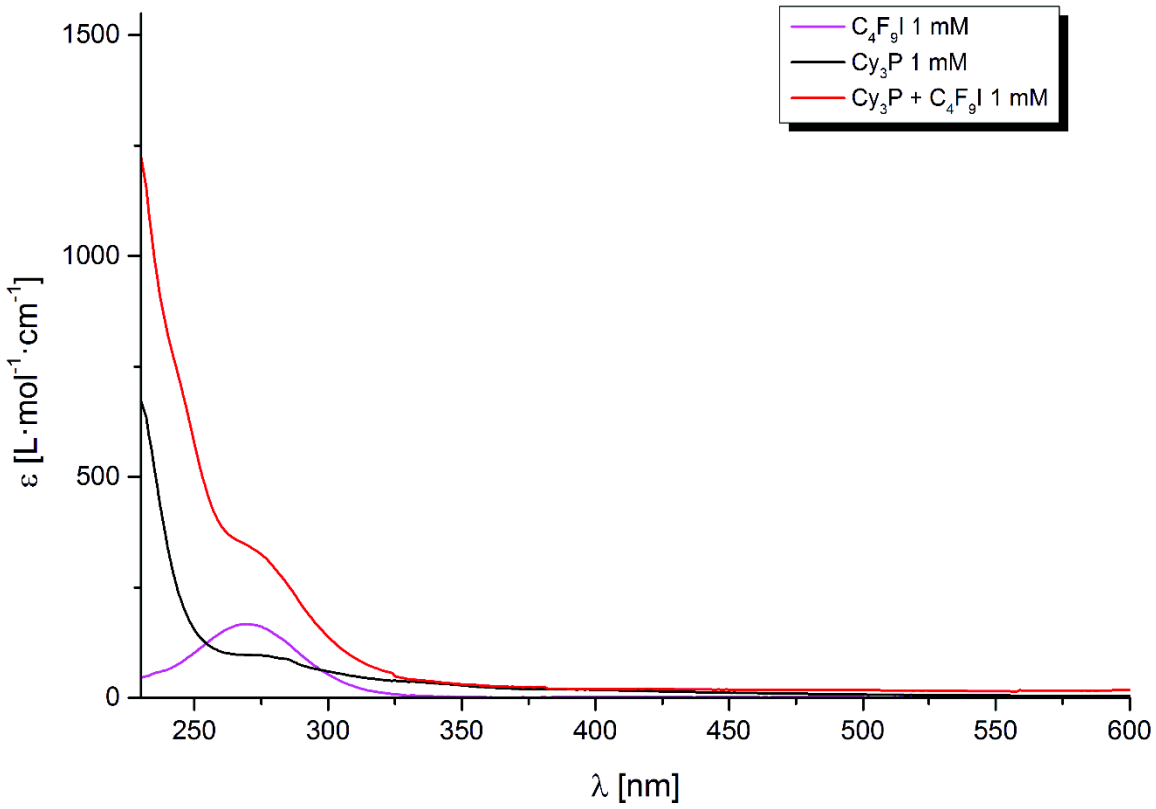

Figure 5: UV-VIS-spectra of C_4F_9I **2** (λ_{max} = 270 nm), Cy_3P (λ_{max} = 227 nm) and a mixture of Cy_3P and C_4F_9I **2** (λ_{max} = 228 nm)

5.6. Triethylamine and mixture of Et_3N and C_4F_9I 2

Et_3N (10.1 mg, 0.100 mmol) was dissolved in CH_2Cl_2 (10.0 ml) in a volumetric. This solution was diluted in a volumetric flask (200 µL in 2.00 ml). The following concentration was present: [Et_3N] = 1 mM

Et_3N (10.1 mg, 0.100 mmol) and C_4F_9I **2** (34.6 mg, 0.100 mmol) were dissolved in CH_2Cl_2 (10.0 ml) in a volumetric flask. This solution was diluted in a volumetric flask (200 µL in 2.00 ml). The following concentration was present: [Et_3N] = 1 mM, [C_4F_9I] = 1 mM.

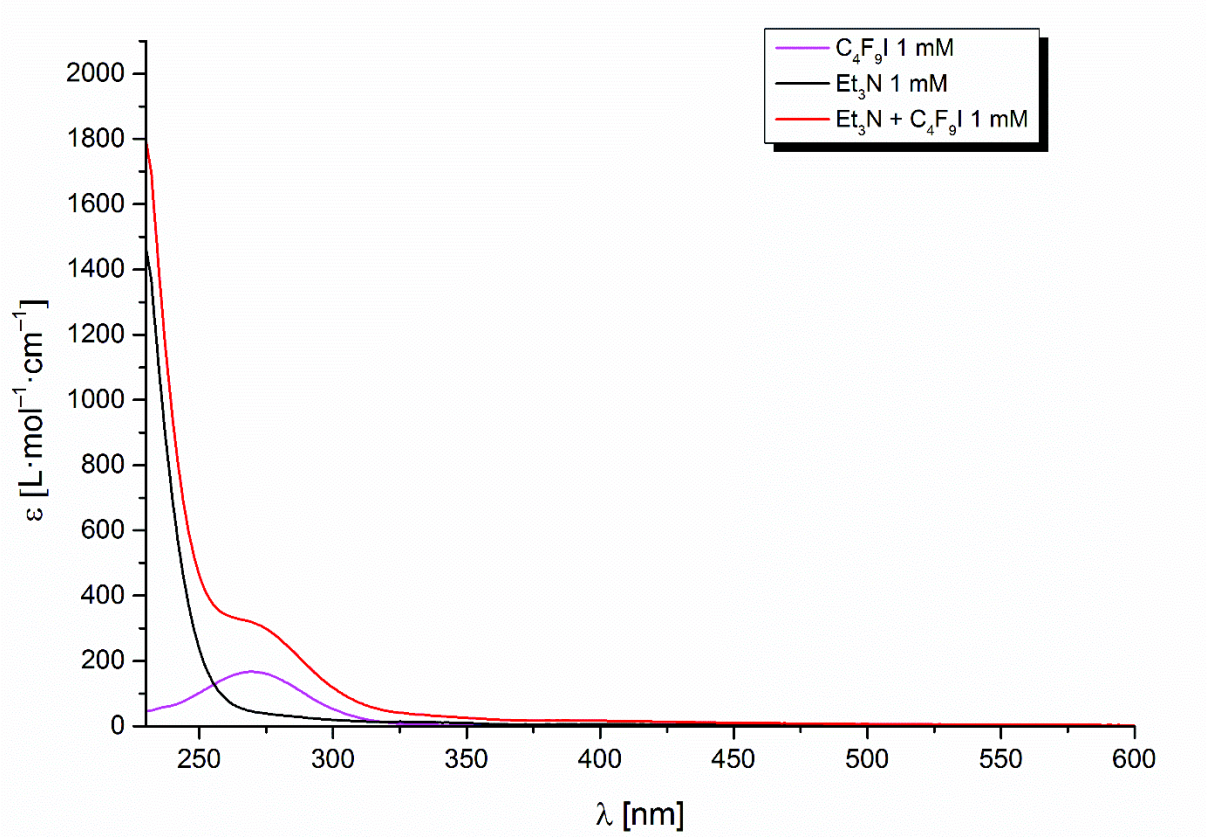

Figure 6: UV-VIS-spectra of C_4F_9I **2** (λ_{max} = 270 nm), Et_3N (λ_{max} = 229 nm) and a mixture of Et_3N and C_4F_9I **2** (λ_{max} = 230 nm)

5.7. Pyrrolidine and mixture of Et_3N and C_4F_9I 2

Pyrrolidine (7.1 mg, 0.100 mmol) was dissolved in CH_2Cl_2 (10.0 ml) in a volumetric. This solution was diluted in a volumetric flask (200 µL in 2.00 ml). The following concentration was present: [Pyrrolidine] = 1 mM

Pyrrolidine (7.1 mg, 0.100 mmol) and C_4F_9I **2** (34.6 mg, 0.100 mmol) were dissolved in CH_2Cl_2 (10.0 ml) in a volumetric flask. This solution was diluted in a volumetric flask (200 µL in 2.00 ml). The following concentration was present: [Pyrrolidine] = 1 mM, [C_4F_9I] = 1 mM.

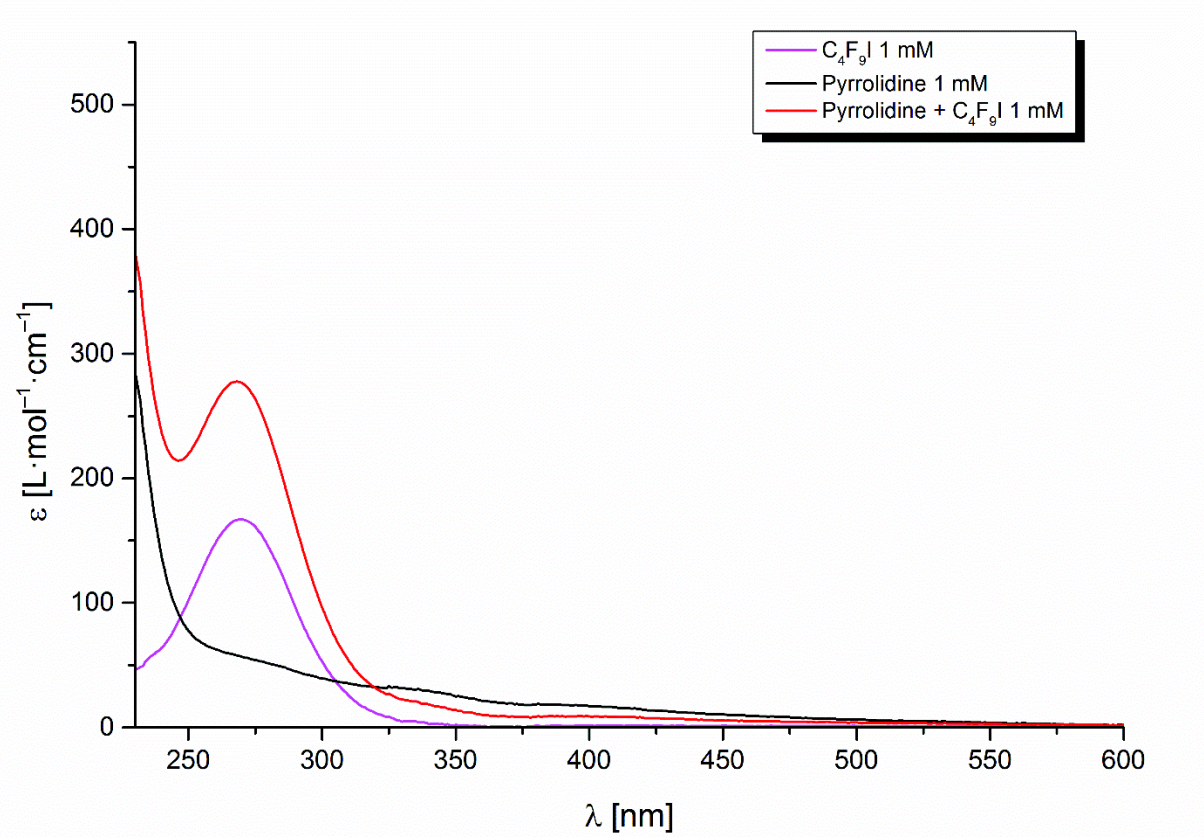

Figure 7: UV-VIS-spectra of C_4F_9I **2** (λ_{max} = 270 nm), Pyrrolidine (λ_{max} = 227 nm) and a mixture of Pyrrolidine and C_4F_9I **2** (λ_{max} = 226 nm)

5.8. TEEDA and mixture of TEEDA and C_4F_9I 2

TEEDA (17.2 mg, 0.100 mmol) was dissolved in CH_2Cl_2 (10.0 ml) in a volumetric. This solution was diluted in a volumetric flask (200 µL in 2.00 ml). The following concentration was present: [TEEDA] = 1 mM

TEEDA (17.2 mg, 0.100 mmol) and C_4F_9I **2** (34.6 mg, 0.100 mmol) were dissolved in CH_2Cl_2 (10.0 ml) in a volumetric flask. This solution was diluted in a volumetric flask (200 µL in 2.00 ml). The following concentration was present: [TEEDA] = 1 mM, [C_4F_9I] = 1 mM.

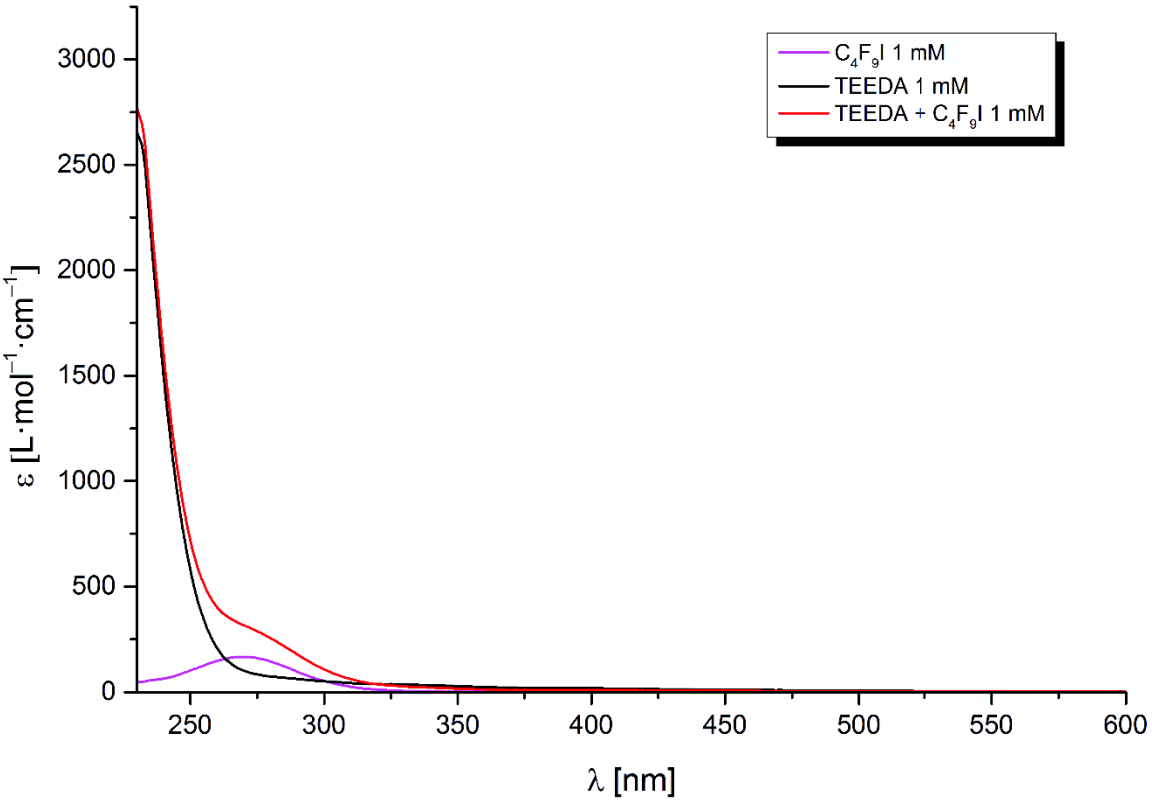

Figure 8: UV-VIS-spectra of C_4F_9I **2** (λ_{max} = 270 nm), TEEDA (λ_{max} = 231 nm) and a mixture of TEEDA and C_4F_9I **2** (λ_{max} = 230 nm)

6. Photoreactor

We designed two different reactor setups which mainly differ regarding their control of the light source. In both cases our light source is a high density RGB LED strip (120 LEDs/m, 12 V). The LED strip was purchased from aliexpress.com. (Brand Name: XUNATA, Size: L500cm (5M) x W1cm x T0.2cm, Protection Rate: not waterproof)

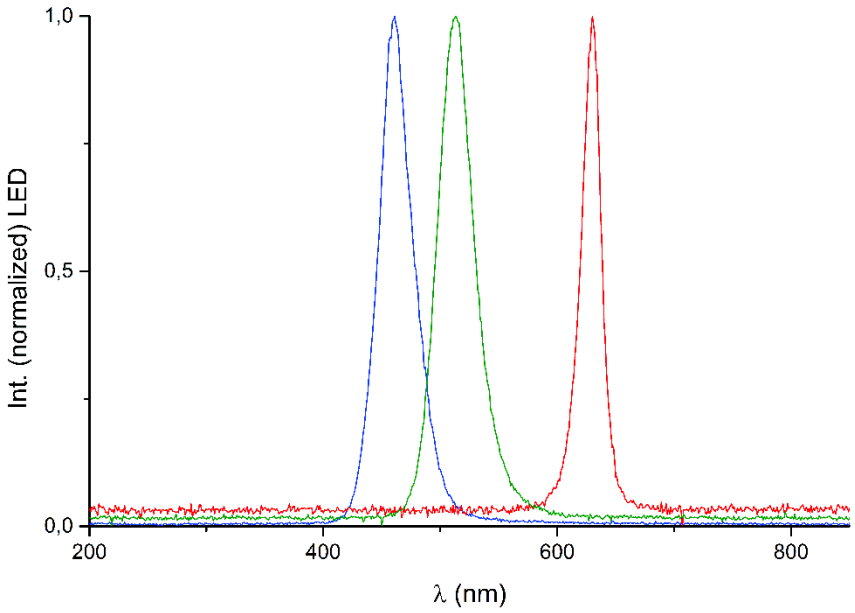

Figure 9: Wavelength of the used LEDs inside the photoreactor:

λ_{max}(blue) = 461 nm, λ_{max}(green) = 513 nm, λ_{max}(red) = 630 nm.

This strip was glued onto a copper pipe (outer diameter: 60 mm, wall thickness: 0.6 mm) or an aluminium pipe (AlMgSi0.5, outer diameter 80 mm, wall thickness: 5 mm) with thermal adhesive to improve heat dissipation. To dissipate the heat efficiently we arranged a cooling fan right below the reaction chamber. Reaction temperatures were determined inside the reactor. They are constantly between 28-32 °C. Since a high intensity light source is used, we designed a special lid for these reactors to prevent eye damage (**Figure**).

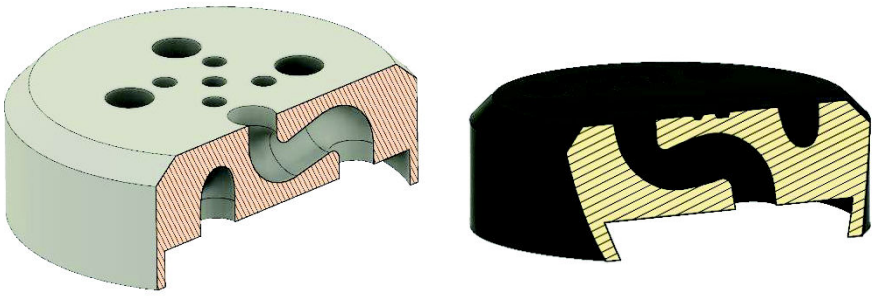

Figure 10: Cut of the modelled lid with holes for NMR-tubes (left) and without (right).

On the one hand, air can flow through specially designed air ducts. On the other hand, no irradiation can exit the reactor. For security reasons we installed a switch in NO-mode (normally open), which is closed by a putting on the lid.

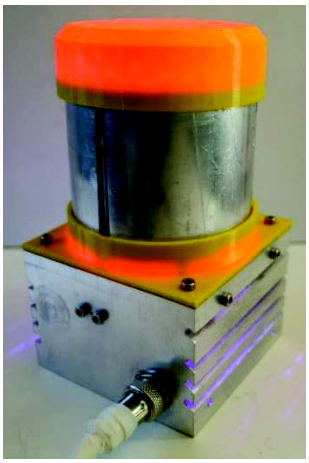

Figure 11: Photoreactor in operation.

Figure 12: Controller using coloured switches.

Figure 13: Combination of the photoreactor and the controller.

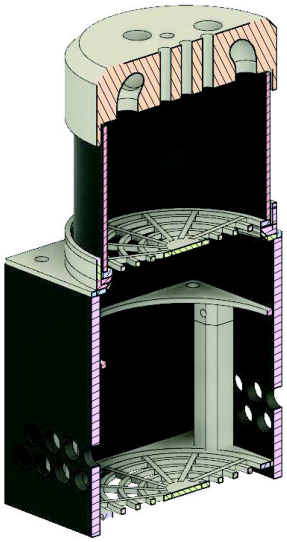

Figure 14: Cut of a modelled photoreactor.

Figure 15: Photoreactor with LCD-display**.**

Figure 16: Active photoreactor.

All used materials are cheap and commercially available. Since 12 V was chosen as the working voltage, no risks arise from this extra-low voltage. As a power source, 12 V power adapters can be used. As connectors, aviation connectors were chosen due to high durability.

Dimensioning of the aluminium parts (AlMgSi0.5 alloy)

aluminium pipe	outer diameter 80 mm, inner diameter 70 mm, wall thickness 5 mm, height 70 mm
bottom squaretube	90 x 90 mm, wall thickness 4 mm, height 65 mm

To achieve a good airflow, holes were drilled or slits were cut into the aluminium socket. All holes were drilled using a drill press and slits were cut with a bench saw (special aluminium saw blade).

All 3D printed parts components designed by us (FreeCAD 0.16 or Fusion 360) from scratch and will be available for free as ".stl" files, which can be processed by common slicers (e.g. Cura, Simplify3D). On demand, we will provide all ".stl" files, detailed information in form of a technical drawing regarding the holes, which need to be drilled, and precise information about suppliers of the utilised materials. We printed components on a modified Anycubic I3 Mega or Creality CR-10S using PLA or PETG as the material.

Disclaimer: Construction and operation of the photoreactor at own risk and safety requirements. We assume no liability for physical damage or damage to property occurring during construction, use, modification and misuse of the photoreactor. Note that we do not have any obligation concerning the effects resulting from the application of this photoreactor.

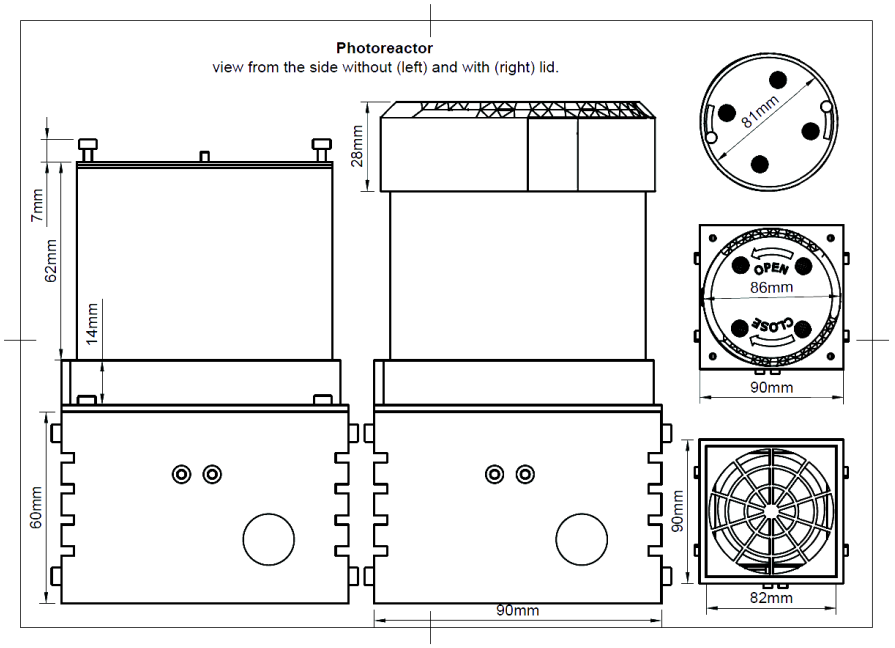

Figure 17: Blue print of a modelled photoreactor with physical dimensions.

7. Spectral Data

7.1. 1,1,1,2,2,3,3,4,4-Nonafluoro-6-iodododecane (3)

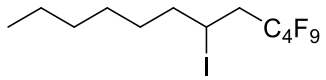

3

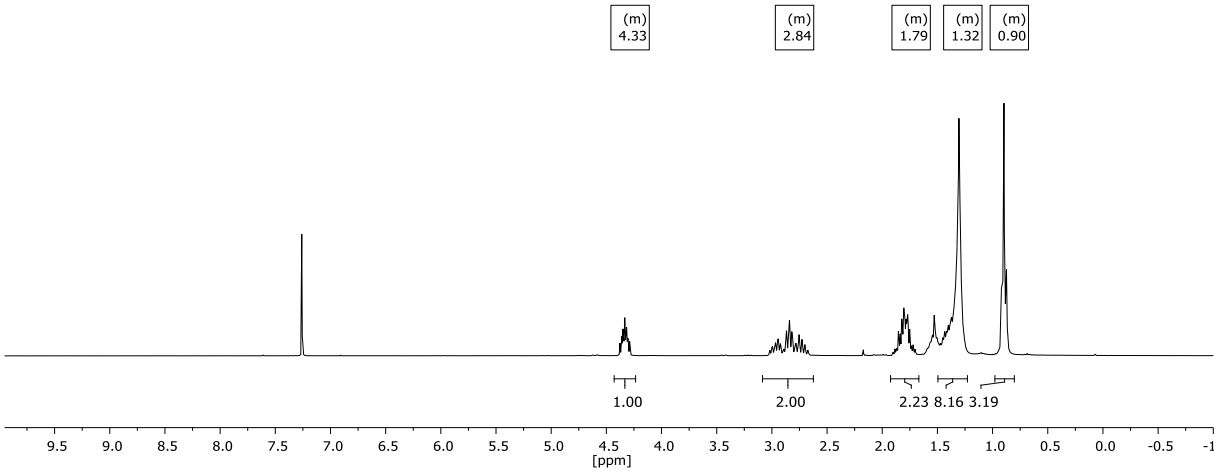

^{1}H-NMR-spectrum (300 MHz, $CDCl_3$)

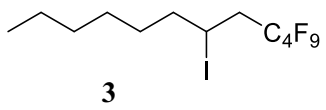

3

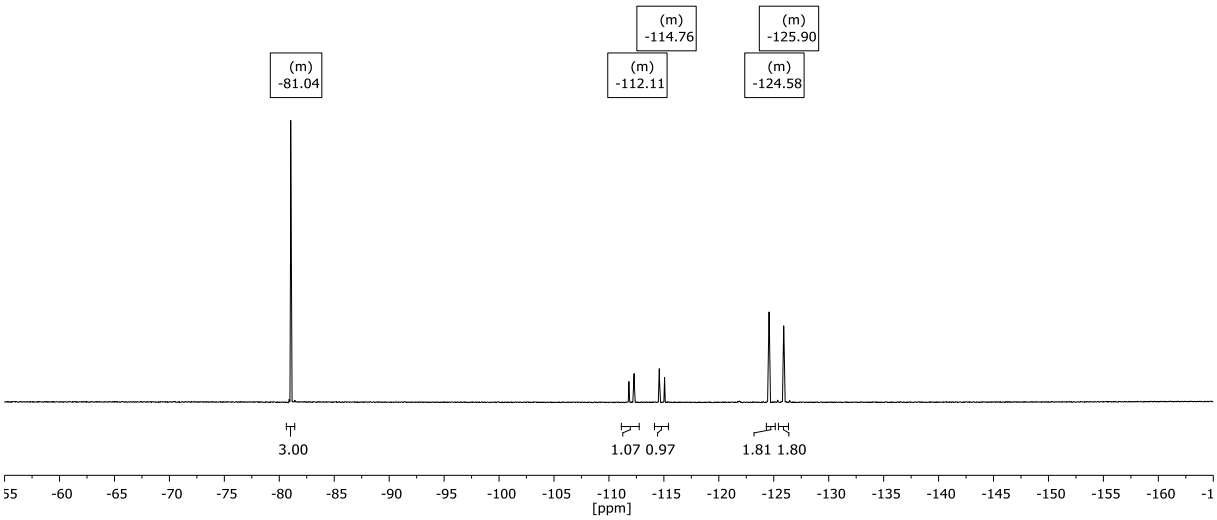

^{19}F-NMR-spectrum (565 MHz, $CDCl_3$)

7.2. 1,1,1-Trifluoro-3-iodononane (5)

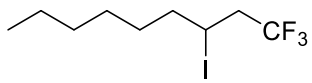

5

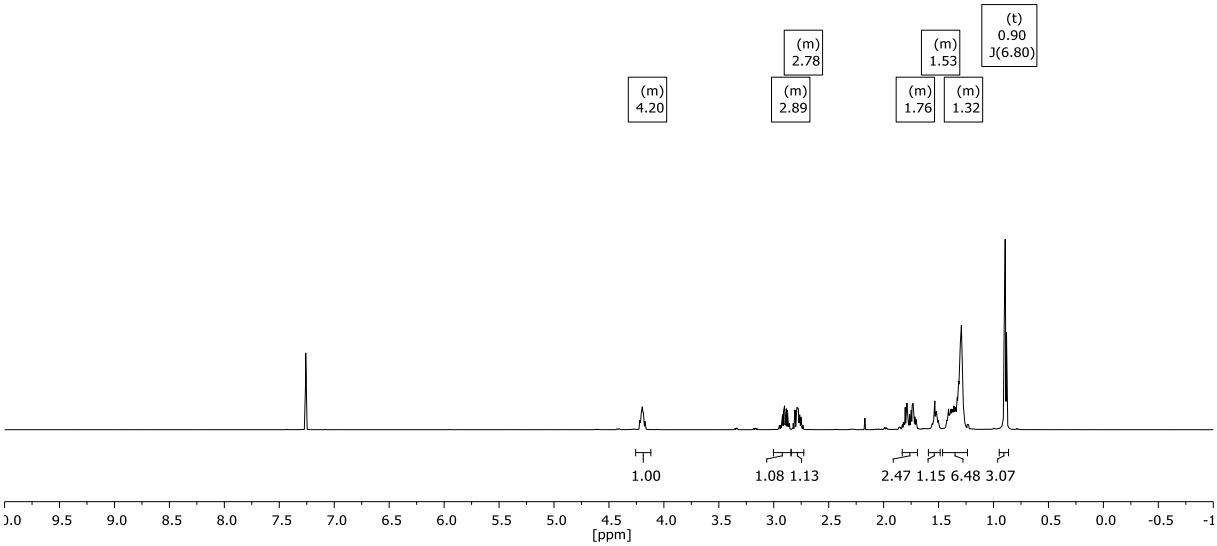

^{1}H-NMR-spectrum (600 MHz, $CDCl_3$)

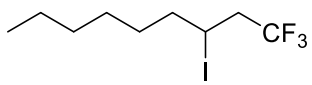

5

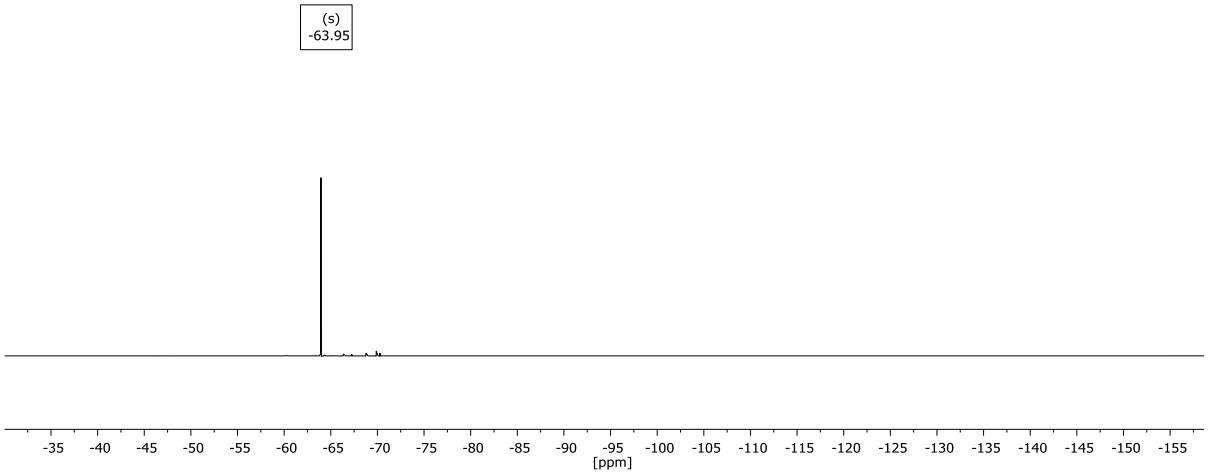

^{19}F-NMR-spectrum (565 MHz, $CDCl_3$)

7.3. 1,1,1,2,2,3,3,4,4,5,5,6,6-Tridecafluoro-8-iodotetradecane (6)

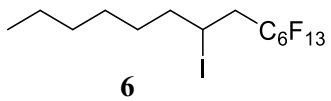

6

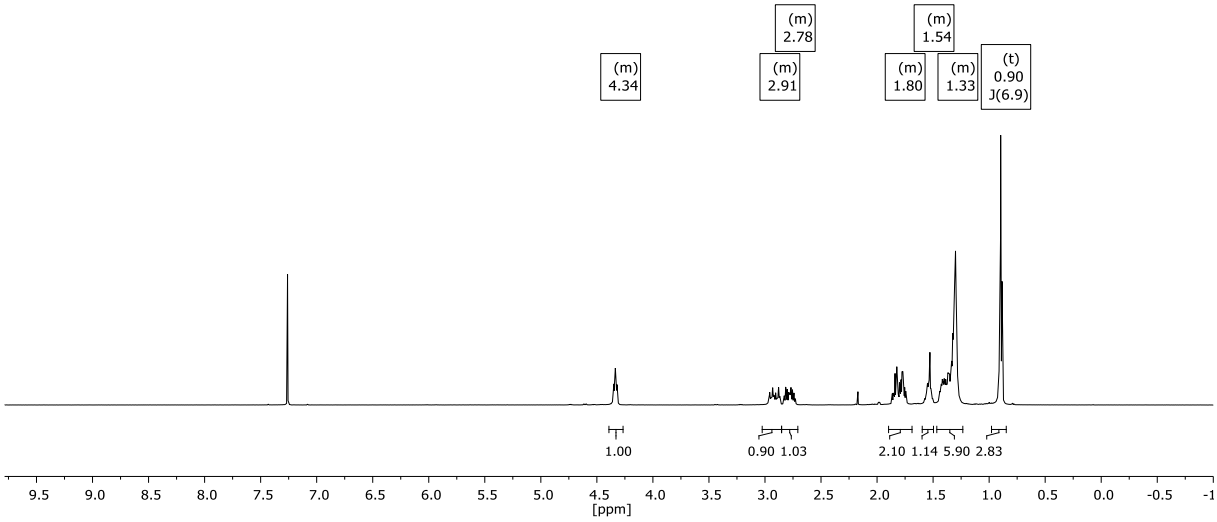

^{1}H-NMR-spectrum (600 MHz, $CDCl_3$)

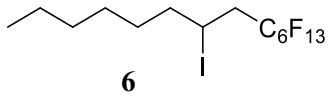

6

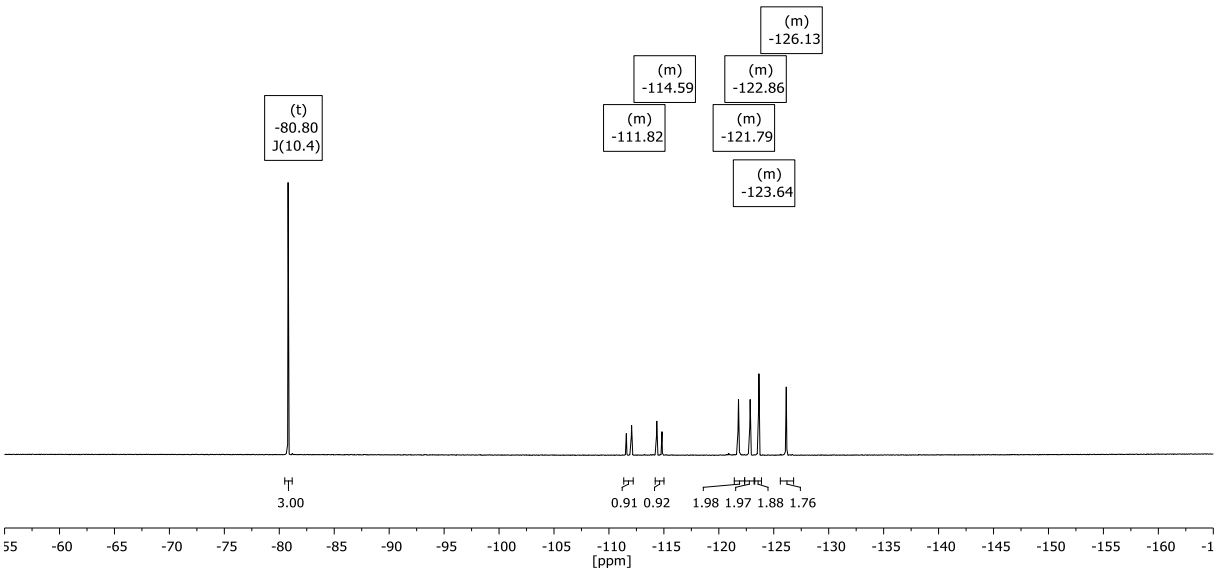

^{19}F-NMR-spectrum (565 MHz, $CDCl_3$)

7.4. 1,1,1,2,2,3,3,4,4,5,6,6,7,8,8,9,9-Heptadecafluoro-11-iodo-5,7-dimethylheptadecane (7)

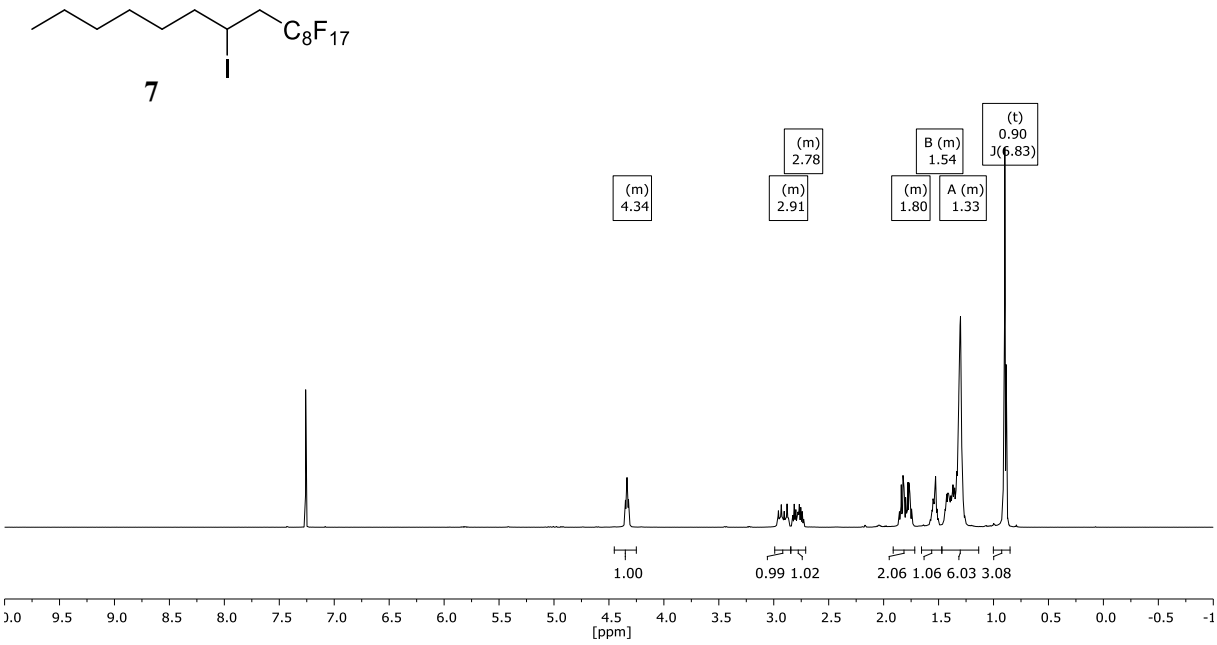

^{1}H-NMR-spectrum (600 MHz, $CDCl_3$)

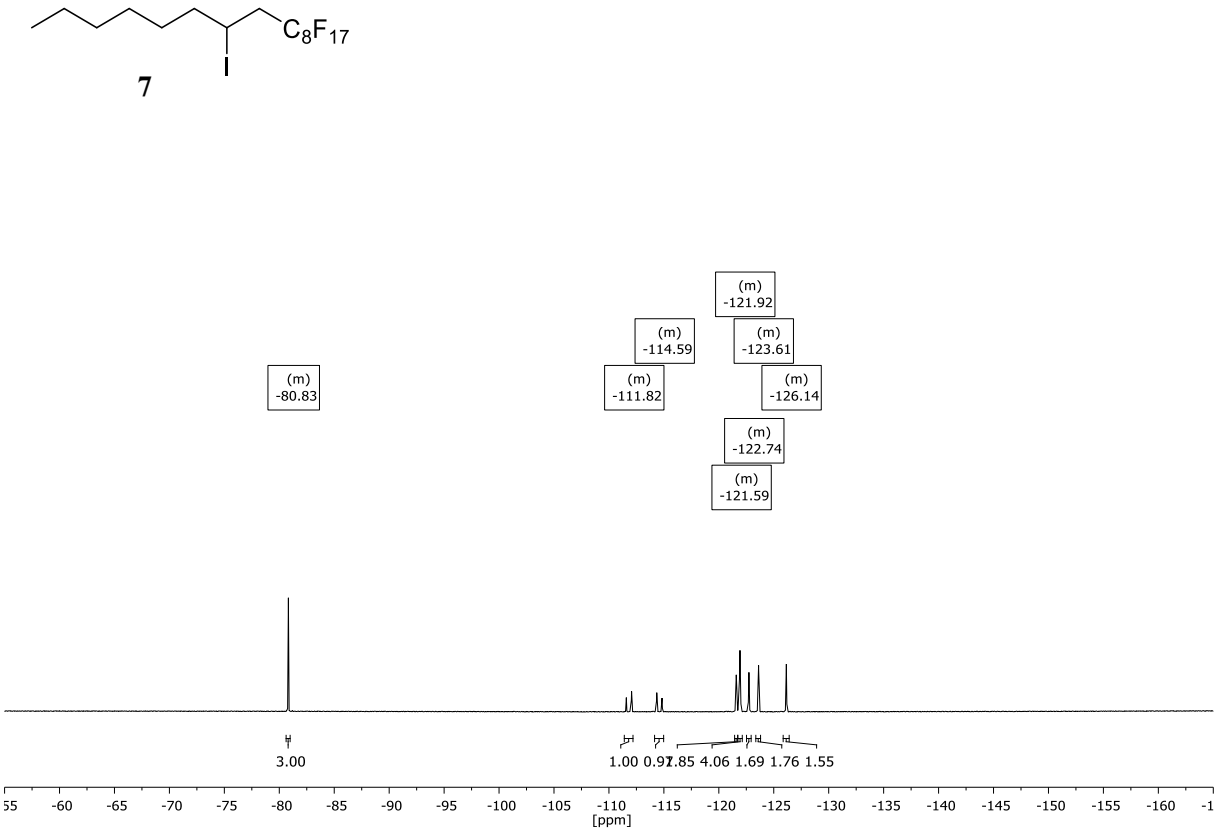

^{19}F-NMR-spectrum (565 MHz, $CDCl_3$)

7.5. (3,3,4,4,5,5,6,6,6-Nonafluoro-1-iodohexyl)cyclohexane (9)

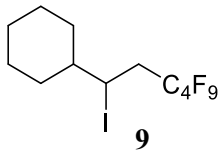

9

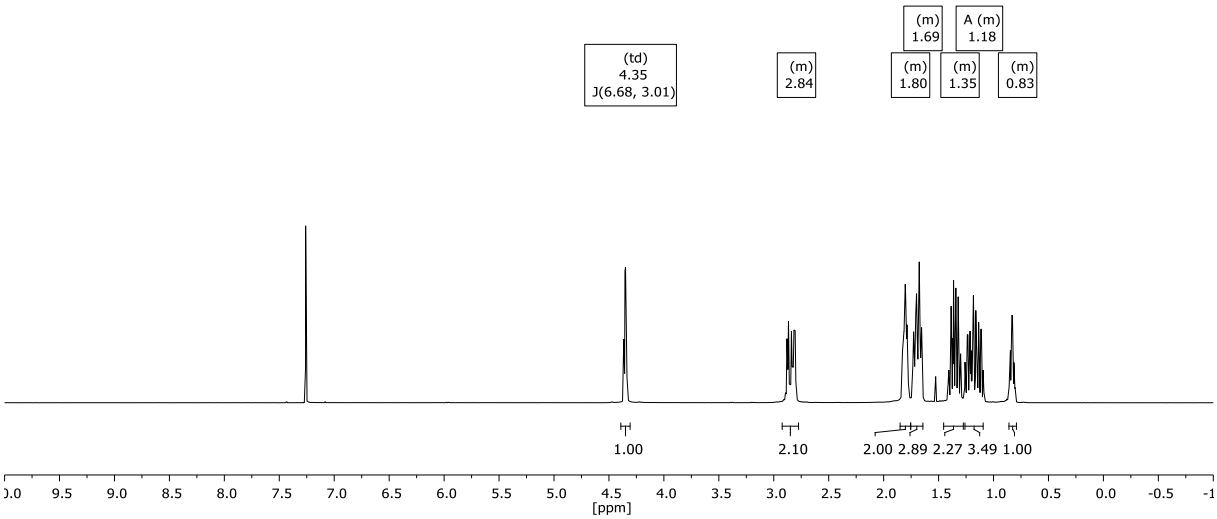

^{1}H-NMR-spectrum (600 MHz, $CDCl_3$)

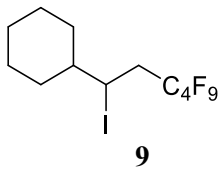

9

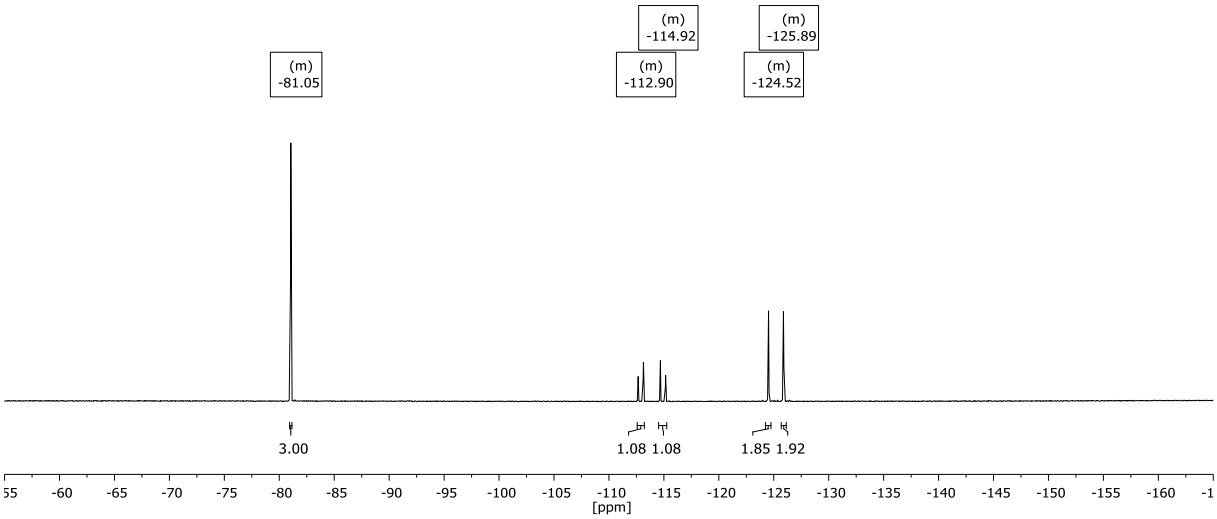

^{19}F-NMR-spectrum (565 MHz, $CDCl_3$)

7.6. (4,4,5,5,6,6,7,7,7-Nonafluoro-2-iodoheptyl)benzene (10)

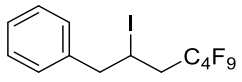

10

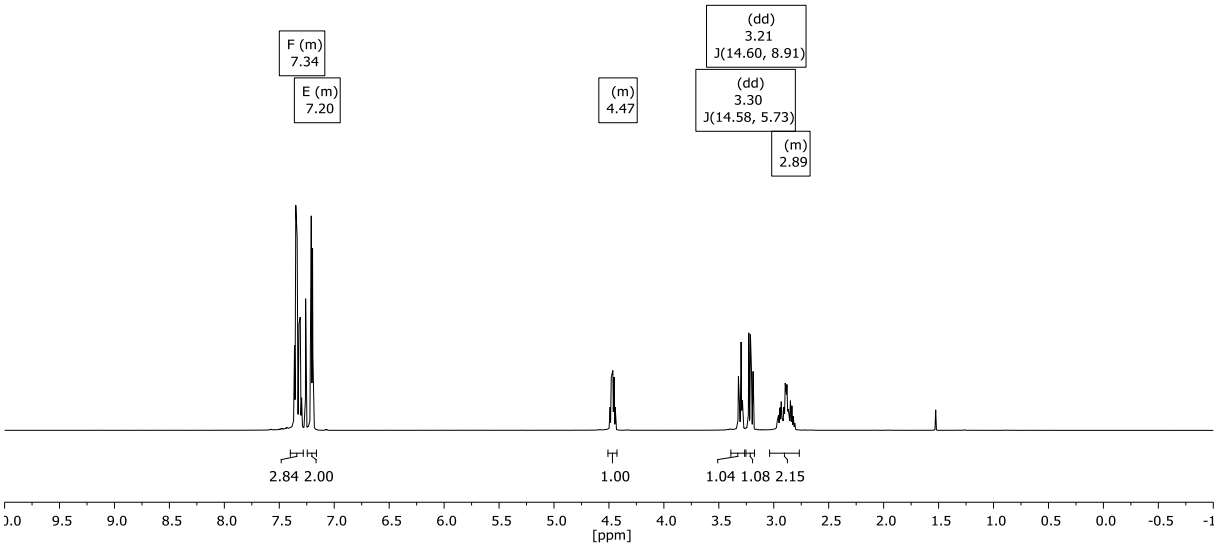

^{1}H-NMR-spectrum (600 MHz, $CDCl_3$)

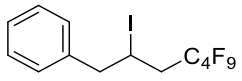

10

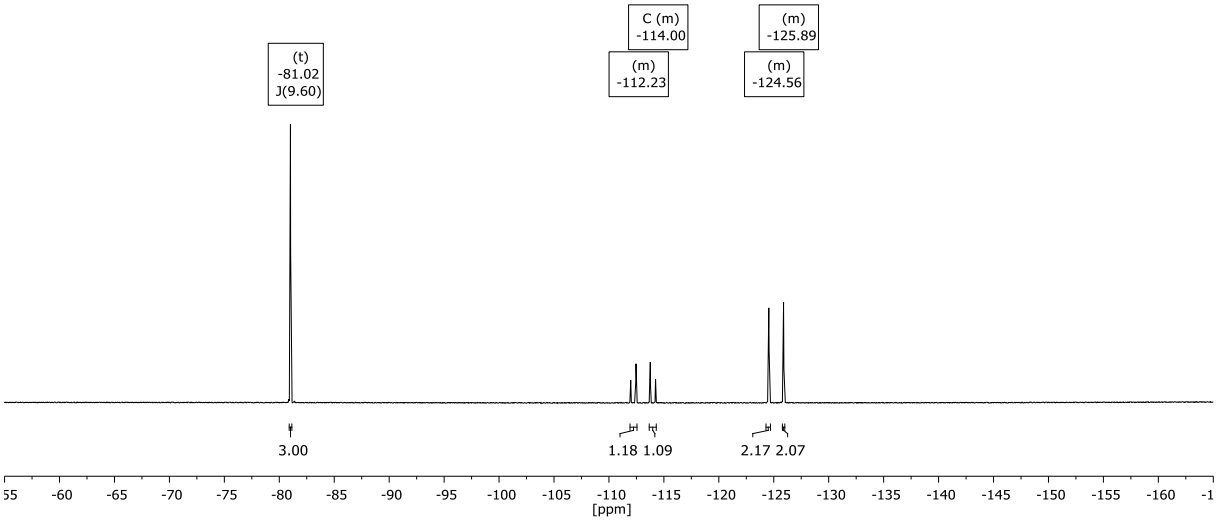

^{19}F-NMR-spectrum (565 MHz, $CDCl_3$)

7.7. 1-Iodo-2-(1,1,2,2,3,3,4,4,4-nonafluorobutyl)cyclooctane (11)

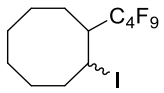

11

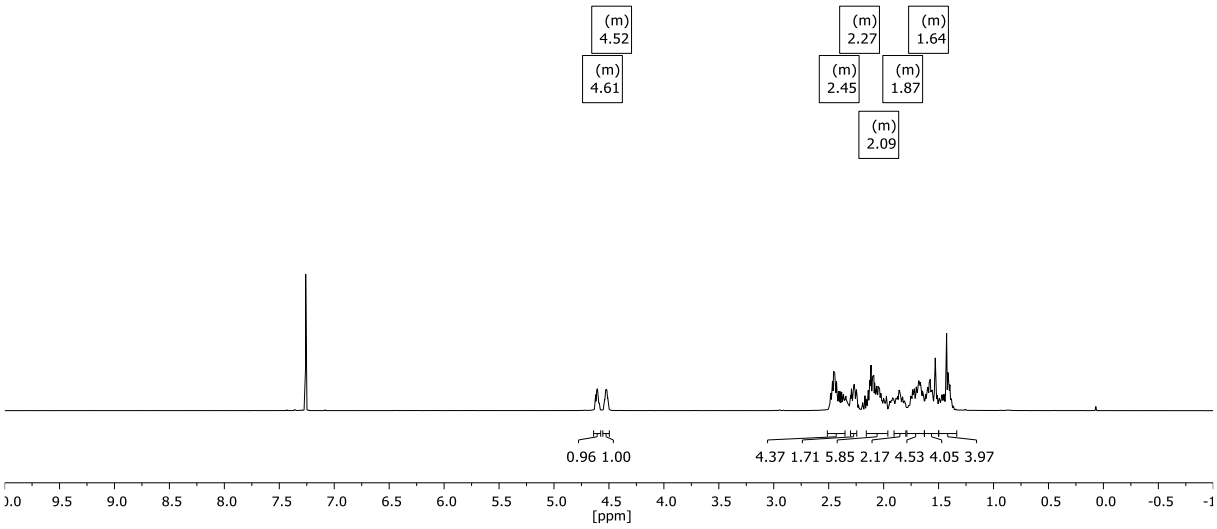

^{1}H-NMR-spectrum (600 MHz, $CDCl_3$)

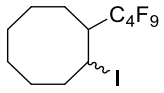

11

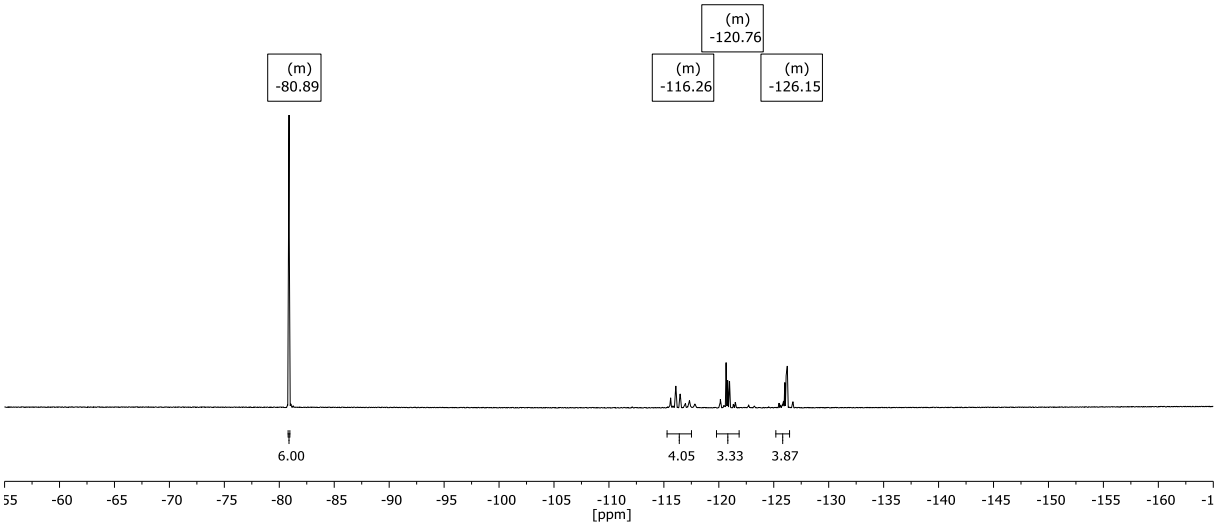

^{19}F-NMR-spectrum (565 MHz, $CDCl_3$)

7.8. 1-Iodo-2-(1,1,2,2,3,3,4,4,4-nonafluorobutyl)cyclopentane (12)

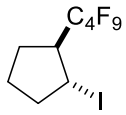

12

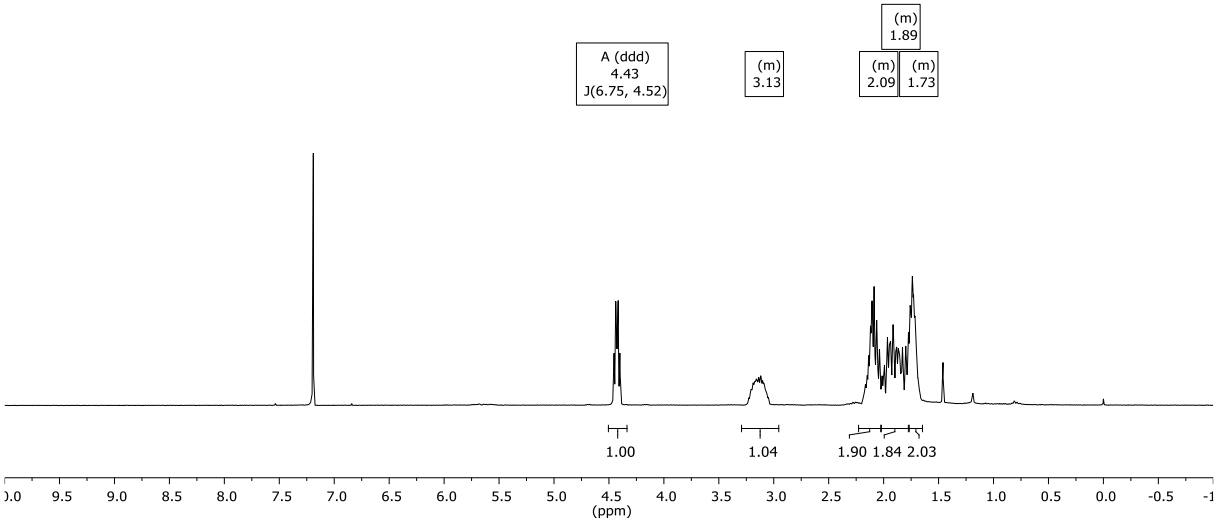

^{1}H-NMR-spectrum (600 MHz, $CDCl_3$)

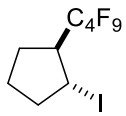

12

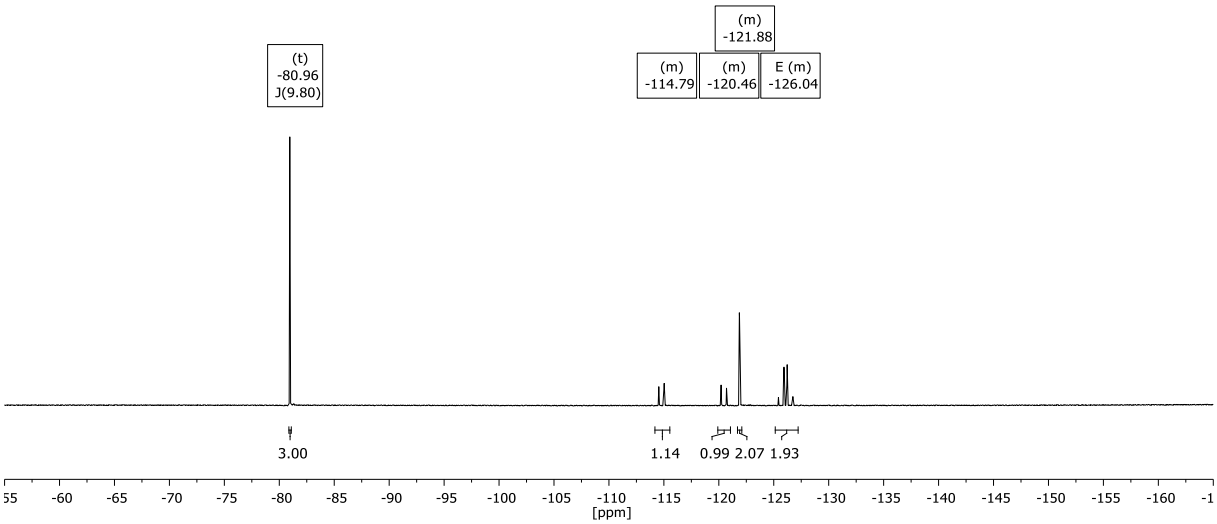

^{19}F-NMR-spectrum (565 MHz, $CDCl_3$)

7.9. 10-Bromo-1,1,1,2,2,3,3,4,4-nonafluoro-6-iododecane (13)

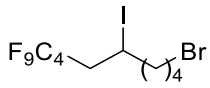

13

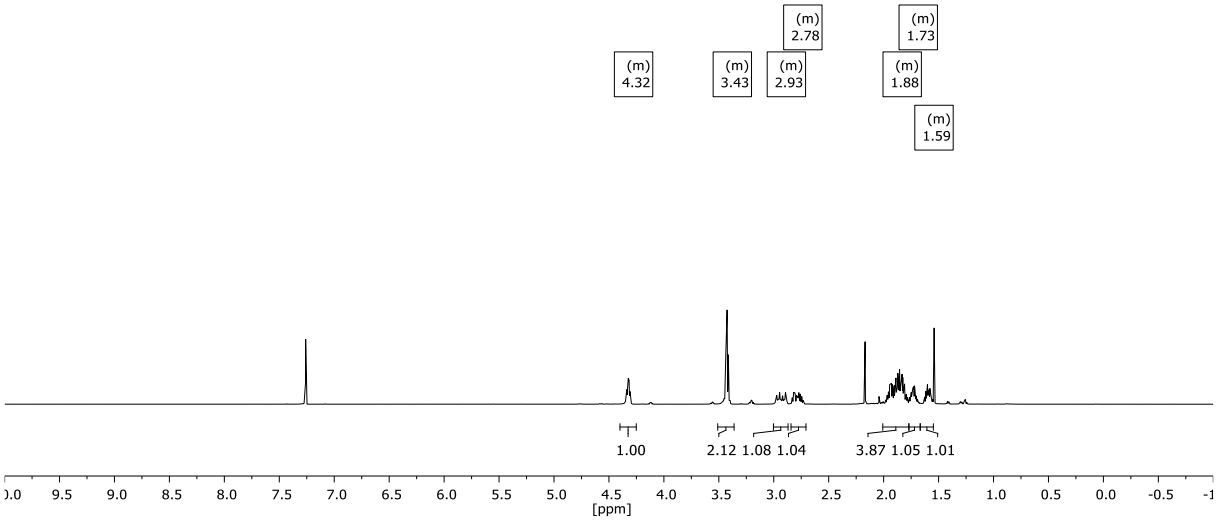

^{1}H-NMR-spectrum (600 MHz, $CDCl_3$)

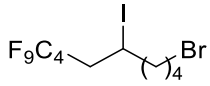

13

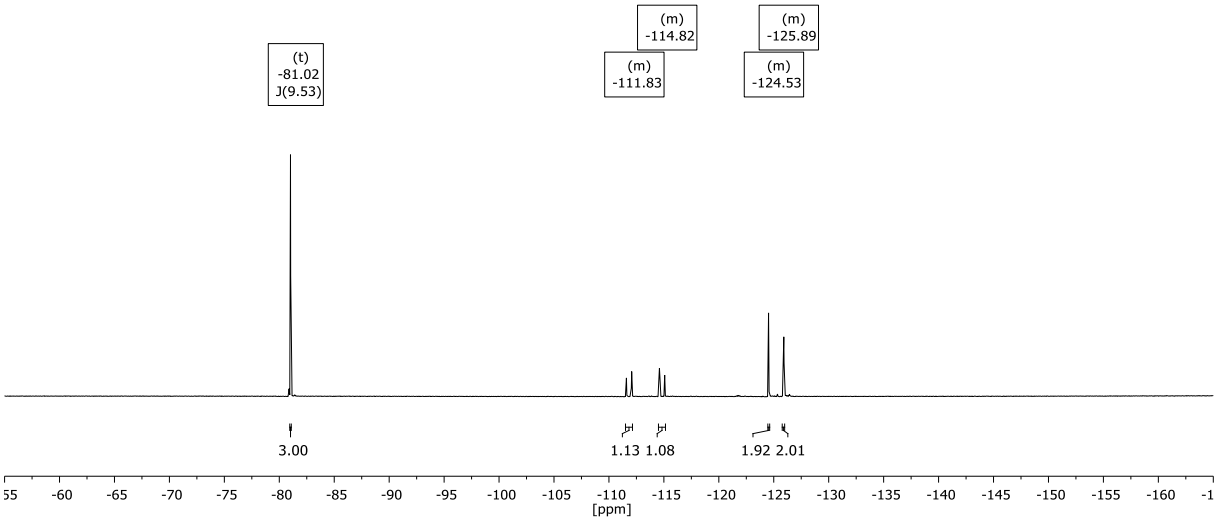

^{19}F-NMR-spectrum (565 MHz, $CDCl_3$)

7.10. 11,11,12,12,13,13,14,14,14-Nonafluoro-9-iodotetradecyl 4-methylbenzenesulfonate (14)

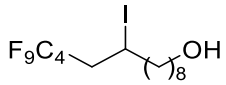

14

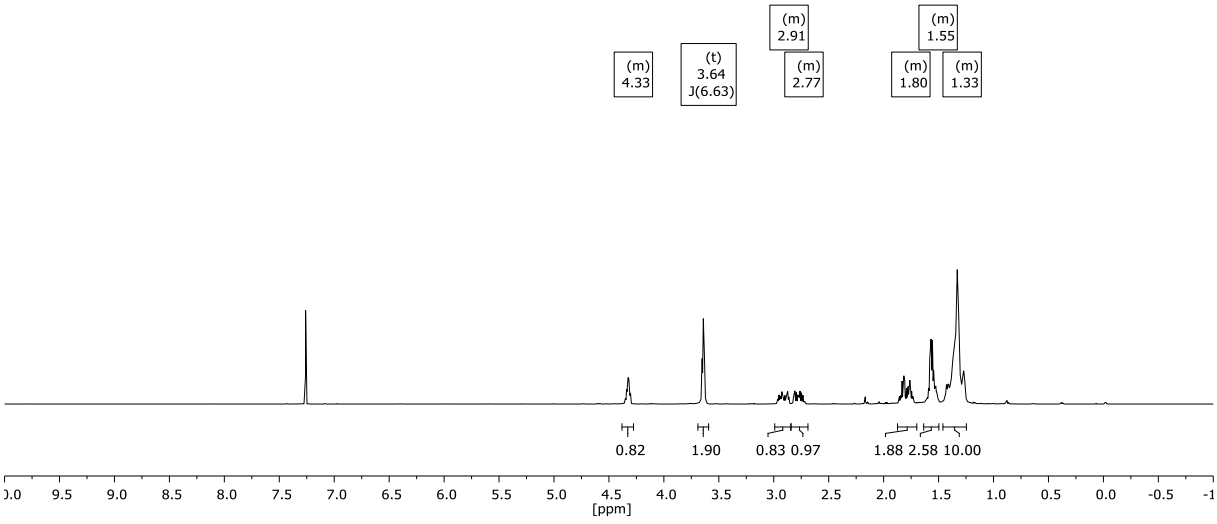

^{1}H-NMR-spectrum (600 MHz, $CDCl_3$)

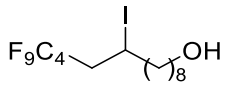

14

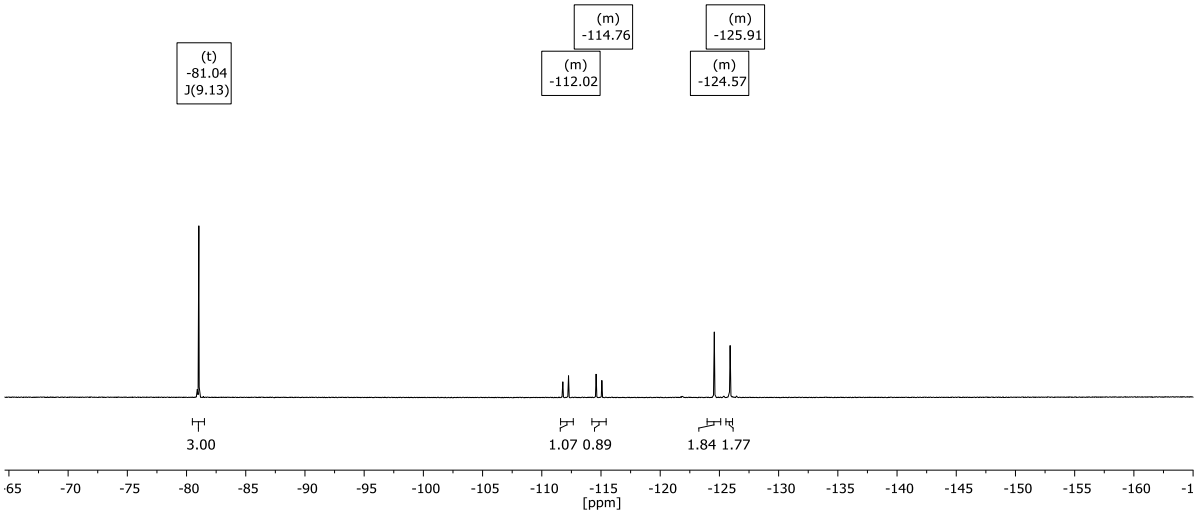

^{19}F-NMR-spectrum (565 MHz, $CDCl_3$)

7.11. 11,11,12,12,13,13,14,14,14-Nonafluoro-9-iodotetradecyl 4-methylbenzenesulfonate (15)

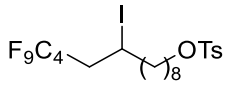

15

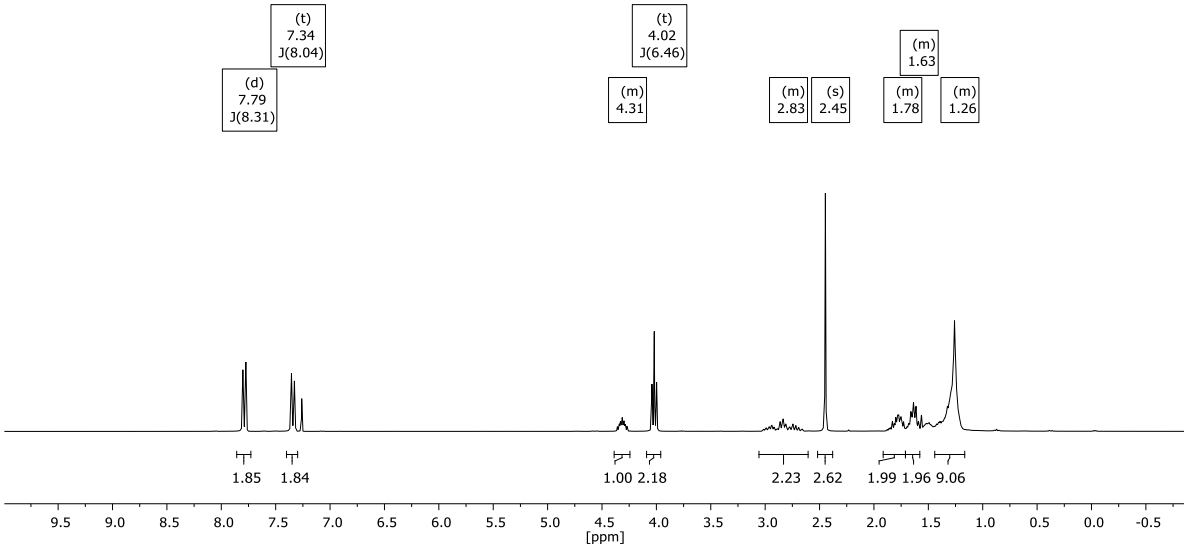

^{1}H-NMR-spectrum (300 MHz, $CDCl_3$)

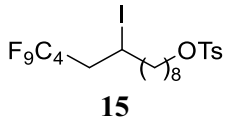

15

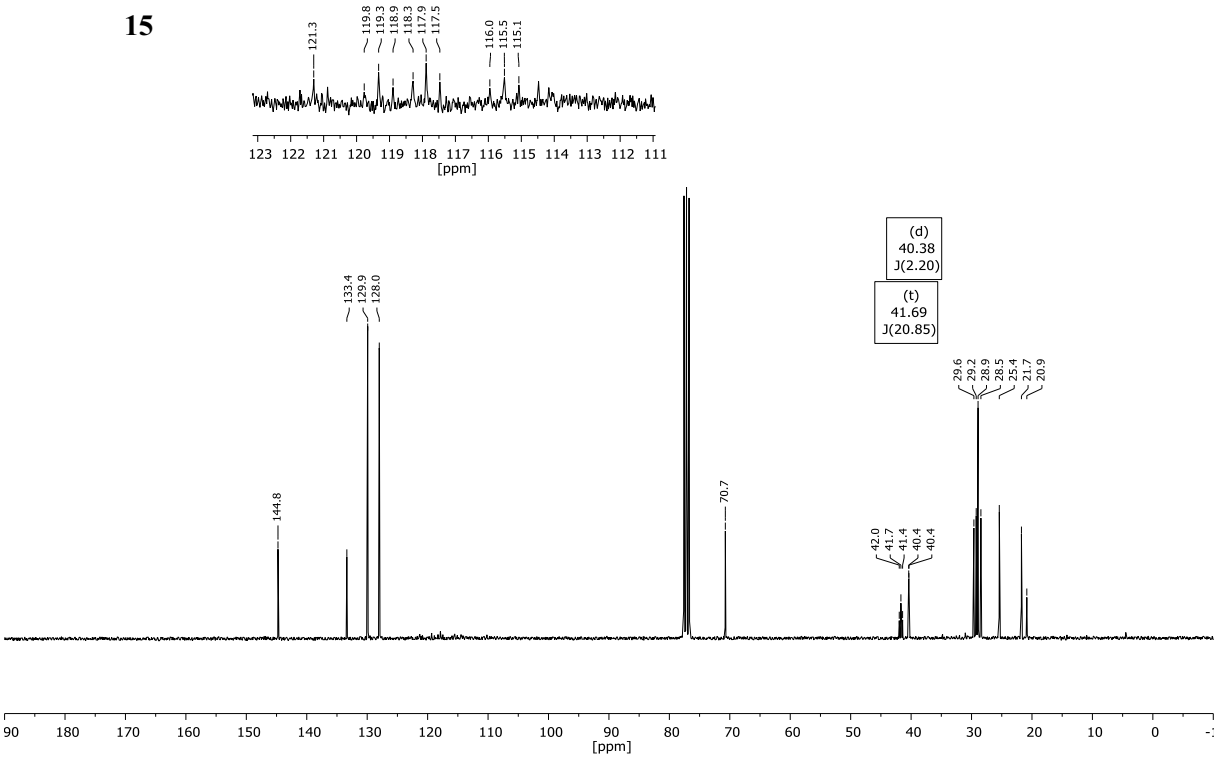

^{13}C-NMR-spectrum (75.5 MHz, $CDCl_3$)

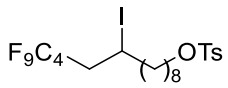

15

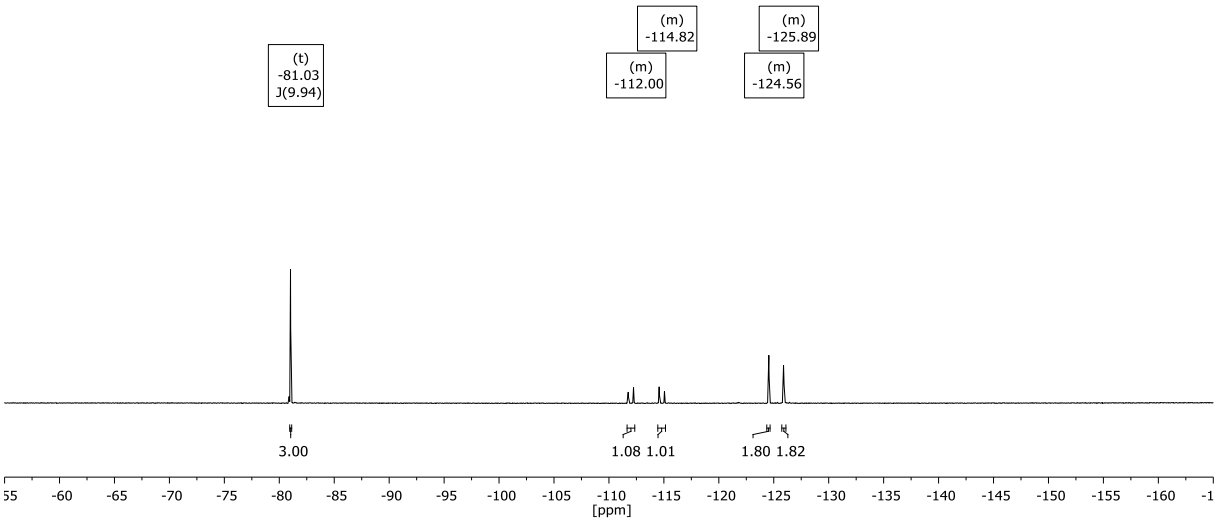

^{19}F-NMR-spectrum (565 MHz, $CDCl_3$)

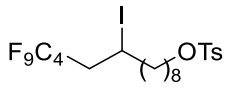

15

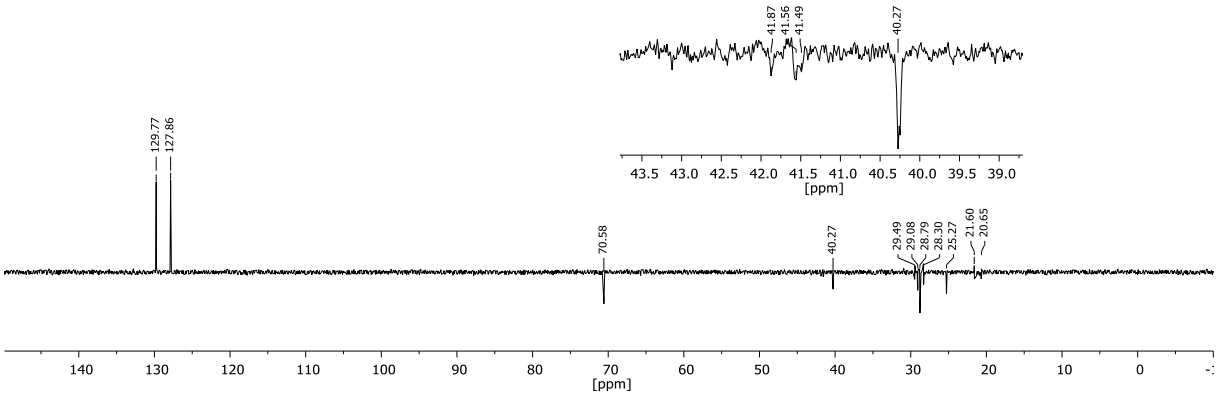

DEPT-NMR-spectrum (75.5 MHz, $CDCl_3$)

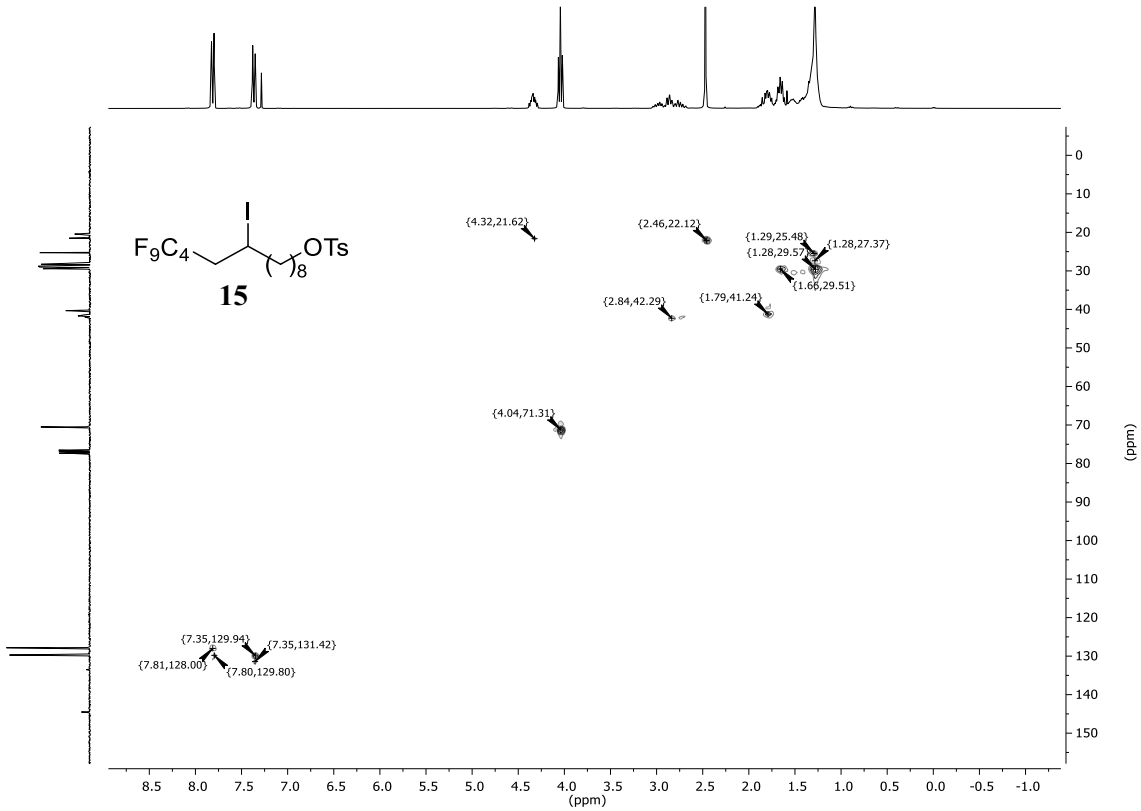

HSQC-spectrum (300, 75.5 MHz, $CDCl_3$)

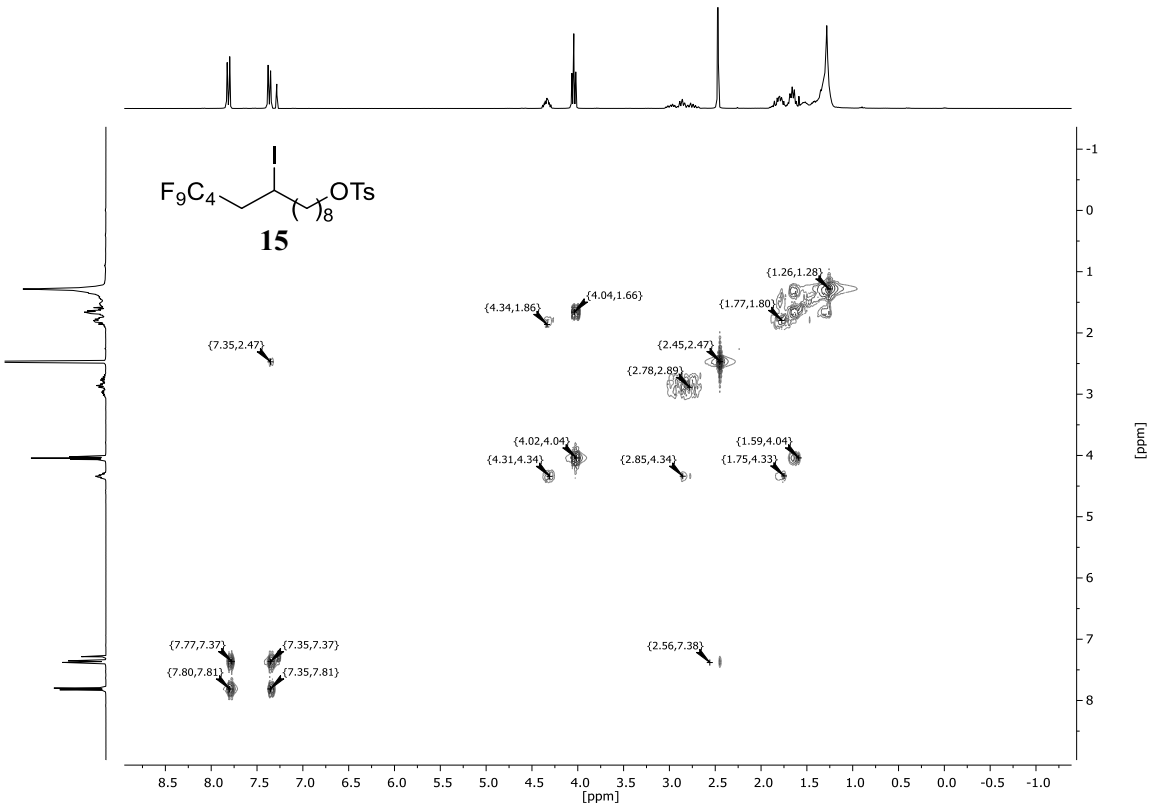

COSY-spectrum (300, 300 MHz, $CDCl_3$)

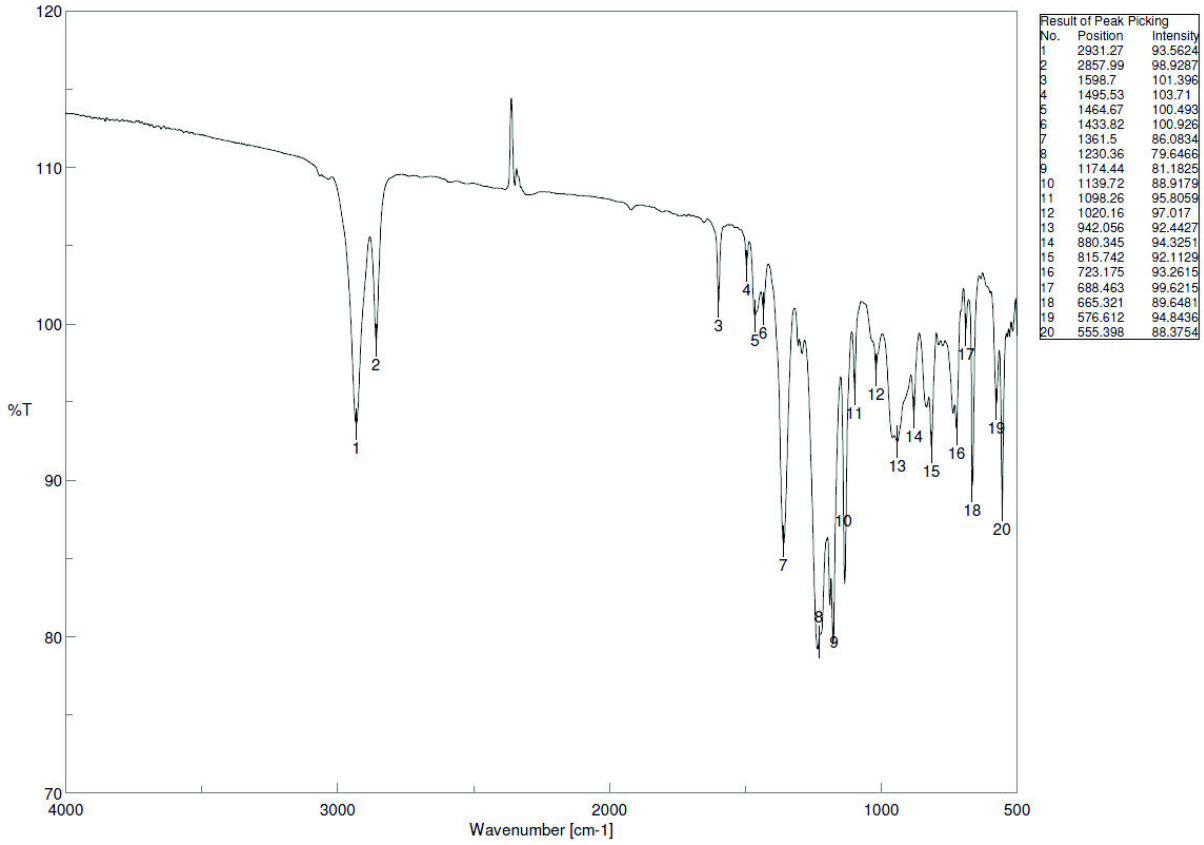

Result of Peak Picking		
No.	Position	Intensity
1	2931.27	93.5624
2	2857.99	98.9287
3	1598.7	101.396
4	1495.53	103.71
5	1464.67	100.493
6	1433.82	100.926
7	1361.5	86.0834
8	1230.36	79.6466
9	1174.44	81.1825
10	1139.72	88.9179
11	1098.26	95.8059
12	1020.16	97.017
13	942.056	92.4427
14	880.345	94.3251
15	815.742	92.1129
16	723.175	93.2615
17	688.463	99.6215
18	665.321	89.6481
19	576.612	94.8436
20	555.398	88.3754

IR-spectrum (film on NaCl)

7.12. 14-Azido-1,1,1,2,2,3,3,4,4-nonafluoro-6-iodotetradecane (16)

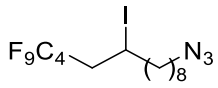

16

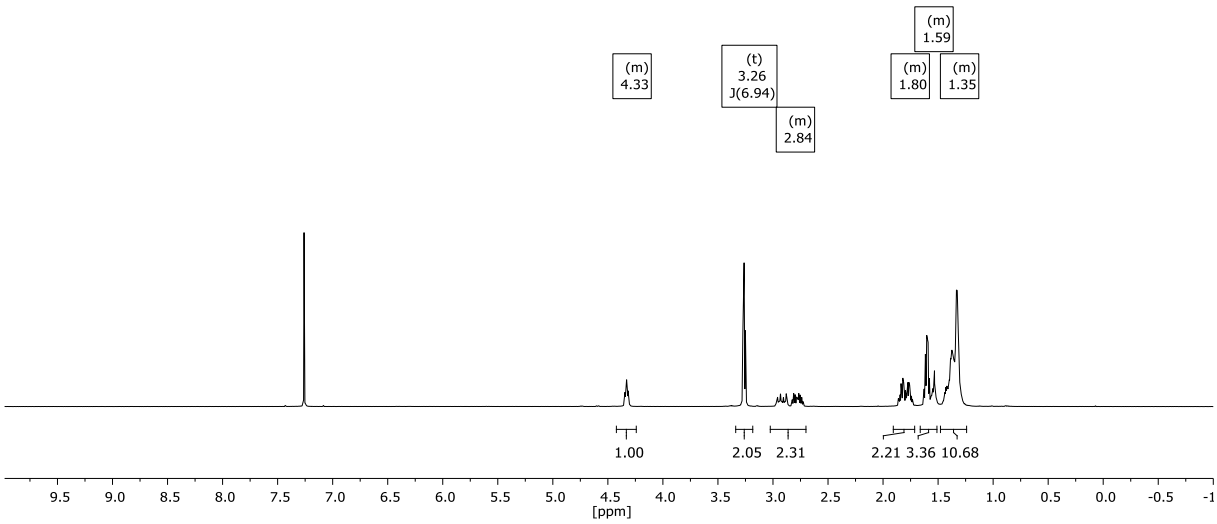

^{1}H-NMR-spectrum (600 MHz, $CDCl_3$)

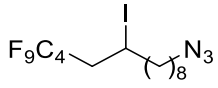

16

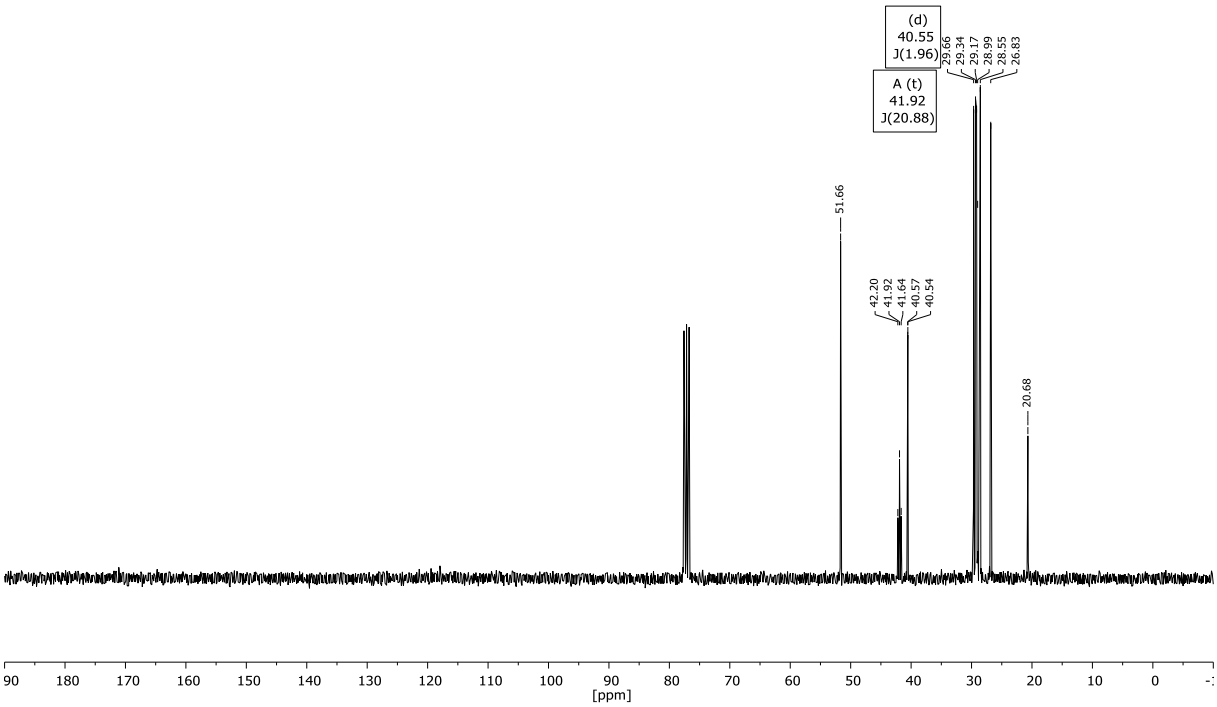

^{13}C-NMR-spectrum (75.5 MHz, $CDCl_3$)

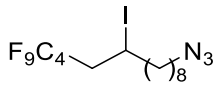

16

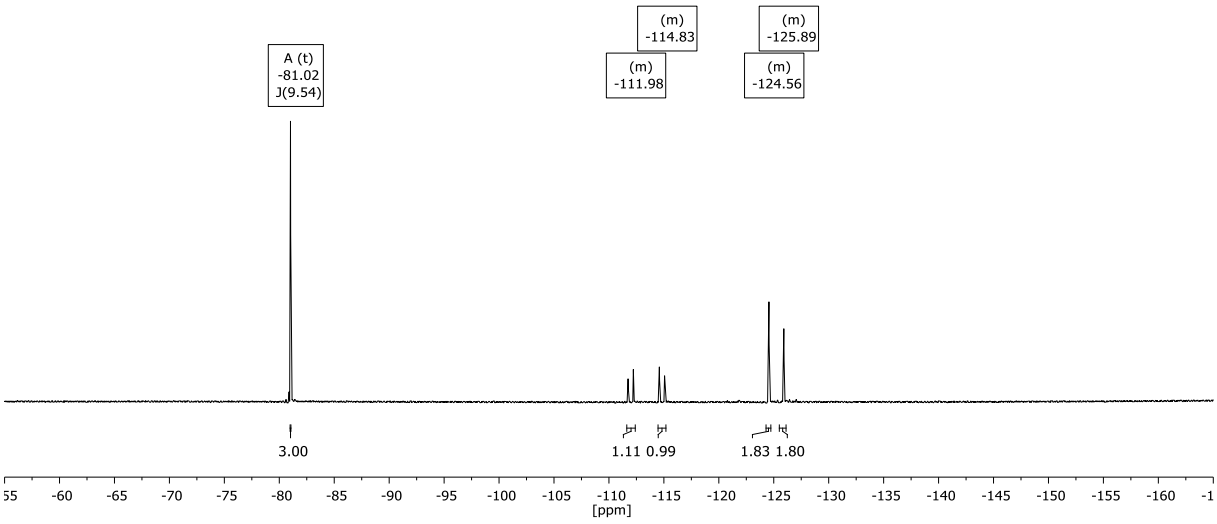

^{19}F-NMR-spectrum (565 MHz, $CDCl_3$)

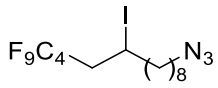

16

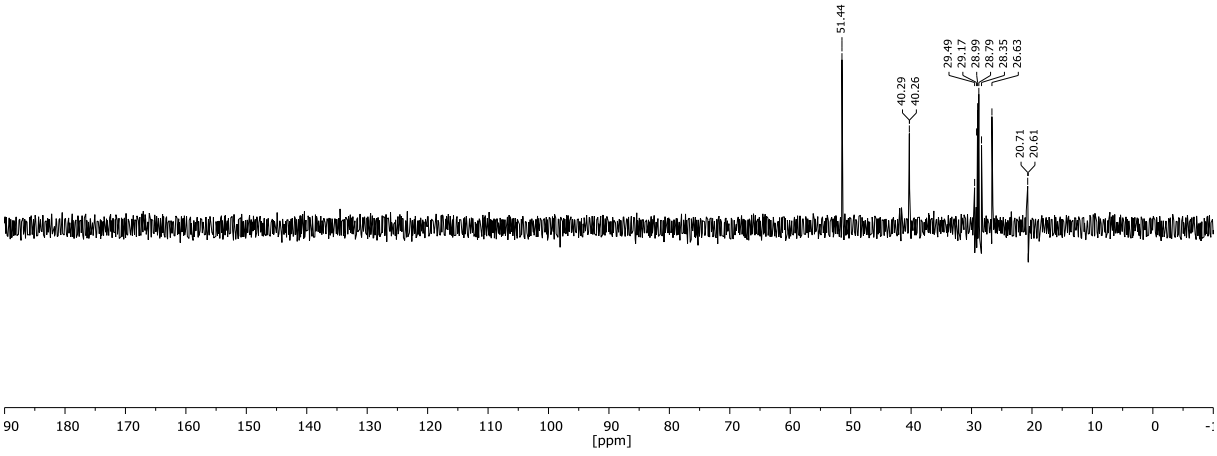

DEPT-NMR-spectrum (75.5 MHz, $CDCl_3$)

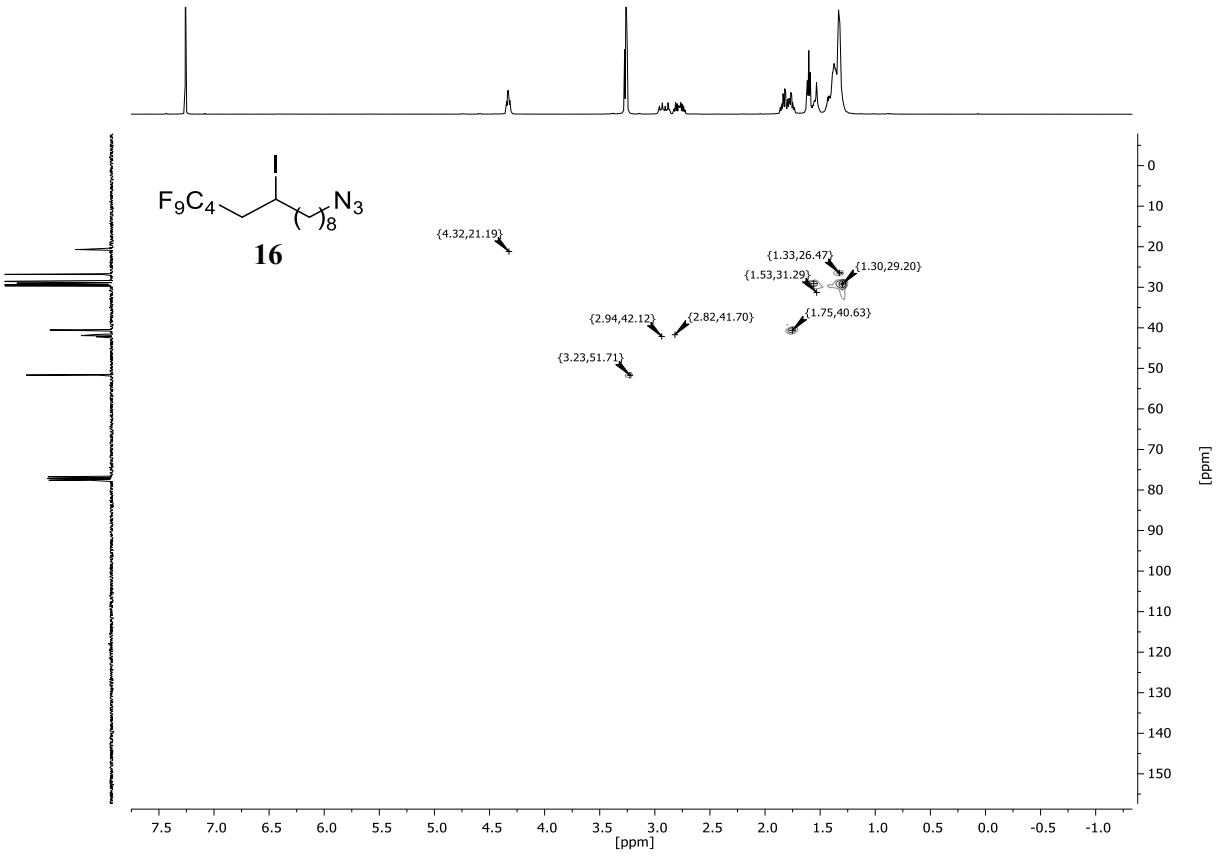

HSQC-spectrum (300, 75.5 MHz, $CDCl_3$)

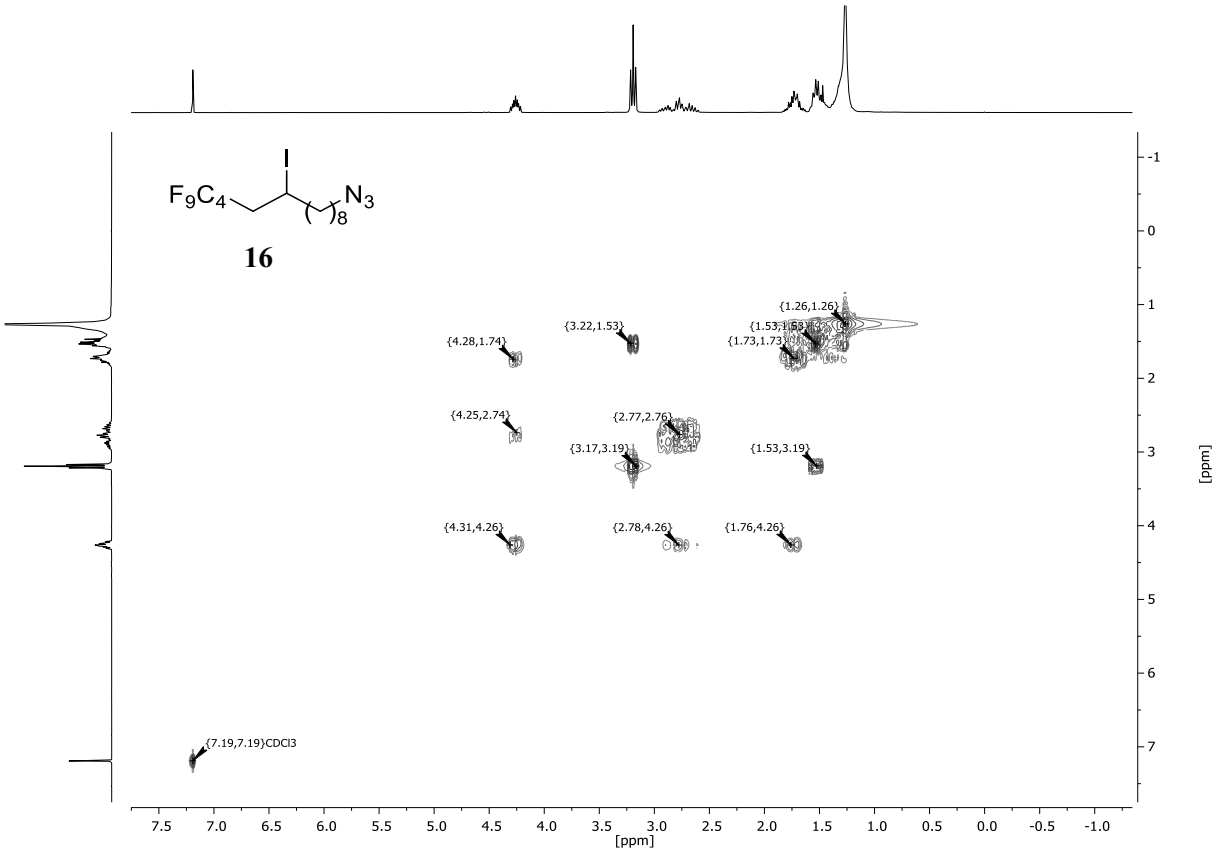

COSY-spectrum (300, 300 MHz, $CDCl_3$)

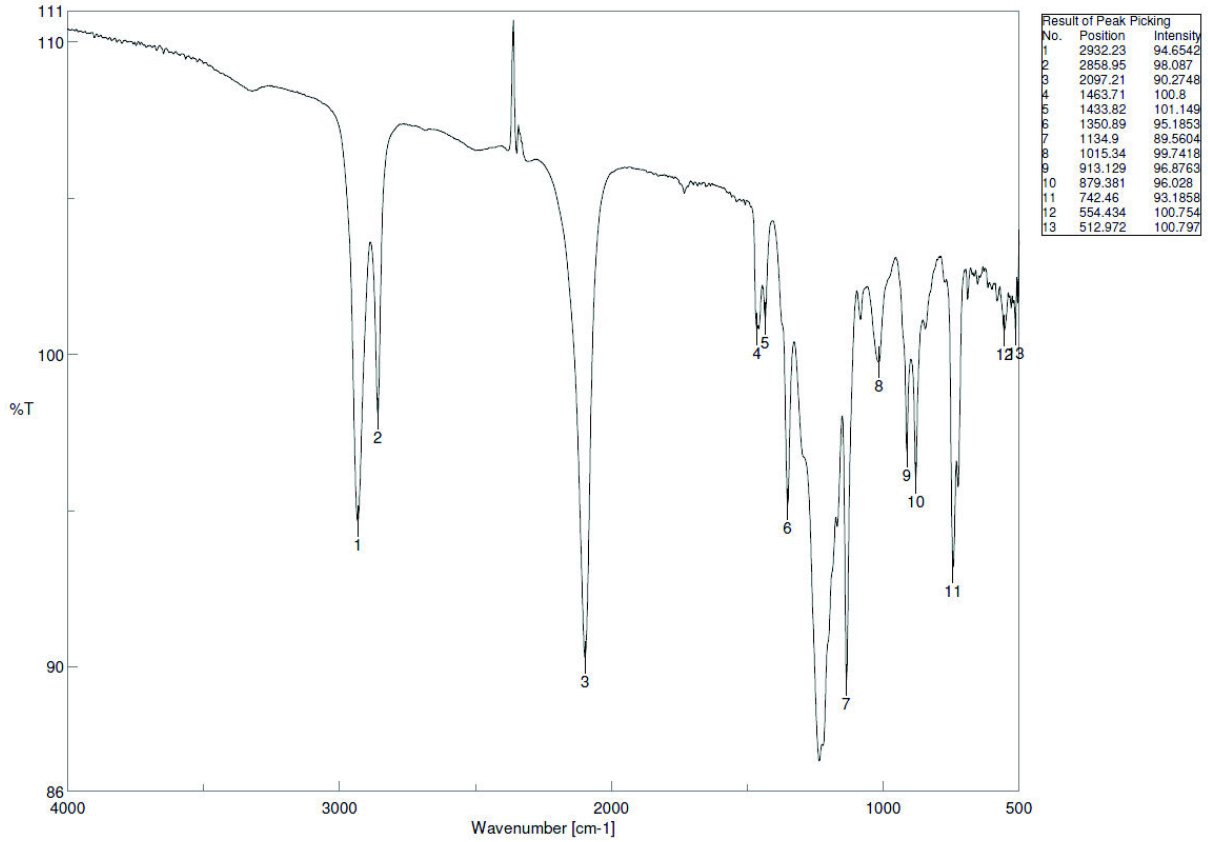

Result of Peak Picking

No.	Position	Intensity
1	2932.23	94.6542
2	2858.95	98.087
3	2097.21	90.2748
4	1463.71	100.8
5	1433.82	101.149
6	1350.89	95.1853
7	1134.9	89.5604
8	1015.34	99.7418
9	913.129	96.8763
10	879.381	96.028
11	742.46	93.1858
12	554.434	100.754
13	512.972	100.797

IR-spectrum (film on NaCl)

7.13. 5,5,6,6,7,7,8,8,9,9,10,10,10-tridecafluoro-3-iododecyl acetate (17)

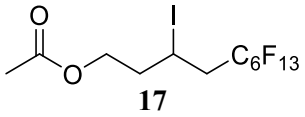

17

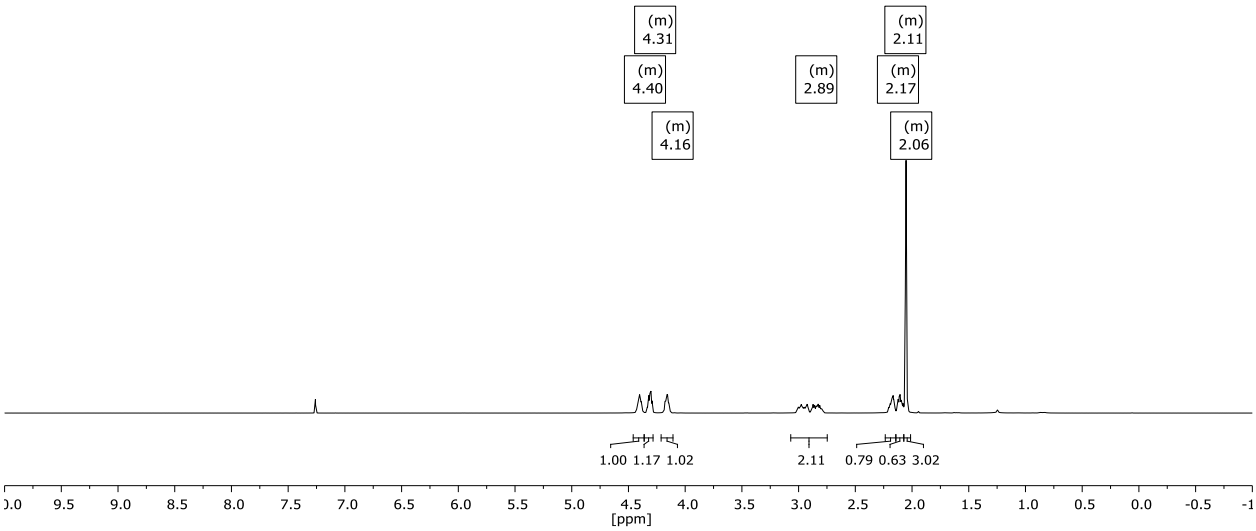

^{1}H-NMR-spectrum (600 MHz, $CDCl_3$)

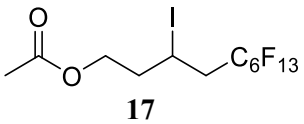

17

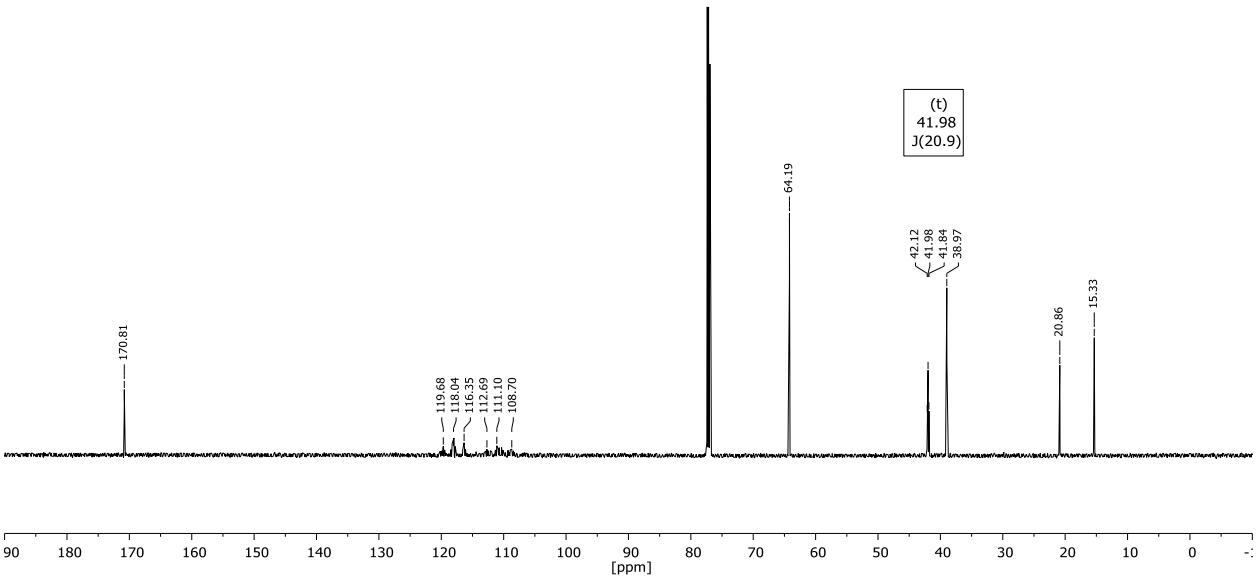

^{13}C-NMR-spectrum (151 MHz, $CDCl_3$)

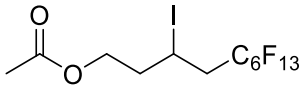

17

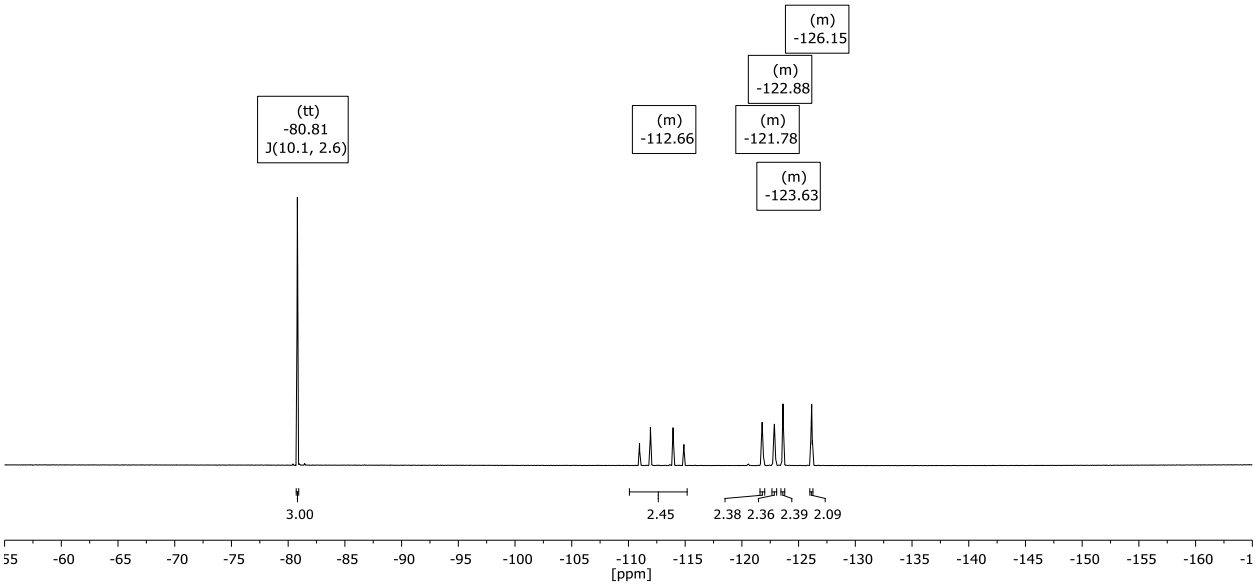

^{19}F-NMR-spectrum (282 MHz, $CDCl_3$)

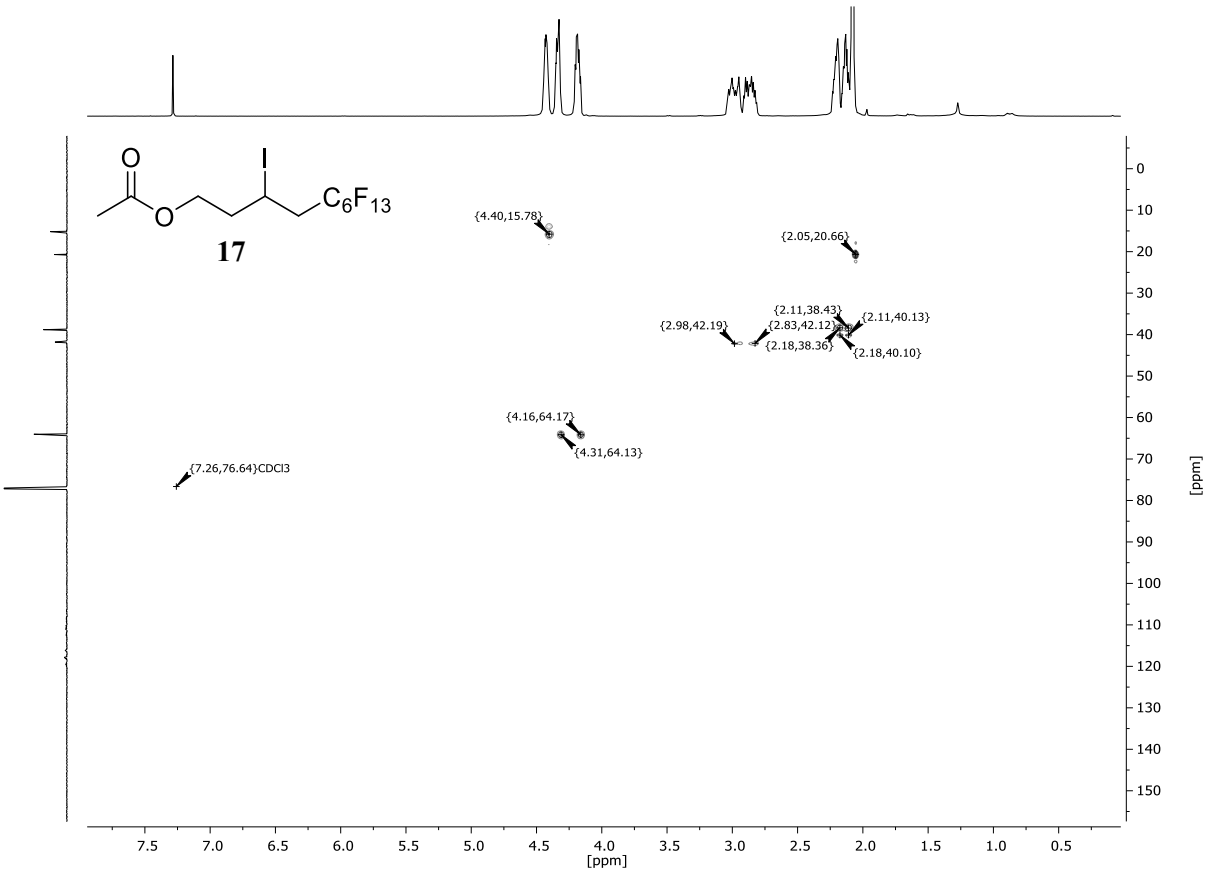

HSQC-NMR-spectrum (600, 150 MHz, $CDCl_3$)

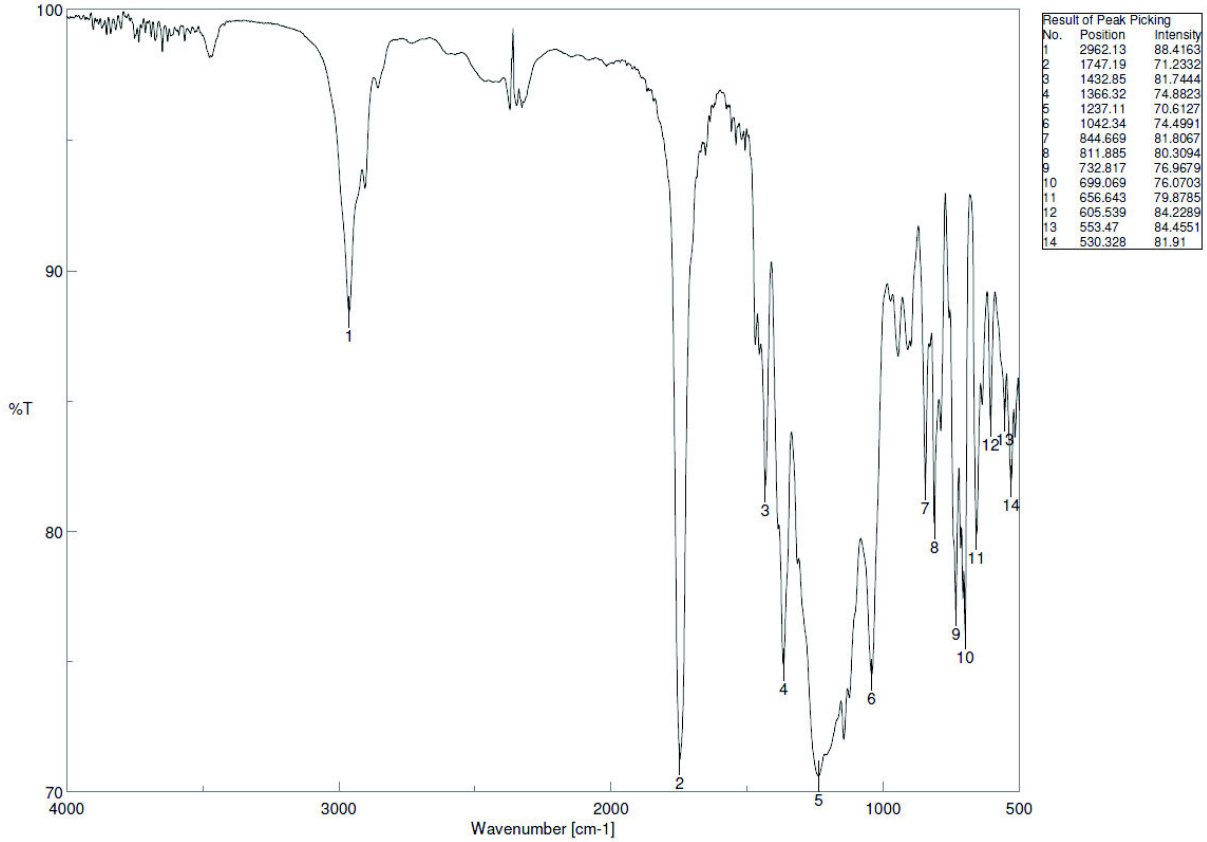

Result of Peak Picking

No.	Position	Intensity
1	2962.13	88.4163
2	1747.19	71.2332
3	1432.85	81.7444
4	1366.32	74.8823
5	1237.11	70.6127
6	1042.34	74.4991
7	844.669	81.8067
8	811.885	80.3094
9	732.817	76.9679
10	699.069	76.0703
11	656.643	79.8785
12	605.539	84.2289
13	553.47	84.4551
14	530.328	81.91

IR-spectrum (film on NaCl)

7.14. 6,6,7,7,8,8,9,9,9-Nonafluoro-4-iodononanamide (18)

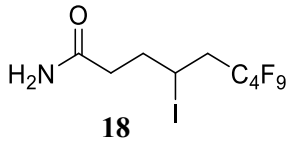

18

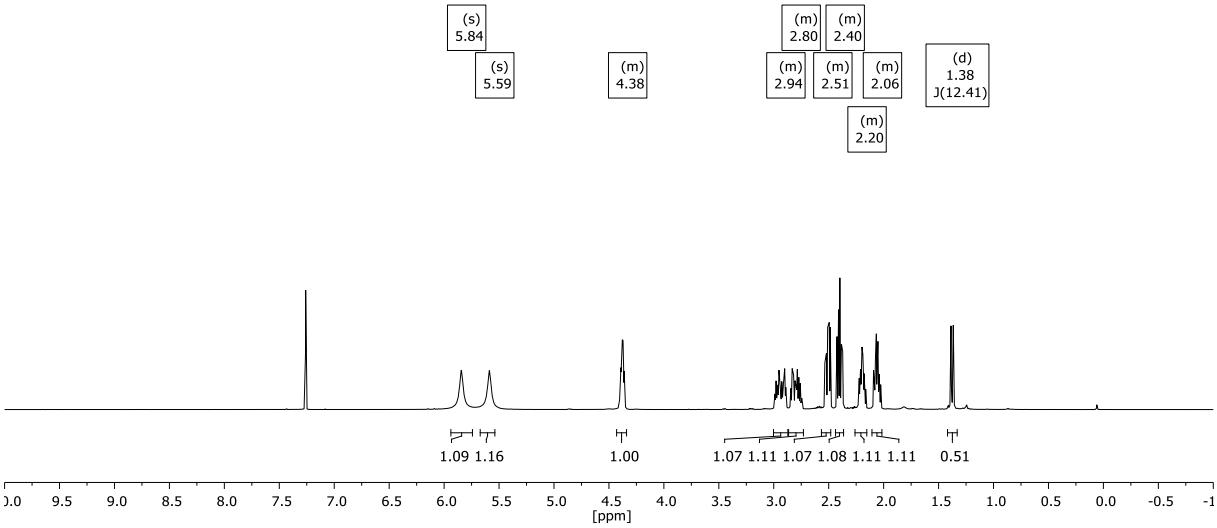

^{1}H-NMR-spectrum (300 MHz, $CDCl_3$)

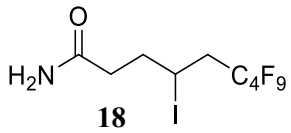

18

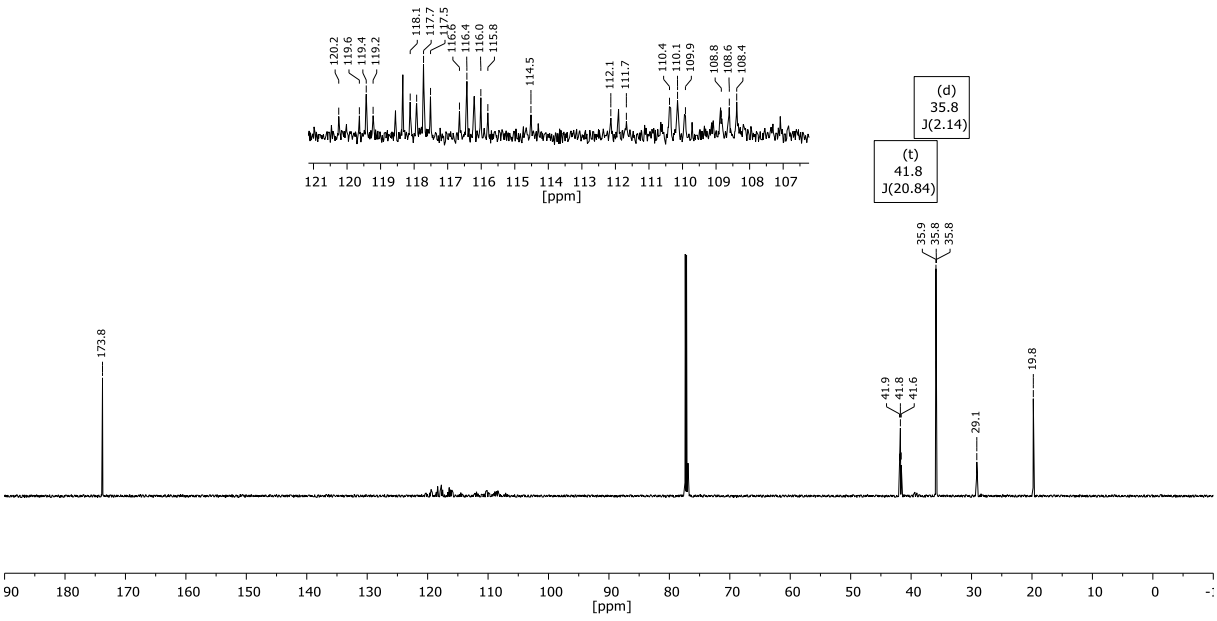

^{13}C-NMR-spectrum (151 MHz, $CDCl_3$)

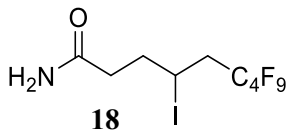

18

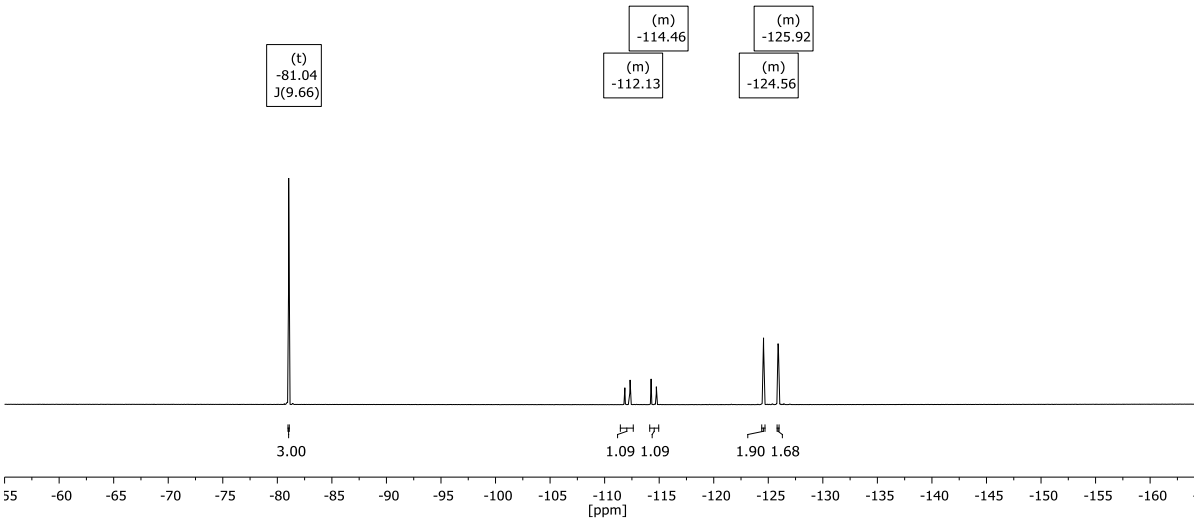

^{19}F-NMR-spectrum (565 MHz, $CDCl_3$)

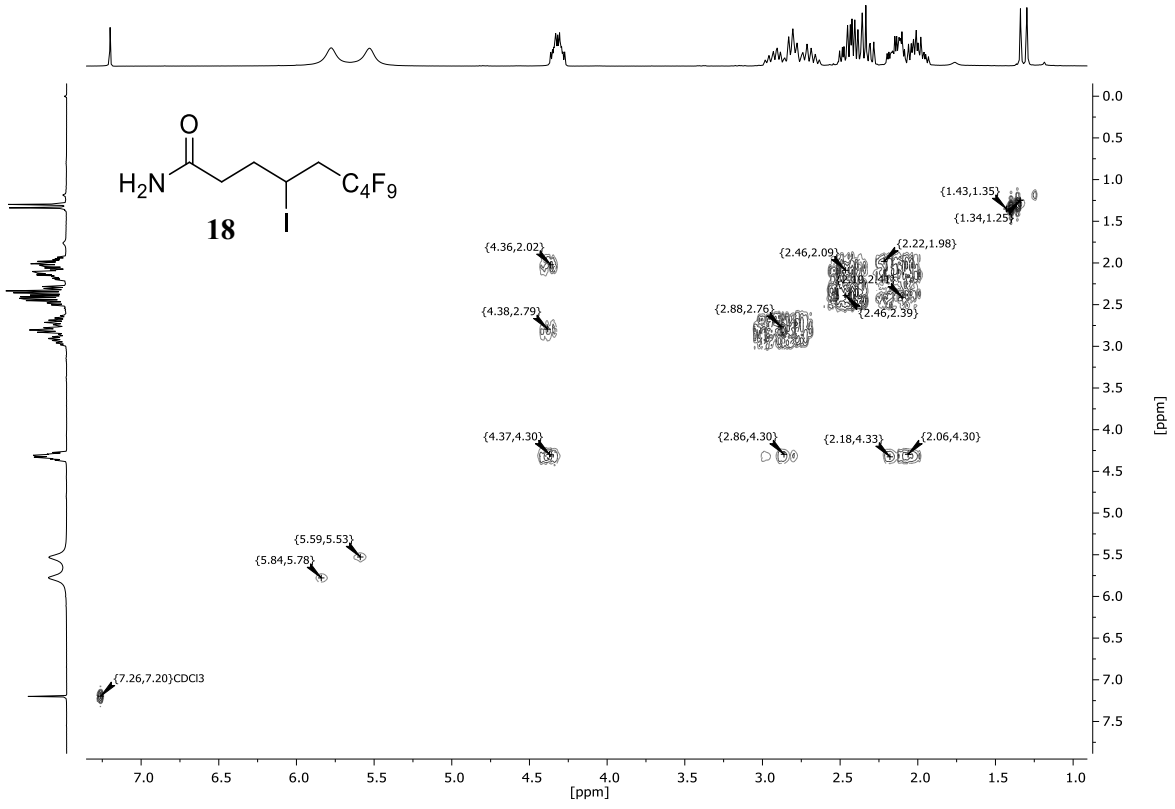

COSY-spectrum (300 MHz, 300 MHz, $CDCl_3$)

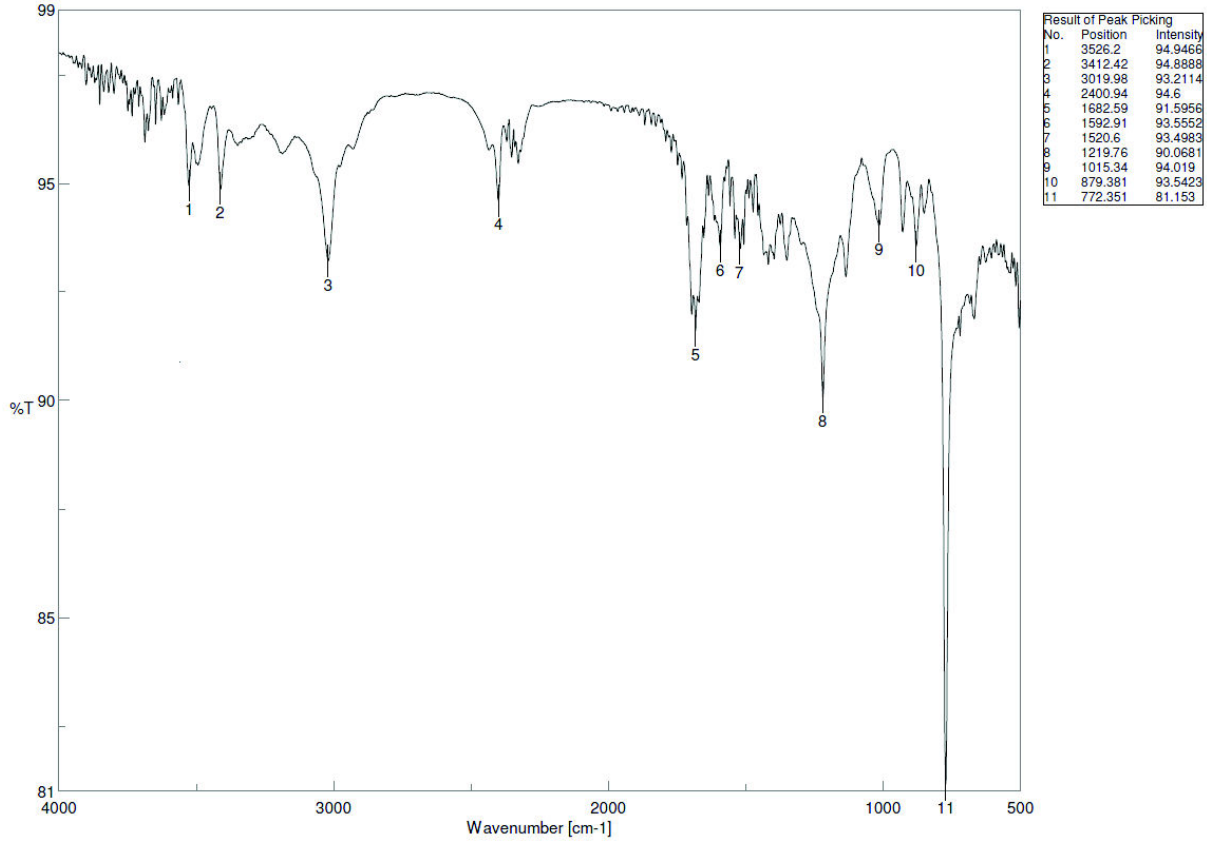

IR-spectrum (film on NaCl)

7.15. 1-(3-(4,4,5,5,6,6,7,7,7-Nonafluoro-2-iodoheptyl)phenyl)ethan-1-one (19)

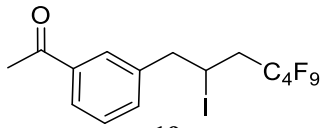

19

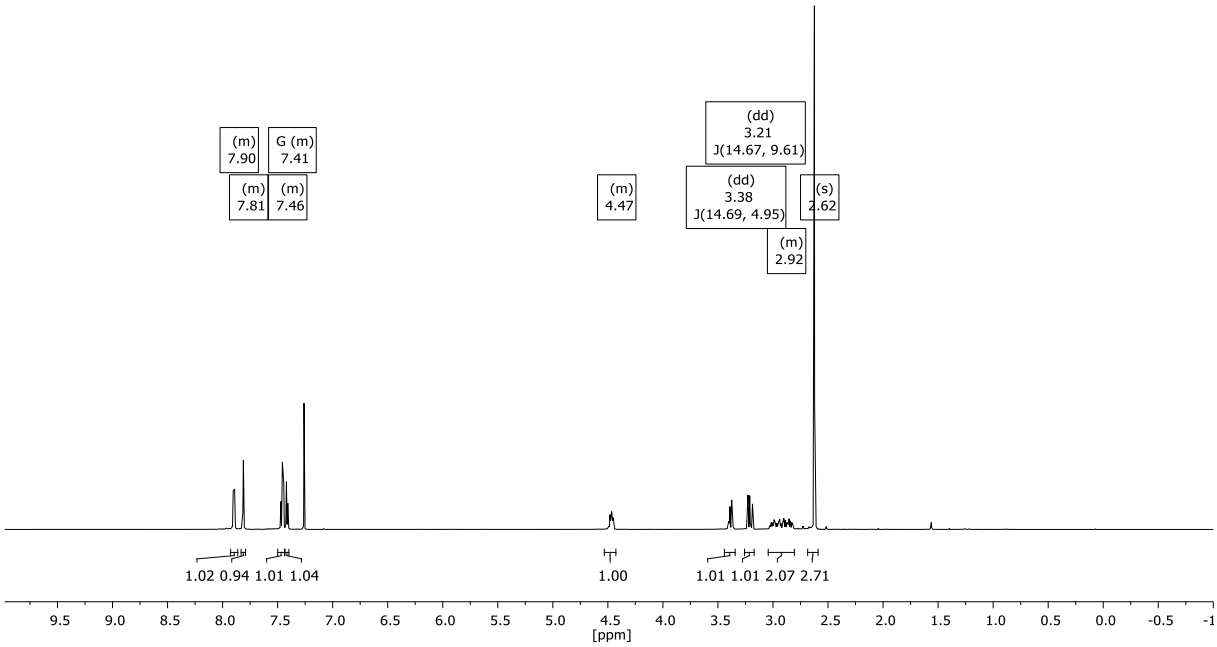

^{1}H-NMR-spectrum (300 MHz, $CDCl_3$)

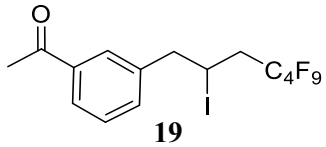

19

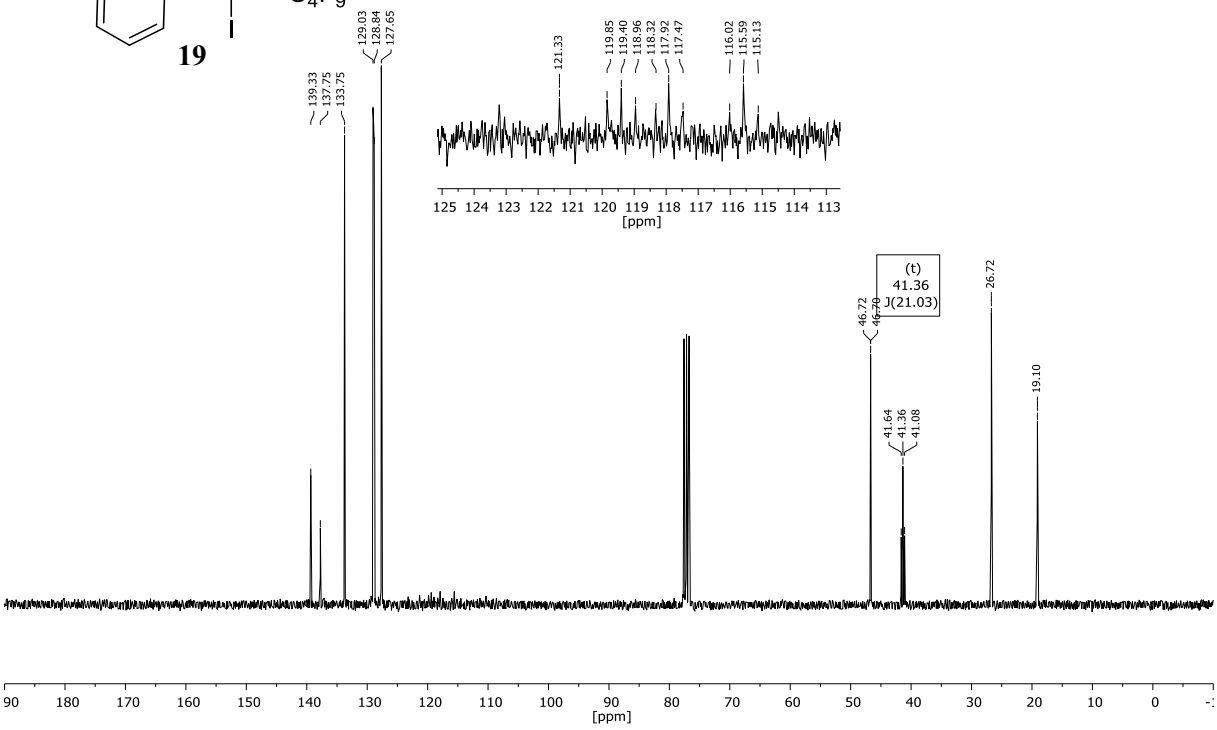

^{13}C-NMR-spectrum (75.5 MHz, $CDCl_3$)

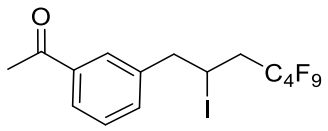

19

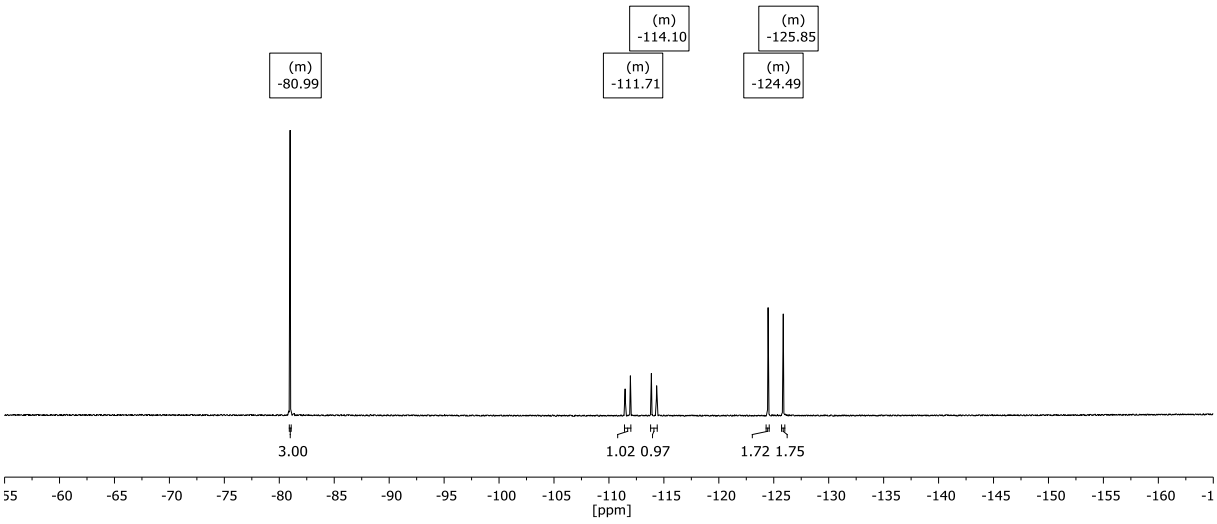

^{19}F-NMR-spectrum (565 MHz, $CDCl_3$)

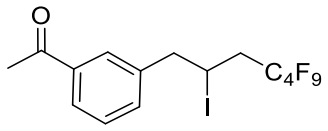

19

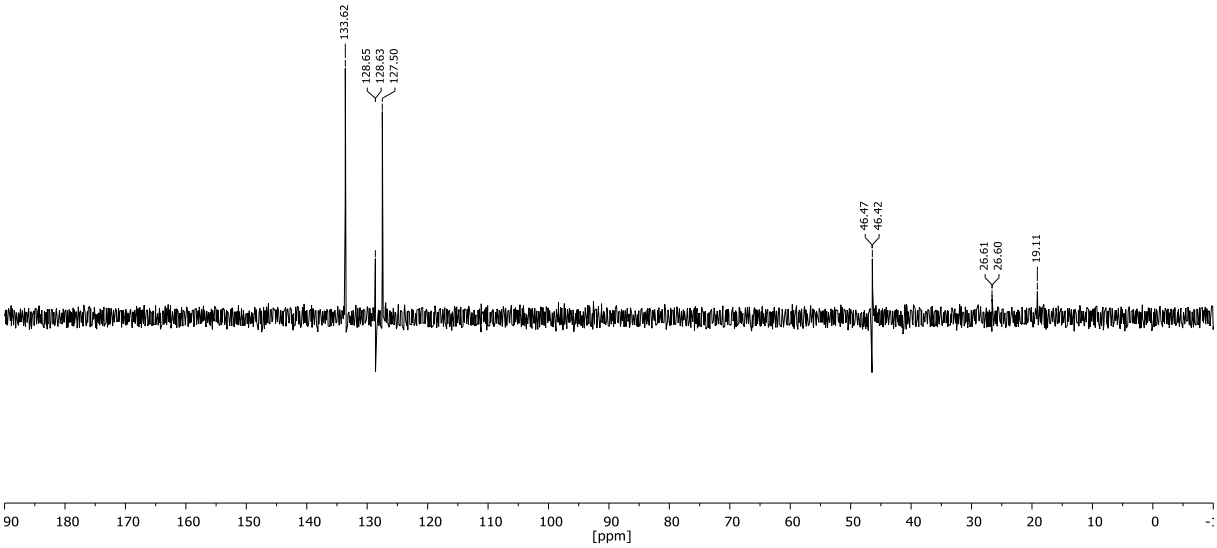

DEPT-spectrum (75.5 MHz, $CDCl_3$)

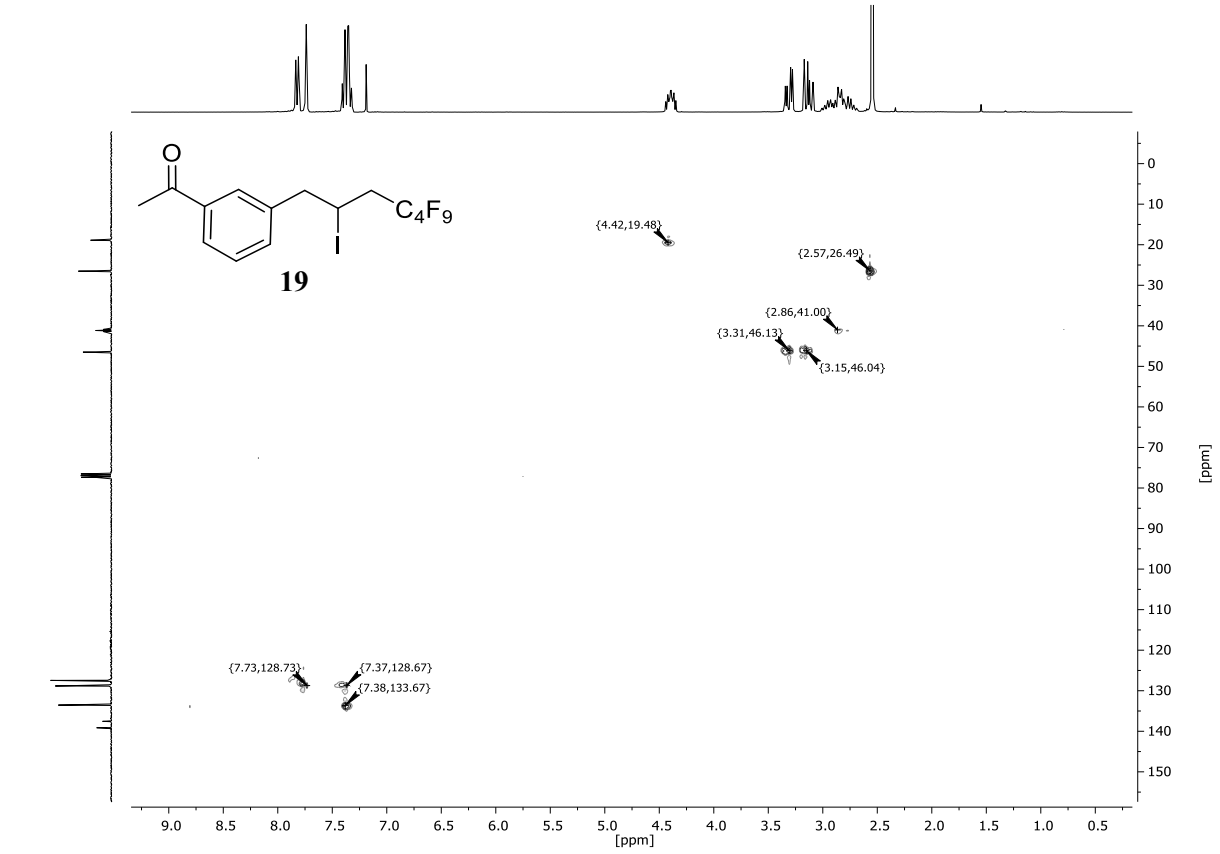

HSQC-spectrum (300, 75.5 MHz, $CDCl_3$)

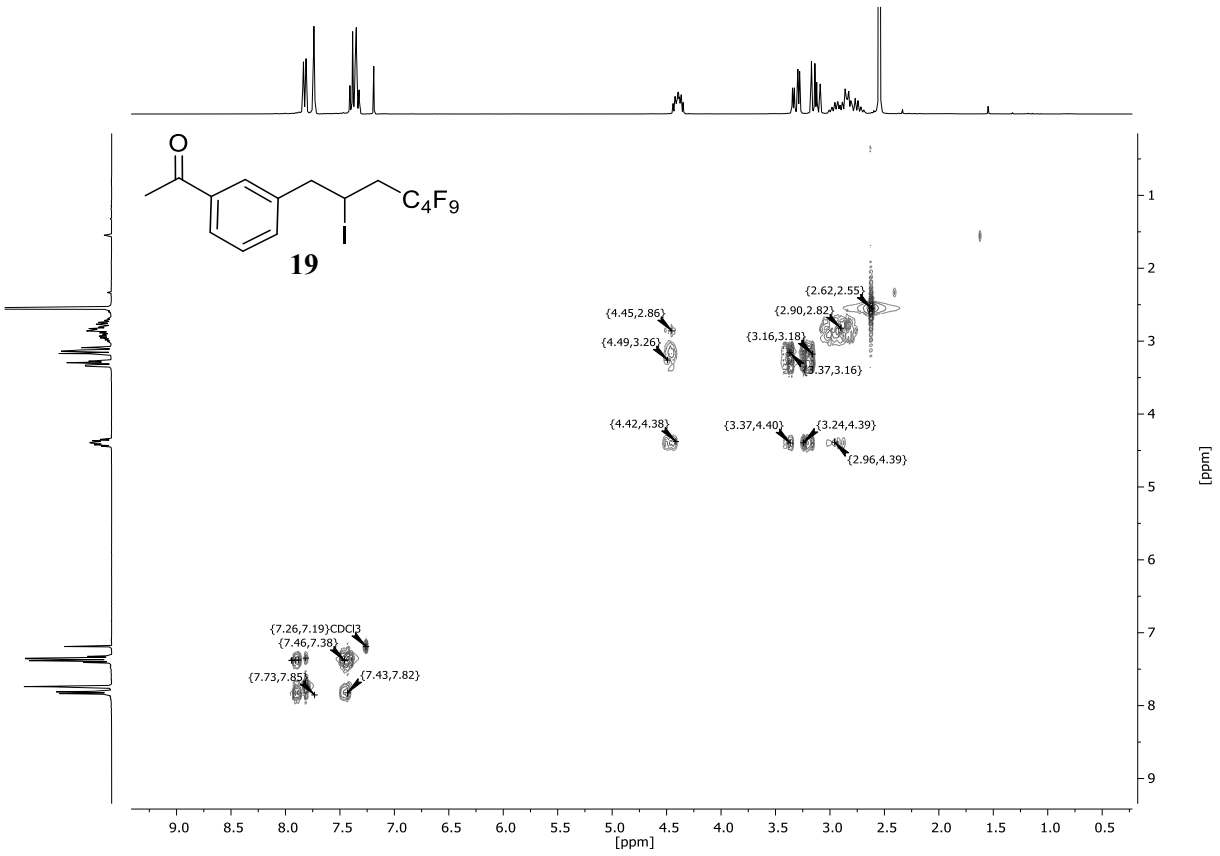

COSY-spectrum (300, 300 MHz, $CDCl_3$)

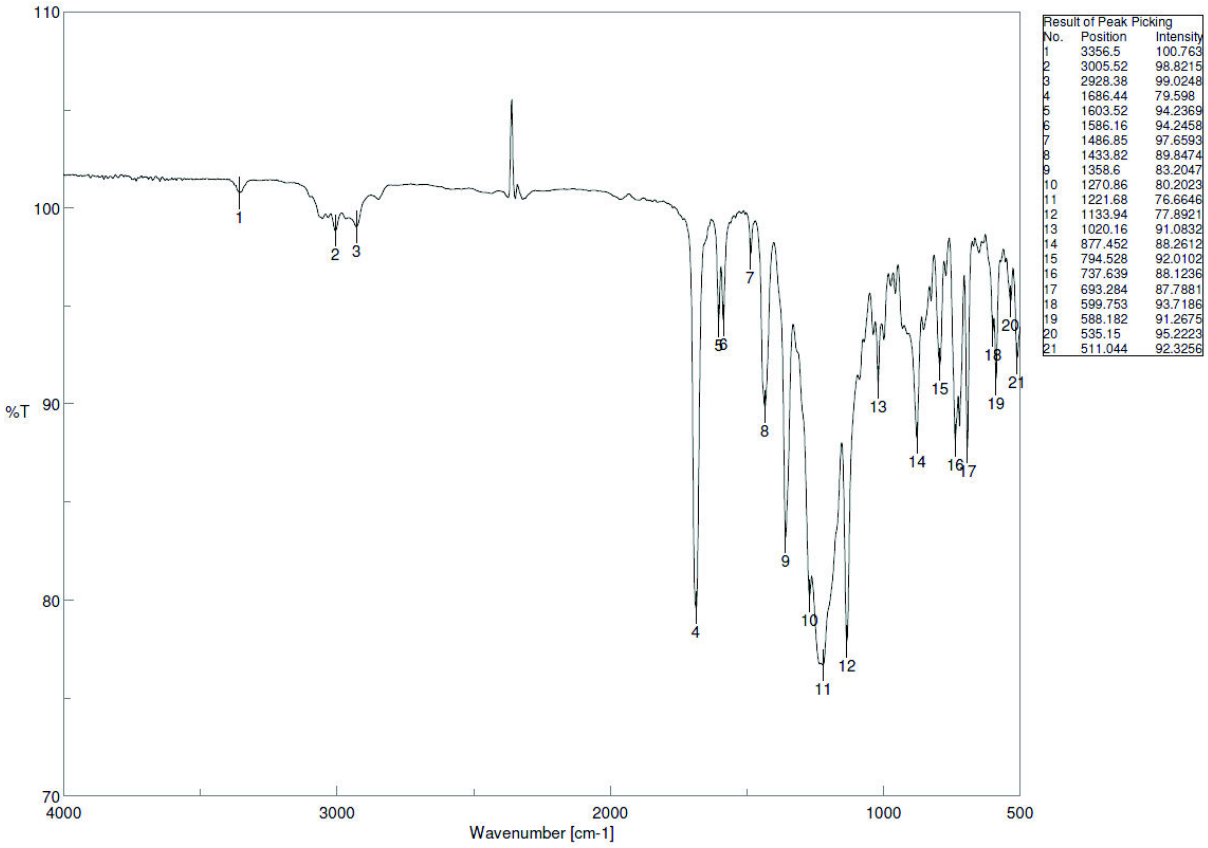

Result of Peak Picking

No.	Position	Intensity
1	3356.5	100.763
2	3005.52	98.8215
3	2928.38	99.0248
4	1686.44	79.598
5	1603.52	94.2369
6	1586.16	94.2458
7	1486.85	97.6593
8	1433.82	89.8474
9	1358.6	83.2047
10	1270.86	80.2023
11	1221.68	76.6646
12	1133.94	77.8921
13	1020.16	91.0832
14	877.452	88.2612
15	794.528	92.0102
16	737.639	88.1236
17	693.284	87.7881
18	599.753	93.7186
19	588.182	91.2675
20	535.15	95.2223
21	511.044	92.3256

IR-spectrum (film on NaCl)

7.16. 2 -(7,7,8,8,9,9,10,10,10-Nonafluoro-5-iododecyl)isoindoline-1,3-dione (20)

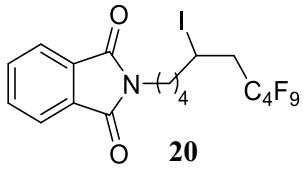

20

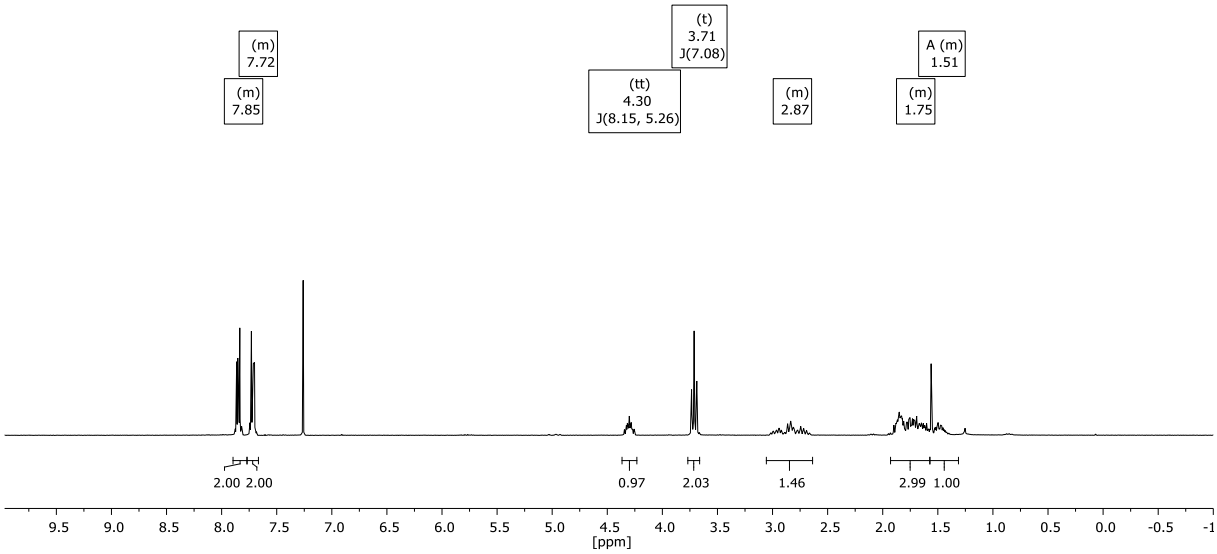

^{1}H-NMR-spectrum (300 MHz, $CDCl_3$)

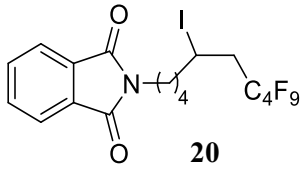

20

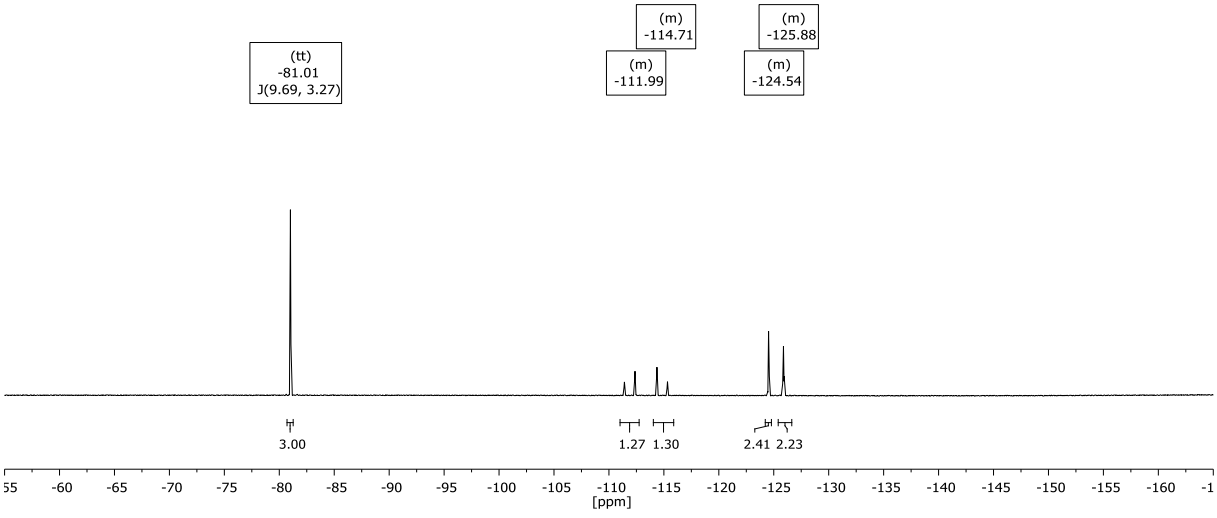

^{19}F-NMR-spectrum (282 MHz, $CDCl_3$)

7.17. 4-Chloro-N-(4,4,5,5,6,6,7,7,7-nonafluoro-2-iodoheptyl)benzamide (21)

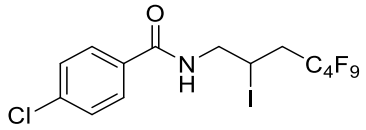

21

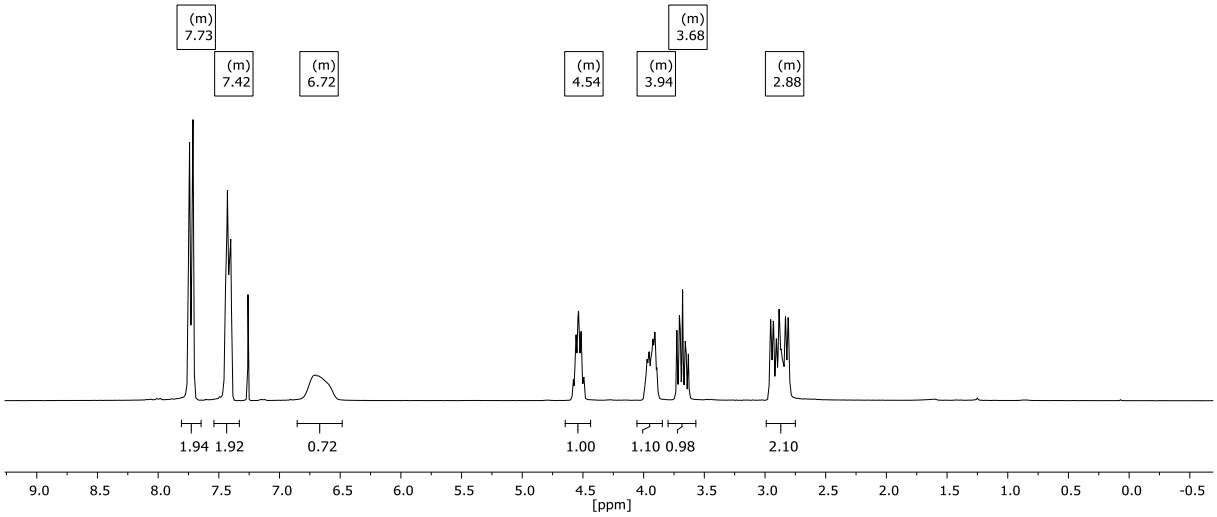

^{1}H-NMR-spectrum (300 MHz, $CDCl_3$)

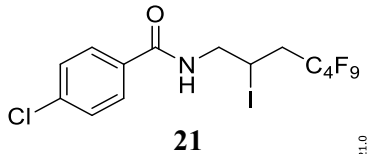

21

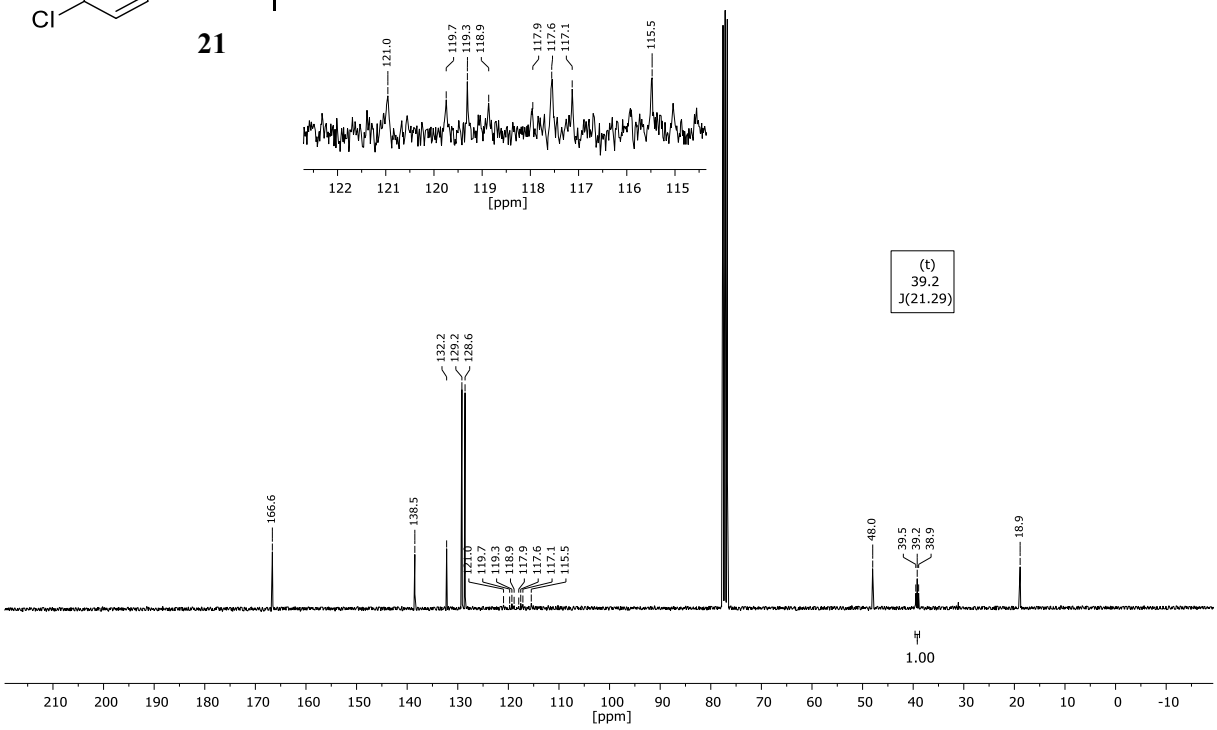

^{13}C-NMR-spectrum (75.5 MHz, $CDCl_3$)

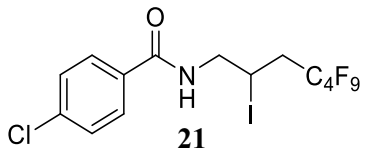

21

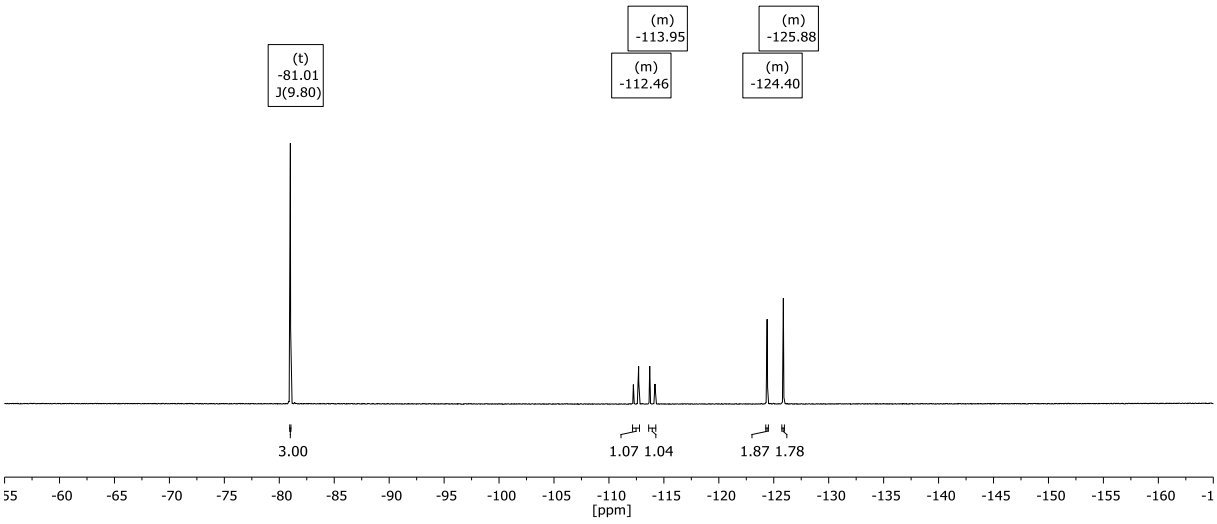

^{19}F-NMR-spectrum (565 MHz, $CDCl_3$)

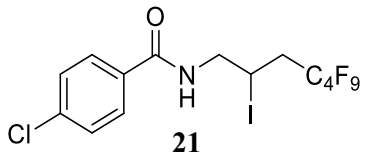

21

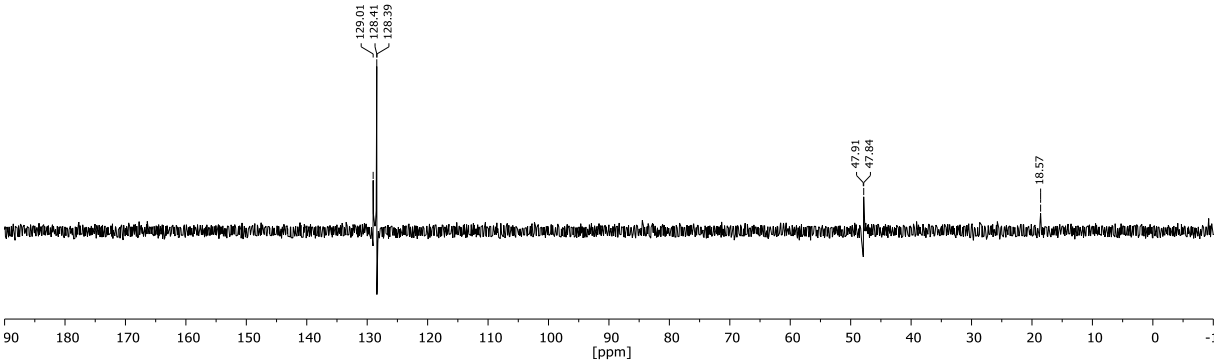

DEPT-spectrum (75.5 MHz, $CDCl_3$)

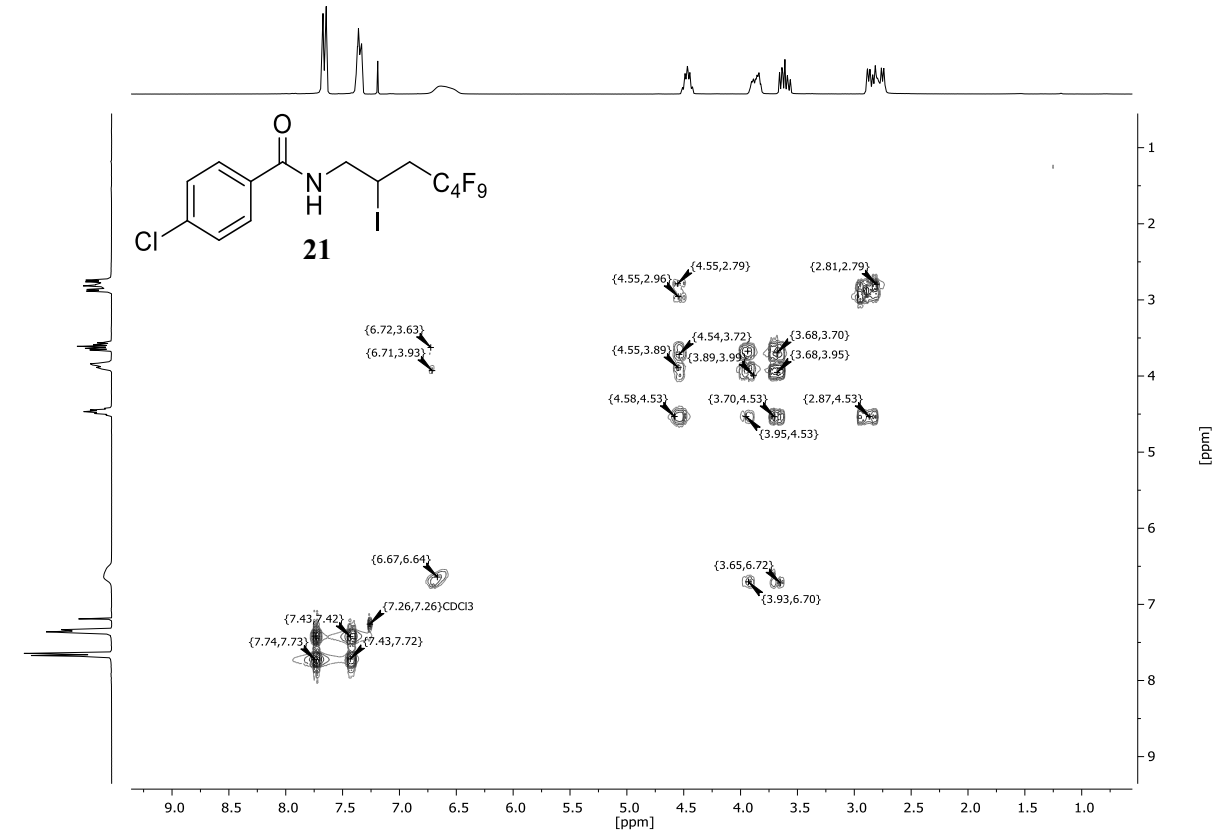

COSY-spectrum (300, 300 MHz, $CDCl_3$)

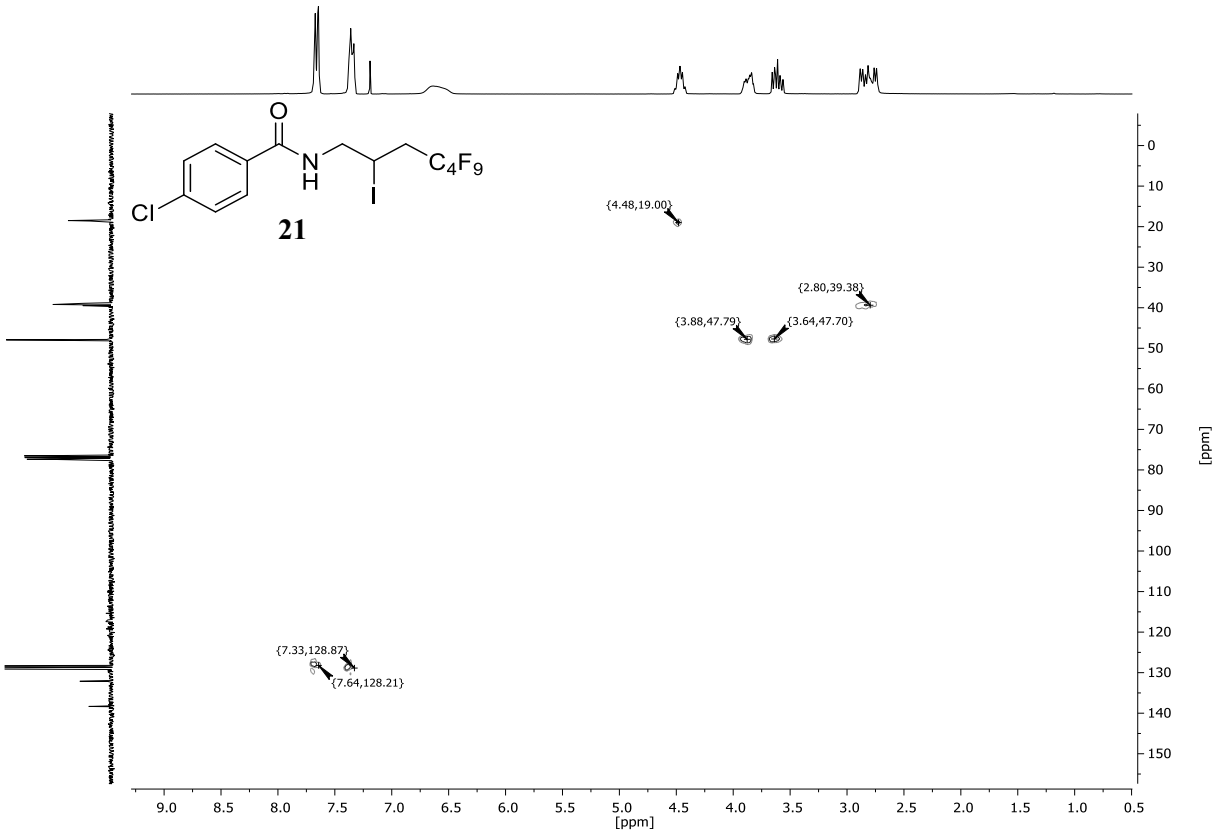

HSQC-spectrum (300, 75.5 MHz, $CDCl_3$)

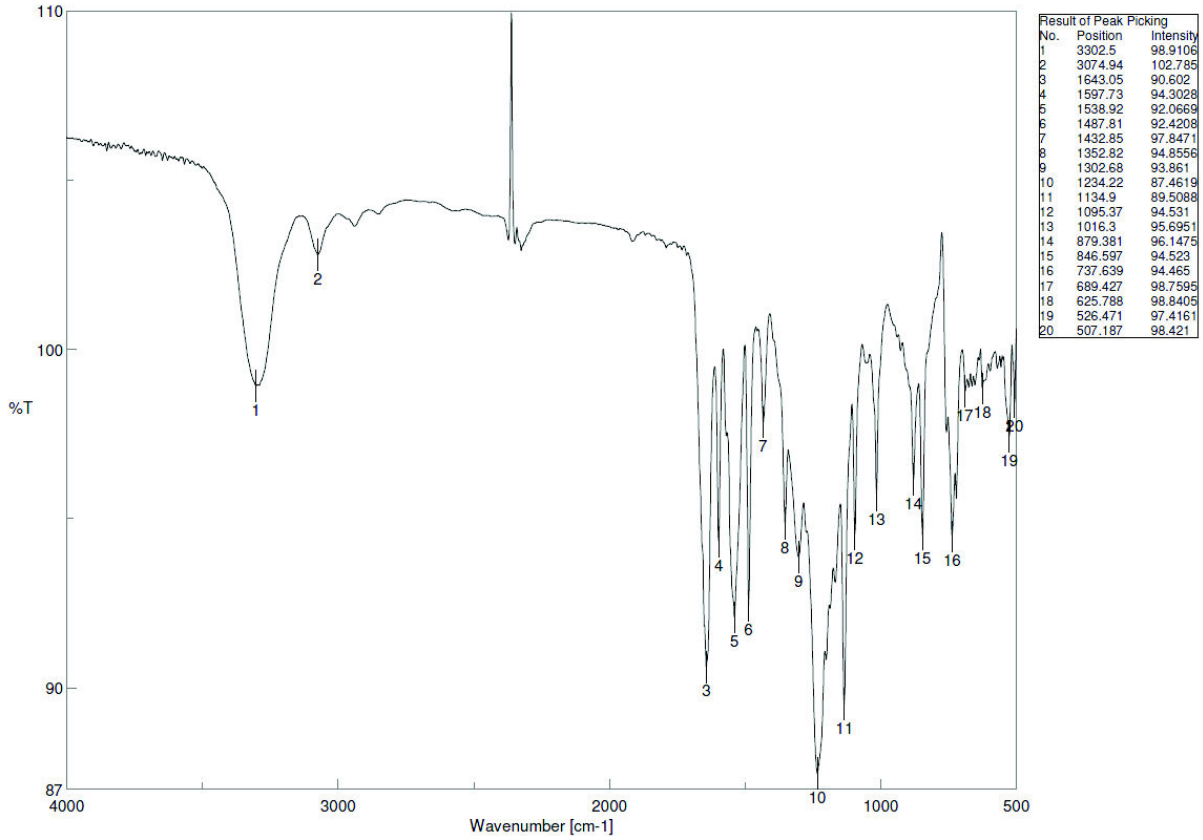

Result of Peak Picking

No.	Position	Intensity
1	3302.5	98.9106
2	3074.94	102.785
3	1643.05	90.602
4	1597.73	94.3028
5	1538.92	92.0669
6	1487.81	92.4208
7	1432.85	97.8471
8	1352.82	94.8556
9	1302.68	93.861
10	1234.22	87.4619
11	1134.9	89.5088
12	1095.37	94.531
13	1016.3	95.6951
14	879.381	96.1475
15	846.597	94.523
16	737.639	94.465
17	689.427	98.7595
18	625.788	98.8405
19	526.471	97.4161
20	507.187	98.421

IR-spectrum (film on NaCl)

7.18. 6,6,7,7,8,8,9,9,9-Nonafluoro-4-iodononyl 4-chlorobenzoate (22)

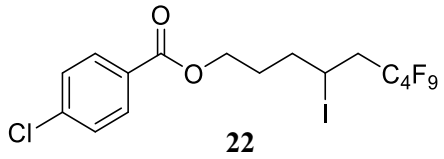

22

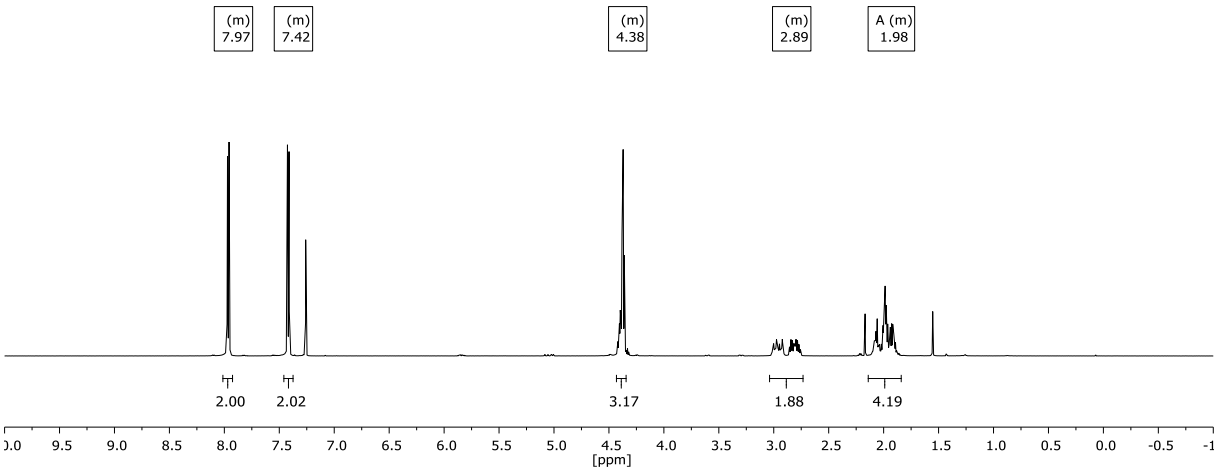

^{1}H-NMR-spectrum (300 MHz, $CDCl_3$)

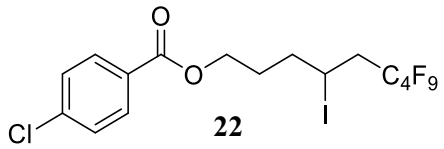

22

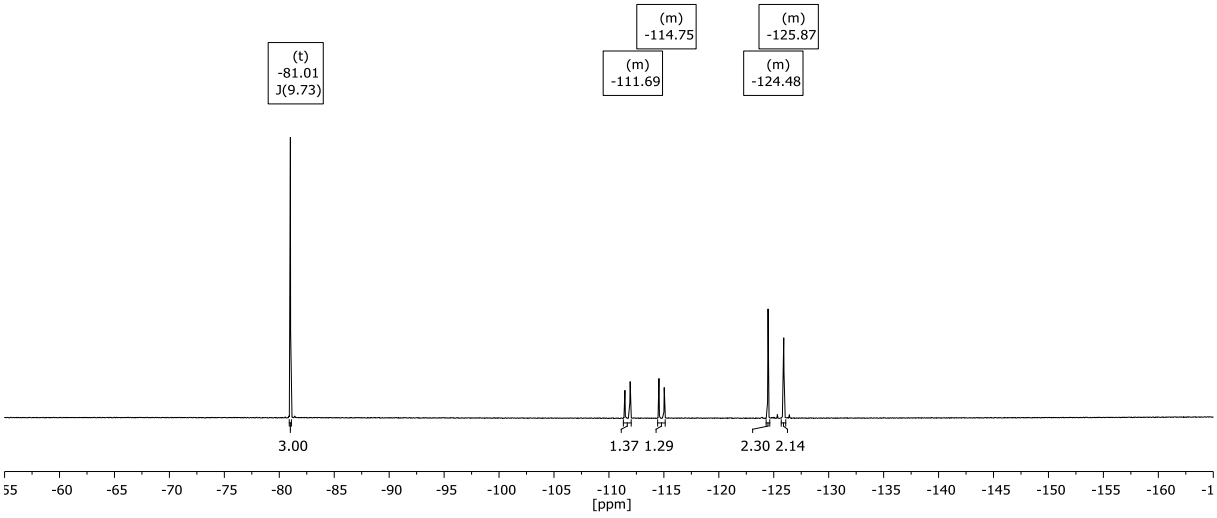

^{19}F-NMR-spectrum (565 MHz, $CDCl_3$)

7.19. 1-Bromo-4-((7,7,8,8,9,9,10,10,10-nonafluoro-5-iododecyl)oxy)benzene (23)

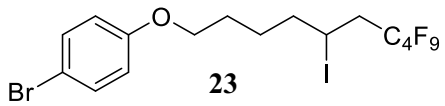

23

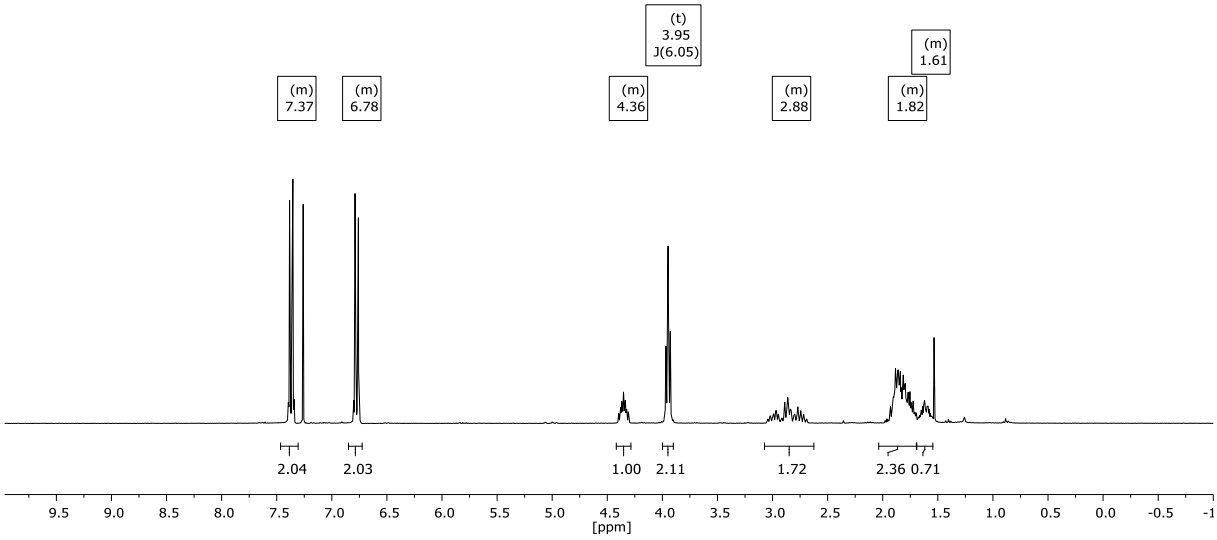

^{1}H-NMR-spectrum (300 MHz, $CDCl_3$)

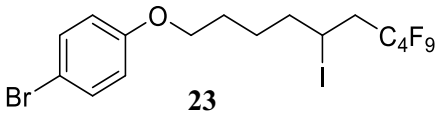

23

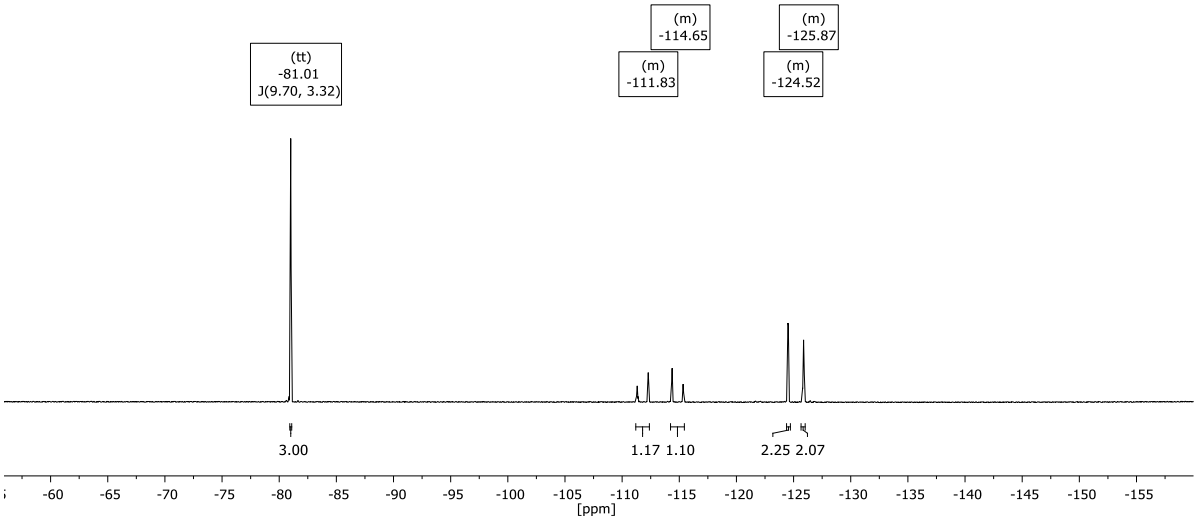

^{19}F-NMR-spectrum (282 MHz, $CDCl_3$)

7.20. 1-Methoxy-4-(4,4,5,5,6,6,7,7,7-nonafluoro-2-iodoheptyl)benzene (24)

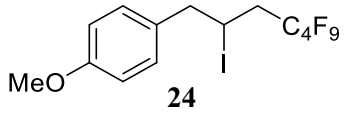

24

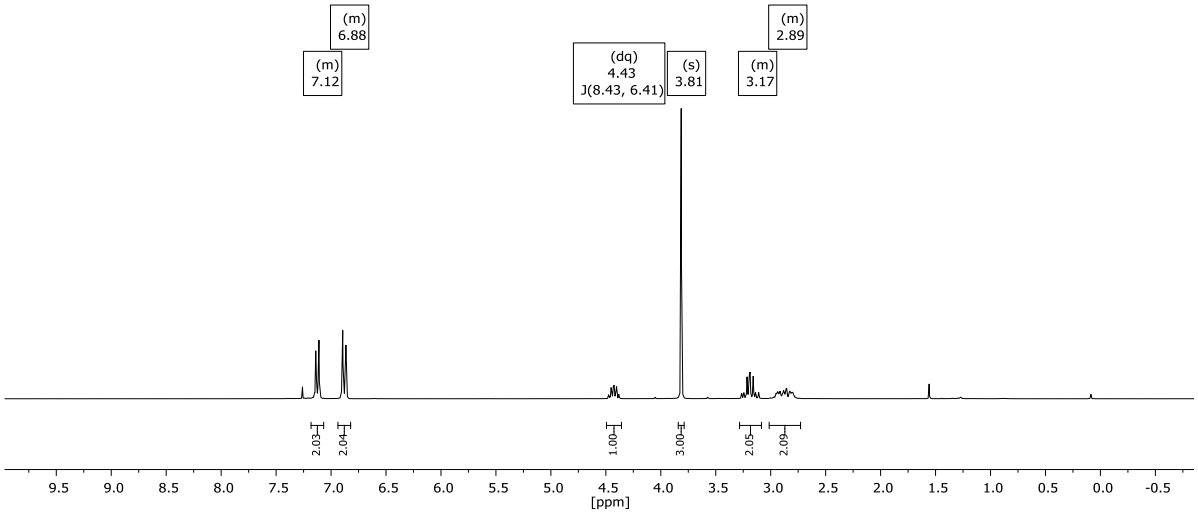

^{1}H-NMR-spectrum (300 MHz, $CDCl_3$)

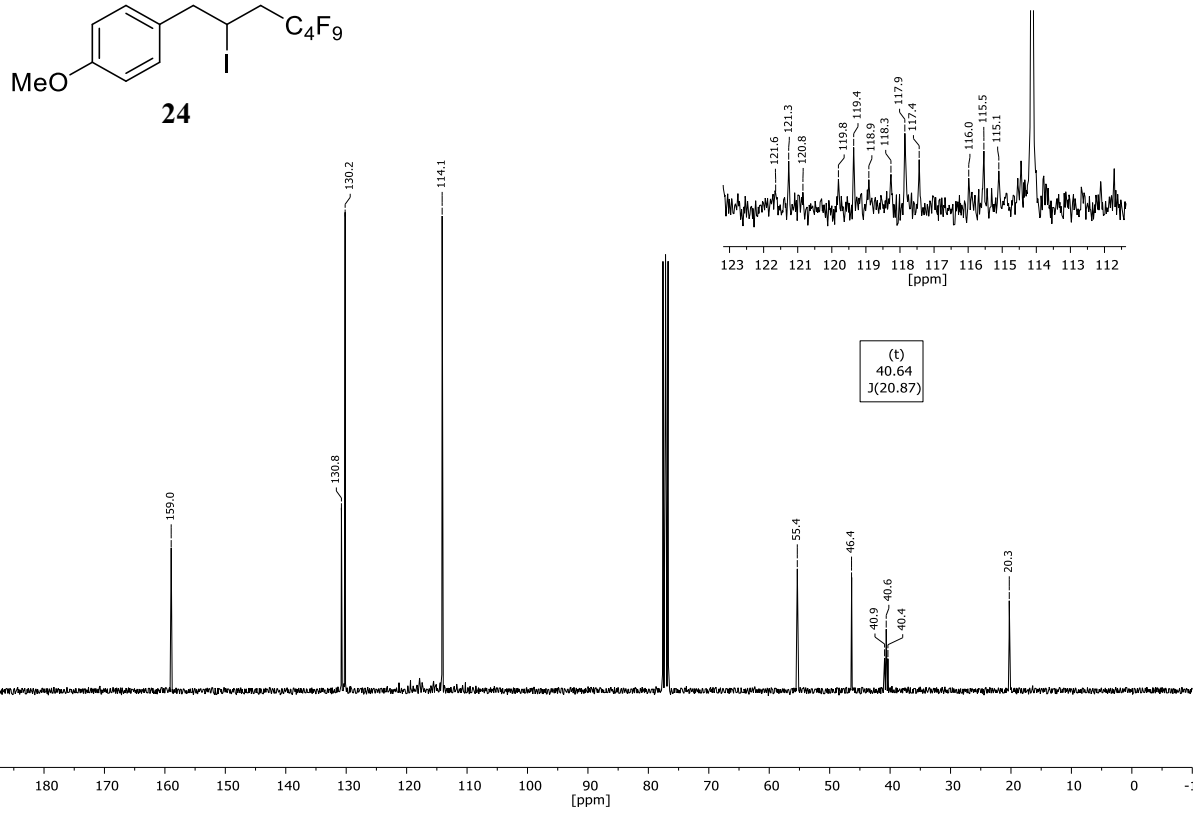

^{13}C-NMR-spectrum (75.5 MHz, $CDCl_3$)

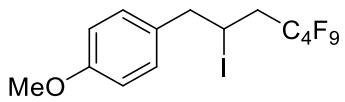

24

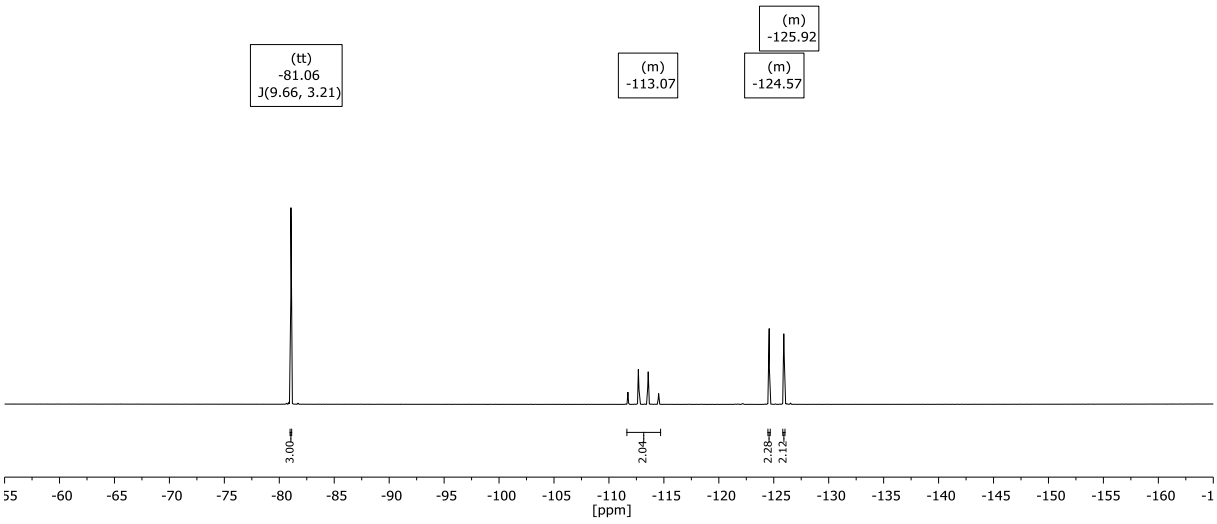

^{19}F-NMR-spectrum (282 MHz, $CDCl_3$)

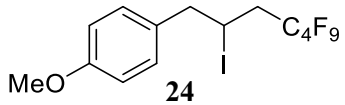

24

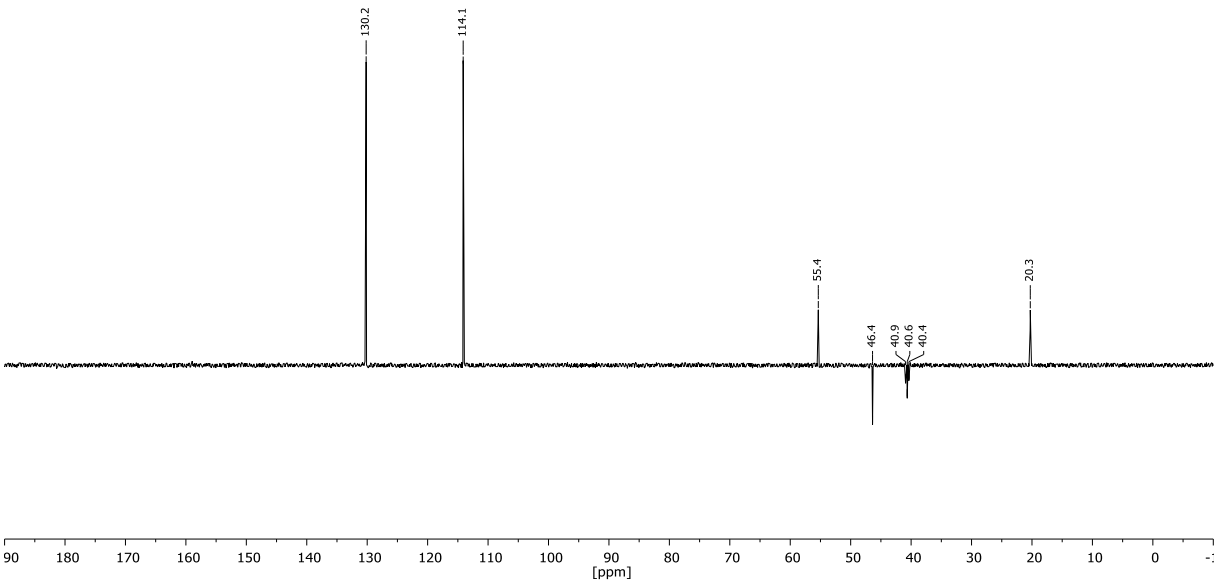

DEPT-spectrum (75.5 MHz, $CDCl_3$)

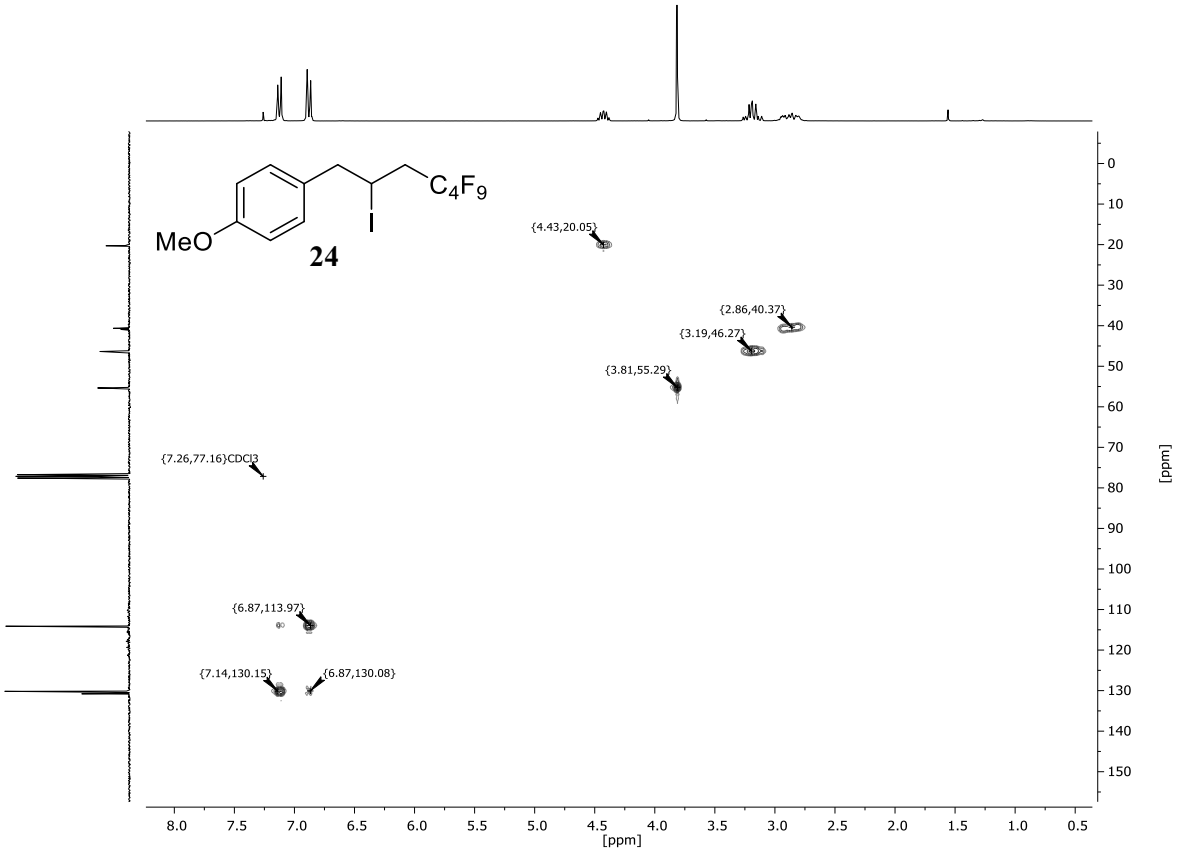

HSQC-spectrum (300, 75.5 MHz, $CDCl_3$)

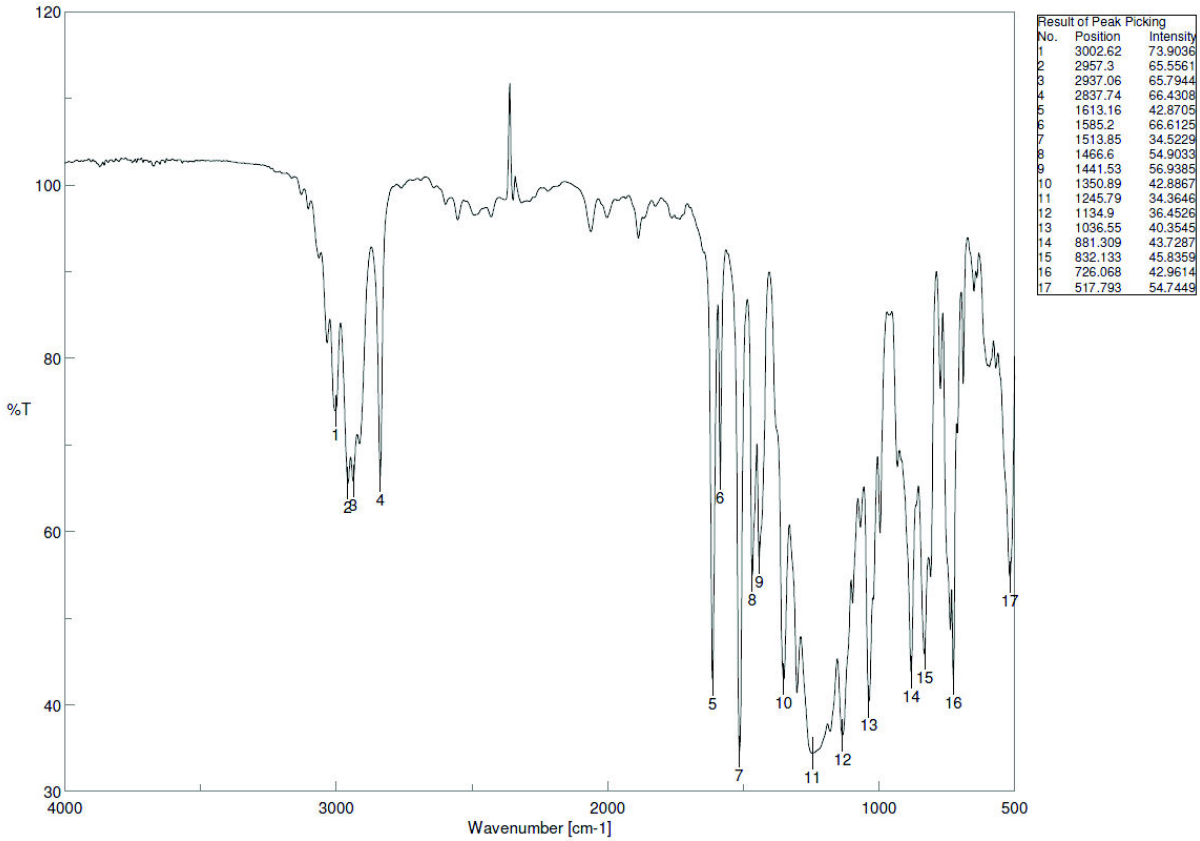

IR-spectrum (film on NaCl)

7.21. Dec-9-en-1-yl-4-methylbenzenesulfonate (39)[7]

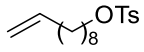

39

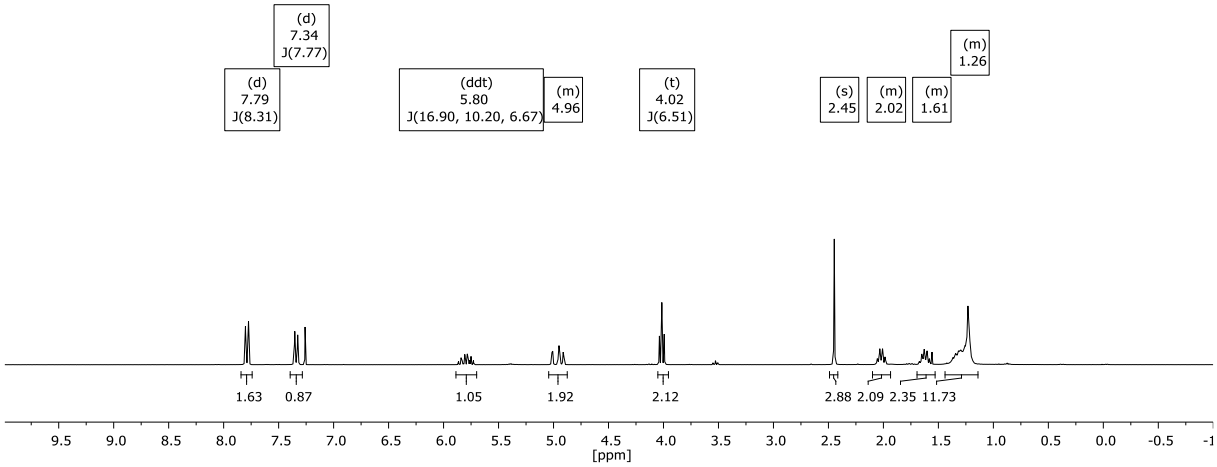

^{1}H-NMR-spectrum (300 MHz, $CDCl_3$)

7.22. 10-Azido-dec-1-ene (41)[8]

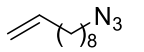

41

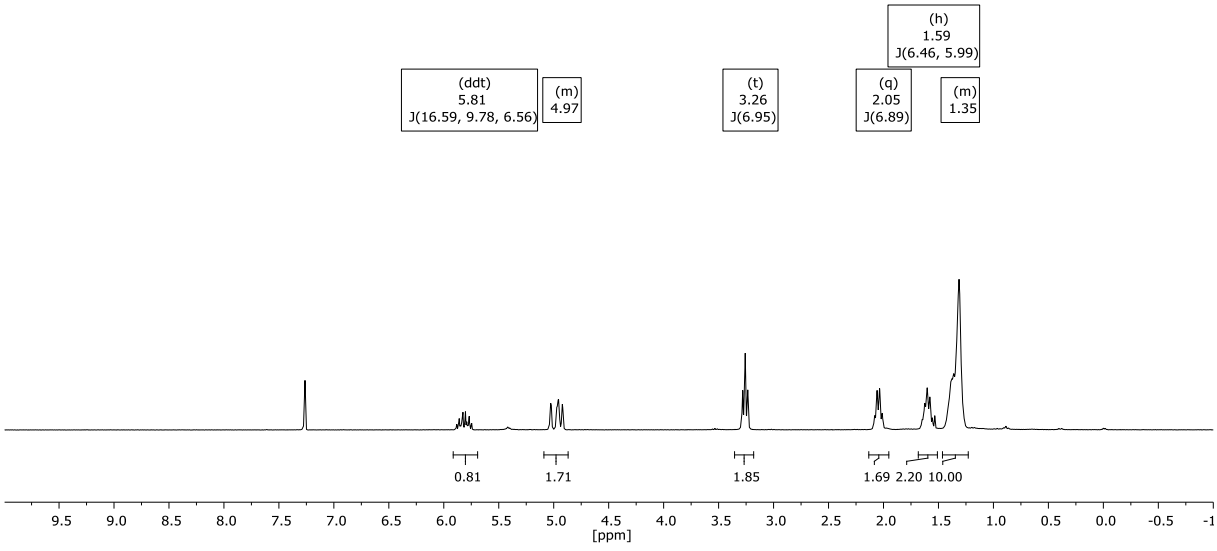

^{1}H-NMR-spectrum (300 MHz, $CDCl_3$)

7.23. Pent-4-enamide (44)[10]

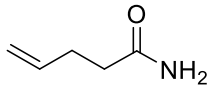

44

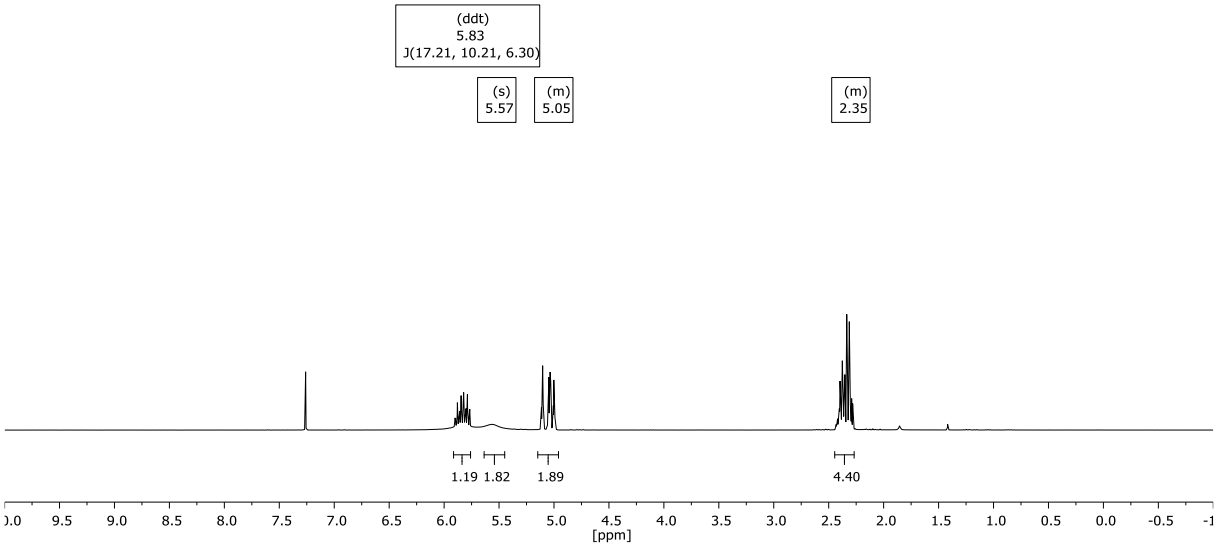

^{1}H-NMR-spectrum (300 MHz, $CDCl_3$)

7.24. 1-(3-Allylphenyl)ethan-1-one (46)[11]

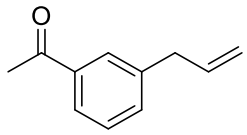

46

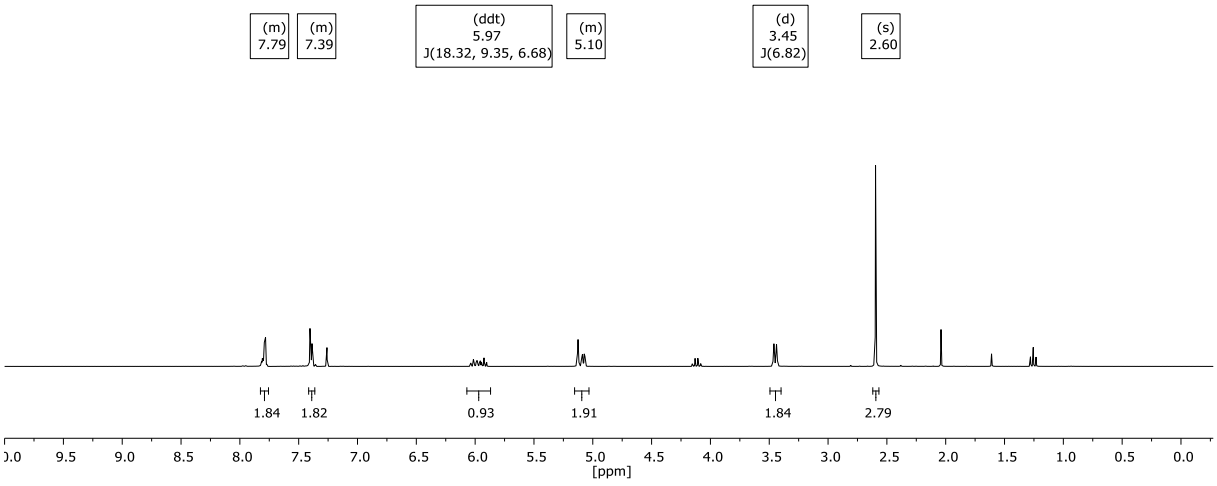

^{1}H-NMR-spectrum (300 MHz, $CDCl_3$)

7.25. 2-(Hex-5-en-1-yl)isoindoline-1,3-dion (49)[12]

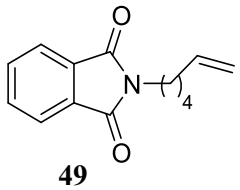

49

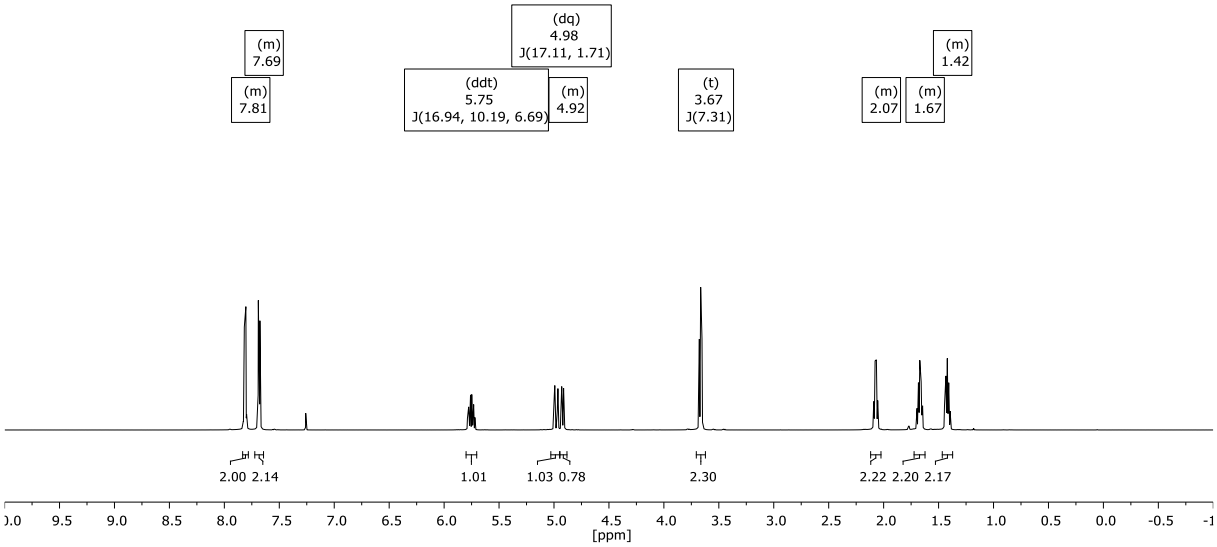

^{1}H-NMR-spectrum (300 MHz, $CDCl_3$)

8. Literature

(1) (a) Armarego, W. L. F.; Chai, C. L. L. In *Purification of Laboratory Chemicals (Sixth Edition)*, Butterworth-Heinemann: Oxford, 2009; pp 88-444; (b) Armarego, W. L. F.; Chai, C. L. L. In *Purification of Laboratory Chemicals (Sixth Edition)*, Butterworth-Heinemann: Oxford, 2009; pp 445-576.

(2) Anthony, F., *Magn. Reson. Chem.* **2004**, *42* (6), 534-555.

(3) Lumbierres, M.; Moreno-Mañas, M.; Vallribera, A., *Tetrahedron* **2002**, *58* (20), 4061-4065.

(4) Mao, L.-L.; Cong, H., *ChemSusChem* **2017**, *10* (22), 4461-4464.

(5) Shi, E.; Liu, J.; Liu, C.; Shao, Y.; Wang, H.; Lv, Y.; Ji, M.; Bao, X.; Wan, X., *J. Org. Chem.* **2016**, *81* (14), 5878-5885.

(6) Lee, J.; Joullié, M. M., *Tetrahedron Lett.* **2015**, *56* (23), 3378-3381.

(7) Montes Vidal, D.; von Rymon-Lipinski, A.-L.; Ravella, S.; Groenhagen, U.; Herrmann, J.; Zaburannyi, N.; Zarbin, P. H. G.; Varadarajan, A. R.; Ahrens, C. H.; Weisskopf, L.; Müller, R.; Schulz, S., *Angew. Chem. Int. Ed.* **2017**, *56* (15), 4342-4346.

(8) Cabezon, B.; Cao, J.; Raymo, F. M.; Stoddart, J. F.; White, A. J. P.; Williams, D. J., *Chem. Eur. J.* **2000**, *6* (12), 2262-2273.

(9) Nicolai, S.; Waser, J., *Org. Lett.* **2011**, *13* (23), 6324-6327.

(10) Raoufmoghaddam, S.; Drent, E.; Bouwman, E. PROCESS TO PREPARE ε-CAPRO LACTAM. 2014.

(11) Thalji, R. K.; Ahrendt, K. A.; Bergman, R. G.; Ellman, J. A., *J. Am. Chem. Soc.* **2001**, *123* (39), 9692-9693.

(12) Fraunhoffer, K. J.; Bachovchin, D. A.; White, M. C., *Org. Lett.* **2005**, *7* (2), 223-226.

(13) Du, Y.; Pearson, R. M.; Lim, C.-H.; Sartor, S. M.; Ryan, M. D.; Yang, H.; Damrauer, N. H.; Miyake, G. M., *Chem. Eur. J.* **2017**, *23* (46), 10962-10968.

(14) Zeng, R.; Fu, C.; Ma, S., *Angew. Chem. Int. Ed.* **2012**, *51* (16), 3888-3891.

(15) Davis, C. R.; Burton, D. J.; Yang, Z.-Y., *J. Fluor. Chem.* **1995**, *70* (1), 135-140.

(16) Rawner, T.; Lutsker, E.; Kaiser, C. A.; Reiser, O., *ACS Catal.* **2018**, *8* (5), 3950-3956.

(17) Behrends, I.; Bähr, S.; Czekelius, C., *Chem. Eur. J.* **2016**, *22* (48), 17177-17181.

(18) Spittler, M.; Helmecke, L.; Czekelius, C., *Eur. J. Org. Chem.* **2019**, 458-468.

(19) Takagi, T.; Kanamori, T., *J. Fluor. Chem.* **2011**, *132* (6), 427-429.

(20) Wang, Y.; Wang, J.; Li, G.-X.; He, G.; Chen, G., *Org. Lett.* **2017**, *19* (6), 1442-1445.

Supplementary Materials: Visible Light-Induced Homolytic Cleavage of Perfluoroalkyl Iodides Mediated by Phosphines

Mario Bracker [1], Lucas Helmecke [2], Martin Kleinschmidt [1]*, Constantin Czekelius [2]* and Christel M. Marian [1]*

March 30, 2020

Contents

S1. General Experimental Procedures

All preparations involving air- and moisture-sensitive compounds were carried out inside a glove box (*Vacuum Atmospheres* model OMNI-LAB) under N_2 atmosphere (*Air Liquide ALPHAGAZ*^{TM} 5.0). Glassware was dried for 2 hours at 120 °C and cooled down in vacuo.

Nonafluoro-1-iodobutane was purchased from TCI and was filtered through a column packed with aluminum oxide 90 basic 0.063 - 0.200 mm (activity stage I) and activated molecular sieve (4 Å) under N_2 atmosphere. The clear and colorless liquid was stored in amber glass vials under N_2 atmosphere. Tri-*tert*-butylphosphine was purchased from Sigma Aldrich.

Pentane and dichloromethane were dried with the solvent purification system MP-SPS 800 from M.Braun and degassed with freeze-pump-thaw.

^{1}H-, ^{13}C, ^{31}P-spectra were recorded on *Bruker* Avance III 300 and 600. Chemical shifts are reported in parts per million (ppm) to the corresponding solvent. The order of citation in parentheses is a) multiplicity (s = singlet, d = doublet, m = multiplet), b) coupling constants, c) number of protons, and d) assignment. Coupling constants (*J*) were reported in Hertz (Hz). If not described differently, the NMR-spectra were measured at 298 K.

UV-VIS spectra were measured on a Perkin Elmer Lamda 2 UV-VIS spectrometer in Hellma cuvettes (10 x 10 mm, Suprasil quartz glass).

GC measurements were performed on a Shimadzu GC-2010 equipped with an auto injector AOC-20i (syringe code: 10R-S-0.63C). A ZB-Wax Plus column (30 × 0.25 mm × 0.25 μm) was used. As internal standard *n*-decane (Acros Organics, purity 99 + %, LOT:1283567) was added to the reaction solution. The used photoreactor is self-assembled and is described in literature. [1]

S2. Synthesis of phosphites

S2.1. 4-Methyl-2,6,7-trioxa-1-phosphabicyclo-[2,2,2]-octane (caged phosphite)

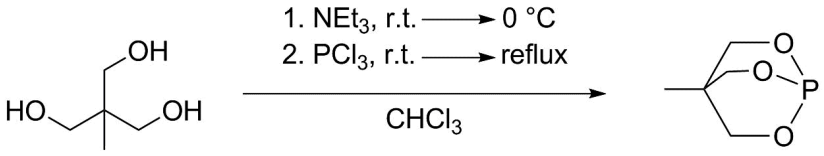

The synthesis of 4-methyl-2,6,7-trioxa-1-phosphabicyclo-[2,2,2]-octane was conducted similar to a literature known procedure. [2] In a 250 ml two-necked round-bottom flask with condenser tris(hydroxymethyl)ethane (7.21 g, 60.0 mmol, 1.0 equiv) and triethylamine (19.2 ml, 138 mmol, 2.3 equiv) were dissolved in $CHCl_3$ (70 ml). PCl_3 (5.2 ml, 59 mmol) in $CHCl_3$ (10 ml) was added dropwise at 0 °C to the cloudy reaction solution. After removing the ice bath the reaction solution was clear and was refluxed for 12 h. The clear reaction solution was extracted with desalinated water (3 × 50 ml), dried over anhydrous $MgSO_4$, filtered and the solvent was evaporated. The obtained colorless gel-like crystals were dissolved in CH_2Cl_2 (4 ml) and the solvent was evaporated again yielding colorless crystals.

yield (148.1 g mol^{-1})	4.70 g (31.7 mmol, 53%)

^{1}H-NMR (600 MHz, $CDCl_3$) δ [ppm] 3.94 (d, J = 1.9 Hz, CH_2, 6H), 0.73 (s, CH_3, 3H)

^{13}C-NMR (75.5 MHz, $CDCl_3$) δ [ppm] 71.94 (s, C—CH_3), 32.13 (d, J = 22.5 Hz, CH_2), 16.82 (d, J = 5.5 Hz, CH_3)

^{31}P-NMR (243 MHz, $CDCl_3$) δ [ppm] 91.2

Mp: 91.2 – 96.9 °C

Analytic data are consistent with literature-known values. [2,3]

S2.2. Tri-tert-*butyl phosphite*

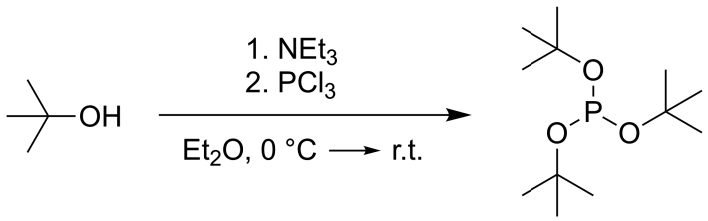

The synthesis of tri-*tert*-butyl phosphite was conducted similar to a literature known procedure. [4] Anhydrous diethyl ether was degassed with freeze-pump-thaw and each educt was degassed in Et_2O again before it was added. *Tert*-butyl alcohol (11.7 ml, 0.125 mol, 2.94 equiv) in Et_2O (25 ml) and triethylamine (17.3 ml, 0.125 mol, 2.94 equiv) in Et_2O (25 ml) were added together at 0 °C. PCl_3 (3.70 ml, 0.0425 mol) in Et_2O (12 ml) was added slowly via a dropping funnel, so that the reaction temperature maintained between 0 °C and 5 °C. After the addition was completed, Et_2O (30 ml) was added to the reaction solution and the reaction mixture was stirred 1 h at 0 °C and 16 h at r.t.. The reaction solution was separated via Schlenk filtration and the solvent was removed in vacuo. While the solvent was removed the round-bottom flask was cooled with an ice/water bath. A pale yellow oil was obtained, transferred into the glovebox and filtered through a syringe filter.

yield (250.3 g mol^{-1})	871.6 mg (3.48 mmol, 8%)

^{1}H-NMR (300 MHz, C_6D_6) δ [ppm] 1.39 (s, (CH_3)$_3$C).

^{13}C-NMR (75.5 MHz, C_6D_6) δ [ppm] 76.1 (s, (CH_3)$_3$*C*), 31.4 (s, (CH_3)$_3$C)

^{31}P-NMR (121 MHz, C_6D_6) δ [ppm] 151.1

^{1}H-NMR (300 MHz, $CDCl_3$) δ [ppm] 1.28 (s, (CH_3)$_3$C).

^{13}C-NMR (75.5 MHz, $CDCl_3$) δ [ppm] 75.8 (d, J = 6.0 Hz, (CH_3)$_3$*C*), 31.1 (d, J = 8.1 Hz, (CH_3)$_3$C)

^{31}P-NMR (121 MHz, $CDCl_3$) δ [ppm] 140.1

Analytic data are consistent with literature-known values. [4–6]

S3. Reactions

S3.1. Reaction with 4-methyl-2,6,7-trioxa-1-phosphabicyclo-[2,2,2]-octane (caged phosphite)

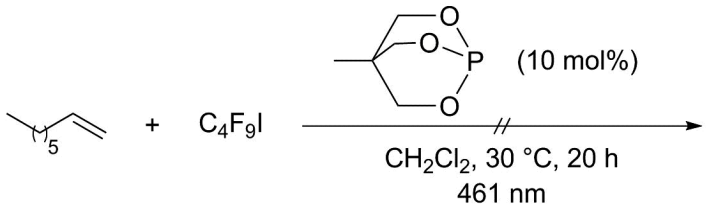

Caged phosphite (8.0 mg, 0.054 mmol, 10 mol%) was weighed into a 4 ml screw neck glass vial. Under a stream of nitrogen 1-octene (84 μl, 0.530 mmol) and CH_2Cl_2 (2 ml) were added. Under red light and the stream of nitrogen C_4F_9I (100 μl, 0.583 mmol, 1.10 equiv) was added, the vial was sealed with a septa screw cap and the reaction solution was irradiated (461 nm) for 20 h. After 1 h, 4 h and 20 h samples for a control by NMR spectroscopy were withdrawn under a stream of nitrogen and under red light. No conversion was observed.

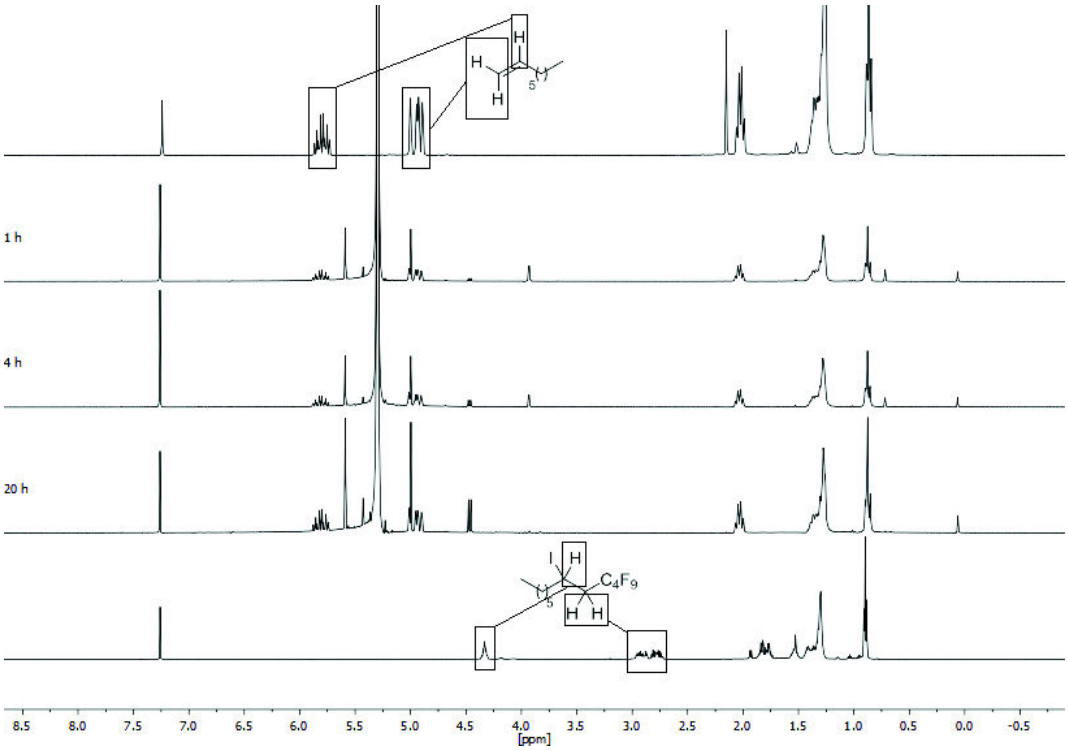

^{1}H-NMR-spectra (300 MHz, $CDCl_3$) of the reaction after 1 h, 4 h and 20 h in comparison with spectra of 1-octene (top) and the iodo perfluoroalkylation products (bottom).

*S3.2. Reaction with tri-*tert*-butylphosphite*

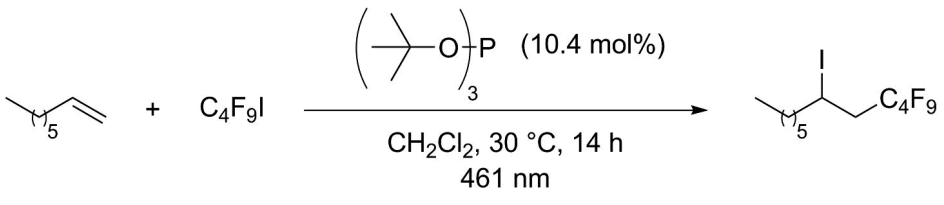

Inside the glovebox tri-*tert*-butylphoshite (14.4 mg, 0.0575 mmol, 10.4 mol%), *n*-decane (29.6 mg) and 1-octene (62.0 mg, 0.552 mmol) were weighed into a 4 ml screw neck glass vial. A Teflon stirring bar and CH_2Cl_2 (2 ml) were added. Under red light C_4F_9I (100 μl, 0.583 mmol, 1.05 equiv) was added, the vial was sealed with a septa screw cap and the reaction solution was irradiated (461 nm) for 14 h. After 1 h (conversion: 31%), 2 h (conversion: 51%) and 14 h (conversion: 56%) samples for a reaction control by GC were withdrawn under a stream of nitrogen. With a 1.0 ml syringe (Braun) flushed with N_2 0.10 ml of the reaction solution were withdrawn and diluted with 0.4 ml CH_2Cl_2 in a short amber thread vial. The vial was sealed with a black screw cap.

S4. NMR Spectra

S4.1. Caged phosphite

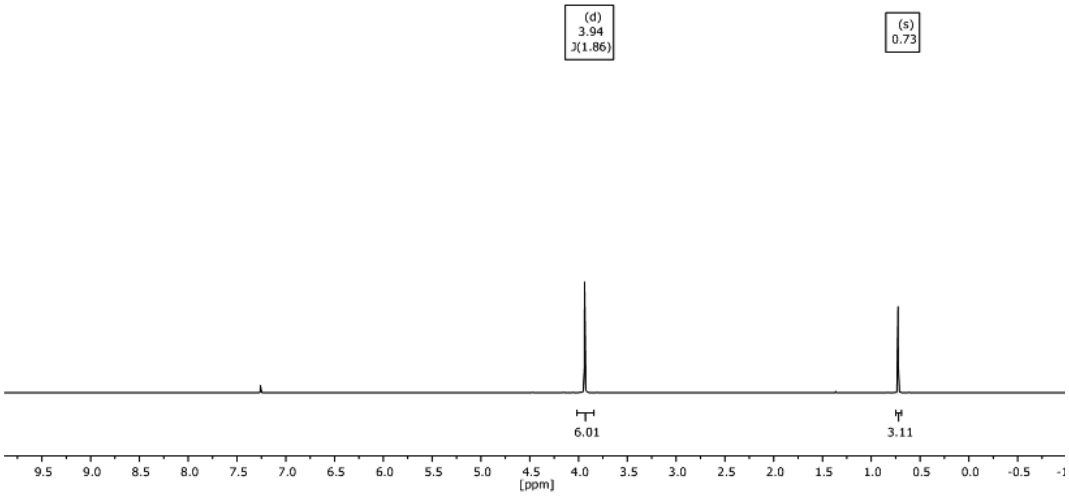

^{1}H-NMR-spectrum (600 MHz. $CDCl_3$)

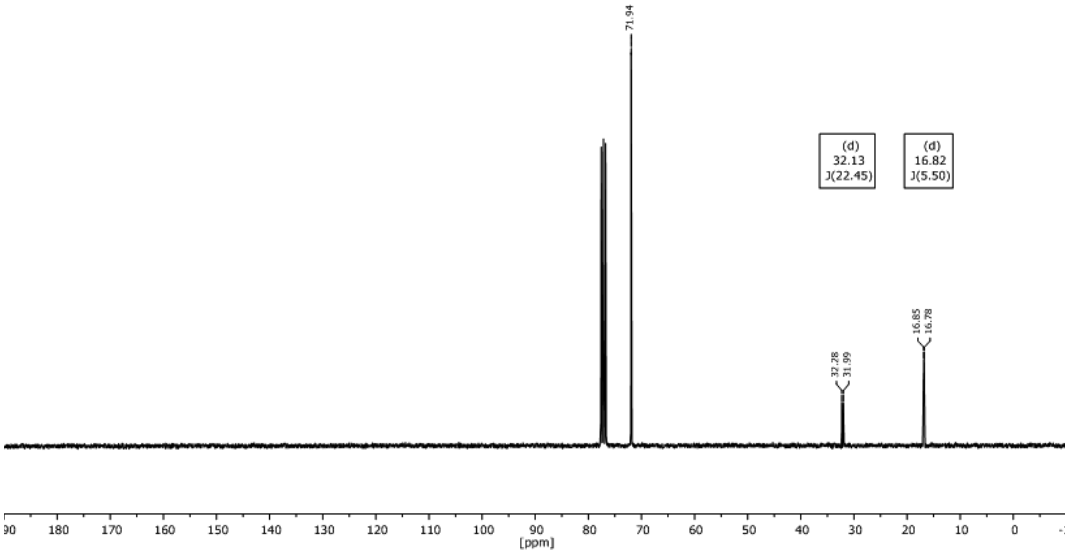

^{13}C-NMR-spectrum (75.5 MHz. $CDCl_3$)

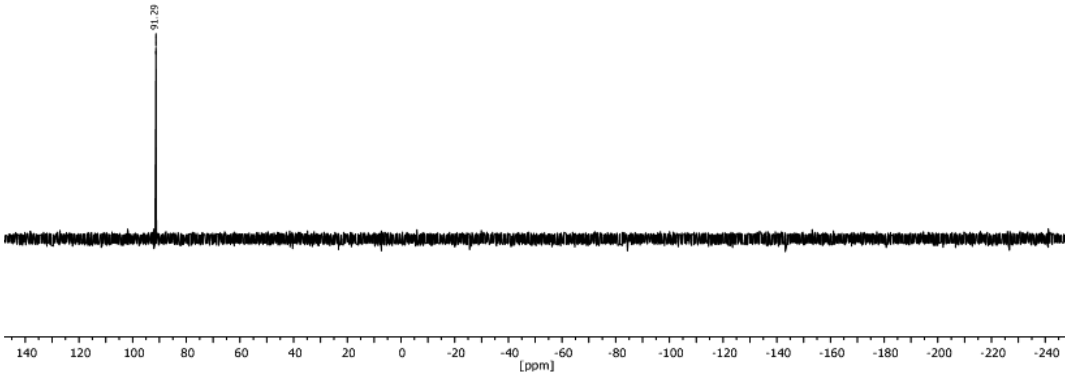

^{31}P-NMR-spectrum (243 MHz. $CDCl_3$)

S4.2. ($^tBuO)_3P$

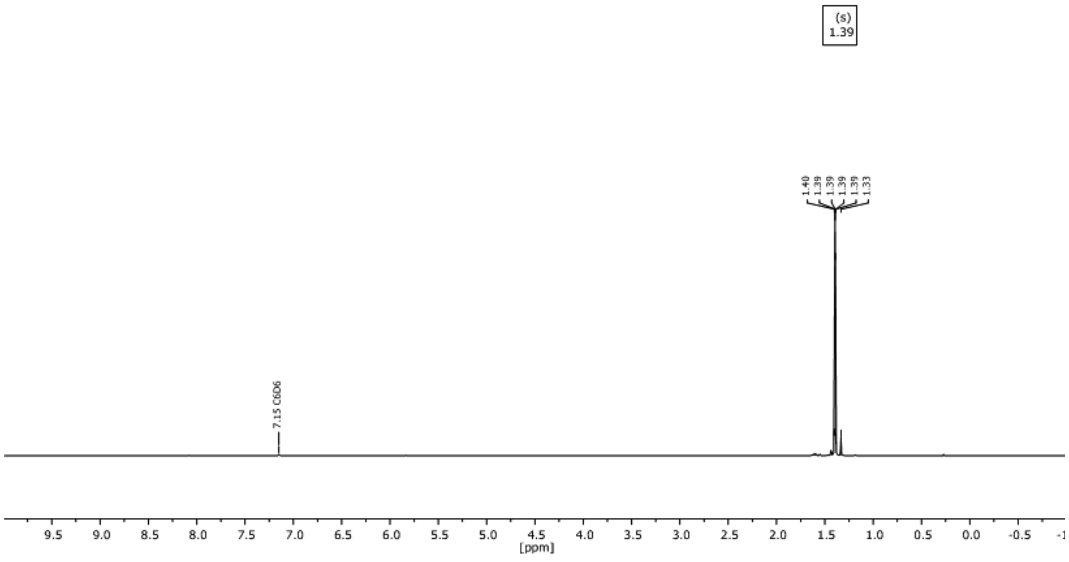

^{1}H-NMR-spectrum (300 MHz. C_6D_6)

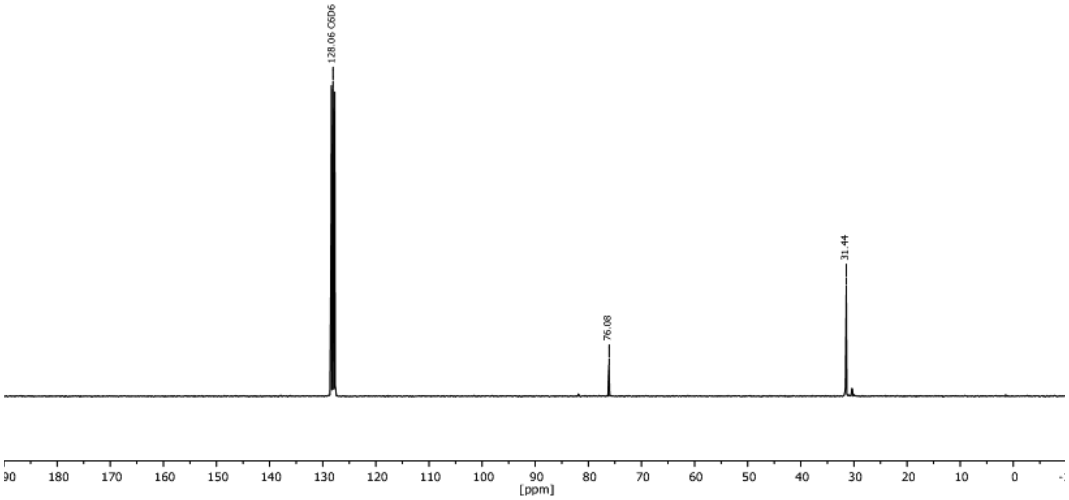

^{13}C-NMR-spectrum (75.5 MHz. C_6D_6)

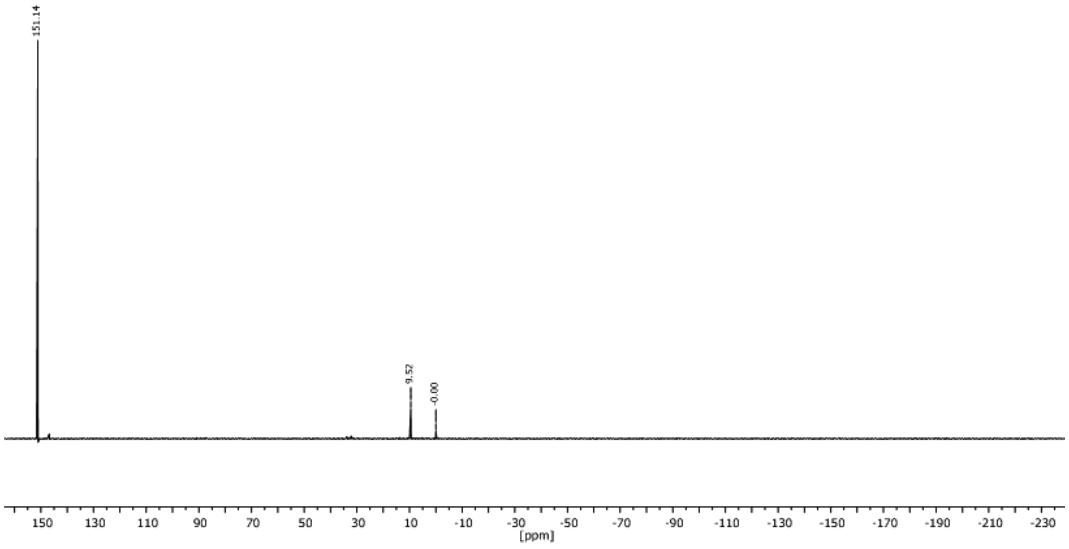

^{31}P-NMR-spectrum (121 MHz. $CDCl_3$)

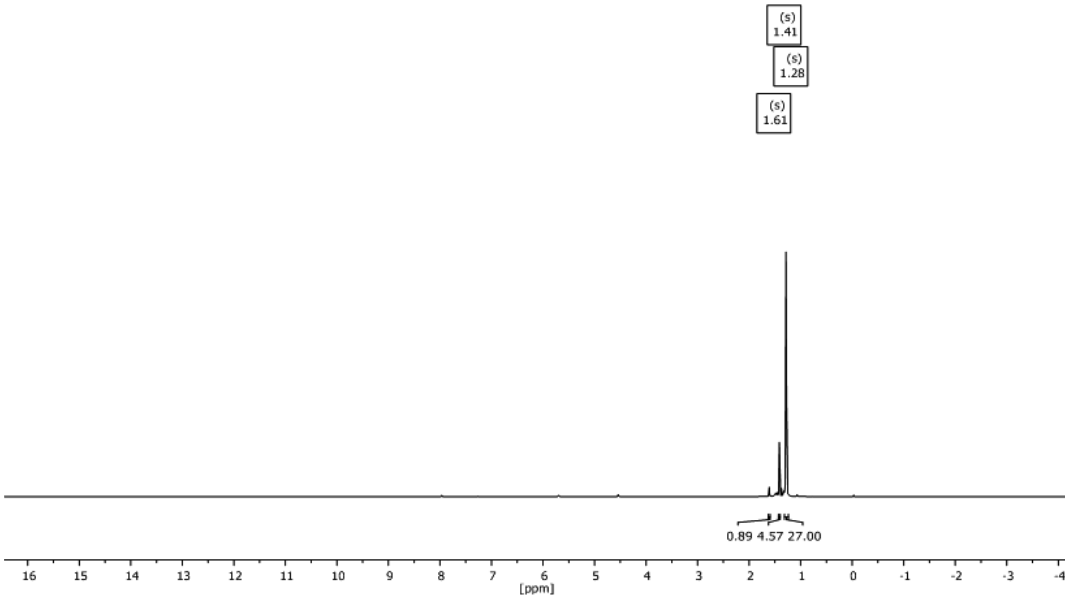

^{1}H-NMR-spectrum (300 MHz. $CDCl_3$)

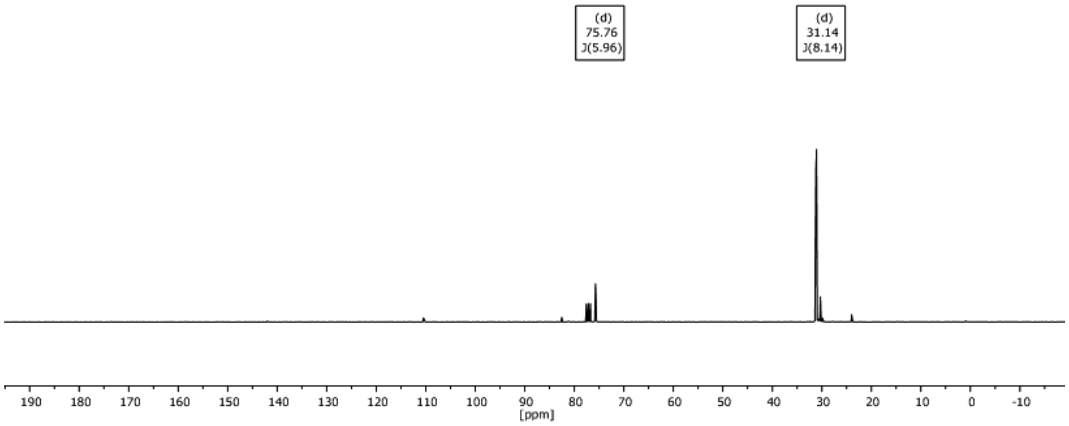

^{13}C-NMR-spectrum (75.5 MHz. $CDCl_3$)

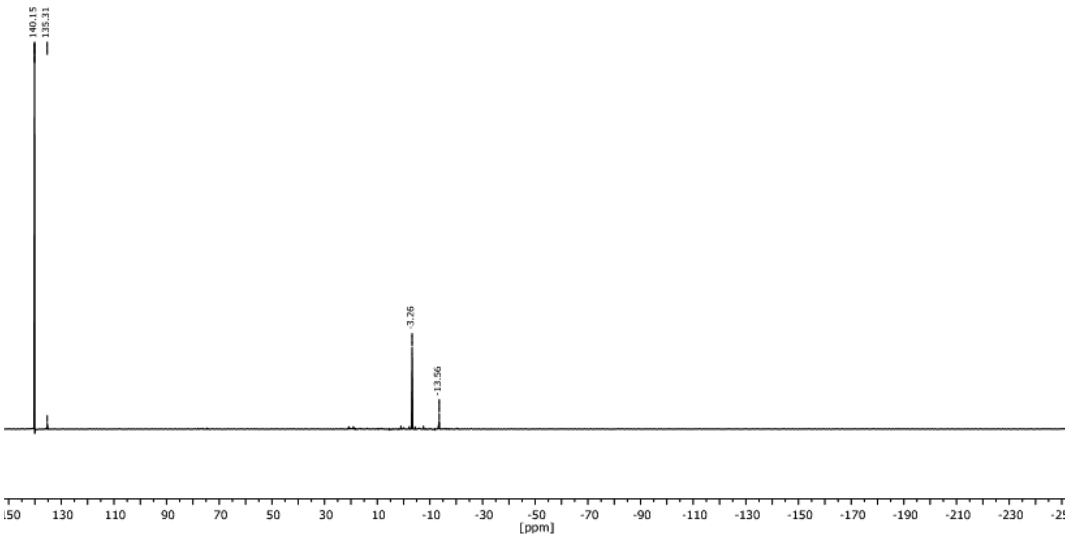

^{31}P-NMR-spectrum (121 MHz. $CDCl_3$)

S5. UV-Vis Measurements

- C_4F_9I (34.6 mg, 0.100 mmol) was dissolved in pentane or CH_2Cl_2 (10.0 ml) inside the glovebox in a volumetric flask. This solution was diluted in a volumetric flask (200 μL in 2.00 ml). The following concentration was present: [C_4F_9I] = 1.0 mM.
- ^{t}Bu$_3$P (20.2 mg, 0.100 mmol) was dissolved in pentane or CH_2Cl_2 (10.0 ml) in a volumetric flask inside the glovebox. This solution was diluted in a volumetric flask (200 μL in 2.00 ml). The following concentration was present: [^{t}Bu$_3$P] = 1 mM.
- ^{t}Bu$_3$P (20.2 mg, 0.100 mmol) and C_4F_9I (34.6 mg, 0.100 mmol) were dissolved in pentane or CH_2Cl_2 (10.0 ml) in a volumetric flask inside the glovebox. This solution was diluted in a volumetric flask (200 μL in 2.00 ml). The following concentration was present: [^{t}Bu$_3$P] = 1 mM, [C_4F_9I] = 1 mM.
- caged phosphine (14.8 mg, 0.100 mmol) was dissolved in CH_2Cl_2 (10.0 ml) in a volumetric flask. This solution was diluted in a volumetric flask (200 μL in 2.00 ml). The following concentration was present: [caged phosphine] = 1.0 mM.
- caged phosphine (14.8 mg, 0.100 mmol) and C_4F_9I (34.6 mg, 0.100 mmol) were dissolved in CH_2Cl_2 (10.0 ml) in a volumetric flask. This solution was diluted in a volumetric flask (200 μL in 2.00 ml). The following concentration was present: [caged phosphine] = 1 mM, [C_4F_9I] = 1 mM.
- $(MeO)_3P$ (12.4 mg, 0.100 mmol) was dissolved in CH_2Cl_2 (10.0 ml) in a volumetric flask. This solution was diluted in a volumetric flask (200 μL in 2.00 ml). The following concentration was present: [$(MeO)_3P$] = 1.0 mM.
- $(MeO)_3P$ (12.4 mg, 0.100 mmol) and C_4F_9I (34.6 mg, 0.100 mmol) were dissolved in CH_2Cl_2 (10.0 ml) in a volumetric flask. This solution was diluted in a volumetric flask (200 μL in 2.00 ml). The following concentration was present: [$(MeO)_3P$] = 1 mM, [C_4F_9I] = 1 mM.
- (^{t}BuO)$_3$P (25.2 mg, 0.100 mmol) was dissolved in CH_2Cl_2 (10.0 ml) inside the glovebox in a volumetric flask. This solution was diluted in a volumetric flask (200 μL in 2.00 ml). The following concentration was present: [(^{t}BuO)$_3$P] = 1.0 mM.
- (^{t}BuO)$_3$P (25.2 mg, 0.100 mmol) and C_4F_9I (34.6 mg, 0.100 mmol) were dissolved in CH_2Cl_2 (10.0 ml) inside the glovebox in a volumetric flask. This solution was diluted in a volumetric flask (200 μL in 2.00 ml). The following concentration was present: [(^{t}BuO)$_3$P] = 1 mM, [C_4F_9I] = 1 mM.

S6. Further Computational Details

All line spectra were broadened by Gaussians with standard deviation $\sigma = 1500$ cm^{-1}. The isovalue for illustrating the molecular orbitals has been set to 0.05.

S7. Absorption Spectra and Molecular Orbitals

S7.1. Perfluorobutyl Iodide

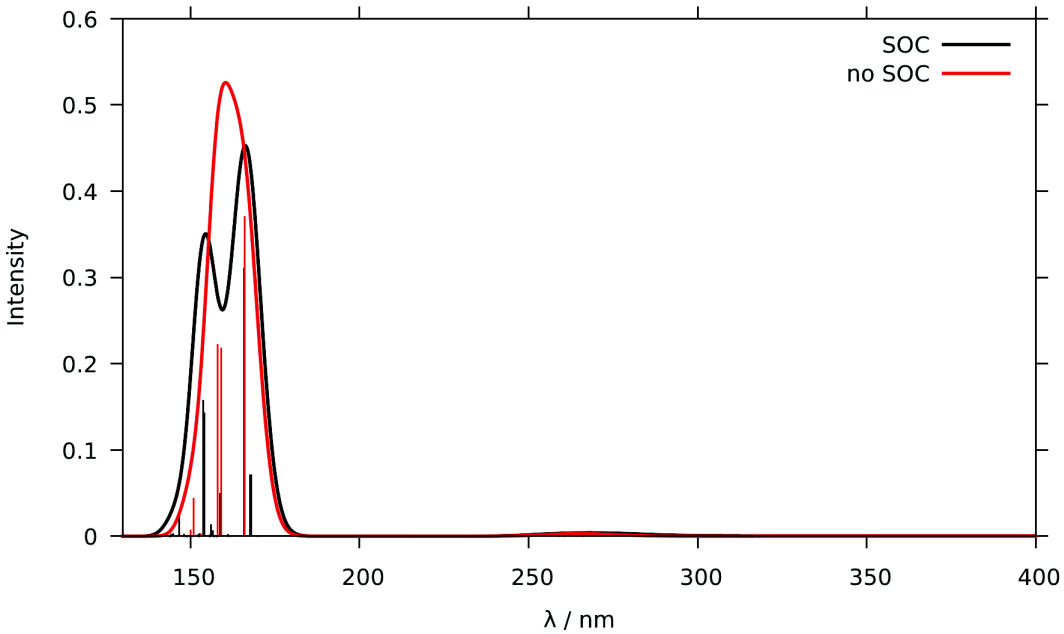

Figure S1. Calculated absorption spectra of C_4F_9I in CH_2Cl_2 with (black) and without (red) spin–orbit coupling (130 – 400 nm).

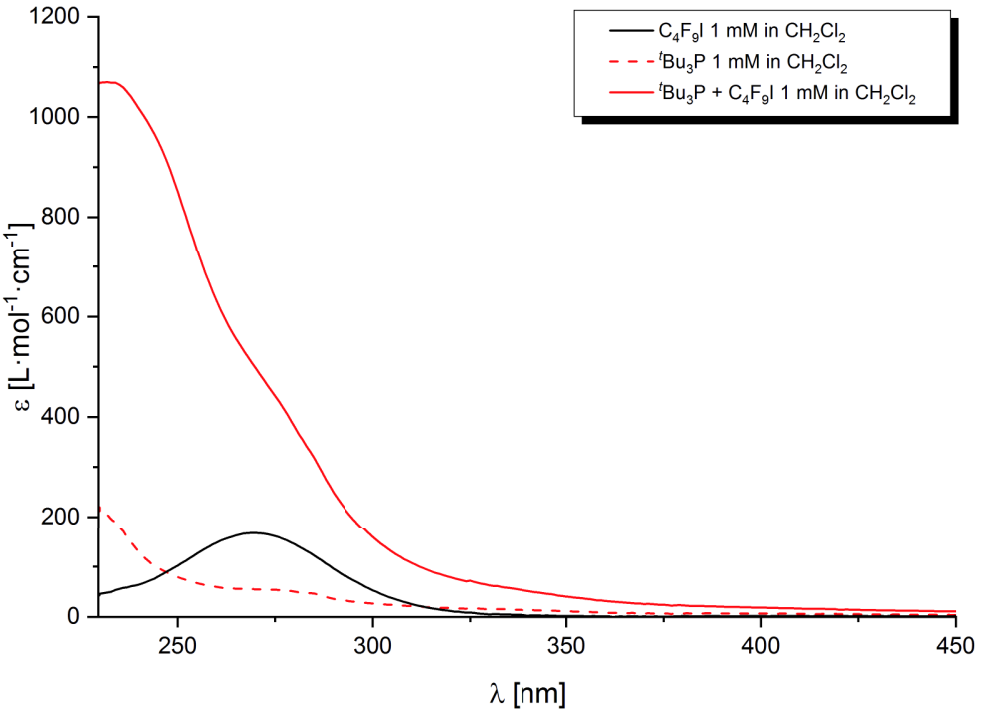

Figure S2. Experimental UV-vis spectra of C_4F_9I (λ_{max} = 270 nm), ^{t}Bu$_3$P (λ_{max} = 227 nm) and ^{t}Bu$_3$P + C_4F_9I (λ_{max} = 232 nm) in CH_2Cl_2.

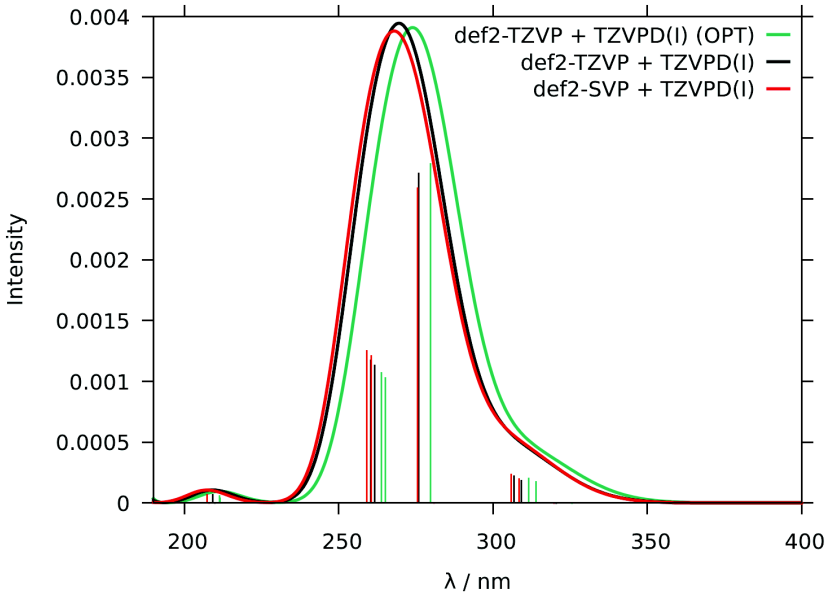

Figure S3. Atomic orbital basis set dependence of the calculated absorption spectrum of C_4F_9I (190 – 400 nm) in CH_2Cl_2 including spin–orbit coupling in quasi-degenerate perturbation theory (DFT/MRCI+SOCQDPT). The red spectrum corresponds to a calculation in the smaller def2-SVP + TZVPD(I) basis set. The black curve, labeled def2-TZVP + TZVPD(I), results from a single-point calculation using the larger def2-TZVP + TZVPD(I) basis set but employing the same geometry parameters as the red one. The green spectrum, labeled def2-TZVP + TZVPD(I) (OPT), was obtained from a set up using the larger def2-TZVP + TZVPD(I) basis set in both, the geometry optimization and DFT/MRCI+SOCQDPT step.

191 *S7.2. Phosphines and Phosphites*

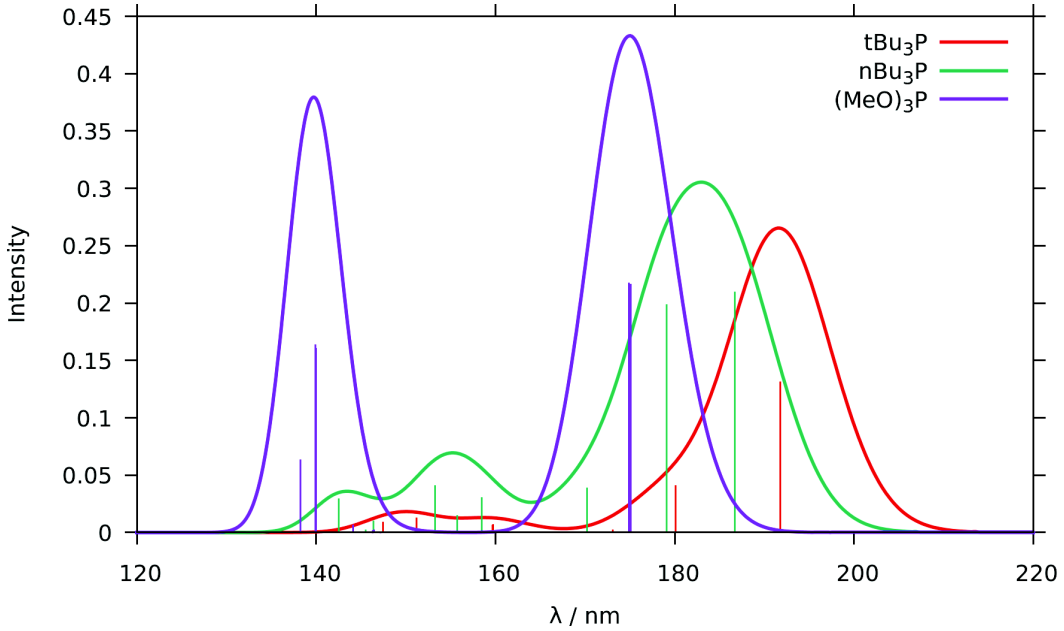

Figure S4. Computed absorption spectra of the phosphines (^{t}Bu$_3$P, ^{n}Bu$_3$P) and the phosphite (MeO)$_3$P in CH_2Cl_2 with spin–orbit coupling (120 – 220 nm).

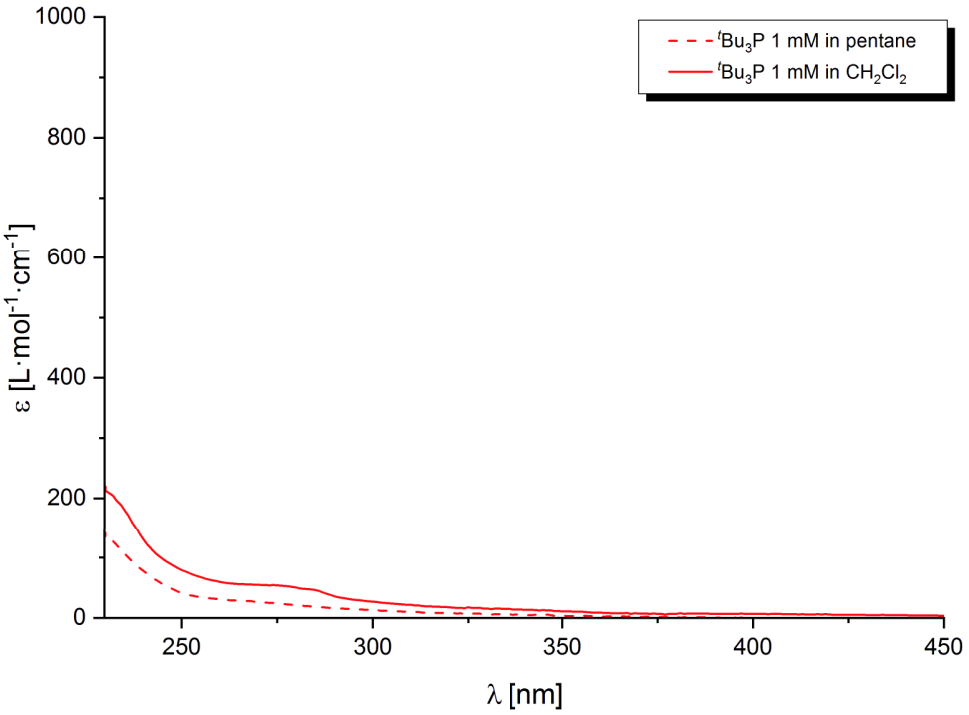

Figure S5. Comparison of the experimental UV-vis spectra of $^{t}Bu_3P$ in pentane (λ_{max} = 227 nm) and in CH_2Cl_2 (λ_{max} = 227 nm).

S7.3. Phosphine and Phosphite Adducts

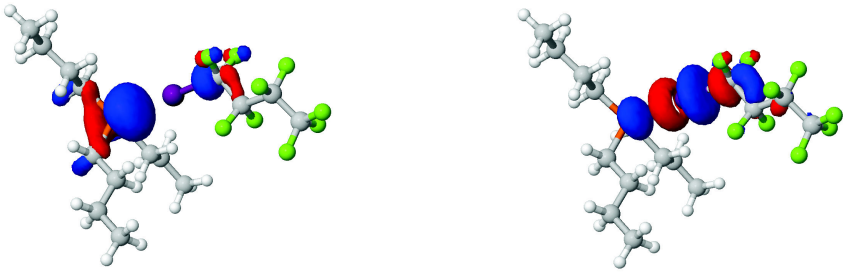

(a) HOMO: n_P (b) LUMO: σ^*

Figure S6. Frontier molecular orbitals of the $^{n}Bu_3P$-IC_4F_9 adduct at the S_0 geometry.

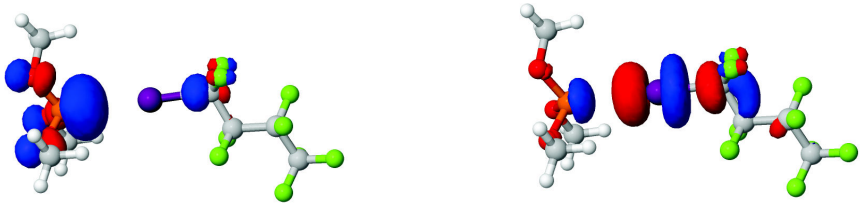

(a) HOMO: n_P (b) LUMO: σ^*

Figure S7. Frontier molecular orbitals of the $(MeO)_3P$-IC_4F_9 adduct at the S_0 geometry.

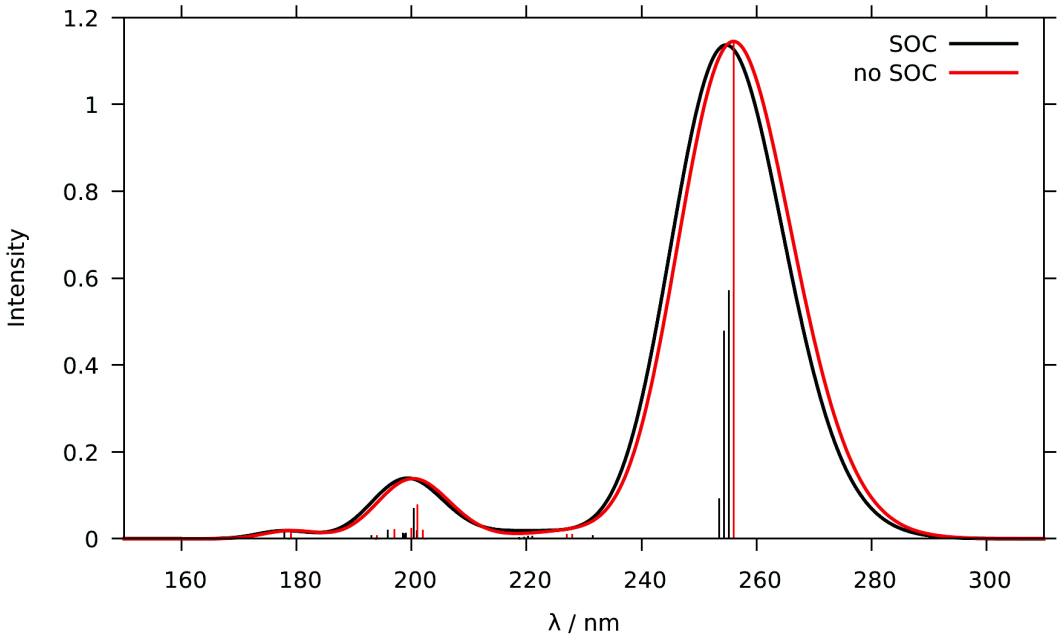

Figure S8. Calculated absorption spectra of $^{t}Bu_3P$–C_4F_9I in CH_2Cl_2 with (black) and without (red) spin–orbit coupling (150 – 310 nm).

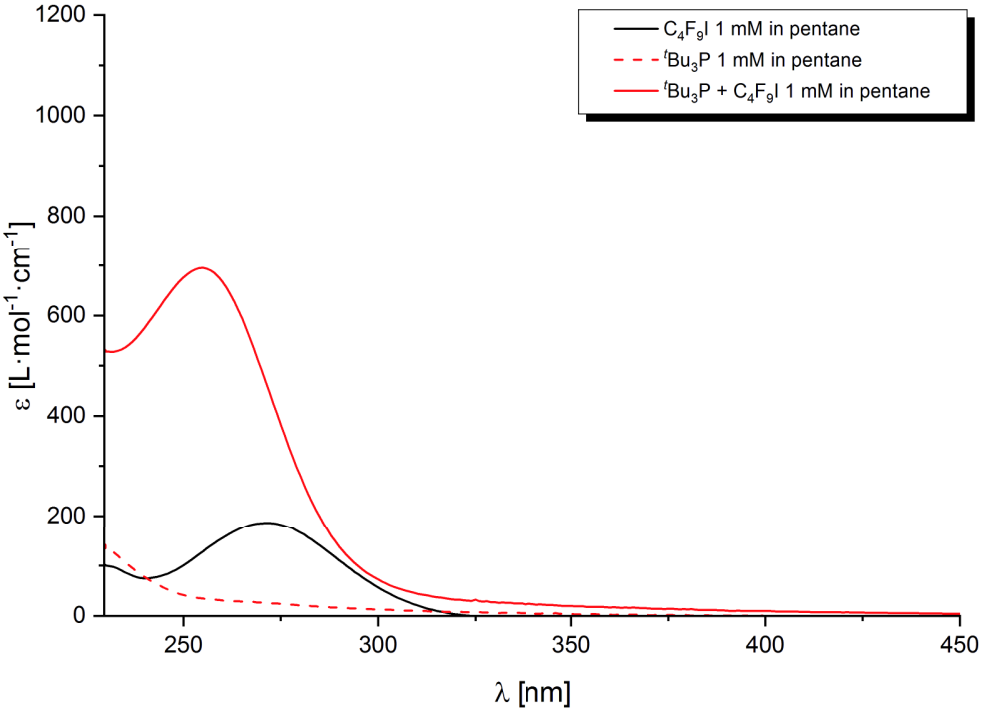

Figure S9. Experimental UV-vis spectra of C_4F_9I (λ_{max} = 270 nm), $^{t}Bu_3P$ (λ_{max} = 227 nm) and $^{t}Bu_3P$ + C_4F_9I (λ_{max} = 255 nm) in pentane.

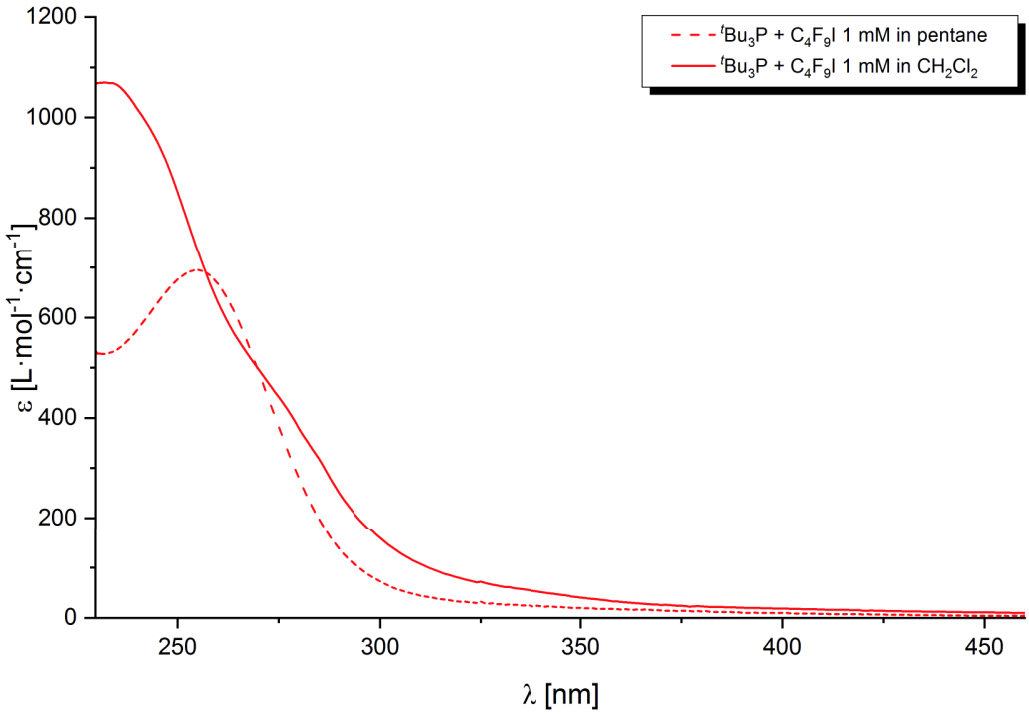

Figure S10. Comparison of the experimental UV-vis spectra of ^{t}Bu$_3$P + C$_4$F$_9$I in pentane (λ_{max} = 255 nm) and in CH_2Cl_2 (λ_{max} = 232 nm).

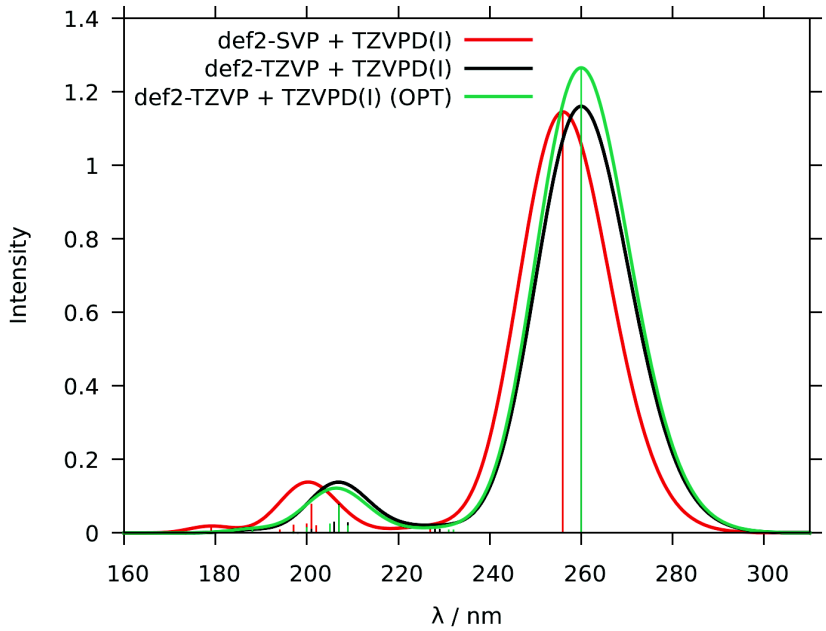

Figure S11. Atomic orbital basis set dependence of the calculated DFT/MRCI singlet absorption spectrum of the ^{t}Bu$_3$P–C$_4$F$_9$I adduct complex (160 – 310 nm). The red spectrum corresponds to a calculation in the smaller def2-SVP + TZVPD(I) basis set. The black curve, labeled def2-TZVP + TZVPD(I), results from a single-point calculation using the larger def2-TZVP + TZVPD(I) basis set but employing the same geometry parameters as the red one. The green spectrum, labeled def2-TZVP + TZVPD(I) (OPT), was obtained from a setup using the larger def2-TZVP + TZVPD(I) basis set in both, the geometry optimization and DFT/MRCI step.

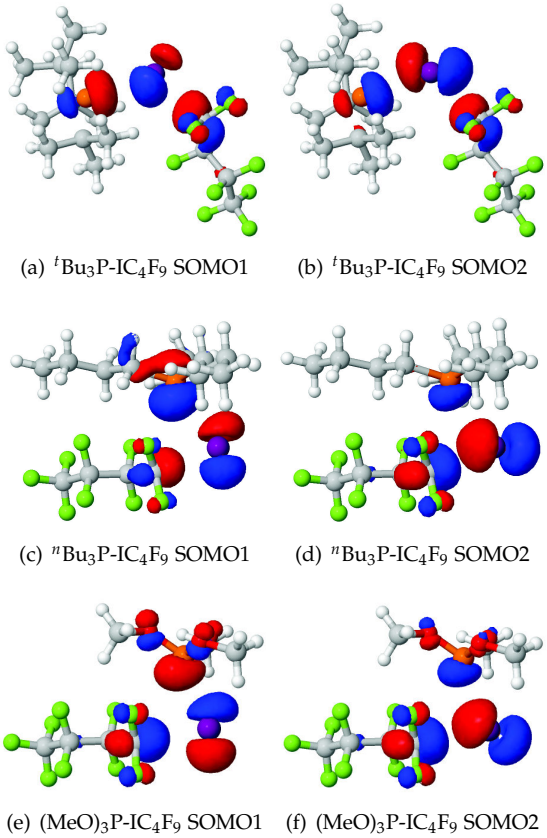

(a) $^{t}Bu_3P\text{-}IC_4F_9$ SOMO1 (b) $^{t}Bu_3P\text{-}IC_4F_9$ SOMO2

(c) $^{n}Bu_3P\text{-}IC_4F_9$ SOMO1 (d) $^{n}Bu_3P\text{-}IC_4F_9$ SOMO2

(e) $(MeO)_3P\text{-}IC_4F_9$ SOMO1 (f) $(MeO)_3P\text{-}IC_4F_9$ SOMO2

Figure S12. Singly occupied MOs (SOMOs) of the phosphine and phosphite adducts in the relaxed T_1 state.

193 *S7.4. Solvent Influence on the Measured Absorption Spectra*

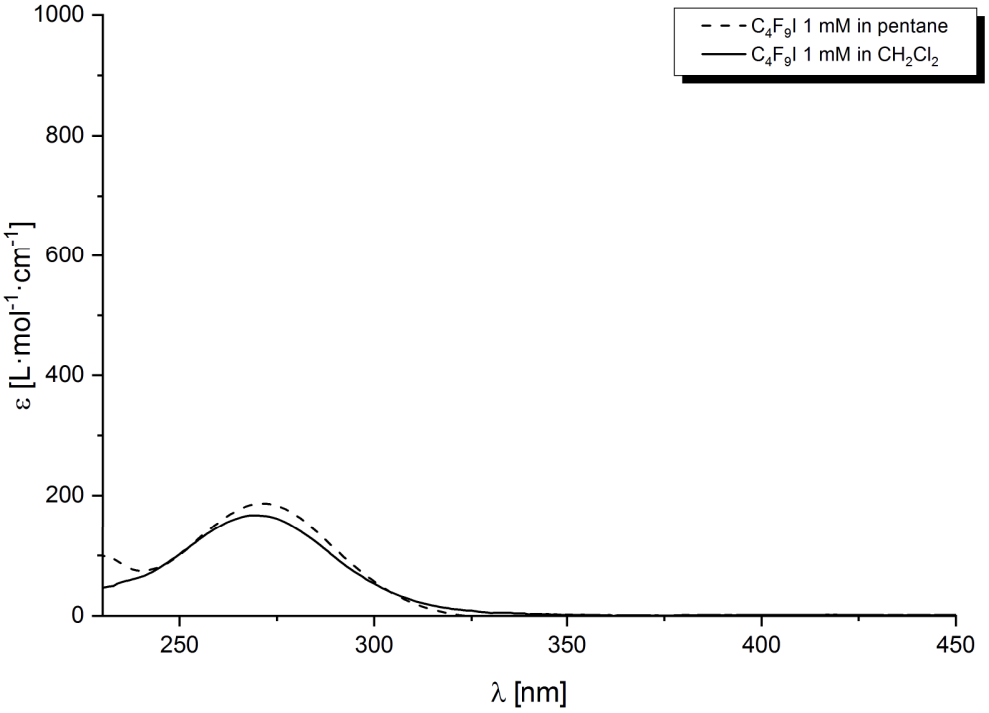

Figure S13. Comparison of the experimental UV-vis spectra of C_4F_9I in pentane (λ_{max} = 270 nm) and in CH_2Cl_2 (λ_{max} = 270 nm).

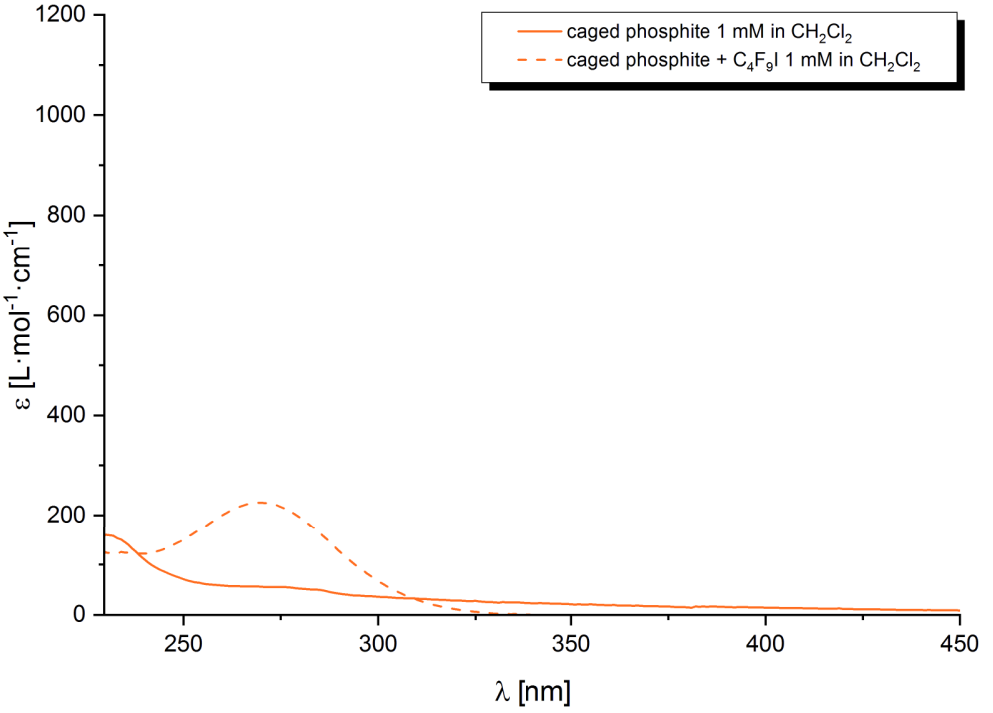

Figure S14. Comparison of the experimental UV-vis spectra of caged phosphite (λ_{max} = 230 nm) and caged phosphite + C_4F_9I (λ_{max} = 270 nm) in CH_2Cl_2.

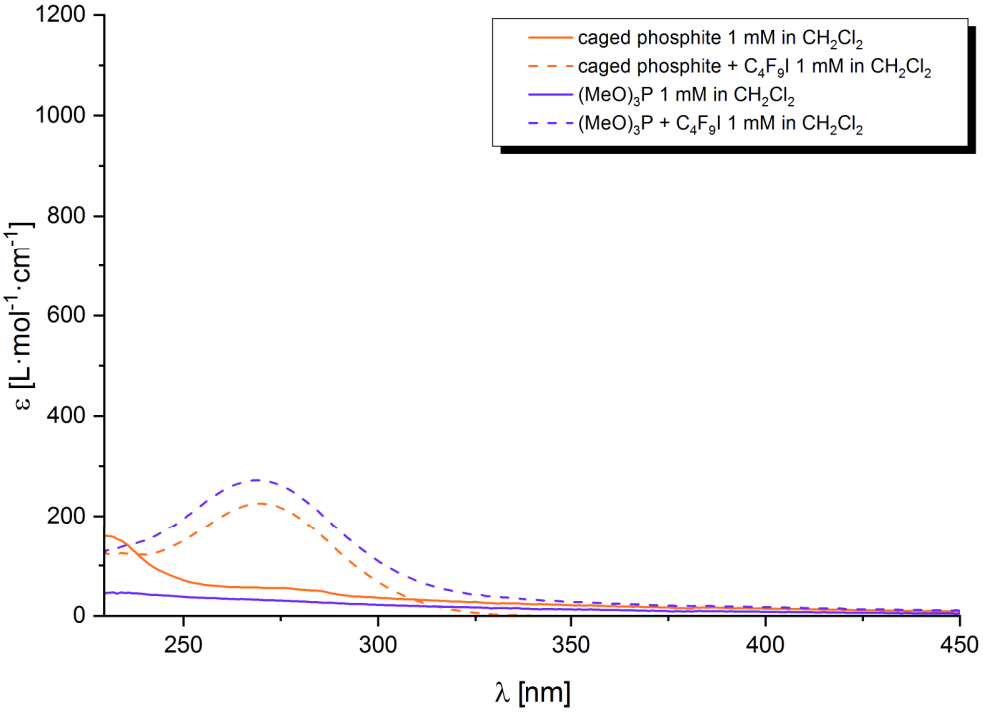

Figure S15. Comparison of the experimental UV-vis spectra of caged phosphite (λ_{max} = 230 nm), caged phosphite + C_4F_9I (λ_{max} = 270 nm), $(MeO)_3P$ ($\lambda_{max} \leq$ 230 nm) and $(MeO)_3P$ + C_4F_9I (λ_{max} = 269 nm) in CH_2Cl_2.

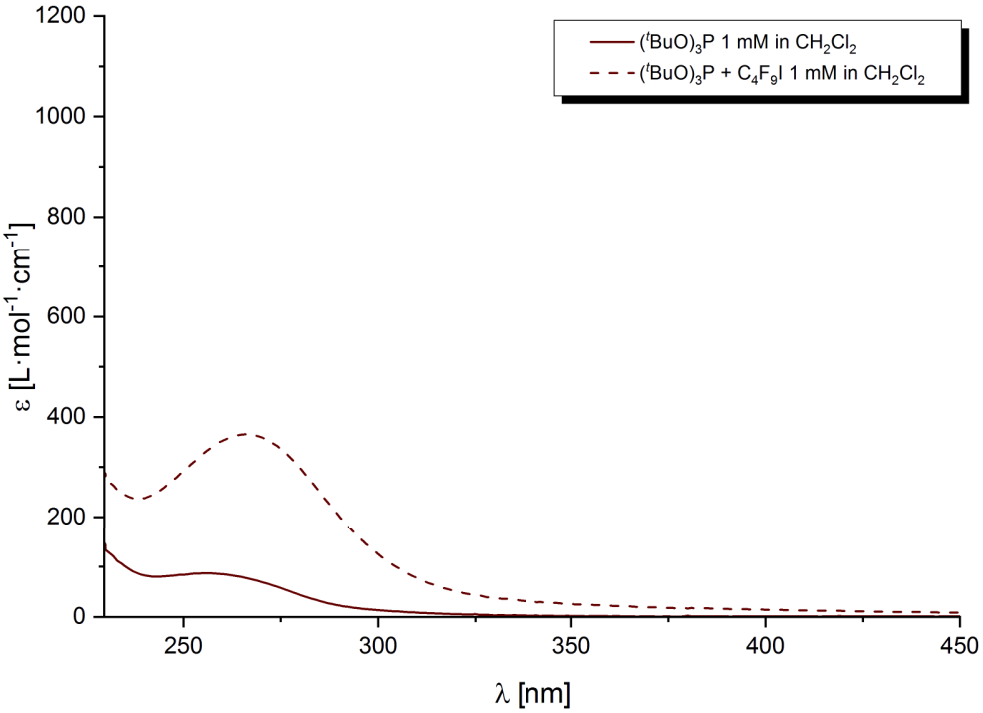

Figure S16. Comparison of the experimental UV-vis spectra of $(^tBuO)_3P$ (λ_{max} = 227 nm) and $(^tBuO)_3P$ + C_4F_9I (λ_{max} = 266 nm) in CH_2Cl_2.

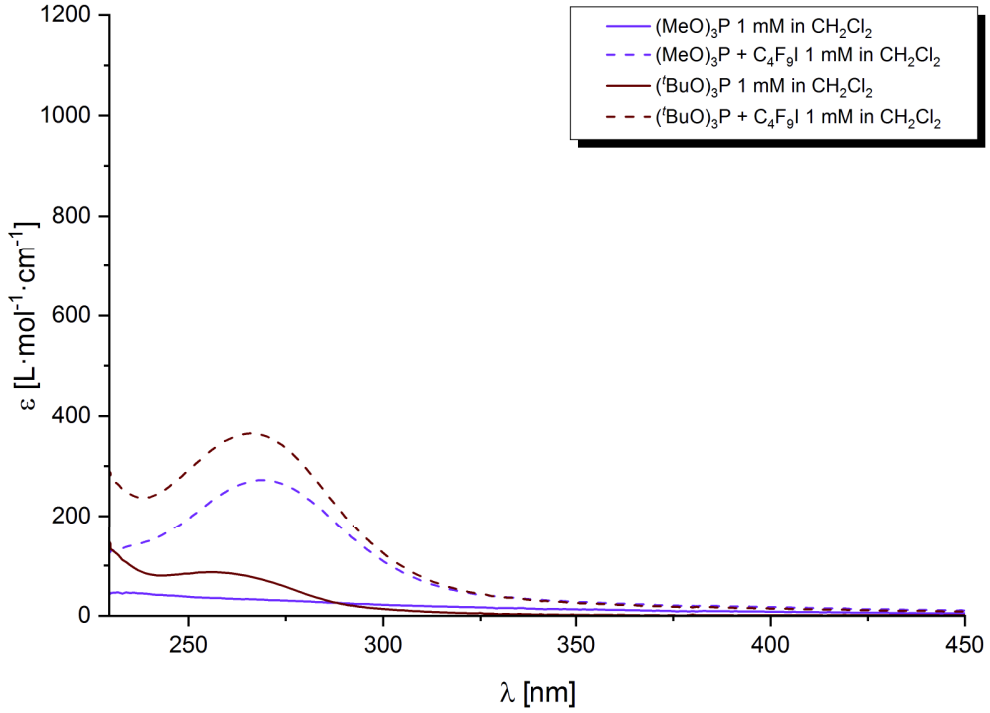

Figure S17. Comparison of the experimental UV-vis spectra of $(MeO)_3P$ ($\lambda_{max} \leq 230$ nm), $(MeO)_3P$ + C_4F_9I ($\lambda_{max} = 269$ nm), $(^tBuO)_3P$ ($\lambda_{max} = 227$ nm) and $(^tBuO)_3P$ + C_4F_9I ($\lambda_{max} = 266$ nm) in CH_2Cl_2.

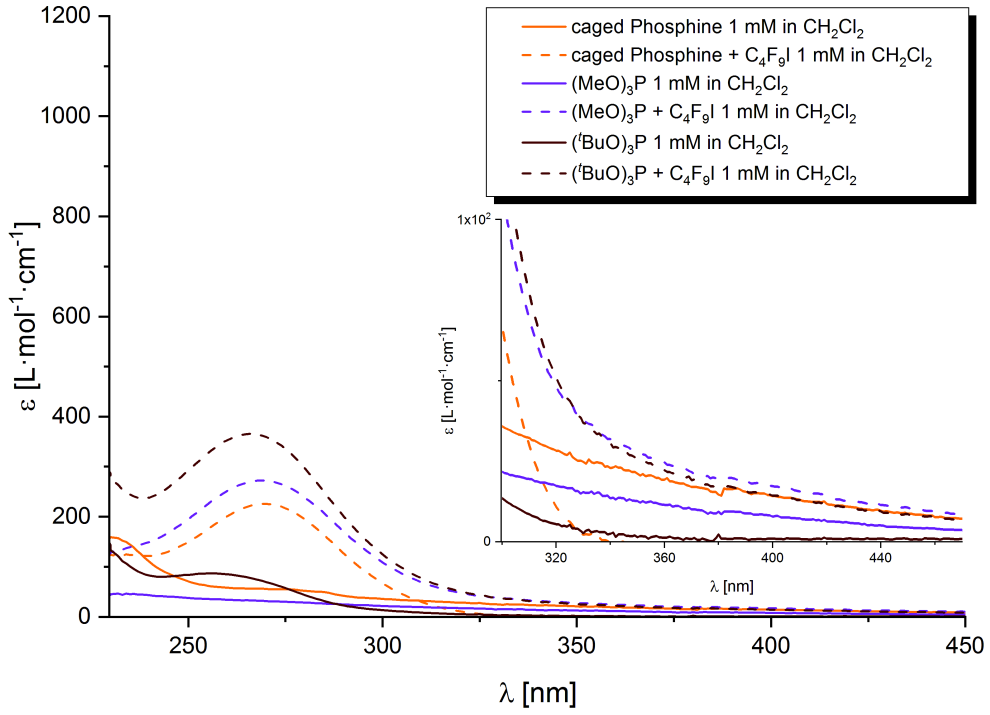

Figure S18. Comparison of the experimental UV-vis spectra of caged phosphite ($\lambda_{max} = 230$ nm), caged phosphite + C_4F_9I ($\lambda_{max} = 270$ nm), $(MeO)_3P$ ($\lambda_{max} \leq 230$ nm), $(MeO)_3P$ + C_4F_9I ($\lambda_{max} = 269$ nm), $(^tBuO)_3P$ ($\lambda_{max} = 227$ nm) and $(^tBuO)_3P$ + C_4F_9I ($\lambda_{max} = 266$ nm) in CH_2Cl_2.

194 *S7.5. Impact of Spin–Orbit Coupling on the Calculated Spectra*

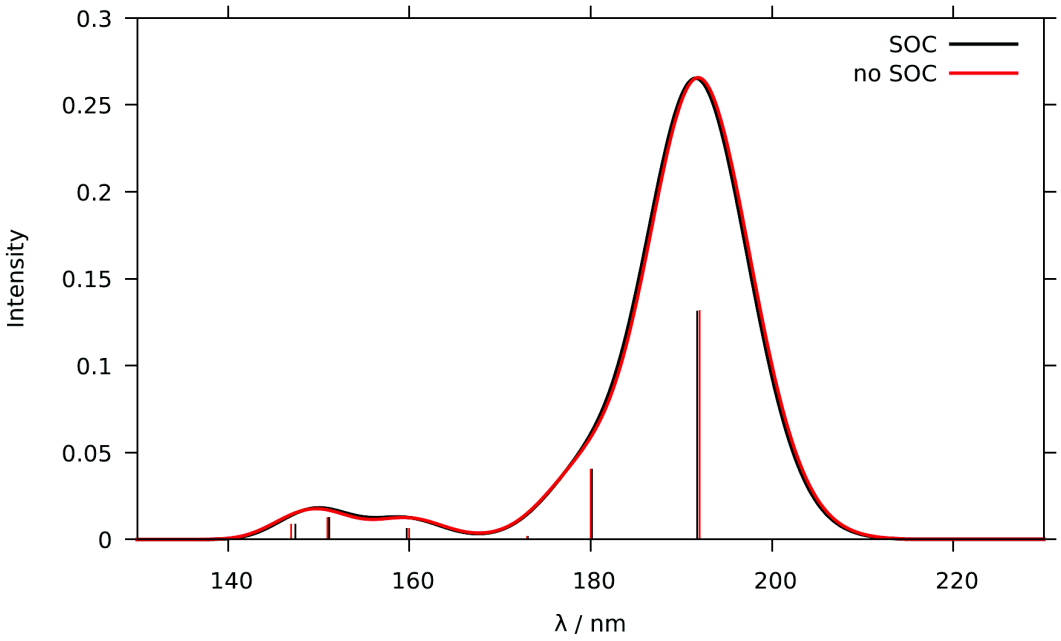

Figure S19. Calculated absorption spectra of $^{t}Bu_3P$ with (black) and without (red) spin–orbit coupling (130 – 230 nm).

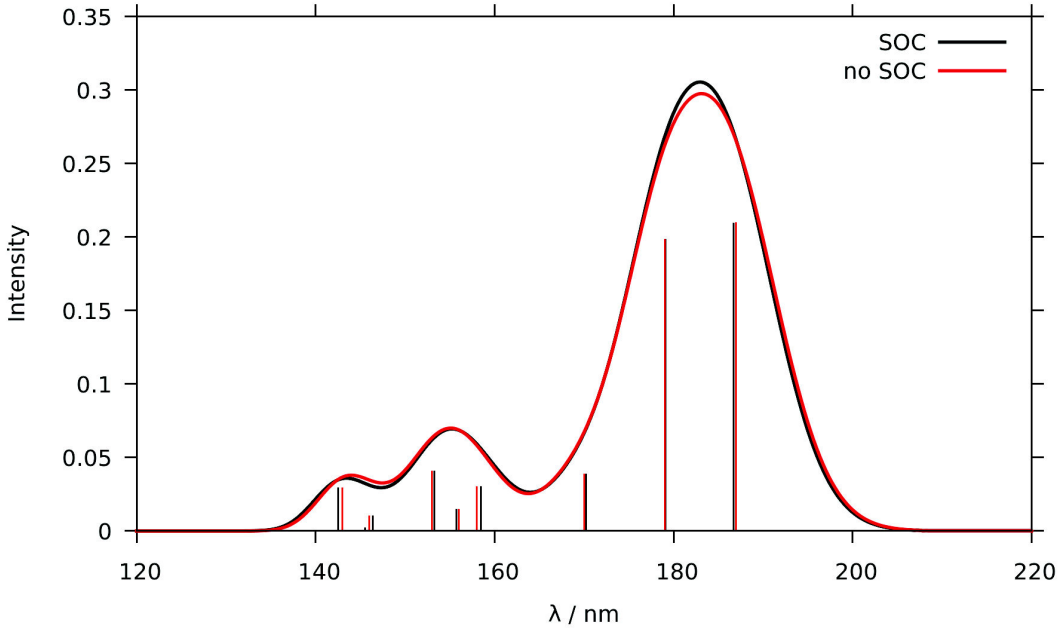

Figure S20. Calculated absorption spectra of $^{n}Bu_3P$ with (black) and without (red) spin–orbit coupling (120 – 220 nm).

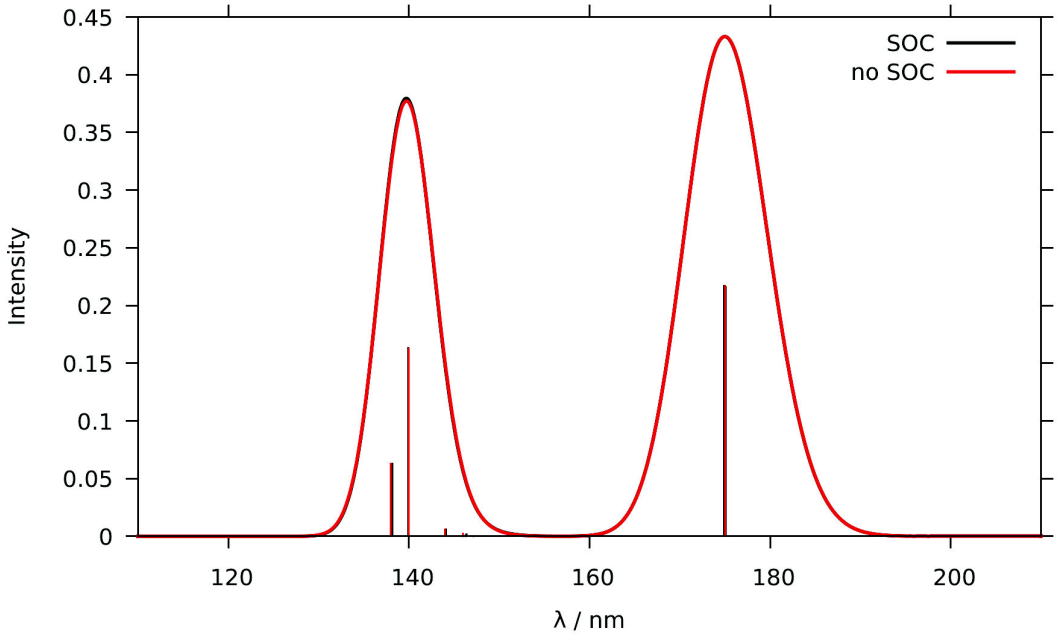

Figure S21. Calculated absorption spectra of $(MeO)_3P$ with (black) and without (red) spin–orbit coupling (110 – 210 nm).

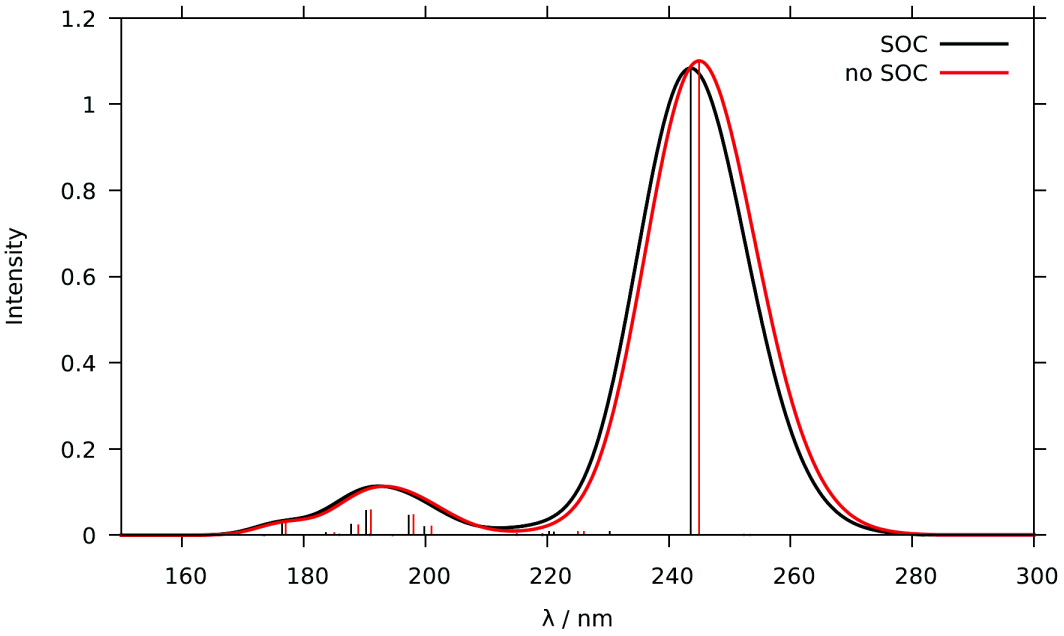

Figure S22. Calculated absorption spectra of $^{n}Bu_3P–C_4F_9I$ with (black) and without (red) spin–orbit coupling (150 – 300 nm).

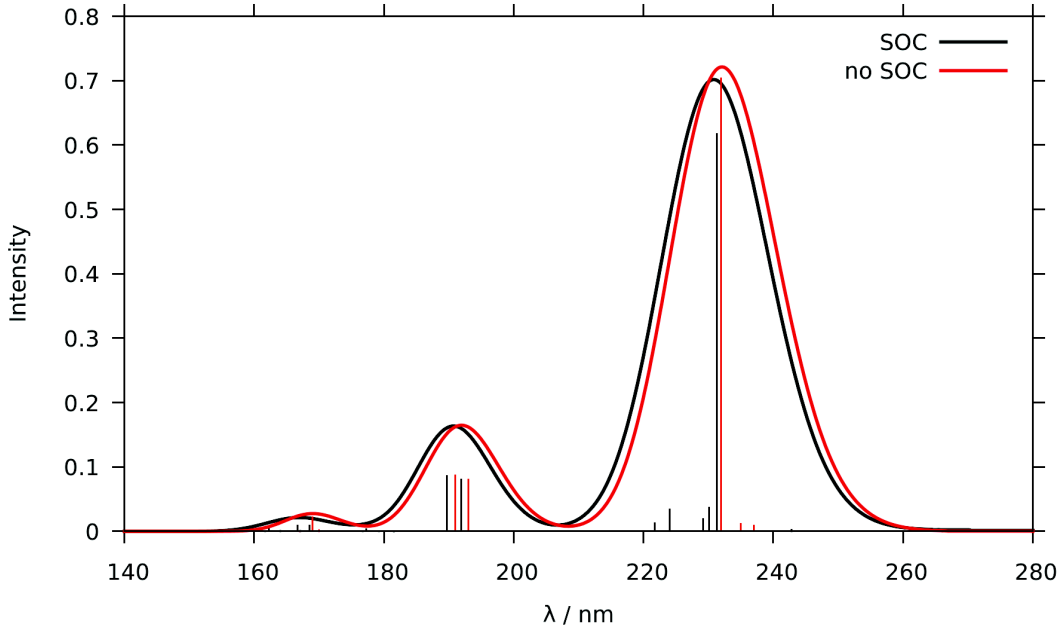

Figure S23. Calculated absorption spectra of $(MeO)_3P–C_4F_9I$ with (black) and without (red) spin–orbit coupling (140 – 280 nm).

S8. Minimum Nuclear Arrangements

S8.1. DFT-Optimized Ground-State Geometries

Perfluoroalkyl Iodide

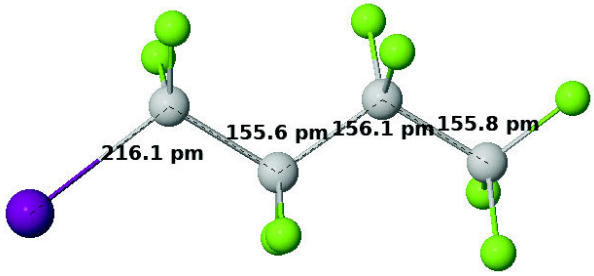

Figure S24. S_0 geometry of C_4F_9I and selected bond lengths in pm.

198 Phosphines

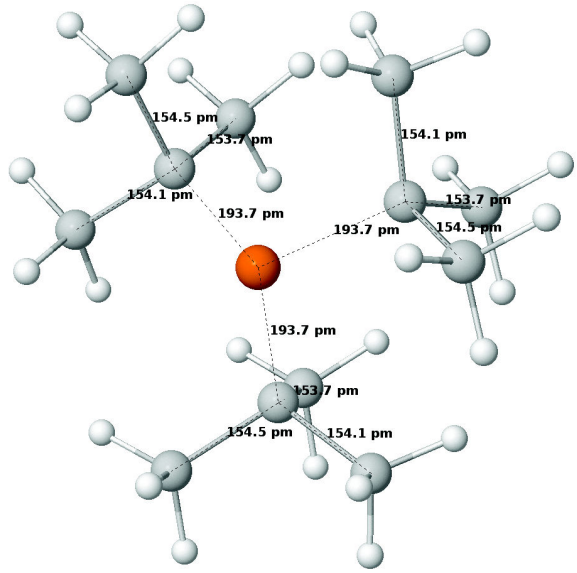

Figure S25. S_0 geometry of $^{t}Bu_3P$ and selected bond lengths in pm.

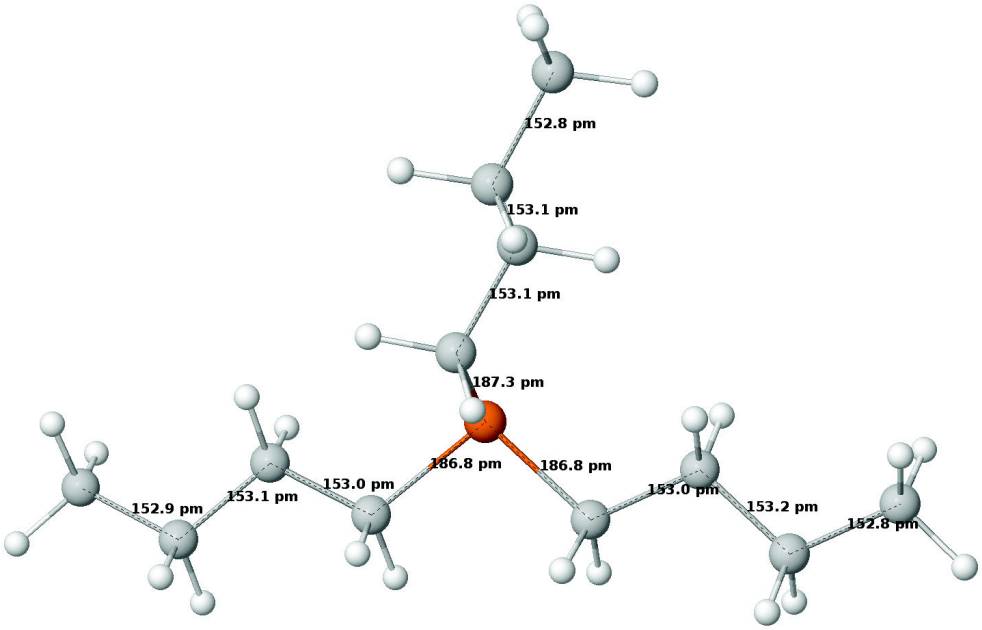

Figure S26. S_0 geometry of $^{n}Bu_3P$ and selected bond lengths in pm.

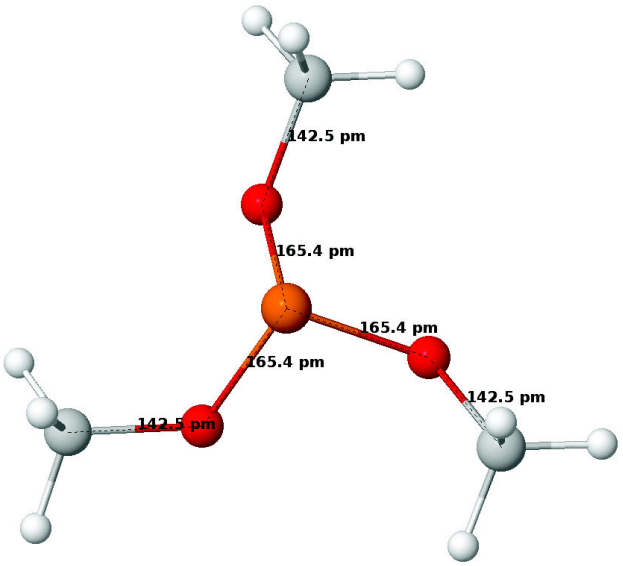

Figure S27. S_0 geometry of $(MeO)_3P$ and selected bond lengths in pm.

Adducts

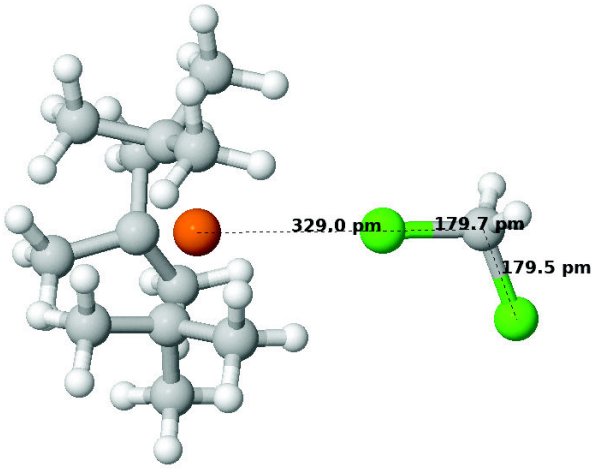

Figure S28. S_0 geometry of $^t Bu_3P–CH_2Cl_2$and selected bond lengths in pm.

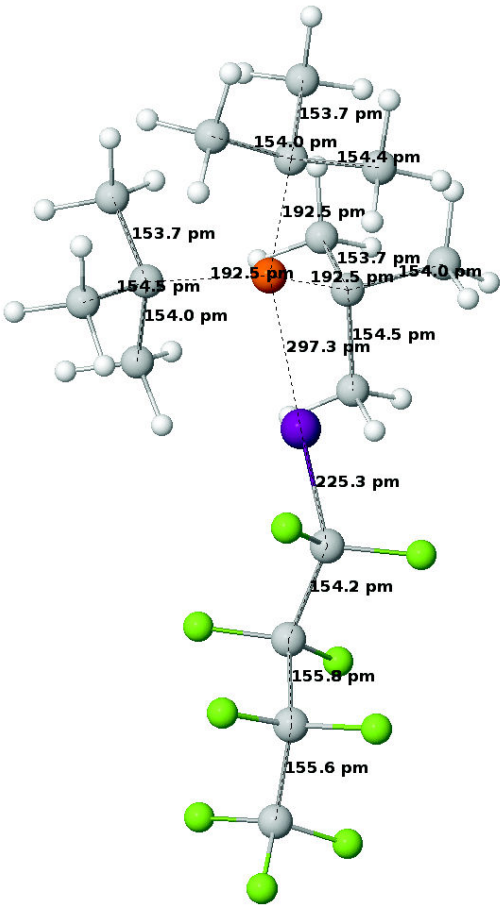

Figure S29. S_0 geometry of ^{t}Bu$_3$P–IC$_4$F$_9$ and selected bond lengths in pm.

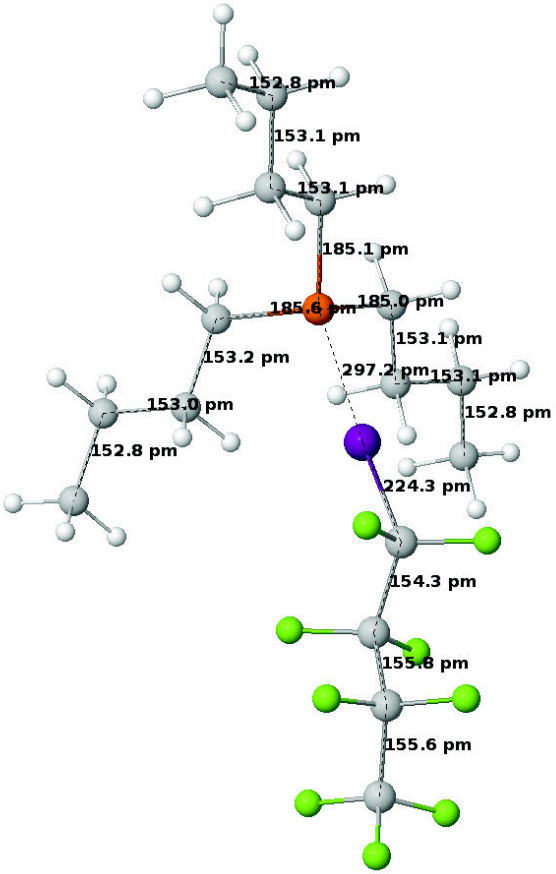

Figure S30. S_0 geometry of $^{n}Bu_3P–IC_4F_9$ and selected bond lengths in pm.

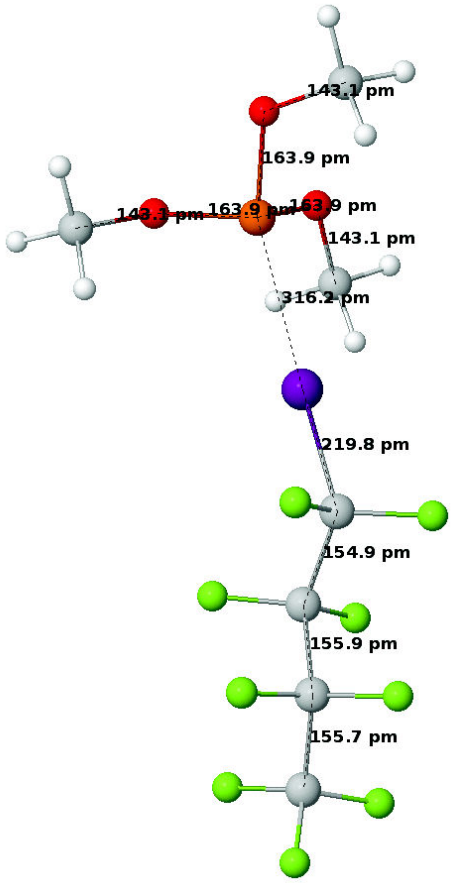

Figure S31. S_0 geometry of $(MeO)_3P–IC_4F_9$ and selected bond lengths in pm.

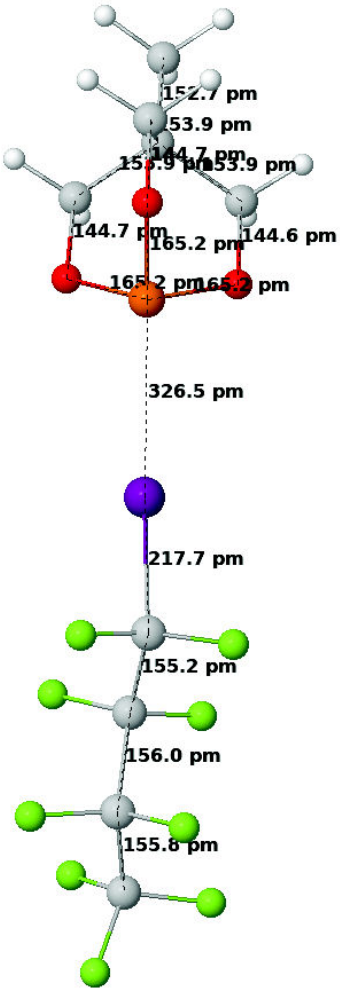

Figure S32. S_0 geometry of the caged phosphite–IC_4F_9 adduct and selected bond lengths in pm.

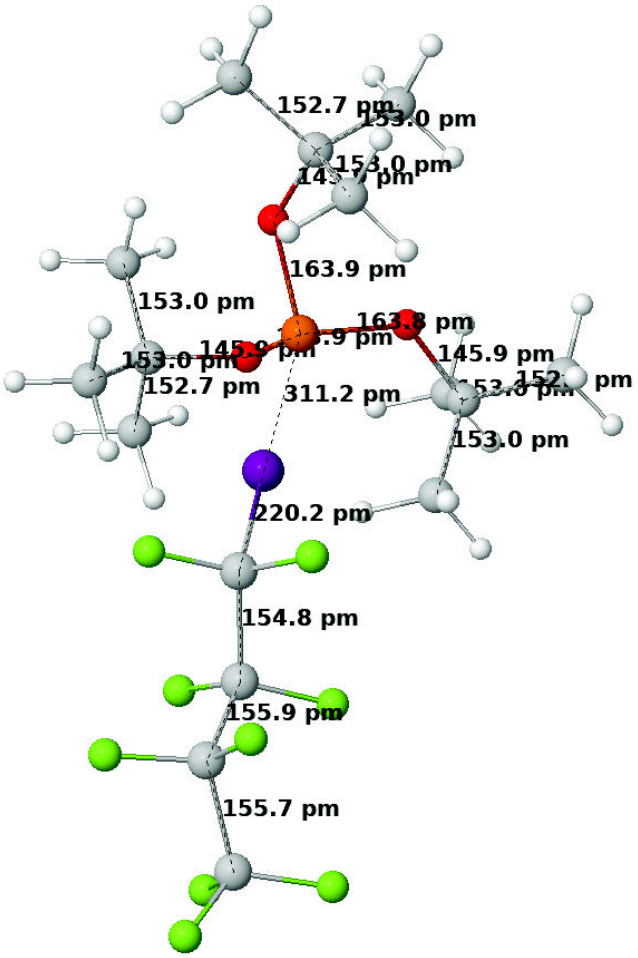

Figure S33. S_0 geometry of $(^t\mathrm{BuO})_3\mathrm{P–IC_4F_9}$ and selected bond lengths in pm.

S8.2. TDDFT/TDA-Optimized Conical Intersection Geometries

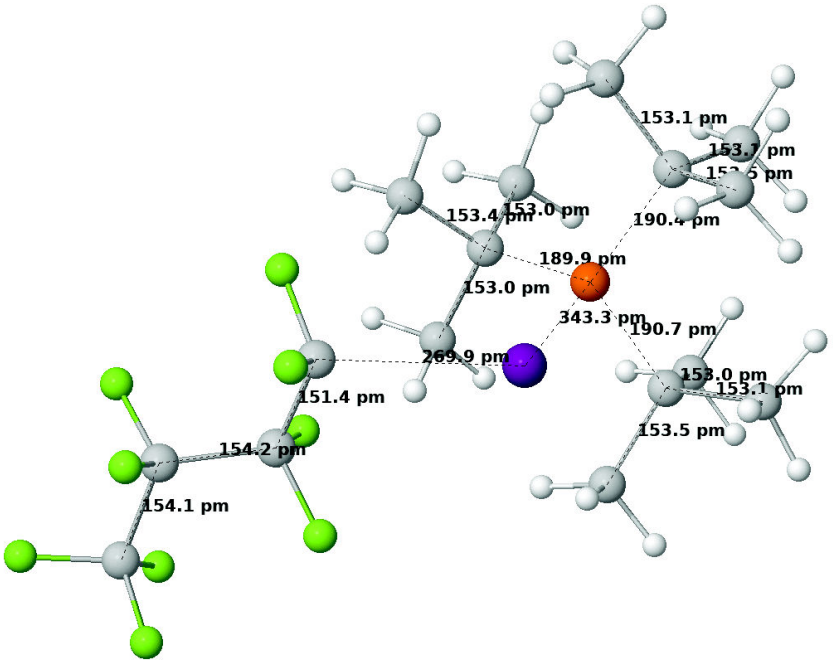

Figure S34. Geometry of the S_1/S_0 conical intersection of $^{t}Bu_3P–IC_4F_9$ and selected bond lengths in pm.

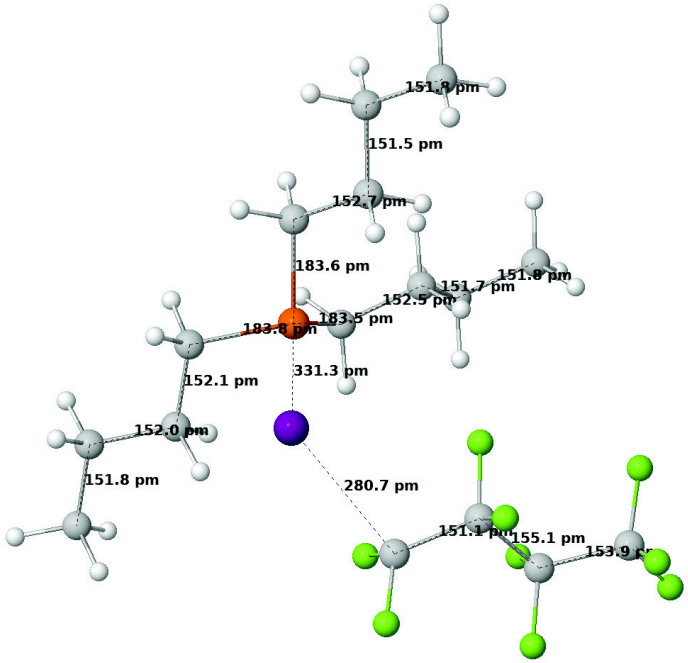

Figure S35. Geometry of the S_1/S_0 conical intersection of $^{n}Bu_3P–IC_4F_9$ and selected bond lengths in pm.

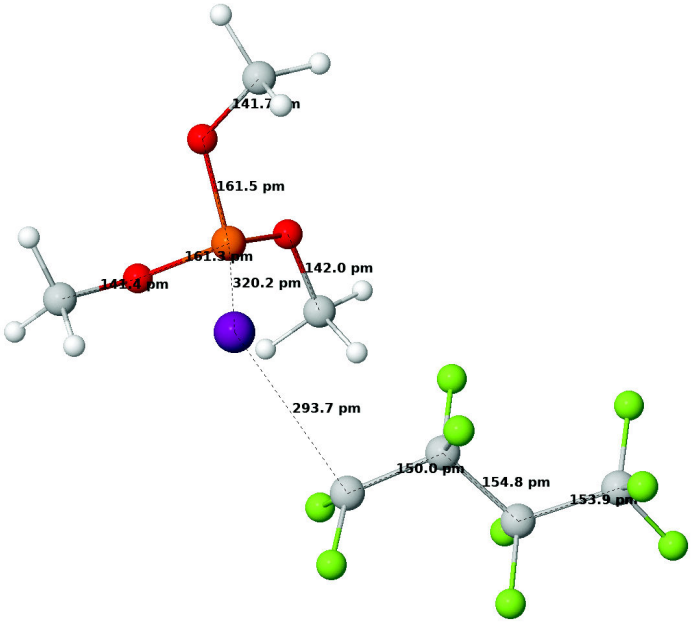

Figure S36. Geometry of the S_1/S_0 conical intersection of $(MeO)_3P–IC_4F_9$ and selected bond lengths in pm.

S8.3. TDDFT/TDA-Optimized Triplet Geometries

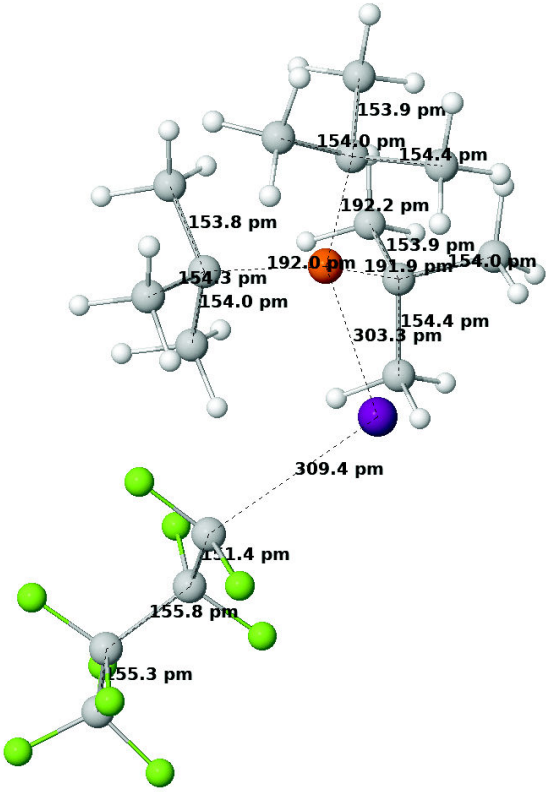

Figure S37. T_1 geometry of $^tBu_3P–IC_4F_9$ and selected bond lengths in pm.

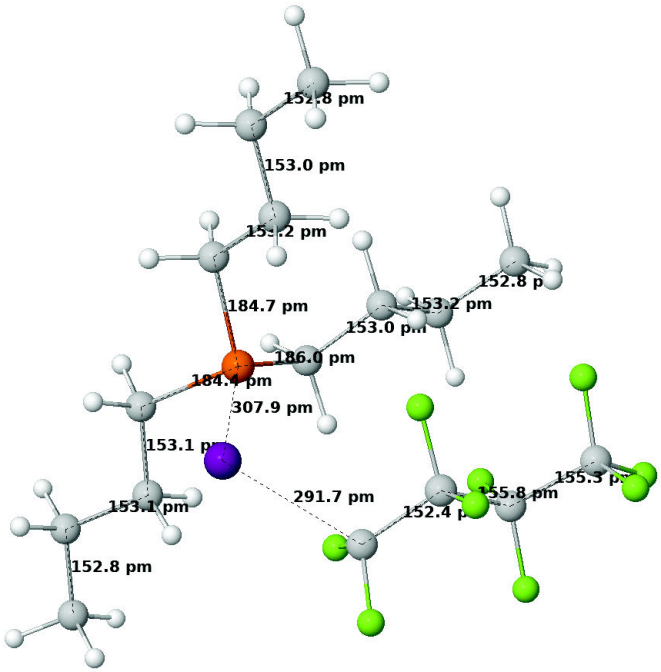

Figure S38. T_1 geometry of $^{n}Bu_3P–IC_4F_9$ and selected bond lengths in pm.

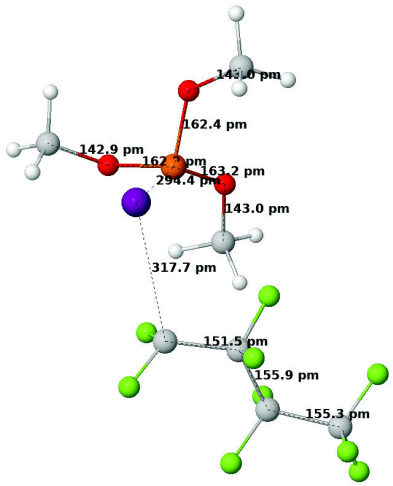

Figure S39. T_1 geometry of $(MeO)_3P–IC_4F_9$ and selected bond lengths in pm.

1. Helmecke, L.; Spittler, M.; Baumgarten, K.; Czekelius, C. Metal-Free Activation of C–I Bonds and Perfluoroalkylation of Alkenes with Visible Light Using Phosphine Catalysts. *Org. Lett.* **2019**, *21*, 7823–7827. doi:10.1021/acs.orglett.9b02812.
2. Cole, J.R.; Dellinger, M.E.; Johnson, T.J.; Reinecke, B.A.; Pike, R.D.; Pennington, W.T.; Krawiec, M.; Rheingold, A.L. Caged phosphite complexes of copper(I) halides. *J. Chem. Crystallogr.* **2003**, *33*, 341–347. doi:10.1023/A:1024217727932.
3. Taira, K.; Mock, W.L.; Gorenstein, D.G. Experimental Tests of the Stereoelectronic Effect at Phosphorus: Nucleophilic Reactivity of Phosphite Esters. *J. Am. Chem. Soc.* **1984**, *106*, 7831–7835. doi:10.1021/ja00337a029.
4. Manning, H.C.; Bai, M.; Anderson, B.M.; Lisiak, R.; Samuelson, L.E.; Bornhop, D.J. Expeditious synthesis of 'P'-protected macrocycles en route to lanthanide chelate metal complexes. *Tetrahedron Lett.* **2005**, *46*, 4707–4710. doi:10.1016/j.tetlet.2005.05.049.
5. Bietti, M.; Calcagni, A.; Salamone, M. The Role of Structural Effects on the Reactions of Alkoxyl Radicals with Trialkyl and Triaryl Phosphites. A Time-Resolved Kinetic Study. *J. Org. Chem.* **2010**, *75*, 4514–4520. doi:10.1021/jo100703b.
6. Mark, V.; Wazer, J.R.V. Tri-*t*-butyl Phosphite and Some of Its Reactions. *J. Org. Chem.* **1964**, *29*, 1006–1008. doi:10.1021/jo01028a005.

10.4. Unpublished Results

10.4.1. Iodoperfluoroalkylation using (*R*)-BINAP as catalyst

Experiment: LH-118

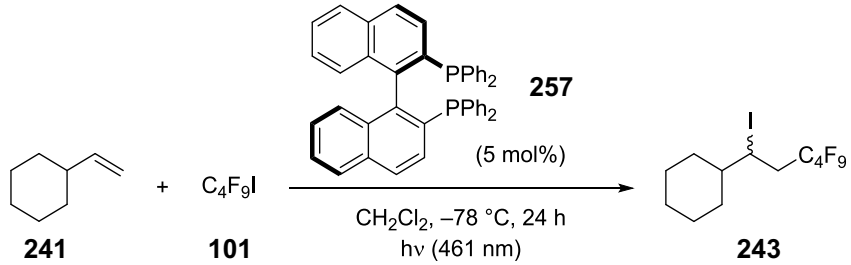

Inside the glovebox (*R*)-BINAP **257** (8.5 mg, 0.014, 4.6 mol%) was weighed inside a vial, dissolved in CH_2Cl_2 (1 mL), transferred in a Schlenk-tube and a stirring bar was added. Vinylcyclohexane (**241**) (40 µL, 0.29 mmol, 1.0 equiv) and nonafluoro-1-iodobutane (**101**) (50 µL, 0.29 mmol, 1.0 equiv) were added under red light and best possible light exclusion. The Schlenk-tube was sealed and covered in aluminum foil. The reaction solution was cooled to –78 °C and irradiated for 24 h. The solvent was evaporated, and purification by chromatography on SiO_2 (pentane) yielded pure product **243** as colorless liquid.

yield (456.13 g mol^{-1}) 35.6 g (0.0780 mmol, 27%)

^{1}H-NMR (300 MHz, Chloroform-*d*) δ [ppm] 4.44 – 4.27 (td, *J* = 6.7, 3.0 Hz, 1H, C*H*I), 2.98 – 2.71 (m, 2H, C*H*$_2$CF$_2$), 1.89 – 1.78 (m, 2H, C*H*$_2$-Cy), 1.73 – 1.63 (m, 3H, C*H*$_2$-Cy), 1.42 – 1.29 (m, 2H), 1.29 – 1.04 (m, 3H, C*H*$_2$-Cy), 0.90 – 0.76 (tq, *J* = 10.6, 3.5 Hz, 1H, *H*-Cy).

^{19}F-NMR (282 MHz, Chloroform-*d*) δ [ppm] –80.89 – –81.24 (t, *J* = 9.7 Hz, 3F, CF_3), –111.97 – –115.64 (m, 2F, CF_2), –124.37 – –124.73 (m, 2F, CF_2), –125.72 – –126.08 (m, 2F, CF_2).

Analytic data are consistent with literature-known values.[1]

10.4.2. Reactions with electron-deficient alkenes and alkynes

Experiment: LH-424

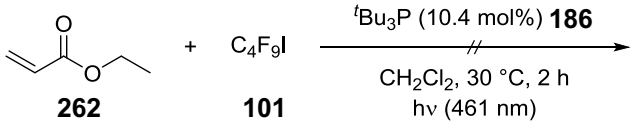

Inside the glovebox ^{t}Bu$_3$P **186** (11.1 mg, 0.0548 mmol, 10.4 mol%) was weighed into a reaction vial and CH_2Cl_2 (2 ml) was added. Outside the glovebox, under a stream of N_2 and under red light ethyl acrylate (**262**) (56 µL, 0.51 mmol, 1.0 equiv) and C_4F_9I **101** (100 µl, 0.583 mmol, 1.10 equiv)

were added and irradiated for 2 h at 461 nm. A sample for the ^{1}H- and ^{19}F-NMR spectroscopy measurements was withdrawn. No conversion was observed.

Experiment: LH-419

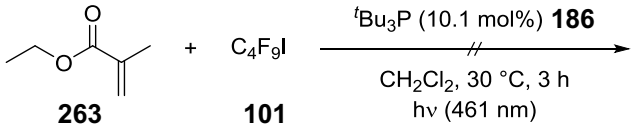

Inside the glovebox ^{t}Bu$_3$P **186** (10.9 mg, 0.0538 mmol, 10.9 mol%) was weighed into a reaction vial and CH_2Cl_2 (2 mL) was added. Outside the glovebox, under a stream of N_2 and under red light ethyl methacrylate (**263**) (66 µL, 0.53 mmol, 1.0 equiv) and C_4F_9I **101** (100 µl, 0.583 mmol, 1.10 equiv) were added and irradiated for 3 h at 461 nm. A sample for the ^{1}H- and ^{19}F-NMR spectroscopy measurements was withdrawn. No conversion was observed.

Experiment: LH-418

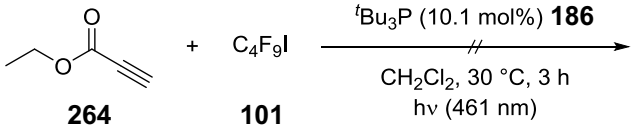

Inside the glovebox ^{t}Bu$_3$P **186** (10.9 mg, 0.0538 mmol, 10.1 mol%) was weighed into a reaction vial and CH_2Cl_2 (2 mL) was added. Outside the glovebox, under a stream of N_2 and under red light ethyl propiolate **264** (54 µL, 0.53 mmol, 1.0 equiv) and C_4F_9I **101** (100 µL, 0.583 mmol, 1.10 equiv) were added and irradiated for 3 h at 461 nm. When C_4F_9I **101** was added, the reaction solution turned dark black. A sample for ^{1}H- and ^{19}F-NMR spectroscopy was withdrawn after the irradiation. No conversion was observed.

Experiment: LH-506

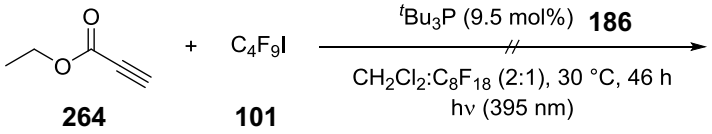

Inside the glovebox ^{t}Bu$_3$P **186** (5.7 mg, 0.028 mmol, 9.5 mol%) was weighed into a reaction vial, CH_2Cl_2 (1 mL) and C_8F_{18} (0.5 mL) were added. Outside the glovebox, under a stream of N_2 and under red light ethyl propiolate (**264**) (27 µL, 0.27 mmol, 1.0 equiv) and C_4F_9I **101** (51 µL, 0.30 mmol, 1.1 equiv) were added and irradiated for 46 h at 395 nm. When C_4F_9I **101** was added, the upper phase turned dark black. A sample of both phases for the ^{1}H- and ^{19}F-NMR spectroscopy was withdrawn after the irradiation. No conversion was observed.

Experiment: LH-428

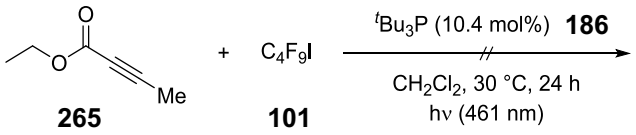

Inside the glovebox $^{t}Bu_3P$ **186** (11.1 mg, 0.0548 mmol, 10.4 mol%) was weighed into a reaction vial and CH_2Cl_2 (2 mL) was added. Outside the glovebox, under a stream of N_2 and under red light 2-butynoic acid (**265**) (44.1 mg, 0.524 mmol, 1.00 equiv) and C_4F_9I **101** (100 µl, 0.583 mmol, 1.11 equiv) were added and irradiated for 24 h at 461 nm. A sample for the ^{1}H- and ^{19}F-NMR spectroscopy was withdrawn. No conversion was observed.

Experiment: LH-429

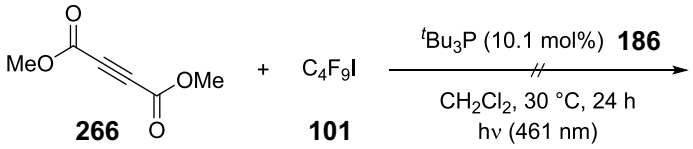

Inside the glovebox $^{t}Bu_3P$ **186** (10.8 mg, 0.0534 mmol, 10.1 mol%) was weighed into a reaction vial and CH_2Cl_2 (2 mL) was added. Outside the glovebox, under a stream of N_2 and under red light dimethyl acetylenedicarboxylate (**266**) (65 µL, 0.53 mmol, 1.0 equiv) and C_4F_9I **101** (100 µl, 0.583 mmol, 1.10 equiv) were added and irradiated for 24 h at 461 nm. A sample for the ^{1}H- and ^{19}F-NMR spectroscopy was withdrawn. No conversion was observed.

Experiment: LH-386

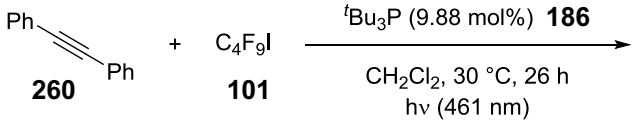

Inside the glovebox $^{t}Bu_3P$ **186** (10.6 mg, 0.0524 mmol, 9.88 mol%) was weighed into a reaction vial. Outside the glovebox, under a stream of N_2 and under red light diphenylacetylene (**260**) (96.9 mg, 0.530 mmol, 1.00 equiv) and C_4F_9I **101** (100 µl, 0.583 mmol, 1.10 equiv) in CH_2Cl_2 (2 mL) were added and irradiated for 26 h at 461 nm. A sample for the ^{1}H- and ^{19}F-NMR spectroscopy was withdrawn. No conversion was observed.

10.4.3. Reactions with 1-bromoperfluorohexane

Experiment: LH-407

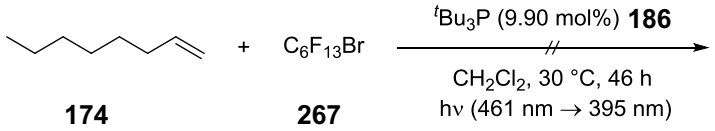

174 **267**

Inside the glovebox $^{t}Bu_3P$ **186** (10.5 mg, 0.0518 mmol, 9.90 mol%), 1-octene (**174**) (58.8 mg, 0.524 mmol, 1.00 equiv) and perfluorohexyl bromide (**267**) (124 µl, 0.583 mmol, 1.11 equiv) were irradiated in CH_2Cl_2 (2 mL) for 2 h at 461 nm. Under red light and a stream of N_2 a sample for the ^{1}H- and ^{19}F-NMR spectroscopy was withdrawn, and the reaction solution was irradiated again for 20 h at 461 nm. After another sample was withdrawn under the same conditions as mentioned before, the reaction solution was irradiated for another 24 h at 395 nm. All NMR-spectra showed no conversion.

Experiment: LH-408

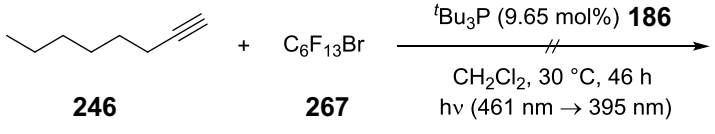

246 **267**

Inside the glovebox $^{t}Bu_3P$ **186** (10.9 mg, 0.0538 mmol, 9.65 mol%), 1-octyne (**246**) (61.5 mg, 0.558 mmol) and perfluorohexyl bromide **267** (124 µl, 0.583 mmol, 1.04 equiv) were irradiated in CH_2Cl_2 (2 mL) for 2 h at 461 nm. Under red light and a stream of N_2 a sample for the ^{1}H- and ^{19}F-NMR spectroscopy was withdrawn, and the reaction solution was irradiated again for 20 h at 461 nm. After another sample was withdrawn under the same conditions as mentioned before, the reaction solution was irradiated for another 24 h at 395 nm. All NMR-spectra showed no conversion.

10.4.4. Crystallization experiments

Experiment: LH-382

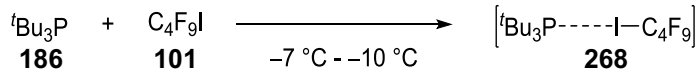

186 **101** **268**

Inside the glovebox $^{t}Bu_3P$ **186** (48.5 mg, 0.240 mmol) and C_4F_9I **101** (70 µl, 0.41 mmol, 1.7 equiv) were weighed into a small glass vial. The vial was placed inside an amber glass and sealed with a lid with Teflon™ inlet. Outside the glovebox one half of the amber glass was placed inside a cooling bath (–7 °C - –10 °C) for two days (see: p. 129, Figure 22, right). Colorless needle-like crystals were formed.

Experiment: LH-392

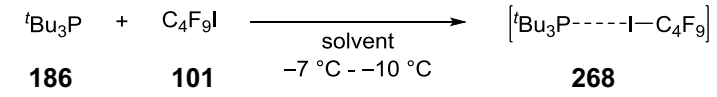

Inside the glovebox $^{t}Bu_3P$ **186** (58.9 mg, 0.291 mmol, 1.00 equiv.) and C_4F_9I **101** (202 mg, 0.583 mmol, 2.00 equiv) were weighed into a small glass vial. The vial was placed inside a screw top glass vial and sealed with a septum. Outside the glovebox one half of the amber glass was placed inside a cooling bath (−7 °C - −10 °C) and a small stream of N_2 was flushed inside the vial. Dried and degassed solvent was added through the septum(see: p. 130, Figure 23) and the samples were cooled for two days.

Table 9: Crystallization experiment of $^{t}Bu_3P$ **186** and C_4F_9I **101** with different solvents.

entry	solvent	[mL]	
1	MeOH	0.5	no crystals
2	MeCN	0.5	dark brown solution
3	Et_2O	0.5	amorphous crystals
4	MeOH + Et_2O	0.25 + 0.25	light yellow crystals
5	MeOH + MeCN	0.25 + 0.25	light yellow crystals

10.4.5. Synthesis of iodoethynyl derivatives

1-Iodohex-1-yne (274)

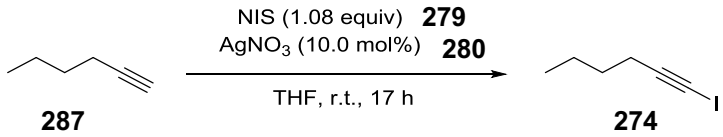

Experiment: LH-493

The synthesis of 1-iodohex-1-yne (**274**) was conducted similar to a literature-known procedure.[116] 1-Hexyne (**287**) (0.7 mL, 6 mmol, 1 equiv) was added to a mixture of $AgNO_3$ **280** (112 mg, 0.661 mmol, 10.0 mol%) and NIS **279** (1.98 g, 8.80 mmol, 1.10 equiv) in dry THF (10 mL). The reaction flask was covered with aluminum foil and was stirred for 17 h. The reaction was quenched with desalinated water (15 mL) and extracted with Et_2O (4 x 25 mL). The combined organic phases were dried over $MgSO_4$. After filtration, volatiles were removed under reduced pressure. Purification was conducted by chromatography on silica gel (pentane) and yielded colorless to slightly yellow liquid as pure product **274**.

yield (208.04 g·mol^{-1}) 1.13 g (5.42 mmol, 89%)

^{1}H-NMR (300 MHz, Chloroform-d) δ [ppm] 2.36 (t, J = 6.9 Hz, 2H), 1.59 – 1.32 (m, 4H), 0.91 (t, J = 7.2 Hz, 3H).

Analytic data are consistent with literature-known values.[116]

(Iodoethynyl)benzene (275)

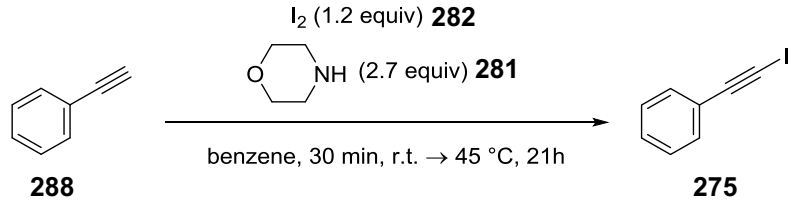

288 **275**

Experiment: LH-496

The synthesis of (iodoethynyl)benzene (**275**) was conducted similar to a literature-known procedure.[117] Iodine (**282**) (2.8 g, 11 mmol, 1.2 equiv) and morpholine (**281**) (2.6 mL, 30 mmol, 2.7 equiv) were dissolved in benzene (20 mL) and the dark red solution was stirred for 30 min at room temperature. Phenylacetylene (**288**) (2.5 mL, 23 mmol, 1.0 equiv.) was added dropwise and the mixture was stirred at 45 °C for 21 h. The yellow suspension was filtered, and the residue was washed with Et_2O (2 x 20 mL). the combined organic layers were washed with saturated aqueous solution of NH_4Cl (20 mL), $NaHCO_3$ (20 mL) and H_2O (20 mL). The combined organic phase was dried over $MgSO_4$. After filtration, volatiles were removed under reduced pressure. Purification was conducted by chromatography on silica gel (pentane) and yielded yellow oil as pure product **275**.

yield (228.0 g·mol^{-1}) 2.73 g (11.9 mmol, 52%)

^{1}H-NMR (300 MHz, Chloroform-d) δ [ppm] 7.54 – 7.27 (m, 5H).

Analytic data are consistent with literature-known values.[117]

Ethyl 3-iodopropiolate (276)

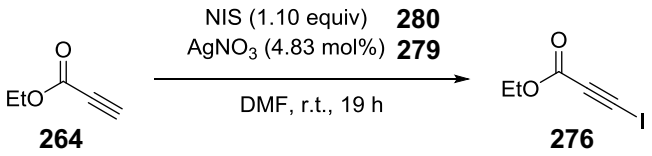

264 **276**

Experiment: LH-485

The synthesis of 3-iodopropiolate (**264**) was conducted similar to a literature-known procedure.[118] To a mixture of $AgNO_3$ **280** (72.2 mg, 0.425 mmol, 4.83 mol%) and ethyl propiolate (**264**) (0.81 mL, 8.0 mmol, 1.0 equiv) in dry and degassed DMF (41 mL) was added NIS **279** (1.98 g, 8.80 mmol, 1.10 equiv) in an N_2-counterflow. The reaction flask was covered with aluminum foil and was stirred for 19 h. The reaction solution was cooled to 0 °C, and ice-cold desalinated water (30 mL) was added. The mixture was extracted with Et_2O (4 x 20 mL), and the combined organic phases were washed with ice-cooled desalinated water (20 mL) and dried over Na_2SO_4. After filtration, volatiles were removed under reduced pressure. Purification was conducted by chromatography on aluminum oxide (90 active

neutral 0.063 - 0.200 mm) (pentane:Et_2O 99:1) yielded colorless to slightly yellow crystals as pure product **276**.

yield (223.93 g·mol^{-1}) 1.68 g (7.50 mmol, 94%)

^{1}H-NMR (300 MHz, Chloroform-d) δ [ppm] 4.23 (q, *J* = 6.9 Hz, 2H, $CH_3CH_2C(O)$-), 1.30 (t, *J* = 7.2 Hz, 3H, $CH_3CH_2C(O)$-).

^{13}C{^{1}H}-NMR (75.5 MHz, Chloroform-*d*) δ [ppm] 152.4, 87.3, 62.6, 14.1, 13.3.

IR (film on NaCl), ν [cm^{-1}] 2999, 2983, 2360, 2340, 2224, 2167, 1683, 1668, 1473, 1453, 1444, 1387, 1368, 1269, 1153, 1112, 1020, 966, 857, 747, 552.

m.p. 75.1 - 76.4 °C.

m/z calculated for $C_5H_6IO_2$ [M + H] 224.9407, found 224.9405.

1,2,3,4,5-pentafluoro-6-(iodoethynyl)benzene (277)

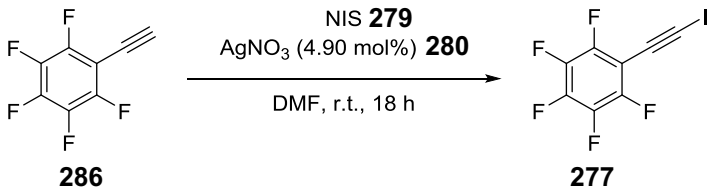

286 **277**

Experiment: LH-486

The synthesis of 1,2,3,4,5-pentafluoro-6-(iodoethynyl)benzene (**277**) was conducted similar to a literature-known procedure.[118] 1-Ethynyl-2,3,4,5,6-pentafluorobenzene (**286**) was contaminated with 1-bromo-2,3,4,5,6-pentafluorobenzene **283** (approx. 69%, determined from the ^{19}F-NMR spectrum).

To a mixture of $AgNO_3$ **280** (50.1 mg, 0.294 mmol) and 1-ethynyl-2,3,4,5,6-pentafluorobenzene (**286**) (1.43 g) in dry and degassed DMF (30 mL) was added NIS **279** (1.35g, 6.00 mmol) in an N_2-counterflow. The reaction flask was covered with aluminum foil and was stirred for 18 h. The reaction solution was cooled to 0 °C, and ice-cold desalinated water (30 mL) was added. The mixture was extracted with EtOAc (4 x 30 mL), and the combined organic phases were washed with ice-cooled desalinated water (20 mL) and dried over Na_2SO_4. After filtration, volatiles were removed under reduced pressure. Purification was conducted by chromatography on SiO_2 (hexane), followed by a second chromatography on aluminum oxide (90 active neutral 0.063 - 0.200 mm) (pentane) yielded colorless to light yellow liquid (628.5 mg). A yield cannot be given in a reasonable fashion. The product **277** was stored at –20 °C.

$^{13}C\{^1H\}$-NMR (300 MHz, Chloroform-d) δ [ppm] 150.3 – 146.8, 143.8 – 140.4, 139.3 – 135.9, 100.3, 77.7, 1 (q, *J* = 3.76 Hz), 21.6 (q, *J* = 3.76 Hz).

^{19}F-NMR (75.5 MHz, Chloroform-*d*) δ [ppm] –161.5 (m, 2F), –151.5 (m, 1F), –136.1 (m, 2F).

Shifts are consistent with literature-known values.[112] The multiplicity of the signals in the ^{19}F-NMR were not consistent with literature-known values.[112]

1-Iodo-2-(trimethylsilyl)acetylene (278)

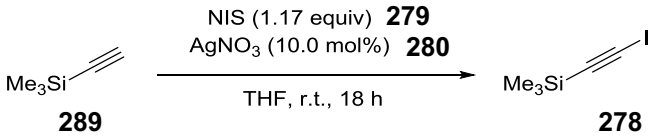

289 **278**

Experiment: LH-501

The synthesis of 1-iodo-2-(trimethylsilyl)acetylene (**278**) was conducted similar to a literature-known procedure.[116]

Trimethylsilylacetylene (**289**) (0.8 mL, 6 mmol, 1 equiv) was added to a mixture of $AgNO_3$ **280** (112 mg, 0.661 mmol, 10.0 mol%) and NIS **279** (1.48 g, 6.58 mmol, 1.17 equiv) in dry THF (10 mL). The reaction flask was covered with aluminum foil and was stirred for 17 h. The reaction was quenched with desalinated water (15 mL) and extracted with Et_2O (3 x 25 mL). The combined organic phases were dried over $MgSO_4$. After filtration, volatiles were removed under reduced pressure. Purification was conducted by chromatography on silica gel (pentane) and yielded colorless to slightly yellow liquid as pure product **274**.

yield (208.04 g·mol^{-1}) 1.04 g (4.64 mmol, 83%)

^1H-NMR (300 MHz, Chloroform-d) δ [ppm] 0.18 (s, 9H).

$^{13}C\{^1H\}$-NMR (500 MHz, Chloroform-d) δ [ppm] 104.4, 20.1, 0.05.

Analytic data are consistent with literature-known values.[116]

10.4.6. Photoreactions with iodoethynyl derivatives

Reaction with ethyl 1-iodohex-1-yne (274) and 1-octene (174)

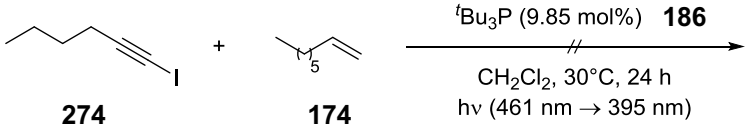

274 **174**

Experiment: LH-497

Inside the glovebox $^tBu_3P$ **186** (10.6 mg, 0.0524 mmol, 9.85 mol%) and 1-octene (**174**) (64.6 mg, 0.576 mmol, 1.08 equiv) were weighed into a reaction glass vial. A Teflon™ stirring bar and CH_2Cl_2

(2 mL) were added, and the vial was sealed with a septa screw cap. Outside the glovebox under a stream of N_2 and under red light 1-iodohex-1-yne (**274**) (111 mg, 0.532 mmol, 1.00 equiv) was added and the reaction vial was sealed. The irradiation was started for 5 h at 461 nm. A sample for the ^{1}H-NMR-spectroscopy was withdrawn under a stream of N_2 and under red light. The reaction solution was further irradiated for 19 h at 395 nm. Another sample for the ^{1}H-NMR-spectroscopy was withdrawn. No conversion was detected.

Reaction with ethyl 1-iodohex-1-yne (274) and 1-octene (174)

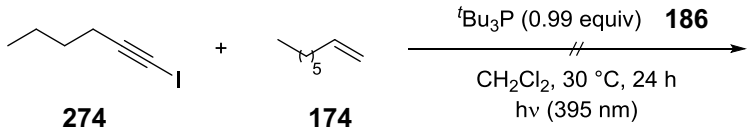

Experiment: LH-499

Inside the glovebox ^{t}Bu$_3$P **186** (110 mg, 0.0545 mmol, 0.99 equiv) and 1-octene (**174**) (63.8 mg, 0.569 mmol, 1.04 equiv) were weighed into a reaction glass vial. A Teflon™ stirring bar and CH_2Cl_2 (2 mL) were added, and the vial was sealed with a septa screw cap. Outside the glovebox under a stream of N_2 and under red light 1-iodohex-1-yne (**274**) (114 mg, 0.548 mmol, 1.00 equiv) was added and the reaction vial was sealed. The irradiation was started for 24 h at 395 nm. A sample for the ^{1}H-NMR-spectroscopy was withdrawn. The reaction solution was dark brown. No conversion was detected.

Reaction with ethyl 1-iodohex-1-yne (274) and 1-octene (174)

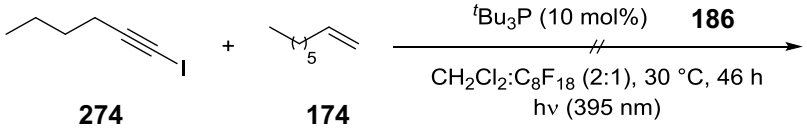

Experiment: LH-503

Inside the glovebox ^{t}Bu$_3$P **186** (5.5 mg, 0.027 mmol, 10 mol%) and 1-octene (**174**) (33.0 mg, 0.294 mmol, 1.12 equiv) were weighed into a reaction glass vial. A Teflon™ stirring bar, CH_2Cl_2 (1 mL) and C_8F_{18} (0.5 mL) were added, and the vial was sealed with a septa screw cap. Outside the glovebox under a stream of N_2 and under red light 1-iodohex-1-yne (**274**) (54.8 mg, 0.263 mmol, 1.00 equiv) was added and the reaction vial was sealed. The irradiation was started for 46 h at 395 nm. A sample of both phases for the ^{1}H-spectroscopy was withdrawn. The upper phase was brown, and the lower phase was colorless clear. No conversion was detected.

Reaction with ethyl 1-iodohex-1-yne (274) and 1-octene (174)

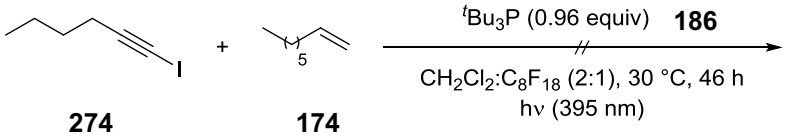

274 174

Experiment: LH-504

Inside the glovebox $^{t}Bu_3P$ **186** (55 mg, 0.27 mmol, 0.96 equiv) and 1-octene (**174**) (33.1 mg, 0.295 mmol, 1.04 equiv) were weighed into a reaction glass vial. A Teflon™ stirring bar, CH_2Cl_2 (1 mL) and C_8F_{18} (0.5 mL) were added, and the vial was sealed with a septa screw cap. Outside the glovebox under a stream of N_2 and under red light 1-iodohex-1-yne (**274**) (58.8 mg, 0.283 mmol, 1.00 equiv) was added and the reaction vial was sealed. The irradiation was started for 46 h at 395 nm. A sample of both phases for the ^{1}H-NMR-spectroscopy were withdrawn. The upper phase was brown, and the lower phase was colorless clear. No conversion was detected.

Reaction with ethyl 1-iodohex-1-yne (274) and 1-octene (174)

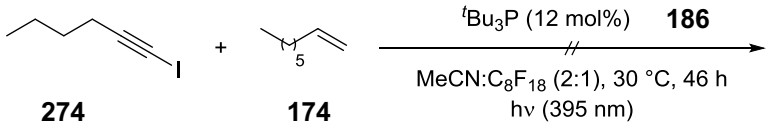

274 174

Experiment: LH-505

Inside the glovebox $^{t}Bu_3P$ **186** (7.0 mg, 0.035 mmol, 12 mol%) and 1-octene (**174**) (32.4 mg, 0.289 mmol, 0.98 equiv) were weighed into a reaction glass vial. A Teflon™ stirring bar and C_8F_{18} (0.5 mL) were added, and the vial was sealed with a septa screw cap. Outside the glovebox under a stream of N_2 and under red light dry MeCN (1 mL) and 1-iodohex-1-yne (**274**) (61.6 mg, 0.296 mmol, 1.00 equiv) were added. The reaction vial was sealed, and the irradiation was started for 46 h at 395 nm. A sample of both phases for the ^{1}H-NMR-spectroscopy were withdrawn. The upper phase was yellow, and the lower phase was colorless clear. No conversion was detected.

Reaction with ethyl 3-iodopropiolate (276) and vinylcyclohexane (241)

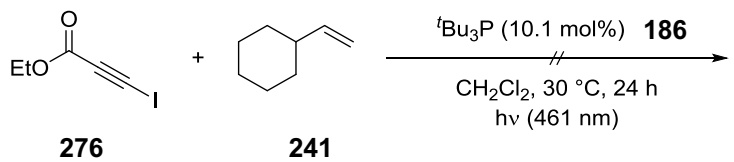

276 241

Experiment: LH-487

Inside the glovebox $^{t}Bu_3P$ **186** (10.9 mg, 0.0539 mmol, 10.1 mol%) and vinylcyclohexane (**241**) (59.6 mg, 0.551 mmol, 1.03 equiv) were weighed into a reaction glass vial. A Teflon™ stirring bar was

added. In another glass vial ethyl 3-iodopropiolate (**264**) (120 mg, 0.535 mmol, 1.00 equiv) was dissolved in CH_2Cl_2 (2 x 1 mL) and transferred into the reaction vial. The solution turned black immediately. The vial was sealed with a septa screw cap and outside the glovebox the irradiation was started for 24 h. A sample for the ^{1}H- and ^{19}F-NMR-spectroscopy was withdrawn. No conversion was detected.

Reaction with ethyl 3-iodopropiolate (276) and 1-octene (174)

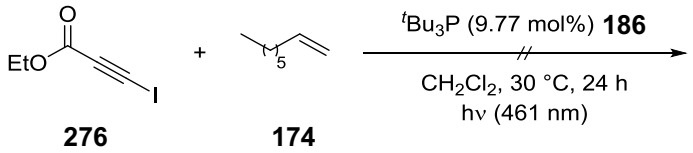

276 **174**

Experiment: LH-488

Inside the glovebox ^{t}Bu$_3$P **186** (10.6 mg, 0.0524 mmol, 9.77 mol%) and 1-octene (**174**) (60.9 mg, 0.542 mmol, 1.01 equiv) were weighed into a reaction glass vial. A Teflon™ stirring bar was added. In another glass vial, ethyl 3-iodopropiolate (**276**) (120 mg, 0.536 mmol, 1.00 equiv) was dissolved in CH_2Cl_2 (2 x 1 mL) and transferred into the reaction vial. The solution turned black immediately. The vial was sealed with a septa screw cap, and outside the glovebox, the irradiation was started for 24 h. A sample for the ^{1}H- and ^{19}F-NMR-spectroscopy was withdrawn. No conversion was detected.

Reaction with 1,2,3,4,5-pentafluoro-6-(iodoethynyl)benzene (277) and vinylcyclohexane (241)

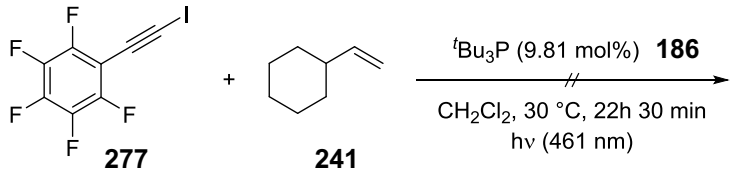

277 **241**

Experiment: LH-491

Inside the glovebox ^{t}Bu$_3$P **186** (10.5 mg, 0.0519 mmol, 9.81 mol%) and vinylcyclohexane (**241**) (55.5 mg, 0.513 mmol, 1.00 equiv) were weighed into a reaction glass vial. A Teflon™ stirring bar and CH_2Cl_2 (2 mL) were added, and the vial was sealed with a septa screw cap. Outside the glovebox under a stream of N_2 and under red light 1,2,3,4,5-pentafluoro-6-(iodoethynyl)benzene (**277**) (187 mg, 0.590 mmol, 1.15 equiv) was added and the reaction vial was sealed. The first colorless reaction solution turned light yellow. The irradiation was started for 1 h. The reaction solution was dark brown. A sample for the ^{1}H- and ^{19}F-NMR-spectroscopy was withdrawn under a stream of N_2 and under red light. The reaction solution was further irradiated for 1:30 h. Another sample for the ^{1}H- and ^{19}F-NMR-

spectroscopy was withdrawn, and the reaction solution was further irradiated for 20 h. One more sample for the ^{1}H- and ^{19}F-NMR-spectroscopy was withdrawn. No conversion was detected.

Reaction with with 1,2,3,4,5-pentafluoro-6-(iodoethynyl)benzene (277) and 1-octene (174)

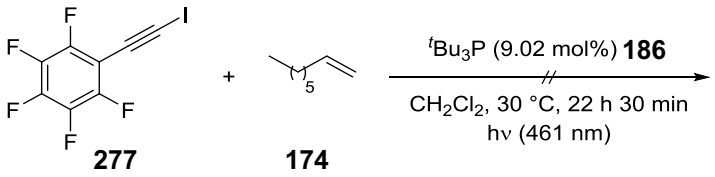

277 **174**

Experiment: LH-492

Inside the glovebox ^{t}Bu$_3$P **186** (10.9 mg, 0.0538 mmol, 9.02 mol%) and 1-octene (**174**) (55.5 mg, 0.494 mmol, 1.00 equiv) were weighed into a reaction glass vial. A Teflon™ stirring bar and CH_2Cl_2 (2 mL) were added, and the vial was sealed with a septa screw cap. Outside the glovebox under a stream of N_2 and under red light 1,2,3,4,5-pentafluoro-6-(iodoethynyl)benzene (**277**) (190 mg, 0.597 mmol, 1.21 equiv) was added and the reaction vial was sealed. The first colorless reaction solution turned light yellow. The irradiation was started for 1 h. The reaction solution was dark brown. A sample for the ^{1}H- and ^{19}F-NMR-spectroscopy was withdrawn under a stream of N_2 and under red light. The reaction solution was further irradiated for 1:30 h. Another sample for the ^{1}H- and ^{19}F-NMR-spectroscopy was withdrawn and the reaction solution was further irradiated for 20 h. One more sample for the ^{1}H- and ^{19}F-NMR-spectroscopy was withdrawn. No conversion was detected.

Reaction with with (iodoethynyl)benzene (275) and 1-octene (174)

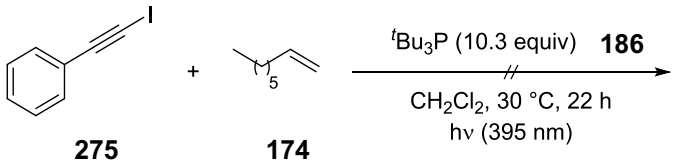

275 **174**

Experiment: LH-498

Inside the glovebox ^{t}Bu$_3$P **186** (11.2 mg, 0.0554 mmol, 10.3 equiv) and 1-octene (**174**) (59 mg, 0.53 mmol, 1.0 equiv) were weighed into a reaction glass vial. A Teflon™ stirring bar and CH_2Cl_2 (2 mL) were added, and the vial was sealed with a septa screw cap. Outside the glovebox under a stream of N_2 and under red light (iodoethynyl)benzene (**275**) (122 mg, 0.537 mmol, 1.00 equiv) was added and the reaction vial was sealed. The irradiation was started for 22 h at 395 nm. A sample for the ^{1}H-NMR-spectroscopy was withdrawn. The reaction solution was dark brown. No conversion was detected.

Reaction with with (iodoethynyl)benzene (275) and 1-octene (174)

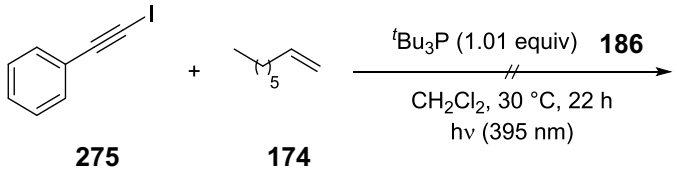

275 **174**

Experiment: LH-500

Inside the glovebox ^{t}Bu$_3$P **186** (110 mg, 0.542 mmol, 1.01 equiv) and 1-octene (**174**) (58.8 mg, 0.524 mmol, 0.98 equiv) were weighed into a reaction glass vial. A Teflon™ stirring bar and CH_2Cl_2 (2 mL) were added, and the vial was sealed with a septa screw cap. Outside the glovebox under a stream of N_2 and under red light (iodoethynyl)benzene (**275**) (122 mg, 0.537 mmol, 1.00 equiv) was added and the reaction vial was sealed. The irradiation was started for 22 h at 395 nm. A sample for the ^{1}H-NMR-spectroscopy was withdrawn. The reaction solution was dark brown. No conversion was detected.

Reaction with with 1-iodo-2-(trimethyl)silylacetylene (278) and 1-octene (174)

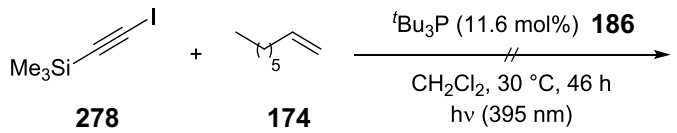

278 **174**

Experiment: LH-507

Inside the glovebox ^{t}Bu$_3$P **186** (12.7 mg, 0.0628 mmol, 11.6 mol%) and 1-octene (**174**) (66.0 mg, 0.589 mmol, 1.09 equiv) were weighed into a reaction glass vial. A Teflon™ stirring bar and CH_2Cl_2 (2 mL) were added, and the vial was sealed with a septa screw cap. Outside the glovebox under a stream of N_2 and under red light 1-iodo-2-(trimethyl)silylacetylene (**278**) (121 mg, 0.540 mmol, 1.00 equiv) was added and the reaction vial was sealed. The irradiation was started for 46 h at 395 nm. A sample for the ^{1}H-NMR-spectroscopy was withdrawn. The reaction solution was slightly brown. No conversion was detected.

NMR experiment of ethyl 3-iodopropiolate (276) with $^{t}Bu_3P$ 186

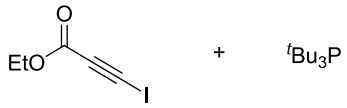

276 **186**

Experiment: LH-489

Inside the glovebox $^{t}Bu_3P$ **186** (11.0 mg, 0.0543 mmol) and ethyl 3-iodopropiolate (**276**) (11.4 mg, 0.0509 mmol, 1.06 equiv) were weighed into a glass vial and dissolved in CH_2Cl_2 (0.6 mL). The dark solution was transferred into a Young valve NMR tube equipped with an external NMR standard (H_3PO_4 in D_2O). The Young NMR tube was sealed, and a ^{1}H- and ^{31}P-NMR spectra were measured.

NMR experiment of 1,2,3,4,5-pentafluoro-6-(iodoethynyl)benzene (277) with $^{t}Bu_3P$ 186

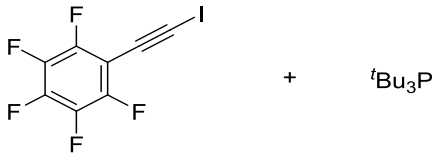

277 **186**

Experiment: LH-490

Inside the glovebox $^{t}Bu_3P$ **186** (11.0 mg, 0.0543 mmol, 1.00 equiv) was weighed into a glass vial and dissolved in CH_2Cl_2 (0.6 mL). The was transferred into a Young valve NMR tube equipped with an external NMR standard (H_3PO_4 in D_2O and $CFCl_3$ in C_6D_6). The Young NMR tube was sealed and outside the glovebox under an N_2-counterflow 1,2,3,4,5-pentafluoro-6-(iodoethynyl)benzene (**277**) (19.0 mg, 0.0597 mmol, 1.10 mmol) was added. The Young NMR tube was sealed again, and a ^{19}F- and ^{31}P-NMR spectra were measured.

11. Spectral Data

11.1.1. Ethyl 3-iodopropiolate (276)

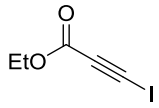

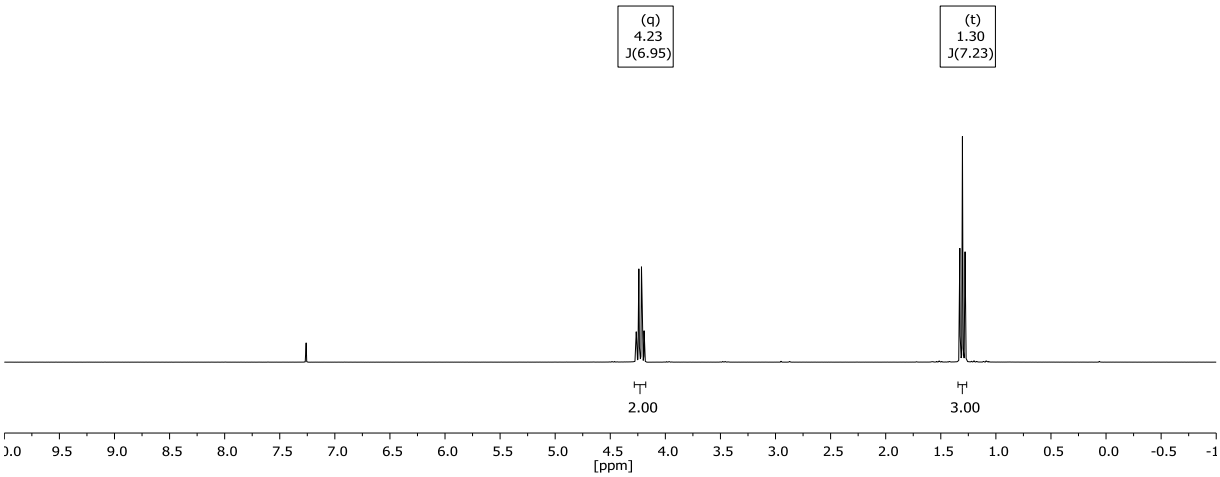

^{1}H-NMR spectrum (300 MHz, $CDCl_3$)

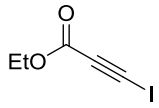

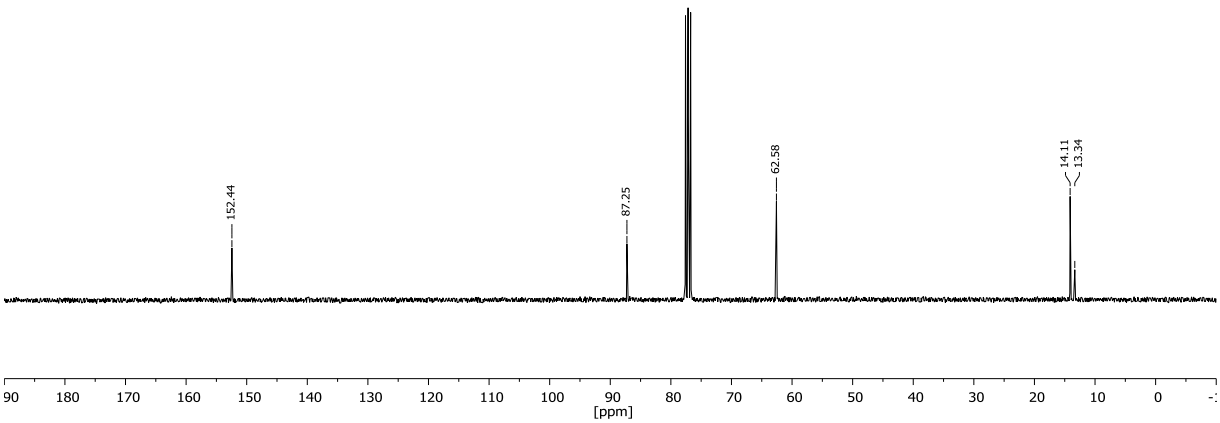

^{13}C{^{1}H}-NMR spectrum (75.5 MHz, $CDCl_3$)

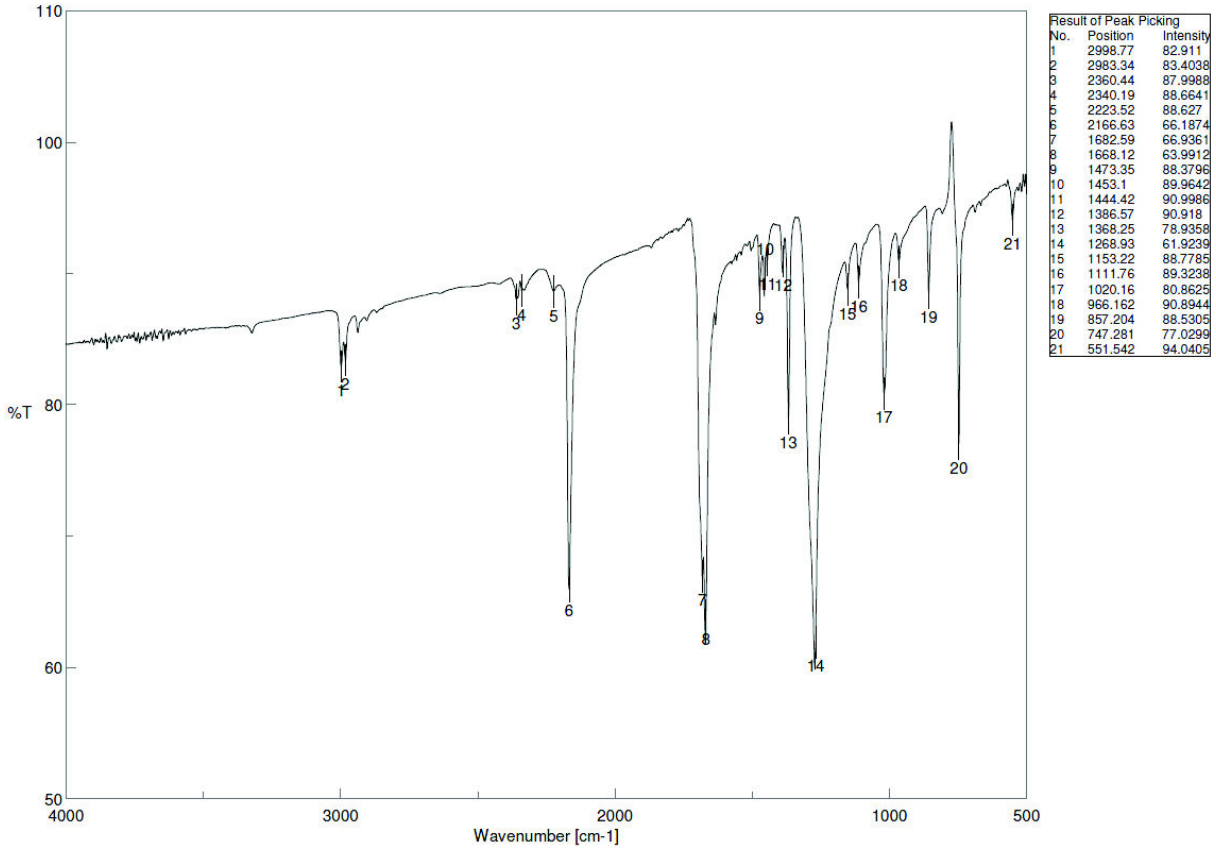

IR-spectrum (film on NaCl)

11.1.2. 1,2,3,4,5-pentafluoro-6-(iodoethynyl)benzene (277)

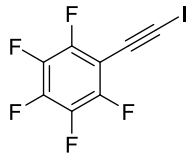

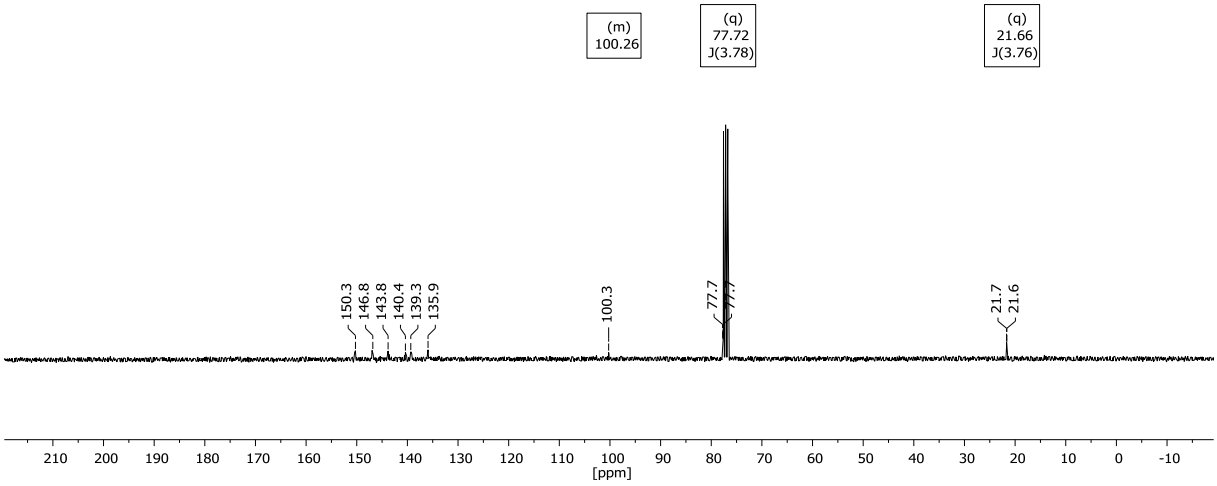

$^{13}C\{^{1}H\}$-NMR spectrum (75.5 MHz, $CDCl_3$)

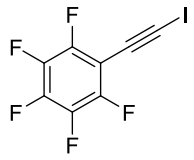

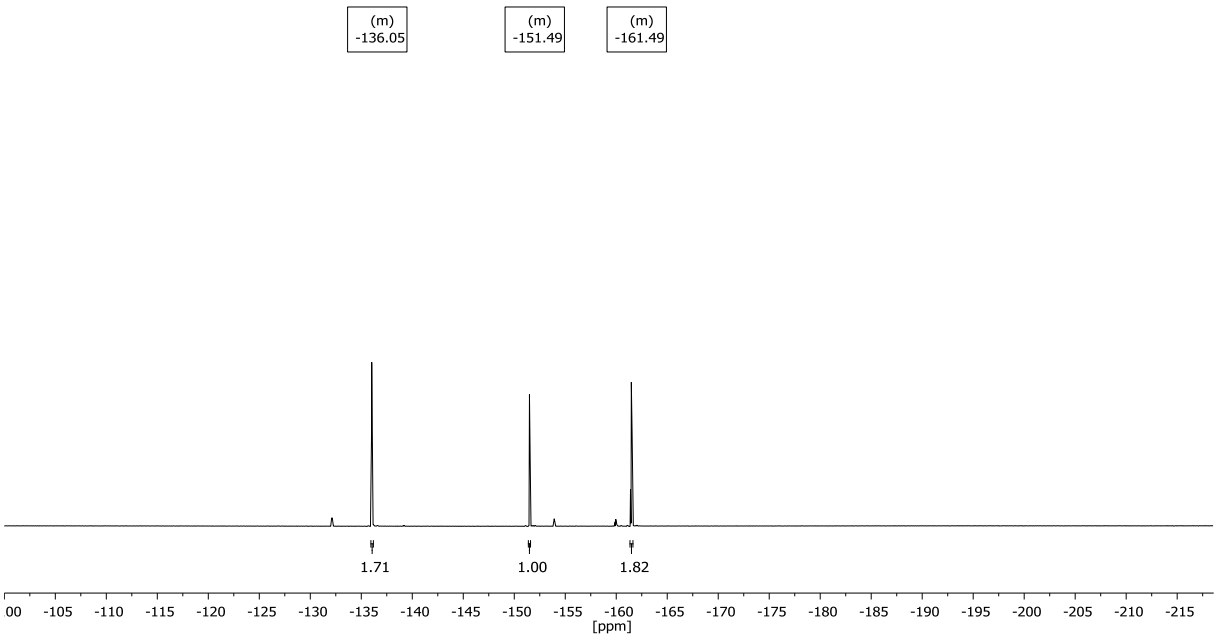

^{19}F-NMR spectrum (282 MHz, $CDCl_3$)

12. Literature

[1] I. Behrends, S. Bähr, C. Czekelius, Perfluoroalkylation of Alkenes by Frustrated Lewis Pairs. *Chem. Eur. J.* **2016**, *22*, 17177-17181.

[2] M. Spittler, L. Helmecke, C. Czekelius, Mechanistic Insights into FLP-Catalyzed Iodoperfluoroalkylations. *Eur. J. Org. Chem.* **2019**, 458-468.

[3] M. Spittler, Frustrated Lewis Pair-Catalysed Functionalisation of Alkenes with Iodoperfluoroalkanes and Gold-Catalysed Desymmetrisation of 1,4-Diynes. Doctoral Dissertation, Heinrich-Heine-Universität Düsseldorf, Düsseldorf, 2018.

[4] L. Helmecke, M. Spittler, K. Baumgarten, C. Czekelius, Metal-Free Activation of C–I Bonds and Perfluoroalkylation of Alkenes with Visible Light Using Phosphine Catalysts. *Org. Lett.* **2019**, *21*, 7823-7827.

[5] M. Bracker, L. Helmecke, M. Kleinschmidt, C. Czekelius, C. M. Marian, Visible Light-Induced Homolytic Cleavage of Perfluoroalkyl Iodides Mediated by Phosphines. *Molecules* **2020**, *25*, 1606.

[6] L. Helmecke, M. Spittler, B. M. Schmidt, C. Czekelius, Metal-Free Iodoperfluoroalkylation: Photocatalysis versus Frustrated Lewis Pair Catalysis. *Synthesis* **2020**, 6; DOI: 10.1055/s-0040-1707232.

[7] J. Wang, M. Sánchez-Roselló, J. L. Aceña, C. del Pozo, A. E. Sorochinsky, S. Fustero, V. A. Soloshonok, H. Liu, Fluorine in Pharmaceutical Industry: Fluorine-Containing Drugs Introduced to the Market in the Last Decade (2001–2011). *Chem. Rev.* **2014**, *114*, 2432-2506.

[8] R. Berger, G. Resnati, P. Metrangolo, E. Weber, J. Hulliger, Organic fluorine compounds: a great opportunity for enhanced materials properties. *Chem. Soc. Rev.* **2011**, *40*, 3496-3508.

[9] W. K. Hagmann, The Many Roles for Fluorine in Medicinal Chemistry. *J. Med. Chem.* **2008**, *51*, 4359-4369.

[10] P. Maienfisch, R. G. Hall, The Importance of Fluorine in the Life Science Industry. *CHIMIA* **2004**, *58*, 93-99.

[11] S. Purser, P. R. Moore, S. Swallow, V. Gouverneur, Fluorine in medicinal chemistry. *Chem. Soc. Rev.* **2008**, *37*, 320-330.

[12] P. Kirsch, *Modern Fluoroorganic Chemistry: Synthesis, Reactivity, Applications*, 2nd ed., Wiley-VCH, Weinheim, **2013**.

[13] B. K. Park, N. R. Kitteringham, P. M. O'Neill, Metabolism of Fluorine-Containing Drugs. *Annu. Rev. Pharmacol. Toxicol.* **2001**, *41*, 443-470.

[14] D. O'Hagan, Understanding organofluorine chemistry. An introduction to the C–F bond. *Chem. Soc. Rev.* **2008**, *37*, 308-319.

[15] K. Müller, C. Faeh, F. Diederich, Fluorine in Pharmaceuticals: Looking Beyond Intuition. *Science* **2007**, *317*, 1881-1886.

[16] D. Seebach, Organic Synthesis—Where now? *Angew. Chem. Int. Ed. Engl.* **1990**, *29*, 1320-1367.

[17] J. E. Huheey, The Electronegativity of Groups. *J. Phys. Chem.* **1965**, *69*, 3284-3291.

[18] M. A. McClinton, D. A. McClinton, Trifluoromethylations and related reactions in organic chemistry. *Tetrahedron* **1992**, *48*, 6555-6666.

[19] D. O'Hagan, Fluorine in health care: Organofluorine containing blockbuster drugs. *J. Fluor. Chem.* **2010**, *131*, 1071-1081.

[20] F. M. D. Ismail, Important fluorinated drugs in experimental and clinical use. *J. Fluor. Chem.* **2002**, *118*, 27-33.

[21] A. M. Thayer, FABULOUS FLUORINE. *Chem. Eng. News* **2006**, *84*, 15-24.

[22] Y. Zhou, J. Wang, Z. Gu, S. Wang, W. Zhu, J. L. Aceña, V. A. Soloshonok, K. Izawa, H. Liu, Next Generation of Fluorine-Containing Pharmaceuticals, Compounds Currently in Phase II–III Clinical Trials of Major Pharmaceutical Companies: New Structural Trends and Therapeutic Areas. *Chem. Rev.* **2016**, *116*, 422-518.

[23] Y. Zhu, J. Han, J. Wang, N. Shibata, M. Sodeoka, V. A. Soloshonok, J. A. S. Coelho, F. D. Toste, Modern Approaches for Asymmetric Construction of Carbon–Fluorine Quaternary Stereogenic Centers: Synthetic Challenges and Pharmaceutical Needs. *Chem. Rev.* **2018**, *118*, 3887-3964.

[24] M. Cametti, B. Crousse, P. Metrangolo, R. Milani, G. Resnati, The fluorous effect in biomolecular applications. *Chem. Soc. Rev.* **2012**, *41*, 31-42.

[25] F. Babudri, G. M. Farinola, F. Naso, R. Ragni, Fluorinated organic materials for electronic and optoelectronic applications: the role of the fluorine atom. *Chem. Commun.* **2007**, 1003-1022.

[26] T. Chatterjee, N. Iqbal, Y. You, E. J. Cho, Controlled Fluoroalkylation Reactions by Visible-Light Photoredox Catalysis. *Acc. Chem. Res.* **2016**, *49*, 2284-2294.

[27] S. Barata-Vallejo, S. M. Bonesi, A. Postigo, Perfluoroalkylation reactions of (hetero)arenes. *RSC Advances* **2015**, *5*, 62498-62518.

[28] G. Ciamician, THE PHOTOCHEMISTRY OF THE FUTURE. *Science* **1912**, *36*, 385-394.

[29] B. König, Photocatalysis in Organic Synthesis – Past, Present, and Future. *Eur. J. Org. Chem.* **2017**, *2017*, 1979-1981.

[30] R. C. McAtee, E. J. McClain, C. R. J. Stephenson, Illuminating Photoredox Catalysis. *Trends Chem.* **2019**, *1*, 111-125.

[31] C. C. Le, M. K. Wismer, Z.-C. Shi, R. Zhang, D. V. Conway, G. Li, P. Vachal, I. W. Davies, D. W. C. MacMillan, A General Small-Scale Reactor To Enable Standardization and Acceleration of Photocatalytic Reactions. *ACS Cent. Sci.* **2017**, *3*, 647-653.

[32] D. A. Nicewicz, T. M. Nguyen, Recent Applications of Organic Dyes as Photoredox Catalysts in Organic Synthesis. *ACS Catal.* **2014**, *4*, 355-360.

[33] J. M. R. Narayanam, C. R. J. Stephenson, Visible light photoredox catalysis: applications in organic synthesis. *Chem. Soc. Rev.* **2011**, *40*, 102-113.

[34] C. K. Prier, D. A. Rankic, D. W. C. MacMillan, Visible Light Photoredox Catalysis with Transition Metal Complexes: Applications in Organic Synthesis. *Chem. Rev.* **2013**, *113*, 5322-5363.

[35] L. Marzo, S. K. Pagire, O. Reiser, B. König, Visible-Light Photocatalysis: Does It Make a Difference in Organic Synthesis? *Angew. Chem., Int. Ed.* **2018**, *57*, 10034-10072.

[36] M. H. Shaw, J. Twilton, D. W. C. MacMillan, Photoredox Catalysis in Organic Chemistry. *J. Org. Chem.* **2016**, *81*, 6898-6926.

[37] D. A. Nicewicz, D. W. C. MacMillan, Merging Photoredox Catalysis with Organocatalysis: The Direct Asymmetric Alkylation of Aldehydes. *Science* **2008**, *322*, 77-80.

[38] M. A. Ischay, M. E. Anzovino, J. Du, T. P. Yoon, Efficient Visible Light Photocatalysis of [2+2] Enone Cycloadditions. *J. Am. Chem. Soc.* **2008**, *130*, 12886-12887.

[39] J. M. R. Narayanam, J. W. Tucker, C. R. J. Stephenson, Electron-Transfer Photoredox Catalysis: Development of a Tin-Free Reductive Dehalogenation Reaction. *J. Am. Chem. Soc.* **2009**, *131*, 8756-8757.

[40] T. Koike, M. Akita, Trifluoromethylation by Visible-Light-Driven Photoredox Catalysis. *Top. Catal.* **2014**, *57*, 967-974.

[41] G. Dagousset, A. Carboni, G. Masson, E. Magnier, in *Modern Synthesis Processes and Reactivity of Fluorinated Compounds, Vol. 3*, 1st ed. (Eds.: H. Groult, F. R. Leroux, A. Tressaud), Elsevier: Amsterdam, Progress in Fluorine Science Series, **2017**, pp. 389-426.

[42] T. Koike, M. Akita, New Horizons of Photocatalytic Fluoromethylative Difunctionalization of Alkenes. *Chem* **2018**, *4*, 409-437.

[43] D. A. Nagib, M. E. Scott, D. W. C. MacMillan, Enantioselective α-Trifluoromethylation of Aldehydes via Photoredox Organocatalysis. *J. Am. Chem. Soc.* **2009**, *131*, 10875-10877.

[44] S. Mizuta, S. Verhoog, K. M. Engle, T. Khotavivattana, M. O'Duill, K. Wheelhouse, G. Rassias, M. Médebielle, V. Gouverneur, Catalytic Hydrotrifluoromethylation of Unactivated Alkenes. *J. Am. Chem. Soc.* **2013**, *135*, 2505-2508.

[45] S. Barata-Vallejo, B. Lantaño, A. Postigo, Recent Advances in Trifluoromethylation Reactions with Electrophilic Trifluoromethylating Reagents. *Chem. Eur. J.* **2014**, *20*, 16806-16829.

[46] G.-R. Park, Y. Choi, M. G. Choi, S.-K. Chang, E. J. Cho, Metal-Free Visible-Light-Induced Trifluoromethylation Reactions. *Asian J. Org. Chem.* **2017**, *6*, 436-440.

[47] N. Iqbal, S. Choi, E. Kim, E. J. Cho, Trifluoromethylation of Alkenes by Visible Light Photoredox Catalysis. *J. Org. Chem.* **2012**, *77*, 11383-11387.

[48] S. P. Pitre, C. D. McTiernan, H. Ismaili, J. C. Scaiano, Metal-Free Photocatalytic Radical Trifluoromethylation Utilizing Methylene Blue and Visible Light Irradiation. *ACS Catal.* **2014**, *4*, 2530-2535.

[49] N. J. W. Straathof, D. J. G. P. van Osch, A. Schouten, X. Wang, J. C. Schouten, V. Hessel, T. Noël, Visible Light Photocatalytic Metal-Free Perfluoroalkylation of Heteroarenes in Continuous Flow. *J. Flow Chem.* **2014**, *4*, 12-17.

[50] R. S. Mulliken, Structures of Complexes Formed by Halogen Molecules with Aromatic and with Oxygenated Solvents[1]. *J. Am. Chem. Soc.* **1950**, *72*, 600-608.

[51] R. S. Mulliken, Molecular Compounds and their Spectra. III. The Interaction of Electron Donors and Acceptors. *J. Phys. Chem.* **1952**, *56*, 801-822.

[52] C. G. S. Lima, T. de M. Lima, M. Duarte, I. D. Jurberg, M. W. Paixão, Organic Synthesis Enabled by Light-Irradiation of EDA Complexes: Theoretical Background and Synthetic Applications. *ACS Catal.* **2016**, *6*, 1389-1407.

[53] A. Postigo, Electron Donor-Acceptor Complexes in Perfluoroalkylation Reactions. *Eur. J. Org. Chem.* **2018**, *2018*, 6391-6404.

[54] G. E. M. Crisenza, D. Mazzarella, P. Melchiorre, Synthetic Methods Driven by the Photoactivity of Electron Donor–Acceptor Complexes. *J. Am. Chem. Soc.* **2020**, *142*, 5461–5476.

[55] Y.-q. Yuan, S. Majumder, M.-h. Yang, S.-r. Guo, Recent advances in catalyst-free photochemical reactions via electron-donor-acceptor (EDA) complex process. *Tetrahedron Lett.* **2020**, *61*, 151506.

[56] S. V. Rosokha, J. K. Kochi, Fresh Look at Electron-Transfer Mechanisms via the Donor/Acceptor Bindings in the Critical Encounter Complex. *Acc. Chem. Res.* **2008**, *41*, 641-653.

[57] R. Rathore, J. K. Kochi, in *Advances in Physical Organic Chemistry, Vol. 35*, Academic Press, **2000**, pp. 193-318.

[58] T. Clark, M. Hennemann, J. S. Murray, P. Politzer, Halogen bonding: the σ-hole. *J. Mol. Model.* **2007**, *13*, 291-296.

[59] P. Politzer, J. S. Murray, T. Clark, Halogen bonding and other σ-hole interactions: a perspective. *Phys. Chem. Chem. Phys.* **2013**, *15*, 11178-11189.

[60] D. Bulfield, S. M. Huber, Halogen Bonding in Organic Synthesis and Organocatalysis. *Chem. Eur. J.* **2016**, *22*, 14434-14450.

[61] P. Politzer, P. Lane, M. C. Concha, Y. Ma, J. S. Murray, An overview of halogen bonding. *J. Mol. Model.* **2007**, *13*, 305-311.

[62] J. S. Murray, P. Lane, T. Clark, P. Politzer, σ-hole bonding: molecules containing group VI atoms. *J. Mol. Model.* **2007**, *13*, 1033-1038.

[63] I. Alkorta, J. Elguero, M. Yáñez, O. Mó, M. M. Montero-Campillo, Relativistic Effects on NMR Parameters of Halogen-Bonded Complexes. *Molecules* **2019**, *24*, 4399.

[64] T. Clark, Halogen bonds and σ-holes. *Faraday Discuss.* **2017**, *203*, 9-27.

[65] R. Sedlak, M. H. Kolář, P. Hobza, Polar Flattening and the Strength of Halogen Bonding. *J. Chem. Theor. Comput.* **2015**, *11*, 4727-4732.

[66] F. Sladojevich, E. McNeill, J. Börgel, S.-L. Zheng, T. Ritter, Condensed-Phase, Halogen-Bonded CF_3I and C_2F_5I Adducts for Perfluoroalkylation Reactions. *Angew. Chem., Int. Ed.* **2015**, *54*, 3712-3716.

[67] H. A. Bent, Structural chemistry of donor-acceptor interactions. *Chem. Rev.* **1968**, *68*, 587-648.

[68] G. Cavallo, P. Metrangolo, R. Milani, T. Pilati, A. Priimagi, G. Resnati, G. Terraneo, The Halogen Bond. *Chem. Rev.* **2016**, *116*, 2478-2601.

[69] S. R. Kandukuri, A. Bahamonde, I. Chatterjee, I. D. Jurberg, E. C. Escudero-Adán, P. Melchiorre, X-Ray Characterization of an Electron Donor–Acceptor Complex that Drives the Photochemical Alkylation of Indoles. *Angew. Chem., Int. Ed.* **2015**, *54*, 1485-1489.

[70] J. Davies, S. G. Booth, S. Essafi, R. A. W. Dryfe, D. Leonori, Visible-Light-Mediated Generation of Nitrogen-Centered Radicals: Metal-Free Hydroimination and Iminohydroxylation Cyclization Reactions. *Angew. Chem., Int. Ed.* **2015**, *54*, 14017-14021.

[71] X. Sun, W. Wang, Y. Li, J. Ma, S. Yu, Halogen-Bond-Promoted Double Radical Isocyanide Insertion under Visible-Light Irradiation: Synthesis of 2-Fluoroalkylated Quinoxalines. *Org. Lett.* **2016**, *18*, 4638-4641.

[72] T. Morack, C. Mück-Lichtenfeld, R. Gilmour, Bioinspired Radical Stetter Reaction: Radical Umpolung Enabled by Ion-Pair Photocatalysis. *Angew. Chem., Int. Ed.* **2019**, *58*, 1208-1212.

[73] Z.-Y. Cao, T. Ghosh, P. Melchiorre, Enantioselective radical conjugate additions driven by a photoactive intramolecular iminium-ion-based EDA complex. *Nat. Commun.* **2018**, *9*, 3274.

[74] M.-C. Fu, R. Shang, B. Zhao, B. Wang, Y. Fu, Photocatalytic decarboxylative alkylations mediated by triphenylphosphine and sodium iodide. *Science* **2019**, *363*, 1429-1434.

[75] Y. Wang, J. Wang, G.-X. Li, G. He, G. Chen, Halogen-Bond-Promoted Photoactivation of Perfluoroalkyl Iodides: A Photochemical Protocol for Perfluoroalkylation Reactions. *Org. Lett.* **2017**, *19*, 1442-1445.

[76] F.-L. Zeng, K. Sun, X.-L. Chen, X.-Y. Yuan, S.-Q. He, Y. Liu, Y.-Y. Peng, L.-B. Qu, Q.-Y. Lv, B. Yu, Metal-Free Visible-Light Promoted Radical Cyclization to Access Perfluoroalkyl-Substituted Benzimidazo[2,1-α]isoquinolin-6(5*H*)-ones and Indolo[2,1-α]isoquinolin-6(5*H*)-ones. *Adv. Synth. Catal.* **2019**, *361*, 5176-5181.

[77] S. Mai, Y. Luo, X. Huang, Z. Shu, B. Li, Y. Lan, Q. Song, Diversity-oriented synthesis of imidazo[2,1-*a*]isoquinolines. *Chem. Commun.* **2018**, *54*, 10240-10243.

[78] Y. Liu, X.-L. Chen, K. Sun, X.-Y. Li, F.-L. Zeng, X.-C. Liu, L.-B. Qu, Y.-F. Zhao, B. Yu, Visible-Light Induced Radical Perfluoroalkylation/Cyclization Strategy To Access 2-Perfluoroalkylbenzothiazoles/Benzoselenazoles by EDA Complex. *Org. Lett.* **2019**, *21*, 4019-4024.

[79] X. Sun, Y. He, S. Yu, Halogen-bond-mediated atom transfer radical addition of perfluoroalkyl iodides to alkynes under visible light irradiation. *J. Photochem. Photobiol. A* **2018**, *355*, 326-331.

[80] Y. Cheng, S. Yu, Hydrotrifluoromethylation of Unactivated Alkenes and Alkynes Enabled by an Electron-Donor–Acceptor Complex of Togni's Reagent with a Tertiary Amine. *Org. Lett.* **2016**, *18*, 2962-2965.

[81] Y. Cheng, X. Yuan, J. Ma, S. Yu, Direct Aromatic C-H Trifluoromethylation via an Electron-Donor–Acceptor Complex. *Chem. Eur. J.* **2015**, *21*, 8355-8359.

[82] M. Nappi, G. Bergonzini, P. Melchiorre, Metal-Free Photochemical Aromatic Perfluoroalkylation of α-Cyano Arylacetates. *Angew. Chem., Int. Ed.* **2014**, *53*, 4921-4925.

[83] G. Filippini, M. Nappi, P. Melchiorre, Photochemical direct perfluoroalkylation of phenols. *Tetrahedron* **2015**, *71*, 4535-4542.

[84] E. Arceo, I. D. Jurberg, A. Álvarez-Fernández, P. Melchiorre, Photochemical activity of a key donor–acceptor complex can drive stereoselective catalytic α-alkylation of aldehydes. *Nat. Chem.* **2013**, *5*, 750-756.

[85] E. Arceo, A. Bahamonde, G. Bergonzini, P. Melchiorre, Enantioselective direct α-alkylation of cyclic ketones by means of photo-organocatalysis. *Chem. Sci.* **2014**, *5*, 2438-2442.

[86] Ł. Woźniak, J. J. Murphy, P. Melchiorre, Photo-organocatalytic Enantioselective Perfluoroalkylation of β-Ketoesters. *J. Am. Chem. Soc.* **2015**, *137*, 5678-5681.

[87] W.-Y. Huang, H.-Z. Zhang, Reaction of perfluoroalkyl iodides with alkenes initiated by organophosphine and related compounds. *J. Fluor. Chem.* **1990**, *50*, 133-140.

[88] D. G. Naae, H. S. Kesling, D. J. Burton, Reversible equilibrium in tertiary phosphine-fluorohalomethane reactions. *Tetrahedron Lett.* **1975**, *16*, 3789-3792.

[89] M. Lumbierres, M. Moreno-Mañas, A. Vallribera, Addition of perfluorooctyl iodide to alkenes. Catalysis by triphenylphosphane. *Tetrahedron* **2002**, *58*, 4061-4065.

[90] H. Lu, D.-y. Wang, A. Zhang, Visible Light-Promoted Phosphine-Catalyzed Difluoroalkylation of Arenes and Heterocycles. *J. Org. Chem.* **2020**, *85*, 942-951.

[91] J.-A. Ma, D. Cahard, Strategies for nucleophilic, electrophilic, and radical trifluoromethylations. *J. Fluor. Chem.* **2007**, *128*, 975-996.

[92] N. Shibata, A. Matsnev, D. Cahard, Shelf-stable electrophilic trifluoromethylating reagents: A brief historical perspective. *Beilstein J. Org. Chem.* **2010**, *6*, 65.

[93] X. Wang, Y. Ye, G. Ji, Y. Xu, S. Zhang, J. Feng, Y. Zhang, J. Wang, Copper-Catalyzed Direct C–H Trifluoromethylation of Quinones. *Org. Lett.* **2013**, *15*, 3730-3733.

[94] A. T. Parsons, S. L. Buchwald, Copper-Catalyzed Trifluoromethylation of Unactivated Olefins. *Angew. Chem., Int. Ed.* **2011**, *50*, 9120-9123.

[95] J. Xu, Y. Fu, D.-F. Luo, Y.-Y. Jiang, B. Xiao, Z.-J. Liu, T.-J. Gong, L. Liu, Copper-Catalyzed Trifluoromethylation of Terminal Alkenes through Allylic C–H Bond Activation. *J. Am. Chem. Soc.* **2011**, *133*, 15300-15303.

[96] X. Liu, X. Wu, Development and Challenges in the Copper-Catalyzed Trifluoromethylation of Alkenes. *Synlett* **2013**, *24*, 1882-1886.

[97] H. Egami, R. Shimizu, Y. Usui, M. Sodeoka, Iron-catalyzed trifluoromethylation with concomitant C–C bond formation *via* 1,2-migration of an aryl group. *Chem. Commun.* **2013**, *49*, 7346-7348.

[98] S. Large, N. Roques, B. R. Langlois, Nucleophilic Trifluoromethylation of Carbonyl Compounds and Disulfides with Trifluoromethane and Silicon-Containing Bases. *J. Org. Chem.* **2000**, *65*, 8848-8856.

[99] X. Liu, C. Xu, M. Wang, Q. Liu, Trifluoromethyltrimethylsilane: Nucleophilic Trifluoromethylation and Beyond. *Chem. Rev.* **2015**, *115*, 683-730.

[100] Q.-Y. Chen, Single Electron Transfer Reactions of Perfluoroalkyl Iodides. *Isr. J. Chem* **1999**, *39*, 179-192.

[101] D. W. Stephan, G. Erker, Frustrated Lewis Pair Chemistry: Development and Perspectives. *Angew. Chem. Int. Ed.* **2015**, *54*, 6400-6441.

[102] D. W. Stephan, G. Erker, Frustrated Lewis Pairs: Metal-free Hydrogen Activation and More. *Angew. Chem., Int. Ed.* **2010**, *49*, 46-76.

[103] G. C. Welch, R. R. S. Juan, J. D. Masuda, D. W. Stephan, Reversible, Metal-Free Hydrogen Activation. *Science* **2006**, *314*, 1124-1126.

[104] L. Helmecke, Mechanismus und Selektivität FLP-katalysierter Perfluoroalkylierungen. Master thesis, Heinrich-Heine-Universität Düsseldorf, Düsseldorf, 2017.

[105] P. E. Sanderson, B. D. Dorsey, T. A. Lyle, M. G. Stanton, D. Staas, A. M. Naylor-Olsen, C. Coburn, M. M. Morrissette Thrombin inhibitors. U.S. Patent 6,610,693 B1, Aug. 26, 2003.

[106] P. Wessig, O. Mühling, Photochemical Synthesis of Highly Functionalized Cyclopropyl Ketones. *Helv. Chim. Acta* **2003**, *86*, 865-893.

[107] C. A. Tolman, Steric effects of phosphorus ligands in organometallic chemistry and homogeneous catalysis. *Chem. Rev.* **1977**, *77*, 313-348.

[108] V. Mark, J. R. V. Wazer, Tri-t-butyl Phosphite and Some of Its Reactions. *J. Org. Chem.* **1964**, *29*, 1006-1008.

[109] T. Allman, R. G. Goel, The basicity of phosphines. *Can. J. Chem.* **1982**, *60*, 716-722.

[110] Y. Xu, J. Huang, B. Gabidullin, D. L. Bryce, A rare example of a phosphine as a halogen bond acceptor. *Chem. Commun.* **2018**, *54*, 11041-11043.

[111] F. Maya, S. H. Chanteau, L. Cheng, M. P. Stewart, J. M. Tour, Synthesis of Fluorinated Oligomers toward Physical Vapor Deposition Molecular Electronics Candidates. *Chem. Mater.* **2005**, *17*, 1331-1345.

[112] O. Dumele, D. Wu, N. Trapp, N. Goroff, F. Diederich, Halogen Bonding of (Iodoethynyl)benzene Derivatives in Solution. *Org. Lett.* **2014**, *16*, 4722-4725.

[113] G. Filippini, M. Silvi, P. Melchiorre, Enantioselective Formal α-Methylation and α-Benzylation of Aldehydes by Means of Photo-organocatalysis. *Angew. Chem., Int. Ed.* **2017**, *56*, 4447-4451.

[114] A. Studer, D. P. Curran, Catalysis of Radical Reactions: A Radical Chemistry Perspective. *Angew. Chem., Int. Ed.* **2016**, *55*, 58-102.

[115] W. L. F. Armarego, *Purification of laboratory chemicals*, 6. ed., Elsevier, Amsterdam u.a., **2009**.

[116] C. Amatore, E. Blart, J. P. Genet, A. Jutand, S. Lemaire-Audoire, M. Savignac, New synthetic applications of water-soluble acetate Pd/TPPTS catalyst generated in Situ. evidence for a true Pd(0) species intermediate. *J. Org. Chem.* **1995**, *60*, 6829-6839.

[117] A. S. K. Hashmi, R. Döpp, C. Lothschütz, M. Rudolph, D. Riedel, F. Rominger, Scope and Limitations of Palladium-Catalyzed Cross-Coupling Reactions with Organogold Compounds. *Adv. Synth. Catal.* **2010**, *352*, 1307-1314.

[118] A. Matsuzawa, S. Takeuchi, K. Sugita, Iodoalkyne-Based Catalyst-Mediated Activation of Thioamides through Halogen Bonding. *Chem. Asian J.* **2016**, *11*, 2863-2866.